UNIVERSIDADE DE SÃO PAULO
Instituto de Ciências Matemáticas e de Computação

Geometrical and topological investigation of some families of quadratic differential systems possessing saddle-nodes or invariant ellipses

Marcos Coutinho Mota

Tese de Doutorado do Programa de Pós-Graduação em Matemática (PPG-Mat)

ICMC USP SÃO CARLOS

Marcos Coutinho Mota

Geometrical and topological investigation of some families of quadratic differential systems possessing saddle-nodes or invariant ellipses

Thesis submitted to the Instituto de Ciências Matemáticas e de Computação – ICMC-USP – in accordance with the requirements of the Mathematics Graduate Program, for the degree of Doctor in Science. *FINAL VERSION*

Concentration Area: Mathematics

Advisor: Profª. Drª. Regilene Delazari dos Santos Oliveira
Co-advisors: Prof. Dr. Alex Carlucci Rezende, Prof. Dr. Joan Carles Artés Ferragud

USP – São Carlos
May 2021

Ficha catalográfica elaborada pela Biblioteca Prof. Achille Bassi
e Seção Técnica de Informática, ICMC/USP,
com os dados inseridos pelo(a) autor(a)

M917g

Mota, Marcos Coutinho
Geometrical and topological investigation of some families of quadratic differential systems possessing saddle-nodes or invariant ellipses / Marcos Coutinho Mota; orientadora Regilene Delazari dos Santos Oliveira; coorientador Alex Carlucci Rezende, Joan Carles Artés Ferragud . -- São Carlos, 2021.
396 p.

Tese (Doutorado - Programa de Pós-Graduação em Matemática) -- Instituto de Ciências Matemáticas e de Computação, Universidade de São Paulo, 2021.

1. quadratic differential system. 2. geometrical and topological classification. 3. phase portrait. 4. invariant polynomial. 5. configuration of invariant ellipses and lines. I. Oliveira, Regilene Delazari dos Santos, orient. II. , Alex Carlucci Rezende, Joan Carles Artés Ferragud, coorient. III. Título.

Bibliotecários responsáveis pela estrutura de catalogação da publicação de acordo com a AACR2:
Gláucia Maria Saia Cristianini - CRB - 8/4938
Juliana de Souza Moraes - CRB - 8/6176

Marcos Coutinho Mota

Investigação geométrica e topológica de algumas famílias de sistemas diferenciais quadráticos possuindo selas-nós ou elipses invariantes

Tese apresentada ao Instituto de Ciências Matemáticas e de Computação – ICMC-USP, como parte dos requisitos para obtenção do título de Doutor em Ciências – Matemática. *VERSÃO REVISADA*

Área de Concentração: Matemática

Orientadora: Profª. Drª. Regilene Delazari dos Santos Oliveira
Coorientadores: Prof. Dr. Alex Carlucci Rezende, Prof. Dr. Joan Carles Artés Ferragud

USP – São Carlos
Maio de 2021

This thesis is dedicated to my parents, sisters, fiance and, of course, to everyone who is interested in the classification of planar quadratic differential systems.

ACKNOWLEDGEMENTS

Depois de quatro anos nessa montanha–russa chamada Doutorado é hora de deixar alguns agradecimentos.

Primeiramente agradeço a Deus pela vida, por todas as oportunidades e por mais esta conquista.

Agradeço aos meus pais, Marta e José Luiz, às minhas irmãs, Maria das Mercês e Elizângela e à minha avó Terezinha (*in memoriam*), por tudo o que fizeram por mim e por sempre me incentivarem a estudar.

Meu mais carinhoso agradecimento é dedicado à minha noiva Mirianne. Meu amor, sem você essa luta certamente seria muito mais difícil! Muito obrigado por sempre estar ao meu lado me dando forças! Você é o melhor presente que a vida me deu durante este Doutorado! Agradeço também aos seus familiares (minha segunda família), por me receberem de braços abertos!

Agradeço também aos amigos da Graduação, Mestrado e Doutorado. Particularmente deixo especial agradecimento ao amigo Marco Antonio. "Primo", desde o Mestrado eu te considero um irmão que a vida me deu! Além disso, você é um dos "culpados" por eu estar concluindo o Doutorado no ICMC. Em 2016 você insistiu tanto até eu fazer minha inscrição, obrigado mesmo por isso e por todo o restante (se eu fosse elencar tudo, certamente não caberia aqui)!

Agradeço a todos os meus ex–professores pelos conhecimentos transmitidos. Em particular, agradeço aos meus ex–orientadores (em Matemática) Marcos Pavani de Carvalho e Liliane Martinez Antonow (Graduação), Denis de Carvalho Braga e Luis Fernando de Osório Mello (Mestrado) por todos os incentivos e ajudas para que eu pudesse chegar até aqui.

Não poderia deixar de agradecer (e muito) à minha orientadora. Regilene, no fim de 2016 eu te escrevi dizendo que havia sido aprovado no processo seletivo para o Doutorado em Matemática do ICMC e perguntei sobre a sua disponibilidade de orientação. Prontamente você me respondeu e já me encaminhou esta proposta de tese (a qual agora se concretiza). Em 2017 iniciei o Doutorado, fiz disciplinas, exames de qualificação, realizamos três estágios de docência e, principalmente, trabalhamos por muitas horas em sua sala (e agora, no fim do Doutorado, virtualmente). Se você tivesse respondido aquele email em 2016 dizendo que não teria disponibilidade para me orientar, certamente eu

não estaria concluindo esta tese. Muito obrigado por todo o seu tempo dedicado a me orientar, por todos os ensinamentos, ajudas, conselhos, incentivos, oportunidades, confiança em meu trabalho, paciência e amizade durante toda a orientação! Espero que nossa amizade e colaborações continuem por muitos anos!

Agradeço muito também ao meu coorientador brasileiro. Alex, depois (e além) da Regilene, você foi de fundamental importância para o andamento e conclusão dos trabalhos desenvolvidos ao longo do meu Doutorado. Você tem grande contribuição nesta tese e, consequentemente, na conclusão dessa etapa da minha vida. Muito obrigado por todas as ajudas, incentivos, conselhos, por todo o seu tempo e, principalmente, por sua amizade no decorrer desta coorientação! Fico muito feliz de ter sido seu (primeiro) aluno de Doutorado! Que nossa amizade e colaborações continuem por muitos anos!

Também deixo um agradecimento aos amigos do nosso "Grupo Dinâmico".

Agradezco mucho a mi codirector catalán Profesor Joan Carles Artés por invitarme a estar en Barcelona para trabajar con él en la Universitat Autònona de Barcelona (UAB). Los seis meses que estuve en Barcelona fue un período muy productivo y significativo para la conclusión de esta tesis. Joan Carles, agradezco mucho todo su tiempo, su paciencia, ayudas con el trabajo, todas las enseñanzas, viajes en coche, compañías en la hora de la comida en el restaurante de la UAB, ¡enfin, por todo! Vuestra ayuda fue fundamental para la conclusión de esta tesis. Mismo con la pandemia del Coronavirus me gustó mucho estar en la magnífica Barcelona y espero que tengamos muchas otras oportunidades de trabajar juntos (claro, sin Coronavirus).

I would like to thank Professor Nicolae Vulpe for the opportunity of working with him during his visit to São Carlos in 2019. Nicolae, I also thank you for the opportunity of learning a little bit about the Invariant Theory and, on behalf of everyone who uses this theory in order to study quadratic systems, thank you very much for having improved these tools!

También tengo mucho que agradecer a mi amigo Laudino (y claro, su familia: Laudy, María, Mirian y Carlos) de Cerdanyola del Vallès. Laudy, muchas gracias por haber abierto las puertas de vuestro piso para yo vivir mientras estuve en Barcelona. Esté cierto de que no voy olvidarme jamás de este período que he estado en vuestra casa. Creo que viví en el mejor piso de Cerdanyola. No voy olvidarme de sus estrellas al sonido de los reggaetones, de su piso, de nuestros paseos en Cerdanyola, del por del sol desde el balcón, de las charlas sobre varios temas y claro, de la pandemia y de los aplausos en el balcón al sonido de la canción *Resistiré*. No olvidaré también a Brenda, que nos ha brindado con su compañía muy graciosa, casi todos los días pacientemente acostada en el balcón mirando el paisaje. Vosotros habéis sido los mejores compañeros de piso, ¡vos agradezco mucho la compañía! ¡Ojalá nos veamos otra vez!

Aos colegas brasileiros Ana Lívia, Luiz Fernando (e familiares), Mariana e Rubem que estiveram em Barcelona durante minha estadia por lá, obrigado pelos bons momentos e passeios juntos!

Deixo também um agradecimento à dona Nair, proprietária do apartamento onde vivi em São Carlos durante o Doutorado, uma pessoa muito bondosa, sempre pronta e disposta a ajudar.

Agradeço a todas as pessoas, as quais não tiveram o nome mencionado aqui, mas que estiveram presente durante toda essa caminhada e que contribuíram de alguma forma para a conclusão desta etapa da minha vida. Em particular, também agradeço a todos os professores e funcionários do ICMC e também do Departamento de Matemática da Universidade Autônoma de Barcelona.

I would like to thank Professors Dr. Alex Carlucci Rezende (UFSCar), Dr. Claudia Valls Angles (Instituto Superior Técnico da Universidade de Lisboa), Dr. Dana Schlomiuk (Université de Montréal), Dr. Fabio Scalco Dias (UNIFEI), Dr. Jaume Llibre (Universitat Autònoma de Barcelona), Dr. Joan Carles Artés (Universitat Autònoma de Barcelona), Dr. Nicolae Vulpe (Institute of Mathematics and Computer Science, Moldova, Chisinau), and Dr. Regilene Delazari dos Santos Oliveira (ICMC-USP) for their availability in participating in my doctoral defense and also for their valuable suggestions and corrections, aiming a higher quality of this thesis.

O presente trabalho foi realizado com apoio da Coordenação de Aperfeiçoamento de Pessoal de Nível Superior – Brasil (CAPES) – Código de Financiamento 001. Deixo meu muito obrigado à CAPES pelos auxílios financeiros recebidos via PROEX (Processo número 88882.328773/2019–01) e PRINT (Processo número 88887.371153/2019–00).

"[...]

Resistiré, erguido frente a todo

Me volveré de hierro para endurecer la piel

Y aunque los vientos de la vida soplen fuerte

Soy como el junco que se dobla

Pero siempre sigue en pie

Resistiré, para seguir viviendo

Soportaré los golpes y jamás me rendiré

Y aunque los sueños se me rompan en pedazos

Resistiré, resistiré [...]"

(Dúo Dinámico, 1988)

El himno de la cuarentena en España en 2020

RESUMO

MOTA, M. C. **Investigação geométrica e topológica de algumas famílias de sistemas diferenciais quadráticos possuindo selas-nós ou elipses invariantes**. 2021. 396 p. Tese (Doutorado em Ciências – Matemática) – Instituto de Ciências Matemáticas e de Computação, Universidade de São Paulo, São Carlos – SP, 2021.

O estudo dos sistemas diferenciais polinomiais quadráticos no plano tem se demonstrado desafiador, existem centenas de artigos datados de mais de um século sobre esse tema e ainda existem muitos tópicos para serem estudados e concluídos. Por exemplo, a caracterização completa dos retratos de fase de sistemas quadráticos permanece desconhecida e a classificação topológica completa de tais sistemas tem sido um trabalho complexo. É bem sabido que a principal dificuldade de se trabalhar com os sistemas quadráticos é a quantidade de parâmetros. Um sistema quadrático (genérico) é definido por 12 parâmetros, entretanto, usando transformações afins e reescala temporal pode–se reduzir este número para cinco, mas ainda são muitos parâmetros, uma vez que o correspondente diagrama de bifurcação é um espaço euclideano de dimensão cinco. Desta forma, faz–se conveniente utilizar algumas ferramentas (a Teoria dos Invariantes, por exemplo) de modo a estudar famílias de sistemas quadráticos com propriedades específicas (por exemplo, de acordo com a estabilidade estrutural ou possuindo classes de curvas algébricas invariantes) para reduzir ainda mais (quando possível) essa quantidade de parâmetros. Nesta tese objetivamos contribuir com a classificação dos sistemas quadráticos no plano. Mais precisamente, apresentamos o estudo completo (módulo ilhas) do diagrama de bifurcação de duas famílias de sistemas quadráticos com propriedades específicas em suas singularidades. Fazemos a classificação topológica completa de todos os retratos de fases (módulo ciclos limites) de dois conjuntos de sistemas quadráticos de codimensão dois e fazemos a classificação de todos os sistemas quadráticos que possuem elipses invariantes de acordo com a chamada configuração de elipses invariantes e retas invariantes. Vale a pena ressaltar que esses trabalhos representam três abordagens distintas para o estudo dos sistemas quadráticos, e cada um deles utiliza técnicas diferentes, que em conjunto são úteis para o objetivo final de classificar retratos de fases.

Palavras-chave: sistema diferencial quadrático, classificação geométrica e topológica, retrato de fase, invariante polinomial, configuração de elipses e retas invariantes.

ABSTRACT

MOTA, M. C. **Geometrical and topological investigation of some families of quadratic differential systems possessing saddle-nodes or invariant ellipses**. 2021. 396 p. Tese (Doutorado em Ciências – Matemática) – Instituto de Ciências Matemáticas e de Computação, Universidade de São Paulo, São Carlos – SP, 2021.

The study of quadratic polynomial differential systems on the plane have been shown a tough challenge, there exist hundreds of papers about them which are dated for over a century and until now there exist several topics to be studied and concluded. For instance, the complete characterization of phase portraits of quadratic systems remains unknown and the complete topological classification of such systems has been a complex work. It is well known that the greatest difficult of working with quadratic systems is the quantity of parameters. A (generic) quadratic system is defined by 12 parameters, however by using affine transformations and time rescaling one can reduce this number by five, but yet this is a very large number, once the corresponding bifurcation diagram is a five–dimensional euclidean space. So, it is convenient to use some tools (as the Invariant Theory) in order to study families of quadratic systems with specific properties (for instance, according to the structural stability or possessing classes of invariant algebraic curves) with the purpose of reducing even more (when it is possible) this quantity of parameters. The main goal of this thesis is to contribute to the classification of the quadratic systems on the plane. More precisely, we present the complete study (modulo islands) of the bifurcation diagram of two families of quadratic systems possessing specific properties on their singularities, we do the complete topological classification (modulo limit cycles) of all the phase portraits of two sets of quadratic systems of codimension two and we perform the classification of quadratic differential systems with invariant ellipses according to their configurations of invariant ellipses and invariant lines. It is worth mentioning that these three works represent three different approaches to the study of quadratic systems and each one of them uses different techniques, which all together are useful towards the final goal of classifying phase portraits.

Keywords: quadratic differential system, geometrical and topological classification, phase portrait, invariant polynomial, configuration of invariant ellipses and lines.

CONTENTS

INTRODUCTION

In Artés, Oliveira and Rezende (2020), the authors present a remarkable introduction to the study of the planar quadratic differential systems. In my point of view, there is no best introduction to this subject. So in the next paragraphs I ask the authors for a permission to use some of their ideas for an introduction to this thesis.

"Mathematicians are fascinated in closing problems. Having a question solved or even sign with a "q.e.d" a question asked in the past is a pleasure which is directly proportional to the time elapsed between the formulation of the question and the moment of the answer" (Artés, Oliveira and Rezende (2020)).

The advent of the Differential Calculus opened the possibility of solving many questions that mathematicians from medieval era asked, but at the same time it opened the possibility of formulating many new other questions. The search for primitive functions that could not be expressed algebraically or with a finite number of analytic terms complicated the future research lines, and even new areas of Mathematics were created to give answers (precise or not) to these questions. And beside the problem of finding a primitive to a differential equation in a single dimension, if we consider a multivariable problem, clearly the study becomes much more difficult.

It is known that it took almost 200 years between the appearance of the first system of linear differential equations and its complete resolution by Laplace in 1812. After the resolution of linear differential systems, for any dimension, it seemed natural to address the classification of *quadratic differential systems*.

However, it was found that the problem would not have an easy solution in a short period of time. An example of this situation occurs with differential equations such as those ones used to solve real–life problems, which may not necessarily be directly solvable, i.e. their solutions do not have an explicit expression. Instead, solutions can be approximated by using numerical methods. Unlike the linear systems that can be solved analytically, quadratic systems (not even, therefore, those of higher degree) generically admit a solution of that kind, at least, with a finite number of terms.

Therefore, during the attempt of solving the non–linear differential systems, another strategy was chosen and that moment allowed the creation of a new area of knowledge in Mathematics, the *Qualitative Theory of Ordinary Differential Equations* (see Poincaré (1885)). Since we are not able to give a precise mathematical expression to the

solution of a system of differential equations, this theory, which became one of the basic tools of pure and applied Mathematics, intends to express by means of a complete and precise drawing the behavior (or evolution in time) of any particle located in a vector field governed by such a differential equation, i.e. its phase portrait.

Even with all the reductions (or simplifications) made to the problem until now, there are still some difficulties. The most expressive one is that the phase portraits of differential systems may have invariant sets as limit cycles and graphics. A linear system cannot generate limit cycles; at most they can present a completely circular phase portrait where all the orbits are periodic. But a differential system in the plane, polynomial or not, and starting with the quadratic ones, may present several limit cycles. It is natural to find an infinite number of these cycles in non–polynomial problems, but the intuition seems to indicate that a polynomial system should not have an infinite number of limit cycles in a similar way as it cannot have an infinite number of isolated singular points. And because the number of singular points is linked to the degree of the polynomial system, it also seems logical to think that the number of limit cycles could also have a similar link, either directly as the number of singular points, or even in an indirect way from the number the parameters of such systems.

In 1900, David Hilbert (Hilbert (1900), Hilbert (1902)) proposed a set of 23 problems to be solved in the 20th century, and among them, the second part of his well–known 16th problem asks for the maximum number of limit cycles that a polynomial differential system in the plane with degree n may have. Even being the polynomial case (i.e. a subfamily of the set of all differential equations) more than one hundred years after, we do not have an uniform upper bound for this generic problem, only for specific families of such systems.

In this thesis we restrict ourselves to the study and to the geometrical and topological classification of *planar quadratic differential systems*, or simply *quadratic systems*, i.e. differential systems of the form

$$\begin{aligned} \dot{x} &= p(x,y), \\ \dot{y} &= q(x,y), \end{aligned} \tag{1}$$

where p and q are polynomials over $\mathbb{R}$ in x and y such that the $\max\{\deg(p),\deg(q)\} = 2$. For system (1) one can always associate the quadratic vector field

$$\xi = p\frac{\partial}{\partial x} + q\frac{\partial}{\partial y}, \tag{2}$$

as well as the differential equation

$$q\,dx - p\,dy = 0. \tag{3}$$

Moreover, we can also write system (1) as

$$\begin{aligned}\dot{x} &= p_0 + p_1(x,y) + p_2(x,y) \equiv p(x,y),\\ \dot{y} &= q_0 + q_1(x,y) + q_2(x,y) \equiv q(x,y),\end{aligned}$$

where p_i and q_i are homogeneous polynomials of degree i in the variables x and y with real coefficients. Along this thesis we use indistinctly the expressions *quadratic systems* (**QS**) and *quadratic vector fields* (**QVF**) to refer to either (1), or (2), or (3).

This family of systems by definition depends on twelve parameters, but due to the action of the group $\mathbf{Aff}(2,\mathbb{R})$ of real affine transformations and time homotheties, the class ultimately depends on five parameters, but this is still a large number.

During discussions, in 1966, Coppel (1966) expressed the belief that we could obtain the classification of phase portraits of quadratic systems by purely algebraic means. That is, by means of algebraic equalities and inequalities, it should be possible to determine the phase portrait of a quadratic system. This claim was not easy to refute at that time, since the isolated finite singular points of a quadratic system can be found by means of the resultant that is of fourth degree, and its solutions can be calculated algebraically, like those ones of infinity. Moreover, at that time it was known how to generate limit cycles by a Hopf bifurcation, whose conditions are also determined algebraically.

On the other hand, in 1991, Dumortier and Fiddelaers (1991) showed that, starting with the quadratic systems (and following with all the higher–degree polynomial systems), there exist geometric and topological phenomena in phase portraits of such systems whose determination cannot be established by means of algebraic expressions. More specifically, most part of the connections among separatrices and the occurrence of double or semi–stable limit cycles cannot be algebraically determined.

Therefore, the complete classification of quadratic systems is a very difficult task at the moment and it depends on the solution of the second part of Hilbert's 16th problem, even at least partially for the quadratic case.

Even so, a lot of problems have been appearing related to quadratic systems to which it has been possible to give an answer, even for specific cases. In fact, there are more than one thousand articles published that are directly related to studies of aspects of quadratic systems. Professor John William Reyn, from Delft University (Netherlands), prepared a bibliography that was published several times until his retirement (see Reyn (1987), Reyn (1994), Reyn (1996), Reyn (1997), Reyn (2007)). It is worth mentioning that in the last two decades many other articles related to quadratic systems have appeared, so that the number of one thousand published papers on the subject may have been widely exceeded.

Many of the questions proposed and the problems solved have dealt with subclassifications of quadratic systems, that is, classifications of systems that shared some specific

characteristic in common. For instance, one can find classifications of quadratic systems having a center type singularity (Vulpe (1983), Żołądek (1994)), having a weak focus of third order (Artés and Llibre (1997), Llibre and Schlomiuk (2004)), having a nilpotent singularity (Jager (1990)), without real singular points (Gasull, Ren and Llibre (1986)), with two invariant straight lines (Reyn (1987)) and so on, up to a thousand articles. In some of them complete answers could be given, including for the problem of limit cycles (existence and number of limit cycles), but in other cases, the classification was done modulo limit cycles, i.e. all the authors present all the possible phase portraits without taking into account the presence and number of limit cycles. Since in quadratic systems a limit cycle can only surround a single finite singular point, which must necessarily be a focus (Coppel (1966)), then it is enough to identify the outermost limit cycle of a nesting of cycles with a point, and interpret the stability of that point as the outer stability of this cycle, and study everything that can happen to the phase portrait in the rest of the phase space.

Within the families of quadratic systems which were studied in the last century, we would highlight the study of the structurally stable quadratic systems, modulo limit cycles (see Artés, Kooij and Llibre (1998)). The goal was to determine how many and which phase portraits of a quadratic system cannot be modified by small perturbations in their parameters. In order to obtain a structurally stable system modulo limit cycles we need a few conditions: we do not allow the existence of multiple singular points and the existence of connections of separatrices. Centers, weak foci, semi–stable cycles, and all other unstable elements belong to the quotient modulo limit cycles. This important study presented in Artés, Kooij and Llibre (1998) showed that the structurally stable quadratic systems have a total of 44 topologically distinct phase portraits. The importance of such a work is reflected in the fact that it completes everything that can happen in a generic form in the huge parameter space $\mathbb{R}^{12}$. Every chosen stable quadratic system is one of these 44, every generic perturbation of a quadratic system is one of these 44, and even some unstable quadratic systems as those ones which possess a weak focus have its phase portrait among these 44.

From this scenario we observe that if we intend to work with classification of phase portraits of quadratic systems before the solution of the second part of Hilbert's 16th problem, this must be done modulo limit cycles.

There are two ways to perform a systematic study of all the phase portraits of the quadratic systems. The first way is the one initiated by Reyn in which he began by studying the phase portraits of all the quadratic systems in which all the finite singular points have coalesced with infinite singular points (see Reyn (1991)). Later, he studied those phase portraits in which exactly three finite singular points have coalesced with points at infinity, so there remains one real finite singularity. And then he completed

the study of the cases in which two finite singular points have coalesced with infinite singularities, originating two real points, or one double point, or two complex points. His work on finite multiplicity three was incomplete and the one on finite multiplicity four was inaccessible.

In another approach, instead of working from the highest degrees of degeneracy to the lower ones, is going in the reverse direction. We already know that the structurally stable quadratic systems produce 44 topologically distinct phase portrait, as already mentioned before. In Artés, Llibre and Rezende (2018) the authors classified the structurally unstable quadratic systems of codimension one modulo limit cycles, which have one and only one of the simplest structurally unstable objects: a saddle–node of multiplicity two (finite or infinite), a separatrix from one saddle point to another, or a separatrix forming a loop for a saddle point with its divergence nonzero. All the phase portraits of codimension one are split into four groups according to the possession of a structurally unstable element: (A) possessing a finite semi–elemental saddle–node, (B) possessing an infinite semi–elemental saddle–node $\overline{\binom{0}{2}}SN$, ($C$) possessing an infinite semi–elemental saddle–node $\overline{\binom{1}{1}}SN$, and ($D$) possessing a separatrix connection. The study of the codimension–one systems was done in approximately 20 years and finally it was obtained at least 204 (and at most 211) topologically distinct phase portraits of codimension one modulo limit cycles (see Artés, Llibre and Rezende (2018)). In Artés, Oliveira and Rezende (2020) and also in a recent study (yet at a preprint level), two mistakes in Artés, Llibre and Rezende (2018) were found and the number of cases was reduced (and confirmed) to at least 202 (and a most 209) topologically distinct phase portraits of codimension one modulo limit cycles.

Once completed the classification of structurally unstable quadratic systems of codimension one, it is time to study the systems of codimension two (considered by the combination of families of codimension one), modulo limit cycles. Even though this work can be exhaustive, it counts with the advantage that how biggest is the degeneration of the systems, bigger is the literature that we have available. Even with the existence of a large literature from which we can take new examples of phase portraits still unknown, new families of quadratic systems must be studied in order to contribute to this systematic process. In fact, the approach is the same as used in the previous two works (Artés, Kooij and Llibre (1998) and Artés, Llibre and Rezende (2018)). One must start by looking for all the potential topological phase portraits (i.e. phase portraits that can be drawn on paper) of codimension two modulo limit cycles, and then try to realize all of them (i.e. to find examples of quadratic differential systems whose phase portraits are exactly those phase portraits obtained previously) or to show that some of them are non–realizable or impossible (i.e. in case of absence of examples for the realization of a phase portrait, say Ψ, it is necessary to prove that there is no quadratic differential system whose phase portrait is topologically equivalent to Ψ). So, it is also very convenient to have studied a bifurcation diagram that helps us in the realization problem. We recall that if we have a

parametric system of differential equations (or, simply, a family of differential equations) the word *bifurcation* usually means a sudden qualitative change in the nature of a solution of the system, as a parameter is varied. The parameter value at which a bifurcation occurs is called a *bifurcation parameter value*. The *bifurcation diagram* shows all the bifurcations of a system as a function of a bifurcation parameter in the system, and corresponding to each choice of the parameter value we can obtain a corresponding phase portrait.

The study of the codimension two systems is already in progress. In Artés, Oliveira and Rezende (2020) the authors have considered the set (AA) obtained by the coalescence of two finite singular points, yielding either a triple saddle, or a triple node, or a cusp point, or two saddle–nodes. They obtained all the potential topological phase portraits of the set (AA) and proved their realization. In their study they got 34 topologically distinct phase portraits (of codimension two) in the Poincaré disc modulo limit cycles.

One of the main goals of this thesis is to contribute to the classification of the phase portraits of planar quadratic differential systems of codimension two, modulo limit cycles. Three of the main results of this thesis are related to the topological classification and realization of phase portraits of the vector fields belonging to sets (AB) and (AC). The set (AB) contains all quadratic systems possessing a finite saddle–node $\overline{sn}_{(2)}$ and an infinite saddle–node of type $\overline{\binom{0}{2}}\,SN$ obtained by the coalescence of an infinite saddle with an infinite node. We point out that the complete bifurcation diagram corresponding to this set was completely studied in Artés, Rezende and Oliveira (2015) and, as we prove in this thesis, the generic phase portraits obtained by these authors are indeed all the phase portraits from the set (AB). The set (AC) describes all quadratic systems possessing a finite saddle–node $\overline{sn}_{(2)}$ and an infinite saddle–node of type $\overline{\binom{1}{1}}\,SN$, obtained by the coalescence of a finite saddle (respectively, a finite node) with an infinite node (respectively, an infinite saddle). Notice that the finite singularity that coalesces with an infinite singularity cannot be the finite saddle–node since then what we would obtain at infinity would not be a saddle–node of type $\overline{\binom{1}{1}}\,SN$ but a singularity of multiplicity three. Even though this is also a case of codimension–two phase portraits and somehow can be considered inside the set (AC), we have preferred to put it into the set (CC), and consider this case in a near future study.

In this thesis we present the study of the bifurcation diagrams corresponding to phase portraits possessing the set of saddle–nodes $\left\{\overline{sn}_{(2)} + \overline{\binom{1}{1}}\,SN\right\}$, i.e. phase portraits belonging to the set (AC) and we also present the study of the topological classification and realization of all of these phase portraits. Additionally, here we present the topological classification and realization of all the phase portraits belonging to the set (AB). The results we have mentioned were obtained thanks to the widely experience and help of Professor Joan Carles Artés, since 2018 collaborating with us. These studies were more intensive and productive during a *sandwich period* at *Universitat Autònoma de Barcelona*

with the supervision of Professor Joan Carles.

The main technique used in this thesis is the *Invariant Theory* for quadratic systems, developed by the Sibirsky's School in Moldova, especially improved by one of his main students, Professor Nicolae Vulpe. In what follows we discuss a little bit about this subject. It is well known that for several years ago there were numerous publications on topological classification of special families of quadratic or cubic vector fields. Such classifications in general were done with respect to chosen normal forms, convenient for studying the specific classification problems. Normal forms are important because they allow us to reduce the number of parameters on which families depend on. A normal form can be effective for studying a problem while for another problem it can be inconvenient and hence another more suitable normal form needs to be found. It is clear that for the study of the whole family of quadratic differential systems a multitude of such normal forms are necessary. But how do we cross the results obtained by using one normal form with those ones obtained by using a different normal form, so as to see the full picture covering the two normal forms, in case they have a nonempty intersection? This is one direction where the algebraic invariant theory of differential equations can be very helpful. This theory has an important role because, unlike other classification results on these systems that were non–intrinsic, the results obtained by using the theory developed by Sibirsky and his students were intrinsic, i.e. they were invariant under allowable coordinate changes and hence independent of the specific presentation of the systems (normal forms) used in the classifications. This is clearly a great advantage.

In order to classify all the global phase portraits obtained by the study of some family, we must verify all the topological changes (bifurcations) in the behavior of solutions of this family depending of course on the real parameters of this family. The bifurcation diagram will be constructed from the behavior of algebraic sets given by the zeroes of the *invariant polynomials* (these are polynomials which have the parameters of the family as variables) or of *comitants* (invariant polynomials which depends also on the variables x and y), and possibly by the existence of some nonalgebraic bifurcation sets numerically found. On these sets one can detect some geometric properties, as for instance whether a singularity goes to infinity or not, if two (or more) points coalesce, if there exist invariant lines, if there exist centers, if there exist weak points (foci or saddles), among others. In short, everything that has been studied in some particular normal form can be viewed in terms of invariants and we can obtain its bifurcations independently of the choice of the normal form.

In this thesis it was possible to classify two families of quadratic systems by using these algebraic tools together with numerical tools to determine the nonalgebraic bifurcations. One of these families possesses five real parameters and the other is four parametric. In the first case we consider the real projective space $\mathbb{RP}^4$ and in the second one we con-

sider $\mathbb{RP}^3$. By considering a convenient foliation of these spaces (indeed, according to the geometric features of the bifurcation surfaces) it was possible to complete the study of the entire bifurcation diagrams, even if they were formed by hundreds of parts (for instance, in the second bifurcation diagram studied in this thesis, corresponding to the closure of the considered family we have obtained 631 parts and 226 topologically distinct phase portraits).

Another way to help in the classification of phase portraits of quadratic systems is to use the Invariant Theory in order to search for the *algebraic invariant curves*, since the knowledge of such curves of a given planar differential system can help us to draw the respective phase portrait. Professors Dana Schlomiuk and Nicolae Vulpe initiated a systematic study of quadratic differential systems with specific invariant algebraic curves. Since the simplest case is of systems with invariant straight lines, their first works involved only invariant lines for quadratic systems (see Schlomiuk and Vulpe (2004), Schlomiuk and Vulpe (2008b), Schlomiuk and Vulpe (2008c), Schlomiuk and Vulpe (2008d), Schlomiuk and Vulpe (2010)). One of the next steps is to study classes of quadratic systems with invariant conics. In this sense, in Oliveira *et al.* (2017) the authors started these studies by considering the class **QSH** of non–degenerate quadratic differential systems having invariant hyperbolas. In 2019, during the visit of Professor Nicolae Vulpe to Instituto de Ciências Matemáticas e de Computação, we have the opportunity to work and learn with him and (at a distance) with Professor Dana Schlomiuk during their study of the class **QSE** of non–degenerate quadratic differential systems having an invariant ellipse. In their *preprint* (Oliveira *et al.* (2021)) they present necessary and sufficient conditions for an existence of an invariant ellipse, in terms of invariant polynomials. Another important result of this thesis deals with the classification of quadratic differential systems with invariant ellipses according to their *configurations of invariant ellipses and invariant lines*. This was a second project developed under the supervision of Professor Nicolae Vulpe during his stay in São Carlos.

It is worth mentioning that these three works represent three different approaches to the study of quadratic systems and each one of them uses different techniques, which all together are useful towards the final goal of classifying phase portraits.

This thesis is organized as follows: In Chap. 1 we present some concepts on Qualitative Theory of Ordinary Differential Equations which are relevant for this thesis. We present some references where the concepts can be found in details. For the reader interested in applications of the general theory, we indicate the results of a paper developed during our studies of the prerequisites from this thesis. Such a paper (already published) is the following one:

C. MOTA, MARCOS, D. S. OLIVEIRA, REGILENE. Dynamic aspects of Sprott BC chaotic system. **Discrete Cont. Dyn.–B**, **26** (2021), 1653-1673.

Chap. 2 describes some basic results on Introduction to Algebraic Geometry and Invariant Theory. As we have said before, the theory of invariant polynomials stated by Sibirsky and his students is one of the most important tools used in this thesis.

In Chap. 3 we present the study of a four–dimensional bifurcation diagram of quadratic systems possessing a finite saddle–node $\overline{sn}_{(2)}$ located at the origin of the plane as the only finite singularity and an infinite saddle–node of type $\overline{\binom{1}{1}}SN$. We highlight that this is the first time that a bifurcation diagram with this high level of dimension is studied by using the Invariant Theory described in Chap. 2. All the phase portraits obtained in this study have codimension at least three. The results presented in this chapter can be found in the paper (already published):

ARTÉS, J.C., MOTA, M.C., REZENDE, A.C. Quadratic differential systems with a finite saddle–node and an infinite saddle–node $(1,1)SN$ - (A), *Internat. J. Bifur. Chaos Appl. Sci. Engrg.*, **31** (2021), 2150026.

In Chap. 4 we exhibit the study of a very beautiful three–dimensional bifurcation diagram of quadratic systems possessing a finite saddle–node $\overline{sn}_{(2)}$ located at the origin of the plane, a finite simple singularity and an infinite saddle–node of type $\overline{\binom{1}{1}}SN$. All the generic phase portraits obtained in this study have codimension two and, as we see in Chap. 5, they provide examples for the realization of all phase portraits from the set (AC). All the results presented in Chap. 4 can be found in the paper:

ARTÉS, J.C., MOTA, M.C., REZENDE, A.C. Quadratic differential systems with a finite saddle–node and an infinite saddle–node $(1,1)SN$ - (B), **to appear at Internat. J. Bifur. Chaos Appl. Sci. Engrg.**, 2021.

In each one of these last two mentioned papers we have dedicated an entire section to present some incompatibilities found in previous classifications of phase portraits possessing specific properties on its singularities. Such incompatibilities are obtained after we compare all of the phase portraits obtained in our bifurcation diagrams with phase portraits from some previous papers which possess the same *topological configuration of singularities*, according to Def. 1 from Artés *et al.* (2020).

In Chap. 5 we present the topological classification and the realization of all the phase portraits belonging to the set (AB) and also the topological classification of phase portraits possessing the set of saddle–nodes $\left\{\overline{sn}_{(2)} + \overline{\binom{1}{1}}SN\right\}$ belonging to the set (AC). These results can also be found in the paper:

ARTÉS, J.C., MOTA, M.C., and REZENDE, A.C. Structurally unstable quadratic vector fields of codimension two: families possessing a finite saddle-node and an infinite saddle-node. *Electron. J. Qual. Theo.* No. 35 **(2021)**, 89pp.

In Chap. 6 we describe the study regarding the classification of quadratic differen-

tial systems with invariant ellipses according to their configurations of invariant ellipses and invariant lines. The results of this chapter are contained in the paper:

MOTA, M.C., OLIVEIRA, R.D.S., REZENDE, A.C., SCHLOMIUK, D., VULPE, N. Geometric analysis of quadratic differential systems with invariant ellipses, <https://repositorio.usp.br/directbitstream/2845e217-374e-4bf0-a229-283b1ff03372/3005920.pdf>, **preprint**, 2021.

Finally we briefly present some concluding comments as well as some ideas for further studies.

CHAPTER

1

PRELIMINARIES

In this chapter we present some results that are tools for a better comprehension of this thesis. Here we recall some basic and specific concepts on Qualitative Theory of Ordinary Differential Equations, we explain the context of our studies and we comment about the problems which we are dealing with in this thesis. The reader with widely experience in this field of study may skip the two first sections of this chapter.

1.1 Standard concepts

In this section we present several results from a first course regarding the qualitative study of the ordinary differential equations. We point out that there are a lot of other important results and what we do here is only to recall some definitions and as well as some results that we consider more relevant to our study. The results presented here can be found in Dumortier, Llibre and Artés (2008) and also in Sotomayor (2011). We strongly recommend these references for all the details.

Definition 1.1.1. Consider Ω an open subset of the space $\mathbb{R}\times\mathbb{R}^n$, being $\mathbb{R}$ the real line and $\mathbb{R}^n$ the n–dimensional euclidean space. A point belonging to $\mathbb{R}\times\mathbb{R}^n$ is denoted by (t,x), with $t\in\mathbb{R}$ and $x=(x_1,\ldots,x_n)\in\mathbb{R}^n$. Let $f:\Omega\to\mathbb{R}^n$ be a continuous map and I a non–degenerate interval of $\mathbb{R}$. A differentiable function $\varphi:I\to\mathbb{R}^n$ is called a *solution* of the differential equation

$$\frac{dx}{dt}=f(t,x) \tag{1.1}$$

on the interval I if

(a) $\mathrm{Gr}(\varphi)=\{(t,\varphi(t));t\in I\}\subset\Omega$;

(b) $\dfrac{d\varphi}{dt}=f(t,\varphi(t))$, for all $t\in I$.

Equation (1.1) is called *first order ordinary differential equation* and it is usually written as

$$x' = f(t,x).$$

Theorem 1.1.2 (Existence and uniqueness of solutions)**.** Let $f : \Omega = [a,b] \times \mathbb{R}^n \to \mathbb{R}^n$ be a continuous function which is Lipschitz on the variable x. Then, for all $(t_0,x_0) \in \Omega$, there exists only one solution for the *Cauchy problem*

$$\begin{cases} x' = f(t,x), \\ x(t_0) = x_0, \end{cases}$$

defined in some interval I contained in $[a,b]$.

Definition 1.1.3. Let Δ be an open subset of the euclidean space $\mathbb{R}^n$. A *vector field* of class $\mathscr{C}^k, 1 \leq k \leq \infty$, in Δ is a map $F : \Delta \to \mathbb{R}^n$.

Definition 1.1.4. Given a vector field $F : \Delta \to \mathbb{R}^n$ one can naturally associate the ordinary differential equation

$$x' = F(x). \tag{1.2}$$

This equation is called *autonomous differential equation* since it is independent on the temporal variable t. Moreover, its solutions, i.e. the differentiable maps $\varphi : I \subset \mathbb{R} \to \Delta$ such that

$$\frac{d}{dt}\varphi(t) = F(\varphi(t)),$$

for all $t \in I$, are called *trajectories* or *integral curves* of the vector field F, or yet of the differential equation (1.2).

Definition 1.1.5. An integral curve $\varphi : I \to \Delta$ of a vector field F is called *maximal* if for every integral curve $\Psi : J \to \Delta$ such that $I \subseteq J$ and $\varphi = \Psi|_I$ we have $I = J$ and, consequently, $\varphi = \Psi$. In this case I is called *maximal interval*.

Theorem 1.1.6. **(a)** (Existence and uniqueness of maximal solutions). For each $x \in \Delta$ there exists an open interval I_x in which it is defined the unique maximal solution φ_x of (1.2) such that $\varphi_x(0) = x$;

(b) (Group property). If $y = \varphi_x(s)$ and $s \in I_x$, so $I_y = I_x - s = \{r - s; r \in I_x\}$, $\varphi_y(0) = y$ and $\varphi_y(t) = \varphi_x(t+s)$ for every $t \in I_y$;

(c) (Differentiability with respect to the initial conditions). The set

$$D = \{(t,x); x \in \Delta, t \in I_x\}$$

is open in $\mathbb{R}^{n+1}$ and the map

$$\begin{aligned} \varphi : \quad D \quad &\to \mathbb{R}^n \\ (t,x) &\mapsto \varphi(t,x) = \varphi_x(t) \end{aligned}$$

is of class $\mathscr{C}^k$. Such a map is called *generated flow* by F and it verifies the following equations

$$D_1D_2\varphi(t,x) = DF(\varphi(t,x)) \cdot D_2\varphi(t,x), \qquad D_2\varphi(t,x)\Big|_{t=0} = E,$$

for every $(t,x) \in D$. Here, E represents the identity of $\mathbb{R}^n$ and D_j stands for the derivative with respect to the j^{th}–variable.

Definition 1.1.7. A map $\varphi : \mathbb{R} \times \mathbb{R}^n \to \mathbb{R}^n$ of class $\mathscr{C}^1$ is said to be a *flow* if

(a) $\varphi(0,x) = x$;

(b) $\varphi(t+s,x) = \varphi(t,\varphi(s,x)), t,s \in \mathbb{R}$.

A flow is called *linear* if for each $t \in \mathbb{R}$, $\varphi_t(x) = \varphi(t,x)$ is a linear map in $\mathbb{R}^n$.

Theorem 1.1.8 (Continuous dependence of solutions)**.** Consider the differential equation $x' = F(x)$ where $F : \Delta \to \mathbb{R}^n$ is of class $\mathscr{C}^1$. Suppose that $x(t)$ is a solution of this equation which is defined on the closed interval $[t_0,t_1]$ with $x(t_0) = x_0$. Then there exist a neighborhood $U \subset \mathbb{R}^n$ of x_0 and a constant k such that if $y_0 \in U$, then there exists a unique solution $y(t)$ also defined on $[t_0,t_1]$ with $y(t_0) = y_0$. Moreover, the solution $y(t)$ verifies

$$|y(t) - x(t)| \leq k|y_0 - x_0| \exp(k(t-t_0)),$$

for all $t \in [t_0,t_1]$.

This result says that, if the solutions $x(t)$ and $y(t)$ start out close to each other, then they remain close for t close to t_0. While these solutions may separate from each other, they do so no faster than exponentially.

Definition 1.1.9. The set $\gamma_p = \{\varphi(t,p); t \in I_p\}$, i.e. the image of the integral curve of the vector field F through the point p is called an *orbit* of F through the point p (in other words, γ_p is the trace of the integral curve of F through the point p). We also define the *positive semi–orbit* through p as the set $\gamma_p^+ = \{\varphi(t,p); t \geq 0\}$.

Proposition 1.1.10. Let $q \in \mathbb{R}^n$. Then $q \in \gamma_p$ if and only if $\gamma_q = \gamma_p$.

Proof. In fact, if $q \in \gamma_p$ there exists $s \in I_p$ such that $q = \varphi(s,p)$ and then

$$\varphi(t,q) = \varphi(t,\varphi(s,p)) = \varphi(t+s,p),$$

for all $t \in I_q = I_p - s$ (i.e. $t+s \in I_p$), so $\gamma_q = \gamma_p$. On the other hand, from the identity $\gamma_q = \gamma_p$ it follows directly that

$$q = \varphi(0,q) \in \gamma_q = \gamma_p.$$

□

The previous proposition implies that there exists an equivalence relation in the set of orbits of a vector field $F:\Delta\to\mathbb{R}^n$. Indeed, either two orbits coincide or they have empty intersection. Therefore, $\Delta\subset\mathbb{R}^n$ can be decomposed in a disjoint union of differentiable curves of F. The following theorem presents a classification of the types of orbits of a vector field F.

Theorem 1.1.11. Let $\Delta\subset\mathbb{R}^n$ be an open set, $F:\Delta\to\mathbb{R}^n$ a vector field of class $\mathscr{C}^k, k\geq 1$, in Δ and $\varphi_x:I_x\to\Delta$ the maximal solution in I_x of the Cauchy problem $x'=F(x), x(0)=x$. Then, one of the following sentences is verified:

(a) φ_x is an injection (in this case the respective orbit is in correspondence with an interval of $\mathbb{R}$);

(b) $I_x=\mathbb{R}$ and φ_x is constant (in this case the orbit is a point);

(c) $I_x=\mathbb{R}$ and φ_x is a periodic function, i.e. there exists $\tau>0$ such that $\varphi_x(t+\tau)=\varphi_x(t)$ for all $t\in I_x$ and $\varphi_x(t_1)\neq\varphi_x(t_2)$ if $|t_1-t_2|<\tau$ (in this case the orbit is diffeomorphic to a circle).

Definition 1.1.12. In case we have $\gamma_p=p$, then the orbit is called a *singular point* (or simply, a *singularity*) and, in case we have γ_p diffeomorphic to a circle we say that γ_p is a *closed* or a *periodic* orbit.

We have that a singularity (stationary orbit) is a zero of the vector field. A point p which is not a singularity of a vector field is called *regular point*.

Example 1.1.13. The singularities of the linear planar systems $x'=Ax$, where A is a 2×2 matrix with $D=\det(A)\neq 0$ are well–known (see Sec. 1.2 of Dumortier, Llibre and Artés (2008), for instance). In fact, consider $T=\text{trace}(A)$. Then:

- if $D<0$ we have a *saddle*;
- if $D>0$ and $T=0$ we have a *linear center*;
- if $D>0$ and $T^2-4D<0$ we have a *focus*, which can be stable or unstable;
- if $D>0$ and $T^2-4D>0$ we have a *node*, which can be stable or unstable.

Note that $T^2=4D$ is a parabola on the TD–plane. Motivated by Figure 4.1 of Hirsch, Smale and Devaney (2004), in Fig. 1 we present the local behavior of each singularity mentioned before, in the TD–plane.

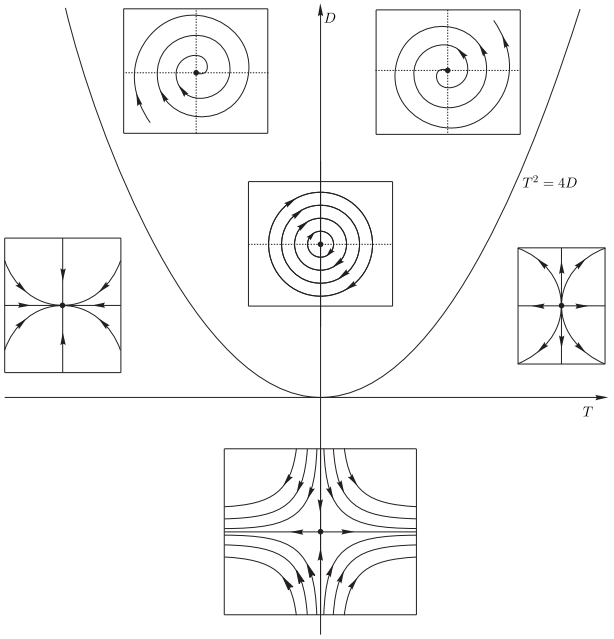

Figure 1 – The trace–determinant plane

Definition 1.1.14. The *phase portrait* of a vector field $F : \Delta \to \mathbb{R}^n$ or of a differential equation $x' = F(x)$ is the decomposition of the open set Δ by the orbits of F, so that all the orbits are orientated in the sense of the integral curves of F and the singularities are endowed with the trivial orientation.

The proof of the following proposition can be found in Sec. 1.4.1 of Chicone (2006).

Proposition 1.1.15 (Reparametrization of Time)**.** Suppose that $\Delta \subset \mathbb{R}^n$ is an open set, $F : \Delta \to \mathbb{R}^n$ is a smooth vector field and define the following Cauchy problem

$$\begin{cases} x' = F(x), \\ x(0) = x_0. \end{cases} \tag{1.3}$$

Assume that $I_{x_0} \subset \mathbb{R}$, $0 \in I_{x_0}$, is the maximal interval of the (maximal) solution $\varphi_{x_0} : I_{x_0} \to \Delta$ of the Cauchy problem (1.3). Let $g : \Delta \to \mathbb{R}$ be a positive smooth function. Then the function

$$\begin{aligned} B : I_{x_0} &\to \mathbb{R} \\ t &\mapsto B(t) = \int_0^t \frac{1}{g(\varphi_{x_0}(s))} ds \end{aligned}$$

is invertible on its range $K \subseteq \mathbb{R}$ and, if $\rho : K \to I_{x_0}$ is the inverse of B, then the identity

$$\rho'(t) = g(\varphi_{x_0}(\rho(t)))$$

holds for all $t \in K$. Moreover, the function

$$\begin{aligned} \sigma : K &\to \mathbb{R}^n \\ t &\mapsto \sigma(t) = \varphi_{x_0}(\rho(t)) \end{aligned}$$

is the solution of the Cauchy problem

$$\begin{cases} x' = g(x)F(x), \\ x(0) = x_0. \end{cases} \tag{1.4}$$

Remark 1.1.16. Prop. 1.1.15 gives us a relationship among the solutions of the Cauchy problems (1.3) and (1.4). The vector fields defined by F and gF have the same direction at each point in Δ, but their sense and lengths may be different. Thus, for a geometrical interpretation of autonomous differential equations, it is clear that the differential equations

$$x' = F(x) \quad \text{and} \quad x' = g(x)F(x)$$

have topologically equivalent phase portraits. Moreover, one can usually say that the first differential equation is obtained from the second one by a *reparametrization of time*. Additionally, in the particular case where $g(x) = c > 0$, the time reparametrization in these case is also called a *time rescaling*.

Definition 1.1.17. Let F_1 and F_2 be two vector fields defined on open sets Δ_1 and Δ_2 of $\mathbb{R}^n$, respectively. We say that F_1 is *topologically equivalent* (respectively $\mathscr{C}^r$*–equivalent*) to F_2 when there exists a homeomorphism (respectively a diffeomorphism of class $\mathscr{C}^r$) $h : \Delta_1 \to \Delta_2$ which takes orbits of F_1 into orbits of F_2 preserving the orientation. More precisely, let $p \in \Delta_1$ and $\gamma^1(p)$ the oriented orbit of F_1 passing through p, then $h(\gamma^1(p))$ is the oriented orbit $\gamma^2(h(p))$ of F_2 passing through $h(p)$.

Observe that this definition establishes an equivalence relation between vector fields defined on open subsets of $\mathbb{R}^n$. The homeomorphism h is called a *topological equivalence* (respectively *differentiable equivalence*) between F_1 and F_2.

Definition 1.1.18. Assume that Δ_1 and Δ_2 are open sets in $\mathbb{R}^n$. Consider $F_1 : \Delta_1 \to \mathbb{R}^n$ and $F_2 : \Delta_2 \to \mathbb{R}^n$ be two vector fields, which generate the corresponding flows $\varphi_1 : D_1 \to \mathbb{R}^n$ and $\varphi_2 : D_2 \to \mathbb{R}^n$. We say that F_1 is *topologically conjugate* (respectively $\mathscr{C}^r$*–conjugate*) to F_2 when there exists a homeomorphism (respectively a diffeomorphism of class $\mathscr{C}^r$) $h : \Delta_1 \to \Delta_2$ such that

$$h(\varphi_1(t,x)) = \varphi_2(t, h(x)),$$

for every $(t,x) \in D_1$.

Observe that in this definition we necessarily have $I_1(x) = I_2(h(x))$, where $I_1(x)$ and $I_2(h(x))$ denote the maximal intervals of the respective maximal solutions. The homeomorphism h is called a *topological conjugation* (respectively $\mathscr{C}^r$*–conjugation*) between F_1 and F_2.

Remark 1.1.19. We observe that the conjugation relation is also an equivalence relation between vector fields defined on open subsets of $\mathbb{R}^n$. It is clear that every conjugation is an equivalence. Moreover, if h is an equivalence between two vector fields F_1 and F_2 and if p is a singularity of F_1, then $h(p)$ is a singularity of F_2. Also, if h is a conjugation and if γ is a closed orbit for the vector field F_1, then $h(\gamma)$ is a closed orbit for the vector field F_2 (in this case $h(\gamma)$ has the same period as γ).

Definition 1.1.20. Assume $F:\Delta\to\mathbb{R}^n$ a vector field of class $\mathscr{C}^k, k\geq 1$ and consider the open sets $\Delta\subset\mathbb{R}^n$ and $A\subset\mathbb{R}^{n-1}$. A map $g:A\to\Delta$, of class $\mathscr{C}^k$, is called a *local transverse section* of F when for all $a\in A$,

$$Dg(a)(\mathbb{R}^{n-1}) \quad \text{and} \quad F(g(a))$$

are linearly independent (or form a basis for $\mathbb{R}^n$). Let $\Sigma=g(A)$ be a set endowed with the induced topology of $\mathbb{R}^n$. If $g:A\to\Sigma$ is a homeomorphism we say that Σ is a *transverse section* of F.

Theorem 1.1.21 (Flow Box Theorem)**.** Let p be a *regular point* and consider $g:A\to\Sigma$ a local transverse section of Σ of class $\mathscr{C}^k$ with $g(0)=p$. Then there exists a neighborhood V of p in Δ and there exists a diffeomorphism $h:V\to(-\varepsilon,\varepsilon)\times B$ of class $\mathscr{C}^k$, with $\varepsilon>0$ and B an open ball in $\mathbb{R}^{n-1}$ centered at the origin $0=g^{-1}(p)$ such that

(a) $h(\Sigma\cap V)=\{0\}\times B$;

(b) h is a $\mathscr{C}^k$–conjugation between $F|_V$ and the constant vector field $Y:(-\varepsilon,\varepsilon)\times B\to\mathbb{R}^n$, with $Y=(1,0,\ldots,0)\in\mathbb{R}^n$.

Remark 1.1.22. Let p be a regular point of a vector field F of class $\mathscr{C}^k$, $k\geq 1$. By the Flow Box Theorem we know that there exists a diffeomorphism of class $\mathscr{C}^k$ which conjugates F, in some neighborhood of p, with the constant vector field $Y=(1,0,\ldots,0)$. As a consequence, two vector fields F and G are locally $\mathscr{C}^k$–conjugate around their regular points.

This remark provides us a satisfactory local qualitative knowledge of the orbits of a vector field near regular points. It is interesting, therefore, the study of the singularities of a vector field. The next theorem tells us that, under certain hypothesis, for the study of a singularity p of a system $x'=F(x)$ it is enough to consider the linear part $x'=DF(p)x$ of the system.

Theorem 1.1.23 (Hartman–Grobman)**.** Consider $F:\Delta\to\mathbb{R}^n$ a vector field of class $\mathscr{C}^1$ and p a singularity which verifies the property that all the eigenvalues of the Jacobian matrix $DF(p)$ have nonzero real part. There exist a neighborhood W of p in Δ and a neighborhood V of 0 in $\mathbb{R}^n$ such that $F|_W$ is topologically conjugate to $DF(p)|_V$.

Note that, if $F|_W$ is topologically conjugate to $DF(p)|_V$, then the singularities of the system $x' = F|_W$ *look like* (in the sense of Rmk. 1.1.19) the singularities of the linear system $x' = DF(p)|_V$, which were presented before in Ex. 1.1.13.

Definition 1.1.24. We say that a singularity p of a vector field $F : \Delta \to \mathbb{R}^n$ of class $\mathscr{C}^1$ is *hyperbolic* if all the eigenvalues of the Jacobian matrix $DF(p)$ have nonzero real part.

Note that, with the exception of the linear center, all the singularities mentioned in Ex. 1.1.13 are hyperbolic.

Definition 1.1.25. Consider $\gamma = \{\varphi_p(t); t \in \mathbb{R}\}$ a τ_0–periodic orbit of a vector field F of class $\mathscr{C}^r$, $r \geq 1$, in an open set $\Delta \subset \mathbb{R}^2$. Let Σ be a transverse section of F in p. Due to the continuity of the flow φ of F, for every point $q \in \Sigma$ sufficiently close to p, the trajectory $\varphi_q(t)$ remains close to γ, with t in a compact interval, for instance, $[0, 2\tau_0]$. We define $\pi(q)$ as the first point in which $\varphi_q(t)$ intersects Σ. Being Σ_0 the domain of π, we clearly have $p \in \Sigma_0$ and $\pi(p) = p$.

Definition 1.1.26. Given Σ a transverse section of a vector field F, we define a *Poincaré map* $\pi : \Sigma_0 \to \Sigma$ as the map of first return of the flow to Σ, i.e for each point of Σ belonging to a specific orbit the map π gives us the first point in which the orbit intersects Σ in positive time. We assume Σ_0 sufficiently small in such a way that π is defined for every point of Σ_0.

Definition 1.1.27. A periodic orbit γ of a vector field $F : \Delta \subset \mathbb{R}^2 \to \mathbb{R}^2$ of class $\mathscr{C}^k, k \geq 1$, in the open set $\Delta \subset \mathbb{R}^2$ is called a *limit cycle* of F if there exists a neighborhood $V \subset \Delta$ of $\gamma \subset \Delta$ such that γ is the only periodic orbit in V, i.e. *a limit cycle is an isolated periodic orbit* in the set of all periodic orbits of the vector field. In addition, a limit cycle is called *simple* or *hyperbolic* if it has multiplicity one.

Proposition 1.1.28. With the same notation used in the previous definition, there exist only three *types* of limit cycles:

1. *Stable,* when $\lim_{t \to +\infty} d(\varphi(t,q), \gamma) = 0$, for all $q \in V$;
2. *Unstable*, when $\lim_{t \to -\infty} d(\varphi(t,q), \gamma) = 0$, for all $q \in V$;
3. *Semi–stable*, when one of the two conditions hold:
   - $\lim_{t \to +\infty} d(\varphi(t,q), \gamma) = 0$, for all $q \in V \cap \mathrm{Ext}(\gamma)$, and $\lim_{t \to -\infty} d(\varphi(t,q), \gamma) = 0$, for all $q \in V \cap \mathrm{Int}(\gamma)$;
   - $\lim_{t \to -\infty} d(\varphi(t,q), \gamma) = 0$, for all $q \in V \cap \mathrm{Ext}(\gamma)$, and $\lim_{t \to +\infty} d(\varphi(t,q), \gamma) = 0$, for all $q \in V \cap \mathrm{Int}(\gamma)$;

where $\mathrm{Ext}(\gamma)$ (respectively $\mathrm{Int}(\gamma)$) means the *exterior* (respectively the *interior*) of the closed curve γ (remember that in this case the very well known Jordan Curve Theorem holds).

Theorem 1.1.29. A periodic orbit $\gamma_p = \{\varphi(t,p); t \in \mathbb{R}\} \subset \Delta$ is a limit cycle of $F : \Delta \to \mathbb{R}^2$ of class $\mathscr{C}^k, k \geq 1$, in the open set $\Delta \subset \mathbb{R}^2$ if and only if $p \in \Delta$ is an isolated fixed point of the Poincaré map $\pi : \Sigma_0 \to \Sigma$, being Σ a transverse section of F in p.

Theorem 1.1.30. Let $\Delta \subset \mathbb{R}^2$ be an open set and consider $F = (F_1, F_2) : \Delta \to \mathbb{R}^2$ a vector field of class $\mathscr{C}^1$. Suppose that γ is a periodic orbit of F of period T and let $\pi : \Sigma_0 \to \Sigma$ be the Poincaré map on a transverse section Σ of F in $p \in \gamma$. Then

$$\pi'(p) = \exp\left(\int_0^T \mathrm{div}F(\gamma(t))dt\right),$$

where

$$\mathrm{div}F(x,y) = \frac{\partial F_1}{\partial x}(x,y) + \frac{\partial F_2}{\partial y}(x,y).$$

In particular, if $\int_0^T \mathrm{div}F(\gamma(t))dt < 0$ we have that γ is *stable* and if $\int_0^T \mathrm{div}F(\gamma(t))dt > 0$ we have that γ is *unstable*.

Definition 1.1.31. Let Δ be an open subset of the euclidean space $\mathbb{R}^n$, $F : \Delta \to \mathbb{R}^n$ a vector field of class $\mathscr{C}^k, k \geq 1$, and $\varphi(t) = \varphi(t,p)$ the integral curve of F passing through a point p, defined on its maximal interval $I_p = (\omega^-(p), \omega^+(p))$. If $\omega^+(p) = +\infty$, we define the ω–limit set corresponding to p (and denoted by $\omega(p)$) as the set of the points $q \in \Delta$ for which there exists a sequence $\{t_n\}$ such that

$$\lim_{n\to\infty} t_n = +\infty, \quad \lim_{n\to\infty} \varphi(t_n) = q.$$

Analogously, if $\omega^-(p) = -\infty$ we define the α–limit set corresponding to p (and denoted by $\alpha(p)$) as the set of the points $q \in \Delta$ for which there exists a sequence $\{t_n\}$ such that

$$\lim_{n\to\infty} t_n = -\infty, \quad \lim_{n\to\infty} \varphi(t_n) = q.$$

Theorem 1.1.32 (Poincaré–Bendixson)**.** Let Δ be an open subset of $\mathbb{R}^2$, F a vector field of class $\mathscr{C}^k$, $k \geq 1$ in Δ and $\varphi(t) = \varphi(t,p)$ an integral curve of F, defined for every $t \geq 0$, in such a way that γ_p^+ be entirely contained in a compact set $K \subset \Delta$. Assume that the vector field F has a finite number of singularities in $\omega(p)$. Then, there exist the following options for $\omega(p)$:

(a) if $\omega(p)$ contains only regular points, then $\omega(p)$ is a periodic orbit;

(b) if $\omega(p)$ contains regular points and also singular points, then $\omega(p)$ consists of a set of orbits with the following property: each one of these orbits tends to one of these singularities when $t \to \pm\infty$. In other words, $\omega(p)$ is a *graphic*;

(c) if $\omega(p)$ does not contain regular points, then $\omega(p)$ is a singularity.

We point out that by a simple reversion on time we clearly have an analogous version of such a theorem if we consider the α–limit set instead of the ω–limit set.

A classical application of the previous result is the following theorem (see Theorem 1.31 from Dumortier, Llibre and Artés (2008)).

Theorem 1.1.33. Let F a vector field of class $\mathscr{C}^1$ in an open set $\Delta \subset \mathbb{R}^2$. If γ is a closed orbit of F such that $\mathrm{Int}(\gamma) \subset \Delta$, then there exists a singularity of F which belongs to $\mathrm{Int}(\gamma)$.

In the case where F is a polynomial vector field on $\mathbb{R}^2$ of the form $X(x,y) = (P(x,y), Q(x,y))$, where P and Q are polynomials in the variables x and y of degree at most 2, in Coppel (1966) it is proved that such a singularity is a focus.

1.2 A summary of the Poincaré compactification technique

In the previous section we presented some general concepts in Qualitative Theory of Ordinary Differential Equations. Briefly summarizing such concepts, we presented the definition of a solution of an ordinary differential equation, we stated the theorem of existence and uniqueness of solutions for a Cauchy problem, we saw the definition of a vector field F together with a classification of the types of its orbits and also the definition of a phase portrait associated to an ordinary differential equation $x' = F(x)$. We finished the mentioned section with the Poincaré–Bendixon Theorem which states that if γ is an orbit of a vector field F such that the positive semi–orbit γ_p^+ is entirely contained in a compact set $K \subset \Delta \subset \mathbb{R}^2$, then the ω–limit set $\omega(p)$ is well characterized. In this context we have a natural question: how can we describe the asymptotic behavior of the semi–orbits which are not contained in compact sets? In other words, how can we study the solutions that "escape to infinity"? With the *Poincaré compactification technique* we can extend analytically the vector field to the compact set

$$\{(x,y,z) \in \mathbb{R}^3;\ x^2+y^2+z^2 = 1,\ z \geq 0\},$$

where one can apply the Poincaré–Bendixon Theorem. In this section we describe briefly such a technique. For the reader interested in more details we indicate Chap. 5 of Dumortier, Llibre and Artés (2008).

We denote by $\mathscr{P}_n(\mathbb{R}^2)$ the polynomial vector fields on $\mathbb{R}^2$ of the form $X(x,y) = (P(x,y), Q(x,y))$, where P and Q are polynomials in the variables x and y of degree at most n (with $n \in \mathbb{N}$). Any such an X is uniquely determinate by the $(n+1)(n+2)$ coefficients of P and Q, hence it may be identified with an unique point of $\mathbb{R}^{(n+1)(n+2)}$. The *coefficient*

topology of $\mathscr{P}_n(\mathbb{R}^2)$ is the induced topology through the mentioned identification by the usual euclidean topology of $\mathbb{R}^{(n+1)(n+2)}$.

For $X \in \mathscr{P}_n(\mathbb{R}^2)$ the *Poincaré compactified vector field* $p(X)$ *corresponding to* X is a vector field induced on $\mathbb{S}^2$ as follows. Let $\mathbb{S}^2 = \{y = (y_1, y_2, y_3) \in \mathbb{R}^3; y_1^2 + y_2^2 + y_3^2 = 1\}$ (the *Poincaré sphere*) and $T_y\mathbb{S}^2$ the tangent space to $\mathbb{S}^2$ at y. Consider the central projections $f_+ : T_{(0,0,1)}\mathbb{S}^2 \to \mathbb{S}^2_+ = \{y \in \mathbb{S}^2; y_3 > 0\}$ and $f_- : T_{(0,0,1)}\mathbb{S}^2 \to \mathbb{S}^2_- = \{y \in \mathbb{S}^2; y_3 < 0\}$, where

$$f^{\pm}(x) = \left(\pm\frac{x_1}{\Delta(x)}, \pm\frac{x_2}{\Delta(x)}, \pm\frac{1}{\Delta(x)}\right), \quad \Delta(x) = \sqrt{x_1^2 + x_2^2 + 1}.$$

These maps define two copies of X, one in the northern hemisphere and the other in the southern hemisphere. Denote by X' the vector field defined on $\mathbb{S}^2$ except on its equator $\mathbb{S}^1 = \{y \in \mathbb{S}^2; y_3 = 0\}$ by $Df_+ \circ X$ and $Df_- \circ X$. Clearly $\mathbb{S}^1$ is identified with the infinity of $\mathbb{R}^2$. In order to extend X' to an analytic vector field on $\mathbb{S}^2$ (including $\mathbb{S}^1$) it is necessary that X satisfies suitable hypotheses. In the case that $X \in \mathscr{P}_n(\mathbb{R}^2)$, the *Poincaré compactification* $p(X)$ of X is the only analytic extension of $y_3^{n-1}X'$ to $\mathbb{S}^2$. For the flow of the compactified vector field $p(X)$, the equator $\mathbb{S}^1$ is invariant. On $\mathbb{S}^2 \setminus \mathbb{S}^1$ there are two symmetric copies of X, and knowing the behavior of $p(X)$ around $\mathbb{S}^1$, we know the behavior of X at the infinity. The projection of the closed northern hemisphere of $\mathbb{S}^2$ on $y_3 = 0$ under $(y_1, y_2, y_3) \mapsto (y_1, y_2)$ is called the *Poincaré disc*, and it is denoted by $\mathbb{D}^2$.

As $\mathbb{S}^2$ is a differentiable manifold, for computing the expression of $p(X)$, we can consider the following six local charts $U_i = \{y \in \mathbb{S}^2; y_i > 0\}$, and $V_i = \{y \in \mathbb{S}^2; y_i < 0\}$ where $i = 1, 2, 3$, and the diffeomorphisms $F_i : U_i \to \mathbb{R}^2$ and $G_i : V_i \to \mathbb{R}^2$ which are the inverses of the central projections from the vertical planes tangents at points

$$(1,0,0),\ (-1,0,0),\ (0,1,0),\ (0,-1,0),\ (0,0,1),\ (0,0,-1),$$

respectively. We denote by $z = (u, v)$ the value of $F_i(y)$ or $G_i(y)$ for any $i = 1, 2, 3$. So z represents different variables, depending on the local chart under consideration. Some straightforward computations give the following expressions for $p(X)$:

$$v^n \cdot \Delta(z) \left[Q\left(\frac{1}{v}, \frac{u}{v}\right) - uP\left(\frac{1}{v}, \frac{u}{v}\right), -vP\left(\frac{1}{v}, \frac{u}{v}\right) \right], \tag{1.5}$$

$$v^n \cdot \Delta(z) \left[P\left(\frac{u}{v}, \frac{1}{v}\right) - uQ\left(\frac{u}{v}, \frac{1}{v}\right), -vQ\left(\frac{u}{v}, \frac{1}{v}\right) \right], \tag{1.6}$$

$$\Delta(z)\left[P(u,v), Q(u,v)\right],$$

in the local charts U_1, U_2 and U_3 respectively, where $\Delta(z) = (u^2 + v^2 + 1)^{\frac{1-n}{2}}$. The expression for V_i is the same as that for U_i except for a multiplicative factor $(-1)^{n-1}$. In these coordinates and in the local charts U_i and V_i for $i = 1, 2$, $v = 0$ always denotes the points of $\mathbb{S}^1$. In what follows we omit the factor $\Delta(z)$ by rescaling the vector field $p(X)$. So, in each local chart we obtain a polynomial vector field. We denote by $\mathscr{P}_n(\mathbb{S}^2)$ all the polynomial vector fields $p(X)$ on $\mathbb{S}^2$ defined as before and endowed with the coefficient topology.

A singularity q of $X \in \mathscr{P}_n(\mathbb{R}^2)$ is called *infinite* (respectively *finite*) if it is a singularity of $p(X)$ in $\mathbb{S}^1$ (respectively in $\mathbb{S}^2 \setminus \mathbb{S}^1$). Then in order to compute all the infinite singularities of X we take the nonzero terms of the expressions (1.5) and (1.6) with $v = 0$ and we obtain

$$F(u) = Q_n(1,u) - uP_n(1,u),$$
$$G(u) = P_n(u,1) - uQ_n(u,1),$$

respectively, where P_n and Q_n are the homogeneous part of degree n of P and Q. Thus, the infinite singularities of X are the points $(u,0)$ satisfying

$$F(u) = 0, \quad \text{if} \quad (u,0) \in U_1,$$
$$G(u) = 0, \quad \text{if} \quad (u,0) \in U_2.$$

Note that the equation $F(u) = 0$ gives us all the infinite singularities of X except, perhaps, the origin of the local chart U_2.

In Sec. 3 of Artés, Llibre and Schlomiuk (2006) the authors explain the Poincaré compactification technique by using another tools. In particular they deal with complex (respectively real) foliation with singularities on $\mathbb{CP}^2$ (respectively $\mathbb{RP}^2$). For the reader interested in this approach we recommend such a reference.

1.3 The context of this thesis

Having seen a little bit about the general frame of the Qualitative Theory of Ordinary Differential Equations, in this section we present the context and the main goals of this thesis. We point out that we are interested in the study of planar polynomial differential systems, more precisely in the problem of classification of phase portraits of such systems according to their structural stability.

Let $\mathscr{P}_n(\mathbb{R}^2)$ be the set of all polynomial vector fields on $\mathbb{R}^2$ of the form $X(x,y) = (P(x,y), Q(x,y))$, with P and Q polynomials in the variables x and y of degree at most n (with $n \in \mathbb{N}$). For $X \in \mathscr{P}_n(\mathbb{R}^2)$, we consider the *Poincaré compactified vector field* $p(X)$ *corresponding to* X as the vector field induced on $\mathbb{S}^2$ as described in our previous section and also in Andronov *et al.* (1973), Artés, Llibre and Rezende (2018), Dumortier, Llibre and Artés (2008), González (1969), Sotomayor (1979). Concerning this, as we saw, a singular point q of $X \in \mathscr{P}_n(\mathbb{R}^2)$ is called *infinite* (respectively *finite*) if it is a singular point of $p(X)$ in $\mathbb{S}^1$ (respectively in $\mathbb{S}^2 \setminus \mathbb{S}^1$).

Using the classical theory of qualitative study of ordinary differential equations we know how to classify the finite and infinite singularities. In this thesis, apart from the classical results, we are interested in the *weak singularities*.

Definition 1.3.1. We call *strong saddle* (respectively *strong focus*) a saddle (respectively focus) with nonzero trace of the linear part at this point. Such a saddle (respectively

focus) is defined to have *order zero*. A saddle (respectively focus) with trace zero is called a *weak saddle* (respectively *weak focus*).

According to this definition, finite saddles and foci (remember Ex. 1.1.13) are classified as strong or weak. When the trace of the Jacobian matrix evaluated at these singular points is not zero, we call them strong saddles and strong foci, respectively, and we denote them by s and f, respectively. But when the trace is zero, except for centers and saddles of infinite order (or integrable saddles, i.e. saddles with all their Poincaré–Lyapounov constants equal to zero (see Llibre and Schlomiuk (2004))), it is known that the saddles and foci of quadratic systems, may have up to order three. We denote them by $s^{(i)}$ and $f^{(i)}$, respectively, where $i = 1,2,3$ is the corresponding order.

The following results hold for any quadratic system. We present a reference where one can find their proofs.

(i) If a quadratic system has a limit cycle, then it surrounds a unique singular point, and this point is a focus, see Coppel (1966).

(ii) A quadratic system with an invariant straight line has at most one limit cycle, see Coll and Llibre (1988).

(iii) A quadratic system with more than one real invariant straight line has no limit cycle, see Bautin (1954).

(iv) In quadratic systems there is at most one limit cycle surrounding a weak focus of second order and when it exists it is hyperbolic (according to the general Def. 1.1.24), see Zhang (2001).

(v) There are no limit cycles in quadratic systems surrounding the weak focus of third order, see Li (1986).

The local classification of the singularities of a vector field $p(X)$ is a well known subject, but we recall such concepts. Let q be a singular point of $p(X)$. The classical definitions are:

- q is *non–degenerate* if $\det(Dp(X)(q)) \neq 0$, i.e. the determinant of the linear part of $p(X)$ at the singular point q is nonzero;
- q is *hyperbolic* if the two eigenvalues of $Dp(X)(q)$ have real part different from 0 (remember the general Def. 1.1.24);
- q is *semi–hyperbolic* if exactly one eigenvalue of $Dp(X)(q)$ is equal to 0.

However, in this thesis we use a new notation introduced in Artés *et al.* (2015), which is directly related to the Jacobian matrix of the singularity:

- q is *elemental* if both eigenvalues of $Dp(X)(q)$ are nonzero;
- q is *semi–elemental* if exactly one of the eigenvalues of $Dp(X)(q)$ is equal to zero;
- q is *nilpotent* if both eigenvalues of $Dp(X)(q)$ are zero, but the Jacobian matrix at this point is non–identically zero;
- q is *intricate* if the Jacobian matrix is identically zero;
- q is an *elemental saddle* if $\det(Dp(X)(q)) < 0$, i.e. the product of the eigenvalues of $Dp(X)(q)$ is negative;
- q is an *elemental antisaddle* if $\det(Dp(X)(q)) > 0$ and the neighborhood of q is not formed by periodic orbits, in which case we would call it a *center*, i.e., it is either a node or a focus.

The *intricate* singularities are usually called in the literature *linearly zero*. As such a kind of singularities usually requires some more sophisticated tools (as the *blow–up technique*, see Dumortier, Llibre and Artés (2008)) in order to be better understood, the term *intricate* indicates the rather complicated behavior of phase curves around such a singularity.

In this thesis we use the pattern established by the mentioned authors and we denote the finite singularities with lower–case letters and the infinite singularities with capital ones (see Sec. 3.7 of Artés *et al.* (2021) for all the details). For instance:

- Elemental singularities: saddles (s and S), nodes (n and N), foci (f) and centers (c). We also have n^d, n^*, N^f and N^∞.
- Semi–elemental singularities (are denoted using a bar): finite saddle–node ($\overline{sn}_{(2)}$), finite triple saddle ($\overline{s}_{(3)}$), infinite saddle–node of type $\overline{\binom{1}{1}}SN$ or $\overline{\binom{0}{2}}SN$, among others.
- Nilpotent singularities (are denoted with a hat): finite elliptic–saddle of multiplicity three ($\widehat{es}_{(3)}$), infinite triple singularity of type $\widehat{\binom{1}{2}}PEP-H$, among others.
- Intricate singularities (are denoted by the sequence formed by the types of their sectors): a finite singularity of multiplicity four $phpphp_{(4)}$, an infinite singularity of multiplicity four $\binom{2}{2}PHP-PHP$, among others.

Regarding the notation presented before, it is worth mentioning that we denote by "$\binom{a}{b}\ldots$" the maximum number a (respectively b) of finite (respectively infinite) singularities which can be obtained by perturbation of an infinite multiple singularity. For

instance, $\overline{\binom{1}{1}}\,SN$ means an infinite saddle–node formed by the coalescence of a finite node (respectively a finite saddle) with an infinite saddle (respectively an infinite node). Additionally, for the infinite nilpotent and intricate singularities, we insert a hyphen between the sectors to split those which appear in one side of the equator of the sphere from those ones which appear in the other side of the equator, and we will always start with a sector bordering the infinity, in order to avoid using two dashes. We also use the notion of *sectorial decomposition* for the infinite nilpotent and intricate singularities, for instance, $\widehat{\binom{1}{2}}\,PHP-E$ indicates a nilpotent infinite singularity for which in one side of the equator we have an elliptic sector (possibly with adjacent parabolic sectors) and on the other side of the equator, corresponding to this point we have two parabolic sectors with a hyperbolic sector between them. The reader is invited to see all the details in Artés *et al.* (2021).

Let $p(X) \in \mathscr{P}_n(\mathbb{S}^2)$ (respectively $X \in \mathscr{P}_n(\mathbb{R}^2)$). A *separatrix* of $p(X)$ (respectively of X) is an orbit which is either a singular point (respectively a finite singular point), or a limit cycle, or a trajectory which lies on the boundary of a hyperbolic sector at a singular point (respectively a finite singular point). Neumann (1975) proved that the set formed by all separatrices of $p(X)$, denoted by $S(p(X))$, is closed. The open connected components of $\mathbb{S}^2 \setminus S(p(X))$ are called *canonical regions* of $p(X)$. We define a *separatrix configuration* as the union of $S(p(X))$ plus one representative solution chosen from each canonical region. Two separatrix configurations S_1 and S_2 of vector fields of $\mathscr{P}_n(\mathbb{S}^2)$ (respectively $\mathscr{P}_n(\mathbb{R}^2)$) are said to be *topologically equivalent* if there exists an orientation–preserving homeomorphism of $\mathbb{S}^2$ (respectively $\mathbb{R}^2$) which maps the trajectories of S_1 onto the trajectories of S_2.

The *skeleton of separatrices* is defined as the union of $S(p(X))$ without the representative solution of each canonical region. Thus, a skeleton of separatrices can still produce different separatrix configurations. Moreover, a *heteroclinic orbit* is a separatrix which starts and ends on different points and a *homoclinic orbit* is a separatrix which starts and ends at the same point. A *loop* is formed by a homoclinic orbit and its associated singular point. These orbits are also called *separatrix connections*.

We now give the notion of *graphics*, which play an important role in obtaining limit cycles when they are due to connection of separatrices, for example.

A *(non–degenerate) graphic* as defined in Dumortier, Roussarie and Rousseau (1994) is formed by a finite sequence of singular points $r_1, r_2, \ldots, r_n$ (with possible repetitions) and non–trivial connecting orbits γ_i for $i = 1, \ldots, n$ such that γ_i has r_i as α–limit set and r_{i+1} as ω–limit set for $i < n$ and γ_n has r_n as α–limit set and r_1 as ω–limit set. Also normal orientations n_j of the non–trivial orbits must be coherent in the sense that if γ_{j-1} has left–hand orientation then so does γ_j. A *polycycle* is a graphic which has a Poincaré return map.

A *degenerate graphic* is formed by a finite sequence of singular points $r_1, r_2, \ldots, r_n$ (with possible repetitions) and non–trivial connecting orbits and/or segments of curves of

singular points γ_i for $i = 1, \ldots, n$ such that γ_i has r_i as α–limit set and r_{i+1} as ω–limit set for $i < n$ and γ_n has r_n as α–limit set and r_1 as ω–limit set. Also normal orientations n_j of the non–trivial orbits must be coherent in the sense that if γ_{j-1} has left–hand orientation then so does γ_j. For more details, see Dumortier, Roussarie and Rousseau (1994).

Remark 1.3.2 (See Artés, Kooij and Llibre (1998))**.** Any graphic or degenerate graphic in a real planar polynomial differential system must either

(a) surround a singular point of index greater than or equal to +1 (see Dumortier, Llibre and Artés (2008), Hirsch (1976) for the definition of index of a singular point), or

(b) contain a singular point having an elliptic sector situated in the region delimited by the graphic (for the definition of characteristic directions and finite sectoral decomposition of vector fields $p(X) \in \mathscr{P}_n(\mathbb{S}^2)$ (or $X \in \mathscr{P}_n(\mathbb{R}^2)$) we indicate Dumortier, Llibre and Artés (2008)), or

(c) contain an infinite number of singular points.

A vector field $p(X) \in \mathscr{P}_n(\mathbb{S}^2)$ is said to be *structurally stable with respect to perturbations in* $\mathscr{P}_n(\mathbb{S}^2)$ if there exists a neighborhood V of $p(X)$ in $\mathscr{P}_n(\mathbb{S}^2)$ such that $p(Y) \in V$ implies that $p(X)$ and $p(Y)$ are topologically equivalent; that is, there exists a homeomorphism of $\mathbb{S}^2$, which preserves $\mathbb{S}^1$, carrying orbits of the flow induced by $p(X)$ onto orbits of the flow induced by $p(Y)$, preserving sense but not necessarily parametrization.

Since in this thesis we are interested in the classification of the structurally unstable quadratic vector fields of codimension two, we recall the concept of quadratic vector fields of lower codimension in structurally stability.

Recalling the works of Peixoto (1962), restricted to the class of the quadratic vector fields, we have the following result.

Theorem 1.3.3. Consider $p(X) \in \mathscr{P}_n(\mathbb{S}^2)$ (or $X \in \mathscr{P}_n(\mathbb{R}^2)$). This system is structurally stable if and only if

(i) the finite and infinite singular points are hyperbolic;

(ii) the limit cycles are hyperbolic (remember Def. 1.1.27);

(iii) there are no saddle connections.

Moreover, the structurally stable systems form an open and dense subset of $\mathscr{P}_n(\mathbb{S}^2)$ (or $\mathscr{P}_n(\mathbb{R}^2)$).

The studies done up to now on structurally stable systems and codimension one systems are modulo limit cycles (see the introduction of this thesis for more details), so it

is sufficient to consider only conditions *(i)* and *(iii)* of Thm. 1.3.3. These conditions are usually called *stable objects*.

According to Artés, Kooij and Llibre (1998) there are 44 topologically distinct structurally stable quadratic vector fields. Concerning the codimension one quadratic vector fields, we allow the break of only one stable object. In other words, a quadratic vector field X is *structurally unstable of codimension one modulo limit cycles* if and only if

(I) It has one and only one structurally unstable object of codimension one, i.e. one of the following types:

(I.1) a saddle–node q of multiplicity two with $\rho_0 = (\partial P/\partial x + \partial Q/\partial y)_q \neq 0$;

(I.2) a separatrix from one saddle point to another;

(I.3) a separatrix forming a loop for a saddle point with $\rho_0 \neq 0$ evaluated at the saddle.

(II) It has no structurally unstable limit cycles, saddle–point separatrices forming a loop, or singular points other than those listed in (I).

(III) If the vector field has a saddle–node, none of its separatrices may go to a saddle point and no two separatrices of the saddle–node are continuation one of the other.

In what follows, instead of talking about codimension one modulo limit cycles, we simply say *codimension one**.

As described in Chap. 5 of Artés, Llibre and Rezende (2018), the *codimension one** quadratic vector fields can be allocated in four sets, according to the bifurcations that occur to the singular points of structurally stable quadratic vector fields X.

(A) When a finite saddle and a finite node of X coalesce (forming a finite saddle–node $\overline{sn}_{(2)}$) and disappear.

(B) When an infinite saddle and an infinite node of X coalesce (forming an infinite saddle–node $\binom{\overline{0}}{2} SN$) and disappear.

(C) When a finite saddle (respectively node) and an infinite node (respectively saddle) of X coalesce (forming an infinite saddle–node $\binom{\overline{1}}{1} SN$) and then they exchange positions.

(D) When we have a saddle–to–saddle connection. This set is split into five subsets according to the type of the connection: (a) finite–finite (heteroclinic orbit), (b) loop (homoclinic orbit), (c) finite–infinite, (d) infinite–infinite between symmetric points, and (e) infinite–infinite between adjacent points.

Recalling the main result in Artés, Llibre and Rezende (2018), as we described before the phase portraits in all these four sets sum up 209 topological distinct ones, where 202 of these total are proved to be realizable (i.e. the authors could exhibit 202 examples of quadratic systems whose phase portraits are topologically equivalent to those ones) and the remaining 7 are conjectured to be impossible (more precisely, the authors provide some arguments indicating that there are no quadratic system whose phase portrait is topologically equivalent to those 7 phase portraits).

The next step is to classify, modulo limit cycles, the quadratic vector fields of codimension two. In what follows we give a more precise definition of codimension, which can be easily extended for higher dimensions.

Definition 1.3.4. We say that a phase portrait of a quadratic vector field is *structurally stable* if any sufficiently small perturbation in the parameter space leaves the phase portrait topologically equivalent the previous one.

Definition 1.3.5. We say that a phase portrait of a quadratic vector field is *structurally unstable of codimension* k if any sufficiently small perturbation in the parameter space either leaves the phase portrait topologically equivalent the previous one or it moves it to a lower codimension one, and there is at least one perturbation that moves it to the codimension $k-1$.

Remark 1.3.6. We point out that all the phase portraits of quadratic systems with centers singularities are in number 31 (see Vulpe (1983)) and here we consider systems without centers.

Then, according to this definition concerning codimension two, we state the following result:

Theorem 1.3.7. A polynomial vector field in $\mathscr{P}_2(\mathbb{R}^2)$ is *structurally unstable of codimension two modulo limit cycles* if and only if all its objects are stable except for the break of exactly two stable objects. In other words, we allow the presence of two unstable objects of codimension one or one of codimension two.

Combining the sets of *codimension one** quadratic vector fields one to each other, we obtain 10 new sets, from which one of them is split into 15 subsets, according to Tables 1 and 2.

As before, instead of talking about codimension two modulo limit cycles, we simply say *codimension two**.

Geometrically, the *codimension two** sets can be described as follows. Let X be a *codimension one** quadratic vector field. We have the following families:

Table 1 – Families of structurally unstable quadratic vector fields of codimension two considered from combinations of the sets of *codimension one**: (A), (B), (C), and (D) (which in turn is split into (a), (b), (c), (d), and (e))

	(A)	(B)	(C)	(D)
(A)	(AA)			
(B)	(AB)	(BB)		
(C)	(AC)	(BC)	(CC)	
(D)	(AD) (5 cases)	(BD) (5 cases)	(CD) (5 cases)	(DD) see Table 2

Table 2 – Families of structurally unstable quadratic vector fields of codimension two in the set (DD) (see Table 1)

	(a)	(b)	(c)	(d)	(e)
(a)	(aa)				
(b)	(ab)	(bb)			
(c)	(ac)	(bc)	(cc)		
(d)	(ad)	(bd)	(cd)	(dd)	
(e)	(ae)	(be)	(ce)	(de)	(ee)

(AA) Either when a finite saddle (respectively a finite node) of X coalesces with the finite saddle–node, giving birth to a semi–elemental triple saddle: $\overline{s}_{(3)}$ (respectively a triple node: $\overline{n}_{(3)}$), or when both separatrices of the saddle–node limiting its parabolic sector coalesce, giving birth to a cusp of multiplicity two: $\widehat{cp}_{(2)}$, or when another finite saddle–node is formed, having then two finite saddle–nodes: $\overline{sn}_{(2)}+\overline{sn}_{(2)}$. We point out that phase portraits with $\overline{s}_{(3)}$ and with $\overline{n}_{(3)}$ are topologically equivalent to structurally stable phase portraits. We may find them in the papers Artés, Rezende and Oliveira (2013) and Artés, Oliveira and Rezende (2016).

(AB) When an infinite saddle and an infinite node of X coalesce plus a finite saddle–node: $\overline{sn}_{(2)}+\overline{\binom{0}{2}}\,SN$.

(AC) When we have a finite saddle–node and when a finite saddle (respectively node) and an infinite node (respectively saddle) of X coalesce: $\overline{sn}_{(2)}+\overline{\binom{1}{1}}\,SN$.

(AD) When we have a finite saddle–node plus a separatrix connection, considering all five types of set D.

(BB) When an infinite saddle (respectively an infinite node) of X coalesces with an existing infinite saddle–node $\overline{\binom{0}{2}}SN$, leading to a triple saddle: $\overline{\binom{0}{3}}S$ (respectively a triple node: $\overline{\binom{0}{3}}N$). This case is irrelevant to the production of new phase portraits since all the possible phase portraits that may be produced are topologically equivalent to a structurally stable one.

(BC) When a finite antisaddle (respectively finite saddle) of X coalesces with an existing infinite saddle–node $\overline{\binom{0}{2}}\,SN$, leading to a nilpotent elliptic saddle $\widehat{\binom{1}{2}}\,E-H$ (respectively nilpotent saddle $\widehat{\binom{1}{2}}\,HHH-H$). Or it may also happen that a finite saddle (respectively node) coalesces with an elemental node (respectively saddle) in a phase portrait already having an $\overline{\binom{0}{2}}\,SN$, having then in total $\overline{\binom{1}{1}}\,SN+\overline{\binom{0}{2}}\,SN$.

(BD) When we have an infinite saddle–node $\overline{\binom{0}{2}}\,SN$ plus a separatrix connection, considering all five types of set D.

(CC) This case has two possibilities:

(a) when a finite saddle (respectively finite node) of X coalesces with an existing infinite saddle–node $\overline{\binom{1}{1}}\,SN$, leading to a semi–elemental triple saddle $\overline{\binom{2}{1}}\,S$ (respectively a semi–elemental triple node $\overline{\binom{2}{1}}\,N$);

(b) when a finite saddle (respectively node) and an infinite node (respectively saddle) of X coalesce plus another existing infinite saddle–node $\overline{\binom{1}{1}}\,SN$, leading to two infinite saddle–nodes $\overline{\binom{1}{1}}\,SN+\overline{\binom{1}{1}}\,SN$.

The first case is irrelevant to the production of new phase portraits since all the possible phase portraits that may be produced are topologically equivalent to a structurally stable one.

(CD) When we have an infinite saddle–node $\overline{\binom{1}{1}}\,SN$ plus a saddle to saddle connection, considering all five types of set D.

(DD) When we have two saddle to saddle connections, which are grouped as follows:

(aa) two finite–finite heteroclinic connections;

(ab) a finite–finite heteroclinic connection and a loop;

(ac) a finite–finite heteroclinic connection and a finite–infinite connection;

(ad) a finite–finite heteroclinic connection and an infinite–infinite connection between symmetric points;

(ae) a finite–finite heteroclinic connection and an infinite–infinite connection between adjacent points;

(bb) two loops;

(bc) a loop and a finite–infinite connection;

(bd) a loop and an infinite–infinite connection between symmetric points;

(be) a loop and an infinite–infinite connection between adjacent points;

(cc) two finite–infinite connections;

(cd) a finite–infinite connection and an infinite–infinite connection between symmetric points;

(ce) a finite–infinite connection and an infinite–infinite connection between adjacent points;

(dd) two infinite–infinite connections between symmetric points;

(de) an infinite–infinite connection between symmetric points and an infinite–infinite connection between adjacent points;

(ee) two infinite–infinite connections between adjacent points.

Some of these cases have also been proved to be empty in an on course paper.

As we already said in the introduction, in Artés, Oliveira and Rezende (2020) the authors obtained 34 phase portraits belonging to the set (AA) and proved their realization. One of the main goals of this thesis is to continue in this direction by presenting the topological classification of all the phase portraits of *codimension two** belonging to the set (AB) and phase portraits of *codimension two** possessing the set of saddle–nodes $\left\{\overline{sn}_{(2)} + \overline{\binom{1}{1}}\, SN\right\}$ belonging to the set (AC). Here we also prove the realization of all of them.

CHAPTER

2

ALGEBRAIC CONCEPTS

In this chapter we present some algebraic concepts, a summary of the Invariant Theory and how this theory is applied in the qualitative study of quadratic systems. These results contribute for understanding the tools used in this thesis. As we did in the previous chapter and since this chapter is not a main goal of this thesis (i.e. we are not interested in indicating here all the details), here we only present the results and we indicate some references for the reader interested in more information.

2.1 Some notions of algebraic curves

In this section we discuss briefly some basic concepts regarding Algebraic Curves. We indicate Fulton (2008) (or any other book on introduction to Algebraic Geometry) for more details.

2.1.1 Intersection number of algebraic curves

The notion of intersection number of two algebraic curves will be very useful in the definition of multiple singularities and also in the description of the bifurcation surfaces combined with the notion of divisors and zero–cyles.

Definition 2.1.1. We define the *affine two–space* over $\mathbb{C}$, or simply the *affine plane* $\mathbb{A}^2(\mathbb{C})$, by the set $\mathbb{C}\times\mathbb{C}$. Its elements are called *points*.

Definition 2.1.2. If $f\in\mathbb{C}[x,y]$, a point $p=(a,b)\in\mathbb{A}^2(\mathbb{C})$ is called a *zero* of f if $f(p)=f(a,b)=0$. We say that two polynomials $f,g\in\mathbb{C}[x,y]$ are *equivalent* if $f=\lambda g$, for some $\lambda\in\mathbb{C}^*$. We define an *affine plane curve* to be an equivalence class of non–constant polynomials under this equivalence relation.

Definition 2.1.3. Let $C : f(x,y) = 0$ and $\widetilde{C} : g(x,y) = 0$ be two affine algebraic curves over $\mathbb{C}$. The *intersection number* of C and $\widetilde{C}$ at a point $a \in \mathbb{A}^2(\mathbb{C})$ is the number

$$I_a(f,g) = \dim_{\mathbb{C}} \frac{O_a}{(f,g)},$$

where O_a is the local ring of the affine complex plane at a, i.e. O_a is the ring of rational functions $p(x,y)/q(x,y)$ which are defined at a (i.e. $q(a) \neq 0$), and (f,g) is the ideal generated by f and g.

Definition 2.1.4. We say that f and g *intersect properly* at a point a if f and g have no common component that passes through a.

One can calculate the intersection number $I_a(f,g)$ of two affine algebraic curves at a point a by using the following seven axioms:

(A1) $I_a(f,g)$ is a non–negative integer for any f,g and a such that f and g intersect properly at a. Moreover $I_a(f,g) = \infty$ if f and g do not intersect properly at a;

(A2) $I_a(f,g) = 0$ if and only if $a \notin f \cap g$;

(A3) If T is an affine translation on $\mathbb{A}^2(\mathbb{C})$ and $T(b) = a$, then $I_a(f,g) = I_b(f \circ T, g \circ T)$;

(A4) $I_a(f,g) = I_a(g,f)$;

(A5) Two curves f and g are said to *intersect transversally* at a if a is a simple point both on f and on g, and if the tangent line to f at a is different from the tangent line to g at a. We want the intersection number to be one exactly if f and g meet transversally at a. More generally, we require $I_a(f,g) \geq m_a(f)m_a(g)$ (where $m_a(f)$ stands for the multiplicity of f at a) and the equality holds if and only if f and g have no tangent lines in common at a;

(A6) The intersection numbers should add when we take unions of curves: if $f = \prod f_i^{r_i}$ and $g = \prod g_j^{s_j}$ then $I_a(f,g) = \sum_{i,j} r_i s_j I_a(f_i, g_j)$;

(A7) $I_a(f,g) = I_a(f,(g+kf))$, for any $k \in \mathbb{C}[x,y]$.

In the case that we have a quadratic polynomial differential system

$$x' = P(x,y), \qquad y' = Q(x,y),$$

the intersection numbers $I_a(P,Q)$ at the singularities $a \in \mathbb{A}^2(\mathbb{C})$ can be computed by using these seven axioms. In this case, we say that a singularity a of the previous system is *simple* if $I_a(P,Q) = 1$, otherwise we say that a has *multiplicity* r if we have $I_a(P,Q) = r$. Roughly speaking, for this last case singularity a produces at most r singularities, as close to a as we desire, by means of polynomial perturbations of this system.

Definition 2.1.5. Consider $\mathbb{A}^{n+1} = \mathbb{A}^{n+1}(\mathbb{K})$, where $\mathbb{K}$ is a field. The set of all lines in $\mathbb{A}^{n+1}$ passing through the origin $0 = (0,\ldots,0)$ is called the *n–dimensional projective space* and it is denoted by $\mathbb{KP}^n$, or simply $\mathbb{P}^n$ when $\mathbb{K}$ is understood.

We identify $\mathbb{P}^n$ with the set of all points in $\mathbb{A}^{n+1}\backslash\{0\}$ modulo the equivalence relation $(x_1,\ldots,x_{n+1}) \sim (\lambda x_1,\ldots,\lambda x_{n+1})$ for all $\lambda \in \mathbb{K}^*$, i.e. two points in $\mathbb{A}^{n+1}\backslash\{0\}$ are equivalent if they are on the same line through the origin. An element of $\mathbb{P}^n$ is called a *point*. If P is a point, then any $(n+1)$–tuple $(a_1,\ldots,a_{n+1})$ in the equivalence class of P is called a set of *homogeneous coordinates* of P. Equivalence classes are usually written as $P = [a_1 : \cdots : a_{n+1}]$ to distinguish from the affine coordinates. Note that

$$[a_1 : \cdots : a_{n+1}] = [\lambda a_1 : \cdots : \lambda a_{n+1}], \quad \forall\ \lambda \in \mathbb{K}^*.$$

We have defined $\mathbb{P}^n$ as the collection of all one–dimensional subspaces of the vector space $\mathbb{A}^{n+1}$, but $\mathbb{P}^n$ may also be thought as $n+1$ (overlapping) copies of affine n–space. In fact, we can express any point

$$[x_1 : \cdots : x_{n+1}] \in U_i = \{[a_1 : \cdots : a_{n+1}] \in \mathbb{P}^n; a_i \neq 0\}$$

in terms of n affine coordinates

$$[x_1 : \cdots : x_{n+1}] = \left[\frac{x_1}{x_i} : \cdots : 1 : \cdots : \frac{x_{n+1}}{x_i}\right],$$

and then, $U_i \cong \mathbb{A}^n$. Projective spaces will be very useful in Chap. 3 and 4.

Definition 2.1.6. A polynomial $f \in \mathbb{K}[x_1,\ldots,x_{n+1}]$ is *homogeneous of degree d* if

$$f(\lambda x_1,\ldots,\lambda x_{n+1}) = \lambda^d f(x_1,\ldots,x_{n+1}), \quad \forall\ \lambda \in \mathbb{K}.$$

Definition 2.1.7. For any set S of polynomials in $\mathbb{K}[x_1,\ldots,x_{n+1}]$ we define the *projective algebraic set*

$$V(S) = \{P \in \mathbb{P}^n; f(P) = 0, \text{ for all homogeneous } f \in S\}.$$

An irreducible projective algebraic set in $\mathbb{P}^n$ is called a *projective variety*.

One can show that an algebraic set $Z \subseteq \mathbb{P}^n$ is irreducible if and only if the ideal generated by Z is prime (i.e. if $ab \in I(Z)$, then $a \in I(Z)$ or $b \in I(Z)$).

Definition 2.1.8. Two non–constant homogeneous polynomials $F, G \in \mathbb{K}[X,Y,Z]$ are said to be *equivalent* if there is a nonzero $\lambda \in \mathbb{K}$ such that $G = \lambda F$. A *projective plane curve* is an equivalence class of homogeneous polynomials.

For two projective curves in $\mathbb{CP}^2$, $F(X,Y,Z) = 0$ and $G(X,Y,Z) = 0$, where F and G are homogeneous polynomials in the variables X, Y, and Z which are relatively prime over

$\mathbb{C}$ we can define $I_W(F,G)$ as follows: suppose for example that $W=[a:b:c]$ where $c\neq 0$, hence $W=[a/c:b/c:1]$. Let $f(x,y)=F(x,y,1)$ and $g(x,y)=G(x,y,1)$. Then $I_W(F,G)=I_w(f,g)$ where $w=(a/c,b/c)$. It is known that $I_W(F,G)$ is independent of the choice of a local chart, and of a projective change of variables (see again Fulton (2008)).

These concepts of intersection multiplicity extend to that of intersection multiplicity of several curves at a point of the projective plane, see Sec. 5 of Artés, Llibre and Schlomiuk (2006) for more details.

2.1.2 Resultants and discriminants

We already know how to compute the intersection number $I_a(f,g)$ between two affine algebraic curves at a point a. The natural question that arises is the following one: how can we proceed in order to find the intersection points between two curves $f,g\in\mathbb{C}[x,y]$? The most general and simple method is to select one of the variables, say y, to act like part of the coefficients, i.e. we consider f and g as polynomials in the variable x with coefficients in the ring $\mathbb{C}[y]$. Then we try to find values of y in such a way that $f(x,y)$ and $g(x,y)$ admit a common root. Geometrically we want to find the projections, over the y axis, of the points of $f\cap g$.

Definition 2.1.9. Let $f(x)=a_nx^n+\cdots+a_0$ and $g(x)=b_mx^m+\cdots+b_0$ be two polynomials of degrees (at most) n and m, respectively, with coefficients in an arbitrary field $\mathbb{K}$ (or, as before, in $\mathbb{C}[y]$). Their *resultant* $R(f,g)=R_{n,m}(f,g)$ is the element of $\mathbb{K}$ given by the determinant of the $(m+n)\times(m+n)$ *Sylvester Matrix*, given by

$$\begin{bmatrix}
a_n & a_{n-1} & a_{n-2} & \cdots & 0 & 0 & 0\\
0 & a_n & a_{n-1} & \cdots & 0 & 0 & 0\\
\vdots & \vdots & \vdots & \ddots & \vdots & \vdots & \vdots\\
0 & 0 & 0 & \vdots & a_1 & a_0 & 0\\
0 & 0 & 0 & \vdots & a_2 & a_1 & a_0\\
a_m & b_{m-1} & b_{m-2} & \cdots & 0 & 0 & 0\\
0 & b_m & b_{m-1} & \cdots & 0 & 0 & 0\\
\vdots & \vdots & \vdots & \ddots & \vdots & \vdots & \vdots\\
0 & 0 & 0 & \vdots & b_1 & b_0 & 0\\
0 & 0 & 0 & \vdots & b_2 & b_1 & b_0
\end{bmatrix},$$

where the m first rows contain the coefficients $a_n,a_{n-1},\ldots,a_0$ of f shifted $0,1,\ldots,m-1$ steps and padded with zeroes, and the n last rows contain the coefficients $b_m,b_{m-1},\ldots,b_0$ of g shifted $0,1,\ldots,n-1$ steps and padded with zeroes (see Garcia and Lequain (2012), for instance, for more details).

The main importance of the resultant lies in the following formula.

Theorem 2.1.10. Let $f(x) = a_n x^n + \cdots + a_0$ and $g(x) = b_m x^m + \cdots + b_0$ be two polynomials of degrees n and m (this means $a_n \neq 0$ and $b_m \neq 0$), respectively, with coefficients in an arbitrary field $\mathbb{K}$. Suppose that, in some extension of $\mathbb{K}$, f has n roots $\alpha_1, \ldots, \alpha_n$ and g has m roots $\beta_1, \ldots, \beta_m$ (not necessarily distinct). Then

$$R(f,g) = a_n^m b_m^n \prod_{i=1}^{n} \prod_{j=1}^{m} (\alpha_i - \beta_j).$$

This theorem implies perhaps the most important result about resultants.

Corollary 2.1.11. Let f and g be two nonzero polynomials with coefficients in a field $\mathbb{K}$. Then f and g have a common non–trivial factor if and only if $R(f,g) = 0$. Equivalently, f and g are coprime if and only if $R(f,g) \neq 0$.

Another important tool that is quite useful in this thesis is the notion of *discriminant* (see Garcia and Lequain (2012), for more details). The discriminant of a polynomial f is generally defined in terms of a polynomial function of its coefficients. The discriminant is widely used in factoring polynomials, number theory, and algebraic geometry, and it gives some information about the nature of the roots of f.

Definition 2.1.12. The discriminant of a polynomial $f(x) = a_n x^n + \cdots + a_1 x + a_0 \in \mathbb{C}[x]$ is a number $\Delta(f)$, which is defined by

$$\Delta(f) = a_n^{2n-2} \prod_{1 \leq i \leq j \leq n}^{n} (\alpha_i - \alpha_j)^2,$$

where α_i are the roots of $f(x) = 0$.

Regarding this definition it is clear that the discriminant $\Delta(f) = 0$ if and only if f has a repeated root.

It is also known that the discriminant of a polynomial f is given in terms of a resultant as

$$\Delta(f) = \frac{(-1)^{n(n-1)/2}}{a_n} R(f, f'),$$

where f' is the derivative of f and n is the degree of f.

We finish this section with the following definition regarding the singularities of an algebraic curve.

Definition 2.1.13. A point a which belongs to an algebraic curve $f \in \mathbb{C}[x,y]$ is said to be *non–singular* (or *regular*) if at least one of the partial derivatives f_x, f_y does not vanish at a.

2.1.3 Zero–cycles and divisors

Here we present the notions of zero–cycle and divisor and we indicate a reference in which the authors use these concepts for the purpose of classifying quadratic systems.

Let V be an irreducible algebraic variety over a field $\mathbb{K}$. A *cycle of dimension r or r–cycle* on V is a formal sum $\sum_W n_W W$, where W is a subvariety of V of dimension r which is not contained in the singular locus of V (i.e. the complement of the regular points of V), $n_W \in \mathbb{Z}$, and only a finite number of n_W's are nonzero. The *support* of a cycle C is the set $Supp(C) = \{W; n_W \neq 0\}$. We denote by $\max(C)$ the maximum value of the coefficients n_W in C. For every $m \leq \max(C)$ let $s(m)$ be the number of the coefficients n_W in C which are equal to m. We call *type* of the cycle C the set of ordered couples $(s(m), m)$ where $1 \leq m \leq \max(C)$. The *degree* of a cycle of $\mathbb{C}^2$, (respectively $\mathbb{R}^2$, $\mathbb{CP}^2$, $\mathbb{RP}^2$) is the sum of its coefficients n_W. If J is a cycle we denote by $\deg(J)$, its degree. An $(n-1)-cycle$ is called a *divisor*.

For a given system S belonging to the family of quadratic systems

$$x' = P(x,y), \quad y' = Q(x,y),$$

we define the algebraic set $Z(P,Q) = \{w \in \mathbb{C}^2; P(w) = Q(w) = 0\}$ and we construct the following zero–cycle

$$\mathscr{D}_S(P,Q) = \sum_{w \in Z(P,Q)} I_w(P,Q) w,$$

where $I_w(P,Q)$ is the intersection number or multiplicity of intersection at w of the projective completions of the curves $P = 0$ and $Q = 0$. It is clear that, for a non–degenerate quadratic system we have $\deg(\mathscr{D}_S) \leq 4$ and the number of points in $Supp(\mathscr{D}_S)$ is lesser than or equal to four. The zero–cycle $\mathscr{D}_S(P,Q)$ is not defined for a degenerate system.

These notions which occur frequently in algebraic geometry (see for instance Hartshorne (1977)), were used for classification purposes of planar quadratic differential systems by Pal and Schlomiuk (see Schlomiuk and Pal (2001)) and by Llibre and Schlomiuk (see Llibre and Schlomiuk (2004)). In Artés, Llibre and Schlomiuk (2006) the authors construct several zero–cycles and divisors related to a real polynomial differential system

$$\dot{x} = f(x,y), \quad \dot{y} = g(x,y),$$

with f and g relatively prime polynomials in $\mathbb{C}[x,y]$ with $\max\{\deg(f), \deg(g)\} = m$.

Remark 2.1.14. In this thesis we shall use routinely the basic concepts of Differential and Integral Calculus, such as *gradient*, *Jacobian matrix* and *Hessian* of a function. We do not mention such results here since they can be found in every Calculus book.

2.2 Affine invariant polynomials

In this section we provide a summary of the *Classical Invariant Theory* and how the concepts are applicable in the qualitative study of differential systems.

The algebraic theory of invariants was originally introduced in Britain in the middle of the nineteenth century. Initially some formal methods of constructing invariants were developed. Then, about one hundred years ago, several fundamental problems of this theory were solved by David Hilbert. In our days the Invariant Theory continues being developed and applied in various branches of Mathematics and Physics. We indicate the book of Olver (1999), in which a very nice historical review and several references are given.

Classical Invariant Theory is the study of intrinsic properties of polynomials. By intrinsic we mean those properties which are unaffected by a change of variables and are then purely geometric, independently to the explicit coordinate system in use. We illustrate with an example. The polynomial

$$f(x) = (x-1)(x+7)^3(x^2+4)^2 \in \mathbb{R}[x]$$

possesses degree 8 and has clearly four roots, namely, $x_1 = 1, x_2 = -7, x_3 = 2i$ and $x_4 = -2i$. The most intuitive changes of variables which preserve the degree of polynomials are the affine transformations $\bar{x} = \alpha x + \beta$ with $\alpha, \beta \in \mathbb{R}$ and $\alpha \neq 0$. By applying this transformation to this polynomial, after a straightforward computation we obtain the polynomial

$$\bar{f}(\bar{x}) = \frac{1}{\alpha^8}(\bar{x} - \alpha - \beta)(\bar{x} + 7\alpha - \beta)^3(\bar{x}^2 - 2\beta\bar{x} + 4\alpha^2 + \beta^2)^2.$$

Thus, properties such as factorizability and multiplicity of the roots are intrinsic, whereas the explicit values of the roots and the particular coefficients of the polynomials are not.

The study of invariants is closely related to the following two problems:

- *the equivalence problem:* when can one polynomial be transformed into another by a suitable change of coordinates?
- *the associated canonical form problem:* how to find a coordinate system in which the polynomial takes a simpler form?

The solution of these intimately related problems, and much more, are governed by the invariants, and so the first goal of the Classical Invariant Theory is to determine the fundamental invariants. With a sufficient number of invariants in hand, one can effectively solve the equivalence, and canonical form problems, and, at least in principle, completely characterize the underlying geometry of a given polynomial.

All these issues appear in the following very simple example. Consider the quadratic binary form

$$f(x,y) = ax^2 + 2bxy + cy^2.$$

The most obvious change of variables which preserves the class of quadratic binary forms are the linear transformations:

$$\bar{x} = \alpha x + \beta y, \quad \bar{y} = \gamma x + \delta y,$$

in which the coefficient matrix

$$A = \begin{pmatrix} \alpha & \beta \\ \gamma & \delta \end{pmatrix}$$

is non–singular, i.e. $\det(A) = \alpha\delta - \beta\gamma \neq 0$. In order to simplify, we assume that the form $f(x,y)$ as well the matrix A are real. Under such a linear transformation, the image of the form $f(x,y)$ is a new form $\bar{f}(\bar{x},\bar{y})$, which is defined so that

$$\bar{f}(\bar{x},\bar{y}) = \bar{f}(\alpha x + \beta y, \gamma x + \delta y) = f(x,y).$$

Then, matrix A induces a transformation on the coefficients a, b, and c of $f(x,y)$, mapping them into the corresponding coefficients $\bar{a}, \bar{b}$, and $\bar{c}$ of $\bar{f}(\bar{x},\bar{y})$. From the previous equation one can write

$$\bar{a}(\alpha x + \beta y)^2 + 2\bar{b}(\alpha x + \beta y)(\gamma x + \delta y) + \bar{c}(\gamma x + \delta y)^2 = f(x,y),$$

and from such an equation we obtain the relation

$$a = \alpha^2\bar{a} + 2\alpha\gamma\bar{b} + \gamma^2\bar{c}, \quad b = \alpha\beta\bar{a} + (\alpha\delta + \beta\gamma)\bar{b} + \gamma\delta\bar{c}, \quad c = \beta^2\bar{a} + 2\beta\delta\bar{b} + \delta^2\bar{c}.$$

From these identities we can conclude that there exists the following relation between the discriminant Δ of $f(x,y)$ with the discriminant $\bar{\Delta}$ of $\bar{f}(\bar{x},\bar{y})$:

$$\Delta = b^2 - ac = (\alpha\delta - \beta\gamma)^2(\bar{b}^2 - \bar{a}\bar{c}) = (\alpha\delta - \beta\gamma)^2\bar{\Delta}.$$

These equations express the underlying invariance of the discriminant of a quadratic form and provide the simplest example of an invariant (in the sense of Classical Invariant Theory). We recall the geometrical meaning of the invariant discriminant: it governs the types of the linear factors of its form. So, it can be applied for the classification of the class of quadratic forms (see Table 3).

Table 3 – Classification of the class of quadratic forms $f(x,y) = ax^2 + 2bxy + cy^2$

Sign of the discriminant	**Number of roots**	**Canonical form**
$\Delta > 0$	2 real (distinct)	xy
$\Delta < 0$	2 complex	$k(x^2+y^2),\ k \in \{-1,1\}$
$\Delta = 0,\ f \not\equiv 0$	1 double (real)	$kx^2,\ k \in \{-1,1\}$
$\Delta = 0,\ f \equiv 0$	–	0

We point out that in this thesis we are not interested in use effectively the Classical Invariant Theory. We only want to use the applications of the *algebraic invariants of differential systems*.

The foundations of the theory of algebraic invariants of differential systems were laid down in the 60's of the last century in the works of Professor Konstantin Sergeevich Sibirsky (see Sibirsky (1988)). He was the founder of the Moldovian School in the Qualitative Theory of Differential Equations. The use of algebraic invariants was prompted by his research (initiated by Professor Nemytsky) in the conditions of the existence of a center for polynomial differential systems. Sibirsky had noticed that the center conditions that he has obtained were invariant under the rotation of the phase plane, and therefore, the rotation invariants of such systems could be used in construction of the center conditions. So, it has arisen the necessity in constructing invariant polynomials depending on the coefficients of differential systems. Since then, Sibirsky and his students (here we highlight Professor Nicolae Vulpe) have been working on the attempt of joining the concepts of invariant polynomials of systems of autonomous differential equations with the action of groups of linear transformations of the phase space.

As it was done before (see for instance Artés, Llibre and Schlomiuk (2006), Artés, Rezende and Oliveira (2015)), in this thesis we apply the results of Sibirsky and his students in order to classify topologically planar differential systems. With the purpose of using this technique we need to introduce some notation and concepts, and also show briefly how the classical theory of invariants and methods are adapted for our aim. In order to adapt and use classical methods and technique we first need to pass to the tensor form of differential systems.

2.2.1 Tensor notation of differential systems

We begin with quadratic systems of the form

$$\begin{aligned}\frac{dx}{dt} &= ax+by+cx^2+dxy+ey^2,\\ \frac{dy}{dt} &= Ax+By+Cx^2+Dxy+Ey^2,\end{aligned}$$

where x and y are unknown functions and t is the independent variable. Denoting by

$$x^1=x,\quad x^2=y,\quad a^1_{12}=a^1_{21}=\frac{1}{2}d,\quad a^2_{12}=a^2_{21}=\frac{1}{2}D,$$

the previous system can be written in the form

$$\begin{aligned}\frac{dx^1}{dt} &= a^1_1x^1+a^1_2x^2+a^1_{11}(x^1)^2+a^1_{12}x^1x^2+a^1_{21}x^2x^1+a^1_{22}(x^2)^2,\\ \frac{dx^2}{dt} &= a^2_1x^1+a^2_2x^2+a^2_{11}(x^1)^2+a^2_{12}x^1x^2+a^2_{21}x^2x^1+a^2_{22}(x^2)^2.\end{aligned}$$

This notation is more convenient, since it is possible to summarize it in the compact way

$$\frac{dx^j}{dt} = \sum_{\alpha=1}^{2} a^j_\alpha x^\alpha + \sum_{\alpha,\beta=1}^{2} a^j_{\alpha\beta} x^\alpha x^\beta, \quad j = 1,2,$$

or, discarding the summation sign, in the form

$$\frac{dx^j}{dt} = a^j_\alpha x^\alpha + a^j_{\alpha\beta} x^\alpha x^\beta, \quad j,\alpha,\beta = 1,2.$$

Another way to write this last system is in the form

$$\frac{dx^j}{dt} = \sum_{\omega=1}^{2} a^j_{j_1 j_2 \dots j_\omega} x^{j_1} x^{j_2} \cdots x^{j_\omega}, \quad j, j_1, j_2, \dots, j_\omega = 1,2,$$

which can be extended to multivariate systems with arbitrary polynomials or series on the right–hand sides

$$\frac{dx^j}{dt} = \sum_{\omega\in\Omega} a^j_{j_1 j_2 \dots j_\omega} x^{j_1} x^{j_2} \cdots x^{j_\omega}, \quad j, j_1, j_2, \dots, j_\omega \in \{1,2,\dots,n\}, \tag{2.1}$$

where Ω is some set of positive distinct integers, while the coefficients $a^j_{j_1 j_2 \dots j_\omega}$ are symmetrical with respect to lower indexes, i.e. their values are not dependent on the order of succession of these indexes.

Definition 2.2.1. The form (2.1) is called a *tensor form.*

We observe that setting $\Omega = \{1,2\}$ and $n = 2$ we obtain the initial quadratic system and if the set Ω is infinite then the right–hand sides of systems (2.1) are formal series.

2.2.2 The definition of an invariant polynomial

In what follows we assume that systems (2.1) are real polynomial systems (in the case when Ω is infinite, remember that a polynomial of an infinite set of variables is a polynomial of any finite subset of these variables). In this case we can identify each system (2.1) to a point $a \in \mathbb{R}^m$, where m is the number of the coefficients of this system.

Consider the group $Q \subseteq GL(n,\mathbb{R})$ of linear transformations of the n–dimensional space X of vectors $x = (x^1, x^2, \dots, x^n)$ (of the phase space of systems (2.1)). We denote a linear transformation $q \in Q$ in the form

$$y = qx,$$

where $y = (y^1, y^2, \dots, y^n)$ is the vector of new unknown functions and q is a $n \times n$–matrix.

Performing this transformation on a system (2.1) corresponding to a point $a \in \mathbb{R}^m$ we arrive at the system

$$\frac{dy^r}{dt} = \sum_{\omega\in\Omega} b^r_{r_1 r_2 \dots r_\omega} y^{r_1} y^{r_2} \cdots y^{r_\omega}, \quad r, r_1, r_2, \dots, r_\omega \in \{1,2,\dots,n\}, \tag{2.2}$$

which corresponds to a point $b \in \mathbb{R}^m$. It is clear that b depends on a and q (i.e. we have $b = b(a,q)$) and we shall sometimes write $b = a(q)$.

Definition 2.2.2. A polynomial $I(a)$ of the coefficients of systems (2.1) is called an *invariant polynomial* for these systems with respect to a group Q if there exists a function $\lambda(q)$ depending only on elements of the group such that for every $(q,a) \in Q \times \mathbb{R}^m$ the following identity holds

$$I(b) = \lambda(q) I(a). \tag{2.3}$$

The function $\lambda(q)$ is called a *multiplicator*. If $\lambda(q) \equiv 1$ then the invariant $I(a)$ is called *absolute*, otherwise it is called *relative*.

In the next subsection we apply directly this definition in order to construct the *GL*–invariants for the simplest class of systems, the linear ones.

2.2.3 Invariants of differential systems

We consider the simplest case, when $\Omega = \{1\}$ and $n = 2$. Then we obtain the linear systems

$$\frac{dx^j}{dt} = a^j_\alpha x^\alpha, \quad j, \alpha = 1,2,$$

which in addition can be written in the vector form

$$\frac{dx}{dt} = ax, \quad a = \begin{pmatrix} a^1_1 & a^1_2 \\ a^2_1 & a^2_2 \end{pmatrix}.$$

We consider the group $GL(2,\mathbb{R})$ of linear transformations. In this case $q \in GL(2,\mathbb{R})$ is a 2×2-matrix which is denoted by

$$q = \begin{pmatrix} \alpha & \beta \\ \gamma & \delta \end{pmatrix},$$

which is non–singular (i.e $\det(q) \neq 0$). Considering the transformation $y = qx$ we obtain the corresponding inverse $x = q^{-1}y$ and then we have

$$\frac{dy}{dt} = q\frac{dx}{dt} = qaq^{-1}y = by$$

which implies

$$\frac{dy}{dt} = by,$$

where $b = \begin{pmatrix} b^1_1 & b^1_2 \\ b^2_1 & b^2_2 \end{pmatrix}$. The equality $b = qaq^{-1}$ is equivalent to $bq = qa$, i.e.

$$\begin{pmatrix} b^1_1 & b^1_2 \\ b^2_1 & b^2_2 \end{pmatrix} \begin{pmatrix} \alpha & \beta \\ \gamma & \delta \end{pmatrix} = \begin{pmatrix} \alpha & \beta \\ \gamma & \delta \end{pmatrix} \begin{pmatrix} a^1_1 & a^1_2 \\ a^2_1 & a^2_2 \end{pmatrix}$$

and this leads us to the following identities

$$\begin{aligned} b_1^1\alpha + b_2^1\gamma = a_1^1\alpha + a_1^2\beta, \qquad & b_1^1\beta + b_2^1\gamma = a_2^1\alpha + a_2^2\beta, \\ b_1^2\alpha + b_2^2\gamma = a_1^1\gamma + a_1^2\delta, \qquad & b_1^2\beta + b_2^2\delta = a_2^1\gamma + a_2^2\delta. \end{aligned}$$

From these equations we obtain

$$\begin{aligned} \det(q)b_1^1 &= \alpha\delta a_1^1 - \alpha\gamma a_2^1 + \beta\delta a_1^2 - \beta\gamma a_2^2, \\ \det(q)b_2^1 &= -\alpha\beta a_1^1 + \alpha^2 a_2^1 - \beta^2 a_1^2 + \alpha\beta a_2^2, \\ \det(q)b_1^2 &= \gamma\delta a_1^1 - \gamma^2 a_2^1 + \delta^2 a_1^2 - \gamma\delta a_2^2, \\ \det(q)b_2^2 &= -\beta\gamma a_1^1 + \alpha\gamma a_2^1 - \beta\delta a_1^2 + \alpha\delta a_2^2. \end{aligned} \tag{2.4}$$

We shall seek for homogeneous invariants of first degree, i.e. invariants of the form

$$I(a) = k_1 a_1^1 + k_2 a_2^1 + k_3 a_1^2 + k_4 a_2^2, \tag{2.5}$$

where k_i $(i = 1,2,3,4)$ are the parameters which we have to determine.

Using Def. 2.2.2, from relation (2.3) we obtain

$$I(b) = k_1 b_1^1 + k_2 b_2^1 + k_3 b_1^2 + k_4 b_2^2 = \lambda(q)(k_1 a_1^1 + k_2 a_2^1 + k_3 a_1^2 + k_4 a_2^2) = \lambda(q) I(a)$$

and this identity must be verified for all values of a_j^i $(i, j = 1,2)$. Considering (2.4) and equating in the previous relation the coefficients in front of a_1^1 and a_2^1 we obtain, respectively

$$\begin{aligned} a_1^1 &: k_1\alpha\delta - k_2\alpha\beta + k_3\gamma\delta - k_4\beta\gamma = \lambda(q)k_1\det(q), \\ a_1^1 &: -k_1\alpha\gamma + k_2\alpha^2 - k_3\gamma^2 + k_4\alpha\gamma = \lambda(q)k_2\det(q). \end{aligned} \tag{2.6}$$

Eliminating the function $\lambda(q)$ from expression (2.6) we arrive at the following relation

$$k_1k_2\alpha\delta - k_2^2\alpha\beta + k_2k_3\gamma\delta - k_2k_4\beta\gamma + k_1^2\alpha\gamma - k_1k_2\alpha^2 + k_1k_3\gamma^2 - k_1k_4\alpha\gamma = 0,$$

which must be satisfied for all values of α, β, γ and δ. Computing the coefficients of $\alpha\beta$ we get $k_2 = 0$. Hence, from the second relation of (2.6) we obtain $k_3 = 0, k_4 = k_1$ and then the first relation of (2.6) becomes

$$k_1(\alpha\delta - \beta\gamma) = k_1\lambda(q)\det(q) = k_1\lambda(q)(\alpha\delta - \beta\gamma).$$

So, $\lambda(q) = 1$ and then, up to a constant $k_1 \neq 0$ we conclude that from (2.5) we have

$$I_1(a) = a_1^1 + a_2^2 = \mathbf{tr}(a),$$

where $\mathbf{tr}(a)$ is the trace of matrix a. This means that $I_1(a)$ is an absolute GL–invariant of degree one.

In a similar way (see Sibirsky (1988)), seeking for invariants of the second degree we obtain that any such an invariant is of the form

$$I(a) = k_1(a_1^1 + a_2^2)^2 + k_2(a_1^1 a_2^2 - a_2^1 a_1^2) = k_1(\mathbf{tr}^2(a)) + k_2 \det(a).$$

So, the polynomial $I_2(a) = \det(a)$ is an absolute invariant and any GL–invariant of second degree for the linear systems is a linear combination of the invariants $\mathbf{tr}^2(a)$ and $\det(a)$. Finally, investigating GL–invariants of third degree it can be shown that any such an invariant is of the form

$$I(a) = k_1 \mathbf{tr}^3(a) + k_2 \mathbf{tr}(a) \det(a).$$

Thus the third degree invariants are expressed polynomially by already obtained invariants of lesser degrees.

Definition 2.2.3. A polynomial invariant $I(a)$ is called *reducible* if it is expressed polynomially by invariants of lesser degrees. In this case we write $I(a) \cong 0$ and we say that $I(a)$ is *congruent* to zero.

In Sibirsky (1988), by using more concepts of tensors and operations with them, it is shown that any GL–invariant for the linear systems is polynomially expressed by means of $I_1(a)$ and $I_2(a)$. In this case we say that these two invariants produce a *polynomial basis* of (affine) invariants for the linear systems.

Definition 2.2.4. The set of polynomials $\{I_\theta(a), \theta \in \Theta\}$ for systems (2.1) with respect to the group Q is called a *polynomial basis of invariants* of these systems if any polynomial invariant $I(a)$ of systems (2.1) with respect to the group Q can be expressed in the form of a polynomial of invariants $I_\theta(a)$. A polynomial basis of invariants of systems (2.1) under the group Q is called *minimal* if after the removing of any invariant polynomial out of the set, it ceases to be a polynomial basis.

Remark 2.2.5. Note that the minimality of a polynomial basis, consisting of invariants $\mathbf{tr}(a)$ and $\det(a)$ follows from the fact that it is impossible to express $\det(a)$ by means of the square of $\mathbf{tr}(a)$.

Sibirsky (1988) concluded that the tensorial method can be applied to construct invariant polynomials which depend not only on the coefficients of differential systems, but also on the unknown functions, i.e. polynomials of the form $K(a,x)$. Such polynomials are called *comitants*. The rule of the invariance of these polynomials is the same as for polynomial invariants, but with a little addition: the identity

$$K(b,y) = \lambda(q) K(a,x)$$

must be verified for every $(a,q,x) \in (\mathbb{R}^m, Q, X)$. So, a GL–invariant is a particular case of a GL–comitant since the first one does not depend on the variable x. It can be shown that

the factor $\lambda(q)$ is of the form (see Sibirsky (1988, Thm. 7.1))

$$\lambda(q) = (\det(q))^{-\chi}, \quad \chi \in \mathbb{Z}.$$

The number $\chi \in \mathbb{Z}$ is called the *weight* of the comitant $K(a,x)$.

Moreover, Sibirsky (1988) made the construction of some basis of invariants and he proved that the polynomial basis of GL–invariants of systems (2.1) consists of 16 invariants (namely, I_1 to I_{16}) and, in addition, if we add 20 more comitants (namely, K_1 to K_{20}) to those 16 invariants we obtain a polynomial basis of GL–comitants of the mentioned systems.

Invariants and comitants have been extensively applied in planar quadratic differential systems (see, for instance, Artés, Llibre and Schlomiuk (2006), Artés, Rezende and Oliveira (2015), Artés *et al.* (2021)). In the next subsection we shall provide the main comitants used in previous studies.

2.2.4 Group actions on quadratic systems

Consider a real quadratic system

$$\begin{cases} \dfrac{dx}{dt} = p_0 + p_1(x,y) + p_2(x,y) \equiv p(x,y), \\ \dfrac{dy}{dt} = q_0 + q_1(x,y) + q_2(x,y) \equiv q(x,y), \end{cases} \tag{2.7}$$

with $\max\{\deg(p), \deg(q)\} = 2$, $\gcd(p,q) = 1$ and

$$\begin{aligned} p_0 &= a_{00}, \quad p_1(x,y) = a_{10}x + a_{01}y, \quad p_2(x,y) = a_{20}x^2 + 2a_{11}xy + a_{02}y^2, \\ q_0 &= b_{00}, \quad q_1(x,y) = b_{10}x + b_{01}y, \quad q_2(x,y) = b_{20}x^2 + 2b_{11}xy + b_{02}y^2. \end{aligned}$$

Let $a = (a_{00}, a_{10}, a_{01}, a_{20}, a_{11}, a_{02}, b_{00}, b_{10}, b_{01}, b_{20}, b_{11}, b_{02})$ be the 12–tuple of the coefficients of system (2.7) and write $\mathbb{R}[a,x,y] = \mathbb{R}[a_{00}, a_{10}, a_{01}, a_{20}, a_{11}, a_{02}, b_{00}, b_{10}, b_{01}, b_{20}, b_{11}, b_{02}, x, y]$. We denote by **QS** the entire class of quadratic systems. Then, to a quadratic system (2.7) we can associate a point of $\mathbb{R}^{12}$, the ordered 12–tuple of the coefficients of $p(x,y)$, $q(x,y)$ and this correspondence is an injection

$$\begin{aligned} \mathscr{B} : \mathbf{QS} &\hookrightarrow \mathbb{R}^{12} \\ S &\mapsto a = \mathscr{B}(S). \end{aligned}$$

The topology of $\mathbb{R}^{12}$ yields an induced topology on **QS**.

On the set **QS** of all quadratic differential systems (2.7) acts (left action) the group $\mathrm{Aff}(2,\mathbb{R})$ of affine transformations on the plane:

$$\begin{aligned} \mathrm{Aff}(2,\mathbb{R}) \times \mathbf{QS} &\to \mathbf{QS} \\ (g,S) &\mapsto \tilde{S} = gS. \end{aligned}$$

This action is defined as follows: Consider an affine transformation $g \in \mathrm{Aff}(2,\mathbb{R})$, $g:\mathbb{R}^2 \to \mathbb{R}^2$. For this transformation we have:

$$g: \begin{pmatrix}\tilde{x}\\ \tilde{y}\end{pmatrix} = M\begin{pmatrix}x\\ y\end{pmatrix} + B; \qquad g^{-1}: \begin{pmatrix}x\\ y\end{pmatrix} = M^{-1}\begin{pmatrix}\tilde{x}\\ \tilde{y}\end{pmatrix} - M^{-1}B, \tag{2.8}$$

where $M = ||M_{ij}||$ is a 2×2 non–singular matrix and B is a 2×1 matrix over $\mathbb{R}$. For every $S \in \mathbf{QS}$ we can form its induced transformed system $\tilde{S} = gS$:

$$\frac{d\tilde{x}}{dt} = \tilde{p}(\tilde{x},\tilde{y}), \qquad \frac{d\tilde{y}}{dt} = \tilde{q}(\tilde{x},\tilde{y}),$$

where

$$\begin{pmatrix}\tilde{p}(\tilde{x},\tilde{y})\\ \tilde{q}(\tilde{x},\tilde{y})\end{pmatrix} = M\begin{pmatrix}(p\circ g^{-1})(\tilde{x},\tilde{y})\\ (q\circ g^{-1})(\tilde{x},\tilde{y})\end{pmatrix}.$$

The map (2.8) verifies the axioms for a left group action. For every subgroup $G \subseteq \mathrm{Aff}(2,\mathbb{R})$ we have an induced action of G on $\mathbf{QS}$.

Definition 2.2.6. Consider a subset $\mathscr{S}$ of $\mathbf{QS}$ and a subgroup G of $\mathrm{Aff}(2,\mathbb{R})$. We say that the subset $\mathscr{S}$ is invariant with respect to the group G if for every $g \in G$ and for every system S in $\mathscr{S}$ the transformed system gS is also in $\mathscr{S}$.

For every $g \in \mathrm{Aff}(2,\mathbb{R})$ let $r_g: \mathbb{R}^{12} \to \mathbb{R}^{12}$ be the map which corresponds to g via this action. We know (see Sibirsky (1988)) that r_g is linear and that the map $r: \mathrm{Aff}(2,\mathbb{R}) \to GL(12,\mathbb{R})$ thus obtained is a group homomorphism. For every subgroup G of $\mathrm{Aff}(2,\mathbb{R})$, r induces a representation of G onto a subgroup $\mathscr{G}$ of $GL(12,\mathbb{R})$.

This group action yields an equivalence relation on $\mathbf{QS}$, namely two systems S_1, S_2 are *affinely equivalent* when there is an affine transformation sending S_1 to S_2. The orbit $Orb(S)$ of a system S under the action of the group is the *affine equivalence class* of S.

2.2.5 Invariants and comitants associated to the group actions

A very useful concept is the notion of polynomial invariant. This kind of invariant sends a polynomial differential system with coefficients a to a polynomial U belonging to the ring $\mathbb{R}[a,x,y]$.

Definition 2.2.7. A polynomial $U(a,x,y) \in \mathbb{R}[a,x,y]$ is called a *comitant* of system (2.7) with respect to a subgroup G of $\mathrm{Aff}(2,\mathbb{R})$, if there exists $\chi \in \mathbb{Z}$ such that for every $(g,a) \in G\times\mathbb{R}^{12}$ and for every $(x,y) \in \mathbb{R}^2$ the following relation holds

$$U(r_g(a),\ g(x,y)) \equiv (\det g)^{-\chi} U(a,x,y),$$

where $\det g = \det M$. If the polynomial U does not explicitly depend on x and y then it is called an *invariant*. The number $\chi \in \mathbb{Z}$ is called the *weight* of the comitant $U(a,x,y)$.

If $G = GL(2,\mathbb{R})$ (or $G = Aff(2,\mathbb{R})$) then the comitant $U(a,x,y)$ of system (2.7) is called *GL–comitant* (respectively *affine comitant*).

These comitants will also be called polynomial invariants. In fact these are the polynomial invariants which we work with.

Definition 2.2.8. A subset $X \subset \mathbb{R}^{12}$ is called *G–invariant* if for every $g \in G$ we have $r_g(X) \subseteq X$.

Let $T(2,\mathbb{R})$ be the subgroup of $\mathrm{Aff}(2,\mathbb{R})$ formed by translations. Consider the linear representation of $T(2,\mathbb{R})$ into its corresponding subgroup $\mathscr{T} \subset GL(12,\mathbb{R})$, i.e. for every $\tau \in T(2,\mathbb{R})$, $\tau:\ x=\tilde{x}+\alpha,\ y=\tilde{y}+\beta$ we consider as before $r_\tau:\ \mathbb{R}^{12} \to \mathbb{R}^{12}$.

Definition 2.2.9. A GL–comitant $U(a,x,y)$ of system (2.7) is called a *T–comitant* if for every $(\tau, a) \in T(2,\mathbb{R}) \times \mathbb{R}^{12}$ and for every $(\tilde{x},\tilde{y}) \in \mathbb{R}^2$ the relation $U(r_\tau \cdot a,\ \tilde{x},\tilde{y}) = U(a,\ \tilde{x},\tilde{y})$ holds.

Let

$$U_i(a,x,y) = \sum_{j=0}^{d_i} U_{ij}(a) x^{d_i-j} y^j, \quad i = 1,\dots,s,$$

be a set of GL–comitants of system (2.7) where d_i denotes the degree of the binary form $U_i(a,x,y)$ in x and y with coefficients in $\mathbb{R}[a] = \mathbb{R}[a_{00},\dots,b_{02}]$. We denote by

$$\mathscr{U} = \left\{ U_{ij}(a) \in \mathbb{R}[a];\ i = 1,\dots,s,\ j = 0,1,\dots,d_i \right\},$$

the set of the coefficients in $\mathbb{R}[a]$ of the GL–comitants $U_i(a,x,y)$, $i = 1,\dots,s$, and by $V(\mathscr{U})$ its associated algebraic set

$$V(\mathscr{U}) = \left\{ a \in \mathbb{R}^{12};\ U_{ij}(a) = 0,\ \forall\ U_{ij}(a) \in \mathscr{U} \right\}.$$

Definition 2.2.10. Let $U_1, U_2, \dots, U_s$ be GL–comitants of a system (2.7). A GL–comitant $U(a,x,y)$ of system (2.7) is called a *conditional T–comitant* (or *CT–comitant*) modulo $\langle U_1, U_2, ..., U_s \rangle$ if the following two conditions are satisfied:

(i) the algebraic subset $V(\mathscr{U}) \subset \mathbb{R}^{12}$ is affinely invariant (see Def. 2.2.8);

(ii) for every $(\tau,\ a) \in T(2,\mathbb{R}) \times V(\mathscr{U})$ we have $U(r_\tau \cdot a,\ \tilde{x},\tilde{y}) = U(a,\ \tilde{x},\tilde{y})$ in $\mathbb{R}[\tilde{x},\tilde{y}]$.

In other words, a CT–comitant $U(a,x,y)$ modulo $\langle U_1, U_2, ..., U_s \rangle$ is a T–comitant on the algebraic subset $V(\mathscr{U}) \subset \mathbb{R}^{12}$.

We consider the polynomials in $\mathbb{R}[a,x,y]$

$$\begin{aligned} C_i(a,x,y) &= y p_i(a,x,y) - x q_i(a,x,y)\ ,\ i = 0,1,2, \\ D_i(a,x,y) &= \frac{\partial}{\partial x} p_i(a,x,y) + \frac{\partial}{\partial y} q_i(a,x,y)\ ,\ i = 1,2. \end{aligned}$$

As it was shown in Vulpe (1986) the polynomials of degree one with respect to the coefficients of the initial system,

$$\Big\{ C_0(a,x,y),\quad C_1(a,x,y),\quad C_2(a,x,y),\quad D_1(a,x,y),\quad D_2(a,x,y) \Big\}, \tag{2.9}$$

are GL–comitants with respect to the coefficients of system (2.7).

Definition 2.2.11. Let $f,\ g \in \mathbb{R}[a,x,y]$ and

$$(f,g)^{(k)} = \sum_{h=0}^{k} (-1)^h \binom{k}{h} \frac{\partial^k f}{\partial x^{k-h}\partial y^h}\ \frac{\partial^k g}{\partial x^h \partial y^{k-h}}\ .$$

Then $(f,g)^{(k)} \in \mathbb{R}[a,x,y]$ is the *transvectant of index* k of (f,g) (see Olver (1999)).

Theorem 2.2.12. (See Vulpe (1986)) Any GL–comitant can be constructed from the elements of the set (2.9) by using the operations: $+$, $-$, $\times$, and by applying the differential operation $(f,g)^{(k)}$.

First, the mentioned authors construct the following GL–comitants of the second degree with respect to coefficients of initial system:

$$\begin{aligned}
&T_1 = (C_0,C_1)^{(1)}, \quad T_2 = (C_0,C_2)^{(1)}, \quad T_3 = (C_0,D_2)^{(1)},\\
&T_4 = (C_1,C_1)^{(2)}, \quad T_5 = (C_1,C_2)^{(1)}, \quad T_6 = (C_1,C_2)^{(2)},\\
&T_7 = (C_1,D_2)^{(1)}, \quad T_8 = (C_2,C_2)^{(2)}, \quad T_9 = (C_2,D_2)^{(1)}.
\end{aligned}$$

In order to be able to calculate the values of the needed invariant polynomials directly for every canonical system they define a family of T–comitants expressed through C_i $(i=0,1,2)$ and D_j $(j=1,2)$:

$$\begin{aligned}
\widetilde{A} &= (C_1, T_8 - 2T_9 + D_2^2)^{(2)}/144,\\
\widetilde{B} &= \Big\{16D_1(D_2,T_8)^{(1)}(3C_1D_1 - 2C_0D_2 + 4T_2) + 32C_0(D_2,T_9)^{(1)}(3D_1D_2 - 5T_6 + 9T_7)\\
&\quad + 2(D_2,T_9)^{(1)}(27C_1T_4 - 18C_1D_1^2 - 32D_1T_2 + 32(C_0,T_5)^{(1)})\\
&\quad + 6(D_2,T_7)^{(1)}\Big[8C_0(T_8 - 12T_9) - 12C_1(D_1D_2 + T_7) + D_1(26C_2D_1 + 32T_5)\\
&\quad + C_2(9T_4 + 96T_3)\Big] + 6(D_2,T_6)^{(1)}\Big[32C_0T_9 - C_1(12T_7 + 52D_1D_2) - 32C_2D_1^2\Big]\\
&\quad + 48D_2(D_2,T_1)^{(1)}(2D_2^2 - T_8) - 32D_1T_8(D_2,T_2)^{(1)} + 9D_2^2T_4(T_6 - 2T_7)\\
&\quad - 16D_1(C_2,T_8)^{(1)}(D_1^2 + 4T_3) + 12D_1(C_1,T_8)^{(2)}(C_1D_2 - 2C_2D_1)\\
&\quad + 6D_1D_2T_4(T_8 - 7D_2^2 - 42T_9) + 12D_1(C_1,T_8)^{(1)}(T_7 + 2D_1D_2) + 96D_2^2[D_1(C_1,T_6)^{(1)}\\
&\quad + D_2(C_0,T_6)^{(1)}] - 16D_1D_2T_3(2D_2^2 + 3T_8) - 4D_1^3D_2(D_2^2 + 3T_8 + 6T_9)\\
&\quad + 6D_1^2D_2^2(7T_6 + 2T_7)252D_1D_2T_4T_9\Big\}/(2^8 3^3),\\
\widetilde{D} &= \big[2C_0(T_8 - 8T_9 - 2D_2^2) + C_1(6T_7 - T_6 - (C_1,T_5)^{(1)}\\
&\quad + 6D_1C_1D_2 - T_5) - 9D_1^2C_2\big]/36,\\
\widetilde{E} &= [D_1(2T_9 - T_8) - 3(C_1,T_9)^{(1)} - D_2(3T_7 + D_1D_2)]/72,
\end{aligned}$$

$$\begin{aligned}\widetilde{F} &= [6D_1^2(D_2^2-4T_9)+4D_1D_2(T_6+6T_7)+48C_0(D_2,T_9)^{(1)}\\ &\quad -9D_2^2T_4+288D_1\widehat{E}-24(C_2,\widehat{D})^{(2)}+120(D_2,\widehat{D})^{(1)}\\ &\quad -36C_1(D_2,T_7)^{(1)}+8D_1(D_2,T_5)^{(1)}]/144,\\ \widetilde{K} &= (T_8+4T_9+4D_2^2)/72,\\ \widetilde{H} &= (8T_9-T_8+2D_2^2)/72.\end{aligned}$$

A minimal polynomial basis of T–comitants of system (2.7) of degrees up to 12 (as polynomials in the coefficients of the systems) was constructed in terms of these T–comitants in Bularas *et al.* (1996). The following 42 polynomials are the elements of this polynomial basis:

$$\begin{aligned}
A_1 &= \tilde{A}, & A_{22} &= \big[C_2,\widetilde{D})^{(1)},D_2\big)^{(1)},D_2\big)^{(1)}D_2\big)^{(1)}/1152,\\
A_2 &= (C_2,D)^{(3)}/12, & A_{23} &= \big[\widetilde{F},\widetilde{H})^{(1)},\widetilde{K}\big)^{(2)}/8,\\
A_3 &= \big[C_2,D_2)^{(1)},D_2\big)^{(1)},D_2\big)^{(1)}/48, & A_{24} &= \big[C_2,\widetilde{D})^{(2)},\widetilde{K}\big)^{(1)},\widetilde{H}\big)^{(2)}/32,\\
A_4 &= (\widetilde{H},\widetilde{H})^{(2)}, & A_{25} &= \big[\widetilde{D},\widetilde{D})^{(2)},\widetilde{E}\big)^{(2)}/16,\\
A_5 &= (\widetilde{H},\widetilde{K})^{(2)}/2, & A_{26} &= (\widetilde{B},\widetilde{D})^{(3)}/36,\\
A_6 &= (\widetilde{E},\widetilde{H})^{(2)}/2, & A_{27} &= \big[\widetilde{B},D_2)^{(1)},\widetilde{H}\big)^{(2)}/24,\\
A_7 &= \big[C_2,\widetilde{E})^{(2)},D_2\big)^{(1)}/8, & A_{28} &= \big[C_2,\widetilde{K})^{(2)},\widetilde{D}\big)^{(1)},\widetilde{E}\big)^{(2)}/16,\\
A_8 &= \big[\widetilde{D},\widetilde{H})^{(2)},D_2\big)^{(1)}/8, & A_{29} &= \big[\widetilde{D},\widetilde{F})^{(1)},\widetilde{D}\big)^{(3)}/96,\\
A_9 &= \big[\widetilde{D},D_2)^{(1)},D_2\big)^{(1)},D_2\big)^{(1)}/48, & A_{30} &= \big[C_2,\widetilde{D})^{(2)},\widetilde{D}\big)^{(1)},\widetilde{D}\big)^{(3)}/288,\\
A_{10} &= \big[\widetilde{D},\widetilde{K})^{(2)},D_2\big)^{(1)}/8, & A_{31} &= \big[\widetilde{D},\widetilde{D})^{(2)},\widetilde{K}\big)^{(1)},\widetilde{H}\big)^{(2)}/64,\\
A_{11} &= (\widetilde{F},\widetilde{K})^{(2)}/4, & A_{32} &= \big[\widetilde{D},\widetilde{D})^{(2)},D_2\big)^{(1)},\widetilde{H}\big)^{(1)},D_2\big)^{(1)}/64,\\
A_{12} &= (\widetilde{F},\widetilde{H})^{(2)}/4, & A_{33} &= \big[\widetilde{D},D_2)^{(1)},\widetilde{F}\big)^{(1)},D_2\big)^{(1)},D_2\big)^{(1)}/128,\\
A_{13} &= \big[C_2,\widetilde{H})^{(1)},\widetilde{H}\big)^{(2)},D_2\big)^{(1)}/24, & A_{34} &= \big[\widetilde{D},\widetilde{D})^{(2)},D_2\big)^{(1)},\widetilde{K}\big)^{(1)},D_2\big)^{(1)}/64,\\
A_{14} &= (\widetilde{B},C_2)^{(3)}/36, & A_{35} &= \big[\widetilde{D},\widetilde{D})^{(2)},\widetilde{E}\big)^{(1)},D_2\big)^{(1)},D_2\big)^{(1)}/128,\\
A_{15} &= (\widetilde{E},\widetilde{F})^{(2)}/4, & A_{36} &= \big[\widetilde{D},\widetilde{E})^{(2)},\widetilde{D}\big)^{(1)},\widetilde{H}\big)^{(2)}/16,\\
A_{16} &= \big[\widetilde{E},D_2)^{(1)},C_2\big)^{(1)},\widetilde{K}\big)^{(2)}/16, & A_{37} &= \big[\widetilde{D},\widetilde{D})^{(2)},\widetilde{D}\big)^{(1)},\widetilde{D}\big)^{(3)}/576,\\
A_{17} &= \big[\widetilde{D},\widetilde{D})^{(2)},D_2\big)^{(1)},D_2\big)^{(1)}/64, & A_{38} &= \big[C_2,\widetilde{D})^{(2)},\widetilde{D}\big)^{(2)},\widetilde{D}\big)^{(1)},\widetilde{H}\big)^{(2)}/64,\\
A_{18} &= \big[\widetilde{D},\widetilde{F})^{(2)},D_2\big)^{(1)}/16, & A_{39} &= \big[\widetilde{D},\widetilde{D})^{(2)},\widetilde{F}\big)^{(1)},\widetilde{H}\big)^{(2)}/64,\\
A_{19} &= \big[\widetilde{D},\widetilde{D})^{(2)},\widetilde{H}\big)^{(2)}/16, & A_{40} &= \big[\widetilde{D},\widetilde{D})^{(2)},\widetilde{F}\big)^{(1)},\widetilde{K}\big)^{(2)}/64,\\
A_{20} &= \big[C_2,\widetilde{D})^{(2)},\widetilde{F}\big)^{(2)}/16, & A_{41} &= \big[C_2,\widetilde{D})^{(2)},\widetilde{D}\big)^{(2)},\widetilde{F}\big)^{(1)},D_2\big)^{(1)}/64,\\
A_{21} &= \big[\widetilde{D},\widetilde{D})^{(2)},\widetilde{K}\big)^{(2)}/16, & A_{42} &= \big[\widetilde{D},\widetilde{F})^{(2)},\widetilde{F}\big)^{(1)},D_2\big)^{(1)}/16.
\end{aligned}$$

In the previous list, the bracket "[" is used in order to avoid placing the otherwise necessary up to five parenthesizes "(".

In order to construct other necessary invariant polynomials one can consider the differential operator $\mathscr{L} = x\cdot\mathbf{L}_2 - y\cdot\mathbf{L}_1$ acting on $\mathbb{R}[a,x,y]$ constructed in Baltag and Vulpe

(1997), where

$$\mathbf{L}_1 = 2a_{00}\frac{\partial}{\partial a_{10}} + a_{10}\frac{\partial}{\partial a_{20}} + \frac{1}{2}a_{01}\frac{\partial}{\partial a_{11}} + 2b_{00}\frac{\partial}{\partial b_{10}} + b_{10}\frac{\partial}{\partial b_{20}} + \frac{1}{2}b_{01}\frac{\partial}{\partial b_{11}},$$
$$\mathbf{L}_2 = 2a_{00}\frac{\partial}{\partial a_{01}} + a_{01}\frac{\partial}{\partial a_{02}} + \frac{1}{2}a_{10}\frac{\partial}{\partial a_{11}} + 2b_{00}\frac{\partial}{\partial b_{01}} + b_{01}\frac{\partial}{\partial b_{02}} + \frac{1}{2}b_{10}\frac{\partial}{\partial b_{11}},$$

as well as the classical differential operator $(f,\varphi)^{(2)}$ acting on $\mathbb{R}[a,x,y]$ (the *transvectant* of the second index):

$$(f,\varphi)^{(2)} = \frac{\partial^2 f}{\partial x^2}\frac{\partial^2 \varphi}{\partial y^2} - 2\frac{\partial^2 f}{\partial x \partial y}\frac{\partial^2 \varphi}{\partial x \partial y} + \frac{\partial^2 f}{\partial y^2}\frac{\partial^2 \varphi}{\partial x^2}.$$

Here $f(x,y)$ and $\varphi(x,y)$ are polynomials in x and y.

In Baltag and Vulpe (1997) it is shown that if a polynomial $U \in \mathbb{R}[a,x,y]$ is a comitant of system (2.7) with respect to the group $GL(2,\mathbb{R})$ then $\mathscr{L}(U)$ is also a GL–comitant. The same is true for the operator transvectant of two comitants f and φ.

Using this operator and the affine invariant $\mu_0 = \mathrm{Res}_x\big(p_2(a,x,y), q_2(a,x,y)\big)/y^4$ define the following polynomials

$$\mu_i(a,x,y) = \frac{1}{i!}\mathscr{L}^{(i)}(\mu_0),\ i = 1,\ldots,4,$$

where $\mathscr{L}^{(i)}(\mu_0) = \mathscr{L}(\mathscr{L}^{(i-1)}(\mu_0))$ and $\mathscr{L}^{(0)}(\mu_0) = \mu_0$.

These polynomials are in fact comitants of systems (2.7), invariant with respect to the group $GL(2,\mathbb{R})$ (see Baltag and Vulpe (1997)). Their geometrical meaning is revealed in the next lemma.

Lemma 2.2.13 (Baltag and Vulpe (1997), Baltag (2003))**.** Assume that a quadratic system S with coefficients a belongs to the family (2.7). Then:

(i) Let λ be an integer such that $\lambda \leq 4$. The total multiplicity of all finite singularities of this system equals $4-\lambda$ if and only if for every $i \in \{0,1,\ldots,\lambda-1\}$ we have $\mu_i(a,x,y) = 0$ in the ring $\mathbb{R}[x,y]$ and $\mu_\lambda(a,x,y) \neq 0$. In this case, the factorization $\mu_\lambda(a,x,y) = \prod_{i=1}^{\lambda}(u_i x - v_i y) \neq 0$ over $\mathbb{C}$ indicates the coordinates $[v_i : u_i : 0]$ of points at infinity which coalesced with finite singularities of system S. Moreover, the number of distinct factors in this factorization is less than or equal to three (the maximum number of infinite singularities of a quadratic system in the projective plane) and the multiplicity of each one of the factors $u_i x - v_i y$ gives us the number of the finite singularities of system S which have coalesced with the infinite singularity $[v_i : u_i : 0]$.

(ii) System S is degenerate (i.e. $\gcd(P,Q) \neq \mathrm{const}$) if and only if $\mu_i(a,x,y) = 0$ in $\mathbb{R}[x,y]$ for every $i = 0,1,2,3,4$.

In Schlomiuk and Vulpe (2004) the authors consider the following GL–comitants for a system (2.7):

$$\begin{aligned}
&M(a,x,y) = 2\,\text{Hess}\big(C_2(x,y)\big), && \eta(a) = \text{Discrim}\big(C_2(x,y)\big),\\
&K(a,x,y) = \text{Jacob}\big(p_2(x,y),q_2(x,y)\big), && \mu(a) = \text{Discrim}\big(K(a,x,y)\big),\\
&H(a,x,y) = -\text{Discrim}\big(C_2(x,y)\big), && N(a,x,y) = K(a,x,y)+H(a,x,y),\\
&\theta(a) = \text{Discrim}\big(N(a,x,y)\big),
\end{aligned}$$

Lemma 2.2.14 (Schlomiuk and Vulpe (2010))**.** The number of infinite singularities (real and complex) of a quadratic system in **QS** is determined by the following conditions:

(i) 3 real if $\eta > 0$;

(ii) 1 real and 2 imaginary if $\eta < 0$;

(iii) 2 real if $\eta = 0$ and $M \neq 0$;

(iv) 1 real if $\eta = M = 0$ and $C_2 \neq 0$;

(v) ∞ if $\eta = M = C_2 = 0$.

Moreover, for each one of these cases the quadratic system (2.7) can be brought via a linear transformation to one of the following 5 normal form, respectively:

$$\begin{cases} \dot{x} = a + cx + dy + gx^2 + (h-1)xy, \\ \dot{y} = b + ex + fy + (g-1)xy + hy^2; \end{cases} \tag{2.10}$$

$$\begin{cases} \dot{x} = a + cx + dy + gx^2 + (h+1)xy, \\ \dot{y} = b + ex + fy - x^2 + gxy + hy^2; \end{cases} \tag{2.11}$$

$$\begin{cases} \dot{x} = a + cx + dy + gx^2 + hxy, \\ \dot{y} = b + ex + fy + (g-1)xy + hy^2; \end{cases} \tag{2.12}$$

$$\begin{cases} \dot{x} = a + cx + dy + gx^2 + hxy, \\ \dot{y} = b + ex + fy - x^2 + gxy + hy^2; \end{cases} \tag{2.13}$$

$$\begin{cases} \dot{x} = a + cx + dy + x^2, \\ \dot{y} = b + ex + fy + xy. \end{cases} \tag{2.14}$$

Lemma 2.2.15. Let $S \in$ **QS** and let $a \in \mathbb{R}^{12}$ be its 12–tuple of coefficients. The common points of $p = 0$ and $q = 0$ on the line $Z = 0$ are given by the common linear factors over

$\mathbb{C}$ of p_2 and q_2. This yields the geometrical meaning of the comitants μ_0, K and H:

$$\gcd(p_2(x,y),q_2(x,y)) = \begin{cases} \text{constant} & \text{iff} \quad \mu_0(a) \neq 0; \\ bx+cy & \text{iff} \quad \mu_0 = 0,\ K(a,x,y) \neq 0; \\ (bx+cy)(dx+ey) & \text{iff} \quad \begin{cases} \mu_0(a) = 0, K(a,x,y) = 0 \\ \text{and} \quad H(a,x,y) \neq 0; \end{cases} \\ (bx+cy)^2 & \text{iff} \quad \begin{cases} \mu_0 = 0, K(a,x,y) = 0, \\ \text{and} \quad H(a,x,y) = 0; \end{cases} \end{cases}$$

where $bx+cy, dx+ey \in \mathbb{C}[x,y]$ are some linear forms and $be-cd \neq 0$.

The invariant polynomials $N(a,x,y)$ and $\theta(a)$ are responsible for detecting parallel invariant lines as we can see in the following lemma.

Lemma 2.2.16. A necessary condition for the existence of one couple (respectively two couples) of parallel invariant straight lines of a system (2.7) corresponding to $a \in \mathbb{R}^{12}$ is the condition $\theta(a) = 0$ (respectively $N(a,x,y) = 0$).

In Schlomiuk and Vulpe (2004) the authors construct the following T–comitants:

$$\begin{aligned} B_3(a,x,y) &= (C_2,D)^{(1)} = Jacob\,(C_2,D)\,, \\ B_2(a,x,y) &= (B_3,B_3)^{(2)} - 6B_3(C_2,D)^{(3)}, \\ B_1(a) &= \mathrm{Res}_x\,(C_2,D)\,/y^9 = -2^{-9}3^{-8}\,(B_2,B_3)^{(4)}\,. \end{aligned}$$

Lemma 2.2.17. (See Schlomiuk and Vulpe (2004)) For the existence of an invariant straight line in one (respectively 2, 3 distinct) directions in the affine plane it is necessary that $B_1 = 0$ (respectively $B_2 = 0$, $B_3 = 0$).

At the moment we only have necessary and not necessary and sufficient conditions for the existence of an invariant straight line or for invariant lines in two or three directions.

We apply the translation $x = x' + x_0$, $y = y' + y_0$ to the polynomials $p(a,x,y)$ and $q(a,x,y)$. Then we obtain $\hat{p}(\hat{a}(a,x_0,y_0),x',y') = p(a,x'+x_0,y'+y_0)$, $\hat{q}(\hat{a}(a,x_0,y_0),x',y') = q(a,x'+x_0,y'+y_0)$. Consider the following polynomials

$$\Gamma_i(a,x_0,y_0) \equiv \mathrm{Res}_{x'}\left(C_i\big(\hat{a}(a,x_0,y_0),x',y'\big), C_0\big(\hat{a}(a,x_0,y_0),x',y'\big)\right)/(y')^{i+1},$$
$$\Gamma_i(a,x_0,y_0) \in \mathbb{R}[a,x_0,y_0], \quad i = 1,2.$$

We denote

$$\tilde{\mathscr{E}}_i(a,x,y) = \Gamma_i(a,x_0,y_0)\big|_{\{x_0=x,\,y_0=y\}} \in \mathbb{R}[a,x,y], \quad i = 1,2.$$

Remark 2.2.18. We note that the polynomials $\tilde{\mathscr{E}}_1(a,x,y)$ and $\tilde{\mathscr{E}}_2(a,x,y)$ are affine comitants of systems (2.7) and they are homogeneous polynomials in the coefficients of p,q and non–homogeneous in x,y and $\deg_a \tilde{\mathscr{E}}_1 = 3$, $\deg_{(x,y)} \tilde{\mathscr{E}}_1 = 5$, $\deg_a \tilde{\mathscr{E}}_2 = 4$, $\deg_{(x,y)} \tilde{\mathscr{E}}_2 = 6$.

Let $\mathscr{E}_i(a,X,Y,Z)$, $i=1,2$, be the homogenization of $\tilde{\mathscr{E}}_i(a,x,y)$, i.e.

$$\mathscr{E}_1(a,X,Y,Z)=Z^5\tilde{\mathscr{E}}_1(a,X/Z,Y/Z),\quad \mathscr{E}_2(a,X,Y,Z)=Z^6\tilde{\mathscr{E}}_1(a,X/Z,Y/Z)$$

The geometrical meaning of these affine comitants is given by the following lemma.

Lemma 2.2.19 (see Schlomiuk and Vulpe (2004))**.** (1) The straight line $\mathscr{L}(x,y)\equiv ux+vy+w=0$, $u,v,w\in\mathbb{C}$, $(u,v)\neq(0,0)$ is an invariant line for a quadratic system (2.7) if and only if the polynomial $\mathscr{L}(x,y)$ is a common factor of the polynomials $\tilde{\mathscr{E}}_1(a,x,y)$ and $\tilde{\mathscr{E}}_2(a,x,y)$ over $\mathbb{C}$, i.e.

$$\tilde{\mathscr{E}}_i(a,x,y)=(ux+vy+w)\widetilde{W}_i(x,y),\quad i=1,2,$$

where $\widetilde{W}_i(x,y)\in\mathbb{C}[x,y]$.

(2) If $\mathscr{L}(x,y)=0$ is an invariant straight line of multiplicity λ for a quadratic system (2.7), then $[\mathscr{L}(x,y)]^\lambda$ divides $\gcd(\tilde{\mathscr{E}}_1,\tilde{\mathscr{E}}_2)$ in $\mathbb{C}[x,y]$, i.e. there exist $W_i(a,x,y)\in\mathbb{C}[x,y]$, $i=1,2$, such that

$$\tilde{\mathscr{E}}_i(a,x,y)=(ux+vy+w)^\lambda W_i((a),x,y),\quad i=1,2.$$

(3) If the line $l_\infty: Z=0$ is of multiplicity $\lambda>1$, then $Z^{\lambda-1}$ divides $\gcd(\mathscr{E}_1,\mathscr{E}_2)$.

The following zero–cycle on the complex plane was introduced in Llibre and Schlomiuk (2004) based on a previous work in Schlomiuk and Pal (2001).

Definition 2.2.20. For a polynomial system (S) we define $\mathscr{D}_{\mathbb{C}^2}(S)=\sum_{s\in\mathbb{C}^2}n_s s$ where n_s is the intersection multiplicity at s of the curves $p(x,y)=0$ and $q(x,y)=0$, with p and q being the polynomials defining equations (2.7).

According to Vulpe (2011) (see also Artés *et al.* (2021)) we have the following proposition.

Proposition 2.2.21. The form of the zero–cycle $\mathscr{D}_{\mathbb{C}^2}(S)$ for non–degenerate quadratic systems (2.7) is determined by the corresponding conditions indicated in Table 4, where we write $p+q+r^c+s^c$ if two of the finite points, i.e. r^c,s^c, are complex but not real, and

$$\begin{aligned}
\mathbf{D}&=\left[3\left((\mu_3,\mu_3)^{(2)},\mu_2\right)^{(2)}-\left(6\mu_0\mu_4-3\mu_1\mu_3+\mu_2^2,\ \mu_4\right)^{(4)}\right]/48,\\
\mathbf{P}&=12\mu_0\mu_4-3\mu_1\mu_3+\mu_2^2,\\
\mathbf{R}&=3\mu_1^2-8\mu_0\mu_2,\\
\mathbf{S}&=\mathbf{R}^2-16\mu_0^2\mathbf{P},\\
\mathbf{T}&=18\mu_0^2(3\mu_3^2-8\mu_2\mu_4)+2\mu_0(2\mu_2^3-9\mu_1\mu_2\mu_3+27\mu_1^2\mu_4)-\mathbf{PR},\\
\mathbf{U}&=\mu_3^2-4\mu_2\mu_4,\\
\mathbf{V}&=\mu_4.
\end{aligned}$$

Table 4 – Number and multiplicity of the finite singularities of **QS**

No.	Zero–cycle $\mathscr{Z}_{\mathbb{C}^2}(S)$	Invariant criteria	No.	Zero–cycle $\mathscr{Z}_{\mathbb{C}^2}(S)$	Invariant criteria
1	$p+q+r+s$	$\mu_0 \neq 0, \mathbf{D} < 0,$ $\mathbf{R} > 0, \mathbf{S} > 0$	10	$p+q+r$	$\mu_0 = 0, \mathbf{D} < 0, \mathbf{R} \neq 0$
2	$p+q+r^c+s^c$	$\mu_0 \neq 0, \mathbf{D} > 0$	11	$p+q^c+r^c$	$\mu_0 = 0, \mathbf{D} > 0, \mathbf{R} \neq 0$
3	$p^c+q^c+r^c+s^c$	$\mu_0 \neq 0, \mathbf{D} < 0, \mathbf{R} \leq 0$ / $\mu_0 \neq 0, \mathbf{D} < 0, \mathbf{S} \leq 0$	12	$2p+q$	$\mu_0 = \mathbf{D} = 0, \mathbf{PR} \neq 0$
4	$2p+q+r$	$\mu_0 \neq 0, \mathbf{D} = 0, \mathbf{T} < 0$	13	$3p$	$\mu_0 = \mathbf{D} = \mathbf{P} = 0, \mathbf{R} \neq 0$
5	$2p+q^c+r^c$	$\mu_0 \neq 0, \mathbf{D} = 0, \mathbf{T} > 0$	14	$p+q$	$\mu_0 = \mathbf{R} = 0, \mathbf{P} \neq 0,$ $\mathbf{U} > 0$
6	$2p+2q$	$\mu_0 \neq 0, \mathbf{D} = \mathbf{T} = 0,$ $\mathbf{PR} > 0$	15	p^c+q^c	$\mu_0 = \mathbf{R} = 0, \mathbf{P} \neq 0,$ $\mathbf{U} < 0$
7	$2p^c+2q^c$	$\mu_0 \neq 0, \mathbf{D} = \mathbf{T} = 0,$ $\mathbf{PR} < 0$	16	$2p$	$\mu_0 = \mathbf{R} = 0, \mathbf{P} \neq 0,$ $\mathbf{U} = 0$
8	$3p+q$	$\mu_0 \neq 0, \mathbf{D} = \mathbf{T} = 0,$ $\mathbf{P} = 0, \mathbf{R} \neq 0$	17	p	$\mu_0 = \mathbf{R} = \mathbf{P} = 0,$ $\mathbf{U} \neq 0$
9	$4p$	$\mu_0 \neq 0, \mathbf{D} = \mathbf{T} = 0,$ $\mathbf{P} = \mathbf{R} = 0$	18	0	$\mu_0 = \mathbf{R} = \mathbf{P} = 0,$ $\mathbf{U} = 0, \mathbf{V} \neq 0$

Along this thesis we use most of the invariants mentioned in this section (and also other invariants) in order to contribute to the classification of phase portraits of quadratic systems. More precisely, in Chap. 3 and 4 we use the geometrical meaning of some of the invariants mentioned along this section in order to construct bifurcation diagrams and in Chap. 6 we use these invariants for the study of quadratic systems with invariant ellipses.

CHAPTER

3

CLASSIFICATION OF QUADRATIC SYSTEMS WITH A FINITE SADDLE–NODE AND AN INFINITE SADDLE–NODE (1,1)SN–(A)

In this chapter we present, for the first time, a study of a five–parametric quadratic system using the Invariant Theory as tools.

3.1 Introduction and statement of the main results

One of the main goals of this thesis is to present the study of the class of all quadratic systems possessing a finite saddle–node $\overline{sn}_{(2)}$ located at the origin of the plane and an infinite saddle–node of type $\overline{\binom{1}{1}}\,SN$. We denote this class by $\mathbf{QsnSN_{11}}$. We recall that a finite saddle–node is a semi–elemental singular point whose neighborhood is formed by the union of two hyperbolic sectors and one parabolic sector. By a semi–elemental singular point we mean a point with zero determinant of its Jacobian matrix with only one eigenvalue equal to zero. These points are known in classical literature as semi–elementary, but we use the term *semi–elemental*, as discussed in page 44. Geometrically, an infinite saddle–node of type $\overline{\binom{1}{1}}SN$ is obtained by the coalescence of a finite antisaddle (respectively finite saddle) with an infinite saddle (respectively infinite node).

Whenever one wants to study a specific family of differential systems sharing a common property, it is necessary to select one (or several) normal form which contains all the phase portraits sharing the desired property. However, except in some trivial cases, it is impossible that the normal form does not contain other phase portraits, normally more degenerate than the cases under study. These other phase portraits are very important to understand the bifurcations that take place inside the chosen normal form. This is why we

always study not just the family of systems that have the desired property, but the closure of the normal form which contains that family. That is, we study all the parameter space of the selected normal form, whether it leads to the desired property or not. However, it is possible that a different normal form could have been chosen and in that case, the generic elements of the family under study should be the same, but the elements in the border might not be. That is, some phase portraits in the border of one normal form could be common or not, with elements in the border of the second normal form.

Inside the class $\overline{\mathbf{QsnSN_{11}}}$ where generically the origin is a saddle–node $\overline{sn}_{(2)}$ and we have an infinite singularity of type $\overline{\binom{1}{1}}\,SN$, we may have or not another simple finite elemental singularity. Then, we split this class into two different families: $\mathbf{QsnSN_{11}(A)}$ of phase portraits possessing the finite saddle–node as the only finite singularity and $\mathbf{QsnSN_{11}(B)}$ of phase portraits possessing the finite saddle–node and also a simple finite elemental singularity. In this chapter we provide the analysis of the closure of the family $\mathbf{QsnSN_{11}(A)}$. The present study in this chapter is part of this attempt of classifying all the codimension–two quadratic systems. All the phase portraits obtained in the study of the class $\overline{\mathbf{QsnSN_{11}(A)}}$ belong to the closure of the set (AC) (see page 49).

For this analysis we follow the pattern set out in Artés, Rezende and Oliveira (2015) and we refer to such a mentioned paper for more complete information. We recall that all the phase portraits are drawn in the Poincaré disc (see page 41).

For the normal form (3.2) from page 82, the class $\overline{\mathbf{QsnSN_{11}(A)}}$ is partitioned into 75 parts: 11 four–dimensional ones, 21 three–dimensional ones, 24 two–dimensional ones, 14 one–dimensional ones and 5 points. This partition is obtained by considering all the bifurcation sets of singularities, one related to the presence of invariant straight lines and one related to connections of separatrices, modulo "islands" (see Sec. 3.6). Due to some values of the parameters, from these 75 parts, four of them correspond to linear systems, being two one–dimensional and two points (see page 104). The corresponding four phase portraits form two classes, as indicated in Fig. 2.

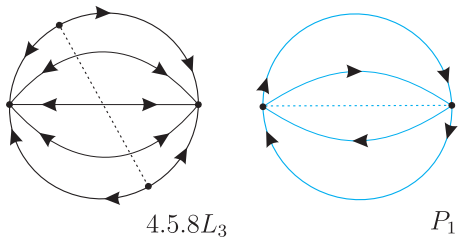

Figure 2 – Phase portraits corresponding to linear systems obtained from normal form (3.2)

Theorem 3.1.1. There are 36 topologically distinct phase portraits for the closure of the family of quadratic vector fields having a finite saddle–node $\overline{sn}_{(2)}$ as the only finite

singularity and an infinite saddle–node of type $\overline{\binom{1}{1}}SN$, and given by the normal form (3.2) (class $\overline{\mathbf{QsnSN_{11}(A)}}$). The bifurcation diagram for this class is given in the parameter space which is the projective four–dimensional space $\mathbb{RP}^4$. All these phase portraits are shown in Figs. 2 and 3. Moreover, the following statements hold:

(a) There are 12 topologically distinct phase portraits in $\mathbf{QsnSN_{11}(A)}$. Precisely we have $H_2, H_3, H_4, H_5, H_6, H_{10}$ plus the systems with the separatrix connection $4V_1, 4V_2, 7V_1$. Moreover, phase portraits $5V_5, 5V_6$ and $5V_7$ also belong to this family since the coalescence of two infinite singular points does not affect one of the double point at infinity. There is one generic region in the closure of $\mathbf{QsnSN_{11}(A)}$, namely H_1, whose phase portrait does not belong to $\mathbf{QsnSN_{11}(A)}$, since H_1 has two double complex singularities at infinity.

(b) There are five phase portraits with more than one non–degenerate graphic, and they are in the parts $5V_5$, $5V_6$, $5V_7$, $2.5S_2$, $4.5S_3$. None of the graphics contain a singularity inside.

(c) There are eight phase portraits with degenerate graphic, and they are in the parts $8V_1$, $2.8S_2$, $5.8S_1$, $5.8S_2$, $8.9S_1$, $2.8.9L_1$, $8.9.9L_1$, P_4.

(d) From the 36 phase portraits, two of them (located in the border of $\mathbf{QsnSN_{11}(A)}$) correspond to linear systems. The corresponding phase portraits are given in Fig. 2.

Corollary 3.1.2. From the class $\overline{\mathbf{QsnSN_{11}(A)}}$, Table 5 compares the number of phase portraits possessing some geometric features between the family $\mathbf{QsnSN_{11}(A)}$ and its border.

Table 5 – Comparison between the family $\mathbf{QsnSN_{11}(A)}$ and its border

	$\mathbf{QsnSN_{11}(A)}$	border of $\mathbf{QsnSN_{11}(A)}$
Distinct phase portraits	12	24
Phase portraits with more than one non–degenerate graphic	3	2
Phase portraits with degenerate graphics	0	8

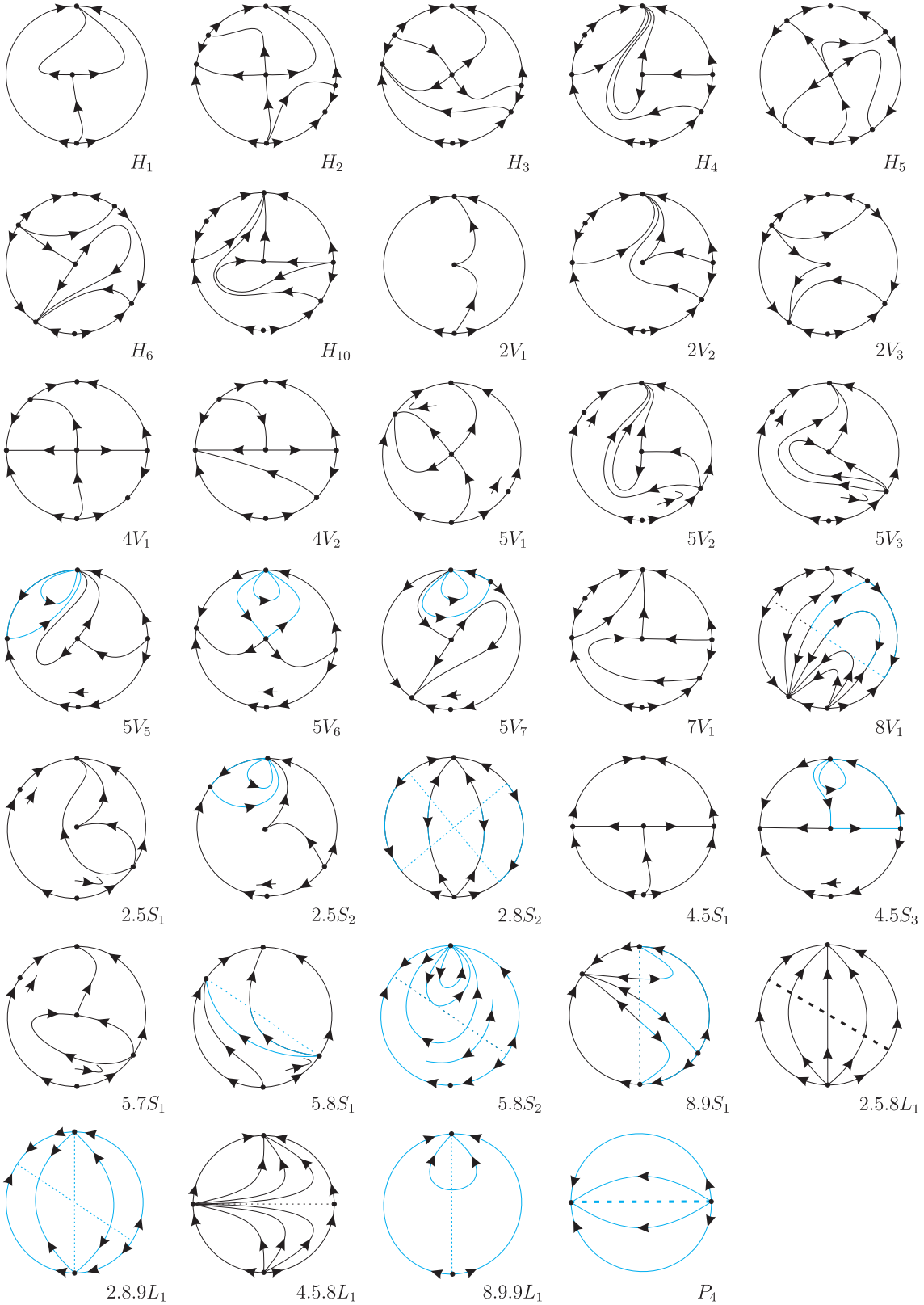

Figure 3 – Phase portraits for quadratic vector fields with a finite saddle–node $\overline{sn}_{(2)}$ and an infinite saddle–node of type $\overline{\binom{1}{1}}\,SN$ from class $\overline{\mathbf{QsnSN_{11}(A)}}$

From the 12 topologically distinct phase portraits of the family $\mathbf{QsnSN_{11}(A)}$, six

occur in four–dimensional parts and six in three–dimensional parts.

From the remaining 24 phase portraits, which are on the border of $\mathbf{QsnSN_{11}(A)}$, one occurs in a four–dimensional part, seven occur in the three–dimensional parts, nine occur in the two–dimensional parts, five occur in the one–dimensional parts and two occur in the zero–dimensional parts.

In Figs. 2 and 3 we have illustrated all the singular points with a small disc. In case of degenerate systems we have also illustrated the infinite singular point belonging to the degenerate set with a small disc only if this point is an infinite singularity of the reduced system. We have drawn with thicker curves the separatrices and also the line filled up with singularities which is double. We have added some thinner orbits to avoid confusion in some required cases. Moreover, we label the phase portraits according to the parts of the bifurcation diagram where they appear. Here we call *hypervolumes* (H) the four–dimensional parts of the bifurcation diagram, *volumes* (V) the three–dimensional ones, *surfaces* (S) the two–dimensional ones, *curves* (L) the one–dimensional ones, and *points* (P) the zero–dimensional ones.

As in Artés, Llibre and Schlomiuk (2006) and Artés, Rezende and Oliveira (2015), we use the same pattern in order to indicate the elements (V), (S), (L) and (P) in the bifurcation diagram. In this chapter we indicate each one of the *hypervolumes* (H) surrounded by a circle, as in Fig. 7.

This chapter is organized as follows. In Sec. 3.2 we describe some basic features regarding normal form (3.2) and we explain the structure of the bifurcation diagram.

In Sec. 3.3, using algebraic invariants and T–comitants as used in Sibirsky's School, we define the algebraic sets that describe the bifurcation diagram for the class $\overline{\mathbf{QsnSN_{11}(A)}}$.

In Secs. 3.4 and 3.5 we explain all the three–dimensional slices (and also the bifurcation planes on them) in the affine part and in the infinite of $\mathbb{RP}^4$, respectively.

In Sec. 3.6 we discuss about the possible existence of "islands" in the bifurcation diagram.

In Sec. 3.7 we introduce a global invariant denoted by $\mathscr{I}$, which classifies completely, up to topological equivalence, the phase portraits that we have obtained for the systems in the class $\overline{\mathbf{QsnSN_{11}(A)}}$. Thm. 3.7.7 shows clearly that they are uniquely determined (up to topological equivalence) by the values of the invariant $\mathscr{I}$.

The bifurcation diagram described in Secs. 3.4 and 3.5, plus Table 6 (from Sec. 3.7) of the geometric invariants distinguishing the 34 phase portraits corresponding to quadratic systems, plus Table 7 giving the equivalences with the remaining phase portraits lead to the proof of the main statement of Thm. 3.1.1.

3.2 Quadratic vector fields with a finite saddle–node $\overline{sn}_{(2)}$ and an infinite saddle–node of type $\overline{\binom{1}{1}}\,SN$

As we mentioned before, for the class $\overline{\mathbf{QsnSN_{11}(B)}}$ (which is presented in the next chapter), we consider quadratic systems possessing a finite saddle–node $\overline{sn}_{(2)}$, a finite elemental singularity and an infinite saddle–node of type $\overline{\binom{1}{1}}\,SN$.

In this chapter, for the class $\overline{\mathbf{QsnSN_{11}(A)}}$ we are considering that the mentioned finite elemental singularity has gone to infinity, i.e. we aim to study quadratic systems having only one finite saddle–node $\overline{sn}_{(2)}$ (which are located at the origin of the plane), an infinite saddle–node of type $\overline{\binom{1}{1}}\,SN$ and other infinite singularities, one of them of at least multiplicity two. Therefore, in this section we are considering quadratic systems of codimension at least three.

Using the T–comitants and invariants for quadratic systems as used in Sibirsky's School, in Artés, Llibre and Vulpe (2008) the authors have obtained two canonical forms for quadratic systems possessing one double real finite singularity and no other finite singularity; see Lemmas 3.24 and 3.25 from Artés, Llibre and Vulpe (2008). In Table 6.1 from Artés *et al.* (2021) these canonical forms are denoted by 16a and 16b, respectively. Family 16a is given by

$$\begin{aligned} \dot{x} &= dy + gx^2 + 2dxy, \\ \dot{y} &= fy + lx^2 + 2fxy, \end{aligned} \tag{3.1}$$

where d, f, g, l are real parameters and $fg - dl \neq 0$. On the other hand, family 16b is described by the differential equations

$$\begin{aligned} \dot{x} &= cx + dy, \\ \dot{y} &= lx^2 + 2mxy + ny^2, \end{aligned} \tag{3.2}$$

where c, d, l, m, n are real parameters and $ld^2 - 2cdm + nc^2 \neq 0$.

For both normal forms we have only one double finite singularity and the two other finite singularities have escaped to infinity. The geometric difference between them is that in normal form (3.1) both singularities coalesce with the same infinite singular point whereas in (3.2) they coalesce with different singular points. These facts are confirmed by Diagram 9.2 from Artés *et al.* (2021), where we can observe that family 16a cannot produce an infinite singularity of type $\overline{\binom{1}{1}}\,SN$ whereas on family 16b one may obtain such a kind of infinite singularity in some of the branches of the diagram. Then, as our main goal is to make a global study of the class $\mathbf{QsnSN_{11}}$ of all real quadratic polynomial differential systems possessing a finite saddle–node $\overline{sn}_{(2)}$ and an infinite saddle–node of type $\overline{\binom{1}{1}}\,SN$, in this chapter we provide the study of the canonical form (3.2).

We observe that canonical form (3.2) depends on five real parameters, namely, c, d, l, m and n. Then, its bifurcation diagram is actually the five–dimensional Euclidean space $\mathbb{R}^5$. Since the case $c=d=l=m=n=0$ corresponds to the null systems and does not belong to our family, we can work with the real projective space $\mathbb{RP}^4$. We point out that this is the first time that a five–dimensional bifurcation diagram is studied using all the ideas and theory described, for instance, in Artés, Llibre and Schlomiuk (2006) and Artés, Rezende and Oliveira (2015). In what follows we describe how we do this work.

Systems (3.2) depend on the parameter $\lambda=(c,l,m,d,n)\in\mathbb{R}^5$. We consider systems (3.2) which are nonzero, i.e. $\lambda=(c,l,m,d,n)\neq 0$. In this case, systems (3.2) can be rescaled with the affine transformation $(x,y,t)\to(x,y,\alpha t)$, $\alpha\neq 0$. In fact, applying this transformation we obtain

$$\begin{aligned}\dot{x}&=\alpha' cx+\alpha' dy,\\ \dot{y}&=\alpha' lx^2+2\alpha' mxy+\alpha' ny^2,\end{aligned}$$

for $\alpha'=1/\alpha$, $\alpha\neq 0$. Then, this transformation takes the systems with parameters (c,l,m,d,n) to systems with parameters $(\alpha' c,\alpha' l,\alpha' m,\alpha' d,\alpha' n)$, with $\alpha'=1/\alpha$. Hence, instead of taking $\mathbb{R}^5$ as the parameter space, we may consider the real projective space $\mathbb{RP}^4$. The four–dimensional projective space $\mathbb{RP}^4$ can be viewed as the quotient space $\mathbb{S}^4/_\sim$ of $\mathbb{S}^4$ by the equivalence relation: (c,l,m,d,n) is equivalent to itself or to $(-c,-l,-m,-d,-n)$. So, our parameter is $[\lambda]=[c:l:m:d:n]\in\mathbb{RP}^4=\mathbb{S}^4/_\sim$. Since for $\alpha'=-1$ the signs of all the parameters change, we may consider $d\geq 0$ in $[c:l:m:d:n]$. Since $c^2+l^2+m^2+d^2+n^2=1$, then $d=\sqrt{1-(c^2+l^2+m^2+n^2)}$, where $0\leq c^2+l^2+m^2+n^2\leq 1$.

We can therefore view the parameter space as a ball: $\overline{\mathscr{B}}=\{(c,l,m,n)\in\mathbb{R}^4; c^2+l^2+m^2+n^2\leq 1\}$ where on the border of this ball, two opposite points are identified. So, we are working with a four–dimensional space. The studies done up to now as Artés, Llibre and Schlomiuk (2006) and Artés, Rezende and Oliveira (2015) were done in a three–dimensional space. The parameter space was divided into specific two–dimensional slices which were of interest for the bifurcation. In our case we must divide the parameter space into three–dimensional slices which later must also be divided into two–dimensional planes in order to be drawn on a paper. We will see that the number of three–dimensional slices (and also the number of planes) is very small. Anyway, as we have mentioned before, this is the first time that this study is done and it is of great interest to have clear ideas when working at this level of dimensions. The different three–dimensional slices that we will detect share one common "top" which can be considered as an $\mathbb{RP}^2$. We have already chosen the parameter d as the parameter to distinguish from the affine space and the infinity. We will chose parameter n to foliate $\mathbb{RP}^4$ into three–dimensional spaces. And we will chose parameter m to split each three–dimensional space into two–dimensional spaces. The complete and general set can be seen as in Fig. 4, where the different k,k_0,k_1,k_α can be a single number or several different numbers if more slices are needed. If more slices were needed, the different cases would correspond alternatively to generic and singular

slices. Since systems (3.2) show different types of symmetries, whenever we change the sign of any of the parameters, each parameter equal to zero will correspond to a singular slice. We will use the parameters c and l as Cartesian coordinates to draw the bifurcation diagram in two dimensions. So, the simplest bifurcation diagram will have at least eight slices of different dimensions. In fact, this will be our case. These slices correspond to the different cases $(d,m,n) \in \{(0,0,0),(0,0,1),(0,1,0),(1,0,0),(0,1,1),(1,0,1),(1,1,0),(1,1,1)\}$. In Fig. 4 we present a general scenario of the partition of the bifurcation diagram.

For $d \neq 0$, we get the affine chart:

$$\begin{aligned}
&\mathbb{RP}^4 \setminus \{d=0\} \leftrightarrow \mathbb{R}^4\\
&[c:l:m:d:n] \to \left(\frac{c}{d},\frac{l}{d},\frac{m}{d},\frac{n}{d}\right) = (\overline{c},\overline{l},\overline{m},\overline{n})\\
&[\overline{c}:\overline{l}:\overline{m}:1:\overline{n}] \leftarrow (\overline{c},\overline{l},\overline{m},\overline{n})
\end{aligned}$$

The subspace $d=0$ in $\mathbb{RP}^4$, which is an $\mathbb{RP}^3$, corresponds to the equation $c^2+l^2+m^2+n^2=1$ (that is, the full sphere $\mathbb{S}^3$ with identification of symmetrical points on the border).

When two parameters are zero, for example, $d=n=0$, we identify the point $[c:l:m:0:0] \in \mathbb{RP}^4$ with $[c:l:m] \in \mathbb{RP}^2$. So, this subset $\{d=n=0\} \subset \overline{\mathscr{B}}$ can be identified with $\mathbb{RP}^2$, which can be viewed as a disc with two opposite points on the circumference (the equator) identified.

Now, when three parameters are zero, for example, the plane $m=d=n=0$ in $\mathbb{RP}^4$ corresponds to the equation $c^2+l^2=1$ which is an $\mathbb{RP}^1$ space, that is a circle with the opposite points identified. The concept of equator which was used in bifurcations in $\mathbb{RP}^3$ (as for instance in Artés, Llibre and Schlomiuk (2006) and Artés, Rezende and Oliveira (2015)) now needs to be enlarged to "equators" of dimension two. More precisely, a one–dimensional equator is when all parameters, except two, are zero. A two–dimensional equator is when all, except three parameters, are zero.

Proposition 3.2.1. By a rescaling in the variables, we may assume $d=0$ or $d=1$ in the normal form (3.2).

Proof. If $d \neq 0$, by the Reparametrization Theorem (see Prop. 1.1.15) we get that systems (3.2) are equivalent to

$$\begin{aligned}
\dot{x} &= Cx+y,\\
\dot{y} &= Lx^2+2Mxy+Ny^2,
\end{aligned}$$

where $C=c/d, L=l/d$, $M=m/d$ and $N=n/d$. By renaming the coefficients $C \to c$, $L \to l$, $M \to m$ and $N \to n$, we obtain systems (3.2) with $d=1$. Moreover, we must also consider the case when $d=0$. □

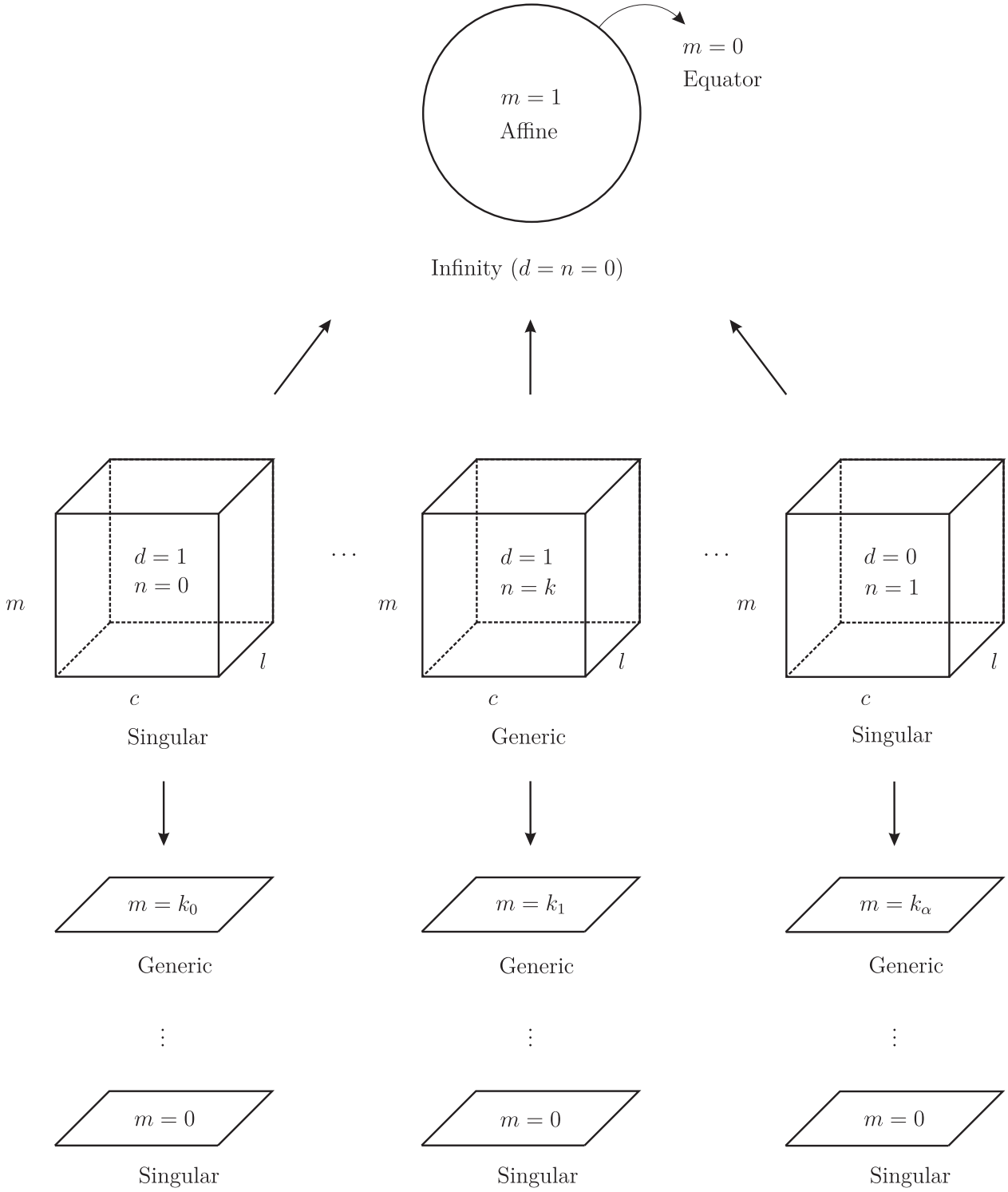

Figure 4 – Scheme of the partition of the bifurcation diagram. The parameter $d = 1$ (respectively $d = 0$) represents the affine (respectively infinite) part of $\mathbb{RP}^4$, the three–dimensional slices are given by the parameter n and from each three–dimensional slice the parameter m indicates the planes that must be studied

3.3 The bifurcation diagram of the systems in $\overline{\mathbf{QsnSN_{11}(A)}}$

In order to construct the bifurcation diagram for systems (3.2), in this chapter we consider the concepts of algebraic invariants and T–comitants as formulated by the Sibirsky's School for differential equations. For a quick summary see for instance Sec. 7 of Artés, Llibre and Schlomiuk (2006) and also and also Sec. 2.2 of this thesis.

3.3.1 Algebraic sets in $\mathbb{RP}^4$

According to Diagram 9.2 from Artés *et al.* (2021), here we define the algebraic sets that are needed for the study of the bifurcation diagram of canonical form (3.2). These algebraic sets are given by the invariants and comitants listed in such a diagram.

Bifurcation set in $\mathbb{RP}^4$ due to degeneracy of systems

$(\mathscr{V}_8)$ Since for systems (3.2) we have a double real finite singularity and two finite singularities have coalesced with different singularities at infinity, according to Diagram 9.2 from Artés *et al.* (2021) one must have $\mu_0 = \mu_1 = \kappa = 0$ and $\mu_2 \neq 0$. Additionally, calculations show that $\mu_3 = \mu_4 = 0$ and

$$\mu_2 = (ld^2 - 2cdm + nc^2)(lx^2 + 2mxy + ny^2).$$

So we define $(\mathscr{V}_8)$ as an algebraic set whose equation is equivalent to $\mu_2 = 0$, i.e.

$$(\mathscr{V}_8): ld^2 - 2cdm + nc^2 = 0,$$

and therefore on this algebraic set we have $\mu_i = 0$, $i = 0,1,2,3,4$, i.e. systems (3.2) are degenerate.

We point out that our aim is to construct a coherent and continuous bifurcation diagram. Although the phase portraits possessing a double finite saddle–node $\overline{sn}_{(2)}$ and an infinite saddle–node $\overline{\binom{1}{1}}SN$ belong to open sets in this bifurcation diagram, in order to have these properties for this diagram, we also need to consider the borders of such sets. In particular, algebraic set $(\mathscr{V}_8)$ borders open sets in this bifurcation diagram.

Remark 3.3.1. According to Diagram 9.2 from Artés *et al.* (2021), for the normal form (3.2) the comitant

$$\widetilde{L} = 8n(lx^2 + 2mxy + ny^2),$$

multiplied by μ_2, allows us to distinguish between different configurations of infinite singularities. More precisely, we have

$$\mu_2\widetilde{L} = 8n(ld^2 - 2cdm + nc^2)(lx^2 + 2mxy + ny^2)^2,$$

and if $\mu_2\widetilde{L} < 0$ we have the configuration of singularities $\overline{\binom{1}{1}}SN$, $\overline{\binom{1}{1}}SN$, N and if $\mu_2\widetilde{L} > 0$ we have the configuration of singularities $\overline{\binom{1}{1}}SN$, $\overline{\binom{1}{1}}NS$, N.

Remark 3.3.2. In some of the equations of the following algebraic sets the factor $ld^2 - 2cdm + nc^2$ is also present. This confirms that the systems on algebraic set $(\mathscr{V}_8)$ are indeed degenerate (possessing curves of singularities) because many geometric features happen at the same time when $ld^2 - 2cdm + nc^2 = 0$. However, we are interested in the other geometric features that the following algebraic sets can provide. In this way, we assume, without loss of generality, that $ld^2 - 2cdm + nc^2 \neq 0$.

Bifurcation set in $\mathbb{RP}^4$ due to the change of topological type of the origin

$(\mathscr{V}_2)$ This is the bifurcation set due to the change of topological type of the origin. On this algebraic set the origin becomes a cusp–type singularity. This phenomenon occurs when two separatrices of a saddle–node coalesce. According to Artés *et al.* (2021), for systems (3.2) a necessary condition for this phenomenon to happen is that the trace of the Jacobian of the finite singularity is zero and it is described by the invariant

$$\mathscr{T}_4 = 4c^2n(d^2l - 2cdm + c^2n)(-m^2 + ln).$$

Taking into consideration Rmk. 3.3.2, we define algebraic set $(\mathscr{V}_2)$ by

$$(\mathscr{V}_2): c^2n(-m^2 + ln) = 0.$$

Remark 3.3.3. We observe that for $n = 0$, we have $(\mathscr{V}_2) \equiv 0$. For normal form (3.2), according to Diagram 9.2 from Artés *et al.* (2021) we must consider the comitant

$$\widetilde{M}\Big|_{n=0} = -32m^2x^2,$$

which vanishes if and only if $m = 0$. Such a mentioned diagram tells us that when $n = 0$ and $m \neq 0$ we can consider the invariant

$$\mathscr{B}_1\Big|_{n=0} = -2c^2dm(-dl + 2cm),$$

and when $n = m = 0$ we can consider the comitant

$$\mathscr{B}_4\Big|_{n=m=0} = 6clx^2(cx + dy).$$

Due to Rmk. 3.3.2 and the diagram under discussion, for $n = 0$ we can define

$$(\mathscr{V}_2): c^2m = 0 \quad \text{if} \quad m \neq 0, \tag{3.3}$$

and

$$(\mathscr{V}_2): c = 0 \quad \text{if} \quad m = 0. \tag{3.4}$$

Bifurcation set in $\mathbb{RP}^4$ due to the presence of invariant straight lines

$(\mathscr{V}_4)$ This algebraic set in $\mathbb{RP}^4$ contains the points of the parameter space where invariant straight lines appear. These straight lines may contain connections of separatrices from different singularities or not. So, in some cases, it may imply a topological bifurcation or not. According to Cor. 4.6 from Schlomiuk and Vulpe (2004) we have necessary conditions for the existence of invariant straight lines, which are given in terms of the zeroes of the comitants B_1, B_2, and B_3. More precisely, such a result tells us that for the existence of an invariant straight line in one (respectively two or three distinct) directions in the affine plane it is necessary that $B_1 = 0$ (respectively $B_2 = 0$ or $B_3 = 0$). For systems (3.2), calculations yield

$$\begin{aligned} B_1 &= 0, \\ B_2 &= -648l^2(ld^2 - 2cdm + nc^2)^2x^4, \\ B_3 &= -6(d^2l - 2cdm + c^2n)x^2y(lx + my). \end{aligned}$$

Taking into consideration Rmk. 3.3.2, we conclude that B_1 is identically zero, B_2 is equivalent to $l = 0$ and B_3 is nonzero. In the case when B_1 is not identically zero, we can simply rely on the bifurcation $B_1 = 0$ to look for the possible existence of invariant straight lines (as for instance in Artés, Rezende and Oliveira (2015)). However, in this case when $B_1 \equiv 0$, we have an invariant line which coalesced with the infinite line $Z = 0$ (i.e. this line is a double one), and we may have invariant straight lines in other directions. Any single affine straight line can be considered "parallel" to the infinity line. Then the invariant $B_2 \equiv 0$ may not cover all the possibilities of existence of a second line. So, we must do the detailed study of whether there can exist or not straight lines. Doing this study it is easy to determine that any invariant straight line must cross the origin and they exist if $l = 0$ or if $ld^2 - 2cdm + nc^2 = 0$ (see Lemma 3.3.4). These are exactly the components of B_2 plus the component $d = 0$. We define algebraic set $(\mathscr{V}_4)$ by the equation

$$(\mathscr{V}_4) : dl(ld^2 - 2cdm + nc^2) = 0.$$

Lemma 3.3.4. Systems (3.2) possess the following invariant straight lines under specific conditions:

1. $\{y = 0\}$, if $l = 0$;
2. $\{x = 0\}$, if $d = 0$;
3. $\{ax + by = 0\}$, if $d = cb/a$ and $n = (2mab - lb^2)/a^2$, for $a \neq 0$. Moreover, these values of d and n satisfy the equation $ld^2 - 2cdm + nc^2 = 0$, i.e. we have degenerate systems.

Proof. We consider the algebraic curves

$$\begin{aligned} f_1(x,y) &\equiv y = 0, \\ f_2(x,y) &\equiv x = 0, \\ f_3(x,y) &\equiv ax + by = 0, \end{aligned}$$

and we show that the polynomials

$$K_1(x,y) = 2mx + ny,$$
$$K_2(x,y) = c,$$
$$K_3(x,y) = c + \frac{lb}{a}x + \frac{b(2ma - lb)}{a^2}y,$$

are the cofactors of $f_1 = 0$, $f_2 = 0$, and $f_3 = 0$, respectively, after restricting systems (3.2) to the respective conditions. □

We shall detect another bifurcation set that is not necessarily algebraic and on which the systems have connection of separatrices different from that ones given by $(\mathscr{V}_4)$. The equations of this bifurcation set can only be determined approximately by means of numerical tools and its existence is proved by using arguments of continuity in the bifurcation diagram. We shall name this set $(\mathscr{V}_7)$.

Bifurcation set in $\mathbb{RP}^4$ due to multiplicities of infinite singularities

$(\mathscr{V}_5)$ This is the bifurcation set due to the coalescence of infinite singularities. This phenomenon is detected by the invariant η which, for systems (3.2), is given by

$$\eta = -4n^2(-m^2 + ln).$$

We define algebraic set $(\mathscr{V}_5)$ by the equation

$$(\mathscr{V}_5) : n^2(-m^2 + ln) = 0.$$

Remark 3.3.5. Again we observe that for $n = 0$, we have $(\mathscr{V}_5) \equiv 0$. According to Diagram 9.2 from Artés *et al.* (2021), for systems (3.2) we must consider the comitant

$$\widetilde{M}\Big|_{n=0} = -32m^2x^2,$$

which vanishes if and only if $m = 0$. Such a mentioned diagram tells us that when $n = 0$ we can define

$$(\mathscr{V}_5) : m = 0 \quad \text{if} \quad n = 0. \tag{3.5}$$

We will see that on the slice $n = 0$ we will always have a coalescence of infinite singularities.

As we said before, we work in the chart of $\mathbb{RP}^4$ corresponding to $d \neq 0$, and we take $d = 1$. In order to perform the analysis, we shall use pictures which are drawn on planes of $\mathbb{RP}^4$, having coordinates $[c : l : m_0 : 1 : n_0]$, with n_0 and m_0 constants, plus the open half sphere $d = 0$ and we shall give pictures of the resulting bifurcation diagram on these planar sections on a disc or in an affine chart of $\mathbb{R}^2$. In these planes the coordinates are (c,l) where the horizontal line is the c–axis.

As in Artés, Llibre and Schlomiuk (2006) and Artés, Rezende and Oliveira (2015), in this chapter we use colors to refer to the bifurcation algebraic sets:

(a) algebraic set ($\mathscr{V}_2$) is drawn in green (the origin becomes a cusp–type singularity);

(b) the non–degenerate part of algebraic set ($\mathscr{V}_4$) is drawn in purple (presence of at least one invariant straight line). We draw it as a continuous curve if it implies a topological change or as a dashed curve otherwise;

(c) algebraic set ($\mathscr{V}_5$) is drawn in red (two infinite singular points coalesce);

(d) set ($\mathscr{V}_7$) is also drawn in purple (connections of separatrices); and

(e) algebraic set ($\mathscr{V}_8$) is drawn in cyan (the systems are degenerate).

We use the same color for ($\mathscr{V}_4$) and ($\mathscr{V}_7$) since both sets deal with connections of separatrices.

3.3.2 Geometric features of the algebraic sets in $\mathbb{RP}^4$

Before we pass to the study of the geometric features of algebraic sets ($\mathscr{V}_2$), ($\mathscr{V}_4$), ($\mathscr{V}_5$), and ($\mathscr{V}_8$), first we remember the definition of a singularity of a several variables smooth map.

Definition 3.3.6. Let $f : U \subset \mathbb{R}^m \to \mathbb{R}^n$ be a smooth map. A point $p \in U$ is a *singular point* of f if the rank of the Jacobian matrix $Df(p)$ is strictly less than $\min\{m,n\}$. More precisely, given $f = (f_1,\ldots,f_n) : U \subset \mathbb{R}^m \to \mathbb{R}^n$ with $f_i = f_i(x_1,\ldots,x_m)$, $i = 1,\ldots,n$, we say that $p \in U$ is a *singular point* for f if the matrix

$$\begin{bmatrix} \frac{\partial f_1}{\partial x_1} & \cdots & \frac{\partial f_1}{\partial x_m} \\ \vdots & \ddots & \vdots \\ \frac{\partial f_n}{\partial x_1} & \cdots & \frac{\partial f_n}{\partial x_m} \end{bmatrix}(p)$$

has rank $r < \min\{m,n\}$.

We have defined the following algebraic sets:

$$\begin{aligned} (\mathscr{V}_8)&: n(ld^2 - 2cdm + nc^2) = 0, \\ (\mathscr{V}_2)&: c^2 n(-m^2 + ln) = 0, \\ (\mathscr{V}_4)&: l = 0, \\ (\mathscr{V}_5)&: n^2(-m^2 + ln) = 0. \end{aligned}$$

Here we are interested in studying the geometric behavior of all of these algebraic sets, that is, their singularities (according to Def. 3.3.6), their intersection points and their "tangencies" (in the affine space) with three–dimensional slices of the type $d = 1$ and constant n. Since this study requires a lot of computations which would take a very

large number of pages to present all the details, in order to be more succinct we have developed an algorithm in software Mathematica and we have created a notebook with all the computations on it. This algorithm is available for free download through the link <http://mat.uab.cat/~artes/articles/qvfsn2SN11A/sn2SN11A.nb> (some previous knowledge of Mathematica is recommended for using this algorithm).

In what follows, we describe the main idea of what we have done in this subsection and we present the results. For more details we recommend the mentioned Mathematica algorithm.

Remark 3.3.7. In $\mathbb{R}^5$ we will create a list of k–dimensional objects, $1 \leq k \leq 4$, in the following way. We denote by $\{Okx_{i(k)}\}_{\{1\leq k\leq 4,\ i(k)\in\mathbb{N}\}}$ a list of k–dimensional objects, where each $Okx_{i(k)}$ is a list of objects of dimension $k \in \{1,\ldots,4\}$. For instance, $O4x_1$ stands for the first element of the list of four–dimensional objects. By "dimension" of an object we mean the number of parameters used for defining it.

In order to proceed with the study of all geometric features (of the algebraic sets) described before, it is interesting to work with the components of each algebraic set (this idea was used explicitly in Artés, Llibre and Schlomiuk (2006) and Artés, Rezende and Oliveira (2015)). Then we generate a list of components, which are denoted according to Rmk. 3.3.7:

- $O4x_1 : c = 0$ which corresponds to the set $\{0,l,m,d,n\}$;
- $O4x_2 : l = 0$ which corresponds to the set $\{c,0,m,d,n\}$;
- $O4x_3 : n = 0$ which corresponds to the set $\{c,l,m,d,0\}$;
- $O4x_4 : m^2 - ln = 0$ which corresponds to the set $\{c,l,m,d,m^2/l\}$;
- $O4x_5 : ld^2 - 2cdm + c^2n = 0$ which corresponds to the set $\{c,(2cdm - nc^2)/d^2,m,d,n\}$;

Now we proceed with the study of the singularities of the four–dimensional components (i.e. the objects $O4x_i, i = 1,\ldots,5$) and their respective intersections. We also study the "tangencies" of these objects in the affine space with slices of the type $d = 1$ and constant n. This study generates a set of three–dimensional or lower objects. More precisely, we have the new objects:

- $O3x_1 = \{0,0,m,d,n\}$;
- $O3x_2 = \{0,l,m,0,n\}$;
- $O3x_3 = \{0,l,m,d,0\}$;
- $O3x_4 = \{0,l,m,d,m^2/l\}$;
- $O3x_5 = \{0,l,m,d,dm^2/l\}$;
- $O3x_6 = \{c,0,0,d,n\}$;
- $O3x_7 = \{c,0,m,d,0\}$;
- $O3x_8 = \{c,0,m,d,2dm/c\}$;

- $O3x_9 = \{c, 0, cdn/2, d, n\}$;
- $O3x_{10} = \{c, l, 0, d, 0\}$;
- $O3x_{11} = \{c, l, dl/2c, d, 0\}$;
- $O3x_{12} = \{c, l, m, 0, 0\}$;
- $O3x_{13} = \{c, cm/d, m, d, dm/c\}$;
- $O3x_{14} = \{c, c^2dn, cdn, d, n\}$;
- $O2x_1 = \{0, 0, 0, d, n\}$;
- $O2x_2 = \{0, 0, m, d, 0\}$;
- $O2x_3 = \{0, l, m, 0, m^2/l\}$;
- $O2x_4 = \{c, 0, 0, d, 0\}$;
- $O2x_5 = \{c, l, 0, 0, 0\}$;
- $O1x_1 = \{0, 0, 0, 0, n\}$.

Now we take the list of three–dimensional objects $O3x_i$ and we study their singularities and their respective intersections. We also study the possibility that any of these objects may be expressed by means of square roots which could produce the change from real solutions to complex ones under some conditions. This generates a set of two–dimensional or lower objects which enlarge the set previously found. More precisely, we have added the new objects:

- $O2x_6 = \{0, 0, m, 0, n\}$;
- $O2x_7 = \{0, l, 0, d, 0\}$;
- $O2x_8 = \{0, l, m, 0, 0\}$;
- $O2x_9 = \{c, 0, 0, 0, n\}$;
- $O2x_{10} = \{c, 0, m, 0, 0\}$;
- $O1x_2 = \{0, 0, 0, d, 0\}$;
- $O1x_3 = \{0, 0, m, 0, 0\}$;
- $O1x_4 = \{0, l, 0, 0, 0\}$;
- $O1x_5 = \{c, 0, 0, 0, 0\}$.

Now we take the list of two–dimensional objects $O2x_i$ and we study their singularities and their respective intersections. Again we consider the possibility of the presence of square roots, which imply real or complex solutions under some conditions. This generates a set of one–dimensional objects which enlarge the set previously found. But we do not have any new element, since we detect that the elements obtained at this stage have already been found previously.

Now, these five one–dimensional objects, which are in $\mathbb{R}^5$ correspond to points in the projective space, which will determine the singular slices that we must take into consideration. As we have said, the bifurcation diagram is very simple and it is described by the next lemma.

Lemma 3.3.8. The parameter space of systems (3.2), which is an $\mathbb{RP}^4$, bifurcates into three spaces $\mathbb{RP}^3$ which are $[c : l : m : 1 : 1]$ (generic), $[c : l : m : 1 : 0]$ and $[c : l : m : 0 : 1]$ (both singular). Then, inside each one of these three–dimensional slices we must only consider two cases: $m = 1$ (generic) and $m = 0$ (singular). Finally, the space $\mathbb{RP}^2$ is given by $[c : l : m : 0 : 0]$ which is border of $[c : l : m : 0 : 1]$.

Even though we have found the existence of a nonalgebraic bifurcation, we have not detected that more slices are needed because of it, i.e. there is complete coherence of continuity of the phase portraits with the slices already provided.

We now begin the analysis of the two–dimensional bifurcation diagrams by studying completely each one of the elements described in Lemma 3.3.8.

We describe first the labels used for each part of the bifurcation space. As we have mentioned before, the subsets of dimensions 4, 3, 2, 1 and 0, of the partition of the parameter space will be denoted respectively by H, V, S, L and P for Hypervolume, Volume, Surface, Line and Point, respectively. The volumes are named using a number which corresponds to each bifurcation volume which is placed on the left side of the letter V and in order to describe the portion of the volume we place an index. The surfaces that are intersection of volumes are named by using their corresponding numbers on the left side of the letter S, separated by a point. The surfaces which are singularities of volumes are named by using the number of the surface twice on the left side of the letter S. To describe the piece of the surface we place an index. The curves that appear can come from different sources: they could be intersection of surfaces, intersection among several volumes, singularities of volumes, and, in general, any object of this classification of dimension one. The curves are named by using their corresponding numbers (of the volumes containing them) on the left side of the letter L, separated by a point. In case we have more than three volumes intersecting on the same curve, we place the three numbers of the surfaces that we consider more relevant. To describe the segment of the curve we place an index. Hypervolumes and Points are simply indexed.

We consider an example: algebraic set ($\mathcal{Y}_2$) splits into 3 different three–dimensional parts labeled as $2V_1$, $2V_2$ and $2V_3$, plus some two–dimensional parts labeled as $2.iS_j$ (where i denotes the other volume intersected by ($\mathcal{Y}_2$) and j is a number), plus some one–dimensional parts labeled as $2.i.kL_j$ (where i and k denote the other volumes intersected by ($\mathcal{Y}_2$) and j is a number), and also some zero–dimensional parts. In order to simplify the labels in all figures we see **H1** which stands for the TEX notation H_1. Analogously, **2V1** (respectively, **2.5S1**) stands for $2V_1$ (respectively $2.5S_1$). And the same happens with many other pictures.

3.4 Bifurcation diagram in the affine part of $\mathbb{RP}^4$

Here we assume that $d = 1$ and we have to consider the three–dimensional slices $n = 1$ and $n = 0$, which indicate, respectively, a generic and a singular slice for $d = 1$.

In Fig. 5 we represent the generic plane $m = 1$ of the parameter space for the generic slice $n = 1$, showing only the algebraic surfaces. We will use lower–case letters provisionally to describe the sets found algebraically in order to not interfere with the final partition

described with capital letters. Moreover, we obtain the global phase portraits with the numerical program P4 (see Artés *et al.* (2005) and Dumortier, Llibre and Artés (2008)). In this slice we have a partition in two–dimensional parts bordered by curved polygons, some of them bounded, others bordered by infinity. For each two–dimensional part we obtain a phase portrait which is coherent with those of all their borders. Except for the part h_9 (the rectangle bordered by green, purple, red and infinity). The study of this part is very important for the coherence of the bifurcation diagram. That is why we have decided to present only this part (and its borders) in Fig. 5.

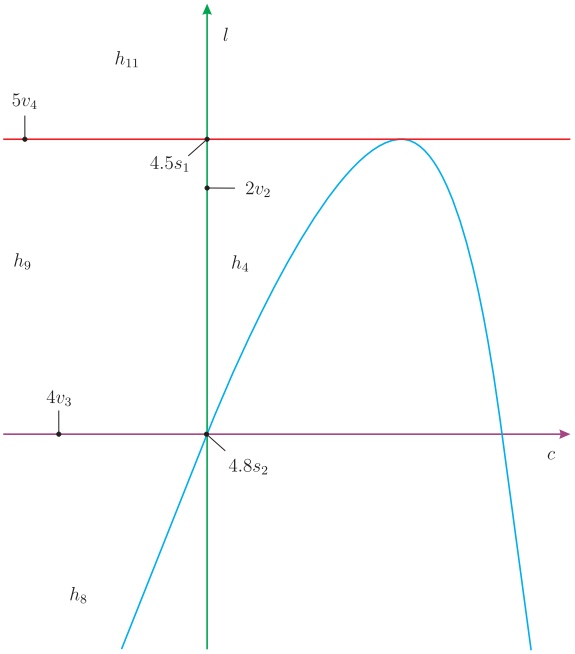

Figure 5 – Plane $m = 1$ on the slice $n = 1$ (only algebraic sets)

We start the analysis of part h_9. The phase portrait in h_9 near $2v_2$ possesses a finite basin passing through the finite saddle–node, i.e. two separatrices of the finite saddle–node start at the same infinite saddle–node, whereas the phase portrait in h_9 away from $2v_2$ does not possess the finite basin. Then, there must exist at least one element $7V_1$ of set $(\mathscr{V}_7)$ dividing part h_9 into two "new" parts, H_9 and H_{10}, which represents a bifurcation due to the connection of a separatrix of a finite saddle–node and a separatrix of an infinite saddle–node (see Fig. 6 for a sequence of phase portraits in these parts). As the segment $5v_4$ corresponds to changes in the infinite singular points, the finite part of the phase portraits remains unchanged and this element of nonalgebraic set $(\mathscr{V}_7)$ must intersect $5v_4$ having this intersection point as one of its endpoints, since in h_{11} we do not have the sufficient number of infinite singularities in order to make this nonalgebraic bifurcation happens. In Lemma 3.4.1 we prove that $7V_1$ is bounded and it has $4.8s_2$ and $5.7S_1$ as endpoints. The complete bifurcation diagram for the generic plane $m = 1$ on the slice $n = 1$ is presented in Fig. 7.

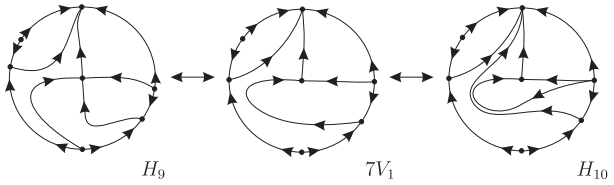

Figure 6 – Sequence of phase portraits in part h_9 of $n = m = 1$

Lemma 3.4.1. The element $7V_1$ of nonalgebraic set $(\mathscr{V}_7)$ is bounded and it has $4.8S_2$ and $5.7S_1$ as endpoints.

Proof. Numerical tools show that this result is true. We have mentioned before that in H_{11} we do not have the sufficient number of infinite singularities in order to make the nonalgebraic bifurcation given by $7V_1$ happens. However, $7V_1$ must intersect $5v_4$ in some point, since some two different phase portraits $5V_3$ and $5V_4$ are detected on this part. Then such a nonalgebraic set has an endpoint at $5.7S_1$. On the other hand, we observe that $4V_3$ represents the existence of an invariant straight line which indicates a topological change between H_8 and H_9. If some point of $4V_3$ were an endpoint of $7V_1$, then the invariant line would necessarily be broken in order to make this nonalgebraic bifurcation happens. Then the second endpoint of $7V_1$ cannot be on $4V_3$. Moreover, it also cannot be on $2V_2$ since on such an algebraic set the finite saddle–node has become a cusp–type singularity. Therefore, the second endpoint of $7V_1$ is $4.8S_2$. See Fig. 7 for the mentioned regions in this proof. □

For the slice $n = 1$, the only singular plane is $m = 0$, in which we observe that the volume regions $4V$ and $5V$ coalesce, making the hypervolume regions H_2, H_3, H_4, H_9, and H_{10} disappear, see Fig. 8.

We now pass to the singular slice $n = 0$. According to the study of the geometric features of the algebraic sets, we must consider the planes $m = 1$ and $m = 0$, which are, respectively, generic and singular planes for this slice.

We start studying the generic plane $m = 1$. According to Rmk. 3.3.5, for this generic plane we have that $(\mathscr{V}_5) \equiv 0$, i.e, there are two infinite singularities that always coalesce. Moreover, in this case we have that $(\mathscr{V}_8)$ is reduced to the line $l = 2c$. In fact, almost all phase portraits from these values of the parameters d, n, m can be obtained from the previous ones via a specific coalescence of infinite singularities. We only have five exceptions, which are the parts which were gone to the infinity during the transition between the generic slice $m = 1$ and the singular one: H_1, H_2, H_5, H_9, and H_{11}. In Fig. 9 we have drawn this generic plane.

Now we discuss the singular plane $m = 0$. In this case, algebraic set $(\mathscr{V}_8)$ is reduced to the line $l = 0$ and this movement makes the volume regions $5V_6$ and $5V_9$ disappear. The

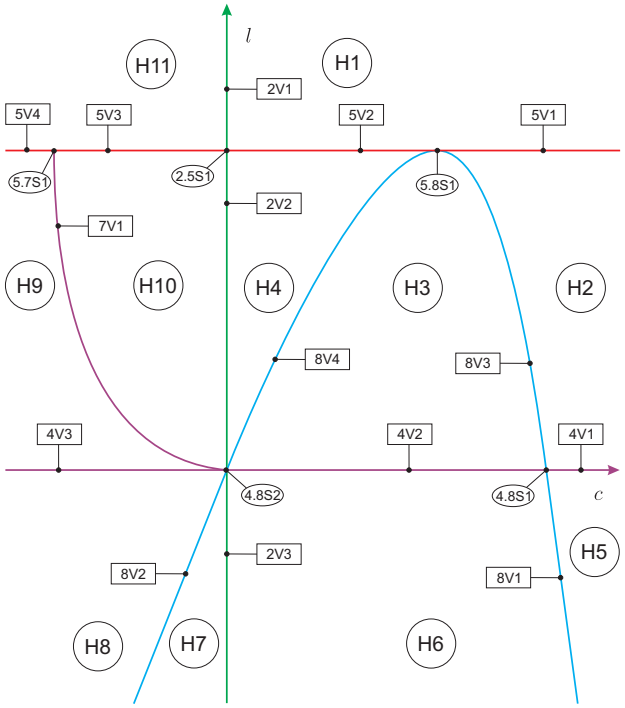

Figure 7 – Plane $m = 1$ on the slice $n = 1$

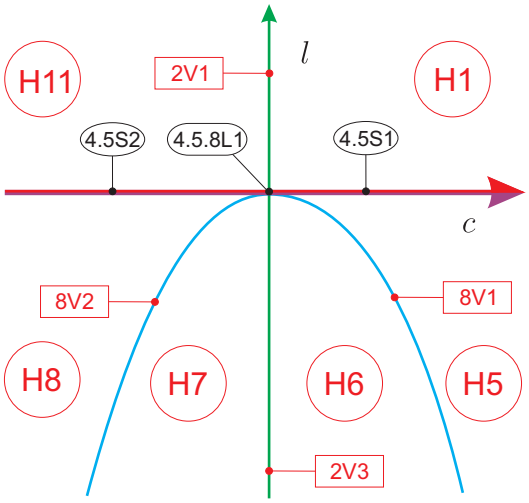

Figure 8 – Plane $m = 0$ on the slice $n = 1$ (see Fig. 7)

new corresponding regions are $4.5.8L_1$, $4.5.8L_2$ and P_1 (see the representation of the plane $m = 0$ in Fig. 10). Moreover, since we are considering $n = 0$, according to Rmk. 3.3.5, for this singular plane we already have that $(\mathcal{Y}_5) \equiv 0$. In addition, equation (3.5) tells us that $\widetilde{M}$ is also 0. Therefore, the phase portraits for the remaining regions of the plane $m = 0$ can be obtained from the corresponding phase portraits from the plane $m = 1$ by performing a convenient coalescence of infinite singularities. In Fig. 10 we have drawn this singular plane.

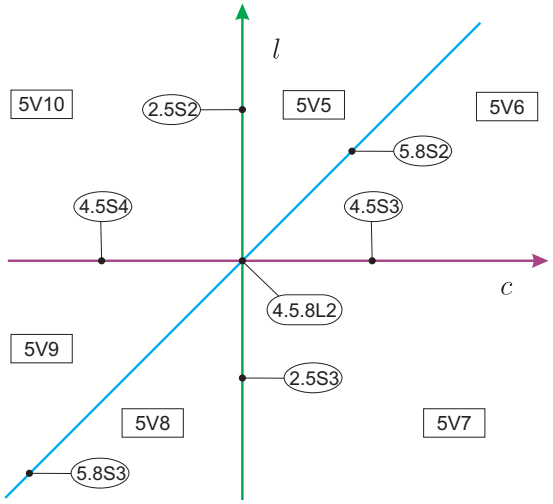

Figure 9 – Plane $m = 1$ on the slice $n = 0$ (see Fig. 8)

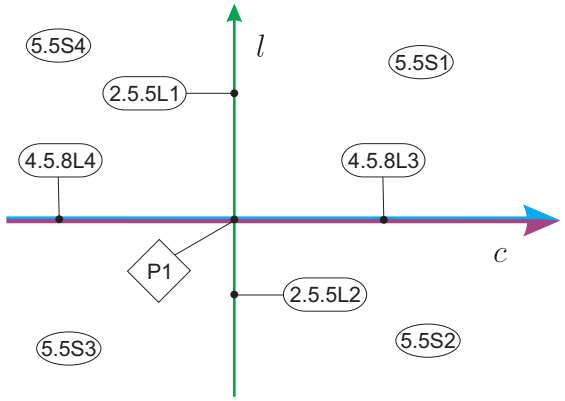

Figure 10 – Plane $m = 0$ on the slice $n = 0$ (see Fig. 9)

3.5 Bifurcation diagram in the infinite part of $\mathbb{RP}^4$

Here we assume that $d = 0$ and again we have to consider the three–dimensional slices $n = 1$ and $n = 0$, which now indicate, respectively, the affine and the infinite part of the infinity of $\mathbb{RP}^4$.

First we consider slice $n = 1$. In this slice we must perform the study of the planes $m = 1$ and $m = 0$, which indicate, respectively, the generic and the singular planes.

For the values of the parameters d and n under consideration, we have that $(\mathcal{Y}_8)$ is reduced to the double line $c^2 = 0$. Therefore, for $m = 1$, this is the only topological change in the bifurcation diagram when we compare this plane with the plane described in Fig. 7 (see Fig. 11).

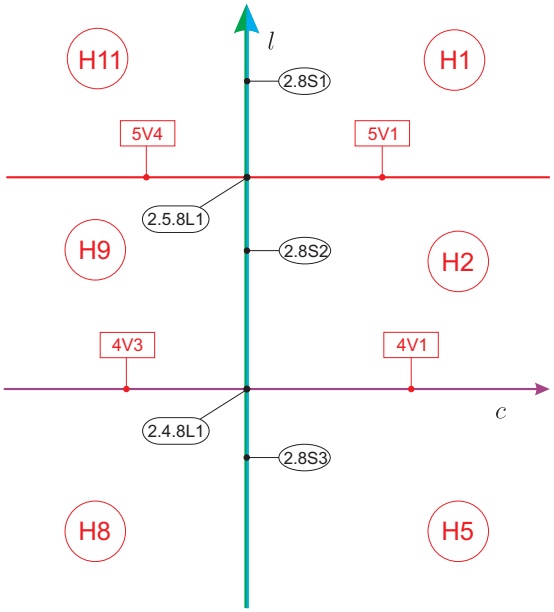

Figure 11 – Plane $m = 1$ on the affine part of the infinity of $\mathbb{RP}^4$ (see Fig. 10)

Using the same arguments as before, we conclude that in the plane $m = 0$ we have only one topological change on the bifurcation diagram when we compare this plane with the plane described in Fig. 8 (see Fig. 12).

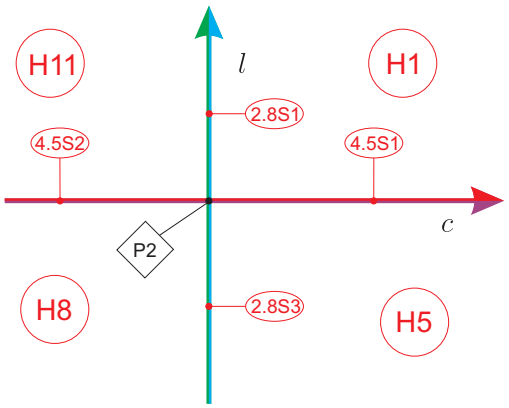

Figure 12 – Plane $m = 0$ on the affine part of the infinity of $\mathbb{RP}^4$ (see Fig. 11)

Remark 3.5.1. The phase portrait corresponding to region $2.8S_1$ in Fig. 11 possesses a pair of complex straight lines filled up with singularities. Such straight lines are described by equations

$$y = (-1 \pm i)x,$$

respectively. We point out that this phase portrait is topologically equivalent to $2V_1$ from Fig. 3. This is a very curious topological coincidence of phase portraits coming from very different quadratic systems. There is even one more quadratic system topologically

equivalent to them but geometrically different, which is the one that has the intricate point $hh_{(4)}$. This fact has already been detected in different papers as Artés and Llibre (1994) or Artés *et al.* (2020).

Now, finally we present the study of the infinity of the infinite part of $\mathbb{RP}^4$. Here we already have $d = n = 0$, i.e. we are in the half–sphere $c^2 + l^2 + m^2 = 1$. Then we proceed as we did in the previous section, that is, here we have to study $m = 1$ (the affine part) and $m = 0$ (the equator). For these values of d and n we have that $(\mathcal{Y}_5) \equiv 0$ and $(\mathcal{Y}_8) \equiv 0$, then all the phase portraits that are obtained here are degenerate. Moreover, equation (3.4) tells us that the vertical axis is still a bifurcation curve because on it the degeneration is of degree two. But we verify that the horizontal axis still produces an invariant straight line but now does not imply any topological change on the bifurcation diagram, this is the reason why we have drawn this axis as a dashed line in Fig. 13. In such a figure, all the "generic" parts are labeled as $8.9S_j$, the lines are labeled as $k.8.9L_j$, where k corresponds to the curve on this compactified plane, and the points are labeled as points. We use the orange color for the equator of $\mathbb{S}^2$, i.e. $d = n = m = 0$.

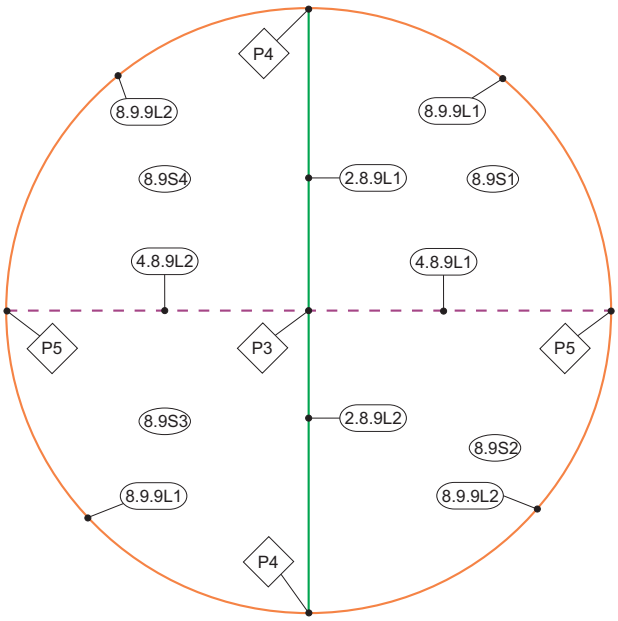

Figure 13 – Compactified plane corresponding to the infinite part of the infinity of $\mathbb{RP}^4$. The affine part is given by $n = 0, m = 1$ and the equator is described by $n = m = 0$ (see Fig. 12)

Since the complete bifurcation diagram is quite simple, the best way to see the continuity between different phase portraits, and the way that they bifurcate ones from the others, is to set all the planes in a single page in a reduced size as we do in Fig. 14.

Because there is coherence among all the slices that we have presented, we conclude that no more slices are needed for the complete coherence of the bifurcation diagram and

therefore we can affirm that we have described a complete bifurcation diagram for family $\overline{\mathbf{QsnSN_{11}(A)}}$ modulo islands, as we discuss in Sec. 3.6.

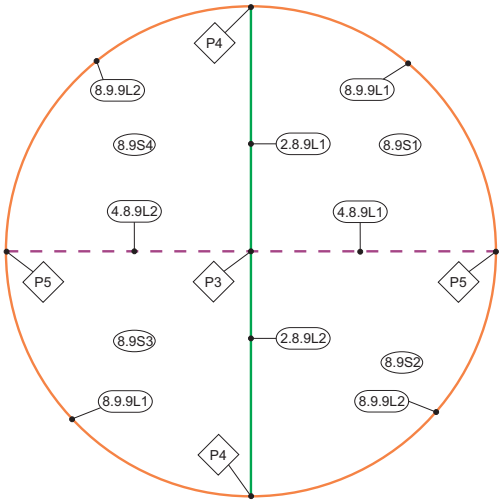

$d = 0, n = 0, m = 1$ (affine)

$d = 0, n = 0, m = 0$ (equator)

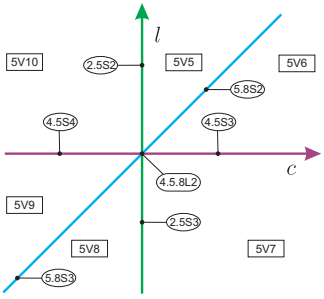

$d = 1, n = 0, m = 1$

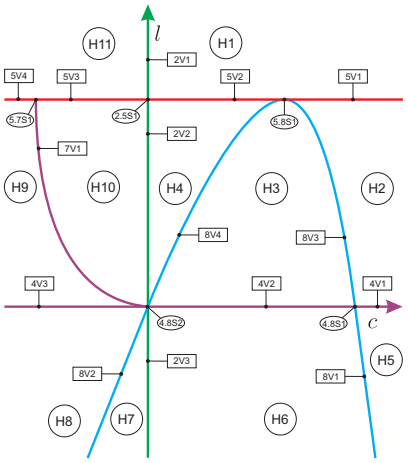

$d = 1, n = 1, m = 1$

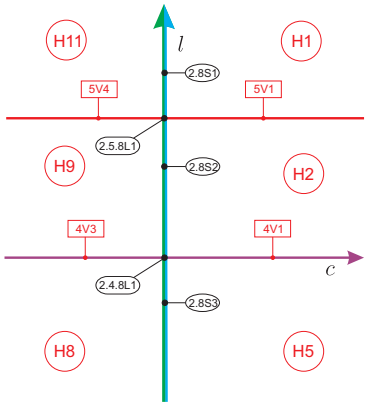

$d = 0, n = 1, m = 1$

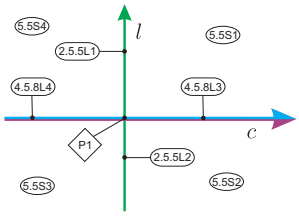

$d = 1, n = 0, m = 0$

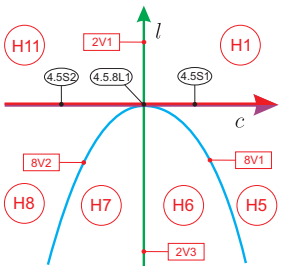

$d = 1, n = 1, m = 0$

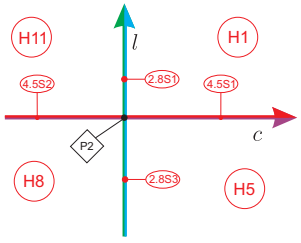

$d = 0, n = 1, m = 0$

Figure 14 – All *cl*–planes of the bifurcation diagram and the corresponding values of the parameters d, m and n

3.6 Other relevant facts about the bifurcation diagram

The bifurcation diagram that we have obtained for the class $\overline{\mathbf{QsnSN_{11}(A)}}$ is completely coherent, i.e. in each plane, by taking any two points in the parameter space and joining them by a continuous curve, along this curve the changes in phase portraits that occur when crossing the different bifurcation surfaces we mention can be completely explained. The same happens when we move from one point of one plane to a close point of another plane.

Nevertheless, we cannot be sure that these bifurcation diagram is the complete bifurcation diagram for $\overline{\mathbf{QsnSN_{11}(A)}}$ due to the possibility of "islands" inside the parts bordered by unmentioned bifurcation sets. In case they exist, these "islands" would not mean any modification of the nature of the singular points.

In case there were more bifurcation sets, we should still be able to join two representatives of any two parts of the 75 parts of $\overline{\mathbf{QsnSN_{11}(A)}}$ found until now with a continuous curve either without crossing such a bifurcation set or, in case the curve crosses it, it must do it an even number of times without tangencies, otherwise one must take into account the multiplicity of the tangency, so the total number must be even. This is why we call these potential bifurcation sets "*islands*". In order to be more precise, we have to answer the following question: which phase portrait could be in such an island? If we consider the phase portraits from Artés, Llibre and Rezende (2018) and from those ones of family (A) of codimension–one (which possess a finite saddle–node $\overline{sn}_{(2)}$, see page 47) and forcing the coalescence of two finite singular points with two different infinite singular points to produce a phase portrait of $\overline{\mathbf{QsnSN_{11}(A)}}$, we can detect up to 8 different phase portraits, in such a way that two of them do not appear here. Under some conditions these phase portraits could live in such an island on the bifurcation diagram. However, using other arguments, it can be proved that they are not realizable. We delay the proof of this fact since this will be the main matter on a future study on the topological classification of all the phase portraits of the class $\mathbf{QsnSN_{11}}$ of *codimension three**.

3.7 Completion of the proof of the main theorem

In the bifurcation diagram we may have topologically equivalent phase portraits belonging to distinct parts of the parameter space. As here we have 75 distinct parts of the parameter space, to help us identify or distinguish phase portraits, we need to introduce some invariants and we actually choose integer valued, character and symbol invariants. Some of them were already used for instance in Artés, Rezende and Oliveira (2015), but we recall them and introduce some needed ones. These invariants yield a classification which is easier to grasp.

First of all we would like to emphasize that due to some values of the parameters, among the 75 phase portraits obtained in the study of the bifurcation diagram, four of them correspond to linear systems (see page 104). These four phase portraits can be clearly divided into two classes as in Fig. 2 (we can distinguish them by considering, for instance, the number of infinite singularities, which is a numeric invariant).

Now we define six invariants I_j, $1 \leq j \leq 6$, that allow us to make the classification of the remaining 71 phase portraits corresponding to quadratic differential systems.

Definition 3.7.1. We denote by $I_1(S)$ the number of the real finite singular points. We note that this number can also be infinity, which is represented by ∞.

Definition 3.7.2. We denote by $I_2(S)$ the number of the real infinite singular points.

Definition 3.7.3. For a given infinite singularity s of a system S, let ℓ_s be the number of global or local separatrices beginning or ending at s and which do not lie on the line at infinity. Then $0 \leq \ell_s \leq 4$. We denote by $I_3(S)$ the sequence of all such ℓ_s when s moves in the set of infinite singular points of system S. We start the sequence at the infinite singular point which receives (or sends) the greatest number of separatrices and take the direction which yields the greatest absolute value, e.g. the values 2110 and 2011 for this invariant are symmetrical (and, therefore, they are the same), so we consider 2110.

Definition 3.7.4. We denote by $I_4(S)$ the total number of local or global separatrices of the finite multiple singular point linking it to the infinite multiple singular points.

Definition 3.7.5. We denote by $I_5(S)$ a character from the set {n,y} describing the nonexistence ("n") or the existence ("y") of elliptic sectors.

Definition 3.7.6. We denote by $I_6(S)$ a symbol from the set $\{[|], [|_2], [\times]\}$ which indicates the following configuration of curves filled up with singularities, respectively: a real straight line, a double real straight line, and two real straight lines intersecting at a finite point. This invariant only makes sense to distinguish the degenerate phase portraits.

Theorem 3.7.7. Consider the class $\overline{\mathbf{QsnSN_{11}(A)}}$ and all the phase portraits that we have obtained for this family. The values of the affine invariant $\mathscr{I} = (I_1, I_2, I_3, I_4, I_5, I_6)$ given in Table 6 yield a partition of these phase portraits of the class $\overline{\mathbf{QsnSN_{11}(A)}}$.

Furthermore, for each value of $\mathscr{I}$ in this diagram there corresponds a single phase portrait; i.e. S and S' are such that $\mathscr{I}(S) = \mathscr{I}(S')$, if and only if S and S' are topologically equivalent.

The bifurcation diagram for $\overline{\mathbf{QsnSN_{11}(A)}}$ has four parts corresponding to two topologically distinct classes of linear systems and also 71 parts corresponding to quadratic ones. As we have said before, the phase portraits corresponding to linear systems can

be easily divided into two different classes, as in Fig. 2. Now we have to work in the classification of the remaining 71 parts. These ones produce 34 topologically different phase portraits as described in Table 7 and the remaining 37 parts do not produce any new phase portrait.

The phase portraits that does not possess graphic have been denoted surrounded by parenthesis, for example $(5V_2)$; the phase portraits having two or more graphics have been denoted surrounded by $\{\{*\}\}$, for example $\{\{P_4\}\}$. Normally we use a single $\{*\}$ when there is just one graphic but this does not happen in the present study.

Proof of Thm. 3.7.7. The mentioned result follows from the results in the previous sections and a careful analysis of the bifurcation planes given in Sec. 3.3, in Figs. 5 to 13, the definition of the invariants I_j and their explicit values for the corresponding phase portraits. □

Regarding the phase portraits corresponding to quadratic systems, in Table 7 we list in the first column 34 parts with all the distinct phase portraits of Fig. 3. Corresponding to each part listed in the first column we have in each row all parts whose phase portraits are topologically equivalent to the phase portrait appearing in the first column of the same row.

In the second column we set all the parts whose systems yield topologically equivalent phase portraits to those in the first column, but which are identical under perturbations.

In the third column we list all parts whose phase portraits possess an invariant curve not yielding a connection of separatrices.

In the fourth column we add the phase portraits, topologically equivalent to those ones from the first column, which corresponds to symmetric parts of the bifurcation diagram.

The last column refers to other reasons associated to different geometric aspects and they are described as follows:

1. the phase portrait possesses a singularity of type $\widehat{\binom{2}{3}}\,PP - PP$ at infinity;
2. the coincidence described in Rmk. 3.5.1.

Whenever phase portraits appear in a row in a specific column, the listing is done according to the decreasing dimension of the parts where they appear, always placing the lower dimensions on lower rows.

Regarding the linear differential systems obtained in this study which correspond to the parts $4.5.8L_3, 4.5.8L_4, P_1, P_5$ of the bifurcation diagram (see Figs. 10 and 12), as we

have mentioned before, we can split them into two different classes as in Fig. 2. By considering, for instance, the number of infinite singularities we obtain that $4.5.8L_3, 4.5.8L_4, P_5$ have two distinct infinite singularities whereas P_1 has only one infinite singularity. Therefore we conclude the classification of all phase portraits obtained by the study of the class $\overline{\mathbf{QsnSN_{11}(A)}}$ with respect to the canonical form (3.2).

Table 6 – Geometric classification for the family $\mathbf{QsnSN_{11}(A)}$

$$
I_1 = \left\{
\begin{array}{l}
1 \,\&\, I_2 = \left\{
\begin{array}{l}
1 \,\&\, I_3 = \left\{
\begin{array}{l}
11\ (2V_1),\\
21\ (H_1),
\end{array}\right.\\
2 \,\&\, I_3 = \left\{
\begin{array}{l}
1110 \,\&\, I_4 = \left\{
\begin{array}{l}
2\ (4.5S_1),\\
3\ \{\{4.5S_3\}\},
\end{array}\right.\\
2100\ (5.7S_1),\\
2101 \,\&\, I_4 = \left\{
\begin{array}{l}
1\ (5V_1),\\
2\ \{\{2.5S_2\}\},\\
3\ \{\{5V_6\}\},
\end{array}\right.\\
2200\ (2.5S_1),\\
2210\ \{\{5V_7\}\},\\
3101\ \{\{5V_5\}\},\\
3200 \,\&\, I_4 = \left\{
\begin{array}{l}
1\ (5V_2),\\
2\ (5V_3),
\end{array}\right.
\end{array}\right.\\
3 \,\&\, I_3 = \left\{
\begin{array}{l}
111010\ (4V_1),\\
111110\ (H_5),\\
210110\ (4V_2),\\
211010\ (7V_1),\\
211110 \,\&\, I_4 = \left\{
\begin{array}{l}
1\ (H_2),\\
2\ (H_3),
\end{array}\right.\\
220110\ (2V_3),\\
311010\ (2V_2),\\
320110\ (H_6),\\
321010\ (H_{10}),\\
411010\ (H_4),
\end{array}\right.
\end{array}\right.\\
\infty \,\&\, I_2 = \left\{
\begin{array}{l}
1 \,\&\, I_5 = \left\{
\begin{array}{l}
\text{n}\ \{\{P_4\}\},\\
\text{y}\ \{\{8.9.9L_1\}\},
\end{array}\right.\\
2 \,\&\, I_3 = \left\{
\begin{array}{l}
0000 \,\&\, I_5 = \left\{
\begin{array}{l}
\text{n} \,\&\, I_6 = \left\{
\begin{array}{l}
[|]\ (4.5.8L_1),\\
[|_2]\ (2.5.8L_1),\\
[\times]\ \{\{2.8.9L_1\}\},
\end{array}\right.\\
\text{y}\ \{\{5.8S_2\}\},
\end{array}\right.\\
1000\ \{\{8.9S_1\}\},\\
1010\ \{\{5.8S_1\}\},
\end{array}\right.\\
3 \,\&\, I_3 = \left\{
\begin{array}{l}
000000\ \{\{2.8S_2\}\},\\
100000\ \{\{8V_1\}\}.
\end{array}\right.
\end{array}\right.
\end{array}\right.
$$

Table 7 – Topological equivalences for the family **QsnSN$_{11}$(A)**

Presented phase portrait	Identical under perturbations	Possessing invariant curve (no separatrix)	Symmetry	Other reasons
H_1	H_{11}			$5.5S_1{}^{(1)}$, $5.5S_2{}^{(1)}$, $5.5S_3{}^{(1)}$, $5.5S_4{}^{(1)}$
H_2	H_9			
H_3				
H_4				
H_5	H_8			
H_6	H_7			
H_{10}				
$2V_1$				$2.8S_1{}^{(2)}$ $2.5.5L_1{}^{(1)}$, $2.5.5L_2{}^{(1)}$
$2V_2$				
$2V_3$				
$4V_1$	$4V_3$			
$4V_2$				
$5V_1$	$5V_4$			
$5V_2$				
$5V_3$				
$5V_5$			$5V_8$	
$5V_6$			$5V_9$	
$5V_7$			$5V_{10}$	
$7V_1$				
$8V_1$	$8V_2$, $8V_3$, $8V_4$	$4.8S_1$, $4.8S_2$		
$2.5S_1$				
$2.5S_2$			$2.5S_3$	
$2.8S_2$	$2.8S_3$	$2.4.8L_1$		
$4.5S_1$			$4.5S_2$	
$4.5S_3$			$4.5S_4$	
$5.7S_1$				
$5.8S_1$				
$5.8S_2$		$4.5.8L_2$	$5.8S_3$	
$8.9S_1$		$4.8.9L_1$, $4.8.9L_2$	$8.9S_2$, $8.9S_3$, $8.9S_4$	
$2.5.8L_1$	P_2			
$2.8.9L_1$		P_3	$2.8.9L_2$	
$4.5.8L_1$				
$8.9.9L_1$			$8.9.9L_2$	
P_4				

CHAPTER

4

CLASSIFICATION OF QUADRATIC SYSTEMS WITH A FINITE SADDLE–NODE AND AN INFINITE SADDLE–NODE (1,1)SN–(B)

In this chapter we present a study of a three–dimensional bifurcation diagram which provides all the representatives for the topological classification of phase portraits belonging to the set (AC), as we see in Chap. 5.

4.1 Introduction and statement of the results

As we have said in the previous chapter, one of the main goals of this thesis is to present the study of the class of all quadratic systems possessing a finite saddle–node $\overline{sn}_{(2)}$ located at the origin of the plane and an infinite saddle–node of type $\overline{\binom{1}{1}}\,SN$. In the previous chapter we have studied family $\mathbf{QsnSN_{11}(A)}$ of all phase portraits possessing a finite saddle–node as the only finite singularity. In this chapter we present the study of family $\mathbf{QsnSN_{11}(B)}$ of phase portraits possessing the finite saddle–node and also a simple finite elemental singularity.

For this study we follow the same pattern as we did in the previous chapter. Moreover, as we have said before, all the generic phase portraits obtained here belong to the set (AC). Additionally, we will see in the next chapter that all the phase portraits belonging to the generic regions of the bifurcation diagram presented in this chapter provide examples for the realization of all the phase portraits from the set (AC).

In the normal form (4.1), see page 119, the class $\overline{\mathbf{QsnSN_{11}(B)}}$ is partitioned into 631 parts: 112 three–dimensional ones, 265 two–dimensional ones, 203 one–dimensional

ones and 51 points. This partition is obtained by considering all the bifurcation surfaces of singularities, one related to the presence of invariant straight lines, one related to connections of separatrices and one related to the presence of a double limit cycle, modulo "islands" (see Sec. 4.4).

We point out that we cannot have a global result about the number of limit cycles that a phase portrait may have. But we can assure that, in some places of the bifurcation diagram, the corresponding phase portraits have a specific number of limit cycles or even a quantity with identical parity (taking into account the multiplicity of limit cycles). More precisely, as we may find an island inside the parameter space for which in its border there exists a double limit cycle and inside the island there are two more limit cycles, all the claims regarding limit cycles always must be formulated with respect to the minimum number of limit cycles (proved to exist), but always having the possibility of the existence of "more" limit cycles, keeping the parity.

Theorem 4.1.1. There are 226 topologically distinct phase portraits for the closure of the family of quadratic vector fields having a finite saddle–node $\overline{sn}_{(2)}$, a finite elemental singularity and an infinite saddle–node of type $\overline{\binom{1}{1}}SN$, and given by the normal form (4.1) (class $\overline{\mathbf{QsnSN_{11}(B)}}$). The bifurcation diagram for this class is given in the parameter space which is the projective three–dimensional space $\mathbb{RP}^3$. All these phase portraits are shown in Figs. 15 to 21. Also the following statements hold:

(a) there are 147 topologically distinct phase portraits in $\mathbf{QsnSN_{11}(B)}$;

(b) there are 32 phase portraits possessing exactly one simple limit cycle (or an odd number of them taking into account their multiplicity), and they are in the parts V_{25}, V_{48}, V_{52}, V_{57}, V_{60}, V_{72}, V_{75}, V_{78}, V_{101}, V_{104}, V_{106}, $2S_{11}$, $2S_{13}$, $4S_{38}$, $4S_{64}$, $4S_{67}$, $5S_{13}$, $5S_{20}$, $5S_{23}$, $5S_{26}$, $5S_{32}$, $5S_{34}$, $7S_{15}$, $7S_{23}$, $9S_{16}$, $9S_{17}$, $9S_{18}$, $2.5L_5$, $4.5L_{13}$, $4.5L_{15}$, $5.7L_8$, $5.9L_3$;

(c) there are three phase portraits with exactly two simple limit cycles (or an even number of them taking into account their multiplicity) surrounding the same focus, and they are in the parts V_{107}, V_{110}, $7S_{24}$;

(d) there is one phase portrait with exactly three simple limit cycles (or a greater odd number of them taking into account their multiplicity) surrounding the same focus, and it is in the part V_{109};

(e) there are two phase portraits possessing one double limit cycle (and no signs of other limit cycles), and they are in the parts $10S_1$, $10S_3$;

(f) there is one phase portrait possessing one double limit cycle and one simple limit cycle (and no signs of other limit cycles) both surrounding the same focus, and it is in the part $10S_2$;

(g) there are 45 phase portraits with exactly one nondegenerate graphic surrounding a focus. These phase portraits are in the parts V_{26}, V_{49}, V_{53}, V_{102}, $4S_{65}$, $5S_{14}$, $5S_{15}$, $5S_{16}$, $5S_{17}$, $5S_{18}$, $5S_{19}$, $5S_{33}$, $7S_3$, $7S_4$, $7S_6$, $7S_7$, $7S_8$, $7S_{11}$, $7S_{13}$, $7S_{14}$, $7S_{22}$, $9S_{21}$, $2.5L_4$, $2.7L_1$, $4.4L_{12}$, $4.5L_8$, $4.5L_9$, $4.5L_{14}$, $5.7L_2$, $5.7L_3$, $5.7L_4$, $5.7L_5$, $5.7L_6$, $5.7L_7$, $5.7L_{11}$, $5.9L_4$, $5.9L_5$, $7.7L_1$, $7.9L_5$, $7.9L_7$, P_7, P_{14}, P_{20}, P_{49}, P_{50}. We highlight that phase portrait $7S_{14}$ is topologically equivalent to phase portrait corresponding to the part P_{27} of the bifurcation diagram (see Table 26), and for this last phase portrait the weak focus is of order two;

(h) there is one phase portrait, namely $7S_{23}$, which possesses one nondegenerate graphic and one simple limit cycle, both surrounding the same focus. This phase portrait is topologically equivalent to phases portraits corresponding to the parts $3.7L_4$ and $3.7L_5$ of the bifurcation diagram (see Table 26), and for each one of these two phase portraits the weak focus is of order one;

(i) there is one phase portrait, namely $7S_{24}$, which possesses one nondegenerate graphic and two simple limit cycles, all of them surrounding the same focus;

(j) there is one phase portrait, namely $7.10L_1$, which possesses one nondegenerate graphic and a double limit cycle, both surrounding the same focus;

(k) there are 18 phase portraits having an infinite family of nondegenerate graphics (with no singularity inside), and these phase portraits are in the parts $9S_3$, $9S_5$, $9S_7$, $9S_{10}$, $9S_{11}$, $9S_{29}$, $9S_{30}$, $9S_{33}$, $9S_{35}$, $9S_{36}$, $2.9L_1$, $2.9L_3$, $2.9L_4$, $4.9L_1$, $4.9L_6$, $4.9L_7$, $7.9L_1$, $7.9L_8$;

(l) phase portraits $9S_{16}$ and $9S_{17}$ possess an infinite family of nondegenerate graphics (with no singularity inside) and also a simple limit cycle;

(m) there are four phase portraits possessing an infinite family of nondegenerate graphics (with no singularity inside) and also another nondegenerate graphic which surrounds a focus. These phase portraits are in the parts $9S_{19}, 9S_{20}, 7.9L_3, 7.9L_4$;

(n) phase portraits $9S_{22}$ and $7.9L_6$ possess two distinct infinite families of nondegenerate graphics, one of them with all the graphics surrounding the same focus and the other having no singularities inside the graphics;

(o) phase portrait $4.9L_4$ possesses two infinite families of nondegenerate graphics (with no singularity inside) plus another nondegenerate graphic which surrounds a focus;

(p) phase portrait $4.9L_5$ possesses three distinct infinite families of nondegenerate graphics, one of them with all the graphics surrounding the same focus and the other two families having no singularities inside the graphics;

(q) there are three phase portraits possessing two infinite families of nondegenerate graphics and there are no singularities inside the graphics. These phase portraits are in the parts $9S_1, 9S_{27}, 9S_{28}$;

(r) there are seven phase portraits with infinite families of degenerate graphics. In fact, such degenerate graphics exist due to a presence of curves filled up with singularities. More precisely:

(r_1) phase portraits $8S_1$ and $5.8L_1$ possess a hyperbola filled up with singularities;

(r_2) phase portraits $9.9L_1$ and P_{29} possess a parabola filled up with singularities;

(r_3) phase portraits $4.8L_1$ and P_3 possess two real straight lines, filled up with singularities, intersecting at a finite point;

(r_4) phase portrait P_{36} possesses the line at infinity filled up with singularities.

Proposition 4.1.2. There are 40 topologically distinct phase portraits of codimension two, modulo limit cycles, in the family $\mathbf{QsnSN_{11}(B)}$.

Corollary 4.1.3. In Table 8 we give the numbers of phase portraits of both families $\mathbf{QsnSN_{11}(B)}$ and its closure for special types of phase portraits.

Corollary 4.1.4. There exist two topologically distinct phase portraits which appear simultaneously in both classes $\overline{\mathbf{QsnSN_{11}(A)}}$ (described in Artés, Mota and Rezende (2021a) and also in the previous chapter) and $\overline{\mathbf{QsnSN_{11}(B)}}$. The correspondences are indicated in Table 9 and the phase portraits in each row are topologically equivalent.

For family $\mathbf{QsnSN_{11}(B)}$, from its 148 topologically different phase portraits, 54 occur in three–dimensional parts, 67 in two–dimensional parts, 24 in one–dimensional parts and three occur in a zero–dimensional parts.

For the border of $\mathbf{QsnSN_{11}(B)}$, from its 78 topologically different phase portraits, 37 occur in two–dimensional parts, 34 in one–dimensional parts and seven occur in zero–dimensional parts.

In Figs. 15 to 21 we have illustrated all the singularities with a small disc. In case of degenerate systems we have also illustrated the infinite singular point belonging to the degenerate set with a small disc only if this point is an infinite singularity of the reduced system. We have drawn with thicker curves the separatrices and we have added some thinner orbits to avoid confusion in some cases.

We have drawn all the limit cycles (and loops) possessing a convex shape (see Lemma 3.31 from Artés, Llibre and Rezende (2018)). The limit cycle is colored in red if it is simple (as in Artés, Rezende and Oliveira (2015), for instance) and it is colored in dark green if it is double. In addition, all the graphics are colored in blue. We notice that weak foci are graphics reduced to a point, so the weak foci could be included in the definition

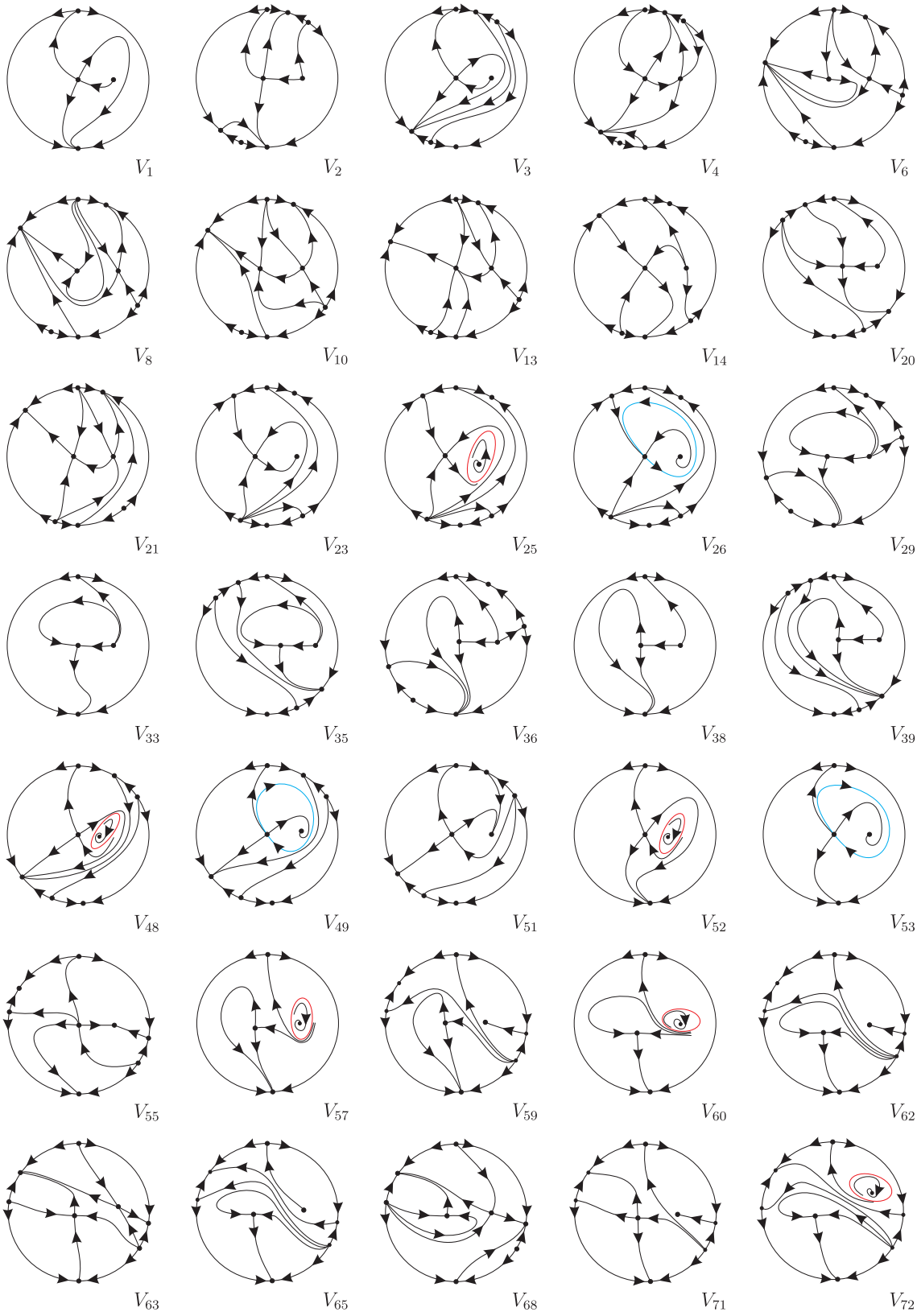

Figure 15 – Phase portraits for quadratic vector fields with a finite saddle–node $\overline{sn}_{(2)}$, a finite elemental singularity and an infinite saddle–node of type $\overline{\binom{1}{1}}$ *SN*, from class $\overline{\mathbf{QsnSN_{11}(B)}}$

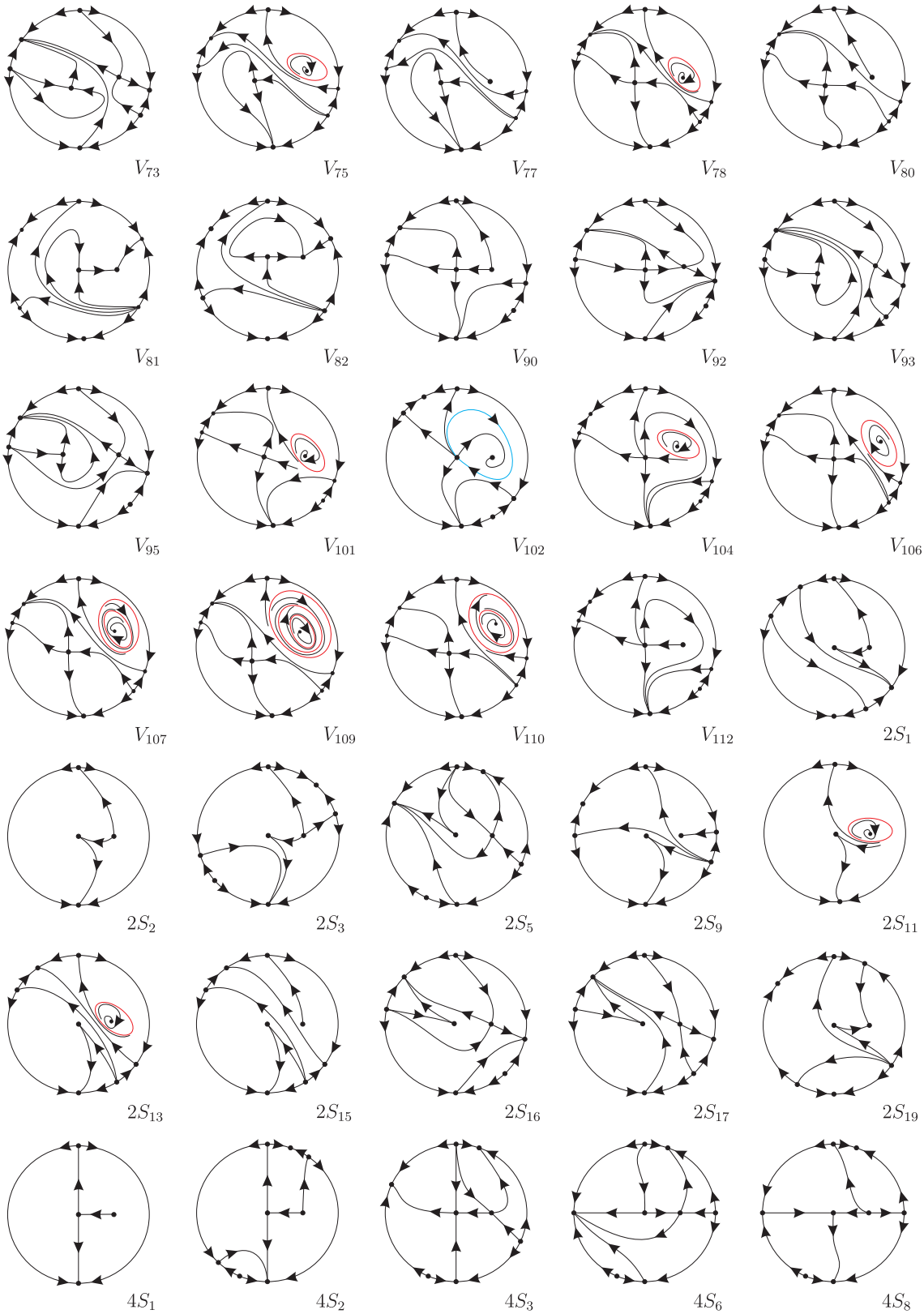

Figure 16 – Continuation of Fig. 15

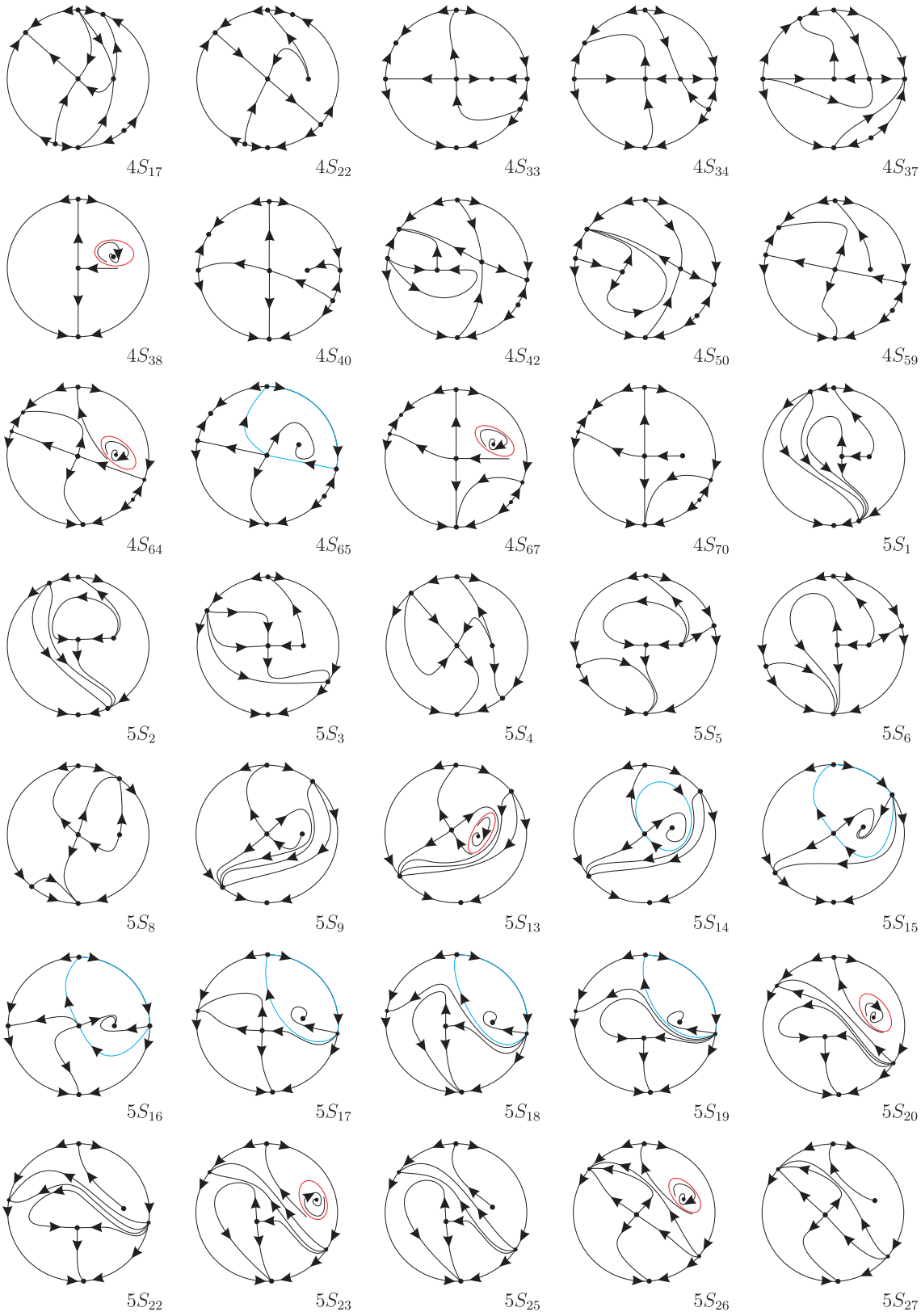

Figure 17 – Continuation of Fig. 16

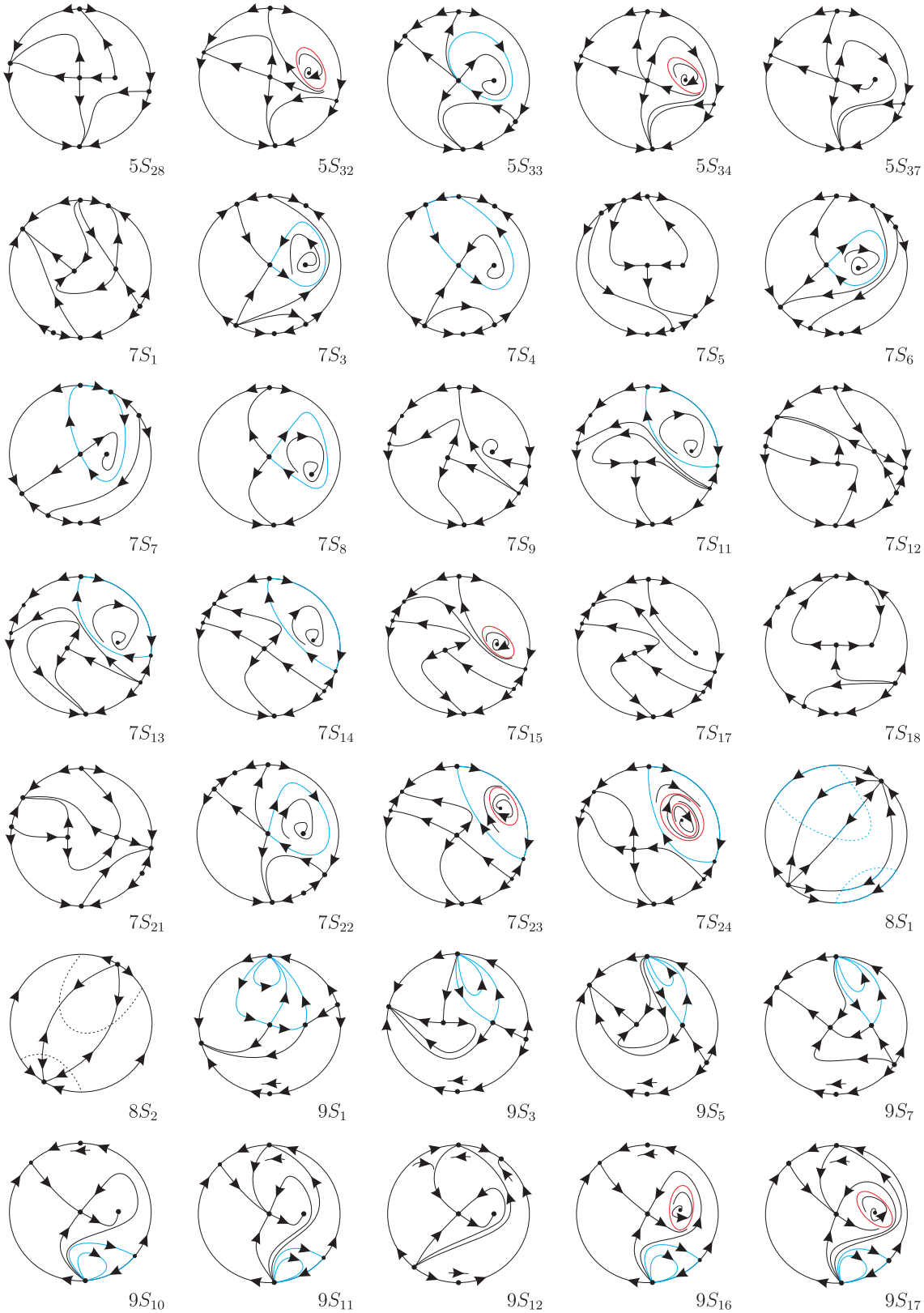

Figure 18 – Continuation of Fig. 17

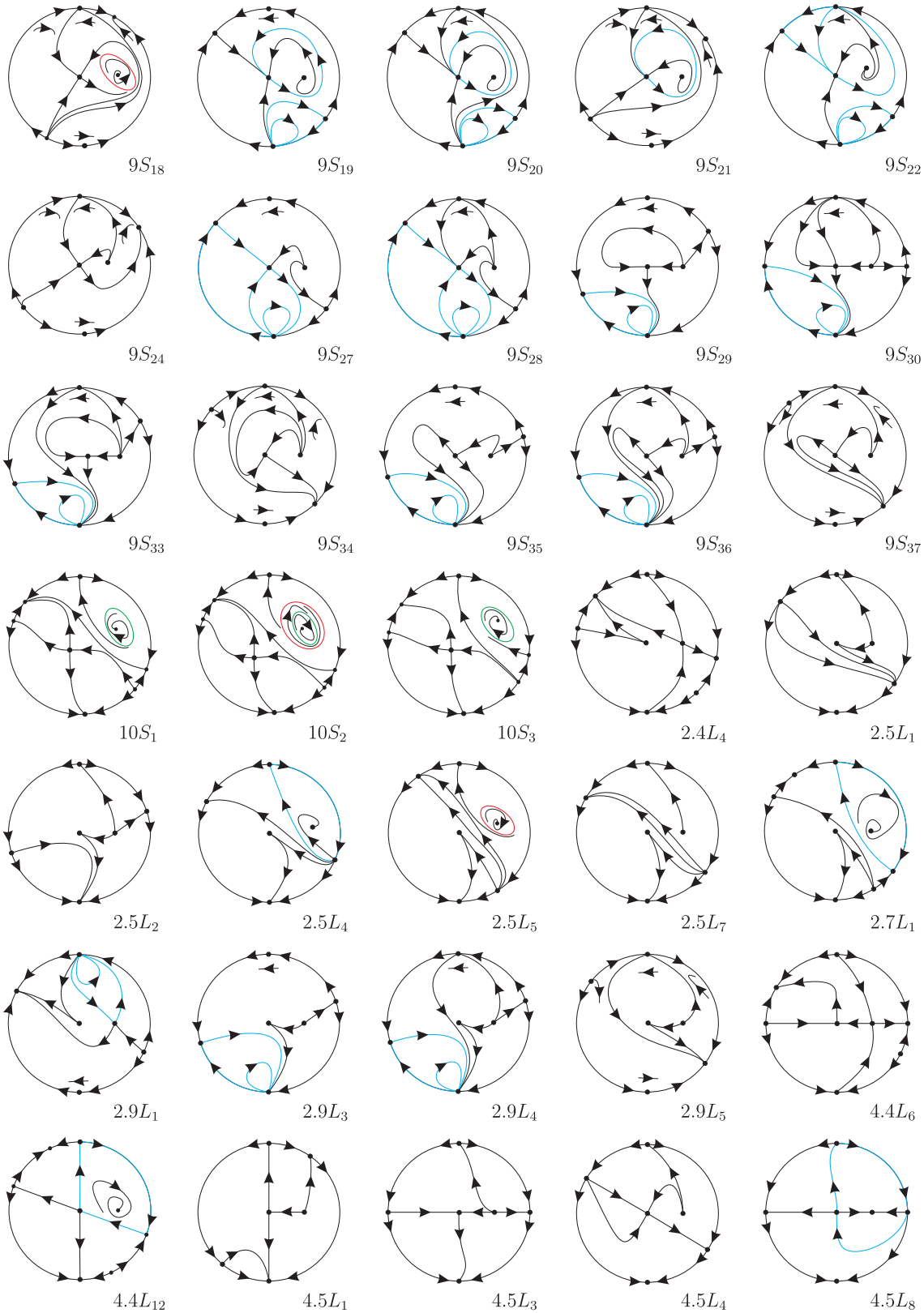

Figure 19 – Continuation of Fig. 18

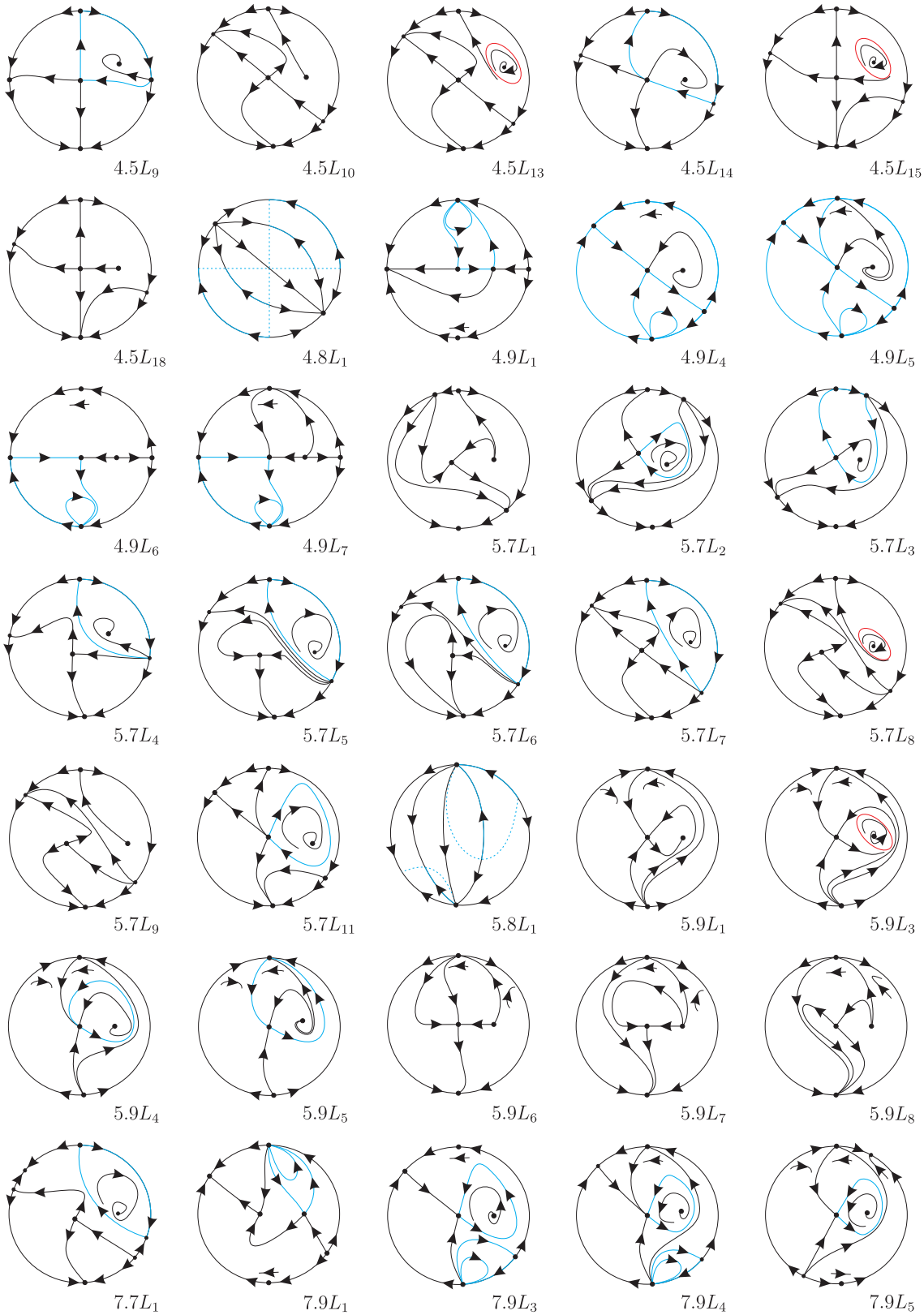

Figure 20 – Continuation of Fig. 19

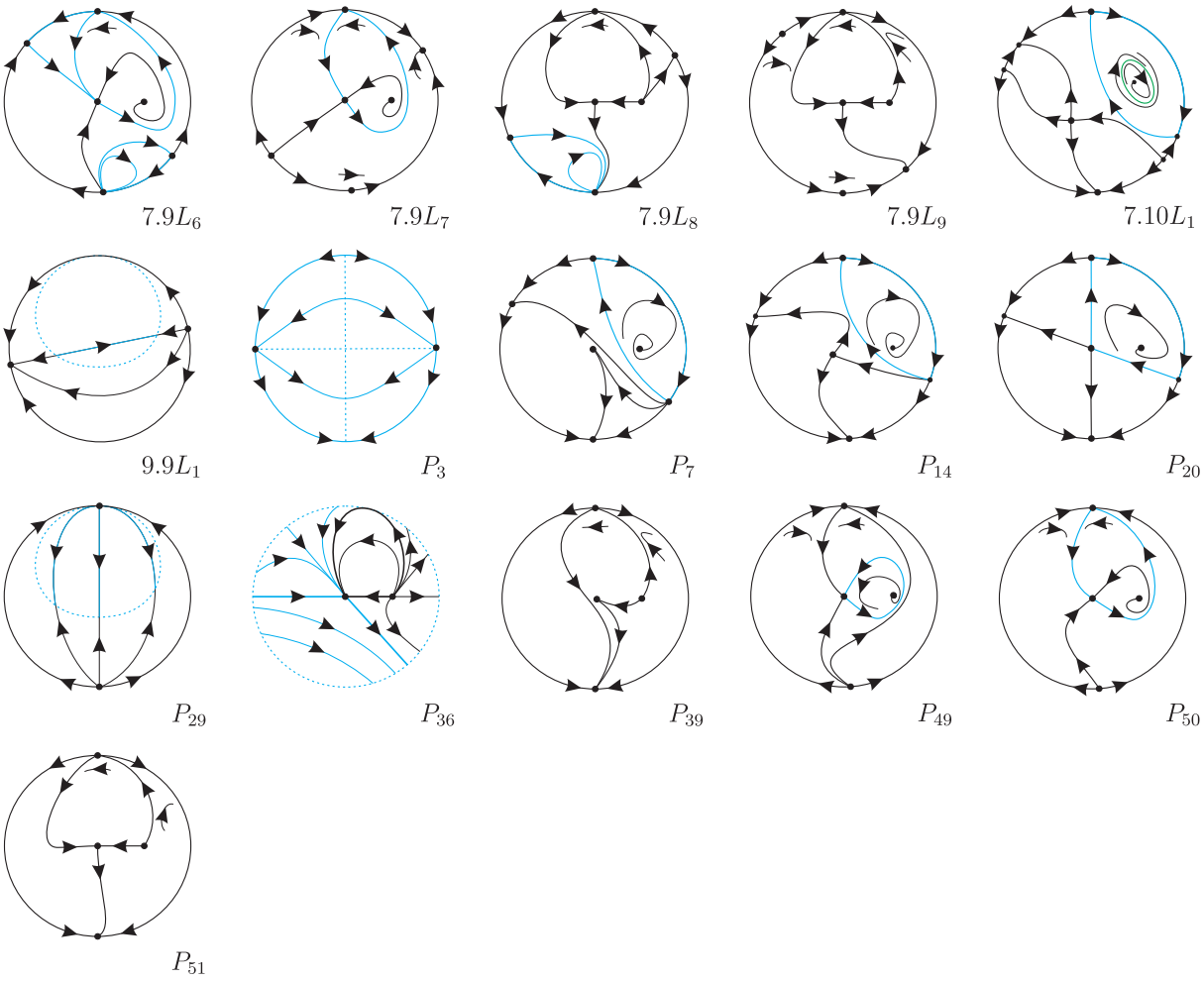

Figure 21 – Continuation of Fig. 20

of graphics and then we should have colored them in blue. However, in order to follow the same pattern as in previous similar studies and according to our definition of graphics we keep all of them in black.

Remark 4.1.5. We label the phase portraits according to the parts of the bifurcation diagram where they occur. Here we call *volumes* (V) the three–dimensional parts of the bifurcation diagram, *surfaces* (S) the two–dimensional ones, *curves* (L) the one–dimensional ones, and *points* (P) the zero–dimensional ones. These labels could be different for two topologically equivalent phase portraits occurring in distinct parts. Some of the phase portraits in three–dimensional parts also occur in some lower dimensional parts bordering these three–dimensional parts. An example occurs when a node turns into a focus. An analogous situation happens for phase portraits in two–dimensional or one–dimensional parts, coinciding with some phase portraits situated on their border. Moreover, as in Artés, Llibre and Schlomiuk (2006) and Artés, Rezende and Oliveira (2015), we use the same pattern in order to indicate the elements (V), (S), (L) and (P) in the bifurcation diagram.

Table 8 – Comparison between the set $\mathbf{QsnSN_{11}(B)}$ and its border (the numbers represent the absolute values in each subclass)

	$\mathbf{QsnSN_{11}(B)}$	Border of $\mathbf{QsnSN_{11}(B)}$
Distinct phase portraits	147	79
Phase portraits with exactly one simple limit cycle	25	7
Phase portraits with exactly two simple limit cycles	3	0
Phase portraits with exactly three simple limit cycles	1	0
Phase portraits with exactly one double limit cycle	2	0
Phase portraits with one double limit cycle and one simple limit cycle	1	0
Phase portraits with exactly one nondegenerate graphic	38	10
Phase portraits with at least one infinite family of nondegenerate graphics	0	31
Phase portraits with degenerate graphics	0	7

Table 9 – Topological equivalence between phase portraits from classes $\overline{\mathbf{QsnSN_{11}(A)}}$ and $\overline{\mathbf{QsnSN_{11}(B)}}$

$\overline{\mathbf{QsnSN_{11}(A)}}$	$\overline{\mathbf{QsnSN_{11}(B)}}$
$2.8S_2$	$4.8L_1$
$2.8.9L_1$	P_3

This chapter is organized as follows. In Sec. 4.2 we describe the normal form for the family of quadratic systems having a finite saddle–node, a simple finite elemental singularity and an infinite saddle–node of type $\overline{\binom{1}{1}}SN$.

In Sec. 4.3, by considering some T–comitants and invariants for quadratic systems as used in Sibirsky's School, we construct the bifurcation surfaces for the class $\overline{\mathbf{QsnSN_{11}(B)}}$.

In Sec. 4.4 we discuss about the possible existence of "islands" in the bifurcation diagram.

In Sec. 4.5 we introduce a global invariant denoted by $\mathscr{I}$, which classifies completely, up to topological equivalence, the phase portraits that we have obtained for the

systems in the class $\overline{\mathbf{QsnSN_{11}(B)}}$. Thm. 4.5.15 shows clearly that they are uniquely determined (up to topological equivalence) by the values of the invariant $\mathscr{I}$.

4.2 Quadratic vector fields with a finite saddle–node $\overline{sn}_{(2)}$, a finite elemental singularity and an infinite saddle–node of type $\overline{\binom{1}{1}}\,SN$

In Artés, Llibre and Vulpe (2008) the authors have constructed the normal form for quadratic systems possessing one double and one simple real finite singularities. In what follows we present an idea of such a construction.

Proposition 4.2.1. Every non–degenerate quadratic system with a finite semi–elemental double saddle–node $\overline{sn}_{(2)}$, a finite elemental singularity and an infinite saddle–node of type $\overline{\binom{1}{1}}\,SN$ can be brought via an affine transformation to the following normal form

$$\begin{aligned} \dot{x} &= cx + cy - cx^2 + 2hxy, \\ \dot{y} &= ex + ey - ex^2 + 2mxy, \end{aligned} \tag{4.1}$$

where c, e, h, m are real parameters and $eh \neq cm$.

Proof. We know that a quadratic system (1) can always be written into the form

$$\begin{aligned} \dot{x} &= p_0 + p_1(x,y) + p_2(x,y) \equiv p(x,y), \\ \dot{y} &= q_0 + q_1(x,y) + q_2(x,y) \equiv q(x,y) \end{aligned}$$

with homogeneous polynomials p_i and q_i $(i = 0,1,2)$ of degree i in x, y:

$$\begin{aligned} p_0 = a_{00}, \quad p_1(x,y) = a_{10}x + a_{01}y, \quad p_2(x,y) = a_{20}x^2 + 2a_{11}xy + a_{02}y^2, \\ q_0 = b_{00}, \quad q_1(x,y) = b_{10}x + b_{01}y, \quad q_2(x,y) = b_{20}x^2 + 2b_{11}xy + b_{02}y^2. \end{aligned}$$

We start supposing that such systems possess four real finite distinct singularities. Assume that one finite singularity has gone to infinity. Then the quadratic polynomials $p_2(x,y)$ and $q_2(x,y)$ have a linear common factor of the form $\alpha x + \beta y$. So this infinite singularity is of the form $N[-\beta : \alpha : 0]$ and via a rotation we can assume that this point is located on the direction $x = 0$, i.e. x is a factor of $p_2(x,y)$ and $q_2(x,y)$. Then, for these systems we can take $a_{02} = b_{02} = 0$. Now, since these systems possess three real finite distinct singularities, we can apply a translation in such a way that one of these singularities can be moved to the origin, i.e. we can assume $a_{00} = b_{00} = 0$. Therefore we obtain the systems:

$$\begin{aligned} \dot{x} &= a_1x + b_1y + c_1x^2 + 2d_1xy, \\ \dot{y} &= a_2x + b_2y + c_2x^2 + 2d_2xy, \end{aligned} \tag{4.2}$$

which, besides the point $M_1(0,0)$, have two other distinct real singularities $M_i(x_i,y_i)$ for $i\in\{2,3\}$. We observe that for systems (4.2), if $x_{2,3}=0$ then we obtain

$$p(0,y_{2,3})=b_1y_{2,3}=0,\quad q(0,y_{2,3})=b_2y_{2,3}=0,$$

and since $y_{2,3}\neq 0$ (otherwise we would have a triple point at the origin) we have $b_1=b_2=0$. This implies that systems (4.2) are degenerate. So we can assume $x_2\neq 0$. Performing the linear transformation

$$\bar{x}=\frac{x}{x_2},\quad \bar{y}=y,\quad \text{if}\quad y_2=0,$$

and

$$\bar{x}=\frac{x}{x_2},\quad \bar{y}=x-\frac{x_2}{y_2}y,\quad \text{if}\quad y_2\neq 0,$$

we keep the form (4.2) and clearly we locate the point $M_2(x_2,y_2)$ at the point $M_2(1,0)$. Imposing that $M_2(x_2,y_2)=(1,0)$ we obtain $a_1=-c_1$ and $a_2=-c_2$. These equalities allow us to write systems (4.2) into the form

$$\begin{aligned}\dot{x}&=a_1x+b_1y-a_1x^2+2d_1xy,\\ \dot{y}&=a_2x+b_2y-a_2x^2+2d_2xy,\end{aligned}\tag{4.3}$$

which have three finite singularities: $M_1(0,0)$, $M_2(1,0)$ and $M_3(x_3,y_3)$. Calculations show that M_3 has the coordinates

$$x_3=\frac{d_{23}}{2d_{45}},\quad y_3=\frac{d_{23}(2d_{45}-d_{23})}{4d_{35}d_{45}},$$

where

$$d_{23}=a_2b_1-a_1b_2,\quad d_{35}=b_1d_2-b_2d_1,\quad d_{45}=a_2d_1-a_1d_2,$$

verifying $d_{23}d_{35}d_{45}(2d_{45}-d_{23})\neq 0$ (i.e. the points are finite and distinct).
For systems (4.3), we observe that $a_1^2+a_2^2\neq 0$, otherwise $d_{23}=0=d_{45}$ what contradicts the previous condition. Finally, in order to have a double finite singularity at the origin, i.e. forcing the point $M_1(0,0)$ to be double, without loss of generality we can make $d_{23}=0$ by taking $b_1=a_1$ and $b_2=a_2$. Therefore, by renaming the coefficients $a_1\to c$, $d_1\to h$, $a_2\to e$, $d_2\to m$, we arrive at normal form (4.1) that we were looking for. Moreover, since $d_{35}d_{45}=-(eh-cm)^2\neq 0$, we conclude that such systems are non–degenerate if and only if $eh-cm\neq 0$. □

In order to complete the study of the closure of family **QsnSN$_{11}$(B)** within the set of representatives of **QsnSN$_{11}$(B)** in the parameter space of normal form (4.1) it is necessary to consider also the case $h=0$.

The next result assures the existence of invariant straight lines under certain conditions for systems (4.1).

Lemma 4.2.2. A non–degenerate system (4.1) possesses the following invariant straight line if and only if the corresponding condition is satisfied:

(i) $\{x=0\} \Leftrightarrow c=0$;

(ii) $\{y=0\} \Leftrightarrow e=0$;

(iii) $\{x=1\} \Leftrightarrow h=-c/2$;

(iv) $\{y=-x\} \Leftrightarrow h=-(c+e+2m)/2$.

Proof. We consider the algebraic curves

$$\begin{aligned} f_1(x,y) &\equiv x=0,\\ f_2(x,y) &\equiv y=0,\\ f_3(x,y) &\equiv x-1=0,\\ f_4(x,y) &\equiv x+y=0, \end{aligned}$$

and we show that the polynomials

$$\begin{aligned} K_1(x,y) &= 2hy,\\ K_2(x,y) &= 2mx,\\ K_3(x,y) &= -c(x+y),\\ K_4(x,y) &= -(c+e)(x-1), \end{aligned}$$

are the cofactors of $f_1=0$, $f_2=0$, $f_3=0$ and $f_4=0$, respectively, after restricting systems (4.1) to the respective conditions. □

We observe that systems (4.1) depend on four real parameters, namely, c, e, h and m. Then, the corresponding bifurcation diagram is actually the four–dimensional Euclidean space $\mathbb{R}^4$. Since the case $c=e=h=m=0$ corresponds to the null system and it does not belong to our family, we can consider the real projective space $\mathbb{RP}^3$. In what follows we describe how we do this study.

Systems (4.1) depend on the parameter $\lambda=(c,e,h,m)\in\mathbb{R}^4$. We consider systems (4.1) which are nonzero, i.e. $\lambda=(c,e,h,m)\neq 0$. In this case, systems (4.1) can be rescaled with the time rescaling $(x,y,t)\to(x,y,t/\alpha)$, $\alpha\neq 0$. In fact, applying this transformation we obtain

$$\begin{aligned} \dot{x} &= \alpha' cx+\alpha' cy-\alpha' cx^2+2\alpha' hxy,\\ \dot{y} &= \alpha' ex+\alpha' ey-\alpha' ex^2+2\alpha' mxy, \end{aligned}$$

for $\alpha'=1/\alpha$, $\alpha\neq 0$. Then, this transformation takes the systems with parameters (c,e,h,m) to systems with parameters $(\alpha' c,\alpha' e,\alpha' h,\alpha' m)$, with $\alpha'=1/\alpha$. Hence, instead of considering as a parameter space the set $\mathbb{R}^4$ we may consider the real projective space $\mathbb{RP}^3$. The three–dimensional projective space $\mathbb{RP}^3$ can be viewed as the quotient space $\mathbb{S}^3/_\sim$ of $\mathbb{S}^3$ by the equivalence relation: (c,e,h,m) is equivalent to itself or to $(-c,-e,-h,-m)$. So, our parameter is $[\lambda]=[c:e:h:m]\in\mathbb{RP}^3=\mathbb{S}^3/_\sim$. Since for $\alpha'=-1$ the signs of all the

parameters change, we may consider $h \geq 0$ in $[c:e:h:m]$. Since $c^2+e^2+h^2+m^2=1$, then $h=\sqrt{1-(c^2+e^2+m^2)}$, where $0 \leq c^2+e^2+m^2 \leq 1$.

We can therefore view the parameter space as a ball: $\overline{\mathscr{B}} = \{(c,e,m) \in \mathbb{R}^3; c^2+e^2+m^2 \leq 1\}$ where on the equator two opposite points are identified. When $m=0$, we identify the point $[c:e:h:\ 0] \in \mathbb{RP}^3$ with $[c:e:h] \in \mathbb{RP}^2$. So, this subset $\{m=0\} \subset \overline{\mathscr{B}}$ can be identified with $\mathbb{RP}^2$, which can be viewed as a disc with two opposite points on the circumference (the equator) identified (see Fig. 22).

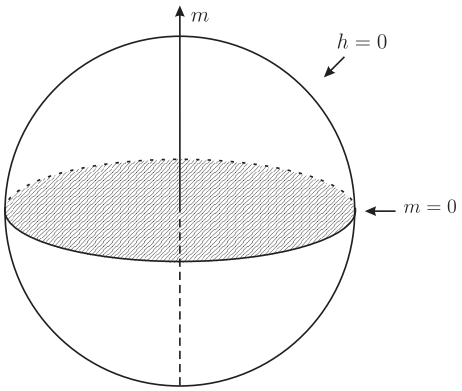

Figure 22 – The parameter space

For $h \neq 0$, we get the affine chart:

$$\begin{aligned} &\mathbb{RP}^3 \setminus \{h=0\} \leftrightarrow \mathbb{R}^3 \\ &[c:e:h:m] \to \left(\frac{c}{h}, \frac{e}{h}, \frac{m}{h}\right) = (\overline{c}, \overline{e}, \overline{m}) \\ &[\overline{c}:\overline{e}:1:\overline{m}] \leftarrow (\overline{c}, \overline{e}, \overline{m}). \end{aligned}$$

The plane $h=0$ in $\mathbb{RP}^3$ corresponds to the equation $c^2+e^2+m^2=1$ (the full sphere $\mathbb{S}^2$) and the line $h=m=0$ in $\mathbb{RP}^3$ corresponds to the equation $c^2+e^2=1$ (the equator $m=0$ of $\mathbb{S}^2$).

We now consider planes in $\mathbb{R}^3$ of the form $\overline{m}=m_0$, where m_0 is a constant. The projective completion of such a plane in $\mathbb{RP}^3$ has the equation $m-m_0h=0$. So we see how the slices $\overline{m}=m_0$ need to be completed in the ball (see Fig. 23). We note that when $h=0$ necessarily we must have $m=0$ on such a slice, and thus the completion of the image of the plane $\overline{m}=m_0$, when visualized in $\mathbb{S}^3$, must include the equator.

The specific equations of the correspondence of the points in the plane $\overline{m}=m_0$ of $\mathbb{R}^3$ (m_0 a constant) onto points in the interior of $\mathbb{S}^2$ ($\mathscr{B} = \{(c,e,m) \in \mathbb{R}^3; c^2+e^2+m^2<1\}$) follows from the bijection:

$$\begin{aligned} &\mathbb{R}^3 \leftrightarrow \mathscr{B} \\ &(\overline{c}, \overline{e}, \overline{m}) \leftrightarrow \left(\frac{\overline{c}}{r}, \frac{\overline{e}}{r}, \frac{\overline{m}}{r}\right), \end{aligned}$$

with $r=\sqrt{\overline{c}^2+\overline{e}^2+\overline{m}^2+1}$. That is, for each plane $\overline{m}=$ constant in $\mathbb{R}^3$, there corresponds an ellipsoid $c^2+e^2+m^2(1+m_0)^2/m_0^2=1, m\geq 0$ (see Fig. 23).

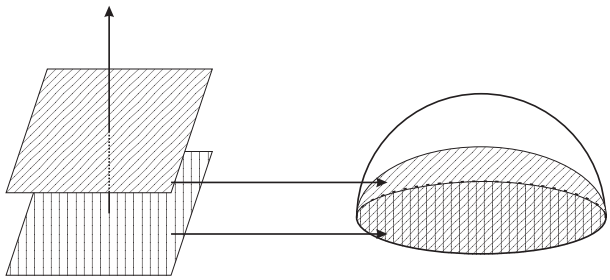

Figure 23 – Correspondence between planes and ellipsoides

Proposition 4.2.3. By a rescaling in the variables, we may assume $h=0$ or $h=1$ in the normal form (4.1).

Proof. If $h\neq 0$, by the Reparametrization Theorem (see Prop. 1.1.15) we get that systems (4.1) are equivalent to

$$\dot{x}=Cx+Cy-Cx^2+2xy,$$
$$\dot{y}=Ex+Ey-Ex^2+2Mxy,$$

where $C=c/h, E=e/h$ and $M=m/h$. By renaming the coefficients $C\to c$, $E\to e$ and $M\to m$, we obtain systems (4.1) with $h=1$. Moreover, we must also consider the case when $h=0$. □

4.3 The bifurcation diagram of the systems in $\overline{\mathbf{QsnSN_{11}(B)}}$

In this chapter we use the concepts of algebraic invariant and T–comitant as formulated by Sibirsky's School for differential equations. For a quick summary see Chap. 2.

In this section we describe the algebraic invariants and T–comitants which are relevant in the study of normal form (4.1).

4.3.1 Algebraic bifurcation surfaces at the affine part of $\mathbb{RP}^3$

From Sec. 7 of Artés, Llibre and Vulpe (2008) and also from Vulpe (2011) we get the formulas which give the bifurcation surfaces of singularities in $\mathbb{R}^{12}$, produced by changes that may occur in the local nature of finite singularities. From Schlomiuk and Vulpe (2005) we get equivalent formulas for the infinite singular points. All of these formulas were lately compiled and improved in the book Artés *et al.* (2021).

Bifurcation surface in $\mathbb{RP}^3$ due to degeneracy of system

$(\mathscr{S}_8)$ Since for systems (4.1) we have an infinite saddle–node of type $\overline{\binom{1}{1}}SN$ we have that $\mu_0 = 0$. Moreover, since

$$\mu_1 = -4(eh - cm)^2 x, \quad \mu_2 = -4(eh - cm)^2 xy,$$

and

$$\mu_3 = \mu_4 = 0,$$

we define $(\mathscr{S}_8)$ as a surface whose equation is given by $\mu_1 = 0$, i.e.

$$(\mathscr{S}_8) : eh - cm = 0,$$

and therefore on this surface we have that $\mu_i = 0$, $i = 0,1,2,3,4$, i.e. systems (4.1) are degenerate (see Artés *et al.* (2021)). We point out that our aim is to construct a coherent and continuous bifurcation diagram. Although the phase portraits possessing a double finite saddle–node $\overline{sn}_{(2)}$, a finite elemental singularity and an infinite saddle–node $\overline{\binom{1}{1}}SN$ are located in open sets in this bifurcation diagram, in order to have these properties for this diagram, we also need to consider the borders of such sets. In particular, surface $(\mathscr{S}_8)$ borders open sets in this bifurcation diagram. In Fig. 24 we present the surface $(\mathscr{S}_8)$ in the three–dimensional affine space which is the hyperplane $h = 1$ in $\mathbb{R}^4$.

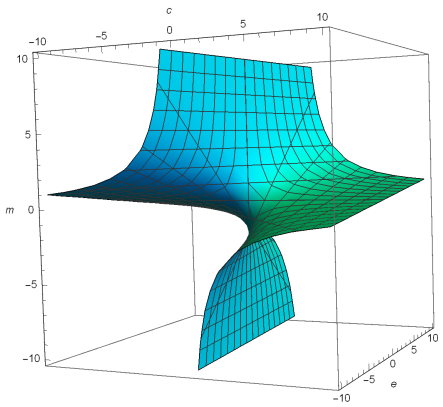

Figure 24 – Surface $(\mathscr{S}_8)$ for $h = 1$

Remark 4.3.1. In the equations of the following surfaces the factor $eh - cm$ is also present. This confirms that the systems on surface $(\mathscr{S}_8)$ are indeed degenerate (possessing curves of singularities) because many geometric features happens at the same time when $eh - cm = 0$. However, we are interested in the other geometric features that the following surfaces can provide. In this way, we assume, without loss of generality, that $eh - cm \neq 0$.

Bifurcation surface in $\mathbb{RP}^3$ due to the change of topological type of the origin

$(\mathscr{S}_2)$ This is the bifurcation surface due to the change of topological type of the origin. On this surface the origin becomes a cusp–type singularity. This phenomenon occurs when two separatrices of a saddle–node coalesce and, according to Artés *et al.* (2021), for normal form (4.1) this phenomenon is described by the invariant E_1 which in this case is given by

$$E_1 = -8(c+e)(-eh+cm)^4.$$

Taking into consideration Rmk. 4.3.1, we define surface $(\mathscr{S}_2)$ by

$$(\mathscr{S}_2): c+e=0.$$

Geometrically, such a surface is a plane on the projective space $\mathbb{RP}^3$ with projective coordinates c, e and m.

The surface of C^∞ bifurcation points due to a strong saddle or a strong focus changing the sign of their traces (weak saddle or weak focus)

$(\mathscr{S}_3)$ This is the bifurcation surface due to weak finite singularities, which occurs when the trace of a finite singular point is zero. According to Vulpe (2011), if the invariant polynomials $\mathscr{T}_4$ and $\mathscr{T}_3$ verify the conditions $\mathscr{T}_4 = 0$ and $\mathscr{T}_3 \neq 0$ then systems (4.1) have exactly one weak singularity. Indeed, for normal form (4.1) the previous conditions are equivalent to

$$\begin{aligned}\mathscr{T}_4 &= -8h(c+e)^2(c-e-2m)(-eh+cm)^2 = 0,\\ \mathscr{T}_3 &= -8h(c+e)(c-3e-4m)(-eh+cm)^2 \neq 0.\end{aligned}$$

Taking into consideration Rmk. 4.3.1 we define surface $(\mathscr{S}_3)$ as

$$(\mathscr{S}_3): c-e-2m=0.$$

We highlight that this bifurcation can produce a topological change if the weak point is a focus or just a C^∞ change if it is a saddle, except when this bifurcation coincides with a loop bifurcation associated with the same saddle, in which case, the change may also be topological (see for instance Artés, Rezende and Oliveira (2015, p. 50)).
We clearly have that such a surface is a plane on the projective space $\mathbb{RP}^3$ with projective coordinates c, e and m.

Bifurcation surface in $\mathbb{RP}^3$ due to the presence of invariant straight lines

$(\mathscr{S}_4)$ This surface contains the points of the parameter space there appear invariant straight lines (see Lemma 4.2.2). This surface is split into some regions. Depending on these regions, the straight line may contain connections of separatrices from different points or not. So, in some cases, it may imply a topological bifurcation and, in others, just a C^∞ bifurcation. According to Artés *et al.* (2021), the equation of this surface is given by the invariant B_1. It is worth mentioning that $B_1 = 0$ is only a necessary condition for

the existence of an invariant straight line, but it is not sufficient (see Corollary 4.6 from Schlomiuk and Vulpe (2004)), i.e. we may find some component of $B_1 = 0$ that does not represent an invariant straight line. For normal form (4.1) the invariant B_1 is given by

$$B_1 = -8c^2e^2(c+2h)(c+e+2h+2m)(-eh+cm)^3.$$

Taking into consideration Rmk. 4.3.1, we define surface $(\mathscr{S}_4)$ by the equation

$$(\mathscr{S}_4): ce(c+2h)(c+e+2h+2m) = 0.$$

In Fig. 25 we present the surface $(\mathscr{S}_4)$ in the three–dimensional affine space which is the hyperplane $h = 1$ in $\mathbb{R}^4$.

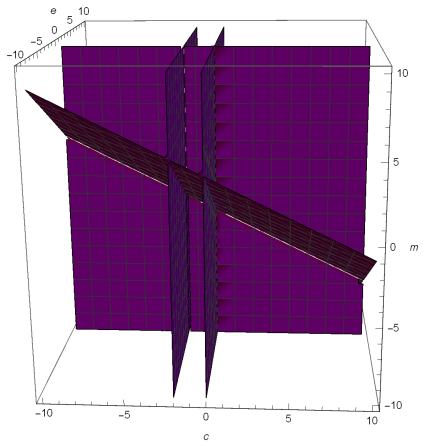

Figure 25 – Surface $(\mathscr{S}_4)$ for $h = 1$

The bifurcation surfaces presented before are all algebraic and they, except $(\mathscr{S}_4)$, are the bifurcation surfaces of finite singularities of systems (4.1) in the parameter space. We shall detect other two bifurcation surfaces not necessarily algebraic. On one of them the systems have global connection of separatrices different from that given by $(\mathscr{S}_4)$ and on the other the systems possess a double limit cycle. The equations of these bifurcation surfaces can only be determined approximately by means of numerical tools. Using arguments of continuity in the phase portraits we can prove the existence of these components not necessarily algebraic in the part where they appear, and we can check them numerically. We shall name them surfaces $(\mathscr{S}_7)$ (connection of separatrices) and $(\mathscr{S}_{10})$ (double limit cycles).

Remark 4.3.2. On surface $(\mathscr{S}_{10})$ the respective systems have at least one double limit cycle. Although this surface is obtained numerically, we can predict in which portion of the bifurcation diagram it can be placed. It must be in the neighborhood of the points of the bifurcation diagram corresponding to a weak focus $f^{(2)}$ of order two. So, according to Vulpe (2011, Main Theorem, item (b_2)), the necessary condition for the existence of weak points of order two or higher is governed by $\mathscr{T}_4 = \mathscr{F}_1 = 0$. Taking into account Rmk. 4.3.1,

for normal form (4.1) the expression of $\mathscr{F}_1$ is given by $\mathscr{F}_1 = c^2 + 2cm + 3ce + 2e$. For $h = 1$, calculations yield

$$\mathscr{T}_4 = \mathscr{F}_1 = 0 \Leftrightarrow c - e - 2m = 2c^2 + (1-2m)c - 2m = 0. \tag{4.4}$$

Such a quadratic equation has discriminant

$$\Delta = 4m^2 + 12m + 1,$$

which is zero if and only if

$$m = \frac{1}{2}\left(\pm 2\sqrt{2} - 3\right).$$

Therefore, for the equation $\mathscr{T}_4 = \mathscr{F}_1 = 0$ we have:

- one double real root if $\Delta = 0$, i.e. $m = \left(\pm 2\sqrt{2} - 3\right)/2$;
- two simple real roots if $\Delta > 0$, i.e. $m < \left(-2\sqrt{2} - 3\right)/2$ or $m > \left(2\sqrt{2} - 3\right)/2$;
- two complex roots if $\Delta < 0$, i.e. $m \in \left(\left(-2\sqrt{2} - 3\right)/2, \left(2\sqrt{2} - 3\right)/2\right)$.

These roots indicate the existence of weak singularities of order two or higher.
On the other hand, for non–degenerate systems (4.1) with $h = 1$ we have that

$$\mathscr{T}_4 = \mathscr{F}_1 = \mathscr{F}_2 = 0$$

if and only if $c = -6/5, e = 36/5$ and $m = -21/5$, and calculations show that $\mathscr{F}_3\mathscr{F}_4 \neq 0$. Then, according to Vulpe (2011, Main Theorem, item (b_3)), we have a third order weak singularity for $m = -21/5$.

Bifurcation surface in $\mathbb{RP}^3$ due to multiplicities of infinite singularities

$(\mathscr{S}_5)$ This is the bifurcation surface due to multiplicity of infinite singularities. This phenomenon is detected by the invariant η (see Lemma 6.1 from Artés *et al.* (2021)), which for normal form (4.1) is given by

$$\eta = -4h^2(-c^2 + 8eh - 4cm - 4m^2) = 0.$$

We define surface $(\mathscr{S}_5)$ by the equation

$$(\mathscr{S}_5) : h(c^2 - 8eh + 4cm + 4m^2) = 0.$$

In Fig. 26 we present the surface $(\mathscr{S}_5)$ in the three–dimensional affine space which is the hyperplane $h = 1$ in $\mathbb{R}^4$.

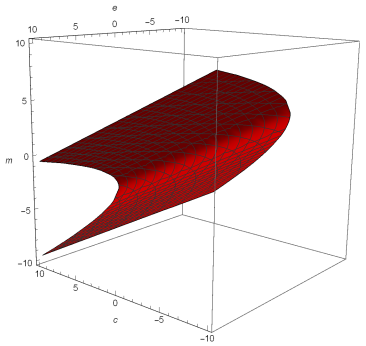

Figure 26 – Surface $(\mathscr{S}_5)$ for $h = 1$

The surface of C^∞ bifurcation due to a node becoming a focus

$(\mathscr{S}_6)$ This surface contains the points of the parameter space where a finite node of the systems turns into a focus. This surface is a C^∞ but not a topological bifurcation surface. In fact, when we only cross the surface $(\mathscr{S}_6)$ in the bifurcation diagram, the topological phase portraits do not change. However, this surface is relevant for isolating the regions where a limit cycle surrounding an antisaddle cannot exist. Using the results of Artés, Llibre and Vulpe (2008), we must consider the invariant W_4. For normal form (4.1), W_4 is given by the polynomial

$$W_4 = 64h^2(c+e)^4(-eh+cm)^4(c^2-2ce+e^2-8eh+4cm+4em+4m^2).$$

Taking into consideration Rmk. 4.3.1 and the fact that W_4 can be considered only when $E_1 \neq 0$, i.e. $c+e \neq 0$ (see Artés *et al.* (2021, Table 6.2)), we define surface $(\mathscr{S}_6)$ as

$$(\mathscr{S}_6): h(c^2-2ce+e^2-8eh+4cm+4em+4m^2) = 0.$$

In Fig. 27 we present the surface $(\mathscr{S}_6)$ in the three–dimensional affine space which is the hyperplane $h = 1$ in $\mathbb{R}^4$.

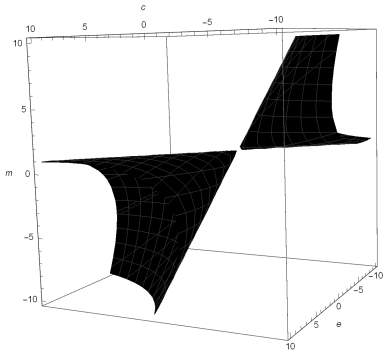

Figure 27 – Surface $(\mathscr{S}_6)$ for $h = 1$

We also must consider the invariant polynomial W_2, which for normal form (4.1) is described by the equation

$$W_2 = 64h^2(eh-cm)^4(3c^2+2ce+3e^2-8eh+4cm+4em+4m^2).$$

This invariant polynomial, according to Artés *et al.* (2021, Table 6.2), can only be considered when $E_1 = c+e = 0$, and W_2 is zero when (for normal form (4.1)) $G_9 = h^2(eh-cm) \neq 0$, i.e. $h \neq 0$. Taking into consideration Rmk. 4.3.1 and the inclusion $\{E_1 = 0\} \subseteq \{\mathscr{T}_4 = 0\}$ we observe that, for normal form (4.1), the solutions of the equation $W_2 = 0$ are indeed the solutions of the system formed by the equations

$$c+e=0, \quad h(c-e-2m)=0, \quad h^2(3c^2+2ce+3e^2-8eh+4cm+4em+4m^2)=0.$$

Calculations yield $W_2 = 0$ as a set with coordinates (c,e,h,m), and such a set is given by

$$\{(-h,h,h,-h); h \in \mathbb{R}\}.$$

In what follows we work at the chart of $\mathbb{RP}^3$ corresponding to $h \neq 0$, and we take $h = 1$. Therefore, $W_2 = 0$ with coordinates (c,e,m) is given by $\{(0,0,0),(-1,1,-1)\}$. We denote this two–point set by $(\mathscr{S}_{6.2})$. More precisely, $(\mathscr{S}_{6.2})$=$\{\mathscr{S}_{6.21},\mathscr{S}_{6.22}\}$, where $\mathscr{S}_{6.21}$=$\{(-1,1,-1)\}$ and $\mathscr{S}_{6.22}$=$\{(0,0,0)\}$.

Remark 4.3.3. As we mentioned before, surface $(\mathscr{S}_6)$ is relevant for isolating the regions where a limit cycle surrounding an antisaddle cannot exist. Then, according to Rmk. 4.3.2 it is interesting to determine the intersection $\mathscr{T}_4 = \mathscr{F}_1 = 0$ with $W_4 = 0$. For normal form (4.1), calculations yield

$$W_4\Big|_{\mathscr{T}_4=\mathscr{F}_1=0} = \frac{4c^2(3+2c)}{1+c},$$

and then W_4 intersects the curve given by $\mathscr{T}_4 = \mathscr{F}_1 = 0$ at $c = 0$ and $c = -3/2$ (which are equivalent to $m = 0$ and $m = -3$, respectively). We observe that W_4 has a relative minimum at $m = 0$, since

$$\frac{\partial W_4}{\partial m}\Big|_{\mathscr{T}_4=\mathscr{F}_1=0|_{c=0}} = 0, \qquad \frac{\partial^2 W_4}{\partial m^2}\Big|_{\mathscr{T}_4=\mathscr{F}_1=0|_{c=0}} = 8,$$

and, moreover, W_4 is decreasing at $m = -3$ because

$$\frac{\partial W_4}{\partial m}\Big|_{\mathscr{T}_4=\mathscr{F}_1=0|_{c=-3/2}} = -12.$$

As a result we conclude, respectively, that:

- if for $m > 0$ we do not have a weak focus of order two (or higher), then for every $m > 0$ we will not find such a kind of singularity, since we will not be "crossing" surface $(\mathscr{S}_6)$;

- if for $m < -3$ we have a weak focus of order two (or higher), then for every $m < -3$ we will find such a kind of singularity.

Remark 4.3.4. Even though we can draw a two–dimensional picture of the algebraic bifurcation surfaces of singularities in affine parts of $\mathbb{RP}^3$ as we did before, it is pointless to see a single two–dimensional image of all these bifurcation surfaces together in an affine part of $\mathbb{RP}^3$. As we shall see later, the full partition of the parameter space obtained from these bifurcation surfaces has 631 parts.

Due to the last remark we shall foliate the three–dimensional bifurcation diagram in $\mathbb{RP}^3$ by the planes $m = m_0$, with m_0 constant, plus the open half sphere $h = 0$ and we shall give pictures of the resulting bifurcation diagram on these planar sections on a disc or in an affine chart of $\mathbb{R}^2$.

As we said before, we work at the chart of $\mathbb{RP}^3$ corresponding to $h \neq 0$, and we take $h = 1$. In order to perform the analysis, we shall use pictures which are drawn on planes $m = m_0$ of $\mathbb{RP}^3$, having coordinates $[c : e : 1 : m_0]$. In these planes the coordinates are (c, e) where the horizontal line is the c–axis.

As the final bifurcation diagram is quite complex, it is useful to introduce colors which will be used to refer to the bifurcation surfaces:

(a) surface ($\mathscr{S}_2$) is drawn in green (the origin becomes a cusp–type singularity);

(b) surface ($\mathscr{S}_3$) is drawn in yellow (when the trace of a singular point becomes zero). We draw it as a continuous curve if the singular point is a focus or as a dashed curve if it is a saddle;

(c) surface ($\mathscr{S}_4$) is drawn in purple (presence of at least one invariant straight line). We draw it as a continuous curve if it implies a topological change or as a dashed curve otherwise;

(d) surface ($\mathscr{S}_5$) is drawn in red (two infinite singular points coalesce);

(e) surface ($\mathscr{S}_6$) is drawn in black (an antisaddle is on the edge of turning from a node to a focus or vice versa);

(f) the two–point set ($\mathscr{S}_{6.2}$) is also drawn in black;

(g) surface ($\mathscr{S}_7$) is also drawn in purple (connections of separatrices);

(h) surface ($\mathscr{S}_8$) is drawn in cyan (the systems are degenerate); and

(i) surface ($\mathscr{S}_{10}$) is drawn in gray (presence of a double limit cycle).

We use the same color for $(\mathscr{S}_4)$ and $(\mathscr{S}_7)$ since both surfaces deal with connections of separatrices mostly.

The following lemmas of this section present the study of the geometric behavior of all of these surfaces for $h \neq 0$ (the case $h = 0$ will be considered separately), that is, their singularities, their intersection points and their extrema (maxima and minima) with respect to the coordinate m.

Lemma 4.3.5. Surface $(\mathscr{S}_2)$ has no singularities.

Proof. Surface $(\mathscr{S}_2)$ is described by the equation $c+e=0$, which is a plane. □

Lemma 4.3.6. For any $m \in \mathbb{R}$, surface $(\mathscr{S}_3)$ has no singularities.

Proof. Surface $(\mathscr{S}_3)$ is given by the equation $c-e-2m=0$, and such an equation describes a plane for each $m \in \mathbb{R}$. □

Lemma 4.3.7. For $h \neq 0$, surface $(\mathscr{S}_4)$ has five straight lines of singularities given by $[0:0:1:m]$, $[0:e:1:-1-e/2]$, $[-2:0:1:m]$, $[-2:e:1:-e/2]$ and $[c:0:1:-1-c/2]$.

Proof. When $h=1$, surface $(\mathscr{S}_4)$ is described by the equation $ce(c+2)(c+e+2m+2)=0$. Such an equation tells us that surface $(\mathscr{S}_4)$ is the union of four planes, namely $\{c=0\}$, $\{e=0\}$, $\{c+2=0\}$ and $\{c+e+2m+2=0\}$. As the planes themselves have no singularities, the singularities of such a surface consist of the intersections among these planes, which are the straight lines $[0:0:1:m]$, $[0:e:1:-1-e/2]$, $[-2:0:1:m]$, $[-2:e:1:-e/2]$ and $[c:0:1:-1-c/2]$. Note that as $\{c=0\}$ and $\{c+2=0\}$ are parallel, they do not provide us any intersection. □

Lemma 4.3.8. For $h \neq 0$, surface $(\mathscr{S}_5)$ has no singularities.

Proof. When $h=1$, surface $(\mathscr{S}_5)$ is written as $c^2-8e+4cm+4m^2=0$. This equation describes a parabolic cylindrical surface which has no singularities. □

Lemma 4.3.9. For $h \neq 0$, $[-2:0:1:1]$ is the only singularity of surface $(\mathscr{S}_6)$.

Proof. When $h=1$, surface $(\mathscr{S}_6)$ is given by the quadric $Q = c^2-8e-2ce+e^2+4cm+4em+4m^2=0$. Computing the derivatives of Q, we obtain:

$$\frac{\partial Q}{\partial c} = 2(c-e+2m), \quad \frac{\partial Q}{\partial e} = -2(4+c-e-2m), \quad \frac{\partial Q}{\partial m} = 4(c+e+2m).$$

These three surfaces (together with Q) have the common point $(-2,0,1)$. We point out that Q is a quadric whose reduced equation is given by

$$\left(\sqrt{3}+2\right)x_2^2 + \frac{1}{2}\left(\sqrt{3}+1\right)y_2^2 - z_2^2 = 0,$$

for some coordinate system (Σ,O), with $O = (x_2, y_2, z_2)$ obtained from (c, e, m) with the rigid movements of translation and rotation. □

Lemma 4.3.10. For $h \neq 0$, surface $(\mathscr{S}_8)$ has no singularities.

Proof. When $h = 1$, surface $(\mathscr{S}_8)$ is described by equation $e - cm = 0$. This equation describes a hyperbolic paraboloid surface, known as a saddle surface, which has no singularities. □

Lemma 4.3.11. For $h \neq 0$, surfaces $(\mathscr{S}_2)$ and $(\mathscr{S}_3)$ intersect along the straight line $[c : -c : 1 : c]$.

Proof. For $h = 1$, solving the system of equations

$$(\mathscr{S}_2) : c + e = 0,$$
$$(\mathscr{S}_3) : c - e - 2m = 0,$$

we obtain $e = -c$ and $m = c$. This result corresponds to the straight line $[c : -c : 1 : c]$. □

Lemma 4.3.12. For $h \neq 0$, surfaces $(\mathscr{S}_2)$ and $(\mathscr{S}_4)$ intersect along the straight lines $[0 : 0 : 1 : m]$, $[-2 : 2 : 1 : m]$ and $[c : -c : 1 : -1]$.

Proof. For $h = 1$, we have the system of equations

$$(\mathscr{S}_2) : c + e = 0,$$
$$(\mathscr{S}_4) : ce(c+2)(c+e+2m+2) = 0.$$

As the equation of surface $(\mathscr{S}_4)$ has four factors, we have to compute the intersection of each one of them with the equation of surface $(\mathscr{S}_2)$. Calculations yield:

- $c = 0$ and $e = 0$. This solution corresponds to the curve $[0 : 0 : 1 : m]$ and it has multiplicity two;
- $c = -2$ and $e = 2$. This solution corresponds to the curve $[-2 : 2 : 1 : m]$;
- $e = -c$ and $m = -1$. This solution corresponds to the curve $[c : -c : 1 : -1]$.

□

Lemma 4.3.13. For $h \neq 0$, surfaces $(\mathscr{S}_2)$ and $(\mathscr{S}_5)$ intersect along the curves $[c : -c : 1 : -\sqrt{-2c} - c/2]$ and $[c : -c : 1 : \sqrt{-2c} - c/2]$. Moreover, the curve $[c : -c : 1 : -\sqrt{-2c} - c/2]$ assumes its extremum (with relation to the coordinate m) for $c = -2$.

Proof. For $h = 1$, we have the system of equations

$$(\mathscr{S}_2) : c + e = 0,$$
$$(\mathscr{S}_5) : c^2 - 8e + 4cm + 4m^2 = 0.$$

Solving this system we obtain the following solutions:

- $e = -c$ and $m = -\sqrt{-2c} - c/2$. This solution corresponds to the curve $[c : -c : 1 : -\sqrt{-2c} - c/2]$;
- $e = -c$ and $m = \sqrt{-2c} - c/2$. This solution corresponds to the curve $[c : -c : 1 : \sqrt{-2c} - c/2]$.

In order to find the extremum of the curve $[c : -c : 1 : -\sqrt{-2c} - c/2]$ we equalize the last coordinate to m and compute the discriminant with respect to c of the obtained function:

$$\mathrm{Discrim}_c(-8c - c^2 - 4cm - 4m^2) = 64(m+1),$$

whose solution is $m = -1$. Finally, solving the equation $-\sqrt{-2c} - c/2 = m$ by substituting m by the zero of the discriminant (i.e. $m = -1$), we obtain $c = -2$, which is the extremum value of the curve with respect to m. □

Lemma 4.3.14. For $h \neq 0$, surfaces $(\mathscr{S}_2)$ and $(\mathscr{S}_6)$ intersect along the curves $[-e : e : 1 : -\sqrt{(2-e)e}]$ and $[-e : e : 1 : \sqrt{(2-e)e}]$. Moreover, these curves assume their extrema (with relation to the coordinate m) for $e = 1$.

Proof. For $h = 1$, we have the system of equations

$$(\mathscr{S}_2) : c + e = 0,$$
$$(\mathscr{S}_6) : c^2 - 8e - 2ce + e^2 + 4cm + 4em + 4m^2 = 0.$$

Solving this system we obtain the following solutions:

- $c = -e$ and $m = -\sqrt{(2-e)e}$. This solution corresponds to the curve $[-e : e : 1 : -\sqrt{(2-e)e}]$;
- $c = -e$ and $m = \sqrt{(2-e)e}$. This solution corresponds to the curve $[-e : e : 1 : \sqrt{(2-e)e}]$.

In order to find the extremum of the curve $[-e : e : 1 : -\sqrt{(2-e)e}]$ we equalize the last coordinate to m and compute the discriminant with respect to e of the obtained function:

$$\mathrm{Discrim}_e(2e - e^2 - m^2) = 4 - 4m^2,$$

whose solutions are $m = \pm 1$. Finally, solving the equation $-\sqrt{(2-e)e} = m$ by substituting m by the zeroes of the discriminant (i.e. $m = \pm 1$), we obtain $e = 1$ for $m = -1$ and we do

not obtain solution for $m=1$.
Analogously, for the curve $[-e:e:1:\sqrt{(2-e)e}]$ calculations yield the same discriminant as before, whose solutions are $m=\pm 1$. Solving the equation $\sqrt{(2-e)e}=m$ by substituting m by the zeroes of the discriminant (i.e. $m=\pm 1$), we obtain $e=1$ for $m=1$ and we do not obtain solution for $m=-1$.
Therefore, $e=1$ is the extremum value of both curves with respect to m. □

Lemma 4.3.15. For $h\neq 0$, the two–point set $(\mathscr{S}_{6.2})$ belongs to the surfaces $(\mathscr{S}_2)$ to $(\mathscr{S}_4)$, $(\mathscr{S}_6)$ and $(\mathscr{S}_8)$. Moreover, $(\mathscr{S}_5)$ intersects the two–point set $(\mathscr{S}_{6.2})$ at $\mathscr{S}_{6.22}$=$\{(0,0,0)\}$.

Proof. For $h=1$, it is easy to show that $\mathscr{S}_{6.21}$=$\{(-1,1,-1)\}$ and $\mathscr{S}_{6.22}$=$\{(0,0,0)\}$ verify this result. □

Lemma 4.3.16. For $h\neq 0$, surfaces $(\mathscr{S}_2)$ and $(\mathscr{S}_8)$ intersect along the straight lines $[0:0:1:m]$ and $[c:-c:1:-1]$.

Proof. For $h=1$, we have the system of equations

$$(\mathscr{S}_2): c+e=0,$$
$$(\mathscr{S}_8): e-cm=0.$$

Solving this system we obtain the following solutions:

- $c=0$ and $e=0$. Then we have the straight line $[0:0:1:m]$;
- $e=-c$ and $m=-1$. This corresponds to the straight line $[c:-c:1:-1]$.

□

Lemma 4.3.17. For $h\neq 0$, surfaces $(\mathscr{S}_3)$ and $(\mathscr{S}_4)$ intersect along the straight lines $[0:e:1:-e/2]$, $[c:0:1:c/2]$, $[-2:e:1:-1-e/2]$ and $[-1:e:1:-(1+e)/2]$.

Proof. For $h=1$, we have the system of equations

$$(\mathscr{S}_3): c-e-2m=0,$$
$$(\mathscr{S}_4): ce(c+2)(c+e+2m+2)=0.$$

As the equation of surface $(\mathscr{S}_4)$ has four factors, we have to compute the intersection of each one of them with the equation of surface $(\mathscr{S}_3)$. Calculations yield the following solutions:

- $c=0$ and $m=-e/2$. This solution corresponds to the straight line $[0:e:1:-e/2]$;
- $e=0$ and $m=c/2$. This solution corresponds to the straight line $[c:0:1:c/2]$;

- $c=-2$ and $m=-1-e/2$. This solution corresponds to the straight line $[-2:e:1:-1-e/2]$;
- $c=-1$ and $m=-(1+e)/2$. This solution corresponds to the straight line $[-1:e:1:-(1+e)/2]$.

□

Lemma 4.3.18. For $h\neq 0$, surfaces $(\mathscr{S}_3)$ and $(\mathscr{S}_5)$ intersect along the curves $[c:2(2+c+2\sqrt{c+1}):1:-2(1+\sqrt{c+1})-c/2]$ and $[c:2(2+c-2\sqrt{c+1}):1:-2(1-\sqrt{c+1})-c/2]$. Moreover, this last curve assumes its extremum (with relation to the coordinate m) for $c=3$.

Proof. For $h=1$, we have the system of equations

$$\begin{aligned}(\mathscr{S}_3) &: c-e-2m=0,\\ (\mathscr{S}_5) &: c^2-8e+4cm+4m^2=0.\end{aligned}$$

Solving this system we obtain the following solutions:

- $e=2(2+c+2\sqrt{c+1})$ and $m=-2(1+\sqrt{c+1})-c/2$. This solution corresponds to the curve $[c:2(2+c+2\sqrt{c+1}):1:-2(1+\sqrt{c+1})-c/2]$;
- $e=2(2+c-2\sqrt{c+1})$ and $m=-2(1-\sqrt{c+1})-c/2$. This solution corresponds to the curve $[c:2(2+c-2\sqrt{c+1}):1:-2(1-\sqrt{c+1})-c/2]$.

In order to find the extremum of the curve $[c:2(2+c-2\sqrt{c+1}):1:-2(1-\sqrt{c+1})-c/2]$, we equalize the last coordinate to m and compute the discriminant with respect to c of the obtained function:

$$\mathrm{Discrim}_c(-2c-c^2/4-4m-cm-m^2)=4-8m,$$

whose solution is $m=1/2$. Finally, solving the equation $-2(1-\sqrt{c+1})-c/2=m$ by substituting $m=1/2$, we obtain $c=3$, which is the extremum value of the curve with respect to m. □

Lemma 4.3.19. For $h\neq 0$, surfaces $(\mathscr{S}_3)$ and $(\mathscr{S}_6)$ intersect along the curves $[(e-\sqrt{e^2+8e})/2:e:1:-(\sqrt{e}+\sqrt{e+8})\sqrt{e}/4]$ and $[(e+\sqrt{e^2+8e})/2:e:1:-(\sqrt{e}-\sqrt{e+8})\sqrt{e}/4]$.

Proof. For $h=1$, we have the system of equations

$$\begin{aligned}(\mathscr{S}_3) &: c-e-2m=0,\\ (\mathscr{S}_6) &: c^2-8e-2ce+e^2+4cm+4em+4m^2=0.\end{aligned}$$

Solving this system we obtain the following solutions:

- $c = (e - \sqrt{e^2+8e})/2$ and $m = -(\sqrt{e}+\sqrt{e+8})\sqrt{e}/4$. This solution corresponds to the curve $[(e - \sqrt{e^2+8e})/2 : e : 1 : -(\sqrt{e}+\sqrt{e+8})\sqrt{e}/4]$;

- $c = (e + \sqrt{e^2+8e})/2$ and $m = -(\sqrt{e}-\sqrt{e+8})\sqrt{e}/4$. This solution corresponds to the curve $[(e + \sqrt{e^2+8e})/2 : e : 1 : -(\sqrt{e}-\sqrt{e+8})\sqrt{e}/4]$.

□

Lemma 4.3.20. For $h \neq 0$, surfaces $(\mathscr{S}_3)$ and $(\mathscr{S}_8)$ intersect along the hyperbola $[c : c^2/(c+2) : 1 : c/(c+2)]$.

Proof. For $h = 1$, we have the system of equations

$$(\mathscr{S}_3) : c - e - 2m = 0,$$
$$(\mathscr{S}_8) : e - cm = 0.$$

Solving this system we obtain $e = c^2/(c+2)$ and $m = c/(c+2)$. Then we have the hyperbola $[c : c^2/(c+2) : 1 : c/(c+2)]$. □

Lemma 4.3.21. For $h \neq 0$, surfaces $(\mathscr{S}_4)$ and $(\mathscr{S}_5)$ intersect along the curves $[0 : m^2/2 : 1 : m]$, $[-2 : (m-1)^2/2 : 1 : m]$, $[c : 0 : 1 : -c/2]$ and $[c : 2 : 1 : -2-c/2]$. Moreover, the straight lines $[c : 0 : 1 : -c/2]$ and $[c : 2 : 1 : -2-c/2]$ correspond to a contact of order two between these two surfaces.

Proof. For $h = 1$, we have the system of equations

$$(\mathscr{S}_4) : c(c+2)e(c+e+2m+2) = 0,$$
$$(\mathscr{S}_5) : c^2 - 8e + 4cm + 4m^2 = 0.$$

As the equation of surface $(\mathscr{S}_4)$ has four factors, we have to compute the intersection of each one of them with the equation of surface $(\mathscr{S}_5)$. Calculations yield the following solutions:

- $c = 0$ and $e = m^2/2$. This solution corresponds to the parabola $[0 : m^2/2 : 1 : m]$;

- $c = -2$ and $e = (m-1)^2/2$. This solution corresponds to the parabola $[-2 : (m-1)^2/2 : 1 : m]$;

- $e = 0$ and $m = -c/2$. This solution corresponds to the straight line $[c : 0 : 1 : -c/2]$;

- $e = 2$ and $m = -2 - c/2$. This solution corresponds to the straight line $[c : 2 : 1 : -2-c/2]$.

Moreover, for $h=1$ surface $(\mathscr{S}_5)$ has a contact of order two with the plane $e=0$ (then with the surface $(\mathscr{S}_4)$) along the straight line $\gamma_1=[c:0:1:-c/2]$. In fact, by computing the resultant with respect to c of $e=0$ and $(\mathscr{S}_5)$ we see that $\mathrm{Res}_c[e,(\mathscr{S}_5)]=e^2$. In order to conclude the proof of this claim it is enough to observe that the gradient vector of the plane $e=0$ in every point $[c:e:1:m]$ is $[0:1:1:0]$ whereas the gradient vector of $(\mathscr{S}_5)$ along the straight line γ_1 is $\nabla\mathscr{S}_5(\gamma_1)=[0:-8:1:0]$, then the surface $(\mathscr{S}_5)$ remains only on one of the two topological subspaces delimited by the plane $e=0$.
Analogously, for $h=1$ surface $(\mathscr{S}_5)$ has a contact of order two with the plane $c+e+2m+2=0$ (then with the surface $(\mathscr{S}_4)$) along the straight line $\gamma_2=[c:2:1:-2-c/2]$. Indeed, as before, by computing the resultant with respect to c of $c+e+2m+2=0$ and $(\mathscr{S}_5)$ we see that $\mathrm{Res}_c[c+e+2m+2,(\mathscr{S}_5)]=(e-2)^2$. Moreover, we observe that the gradient vector of the plane $c+e+2m+2=0$ in every point $[c:e:1:m]$ is $[1:1:1:2]$ whereas the gradient vector of $(\mathscr{S}_5)$ along the straight line γ_2 is $\nabla\mathscr{S}_5(\gamma_2)=[-8:-8:1:-16]$, then the surface $(\mathscr{S}_5)$ remains only on one of the two topological subspaces delimited by the plane $c+e+2m+2=0$. □

Lemma 4.3.22. For $h\neq 0$, surfaces $(\mathscr{S}_4)$ and $(\mathscr{S}_6)$ intersect along the curves $[0:e:1:-\sqrt{2e}-e/2]$, $[0:e:1:\sqrt{2e}-e/2]$, $[-2:e:1:1-e/2]$, $[c:0:1:-c/2]$ and $[-2+1/e:e:1:-(e^2+1)/(2e)]$. Moreover, the curve $[0:e:1:\sqrt{2e}-e/2]$ has its extremum (with relation to the coordinate m) for $e=2$ and the curve $[-2+1/e:e:1:-(e^2+1)/(2e)]$ has its extremum for $e=\pm 1$. In addition, the straight lines $[-2:e:1:1-e/2]$ and $[c:0:1:-c/2]$ correspond to a contact of order two between these two surfaces.

Proof. For $h=1$, we have the system of equations

$$\begin{aligned}(\mathscr{S}_4) &: c(c+2)e(c+e+2m+2)=0,\\ (\mathscr{S}_6) &: c^2-8e-2ce+e^2+4cm+4em+4m^2=0.\end{aligned}$$

As the equation of surface $(\mathscr{S}_4)$ has four factors, we have to compute the intersection of each one of them with the equation of surface $(\mathscr{S}_6)$. Calculations yield the solutions:

- $c=0$ and $m=-\sqrt{2e}-e/2$. This solution corresponds to the curve $[0:e:1:-\sqrt{2e}-e/2]$;
- $c=0$ and $m=\sqrt{2e}-e/2$. This solution corresponds to the curve $[0:e:1:\sqrt{2e}-e/2]$;
- $c=-2$ and $m=1-e/2$. This solution corresponds to the straight line $[-2:e:1:1-e/2]$;
- $e=0$ and $m=-c/2$. This solution corresponds to the straight line $[c:0:1:-c/2]$;
- $c=-2+1/e$ and $m=-(e^2+1)/(2e)$. This solution corresponds to the hyperbola $[-2+1/e:e:1:-(e^2+1)/(2e)]$.

In order to find the extremum of the curve $[0:e:1:\sqrt{2e}-e/2]$ we equalize the last coordinate to m and compute the discriminant with respect to e of the obtained function:

$$\text{Discrim}_e(8e-e^2-4em-4m^2) = -64(m-1),$$

whose solution is $m=1$. Now, solving the equation $\sqrt{2e}-e/2=m$ by substituting $m=1$, we obtain $e=2$, which is the extremum value of the curve with respect to m.
Analogously, in order to find the extrema of the curve $[-2+1/e:e:1:-(e^2+1)/(2e)]$ we equalize the last coordinate to m and compute the discriminant with respect to e of the obtained function:

$$\text{Discrim}_e(-1-e^2-2em) = 4(m^2-1),$$

whose solutions are $m=\pm 1$. Proceeding, solving the equation $-(e^2+1)/(2e)=m$ by substituting $m=1$ we obtain $e=-1$, and by substituting $m=-1$ we obtain $e=1$. Therefore, $e=\pm 1$ are the extrema values of the curve with respect to m.
It remains to show that the straight lines $[-2:e:1:1-e/2]$ and $[c:0:1:-c/2]$ correspond to a contact of order two between surfaces $(\mathscr{S}_4)$ and $(\mathscr{S}_6)$.
In fact, for $h=1$ surface $(\mathscr{S}_6)$ has a contact of order two with the plane $e=0$ (then with the surface $(\mathscr{S}_4)$) along the straight line $\gamma_3=[c:0:1:-c/2]$. Indeed, by computing the resultant with respect to c of $e=0$ and $(\mathscr{S}_6)$ we see that $\text{Res}_c[e,(\mathscr{S}_6)]=e^2$. In order to conclude the proof of this claim we observe that the gradient vector of the plane $e=0$ in every point $[c:e:1:m]$ is $[0:1:1:0]$ whereas the gradient vector of $(\mathscr{S}_6)$ along the straight line γ_3 is $\nabla\mathscr{S}_6(\gamma_3)=[0:-4(2+c):1:0]$, then, for each fixed value of the parameter c the surface $(\mathscr{S}_6)$ remains only on one of the two topological subspaces delimited by the plane $e=0$.
Analogously, for $h=1$ surface $(\mathscr{S}_6)$ has a contact of order two with the plane $c+2=0$ (then with the surface $(\mathscr{S}_4)$) along the straight line $\gamma_4=[-2:e:1:1-e/2]$. In fact, as before, by computing the resultant with respect to e of $c+2=0$ and $(\mathscr{S}_6)$ we see that $\text{Res}_e[c+2,(\mathscr{S}_6)]=(c+2)^2$. Moreover, we observe that the gradient vector of the plane $c+2=0$ in every point $[c:e:1:m]$ is $[1:0:1:0]$ whereas the gradient vector of $(\mathscr{S}_6)$ along the straight line γ_4 is $\nabla\mathscr{S}_6(\gamma_4)=[-4e:0:1:0]$, then, for each fixed value of the parameter e the surface $(\mathscr{S}_6)$ remains only on one of the two topological subspaces delimited by the plane $c+2=0$. □

Lemma 4.3.23. For $h\neq 0$, surfaces $(\mathscr{S}_4)$ and $(\mathscr{S}_8)$ intersect along the straight lines $[c:0:1:0]$, $[0:0:1:m]$, $[-2:-2m:1:m]$ and $[c:-c:1:-1]$.

Proof. For $h=1$, we have the system of equations

$$(\mathscr{S}_4): c(c+2)e(c+e+2m+2)=0,$$
$$(\mathscr{S}_8): e-cm=0.$$

As the equation of surface $(\mathscr{S}_4)$ has four factors, we have to compute the intersection of each one of them with the equation of surface $(\mathscr{S}_8)$. Calculations yield the solutions:

- $e=0$ and $m=0$. This solution corresponds to the straight line $[c:0:1:0]$.
- $c=0$ and $e=0$. This solution corresponds to the straight line $[0:0:1:m]$ and it has multiplicity three;
- $c=-2$ and $e=-2m$. This solution corresponds to the straight line $[-2:-2m:1:m]$ and it has multiplicity two;
- $e=-c$ and $m=-1$. This solution corresponds to the straight line $[c:-c:1:-1]$.

□

Lemma 4.3.24. For $h\neq 0$, surfaces $(\mathscr{S}_5)$ and $(\mathscr{S}_6)$ intersect along the curves $[c:0:1:-c/2]$, $[c:4(4+c+2\sqrt{2c+4}):1:-2\sqrt{2c+4}-c/2-4]$, and $[c:4(4+c-2\sqrt{2c+4}):1:2\sqrt{2c+4}-c/2-4]$. Moreover, this last curve takes its extremum (with relation to the coordinate m) for $c=6$. In addition, the straight line $[c:0:1:-c/2]$ corresponds to a contact of order two between these two surfaces.

Proof. For $h=1$, we have the system of equations

$$\begin{aligned}(\mathscr{S}_5):\ & c^2-8e+4cm+4m^2=0,\\ (\mathscr{S}_6):\ & c^2-8e-2ce+e^2+4cm+4em+4m^2=0.\end{aligned}$$

Solving this system we obtain:

- $e=0$ and $m=-c/2$. This solution corresponds to the straight line $[c:0:1:-c/2]$;
- $e=4(4+c+2\sqrt{2c+4})$ and $m=-2\sqrt{2c+4}-c/2-4$. This solution corresponds to the curve $[c:4(4+c+2\sqrt{2c+4}):1:-2\sqrt{2c+4}-c/2-4]$;
- $e=4(4+c-2\sqrt{2c+4})$ and $m=2\sqrt{2c+4}-c/2-4$. This solution corresponds to the curve $[c:4(4+c-2\sqrt{2c+4}):1:2\sqrt{2c+4}-c/2-4]$.

In order to find the extremum of the curve $[c:4(4+c-2\sqrt{2c+4}):1:2\sqrt{2c+4}-c/2-4]$, we equalize the last coordinate to m and compute the discriminant with respect to c of the obtained function:

$$\mathrm{Discrim}_c(4c-c^2/4-8m-cm-m^2)=-16(m-1),$$

whose solution is $m=1$. Finally, solving the equation $2\sqrt{2c+4}-c/2-4=m$ by substituting m by the zero of the discriminant (i.e. $m=1$), we obtain $c=6$, which is the extremum value of the curve with respect to m.
To prove the contact between both surfaces along the straight line $\gamma=[c:0:1:-c/2]$, we start by computing the resultant of these two surfaces with respect to c. As a result we obtain $\mathrm{Res}_c[(\mathscr{S}_5),(\mathscr{S}_6)]=e^2(e^2+16e(m-2)+64m^2)$. In order to conclude the proof of this

claim we apply the affine change of coordinates given by $m=-(c+2v)/2$, $v\in\mathbb{R}$. Under this transformation, the gradient vector of $(\mathscr{S}_5)$ along the curve γ is $\nabla\mathscr{S}_5(\gamma)=[0:-8:1:0]$, whereas the gradient vector of $(\mathscr{S}_6)$ along the curve γ is $\nabla\mathscr{S}_6(\gamma)=[0:-8-4c:1:0]$, whose second coordinate is positive or negative, for each fixed value of the parameter c. As $\nabla\mathscr{S}_5(\gamma)$ does not change its sign, this vector will point to the same direction (or to the contrary direction, depending on the value of the parameter c) in relation to $(\mathscr{S}_6)$ restricted to the previous change of coordinates. Then, for each fixed value of the parameter c, the surface $(\mathscr{S}_6)$ remains only on one of the two topological subspaces delimited by the plane $e=0$, and for all values of the parameter c the surface $(\mathscr{S}_5)$ remains only on one of the two topological subspaces delimited by the plane $e=0$. □

Lemma 4.3.25. For $h\neq 0$, surfaces $(\mathscr{S}_5)$ and $(\mathscr{S}_8)$ intersect along the parabola $[c:c^2/2:1:c/2]$. In addition, this parabola corresponds to a contact of order two between these two surfaces.

Proof. For $h=1$, we have the system of equations

$$(\mathscr{S}_5): c^2-8e+4cm+4m^2=0,$$
$$(\mathscr{S}_8): e-cm=0.$$

Solving this system we obtain $e=c^2/2$ and $m=c/2$. This solution corresponds to the parabola $[c:c^2/2:1:c/2]$.
In order to prove the contact between both surfaces along the parabola $\gamma=[c:c^2/2:1:c/2]$, we start by computing the resultant of these two surfaces with respect to m. As a result we obtain $\mathrm{Res}_m[(\mathscr{S}_5),(\mathscr{S}_8)]=(c^2-2e)^2$. In order to conclude the proof of this claim we apply the affine change of coordinates given by $m=(c-2v)/2$, $v\in\mathbb{R}$. Under this transformation, the gradient vector of $(\mathscr{S}_8)$ along the curve γ is $\nabla\mathscr{S}_8(\gamma)=[-c:1:1:c]$, whereas the gradient vector of $(\mathscr{S}_5)$ along the curve γ is $\nabla\mathscr{S}_5(\gamma)=[8c:-8:1:-8c]$, whose second coordinate is always negative. As for each fixed value of the parameter c we have that $\nabla\mathscr{S}_8(\gamma)$ does not change its sign, this vector will always point to the opposite direction in relation to $(\mathscr{S}_5)$ restricted to the previous change of coordinates. Then, the surface $(\mathscr{S}_8)$ remains only on one of the two topological subspaces delimited by the surface $(\mathscr{S}_5)$. □

Lemma 4.3.26. For $h\neq 0$, surfaces $(\mathscr{S}_6)$ and $(\mathscr{S}_8)$ intersect along the hyperbola $[c:c^2/(c+2):1:c/(c+2)]$. Moreover, this hyperbola corresponds to a contact of order two between these two surfaces.

Proof. For $h=1$, we have the system of equations

$$(\mathscr{S}_6): c^2-8e-2ce+e^2+4cm+4em+4m^2=0,$$
$$(\mathscr{S}_8): e-cm=0.$$

Solving this system we obtain $e = c^2/(c+2)$ and $m = c/(c+2)$. This solution corresponds to the hyperbola $[c : c^2/(c+2) : 1 : c/(c+2)]$, for $c \neq -2$.
In order to prove the contact between both surfaces along the hyperbola $\gamma = [c : c^2/(c+2) : 1 : c/(c+2)]$, we start by computing the resultant of these two surfaces with respect to m. As a result we obtain $\mathrm{Res}_m[(\mathscr{S}_6),(\mathscr{S}_8)] = (c^2-(c+2)e)^2$. In order to conclude the proof of this claim we apply the affine change of coordinates given by $m = (c-2v-cv)/(c+2)$, $v \in \mathbb{R}, c \neq -2$. Under this transformation, the gradient vector of $(\mathscr{S}_8)$ along the curve γ is $\nabla\mathscr{S}_8(\gamma) = [-1+4/(c+2)^2 : 1 : 1 : c]$, whereas the gradient vector of $(\mathscr{S}_6)$ along the curve γ is $\nabla\mathscr{S}_6(\gamma) = [(8c(c+4))/(c+2)^2 : -8 : 1 : -8c]$, whose second coordinate is always negative. As for each fixed value of the parameter c we have that $\nabla\mathscr{S}_6(\gamma)$ does not change its sign, this vector will always point to the opposite direction in relation to $(\mathscr{S}_8)$ restricted to the previous change of coordinates. Then, the surface $(\mathscr{S}_6)$ remains only on one of the two topological subspaces delimited by the surface $(\mathscr{S}_8)$. □

The purpose now is to find the slices in which the intersection among at least three surfaces or other equivalent phenomena happen. Since there are 36 distinct curves of intersections or contacts between any two surfaces, we need to study 666 different possible intersections of these surfaces. As the relation is very long, we indicate only a few of them deploying the different algebraic techniques used to solve them. The full set of proves can be found in the Mathematica file available at the link <http://mat.uab.es/~artes/articles/qvfsn2SN11B/sn2SN11B.nb>.

Remark 4.3.27. In the next five lemmas we use the following notation. A curve of singularities of a surface or a curve of intersection or contact between two surfaces will be denoted by sol*AB*x*C*, where $A < B$ are the numbers of the surfaces involved in the intersection or contact and C is a cardinal. We point out that on such lemmas we indicate only one value of the parameter m where the respective intersection occurs, i.e. the corresponding surfaces may have intersection in other value of m. Moreover, these five lemmas illustrate how we obtain the intersection among at least three surfaces or other equivalent phenomena.

Lemma 4.3.28. Surfaces $(\mathscr{S}_2)$, $(\mathscr{S}_3)$ and $(\mathscr{S}_4)$ intersect in slice when $m = 0$.

Proof. By Lemmas 4.3.11 and 4.3.12, we have the curves sol23x1 $= [c : -c : 1 : c]$ and sol24x1 $= [0 : 0 : 1 : m]$. Equalizing each corresponding coordinate:

$$c = 0, \quad -c = 0, \quad c = m,$$

and solving the obtained system, we have the solution $c = 0, m = 0$. Since the curves are parametrized by c and m, we must substitute the solutions of the system in the expressions of the curves and consider the value of the coordinate m. Then,

$$\text{sol23x1}|_{c=0} = [0 : 0 : 1 : 0] \qquad \text{and} \qquad \text{sol24x1}|_{m=0} = [0 : 0 : 1 : 0],$$

implying that the value of m where the three surfaces intersect is $m = 0$. □

Lemma 4.3.29. Surfaces $(\mathscr{S}_2)$, $(\mathscr{S}_4)$ and $(\mathscr{S}_5)$ intersect in slice when $m = 3$.

Proof. By Lemmas 4.3.12 and 4.3.13, we have the curves $\text{sol24x2} = [-2 : 2 : 1 : m]$ and $\text{sol25x2} = [c : -c : 1 : \sqrt{-2c} - c/2]$. Equalizing each corresponding coordinate:

$$c = -2, \quad -c = 2, \quad m = \sqrt{-2c} - c/2,$$

and solving the obtained system, we have the solution $c = -2, m = 3$. Since the curves are parametrized by c and m, we must substitute the solutions of the system in the expressions of the curves and consider the value of the coordinate m. Then,

$$\text{sol24x2}|_{m=3} = [-2 : 2 : 1 : 3]$$

and

$$\text{sol25x2}|_{c=-2} = [-2 : 2 : 1 : 3],$$

implying that the value of m where the three surfaces intersect is $m = 3$. □

Lemma 4.3.30. Surfaces $(\mathscr{S}_2)$, $(\mathscr{S}_4)$ and $(\mathscr{S}_6)$ intersect in slice when $m = -1$.

Proof. By Lemmas 4.3.12 and 4.3.14, we have the curves $\text{sol24x3} = [c : -c : 1 : -1]$ and $\text{sol26x1} = [-e : e : 1 : -\sqrt{(2-e)e}]$. Equalizing each corresponding coordinate:

$$c = -e, \quad -c = e, \quad -\sqrt{(2-e)e} = -1,$$

and solving the obtained system, we have the solution $c = -1, e = 1$. Since the curves are parametrized by c and e, we must substitute the solutions of the system in the expressions of the curves and consider the value of the coordinate m. Then,

$$\text{sol24x3}|_{c=-1} = [-1 : 1 : 1 : -1]$$

and

$$\text{sol26x1}|_{e=1} = [-1 : 1 : 1 : -1],$$

implying that the value of m where the three surfaces intersect is $m = -1$. □

Lemma 4.3.31. Surfaces $(\mathscr{S}_3)$, $(\mathscr{S}_4)$ and $(\mathscr{S}_5)$ intersect in slice when $m = -4$.

Proof. By Lemmas 4.3.17 and 4.3.18, we have the curves $\text{sol35x1} = [c : 2(2+c+2\sqrt{c+1}) : 1 : -2(\sqrt{c+1}+1) - c/2]$ and $\text{sol45x1} = [0 : m^2/2 : 1 : m]$. Equalizing each corresponding coordinate:

$$c = 0, \quad m^2/2 = 2(2+c+2\sqrt{c+1}),$$

and

$$m = -2(\sqrt{c+1}+1) - c/2,$$

and solving the obtained system, we have the solution $c=0, m=-4$. Since the curves are parametrized by c and m, we must substitute the solutions of the system in the expressions of the curves and consider the value of the coordinate m. Then,

$$\text{sol35x1}|_{c=0} = [0:8:1:-4]$$

and

$$\text{sol45x1}|_{m=-4} = [0:8:1:-4],$$

implying that the value of m where the three surfaces intersect is $m=-4$. □

Lemma 4.3.32. Surfaces $(\mathscr{S}_4)$, $(\mathscr{S}_5)$ and $(\mathscr{S}_6)$ intersect in slice when $m=1$.

Proof. By Lemmas 4.3.21 and 4.3.22, we have the curves $\text{sol45x3} = [c:0:1:-c/2]$ and $\text{sol46x3} = [-2:e:1:1-e/2]$. Equalizing each corresponding coordinate:

$$c=-2, \quad e=0, \quad -c/2 = 1-e/2,$$

and solving the obtained system, we have the solution $c=-2, e=0$. Since the curves are parametrized by c and e, we must substitute the solutions of the system in the expressions of the curves and consider the value of the coordinate m. Then,

$$\text{sol45x3}|_{c=-2} = [-2:0:1:1]$$

and

$$\text{sol46x3}|_{e=0} = [-2:0:1:1],$$

implying that the value of m where the three surfaces intersect is $m=1$. □

The next result presents all the algebraic values of m corresponding to singular slices in the bifurcation diagram. Its proof follows from Rmk. 4.3.2, Lemmas 4.3.28 to 4.3.32 and by computing all the remaining different possible intersections, singularities or contacts among three or more surfaces.

Lemma 4.3.33. The full set of needed algebraic singular slices in the bifurcation diagram of family $\mathbf{QsnSN_{11}(B)}$ is formed by 18 elements which correspond to the values of m in (4.5). These elements indicate the 17 finite slices plus the infinite one.

$$\begin{aligned} &m_1 = +\infty,\ m_3 = 3,\ m_5 = 1,\ m_7 = \frac{1}{2},\ m_{13} = 0,\ m_{15} = \frac{1}{2}\left(2\sqrt{2}-3\right),\ m_{17} = -\frac{1}{2} \\ &m_{21} = -\frac{8}{9},\ m_{23} = -\frac{24}{25},\ m_{25} = -1,\ m_{35} = -\frac{5}{4},\ m_{37} = -\frac{3}{2},\ m_{39} = -2, \\ &m_{41} = \frac{1}{2}\left(-2\sqrt{2}-3\right),\ m_{43} = -3,\ m_{45} = -4,\ m_{47} = -\frac{21}{5},\ m_{53} = -8. \end{aligned} \tag{4.5}$$

The numeration in (4.5) is not consecutive since we reserve numbers for other slices not algebraically determined and for generic slices.

Now we sum up the content of the previous lemmas. In (4.5) we list all the algebraic values of m where significant phenomena occur for the bifurcation diagram generated by singularities. We first have the two extreme values for m, i.e. $m=+\infty$ (corresponding to $h=0$) and $m=-8$. We remark that to perform the bifurcation diagram of all singularities for $m=+\infty$ we set $h=0$ and, in the remaining three variables (c,e,m), yielding the point $[c:e:m]$ in $\mathbb{RP}^2$, we take the chart $m\neq 0$ in which we may assume $m=1$.

In order to determine all the parts generated by the bifurcation surfaces from $(\mathscr{S}_2)$ to $(\mathscr{S}_{10})$, we first draw the horizontal slices of the three–dimensional parameter space which correspond to the explicit values of m obtained in Lemma 4.3.33. However, as it will be discussed later, the presence of nonalgebraic bifurcation surfaces will be detected and the singular slices corresponding to their singular behavior as we move from slice to slice will be approximately determined. We add to each interval of singular values of m an intermediate value for which we represent the bifurcation diagram of singularities. The diagram will remain essentially unchanged in these open intervals except for the parts affected by the bifurcation. All the sufficient values of m are shown in (4.6).

$$
\begin{array}{lll}
m_1=+\infty & m_{19}=-1/2-\varepsilon_4^* & m_{37}=-3/2\\
m_2=4 & m_{20}=-1/2-\varepsilon_5 & m_{38}=-7/4\\
m_3=3 & m_{21}=-8/9 & m_{39}=-2\\
m_4=2 & m_{22}=-9/10 & m_{40}=-5/2\\
m_5=1 & m_{23}=-24/25 & m_{41}=(-2\sqrt{2}-3)/2\\
m_6=3/4 & m_{24}=-98/100 & m_{42}=-295/100\\
m_7=1/2 & m_{25}=-1 & m_{43}=-3\\
m_8=1/2-\varepsilon_1 & m_{26}=-1-\varepsilon_6 & m_{44}=-7/2\\
m_9=1/2-\varepsilon_1^* & m_{27}=-1-\varepsilon_6^* & m_{45}=-4\\
m_{10}=1/2-\varepsilon_2 & m_{28}=-1-\varepsilon_7 & m_{46}=-4-\varepsilon_{11}\\
m_{11}=1/2-\varepsilon_2^* & m_{29}=-1-\varepsilon_7^* & m_{47}=-21/5\\
m_{12}=1/2-\varepsilon_3 & m_{30}=-1-\varepsilon_8 & m_{48}=-21/5-\varepsilon_{12}\\
m_{13}=0 & m_{31}=-1-\varepsilon_8^* & m_{49}=-21/5-\varepsilon_{12}^*\\
m_{14}=-5/100 & m_{32}=-1-\varepsilon_9 & m_{50}=-21/5-\varepsilon_{13}\\
m_{15}=(2\sqrt{2}-3)/2 & m_{33}=-1-\varepsilon_9^* & m_{51}=-21/5-\varepsilon_{13}^*\\
m_{16}=-1/4 & m_{34}=-1-\varepsilon_{10} & m_{52}=-21/5-\varepsilon_{14}\\
m_{17}=-1/2 & m_{35}=-5/4 & m_{53}=-8\\
m_{18}=-1/2-\varepsilon_4 & m_{36}=-13/10 & m_{54}=-10
\end{array}
\tag{4.6}
$$

The values indexed by positive odd indexes in (4.6) correspond to explicit values of m for which there exists a bifurcation in the behavior of the systems on the slices. Those indexed by even values are just intermediate points which are necessary to the coherence of the bifurcation diagram.

Due to the presence of many branches of nonalgebraic bifurcation surfaces, we cannot point out exactly neither predict the specific value of m where the changes in the parameter space happen. Thus, with the purpose to set an order for these changes in the parameter space, we introduce the following notation. If the bifurcation happens between two specific values of m, then we add or subtract a sufficiently small positive value ε_i or ε_j^* to/from a specific value of m; this specific value of m (which is a reference value) can be any of the two values that define the range where the non–specific values of m are inserted. The representation ε_i means that the m_i refers to a generic slice, whereas ε_j^* means that the m_j refers to a singular slice. Moreover, considering the values ε_i, ε_i^*, ε_{i+1} and ε_{i+1}^*, it means that $\varepsilon_i < \varepsilon_i^* < \varepsilon_{i+1} < \varepsilon_{i+1}^*$ meanwhile they belong to the same interval determined by algebraic bifurcations.

We now begin the analysis of the bifurcation diagram by studying completely one generic slice and after by moving from slice to slice and explaining all the changes that occur. As an exact drawing of the curves produced by intersecting the surfaces with the slices gives us very small parts which are difficult to distinguish, and points of tangency are almost impossible to recognize, we have produced topologically equivalent figures where parts are enlarged and tangencies are easy to observe.

The reader may find the exact pictures of the 17 finite singular slices described in (4.5) in a PDF file available at the link <http://mat.uab.es/~artes/articles/qvfsn2SN11B/sn2SN11B.pdf>. We point out that these 17 slices contain only the algebraic surfaces.

We now describe the labels used for each part of the bifurcation space. As we have mentioned in Rmk. 4.1.5, the subsets of dimensions 3, 2, 1 and 0, of the partition of the parameter space will be denoted respectively by V, S, L and P for Volume, Surface, Line and Point, respectively. The surfaces are named using a number which corresponds to each bifurcation surface which is placed on the left side of the letter S. To describe the portion of the surface we place an index. The curves that are intersection of surfaces are named by using their corresponding numbers on the left side of the letter L, separated by a point. To describe the segment of the curve we place an index. Volumes and Points are simply indexed (since three or more surfaces may be involved in such an intersection).

We consider an example: surface $(\mathscr{S}_2)$ splits into 20 different two–dimensional parts labeled from $2S_1$ to $2S_{20}$, plus some one–dimensional arcs labeled as $2.iL_j$ (where i denotes the other surface intersected by $(\mathscr{S}_2)$ and j is a number), and some zero–dimensional parts. In order to simplify the labels in all figures we see **V1** which stands for the TEX notation V_1. Analogously, **2S1** (respectively **2.3L1**) stands for $2S_1$ (respectively $2.3L_1$), see Fig. 30 for example. And the same happens with many other pictures.

In Fig. 28 we represent the generic slice of the parameter space when $m = m_2 = 4$, showing only the algebraic surfaces.

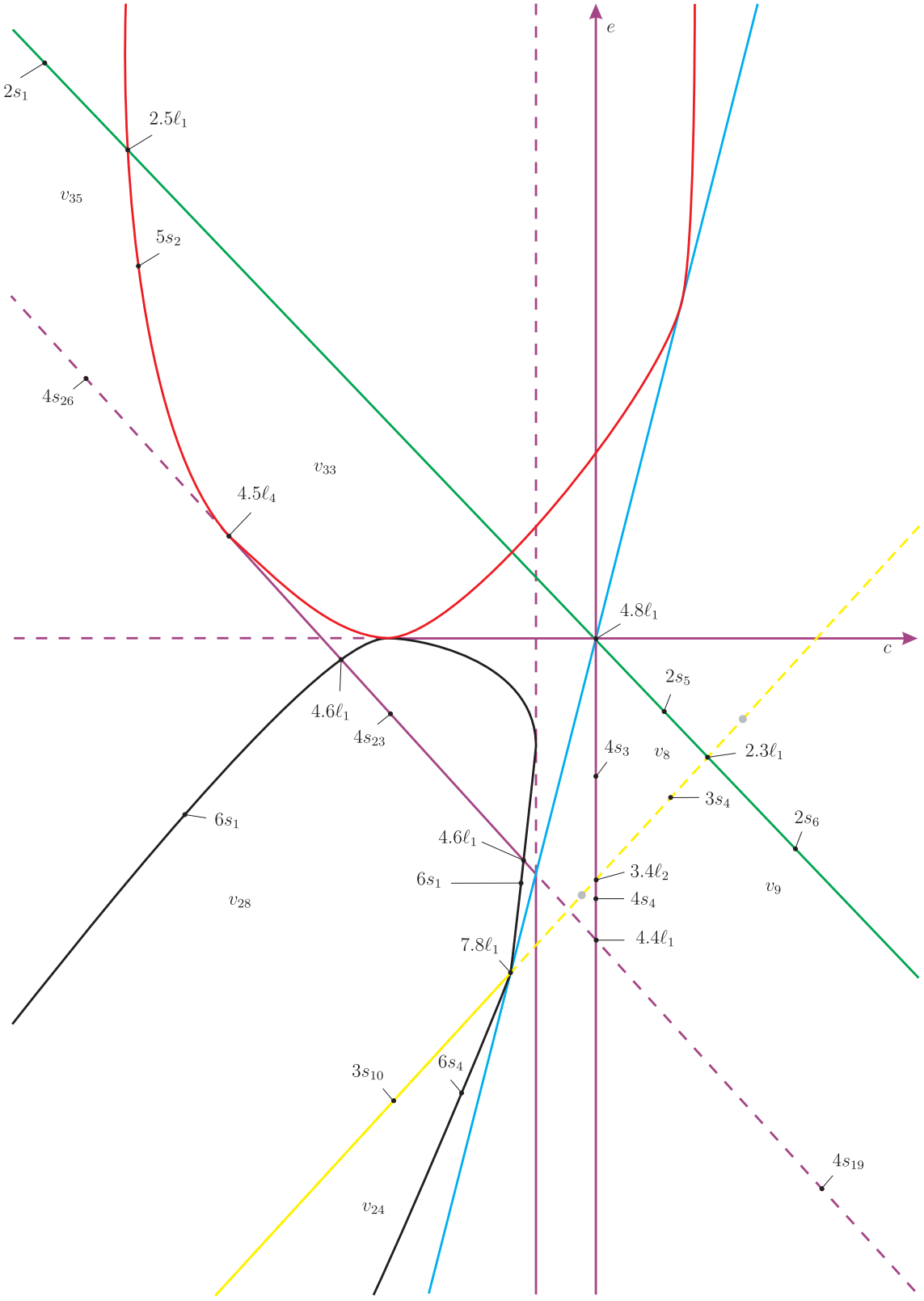

Figure 28 – Slice of parameter space when $m = 4$ (only algebraic surfaces)

In Fig. 28 we point out that there are some dashed branches of surface $(\mathscr{S}_3)$ (in yellow) and $(\mathscr{S}_4)$ (in purple). This means the existence of a weak saddle, in the

case of surface ($\mathscr{S}_3$), and the existence of an invariant straight line without separatrix connection, in the case of surface ($\mathscr{S}_4$); they do not mean a topological change in the phase portraits but a C^∞ change. In the next figures we will use the same representation for these characteristics of these two surfaces.

We also point out that the gray dots that appear in surface ($\mathscr{S}_3$) indicate weak singularities of order two or higher, according to Rmk. 4.3.2 and 4.3.3.

With the purpose of explaining all the changes in the bifurcation diagram, we would have to present two versions of the picture of each slice: one of them without labels and the other with labels in each new part (as it was done, for instance, in Artés, Rezende and Oliveira (2013) and Artés, Rezende and Oliveira (2014)). However, as the number of slices is considerably large (see equation (4.6) – 54 slices to be more precise) we would have to present 108 pictures, which would occupy a large number of pages. Then, we will present only the labeled drawings (just the "important part" in each slice) containing the algebraic and nonalgebraic bifurcation surfaces. In the next section, we prove the existence of such nonalgebraic surfaces and their necessity for the coherence of the bifurcation diagram.

Remark 4.3.34. Wherever two parts of equal dimension d are separated only by a part of dimension $d-1$ of the black bifurcation surface ($\mathscr{S}_6$), their respective phase portraits are topologically equivalent since the only difference between them is that a finite antisaddle has turned into a focus without change of stability and without appearance of limit cycles. We denote such parts with different labels, but we do not give specific phase portraits in pictures attached to Thm. 4.1.1 for the parts with the focus. We only give portraits for the parts with nodes, except in the case of existence of a limit cycle or a graphic where the singular point inside them is portrayed as a focus. Neither do we give specific invariant description in Sec. 4.5 distinguishing between these nodes and foci.

4.3.2 Bifurcation surfaces due to connections (nonalgebraic) in the affine part of $\mathbb{RP}^3$

We start this section explaining the generic slice when $m=4$ presented in Fig. 28. In this slice we make a complete study of all its parts, whereas in the next slices we only describe the changes. Some singular slices will produce only few changes which are easy to describe, but others can produce simultaneously many changes, even a complete change of all parts and these will need a more detailed description.

As said in last section, in Fig. 28 we present the slice when $m=4$ with only the algebraic surfaces. We now place for each set of the partition on this slice the local behavior of the flow around the singular points. For a specific value of the parameters of each one of the sets in this partition we compute the global phase portrait with the

numerical program P4 (see Artés *et al.* (2005) and Dumortier, Llibre and Artés (2008)).

In this slice we have a partition in two–dimensional parts bordered by curved polygons, some of them bounded, others bordered by infinity. From now on, we use lower–case letters provisionally to describe the sets found algebraically in order to not interfere with the final partition described with capital letters. For each two–dimensional part we obtain a phase portrait which is coherent with those of all their borders, except for four parts, which are shown in Fig. 28 and named as follows:

- v_8: the triangle bordered by green, purple and yellow curves;
- v_9: the pentagon bordered by green, yellow and purple curves and infinity;
- v_{28}: the curved pentagon bordered by black, purple and yellow curves and infinity;
- v_{35}: curved quadrilateral bordered by green, red and purple curves and infinity.

The study of these parts is quite important for the coherence of the bifurcation diagram. That is why we have decided to present only these parts in Fig. 28.

We begin with the analysis of the parts v_8 and v_9. First we consider part v_8. If we are sufficiently close to part $2s_5$, the respective phase portrait is topologically equivalent to the one in V_8, because in $2s_5$ we have the phase portrait topologically equivalent to $2S_5$, see Fig. 16. However, on $4s_3$, the separatrix of the infinite saddle–node connects with a separatrix of the finite saddle–node producing an invariant straight line linking the pair of infinite saddle–nodes. When perturbing this straight line by entering part v_8, this connection is broken and the separatrix of the infinite saddle–node connects with the infinite stable node and the separatrix of the finite saddle–node connects with the infinite unstable node, leading to a phase portrait topologically different from V_8. This proves that the region v_8 must be split into at least two connected regions. On the other hand, on $2s_5$ the phase portrait possesses a cusp point and all the canonical regions in its corresponding phase portrait are topologically the same as in phase portrait V_8, except for the *infinite basin* involving the finite saddle–node which became the cusp point. By a *basin* we understand a region bordered by two separatrices of a same singularity which have the same limit–object, most commonly, they end at an infinite singularity and we call it an *infinite basin* or they end at a finite singularity and we call it a *finite basin*.

As we have concluded that we have at least two different phase portraits inside region v_8, there must exist at least one element $7S_1$ of surface $(\mathscr{S}_7)$ dividing part v_8 into two "new" parts, V_8 and V_{10}, which represents a bifurcation due to the connection between a separatrix of a finite saddle–node with a separatrix of a finite saddle. It is worth mentioning that the segment $3s_4$ refers to the presence of weak saddle which shows that the movement from v_8 to v_9 does not imply a topological change. Then, part v_9 must also

be divided into V_9 and V_{11} by an element $7S_2$ of surface $(\mathscr{S}_7)$ with the same bifurcation as $7S_1$. In fact, $7S_2$ is clearly a "continuation" of $7S_1$. Coupled with this idea, we have parametrized the yellow surface, "walked" on it and found that there exists a topological change in the corresponding phase portraits. Then, $7S_1$ has one of its endpoints on $3s_4$ (dividing it into $3S_4$ and $3S_5$) and Lemma 4.3.35 assures that the other endpoint is $4.8\ell_1$.

Lemma 4.3.35. The endpoint of $7S_1$ (rather than the one which is on $3s_4$) is $4.8\ell_1$. Moreover, $7S_2$ is not bounded.

Proof. Numerical tools show that the endpoint of $7S_1$, rather than the one which is on $3s_4$, is $4.8\ell_1$. In what follows, we prove that this endpoint cannot be on segments $4s_3$ and $2s_5$. Moreover, $7S_2$ is not bounded.
If this endpoint was located on $4s_3$, as we said before, there must exist a connection between a separatrix of a finite saddle–node with a separatrix of a finite saddle. Then, in this case, the invariant line would be broken in order to make this bifurcation happens.
We point out that the endpoint of $7S_1$ also cannot be located on $2s_5$, since $7S_1$ describes a connection between a separatrix of a finite saddle with a separatrix of a finite saddle–node and this separatrix (of the saddle–node) disappears when on $2s_5$ the finite saddle–node becomes a cusp–type singularity.
Therefore, as the endpoint of $7S_1$ is neither on $4s_3$ nor on $2s_5$, this confirms the evidence pointed out by the numerical calculations that $7S_1$ ends at $4.8\ell_1$.
Moreover, as we know that on $4s_{19}$ there is no invariant straight line that produces a topological change, it is not relevant whether $7S_2$ crosses $4s_{19}$ or not. □

We show the sequence of phase portraits along these subsets in Fig. 29. We also draw the complete bifurcation diagram for these two parts in Fig. 30.

We have added in the bifurcation diagram a label associated to each part of the bifurcation $(\mathscr{S}_7)$ indicating the type of connection produced by this bifurcation. The possibilities are "(ℓoop)", "(f–f)" (for a connection between different finite singularities), "(f–∞)" (for a connection between a finite singularity and an infinite one), and "(∞–∞)" (for a connection between different infinite singularities). These labels are indicated only in the first time that the corresponding nonalgebraic bifurcation is detected.

We now perform the study of part v_{28}. We consider the segment $3s_{10}$ in Fig. 28, which is one of the borders of part v_{28}. On this segment, the corresponding phase portrait possesses a weak focus (of order one) and, consequently, this branch of surface $(\mathscr{S}_3)$ corresponds to a Hopf bifurcation. This means that either in v_{24} or in v_{28} we must have a limit cycle; in fact it is in v_{28}.

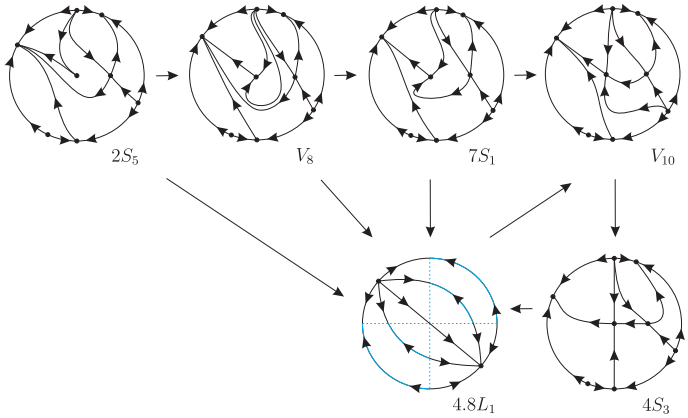

Figure 29 – Sequence of phase portraits in parts v_8 and v_9 of slice $m = 4$ (the labels are according to Fig. 30). We start from v_8. We recall that the phase portrait $3S_4$ (respectively $3.7L_1$ and $3S_5$) is equivalent to the phase portrait V_8 (respectively $7S_1$ and V_{10}) up to a weak saddle. If we start on $2s_5$ we can reach V_{10} by the path $2S_5 \to 4.8L_1 \to V_{10}$. When crossing $2s_5$, we shall obtain the phase portrait V_8 in a subset of v_8. From this point we may choose three different ways to reach the subset V_{10} by crossing the purple surface: (1) from the phase portrait $3.7L_1$ to the V_{10}; (2) from the phase portrait $7S_1$ to the V_{10}; and (3) from the degenerate phase portrait $4.8L_1$ to the V_{10}. Now, from v_9, when crossing $2s_6$ (topologically equivalent to $2s_5$), we shall obtain the phase portrait V_9 (topologically equivalent to V_8) in a subset of v_9. From this point we may choose two different ways to reach the subset V_{11} (topologically equivalent to V_{10}) by crossing the purple surface: (1) from the phase portrait $3.7L_1$ to the V_{11} or (2) from the phase portrait $7S_2$ (topologically equivalent to $7S_1$) to the V_{11}

However, when we get close to $6s_1$ and $4s_{23}$, the limit cycle has been lost, which implies the existence of at least one more element of surface $(\mathscr{S}_7)$ (see $7S_3$ in Fig. 30) in a neighborhood of $3s_{10}$; furthermore, the phase portrait in a small neighborhood of $6s_1$ (respectively $4s_{23}$) is not coherent to that obtained just after making the limit cycle disappears. If we fix a value for the parameter c in order to be in this part and we make the parameter e increases from $3s_{10}$ towards $4s_{23}$, then we obtain generically three topologically distinct phase portraits inside part v_{28}, which implies the existence of not only one but at least two elements of surface $(\mathscr{S}_7)$, namely, $7S_3$ and $7S_4$ in Fig. 30. Such new phase portraits are V_{25}, with limit cycle, V_{26} and V_{28}, without limit cycles (see Fig. 31 for a sequence of phase portraits in these parts). Even though parts V_{26} and V_{28} have no limit cycles, they provide topologically distinct phase portraits since the connection of separatrices on $7S_4$ is due to the saddle–node $\overline{\binom{1}{1}}$ SN and the finite saddle–node, i.e. connection of separatrices from different points, whereas the connection on $7S_3$ is due to a saddle–node to itself (i.e. a loop–type connection). In Lemma 4.3.36 we show that $7S_3$ and $7S_4$ have one of its ends at the curve $7.8\ell_1$ and, in addition, they are not bounded. We plot the complete bifurcation diagram for these two parts in Fig. 30.

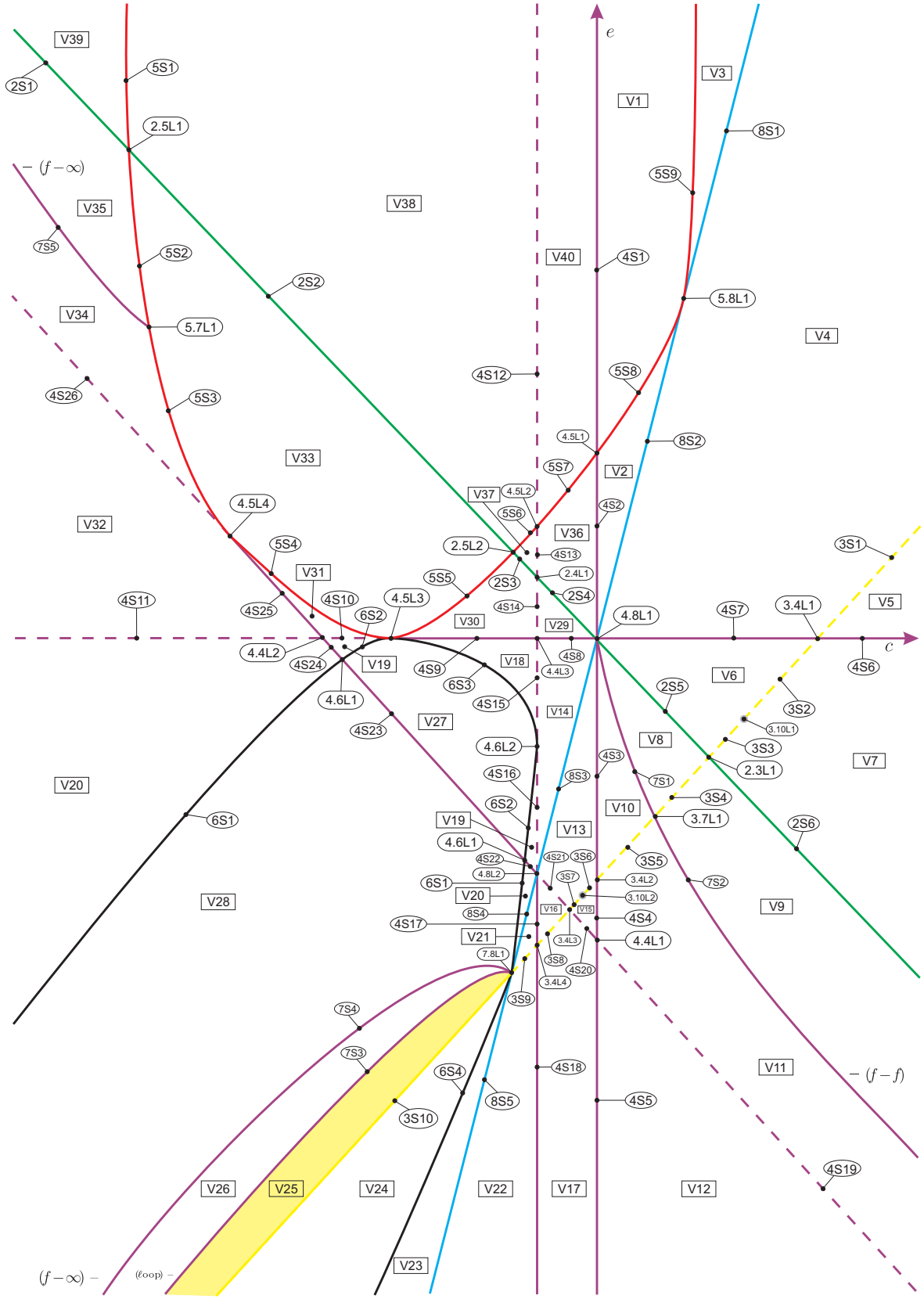

Figure 30 – Complete bifurcation diagram for slice $m = 4$

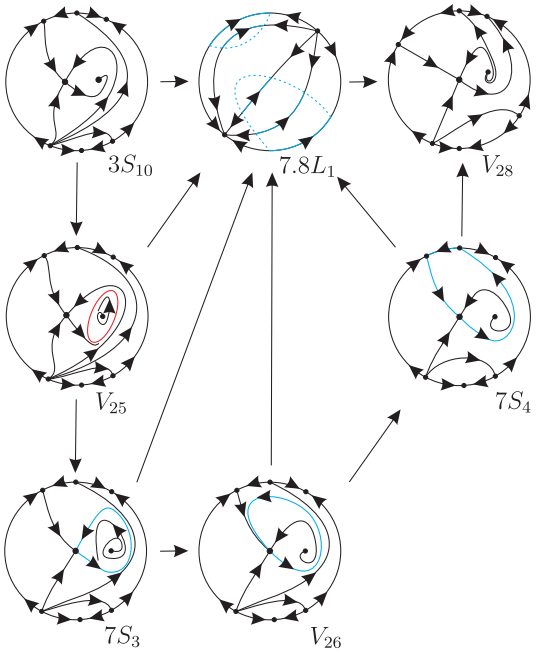

Figure 31 – Sequence of phase portraits in part v_{28} of slice $m = 4$ (the labels are according to Fig. 30). By starting on $3s_{10}$ we can reach V_{28} by the path $3S_{10} \to 7.8L_1 \to V_{28}$. Now, when crossing $3s_{10}$, we shall obtain phase portrait V_{25} (with limit cycle) in a subset of v_{28}. From this point we may choose at least five different ways to reach the phase portrait of the region V_{28}: (1) $V_{25} \to 7.8L_1 \to V_{28}$; (2) $V_{25} \to 7S_3 \to 7.8L_1 \to V_{28}$; (3) $V_{25} \to 7S_3 \to V_{26} \to 7.8L_1 \to V_{28}$; (4) $V_{25} \to 7S_3 \to V_{26} \to 7S_4 \to 7.8L_1 \to V_{28}$; and (5) $V_{25} \to 7S_3 \to V_{26} \to 7S_4 \to V_{28}$

Lemma 4.3.36. One of the endpoints of $7S_3$ and $7S_4$ is $7.8\ell_1$. Moreover, $7S_3$ and $7S_4$ are not bounded.

Proof. Numerical analysis suggest that surfaces $7S_3$ and $7S_4$, which corresponds to a loop–type bifurcation and finite–infinite separatrix connection, respectively, have one of its ends on the curve $7.8\ell_1$. Indeed, if the starting point of any of these surfaces is any point of $3s_{10}$, then a portion of this subset must not refer to a Hopf bifurcation, which contradicts the fact that on $3s_{10}$ we have a weak focus of order one. On the other hand, we observe that it is not possible that the starting point of these surfaces is on $6s_1$, since on black surfaces we have only a C^∞ node–focus bifurcation. In fact, this can happen only if surface $(\mathscr{S}_6)$ intersects other surfaces like $(\mathscr{S}_3)$ and $(\mathscr{S}_8)$. Moreover, the endpoint of $7S_3$ and $7S_4$ cannot be on $4s_{23}$ because, in order to have this, in any case, first we need to break the invariant straight line. Then, the only possible endpoint of surfaces $7S_3$ and $7S_4$ is $7.8\ell_1$. Using the same arguments we can conclude that such surfaces are not bounded. □

Now, we carry out the analysis of part v_{35}. The phase portrait in v_{35} near $2s_1$ possesses a finite basin passing through the finite saddle–node, i.e. two separatrices of the finite saddle–node start at the same finite antisaddle, whereas the phase portrait in v_{35}

near $4s_{26}$ does not possess the finite basin. Then, there must exist at least one element $7S_5$ of surface $(\mathscr{S}_7)$ dividing part v_{35} into two "new" parts, V_{34} and V_{35}, which represents a bifurcation due to the connection between a separatrix of a finite saddle–node with a separatrix of an infinite saddle (see Fig. 32 for a sequence of phase portraits in these parts). As the segment $5s_2$ corresponds to changes in the infinite singular points, the finite part of the phase portraits remains unchanged and this element of surface $(\mathscr{S}_7)$ must intersect $5s_2$ having this intersection point as one of its endpoints, since in v_{33} we have only one infinite singularity, namely, the infinite saddle–node. With these arguments we have parametrized the red surface, "walked" on it and found that there exists a topological change in the phase portraits obtained. In Lemma 4.3.37 we prove that $7S_5$ is unbounded and it has $5.7\ell_1$ as endpoint. We plot the complete bifurcation diagram for these two parts in Fig. 30.

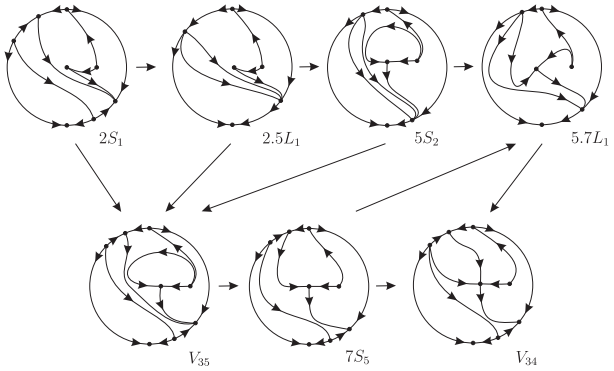

Figure 32 – Sequence of phase portraits in part v_{35} of slice $m = 4$ (the labels are according to Fig. 30). By starting on $2s_1$ we can reach V_{34} by one of the following paths: (1) $2S_1 \to 2.5L_1 \to 5S_2 \to 5.7L_1 \to V_{34}$; (2) $2S_1 \to 2.5L_1 \to 5S_2 \to V_{35} \to 7S_5 \to V_{34}$; (3) $2S_1 \to 2.5L_1 \to 5S_2 \to V_{35} \to 7S_5 \to 5.7L_1 \to V_{34}$; (4) $2S_1 \to 2.5L_1 \to V_{35} \to 7S_5 \to V_{34}$; and (5) $2S_1 \to V_{35} \to 7S_5 \to V_{34}$

Lemma 4.3.37. The element $7S_5$ of surface $(\mathscr{S}_7)$ is unbounded and it has $5.7\ell_1$ as endpoint.

Proof. Numerical tools indicate that one of the endpoints of $7S_5$ is $5.7\ell_1$. In what follows, we prove that it cannot be on $4s_{26}$ and $2s_1$.

In fact, as $4s_{26}$ represents the existence of an invariant line which does not indicate a topological change, it cannot contain an endpoint of $7S_5$, unless there exists a degenerate portion of $4s_{26}$ where this endpoint is located. Moreover, as on $2s_1$ the finite saddle–node already has become a cusp–type singularity, we do not have a finite saddle–node in order to perform the topological changes given by $7S_5$. Then, $7S_5$ must intersect the red surface. In fact, its endpoint is $5.7\ell_1$ because in v_{33} we do not have the necessary number of infinite singularities in such a way that the bifurcations given by $7S_5$ could happen.

Therefore, we confirm the evidence pointed out by the numerical calculations that $7S_5$

has $5.7\ell_1$ as an endpoint. By the same arguments we conclude that such a surface is unbounded. □

Having analyzed all the parts pointed out on page 148 and explained the existence of all possible nonalgebraic surfaces in there (modulo islands), we have finished the study of the generic slice $m = 4$. However, we cannot be sure that these are all the additional bifurcation surfaces in this slice. There could exist others which are closed surfaces small enough to escape our numerical research. For all other two–dimensional parts of the partition of this slice, whenever we join two points which are close to different borders of the part, the two phase portraits are topologically equivalent. So, we do not encounter more situations than the ones mentioned before. In short, it is expected that the complete bifurcation diagram for $m = 4$ is the one shown in Fig. 30. In this and the next figures, we have colored in light yellow the open regions with one limit cycle, in black the labels referring to new parts which are created in a slice and in red the labels corresponding to parts which has already appeared in previous slices.

We already know that there are no more singular slices for $m > 3$. We have to prove also that there are no other significant nonalgebraic slices for $m \geq 4$. In order to do this we must describe the slice at infinity, which correspond to the case $h = 0$ and $m = 1$. By studying and describing all the phase portraits in these slices and finding coherence in continuity between the phase portraits on the infinite slice and the slice $m = 4$, we have proved that we do not need more singular slices. In the limit to infinity, the bifurcation diagram (of the algebraic surfaces) tends to be the one shown in Fig. 33.

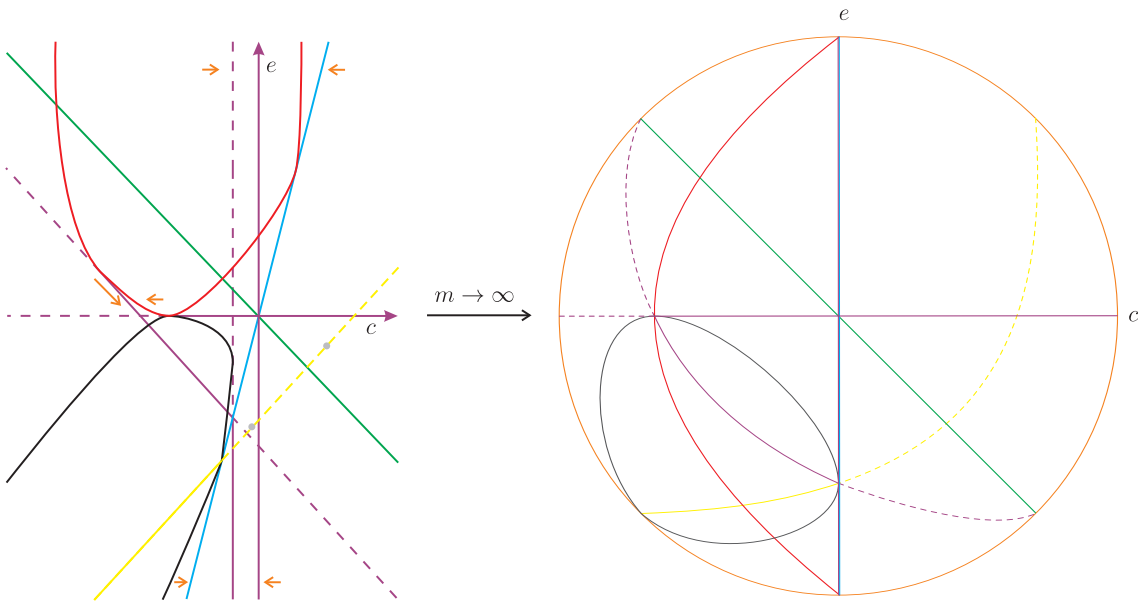

Figure 33 – The transition from $m > 4$ to infinity. The orange arrows show the movement that the surfaces must do as $m \to \infty$

4.3.3 Bifurcation surfaces at the infinite part of $\mathbb{RP}^3$

In order to make this transition (or convergence) clearer, we need to describe the algebraic curves which appear in the slice $m = +\infty$. In fact, as we said before, the slice $m = +\infty$ is obtained by considering $h = 0$ and $m = 1$ in the normal form (4.1), which becomes

$$\begin{aligned} \dot{x} &= cx + cy - cx^2, \\ \dot{y} &= ex + ey - ex^2 + 2xy. \end{aligned} \tag{4.7}$$

In this way, according to the definition of surfaces $(\mathscr{S}_2)$ to $(\mathscr{S}_{10})$ we observe that, under these conditions of the parameters h and m, we have:

- surface $(\mathscr{S}_2)$ remains the same;
- surface $(\mathscr{S}_3)$ needs to be redefined since now we have $\mathscr{T}_i = 0, i = 1, \ldots, 4$;
- surface $(\mathscr{S}_4)$ reduces to $ce(c+e+2) = 0$;
- surfaces $(\mathscr{S}_5)$ and $(\mathscr{S}_6)$ must also be redefined since now we have $\eta = W_4 = 0$, respectively;
- two–point set $(\mathscr{S}_{6.2})$ does not make sense here, since $G_9 = 0$; and
- surface $(\mathscr{S}_8)$ reduces to $c = 0$.

Then, we must define surfaces $(\mathscr{S}_3)$, $(\mathscr{S}_5)$ and $(\mathscr{S}_6)$ in terms of other nonzero invariants (or comitants) which represent the same geometrical meaning as those ones that vanish.

The curve at slice $m = +\infty$ of C^∞ bifurcation due to a strong saddle or a strong focus changing the sign of their traces (weak saddle or weak focus)

$(\mathscr{S}_3')$ This is the bifurcation surface due to finite weak singularities, which occurs when the trace of a finite singular point is zero. Calculations yield

$$\mathscr{T}_4 = \mathscr{T}_3 = \mathscr{T}_2 = \mathscr{T}_1 = 0, \quad \sigma = c + e + 2x(1-c) \neq 0.$$

According to Vulpe (2011), Main Theorem, item (e), under these conditions, systems (4.1) could possess one and only one weak singularity. Moreover these systems have one weak singularity, which is of the type indicated in the sequence if and only if one of the following conditions holds:

- $s^{(1)} \Leftrightarrow \mathscr{F}_1 \neq 0, \mathscr{H} = \mathscr{B}_1 = 0, \mathscr{B}_2 > 0$;
- $f^{(1)} \Leftrightarrow \mathscr{F}_1 \neq 0, \mathscr{H} = \mathscr{B}_1 = 0, \mathscr{B}_2 < 0$.

Therefore, for $h=0$ and $m=1$ systems (4.1) do not have weak singularities of order two or higher. Moreover, under these conditions we have:

$$\begin{aligned}\mathscr{F}_1 &= -2c^2(c+3e+2), \quad \mathscr{H} = 0,\\ \mathscr{B}_1 &= 2c^2(c+e)^2(c-e-2),\\ \mathscr{B}_2 &= -2c^3(c+e)(c-3e-4)(c-1)^2.\end{aligned}$$

According to the Main Theorem just mentioned, if the conditions $\mathscr{F}_1 \neq 0$ and $\mathscr{B}_1 = 0$ imply $\mathscr{B}_2 \neq 0$, then we have a weak focus or a weak saddle. In fact, the condition $\mathscr{B}_1 = 0$ implies $c = e+2$ and the condition $\mathscr{F}_1 \neq 0$ implies $c \neq 0$ and $c+3e+2 \neq 0$ (i.e. $e+1 \neq 0$). So, from the expression of $\mathscr{B}_2$ we have

$$c-3e-4 = -2(e+1) \neq 0.$$

Therefore, in the slice $m=+\infty$ we define surface $(\mathscr{S}_3')$ by the equation of the straight line

$$(\mathscr{S}_3'): c-e-2=0.$$

The bifurcation curve in slice $m=+\infty$ due to multiplicities of infinite singularities

$(\mathscr{S}_5')$ This is the bifurcation surface due to multiplicity of infinite singularities. As we said before, under the conditions $h=0$ and $m=1$ we have that $\eta=0$. Then, we already have that two infinite singularities have coalesced. In order to detect when we have a triple infinite singularity, we calculate

$$\widetilde{M} = -8(c+2)^2x^2, \quad C_2 = x^2(ex-y(2+c)).$$

According to Lemma 5.5 from Artés *et al.* (2021), a triple infinite singularity occurs if and only if $\widetilde{M}=0$ and $C_2 \neq 0$. Therefore, in the slice $m=+\infty$ we have a coalescence of infinite singularities on the straight line

$$(\mathscr{S}_5'): c+2=0.$$

In fact, this argument shows the reason why we have drawn a red straight line instead of a parabola in Fig. 33.
On the other hand, according to the mentioned Lemma, if $(c,e)=(-2,0)$, then the line at infinity is filled up with singularities, since $C_2=0$.

The curve in slice $m=+\infty$ of C^∞ bifurcation due to a node becoming a focus

$(\mathscr{S}_6')$ This surface contains the points of the parameter space where a finite node of the systems turns into a focus. This surface is a C^∞ but not a topological bifurcation surface. In fact, when we cross surface $(\mathscr{S}_6')$ in the bifurcation diagram, the topological phase

portraits do not change. However, as in the affine part of $\mathbb{RP}^3$, this surface is relevant for isolating the regions where a limit cycle surrounding an antisaddle cannot exist. According to Artés, Llibre and Vulpe (2008) and Artés *et al.* (2021), as we have (assuming $h=0$ and $m=1$) $G_9 = W_4 = 0$, we must consider the invariant $W_7 = 0$, which defines a parabola

$$(\mathscr{S}_6'): c^2 - 2c(e-2) + (e+2)^2 = 0.$$

Since these curves have the same geometrical meaning as those previous ones that became zero, we keep the respective colors for these curves as we have described before.

Another important bifurcation algebraic curve for this slice is the following one.

Bifurcation algebraic curve in the slice $m=+\infty$ due to the presence of an infinite nilpotent singularity of type $\widehat{\binom{1}{2}}\,E-H$

$(\mathscr{L}_0)$ For $h=0$ and $m=1$, the corresponding phase portraits on the line $c+1=0$ in the bifurcation diagram possess an infinite singularity of the type $\widehat{\binom{1}{2}}\,E-H$, which is the transition between the singularities $\widehat{\binom{1}{2}}\,PEP-H$ and $\widehat{\binom{1}{2}}\,E-PHP$. Such a straight line is needed for the coherence of the bifurcation diagram. In fact, according to Artés *et al.* (2021) we know that the comitant $\widetilde{N}$ is related to a triple infinite singularity and such a comitant only makes sense in the slices where such a kind of singularity appears, i.e. in the slices where we do not have a triple infinite singularity this comitant does not affect at all. Moreover, $\widetilde{N}$ "works like" $\mathscr{T}_4$, in the sense that the curve $\widetilde{N}=0$ splits the parameter space into two distinct canonical regions and the phase portrait over $\widetilde{N}=0$ is topologically equivalent to the phase portrait in one of its sides and topologically distinct to the one in the other side. In such a way we need to determine the points on the parameter space that verifies the equation $\widetilde{N}=0$. Calculations yield

$$\widetilde{N} = -4(c+1)x^2.$$

It is clear that the straight line $c+1=0$ verifies this equation. Therefore we define the curve $(\mathscr{L}_0)$ by the equation

$$(\mathscr{L}_0): c+1=0,$$

and we draw such a straight line with the brown color.

In order to determine the endpoints of each one of these curves, we take the respective projective equation with homogeneous coordinates C, E and M, we put $M=0$ and then we calculate the roots of the resulting polynomial.

As in slice $m=+\infty$ we are in a surface, in fact the upper half–sphere $\mathbb{S}^2$, we point out that all the "generic" parts in this slice are labeled as $9S_j$, the lines are labeled as $9.iL_j$ and the points as points. We use the orange color for the equator of $\mathbb{S}^2$, i.e. $h=m=0$.

We now have finished describing the algebraic curves that appear in slice $m = +\infty$. In Fig. 34 we present this slice completely and properly labeled. We draw special attention to the fact that the nonalgebraic curves (numerically detected and which existence was proved before) still remain in this slice and they maintain the same relative positions with respect to the algebraic curves in the transition from slice $m = 4$ to slice $m = +\infty$, numerical tools support this claim.

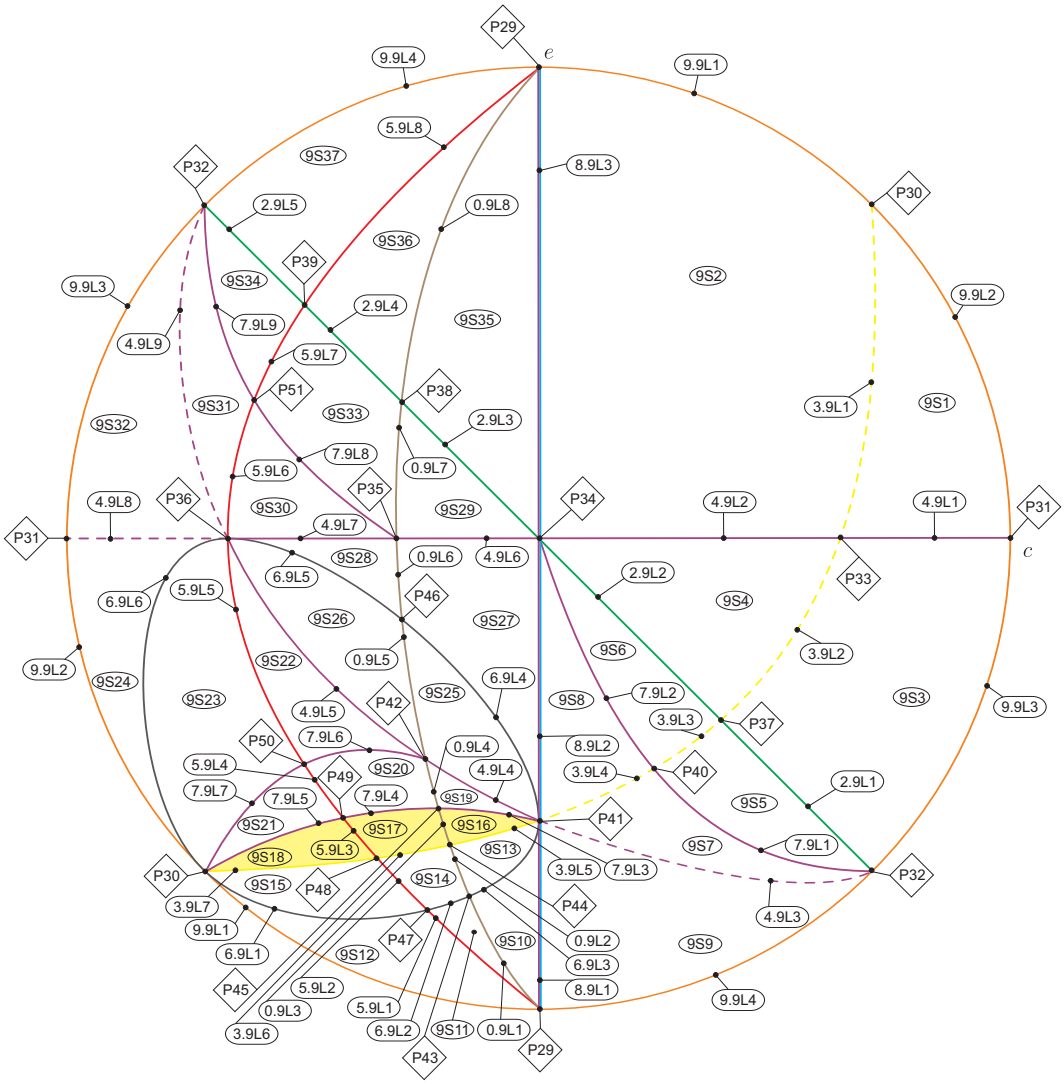

Figure 34 – Slice of parameter space when $m = +\infty$

There are some relevant facts on the bifurcation diagram that are worth being remarked. On one side we already have the curve $(\mathscr{L}_0)$ which has topological relevance only on $h = 0$, as we already have described. Moreover, we also have that surface $(\mathscr{S}_5)$ which is a parabola in the affine slices degenerates as a double line when $h = 0$. This degeneration apart from collapsing some parts of the bifurcation diagram, introduces a new bifurcation in some other parts where before it did not exist. Such bifurcations will also be relevant for large negative values of m.

Even more, we also have surface ($\mathscr{S}_7$) which in slice $m=4$, its part $7S_5$ borders V_{34} and V_{35}, but it does not affect either part V_{33} or V_{30}. However, at infinity, after the collapse of the parabola ($\mathscr{S}_5$) the border of region V_{30} on $h=0$ is also split into two because of $7.9L_8$. The difference between the topological behavior in $9S_{30}$ and $9S_{33}$ deals with the existence of separatrices of an elliptic–saddle at infinity. This allows the possibility of a separatrix connection between one of this separatrices and a separatrix of the finite saddle–node. Since the elliptic–saddle does not exist for $h=1$ this bifurcation looses all the sense in the affine space. Since we have detected the two possible bifurcations from the separatrix connection implied by $7.9L_8$, we then prove its existence. See all the respective phase portraits in Figs. 15 to 21. These are the reasons why some three–dimensional parts of the affine space which have their border on $h=0$ split into several two–dimensional regions (plus the corresponding one–dimensional borders).

In Table 10 we indicate the "death" of all volume parts from slice $m=4$ to $m=+\infty$. Then we have established the correspondence between the phase portraits of the slices $m=4$ and $m=+\infty$. Therefore, the convergence presented in Fig. 33 is coherent.

Table 10 – Transition from slice $m=4$ to $m=+\infty$. Here we present the correspondence between the volume regions from slice $m=4$ and the respective parts from slice $m=+\infty$

Parts in slice $m=4$	Parts in slice $m=+\infty$	Parts in slice $m=4$	Parts in slice $m=+\infty$
V_1	$8.9L_3$	V_{21}	P_{41}
V_2	$8.9L_3$	V_{22}	$8.9L_1$
V_3	$8.9L_3$	V_{23}	$9S_{10}$, $9S_{11}$, $9S_{12}$
V_4	$9S_2$	V_{24}	$9S_{13}$, $9S_{14}$, $9S_{15}$
V_5	$9S_1$	V_{25}	$9S_{16}$, $9S_{17}$, $9S_{18}$
V_6	$9S_4$	V_{26}	$9S_{19}$, $9S_{20}$, $9S_{21}$
V_7	$9S_3$	V_{27}	$9S_{25}$, $9S_{26}$
V_8	$9S_6$	V_{28}	$9S_{22}$, $9S_{23}$
V_9	$9S_5$	V_{29}	P_{34}
V_{10}	$9S_8$	V_{30}	$9S_{29}$, $9S_{30}$, $9S_{33}$
V_{11}	$9S_7$	V_{31}	P_{36}
V_{12}	$9S_9$	V_{32}	$9S_{32}$
V_{13}	$8.9L_2$	V_{33}	$5.9L_6$, $5.9L_7$, P_{51}
V_{14}	$8.9L_2$	V_{34}	$9S_{31}$
V_{15}	P_{41}	V_{35}	$9S_{34}$
V_{16}	P_{41}	V_{36}	$8.9L_3$
V_{17}	$8.9L_1$	V_{37}	$9S_{35}$, $9S_{36}$
V_{18}	$9S_{27}$, $9S_{28}$	V_{38}	$5.9L_8$
V_{19}	P_{36}, P_{41}	V_{39}	$9S_{37}$
V_{20}	$9S_{24}$, P_{41}	V_{40}	$8.9L_3$

4.3.4 Transition from slice to slice in the affine part of $\mathbb{RP}^3$

Since there is coherence (modulo islands, as we discuss in Sec. 4.4) between the slices $m = +\infty$ and $m = 4$, no more slices $m > 4$ are needed.

Having finished the complete study of slice $m = 4$ and having presented the transition from $m = 4$ to $m = +\infty$, the next step is to decrease the values of m, according to equation (4.6), and make an analogous study for each one of the slices that we need to consider and also search for changes when going from one slice to the next one.

We now start decreasing the values of the parameter m in order to explain as much as we can the bifurcations in the parameter space.

We consider the curved triangle V_{37} in the second quadrant of slice $m = 4$ (see Fig. 30), having $2.4L_1$ as a vertex. As we move down from $m = 4$ to $m = 3$ (a singular slice), this triangle collapses to a single point, which we denote by P_1 in Fig. 35.

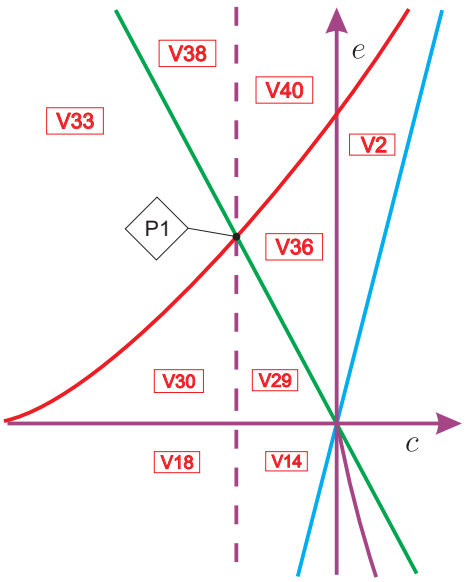

Figure 35 – Slice of parameter space when $m = 3$ (see Fig. 30)

When we go to the next generic slice, $m = 2$, we observe that from this P_1 a new curved triangle V_{41} is born, "pushing to the right" the old curved triangle V_{36}, as we can see in Fig. 36.

Now, studying the singular slice $m = 1$ we observe the following phenomena (compare Figs. 30 and 37):

- the curve $4.5L_3$ of the red parabola coalesces with $4.4L_3$ (see Fig. 30) and also with $4.5L_5$ (see Fig. 36), forming the point P_2 presented in Fig. 37. This movement makes region V_{30} vanishes;

- the black parabola degenerates and becomes a double straight line, which is now parallel to the yellow straight line and it still intersects the red parabola at P_2 (this fact was expected by the shape of the black surface shown in Fig. 27);

- the cyan straight line is parallel to the black and yellow surfaces.

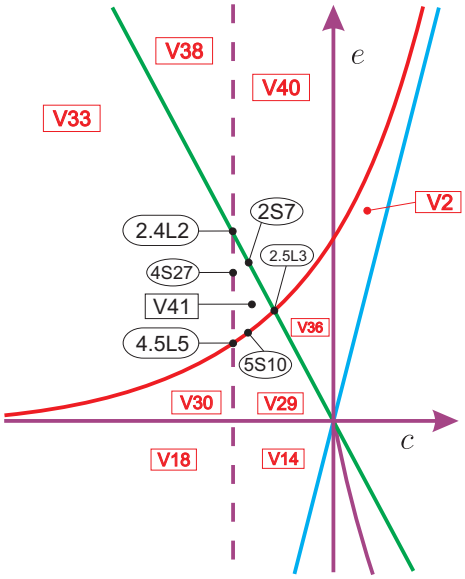

Figure 36 – Slice of parameter space when $m = 2$ (see Fig. 35)

Having in mind all these movements together, we observe from Fig. 30 that it is clear that the regions $V_{30}, V_{18}, V_{27}, V_{28}, V_{24}, V_{25}$ and V_{26} must vanish. As we now have that the black, cyan and yellow surfaces intersect at infinity (because they are parallel), the nonalgebraic surfaces $7S_3$ and $7S_4$ "have gone" to infinity of the third quadrant of the bifurcation diagram. In fact, later we will detect that they will "return" at the first quadrant of the next generic slice, $m = 3/4$. Moreover, the appearance of the black surface as a double straight line splits each one of the regions V_1, V_3, V_{40} and V_{41} into two regions each, which are separated in this slice but which are continuous in the three–dimensional space. So they received the same label. About the respective borders, we will indicate (in black color) only those containing the black straight line, since the others already have been defined previously and they were not "modified" by the presence of the black straight line. In addition, we observe that the nonalgebraic surfaces $7S_1$, $7S_2$ and $7S_5$ still remain in this slice. As in this slice we detect significant changes in the bifurcation diagram, in Fig. 37 we present one picture that gives a global idea of the bifurcation diagram when $m = 1$.

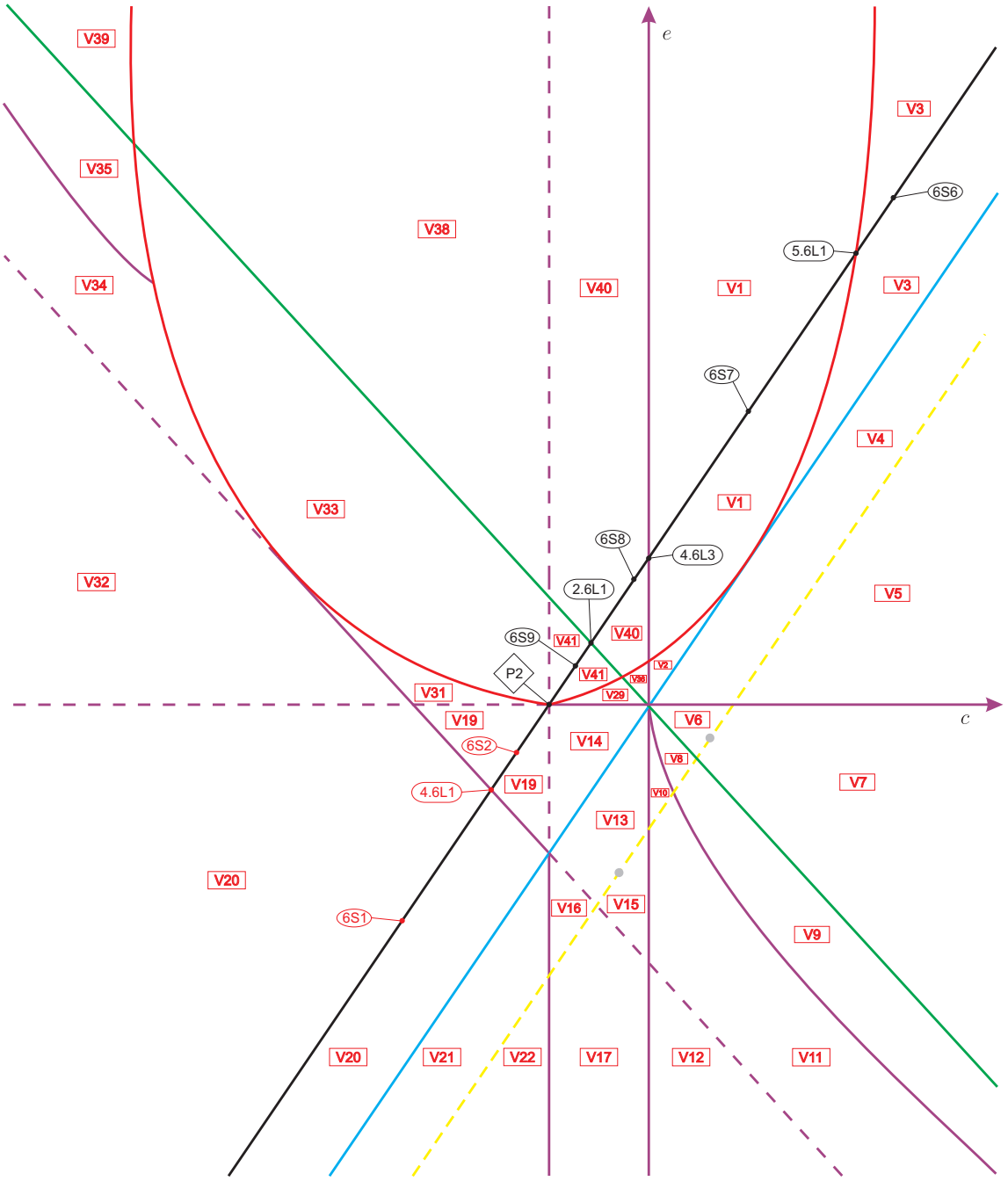

Figure 37 – Slice of parameter space when $m = 1$ (see Fig. 36)

Going on with the study of the slices, we pass to the study of the generic slice $m = 3/4$, see Fig. 40. This is a very interesting slice. Here we observe that the black straight line again has become a parabola, now in the semi–positive plane (in fact, this was expected by Fig. 27). Such a parabola generates six new volume regions, namely, v_{44} to v_{48} plus v_{51} (see Fig. 38). This is implied by the fact that as in the slice $m = 4$, one of its branches intersects the cyan and the yellow straight line in a point, namely, $7.8L_1$. Because of this triple intersection there must exist the new volume regions v_{48} and v_{51}, see Fig. 38. We have denoted them in lower–case letters and we have produced a gap

in the numeration because we detect that some new nonalgebraic surface will be needed, producing new volume regions.

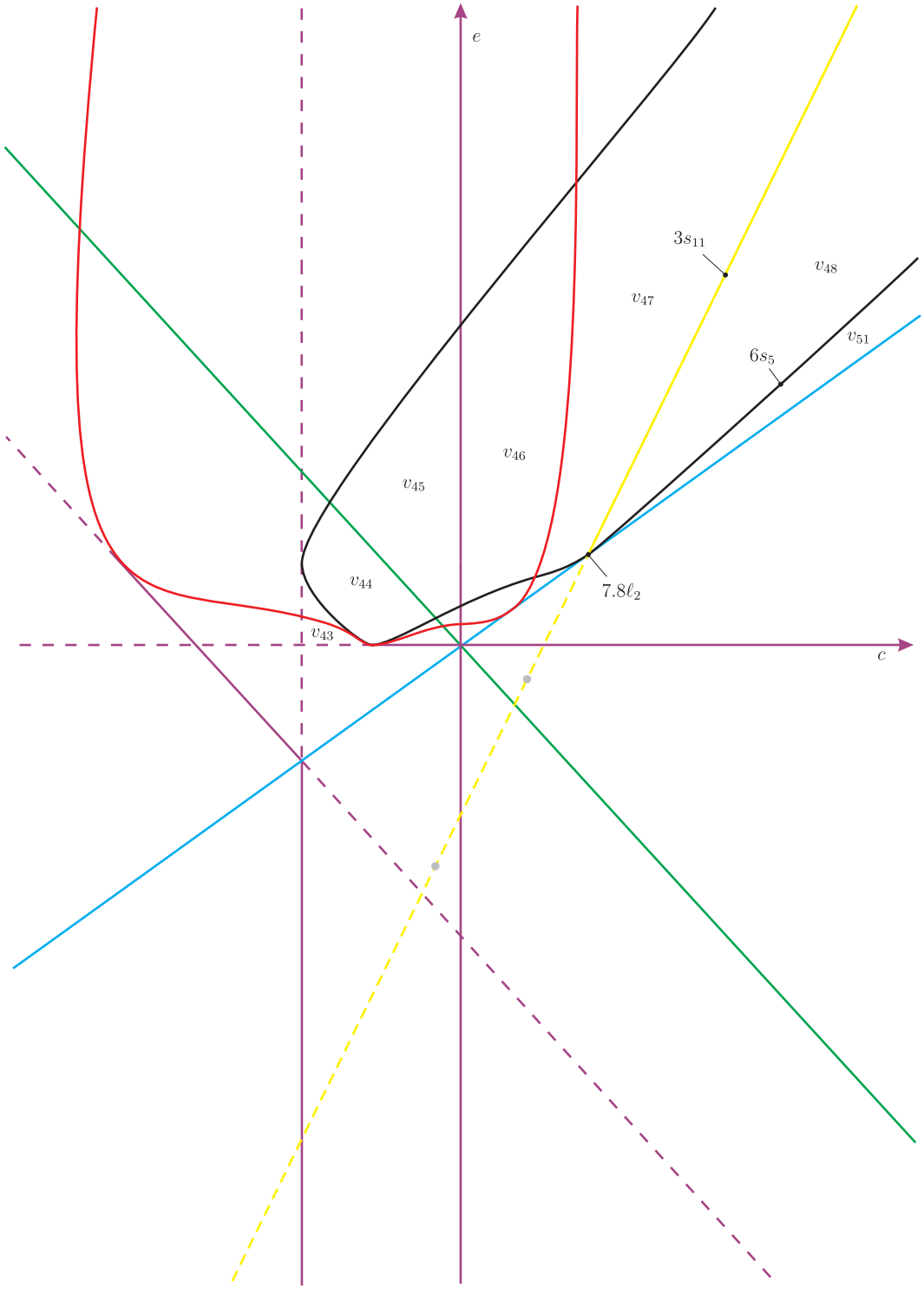

Figure 38 – Slice of parameter space when $m = 3/4$ (only algebraic surfaces)

Performing an analysis of this slice we note that the nonalgebraic surfaces $7S_1$, $7S_2$ and $7S_5$ remain. In addition, for each two–dimensional part we obtain a phase portrait

which is coherent with those of all their borders. Except for the part v_{48} (the curved triangle bordered by the black, yellow and infinite line in Fig. 38), which corresponds to part V_{48} in Fig. 40, which as we will see, will be split into several regions. Consider the segment $3s_{11}$ in Fig. 38, which is one of the borders of part v_{48}. On this segment the corresponding phase portrait possesses a weak focus (of order one) and, consequently, this branch of surface $(\mathscr{S}_3)$ corresponds to a Hopf bifurcation. This means that either in v_{47} or in v_{48} we must have a limit cycle; in fact it is in v_{48}. However, approaching $6s_5$, the limit cycle has been lost, which implies the existence of at least one more element of surface $(\mathscr{S}_7)$ (surface $7S_6$ in Fig. 40) in a neighborhood of surface $3S_{11}$; furthermore, the phase portrait in a small neighborhood of $6s_5$ is not coherent to that one obtained just after making the limit cycle disappears. If we fix a value of the parameter c in order to be in this part and we make the parameter e decreases from $3s_{11}$ towards $6s_5$, then we obtain three topologically distinct phase portraits inside part v_{48}, which implies the existence of not only one but at least two elements of surface $(\mathscr{S}_7)$, the surfaces $7S_6$ and $7S_7$ in Fig. 40; such new phase portraits are V_{48}, with limit cycle, V_{49} and V_{50}, without limit cycles (see Fig. 39 for a sequence of phase portraits in these parts).

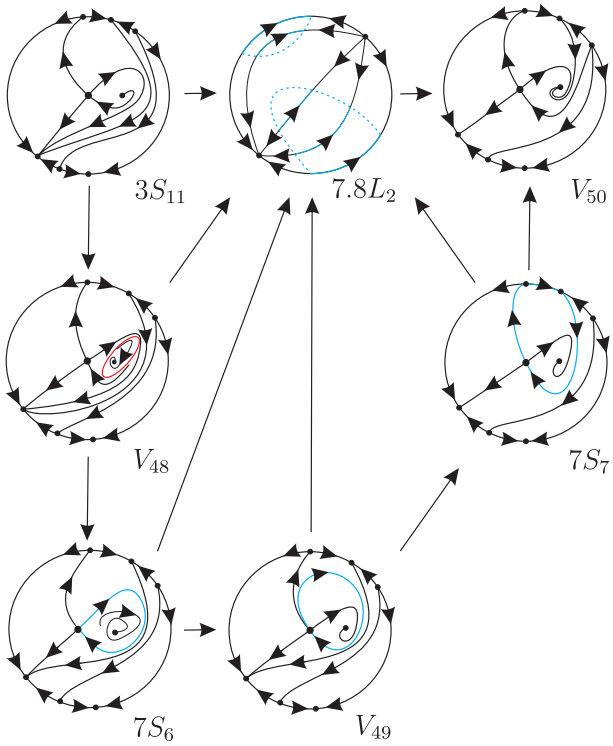

Figure 39 – Sequence of phase portraits in part v_{48} of slice $m = 3/4$ (the labels are according to Fig. 40). By starting on $3s_{11}$ we can reach region V_{50} by the path $3S_{11} \to 7.8L_2 \to V_{50}$. Now, when crossing $3s_{11}$, we shall obtain the phase portrait V_{48} (containing a limit cycle) in a subset of v_{48}. From this point we may choose five different ways to reach the subset V_{50}: (1) $V_{48} \to 7.8L_2 \to V_{50}$; (2) $V_{48} \to 7S_6 \to 7.8L_2 \to V_{50}$; (3) $V_{48} \to 7S_6 \to V_{49} \to 7.8L_2 \to V_{50}$; (4) $V_{48} \to 7S_6 \to V_{49} \to 7S_7 \to 7.8L_2 \to V_{50}$; and (5) $V_{48} \to 7S_6 \to V_{49} \to 7S_7 \to V_{50}$

Even though parts V_{49} and V_{50} have no limit cycles, they provide topologically distinct phase portraits since the connection on $7S_6$ is due to a saddle–node to itself, whereas the connection of separatrices on $7S_7$ is due to the finite saddle–node and the infinite saddle, i.e. connection of separatrices from different points. In Lemma 4.3.38 we show that $7S_6$ and $7S_7$ have one of its endpoints at the point $7.8\ell_2$ and, in addition, they are not bounded. We plot the complete bifurcation diagram for these two parts in Fig. 40.

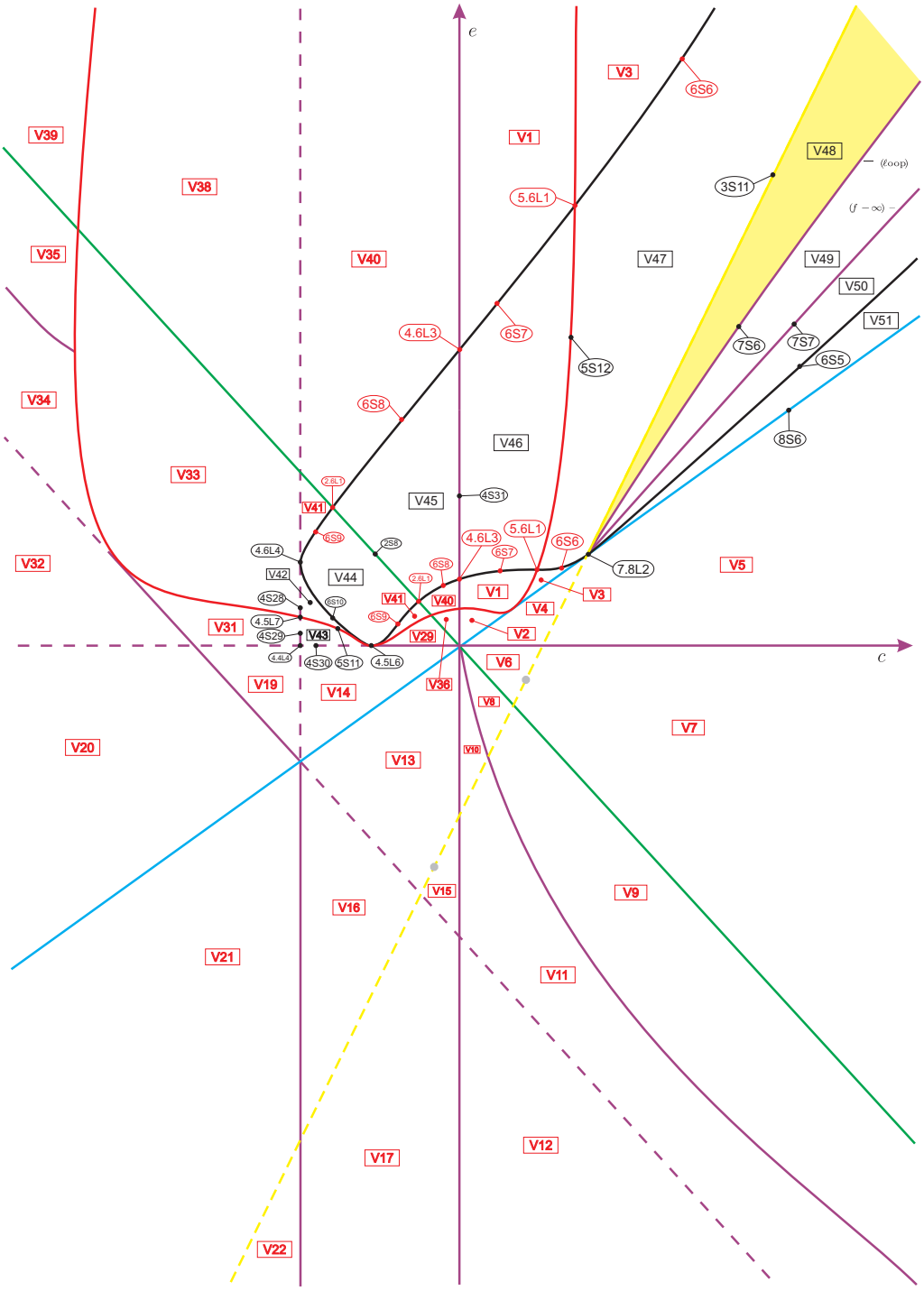

Figure 40 – Slice of parameter space when $m = 3/4$ (see Fig. 37)

Lemma 4.3.38. One of the endpoints of $7S_6$ and $7S_7$ is $7.8\ell_2$. Moreover, $7S_6$ and $7S_7$ are not bounded.

Proof. We proceed exactly as in the proof of Lemma 4.3.36. In fact, numerical analysis suggests that $7S_6$ and $7S_7$, which correspond to a loop–type bifurcation and a finite–infinite separatrix connection, respectively, have one of its ends in the curve $7.8\ell_2$. Indeed, if the starting point of any of these surfaces were any point of segment $3s_{11}$, then a portion of this subset must not refer to a Hopf bifurcation, which contradicts the fact that on $3s_{11}$ we have a weak focus of order one. On the other hand, we observe that it is not possible that the starting point of these surfaces be on $6s_5$, since on black surfaces we only have a C^∞ node–focus bifurcation. In fact, this could happen unless we have a degenerate portion of black surface in which these surfaces would start. Then, the only possible endpoint of surfaces $7S_6$ and $7S_7$ is $7.8\ell_2$. Using the same arguments we can conclude that such surfaces are not bounded. □

The regions V_{44} to V_{47} do not bring any new topologically distinct phase portrait since all of them border already known phase portraits by a node–focus bifurcation. Also the borders $2S_8$, $4S_{31}$ and $5S_{12}$ are already known phase portraits. In fact, the only new phase portraits discovered in this slice are those ones in Fig. 39.

We will follow the list of slices presented in (4.6) and now we study the singular slice $m = 1/2$. Here we observe the existence of a contact point between the red parabola and the yellow straight line. We denote this contact by $3.5L_1$, see Fig. 41. In fact, for $m = 1/2$ this is the only significant change in the bifurcation diagram.

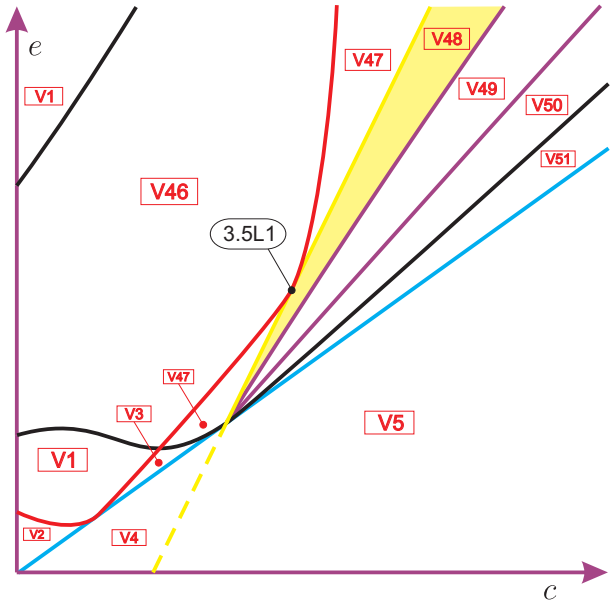

Figure 41 – Slice of parameter space when $m = 1/2$ (see Fig. 40)

Now, moving down from $m = 1/2$ we observe that, from values of m less than but very close to $1/2$ the red parabola "keeps moving" and makes $3.5L_1$ generates a new volume region. Such a region has a semi–circumference shape and we denote it by V_{52}, see Fig. 42. As we have already proved, there exist two elements of surface $(\mathscr{S}_7)$ in region V_{48} (which now contains V_{52}) and after numerical analysis for values of m less than $1/2$, but very close to it, we still verify the same changes in the phase portraits as shown in the sequence in Fig. 39. We also verify that it does not occur any topological change in the phase portrait described by $5S_{13}$. Then we conclude that the red parabola has "crossed" the yellow straight line, but it did not touch the purple surface $7S_6$.

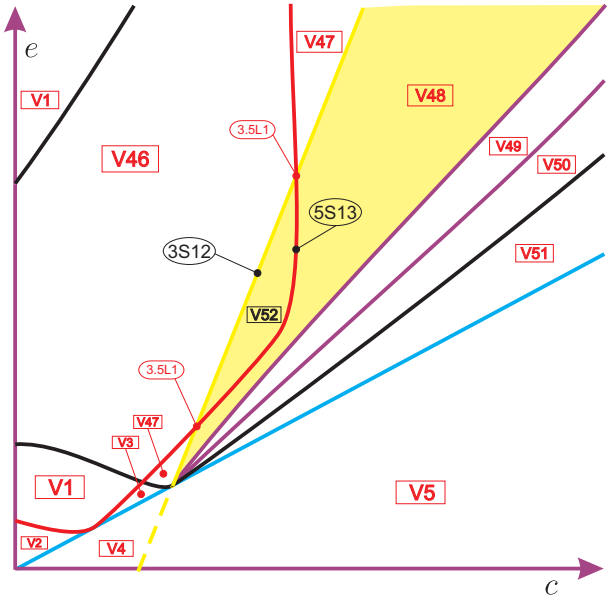

Figure 42 – Slice of parameter space when $m = 1/2 - \varepsilon_1$ (see Fig. 41)

In order to obtain a coherence of the bifurcation diagram, due to the presence of two nonalgebraic surfaces in region V_{48}, we did a careful study of this region. After obtaining the last generic slice, numerical analysis suggest that the red parabola, for a smaller and close value of m, must touch surface $7S_6$ in a curve (see $5.7L_2$ in Fig. 43).

Going further with our numerical analysis, we observe that after decreasing a little bit the values of m, a new volume region V_{53} appears, limited by the two surfaces which are $5S_{14}$ and $7S_8$ and the curve $5.7L_2$ (as always the representation that we see in figures are one–dimensional less). Surface $5S_{14}$ separates region V_{49} from V_{53} and surface $7S_8$ separates region V_{52} from V_{53}, see Fig. 44. We point out that our numerical analysis is a valid argument, since we have the coherence of the obtained phase portraits.

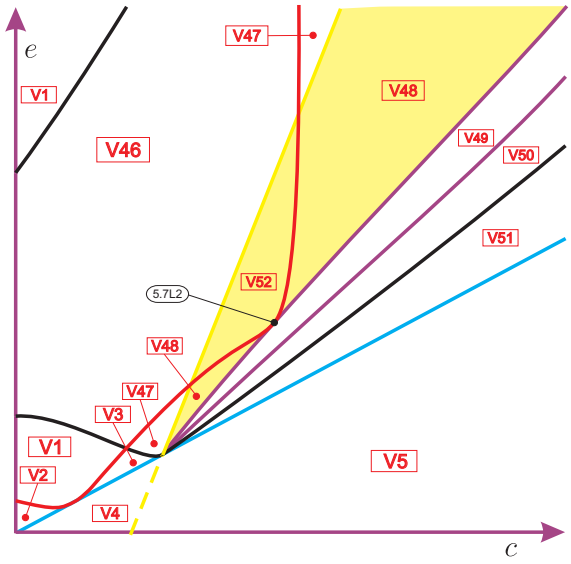

Figure 43 – Slice of parameter space when $m = 1/2 - \varepsilon_1^*$ (see Fig. 42)

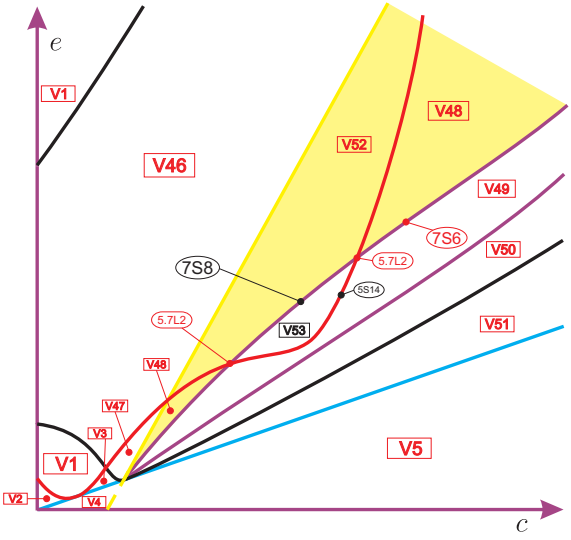

Figure 44 – Slice of parameter space when $m = 1/2 - \varepsilon_2$ (see Fig. 43)

For a better comprehension of the graphics producing limit cycles in perturbations, in Fig. 45 we present an amplification of the neighborhood in the parameter space of the curve $5.7L_2$ (see Fig. 44) with the corresponding phase portraits.

Now, for the next singular slice, numerical analysis suggest that surface $5S_{14}$ must touch surface $7S_7$ again in a curve, namely, $5.7L_3$, splitting the part $7S_7$ as in Fig. 46.

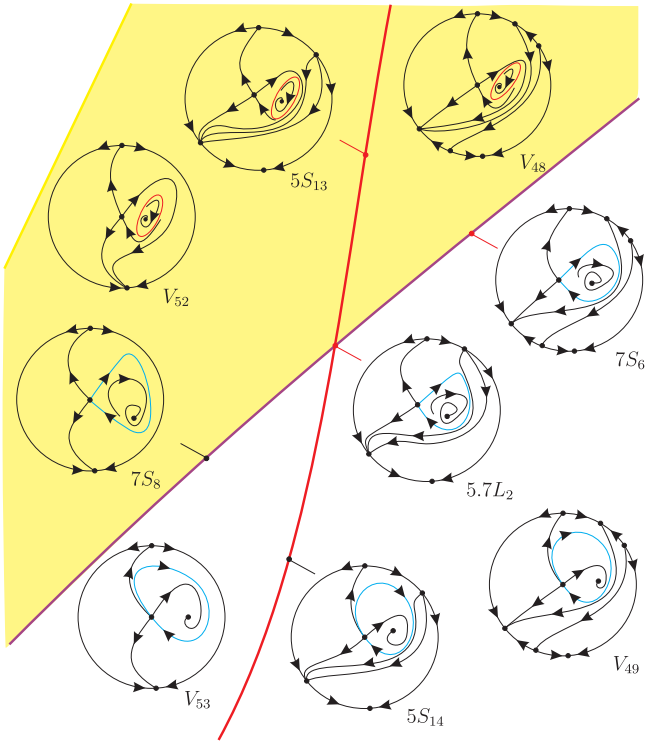

Figure 45 – Graphics producing limit cycles: neighborhood of $5.7L_2$ (see Fig. 44)

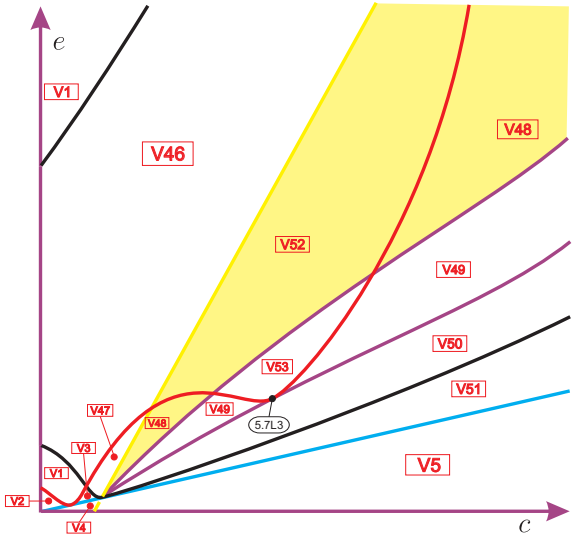

Figure 46 – Slice of parameter space when $m = 1/2 - \varepsilon_2^*$ (see Fig. 44)

We detect that for an even smaller value of m, surface $(\mathscr{S}_5)$ crosses surface $(\mathscr{S}_7)$ but this does not generate a new volume region, because the bifurcation given by the part $7S_7$ deals with a separatrix of an infinite singularity which does not exist in region V_{53}. However, it does generate a new bifurcation surface, namely, $5S_{15}$, which is the border between V_{50} and V_{53}. All the respective phase portraits are coherent with their neighbors

and this generic slice is presented in Fig. 47. In such a figure we intend to give an idea of the global bifurcation diagram, specially to show how "close" to the origin some surfaces are. This notion is very important in order to better understand the singular slice $m = 0$.

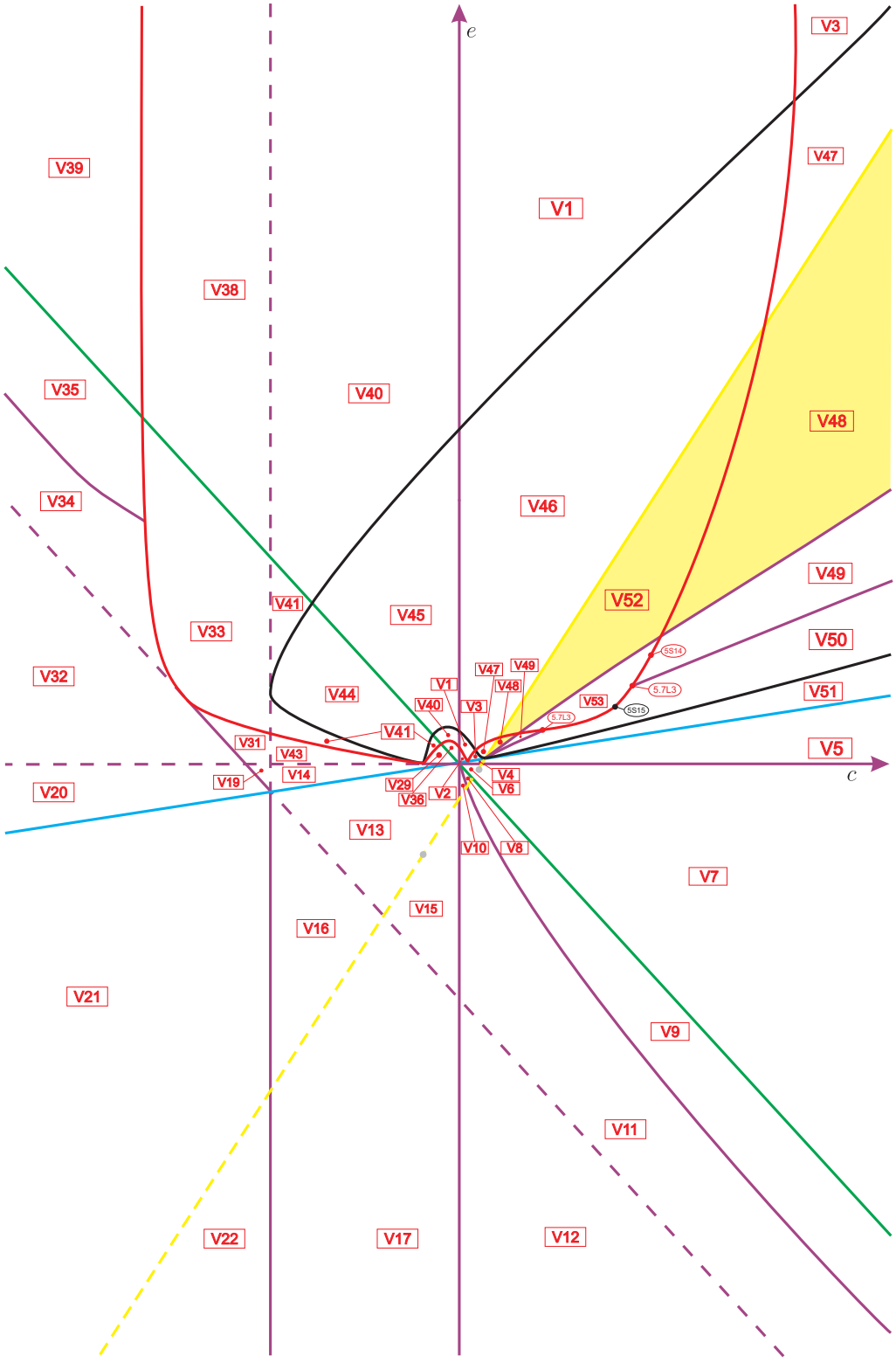

Figure 47 – Slice of parameter space when $m = 1/2 - \varepsilon_3$ (see Fig. 46)

The next slice to be analyzed is the singular slice $m = 0$ (see Fig. 48).

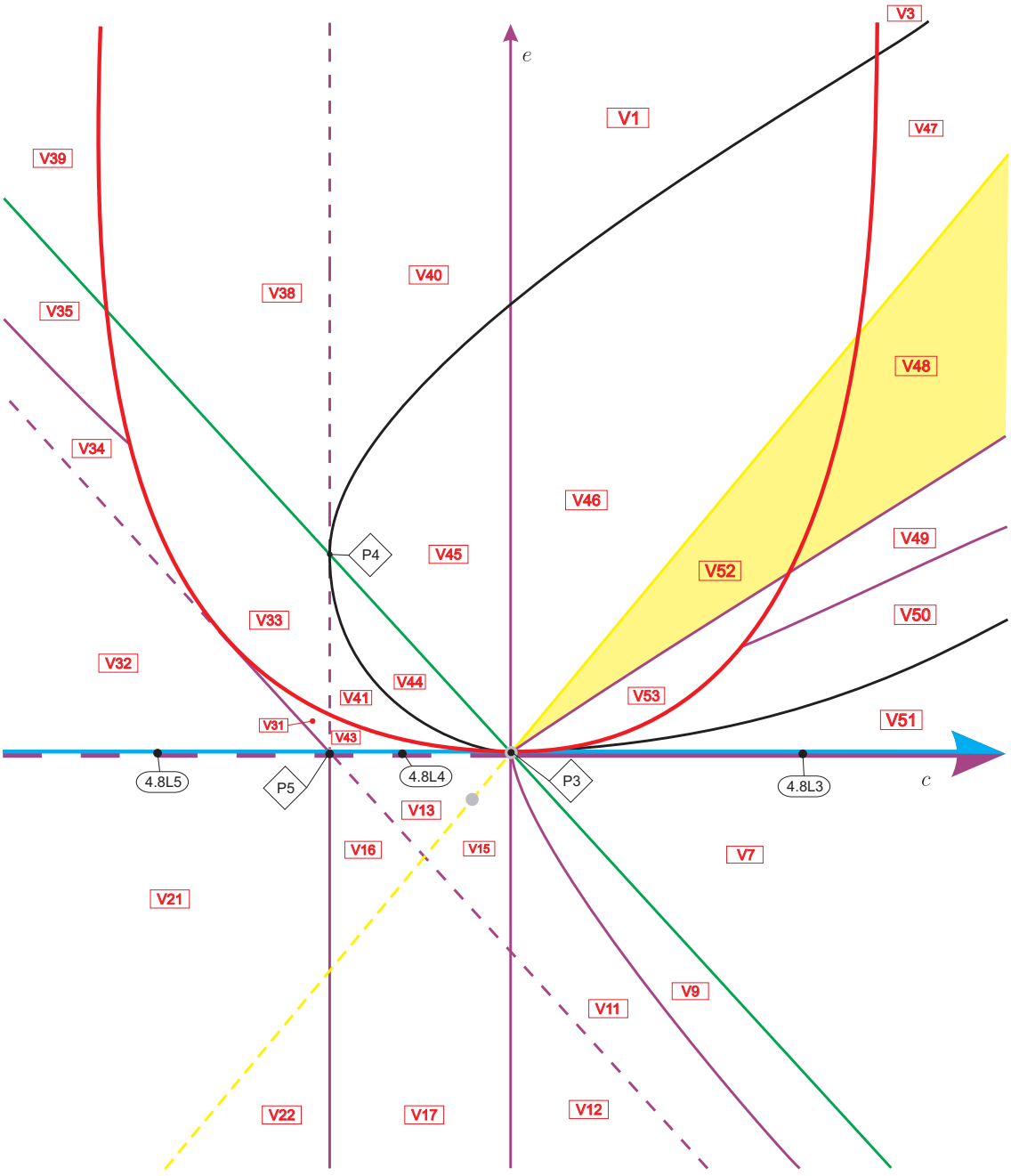

Figure 48 – Slice of parameter space when $m = 0$ (see Fig. 47)

As we mentioned before and we saw in Fig. 47, several surfaces were "very close" to the origin. When $m = 0$, several things happen simultaneously:

- the cyan straight line coalesce with the c–axis. This movement makes regions V_4, V_5, V_{14}, V_{19}, and V_{20} vanish. We denote by $4.8L_3$ to $4.8L_5$ the three new one–dimensional parts of c–axis, by P_3 the origin and by P_5 the point $(c,e) = (-2,0)$;

- the red parabola now is tangent to the c–axis at the origin. This makes regions V_2, V_{29}, and V_{36} vanish;

- the black parabola is also tangent to the c–axis at the origin and this makes regions V_1 (curved quadrilateral bordered by black, red and purple surfaces), V_3 (curved triangle bordered by black, cyan and red surfaces), and V_{40} (curved quadrilateral bordered by black, green, red and purple surfaces) vanish. Moreover, the black parabola is also tangent to the straight line $c = -2$ at the point P_4 making the region V_{41} vanishes;

- the yellow straight line now passes through the origin, making V_6, V_8, and V_{10} vanish, and it coalesces $3.10L_1$ to P_3;

- the curve $5.7L_3$ shrinks to the origin, making V_{47} (curved triangle bordered by black, red and yellow surfaces), V_{48} (curved triangle bordered by purple, red and yellow surfaces), and V_{49} (curved triangle bordered by red and purple surfaces) vanish;

- the purple straight line, which is parallel to the green one, passes through P_5.

The critical slice $m = 0$ is shown in Fig. 48, where, as usual, we indicate in red colors the old labels and in black color the new ones.

Now we begin the study of slices corresponding to negative values of m, see (4.6). The first slice to be considered is $m = -5/100$. As we saw in the slice $m = 0$, the displacement of the black, cyan, yellow and red surfaces caused the "death" of several regions. As we move down, such surfaces keep moving themselves and it is natural to expect that several regions arise when we go from $m = 0$ to $m = -5/100$. In fact, in this new slice we observe that such surfaces (and also the purple one that crossed the c–axis at P_5 when $m = 0$) moved and gave "birth" to the following 20 volume regions v_{54} to v_{73}, and all their borders, as in Fig. 53. Moreover, the curve $3.10L_1$ (from slice $m = 1/2 - \varepsilon_3$) that was carried to the origin when $m = 0$ now becomes $3.10L_2$, which already appeared in previous slices. The reason why it belongs to the same curve is that in the next slice we will find a single point which here is split into two. This also makes that the segment in surface $(\mathscr{S}_3)$ that we see in this slice between $3.4L_6$ and $3.10L_2$ which appears from the bifurcation, is linked in a lower slice to part $3S_7$ and so it receives the same name. On the other hand, due to the presence of the cyan straight line (in which systems (4.1) are degenerate) and due to its movement between two slices, we can found new nonalgebraic surfaces splitting some volume regions. This phenomena happens here. Indeed, almost the phase portraits obtained from each "new" two–dimensional part is coherent with those of all their borders. We have only four exceptions, which are shown in Fig. 49 and named as follows:

- v_{58}: the curved quadrilateral bordered by black, green, purple and red surfaces;

- v_{59}: the curved triangle bordered by black, green and purple surfaces;
- v_{61}: the curved quadrilateral bordered by black, green, yellow and red surfaces;
- v_{67}: the right triangle bordered by purple surfaces.

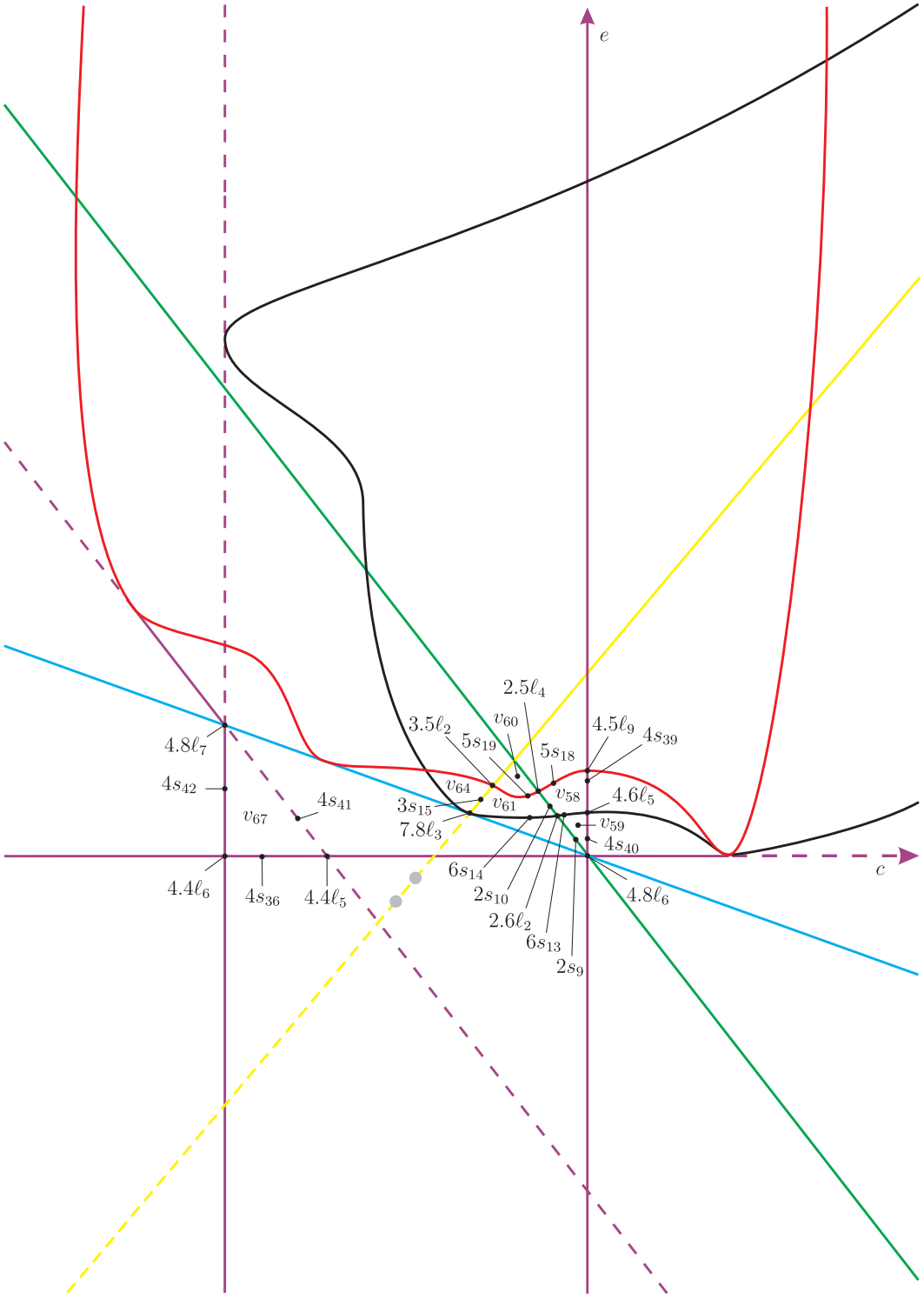

Figure 49 – Slice of parameter space when $m = -5/100$ (only algebraic surfaces)

We start analyzing parts v_{58} and v_{59}. First we consider part v_{59}. The respective phase portrait is topologically equivalent to the one in V_{59}. On $4s_{40}$, the separatrix of the infinite saddle–node connects with a separatrix of the finite saddle–node producing an invariant straight line linking the pair of infinite saddle–nodes. When entering part v_{59}, this connection is broken and the separatrix of the infinite saddle–node connects with the infinite unstable node and the separatrix of the finite saddle–node connects with the infinite stable node. However, when we approach $2s_9$, the phase portrait in a neighborhood of this segment is topologically different from the one we described just after entering part v_{59}. Indeed, the phase portrait in v_{59} near $2s_9$ possesses an infinite basin passing through the finite saddle–node, i.e. two separatrices of the finite saddle–node end at the same infinite singular point (in this case, the infinite saddle–node), whereas the phase portrait in v_{59} near $4s_{40}$ does not possess the infinite basin and each one of the same two separatrices of the saddle–node ends in different infinite singular points. Then, there must exist at least one element $7S_{10}$ of surface $(\mathscr{S}_7)$ dividing part v_{59} into two "new" parts, V_{59} and V_{71}, which represents a bifurcation due to the connection between a separatrix of a finite saddle–node with a separatrix of an infinite saddle. It is worth mentioning that the segment $6s_{13}$ refers to the C^∞ surface of node–focus bifurcation, which implies that whatever we find in part v_{58} there must exist in part v_{59} and viceversa. Then, part v_{58} must also be divided into V_{58} and V_{70} by an element $7S_9$ of surface $(\mathscr{S}_7)$ with the same bifurcation as $7S_{10}$. Clearly we have that $7S_9$ is a "continuation" of $7S_{10}$. Coupled with this idea, we have parametrized the black surface, "walked" on it and found that there exists a topological change in the phase portraits obtained.

Then, we know that $7S_{10}$ has one of its endpoints on $6s_{13}$ (dividing it into $6S_{13}$ and $6S_{12}$) and Lemma 4.3.39 assures that the other endpoint is $4.8\ell_6$. We show the sequence of phase portraits along these subsets in Fig. 50.

Moreover, as the segment $5s_{18}$ corresponds to changes in the infinite singular points, the finite part of the phase portraits remains unchanged and then segment $7s_9$ must intersect $5s_{18}$ having this intersection point as one of its endpoints, since in v_{57} we have only one infinite singularity, namely, the infinite saddle–node. With these arguments we also have parametrized the red surface, "walked" on it and found that there exists a topological change in the phase portraits obtained. In fact, in Lemma 4.3.40 we prove that surface $7S_9$ has $5.7\ell_4$ as endpoint. As V_{58} is topologically equivalent to V_{59} and V_{70} is topologically equivalent to V_{71}, the sequence of phase portraits along these subsets then is given by the path $V_{71} \to V_{59}$ presented in Fig. 50.

We plot the complete bifurcation diagram for these two parts in Fig. 53.

Lemma 4.3.39. The endpoint of $7S_{10}$ (rather than the one which is on $6s_{13}$) is $4.8\ell_6$.

Proof. Numerical tools evidence that the endpoint of $7S_{10}$, rather than the one which is

on $6s_{13}$, is $4.8\ell_6$. In what follows, we prove that this endpoint cannot be on segments $4s_{40}$ and $2s_9$. In fact, if this endpoint was located on $4s_{40}$, then there should exist a portion of this segment in which the separatrix of the infinite saddle–node connects with the infinite unstable node, causing the break of the invariant straight line. As we are considering projective coordinates, this fact contradicts Lemma 4.2.2. On the other hand the endpoint of $7S_{10}$ cannot be located on $2s_9$, since $7S_{10}$ describes a connection between a separatrix of a finite saddle–node with a separatrix of an infinite saddle and on $2s_9$ the finite saddle–node already has become a cusp–type singularity. Therefore, as the endpoint of $7S_{10}$ is not on $4s_{40}$ nor in $2s_9$, this confirms the evidence pointed out by the numerical calculations that $7S_{10}$ ends at $4.8\ell_6$. □

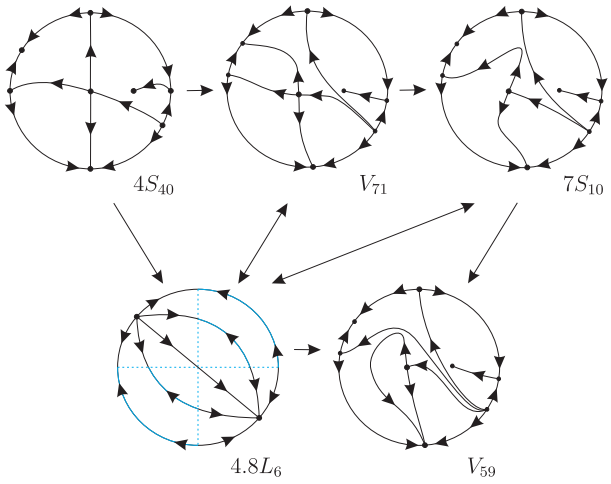

Figure 50 – Sequence of phase portraits in parts v_{59} and v_{58} of slice $m = -5/100$ (the labels are according to Fig. 53). We start by analyzing v_{59}. First we recall that the phase portrait $4S_{40}$ (respectively V_{71}, $7S_{10}$ and V_{59}) is topologically equivalent to the phase portrait $4S_{39}$ (respectively V_{70}, $7S_9$ and V_{58}) due to a node–focus bifurcation. If we start on $4s_{40}$ we can reach V_{59} by one of the six following paths: (1) $4S_{40} \to 4.8L_6 \to V_{59}$; (2) $4S_{40} \to 4.8L_6 \to 7S_{10} \to V_{59}$; (3) $4S_{40} \to 4.8L_6 \to V_{71} \to 7S_{10} \to V_{59}$; (4) $4S_{40} \to V_{71} \to 4.8L_6 \to 7S_{10} \to V_{59}$; (5) $4S_{40} \to V_{71} \to 7S_{10} \to 4.8L_6 \to V_{59}$; and (6) $4S_{40} \to V_{71} \to 7S_{10} \to V_{59}$

Lemma 4.3.40. The endpoint of $7S_9$ (rather than the one which is on $6s_{13}$) is $5.7\ell_4$.

Proof. Numerical tools evidence that the endpoint of $7S_9$ is $5.7\ell_4$. As V_{58} is topologically equivalent to V_{59} and V_{70} is topologically equivalent to V_{71}, repeating the same arguments used in the proof of Lemma 4.3.39 we conclude that $7S_9$ must intersect the red surface. In fact, its endpoint is $5.7\ell_4$ because on v_{57} we do not have the necessary number of infinite singularities in such a way that the bifurcation given by $7S_9$ could happen. □

We now present the study of part v_{61}. We consider the segment $2s_{10}$ in Fig. 49, which is one of the borders of part v_{61}. The respective phase portrait in this border is

topologically equivalent to the one in $2S_{10}$, with the origin being a cusp–type singularity. When entering part v_{61} near $2s_{10}$ the infinite saddle–node has a separatrix starting at the infinite unstable node. On the other hand, in the phase portrait in v_{61} near $3s_{15}$ such a separatrix has a limit cycle as its α–limit. Then, there must exist at least one element $7S_{11}$ of surface $(\mathscr{S}_7)$ dividing part v_{61} into two "new" parts, V_{61} and V_{72}, which represents a bifurcation due to the connection between a separatrix of an infinite saddle–node with a separatrix of an infinite saddle. Moreover, as the segment $5s_{19}$ corresponds to changes in the infinite singular points, the finite part of the phase portraits remain unchanged and then $7S_{11}$ must intersect $5s_{19}$ having this intersection point as one of its endpoints, since in v_{60} we have only one infinite singularity, namely, the infinite saddle–node. In Lemma 4.3.41 we prove that surface $7S_{11}$ has $7.8\ell_3$ as endpoint. We show the sequence of phase portraits along these subsets in Fig. 51 and the complete bifurcation diagram for this part is presented in Fig. 53.

Lemma 4.3.41. The endpoint of $7S_{11}$ (rather than the one which is on $5s_{19}$) is $7.8\ell_3$.

Proof. Numerical tools evidence that the endpoint of $7S_{11}$, rather than the one which is on $5s_{19}$, is $7.8\ell_3$. In fact, as we saw before, $7S_{11}$ indicates a bifurcation due to the connection between a separatrix of an infinite saddle–node with a separatrix of an infinite saddle. We point out that it is not possible that the endpoint of this surface is on $6s_{14}$, since on black surfaces we have only a C^∞ node–focus bifurcation. Indeed, this could happen unless we have a degenerate portion of black surface in which $7S_{11}$ would start. On the other hand, if the endpoint was on $3s_{15}$ then there should exist a degenerate portion of $3s_{15}$ in which $7S_{11}$ ends, otherwise a portion of this subset must not refer to a Hopf bifurcation, which contradicts the fact that on $3s_{15}$ we have a weak focus of order one. □

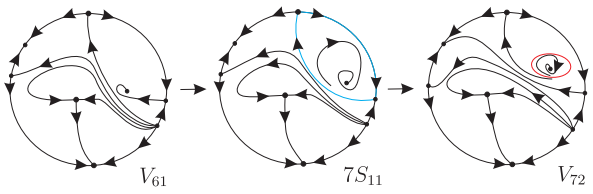

Figure 51 – Sequence of phase portraits in part v_{61} of slice $m = -5/100$ (the labels are according to Fig. 53). When crossing $2s_{10}$, we shall obtain the phase portrait V_{61} in a subset of v_{61}. From this point we can reach the subset V_{72} by crossing the purple surface $7S_{11}$. We observe that the separatrix of the infinite saddle–node coalesces with the separatrix of the infinite saddle, forming a closed graph, which breaks, given birth to a limit cycle

The last case to be considered is part v_{67}. The respective phase portrait on surface $4S_{41}$ is topologically equivalent to V_{66} because on this point, surface $(\mathscr{S}_4)$ produces a straight line not formed by separatrices. On the other hand, on $4s_{42}$ there exists a

connection between the separatrix of the infinite saddle–node with the separatrix of the finite saddle, forming an invariant straight line. Moreover, the phase portrait possesses an infinite basin passing through the infinite unstable node, i.e. two separatrix of the finite saddle–node start at the infinite unstable node. When entering part v_{67} the separatrix connection is broken and the separatrix of the finite saddle starts at the unstable infinite node and the separatrix of the infinite saddle–node ends at the infinite stable node. In addition, the infinite basin remains on this phase portrait. But this is not the same when we are close to $4s_{36}$ and $4s_{41}$, since when we approach them, we detect that the infinite basin is lost and the separatrix of the infinite saddle–node now ends at the finite saddle–node. This topological change suggests that there must exist at least one element $7S_{12}$ of surface $(\mathscr{S}_7)$ dividing part v_{67} into two "new" parts, V_{67} and V_{73}, which represents a bifurcation due to the connection between a separatrix of a finite saddle–node with a separatrix of an infinite saddle–node (see Fig. 52 for a sequence of phase portraits in these parts).

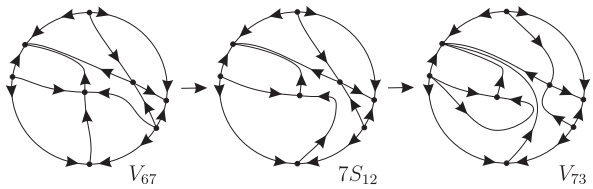

Figure 52 – Sequence of phase portraits in part v_{67} of slice $m = -5/100$ (the labels are according to Fig. 53). When crossing $4s_{41}$, we shall obtain the phase portrait V_{67} in a subset of v_{67}. From this point we can reach the subset V_{73} by crossing the purple surface $7S_{12}$. We observe that the separatrix of the infinite saddle–node coalesces with the separatrix of the finite saddle–node, and then such a connection is broken, forming an infinite basin passing through the infinite unstable node

In Lemma 4.3.42 we prove that $7S_{12}$ has $4.4\ell_6$ and $4.8\ell_7$ as start/endpoints. The complete bifurcation diagram for these two parts is shown in Fig. 53.

Lemma 4.3.42. The nonalgebraic surface $7S_{12}$ has $4.4\ell_6$ and $4.8\ell_7$ as start/endpoints.

Proof. Numerical tools evidence that this result is valid. Indeed, as we mentioned before, $7S_{12}$ represents a bifurcation due to the connection between a separatrix of an infinite saddle–node with a separatrix of a finite saddle–node. We start by observing that if $7S_{12}$ has one of its start/endpoints at any point of the segment $4s_{42}$ (without the extreme points) then there would exists a portion of such a segment in which the invariant line is broken, contradicting the fact that on $4S_{42}$ we have an invariant straight line. Analogously we conclude that $7S_{12}$ cannot have one of its start/endpoints at any point of segment $4s_{36}$ (without the extreme points). Finally, the endpoint cannot be on $4s_{41}$ (or even in the point $4.4\ell_5$) since $4s_{41}$ represents only an invariant straight line without separatrices connection (otherwise it would exist a degenerate portion of $4s_{41}$ in which $7S_{12}$ would

have its start/endpoint). Therefore, the nonalgebraic surface $7S_{12}$ has $4.4\ell_6$ and $4.8\ell_7$ as start/endpoints. □

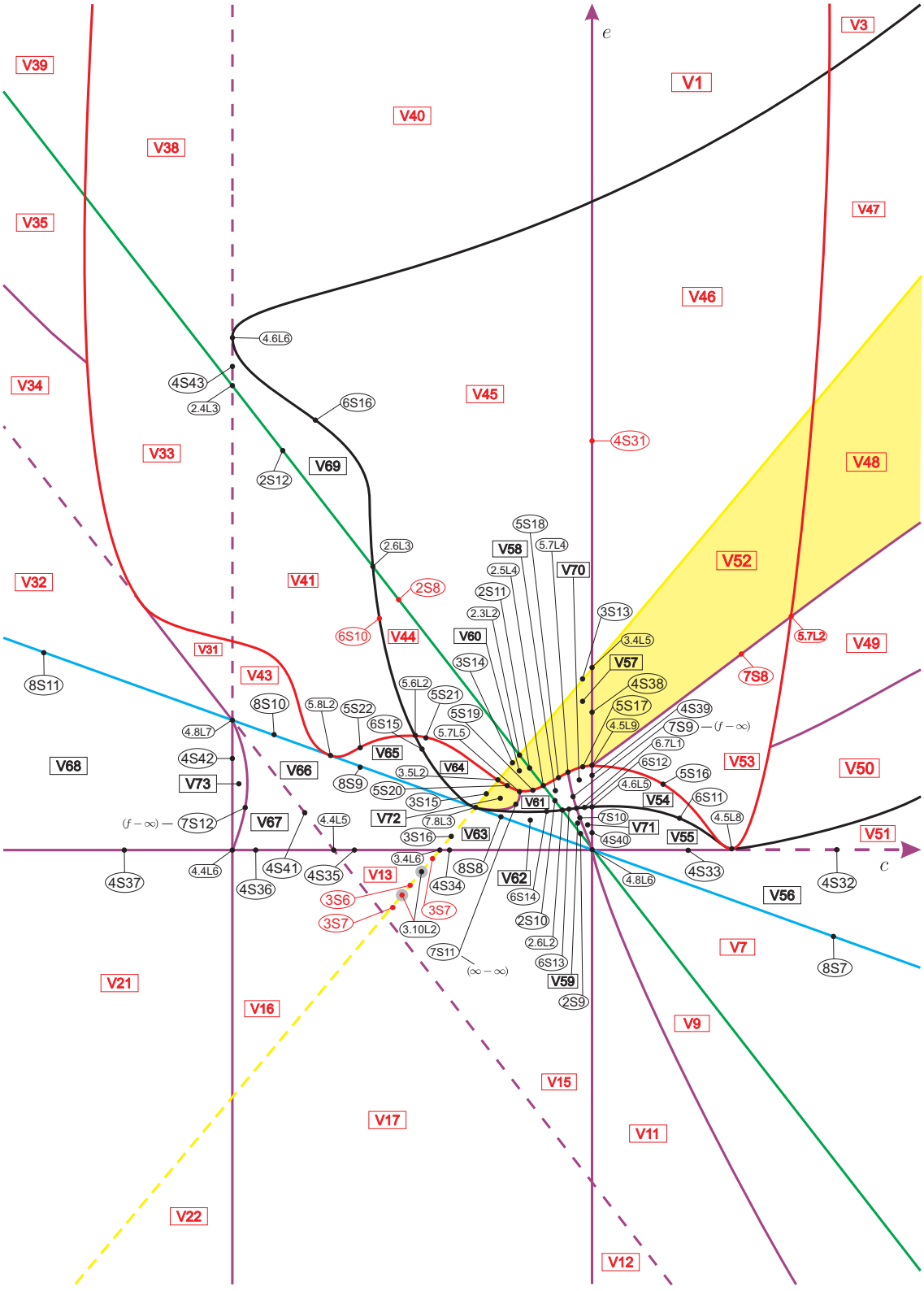

Figure 53 – Complete bifurcation diagram for slice $m = -5/100$ (see Fig. 48)

Before we go to the next slice, in order to finish describing the complete slice $m = -5/100$, we point out that in this slice we have limit cycles at the following new regions: V_{57}, V_{60} and V_{72}. In addition, numerical analysis confirm that the nonalgebraic surfaces $7S_2$ and $7S_5$ to $7S_8$ are still present at this slice. In particular, surfaces $7S_6$ and $7S_8$ still intersect along the curve $5.7L_2$. The only thing that remains to be proved is that, according to Fig. 53, the nonalgebraic surface $7S_8$ has $4.5\ell_9$ as an endpoint, see Lemma 4.3.43.

Lemma 4.3.43. For $m = -5/100$, the endpoint of $7S_8$ (rather than $5.7\ell_2$) is $4.5\ell_9$.

Proof. Numerical analysis suggests that surface $7S_8$, which corresponds to a loop–type bifurcation, have one of its ends at the point $4.5\ell_9$. Indeed, using the same argument as in the proof of Lemma 4.3.38 we conclude that the endpoint of this surface is not on $3s_{12}$. Now, if the endpoint is on $4s_{38}$ then there should exist a portion of this segment in which the respective invariant straight line would be broken. Finally, if the endpoint is on $5s_{16}$, then there should exist a portion of red parabola which is a "path" between V_{52} and V_{54}. We know that crossing the red parabola means that two infinite singularities coalesce. Then, if in V_{54} we make the infinite saddle and the infinite node coalesce, then we would have a saddle–node of type $\overline{\binom{0}{2}}\,SN$. Even if this infinite singularity disappears, we would be crossing the red parabola, going to V_{52} and arriving there without limit cycle (since this transition does not change the finite part, for instance, the separatrix of the finite saddle–node which has the finite antisaddle as a ω–limit does not disappear), a contradiction, since we already know that on V_{52} the respective phase portrait has a limit cycle. □

Remark 4.3.44. In the next figures we present some regions without labels, just for the reader follows the movement of the surfaces. Of course, the respective red labels can be found looking for previous figures. For instance, in Fig. 54 the curved quadrilateral region bordered by black, green, red and yellow surfaces corresponds to the region V_{44} in Fig. 53.

In Rmk. 4.3.2 we have concluded that the equation $\mathscr{T}_4 = \mathscr{F}_1 = 0$ has one double root if $\Delta = 0$, i.e. $m = \left(\pm 2\sqrt{2} - 3\right)/2$. In this way, the slice $m = \left(2\sqrt{2} - 3\right)/2$ is singular because the curve $3.10L_2$, which cuts twice the slices with $m \in \left(\left(2\sqrt{2} - 3\right)/2, 0\right)$, cuts the slice when $m = \left(2\sqrt{2} - 3\right)/2$ in a single point. Moreover, the part $3S_6$ vanishes. The result can be seen in Fig. 54.

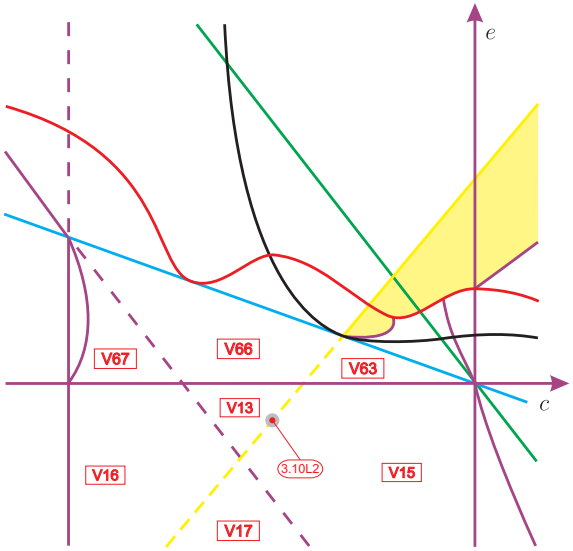

Figure 54 – Slice of parameter space when $m = \left(2\sqrt{2}-3\right)/2$ (see Fig. 53)

Analogously, again according to Rmk. 4.3.2 we proved that the equation described by $\mathscr{T}_4 = \mathscr{F}_1 = 0$ has no real roots for $\Delta < 0$, i.e. for $m \in \left(\left(-2\sqrt{2}-3\right)/2, \left(2\sqrt{2}-3\right)/2\right)$. Therefore, on the next generic slice, namely, $m = -1/4$, the only important thing that we observe is that the curve $3.10L_2$ does not cut these slices, see Fig. 55.

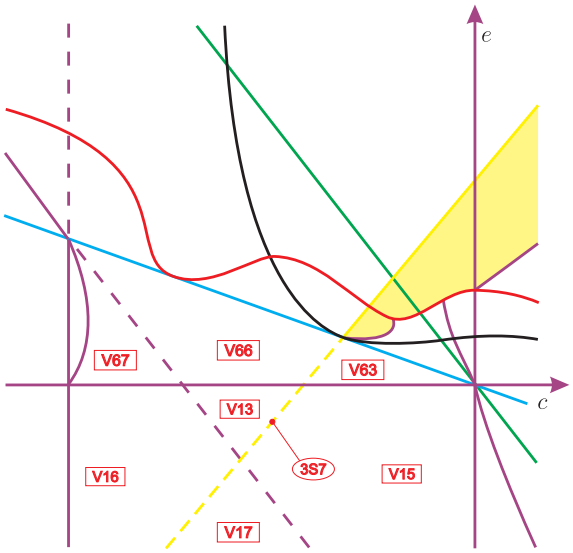

Figure 55 – Slice of parameter space when $m = -1/4$ (see Fig. 54)

Proceeding with the study of the next singular slice, $m = -1/2$, we observe that triangle V_{13} (see Fig. 55) collapses into a point, namely, P_6. This is caused by the displacement of yellow and purple algebraic surfaces. The rest of the bifurcation diagram remains topologically equivalent to the previous one. We present this result in Fig. 56.

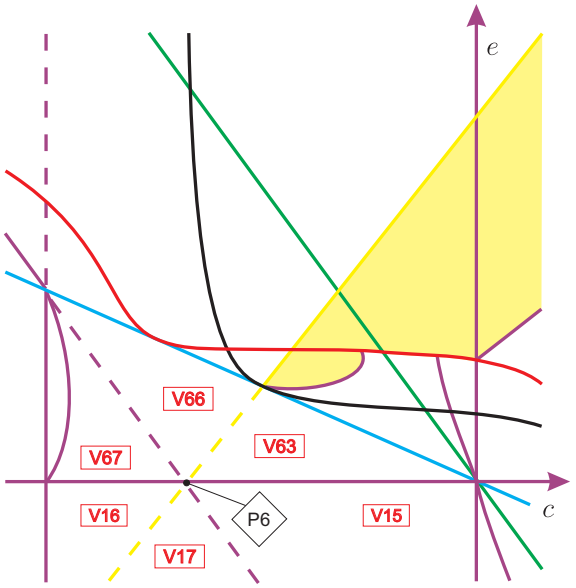

Figure 56 – Slice of parameter space when $m = -1/2$ (see Fig. 55)

When we move down with values of the parameter m very close to $m = -1/2$, we verify that the yellow and purple surfaces mentioned before keep their movement and from the point P_6 arises a new volume region which we denote by V_{74}. We denote this generic slice by $m = -1/2 - \varepsilon_4$ and we present it in Fig. 57. The phase portrait will be equivalent to the one in V_{63} since the bifurcation that splits them is just due to a straight line that does not represent a separatrix connection.

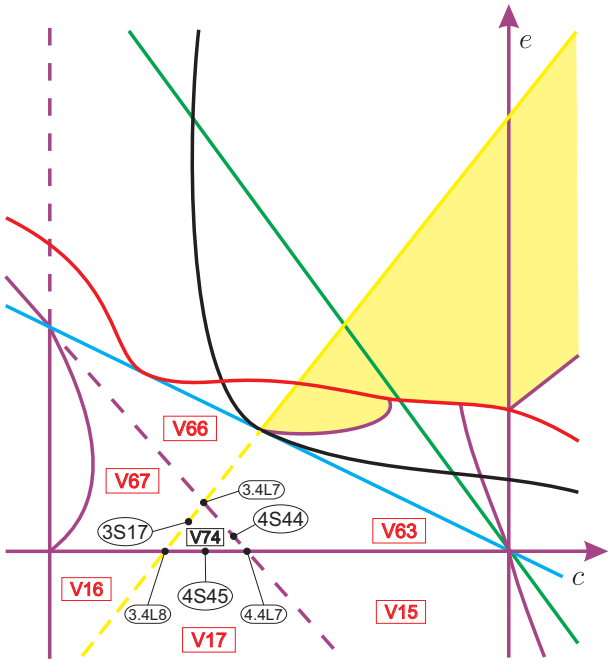

Figure 57 – Slice of parameter space when $m = -1/2 - \varepsilon_4$ (see Fig. 56)

Following the study of values of m less than but closer to $m = -1/2$ numerical analysis indicates that there must exist a point (see P_7 in Fig. 58) in which $5.7L_5$ coalesces with $2.5L_4$ (see Fig. 53). This situation gives a singular slice $m = -1/2 - \varepsilon_4^*$ which we describe in Fig. 58.

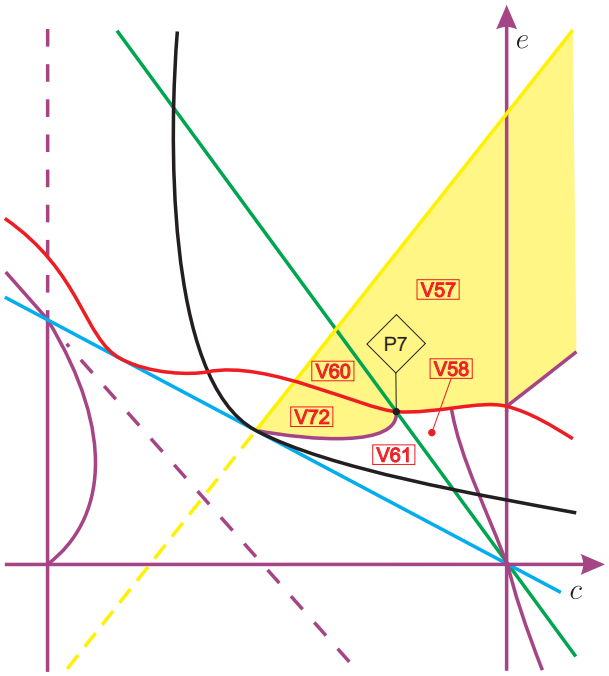

Figure 58 – Slice of parameter space when $m = -1/2 - \varepsilon_4^*$ (see Fig. 57)

We detect that from point P_7, due to the displacement of the surfaces, even for values less than but closer to $m = -1/2$, we now have a new volume region with a curved triangle shape which we denote by V_{75}. Such a region is detected by taking a small neighborhood of $2S_{10}$ (over it) and of $5S_{18}$ (under it) and then by decreasing the value of the parameter c up to the intersection point between these two surfaces (see Fig. 53). Moreover, this region contains a limit cycle and one of its edges (namely, $7S_{13}$) must be a continuation of the nonalgebraic surface $7S_{11}$. In fact, both pieces of nonalgebraic surface indicate a connection between a separatrix of the infinite saddle–node of type $\overline{\binom{1}{1}}\,SN$ and a separatrix of the infinite saddle. This nonalgebraic bifurcation given by $7S_{13}$ is exactly what we need in order to have a coherent transition between V_{58} and V_{75}. In addition, as in V_{57} we only have the infinite saddle–node of type $\overline{\binom{1}{1}}\,SN$, as it was expected by Fig. 57, the nonalgebraic surface $7S_{13}$ must have one of its ends now on $5.7L_6$, which separates the already known part $5S_{18}$ from the new part $5S_{23}$. In Fig. 59 we present this generic slice and we denote it by $m = -1/2 - \varepsilon_5$.

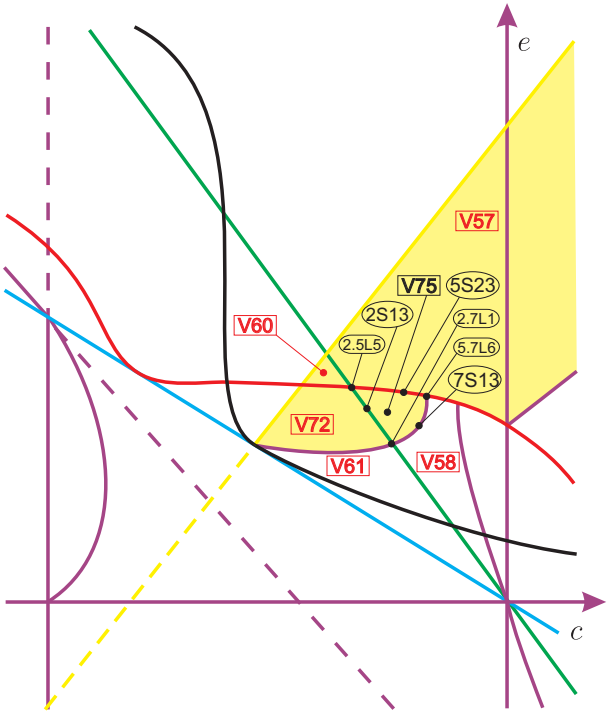

Figure 59 – Slice of parameter space when $m = -1/2 - \varepsilon_5$ (see Fig. 58)

Now we observe that for $m = -8/9$, the volume region V_{60} disappeared. Indeed, it was reduced to the point P_8, as in Fig. 60.

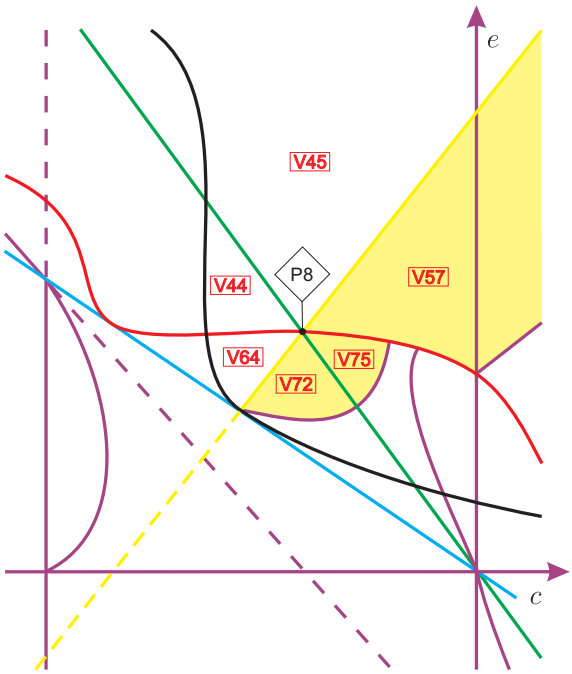

Figure 60 – Slice of parameter space when $m = -8/9$ (see Fig. 59)

Proceeding with the study of the next generic slice, $m = -9/10$, from the point P_8

arises a new volume region, which we denote by V_{76}, see Fig. 61.

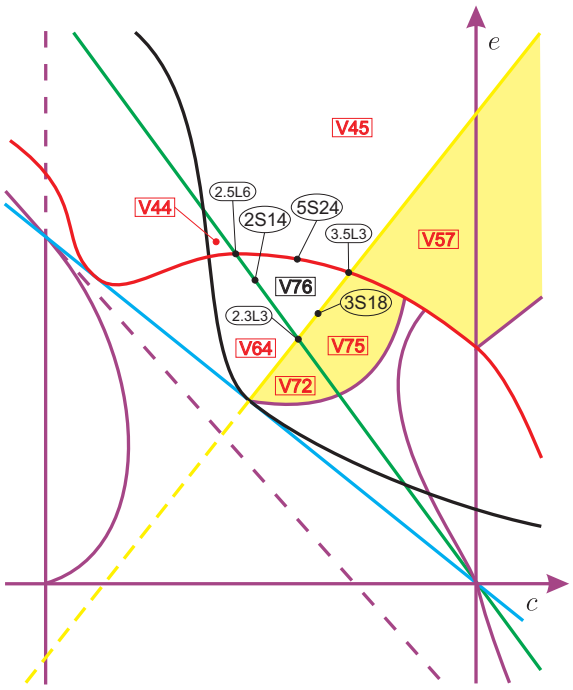

Figure 61 – Slice of parameter space when $m = -9/10$ (see Fig. 60)

When $m = -24/25$, the volume region V_{44} disappears. In fact, it is reduced to the point P_9, as in Fig. 62.

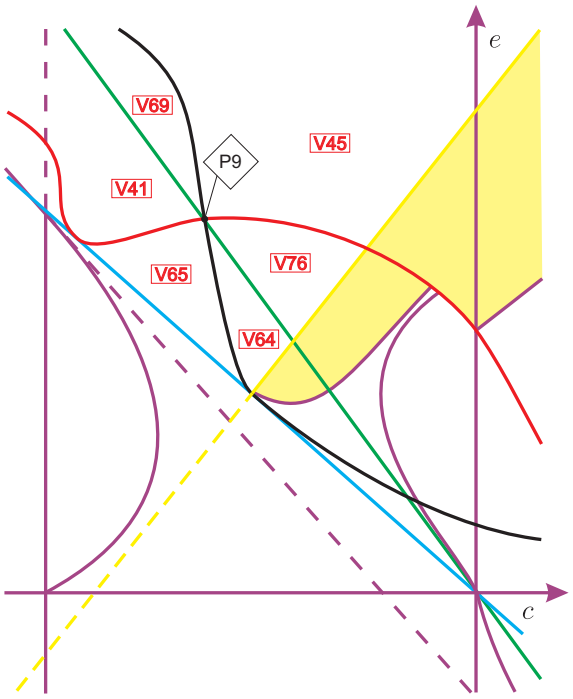

Figure 62 – Slice of parameter space when $m = -24/25$ (see Fig. 61)

In the next generic slice, $m = -98/100$, from the point P_9 arises a new volume region, which we denote by V_{77}, see Fig. 63.

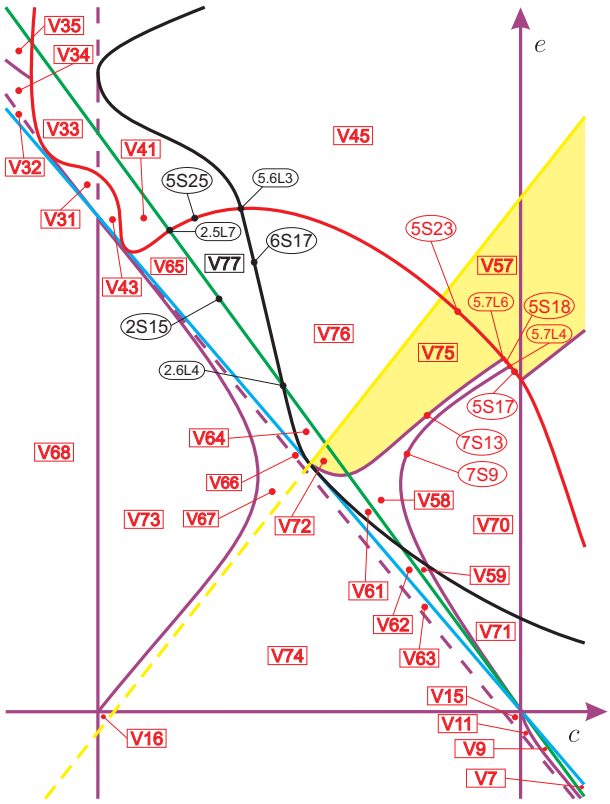

Figure 63 – Slice of parameter space when $m = -98/100$ (see Fig. 62)

In the next singular slice, $m = -1$, we have a coalescence of the cyan, green and purple surfaces and this displacement kills the following 18 volume regions: V_7, V_9, V_{11}, V_{15}, V_{31}, V_{32}, V_{33}, V_{34}, V_{35}, V_{41}, V_{43}, V_{61}, V_{62}, V_{63}, V_{64}, V_{65}, V_{66} and V_{72} (see these regions in Fig. 63). Moreover, when $m = -1$ we also have that the yellow surface passes trough P_{13}, making the volume region V_{16} disappears. In addition, by using numerical tools, we detect the death of the volume regions V_{58} and V_{59}. In fact, this phenomenon is caused by the coalescence of the two pieces $7S_9$ and $7S_{13}$ of the nonalgebraic surface ($\mathscr{S}_7$). This is why we have drawn these two surfaces very close to each other up to Fig. 63. We denote by $7.7L_1$ the nonalgebraic surface that corresponds to this coalescence and in Fig. 64 we indicate it with ticker line. It is clear that such a surface has one of its ends on the red surface (more precisely, at the point P_{14}, which represents the coalescence of $5.7L_4$ and $5.7L_6$, respectively) and due to the nature of the bifurcation described by $7S_9$, the other endpoint of $7.7L_1$ is P_{11}. On the other hand, again by using numerical tools, we detect that the nonalgebraic surface $7S_{12}$ now has one of its endpoints also at P_{11} (the other endpoint remains at P_{13}). In Fig. 64 we present this slice properly labeled.

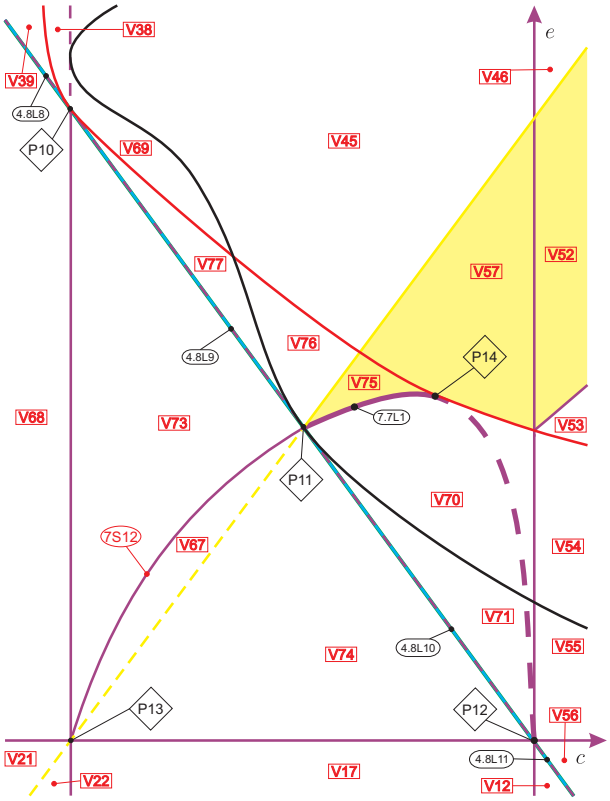

Figure 64 – Slice of parameter space when $m=-1$ (see Fig. 63)

Additionally, by using carefully the numerical program P4 (see Artés *et al.* (2005) and Dumortier, Llibre and Artés (2008)) we take a small neighborhood under the yellow surface, i.e. $e=c-2m-\varepsilon$ and $m=-1$, and we detect that for

$$c=\delta-1, \quad \varepsilon=\delta+\delta^2, \quad \delta\in\mathbb{R},$$

we have that

$$(c,e)=(\delta-1,1-\delta^2), \quad \delta\in\mathbb{R},$$

and then, surface $7S_{12}$ together with $7.7L_1$ could be approximated by the equation

$$e=-c^2-2c,$$

which is a parabola (an algebraic equation) on the ce–plane. Then we can also have an approximation for the point P_{14} (the tangent point of such a parabola with the red surface). On the other hand, we detect that, under the previous conditions over the parameters c,e,m (and from the beginning, $h=1$) we have the algebraic invariant curve

$$g(x,y)=(1+\delta)(-1+\delta+x)x+(-1+\delta+2x)y, \quad \delta\in\mathbb{R},$$

with cofactor $2y$. These facts are particularly amazing, since therefore $7.7L_1$ is algebraic and represents an algebraic connection given by the coalescence of the two pieces $7S_9$

and $7S_{13}$ of the nonalgebraic surface $(\mathscr{S}_7)$. The resulting parabola has one piece which represents a single connection of separatrices (namely, $7S_{12}$), one piece which represents simultaneously two distinct connections of separatrices (namely, $7.7L_1$) and the remaining part of this parabola does not indicate any additional topological change for the bifurcation diagram. But in order to indicate the existence of such a parabola, in Fig. 64 we have drawn $7S_{12}$ together with $7.7L_1$ resembling a parabola and the respective piece that does not represent any topological change is drawn as a dashed curve.

By finishing analyzing this singular slice, when we keep going down with the values of the parameter m, due to the continuous displacement of such surfaces it is natural to expect the birth of several new volume regions. In fact, when we consider a generic slice $m = -1 - \varepsilon_6$, very close to $m = -1$, we get the following 21 new volume regions: V_{78} to V_{98}. Such regions and their respective borders are drawn in Fig. 65. In what follows we explain a little bit about the existence of the pieces of nonalgebraic surfaces $7S_{14}$ to $7S_{21}$ presented in such a figure.

Numerical analysis indicates that surface $7.7L_1$ (from Fig. 64) splits itself into two new pieces of nonalgebraic surface $(\mathscr{S}_7)$, as in Fig. 65. Moreover, we also have the birth of the following three volume regions: V_{78}, V_{79}, and V_{80}. In what follows we justify the existence of such nonalgebraic surfaces and, consequently, of these new volume regions.

We begin by recalling that before the slice $m = -1$, we had that the nonalgebraic surface $7S_{13}$ had a continuation $7S_{11}$ (which was "squeezed" in the slice $m = -1$ by the triple surface). Numerical analysis suggests that, after the splitting of the triple surface, the nonalgebraic surface $7S_{14}$ has a continuation, which we denote by $7S_{20}$. In fact, by taking a small neighborhood of $4S_{55}$ and start decreasing the value of the parameter c, we detect that, at some moment, the region over V_{70} becomes V_{78} and the region under V_{86} becomes V_{87}. As V_{70} is topologically equivalent to V_{86} and V_{78} is topologically equivalent to V_{87} then we have the existence of some element of surface $(\mathscr{S}_7)$, namely $7S_{20}$, being a continuation of $7S_{14}$. Both nonalgebraic surfaces describe a connection between a separatrix of the infinite saddle–node and a separatrix of the infinite saddle. So, $7S_{20}$ has one endpoint on $4.7L_1$. We observe that the nonalgebraic surface $7S_{20}$ cannot have its other endpoint neither on surface $6S_{18}$ (which represents only a $\mathscr{C}^\infty$ node–focus bifurcation, unless there exists a degenerate portion of such a surface being an endpoint of $7S_{20}$) nor on $3S_{20}$ (since otherwise a portion of this subset must not refer to a Hopf bifurcation, which contradicts the fact that on $3S_{20}$ we have a weak focus of order one). Then, the other endpoint of $7S_{20}$ is $7.8L_4$.

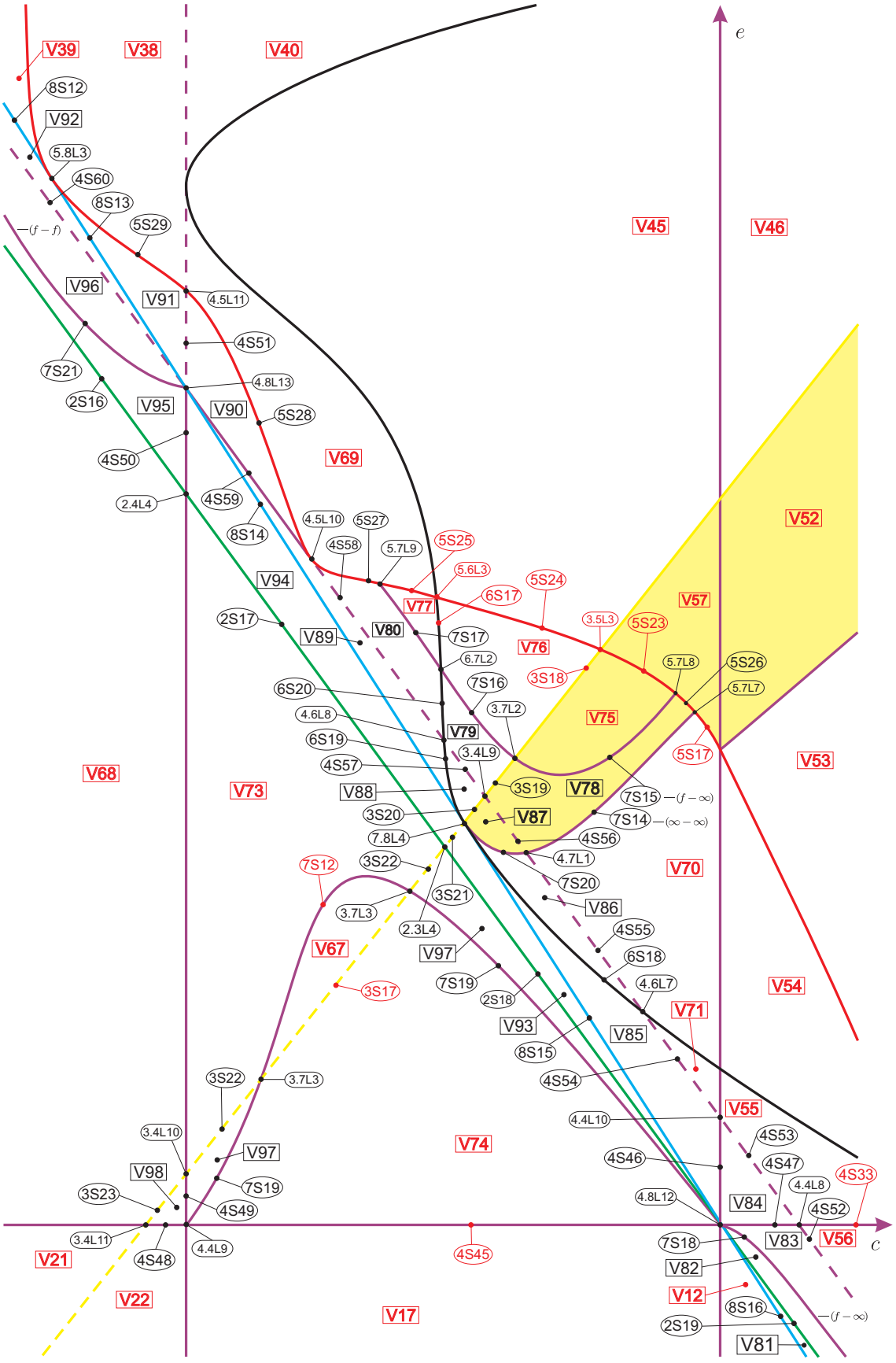

Figure 65 – Slice of parameter space when $m = -1 - \varepsilon_6$ (see Fig. 64)

We now pass to analyze V_{78}. As before, when we approach $5S_{23}$ under it, we obtain a phase portrait that is topologically equivalent to V_{75}. However, by taking a small neighborhood of $5S_{17}$ (respectively $5S_{23}$) and by decreasing (respectively increasing) the value of the parameter c, we obtain a phase portrait that does not belong either to V_{70} or to V_{75}. In fact, this phase portrait contains a limit cycle (as in V_{75}) but it does not contain the infinite basin (presented in V_{75}) as in V_{70}. These facts suggest that there must exist a new volume region (which we denote by V_{78} in Fig. 65) "between" V_{70} and V_{75}. Consequently, there must exist two pieces of nonalgebraic surface ($\mathscr{S}_7$) bordering this new region. We denote such surfaces by $7S_{14}$ (which describes a connection between a separatrix of the infinite saddle–node and a separatrix of the infinite saddle) and $7S_{15}$ (which indicates a connection between a separatrix of the finite saddle–node and a separatrix of the infinite saddle). Since in V_{57} we do not have a sufficient number of infinite singularities in order to make the bifurcation given by these two nonalgebraic surfaces happens, we conclude that these surfaces must have one of their endpoints on the red surface, indeed, on the curves $5.7L_7$ and $5.7L_8$, respectively. Then we also have a new piece $5S_{26}$ of surface ($\mathscr{S}_5$) bordering this new region. We know that there exist two other borders of V_{78} (and also of V_{87}). On the other hand, when we approach $3S_{18}$ under it, we obtain a phase portrait that is topologically equivalent to V_{75} and, by taking a small neighborhood under $3S_{18}$, when we decrease the value of parameter e we get a phase portrait that is topologically equivalent to V_{78}. So, the nonalgebraic surface $7S_{15}$ must intersect the yellow surface, splitting $3S_{18}$ into two parts, namely, $3S_{18}$ and $3S_{19}$. This is confirmed if we parametrize and "walk above" the yellow surface between its intersection with the red surface and the purple one. Therefore, we have obtained all the borders of regions V_{78} (and V_{87}).

We now pass to describe the existence of the volume region V_{79} and also the nonalgebraic surface $7S_{16}$. In fact, when we approach $5S_{24}$ under it, we obtain a phase portrait that is topologically equivalent to V_{76}, but when we approach $4S_{57}$ over it, we obtain a phase portrait that is different from the previous one (which we denote by V_{79}). In fact, if in region V_{76} we fix a value of the parameter c and start decreasing the parameter e, we observe that, in some moment, the infinite basin from V_{76} is lost. This phenomenon happens due to a connection between a separatrix of the finite saddle–node and a separatrix of the infinite saddle. Then there must exist a nonalgebraic surface $7S_{16}$ splitting the volume region V_{76} into two parts, namely, V_{76} and V_{79}. Moreover, if we take a small neighborhood over the yellow surface, we detect that surface $7S_{16}$ has one of its endpoints on the yellow surface. Indeed, surface $7S_{16}$ is clearly a continuation of surface $7S_{15}$, because both surfaces represent the same nonalgebraic bifurcation and they have endpoints on the yellow surface, in fact, at the curve $3.7L_2$. We also observe that surface $7S_{16}$ has its another endpoint on the black surface, indeed, at the curve $6.7L_2$. On the other hand, as the black surface only represents a $\mathscr{C}^\infty$ node–focus bifurcation, we conclude that surface $7S_{16}$ must cross the black surface and, indeed, a careful numerical analysis

indicates that there exists a piece of nonalgebraic surface $7S_{17}$ being a continuation of $7S_{16}$ and splitting V_{77} into V_{77} and V_{80}. Moreover, if we parametrize surface $5S_{25}$ we detect that, for some negative value of the parameter c, the same bifurcation described by $7S_{17}$ happens at $5.7L_9$, which splits $5S_{25}$ into $5S_{25}$ and $5S_{27}$. Since as in V_{69} we do not have the sufficient number of separatrices in order to perform the bifurcation described by $7S_{17}$ we conclude that $5.7L_9$ is, in fact, the other endpoint of $7S_{17}$. As in Fig. 65, this nonalgebraic surface is a border of V_{80} which is topologically equivalent to V_{89} (since surface $4S_{58}$ represents an invariant straight line which does not indicate a separatrix connection).

We have seen that up to slice $m = -98/100$, we had the existence of the nonalgebraic surface $7S_2$ being a common border of the regions V_9 and V_{11}. Such a surface was "squeezed" in the slice $m = -1$ by the triple surface (formed by cyan, green and purple surfaces) and, it is natural to expect that after the splitting of this triple surface, it arises a new piece of nonalgebraic surface in the neighborhood of the region where $7S_2$ was located. In fact, it happens here. If we approach $4S_{52}$ under it, we obtain a phase portrait that is topologically equivalent to V_{83} and, when we approach $2S_{19}$ over it we obtain a phase portrait which is topologically equivalent to V_{82}. This suggests that there exists some element of surface $(\mathscr{S}_7)$ between $4S_{52}$ and $2S_{19}$, which represents a nonalgebraic bifurcation due to the connection between a separatrix of the finite saddle–node with a separatrix of the infinite saddle–node. We denote such a nonalgebraic surface by $7S_{18}$. We observe that as in $2S_{19}$ the finite saddle–node has become a cusp–type singularity, then $7S_{18}$ cannot have an endpoint on $2S_{19}$. Moreover, as the dashed surface $4S_{52}$ only represents a $\mathscr{C}^\infty$ bifurcation, then $7S_{18}$ cannot have an endpoint on it either. On the other hand, if $7S_{18}$ has an endpoint on $4S_{47}$, then in order to make the respective bifurcation happens, the corresponding invariant straight line would be broken. Therefore, $7S_{18}$ has $4.8L_{12}$ as an endpoint and by using the same arguments we conclude that such a surface is unbounded.

On the other hand in slice $m = -1$ (and before it), we had the existence of the nonalgebraic surface $7S_{12}$ being a common border of the regions V_{67} and V_{73} and describing a connection between a separatrix of the finite saddle–node with a separatrix of the infinite saddle–node. We observe that even after the splitting of the triple surface, this nonalgebraic surface remains in this region, but now numerical analysis indicates that it intersects the yellow surface at two curves, which are denoted by $3.7L_3$. Indeed, when we are "close" to the curve $4.4L_9$ (see Fig. 65), due to the displacement of the yellow surface, numerical analysis suggests that it "cuts" the nonalgebraic surface $7S_{12}$. In fact, when we take a small neighborhood over $3S_{17}$ and start decreasing the value of the parameter c, we observe that, at some moment, the region V_{67} becomes V_{73} and, if we take the same neighborhood under $3S_{17}$ and start decreasing the value of the parameter c, we observe that, at some moment, the region V_{74} becomes V_{97}. As V_{73} is topologically equivalent to V_{97} and V_{67} is topologically equivalent to V_{74} then we have the existence of some element

of surface ($\mathscr{S}_7$), namely $7S_{19}$, being a continuation of $7S_{12}$. So, $7S_{19}$ has one endpoint on $3.7L_3$. We note that $7S_{19}$ cannot have its other endpoint either on $4S_{49}$ or on $4S_{45}$, since otherwise the respective invariant lines would be broken in order to make the respective nonalgebraic bifurcation happens (as we already proved before for surface $7S_{12}$). Then, the other endpoint of $7S_{19}$ is $4.4L_9$. Now, if we are "close" to the curve $2.3L_4$ (see Fig. 65) and we take a small neighborhood over the yellow surface and start decreasing the value of the parameter c, we observe that, in some moment, the region V_{73} becomes V_{67} and if we take a small neighborhood under the yellow surface we obtain the same sequence of phase portraits. These facts suggest that the nonalgebraic surface $7S_{12}$ has another piece of nonalgebraic surface (which we also denote by $7S_{19}$) being its continuation and which due to the bifurcation that it represents, it cannot intersect surfaces $2S_{18}$ and $4S_{45}$, then it must have its other endpoint on $4.8L_{12}$.

Moreover, up to slice $m = -98/100$, we had the existence of the nonalgebraic surface $7S_5$ being a common border of the regions V_{34} and V_{35}. Such a surface was "squeezed" in the slice $m = -1$ by the triple surface and, it is natural to expect that after the splitting of this triple surface, it arises a new piece of nonalgebraic surface in the neighborhood of the region where $7S_5$ was located. In fact, it happens here. If we approach $4S_{60}$ under it, we obtain a phase portrait that is topologically equivalent to V_{96} and, when we approach $2S_{16}$ over it we obtain a phase portrait which is topologically equivalent to V_{95}. This suggests that there exists some element of surface ($\mathscr{S}_7$) between $4S_{60}$ and $2S_{16}$, which represents a nonalgebraic bifurcation due to the connection between a separatrix of the finite saddle–node with a separatrix of the finite saddle. We denote such a nonalgebraic surface by $7S_{21}$. We observe that as in $2S_{16}$ the finite saddle–node has become a cusp–type singularity, then $7S_{21}$ cannot have an endpoint on $2S_{16}$. In addition, as the dashed surface $4S_{60}$ only represents a $\mathscr{C}^\infty$ bifurcation, then $7S_{16}$ cannot have an endpoint on it either. On the other hand, if $7S_{18}$ has an endpoint on $4S_{50}$, then in order to make the respective bifurcation happens, the invariant straight line would be broken. Therefore, $7S_{21}$ has $4.8L_{13}$ as an endpoint and such a surface is unbounded.

In Fig. 65 we sum up all the information given on the previous paragraphs.

After numerical analysis for values of m less than $m = -1 - \varepsilon_6$, but very close to it, we observe that there must exist a singular value of the parameter m in which the curves $3.5L_3$ and $5.7L_8$ coalesce and this makes the volume region V_{75} disappears. In fact, such a region is reduced to the point P_{15} from slice $m = -1 - \varepsilon_6^*$, as in Fig. 66.

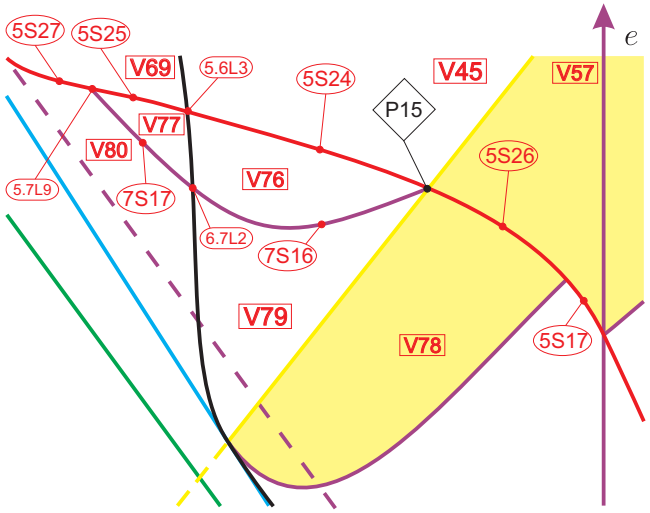

Figure 66 – Slice of parameter space when $m = -1 - \varepsilon_6^*$ (see Fig. 65)

Numerical analysis suggests that for a little bit smaller value of the parameter m, namely $m = -1 - \varepsilon_7$, corresponding to the point P_{15} we now have two curves and a piece of the red surface (namely, $3.5L_4$, $5.7L_{10}$, and $5S_{30}$, respectively) as in Fig. 67.

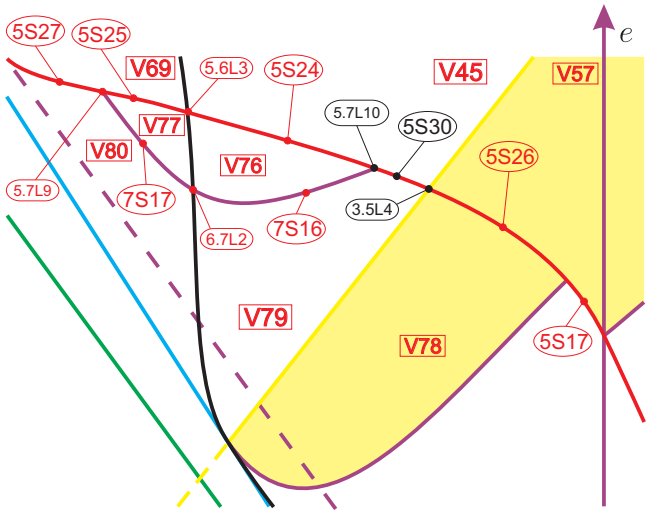

Figure 67 – Slice of parameter space when $m = -1 - \varepsilon_7$ (see Fig. 66)

Again by using numerical tools we detect that there must exist a singular value $m = -1 - \varepsilon_7^*$ in which the curves $5.6L_3$ and $5.7L_9$ coalesce, making the volume region V_{77} disappears. Indeed, such a region is reduced to the point P_{16}, as in Fig. 68.

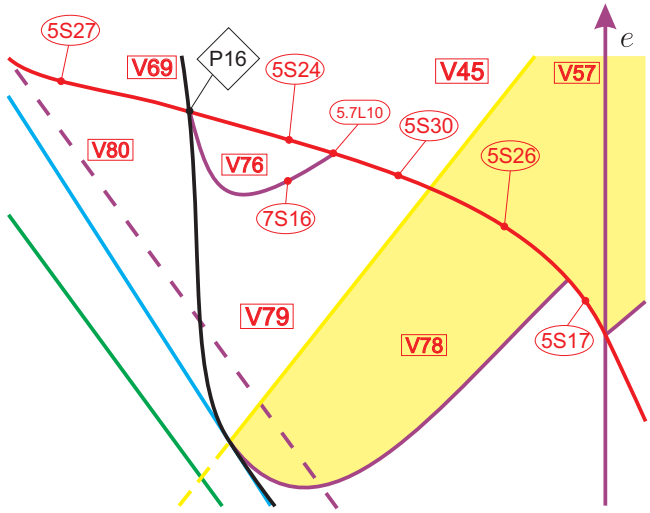

Figure 68 – Slice of parameter space when $m = -1 - \varepsilon_7^*$ (see Fig. 67)

Moving on with our numerical analysis, we observe that in generic slice $m = -1 - \varepsilon_8$, from the point P_{16} we now have two curves and a piece of the red surface (namely, $5.6L_4$, $5.7L_{10}$, and $5S_{30}$, respectively) as in Fig. 69.

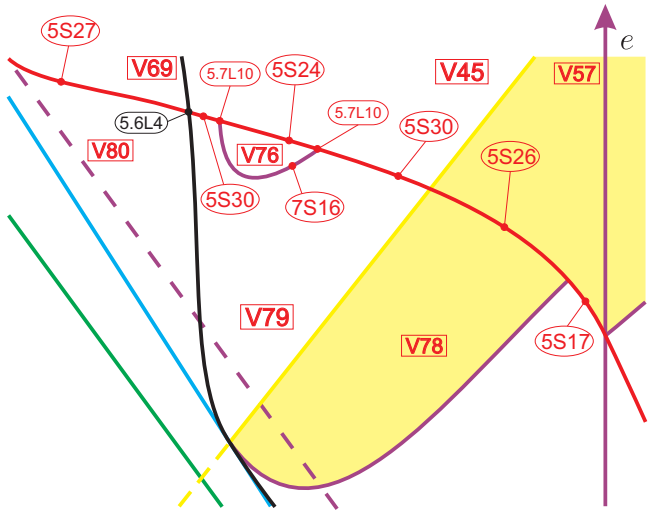

Figure 69 – Slice of parameter space when $m = -1 - \varepsilon_8$ (see Fig. 68)

Now, we detect that there must exist a singular value $m = -1 - \varepsilon_8^*$ in which the curves $5.7L_{10}$ coalesce, making the volume region V_{76} disappears, see Fig. 70.

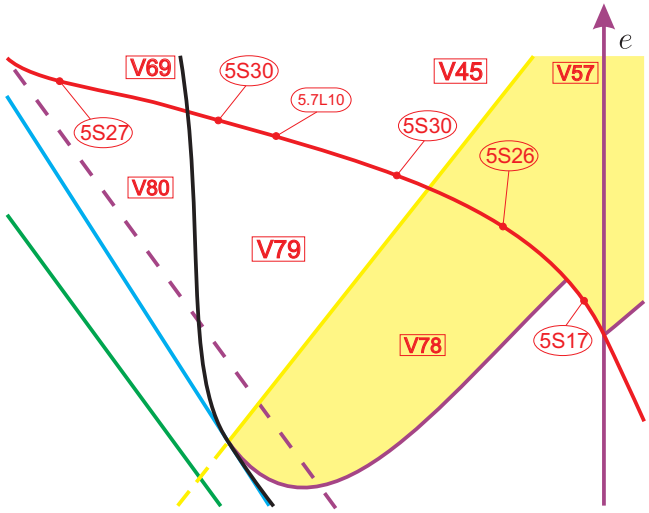

Figure 70 – Slice of parameter space when $m = -1 - \varepsilon_8^*$ (see Fig. 69)

The next nonalgebraic generic slice, $m = -1 - \varepsilon_9$, is again obtained by numerical tools and it represents the absence of the curve $5.7L_{10}$ and the displacement of the nonalgebraic surface $7S_{12}$ towards $3S_{17}$, making the volume region V_{67} "smaller". See the representation in Fig. 71.

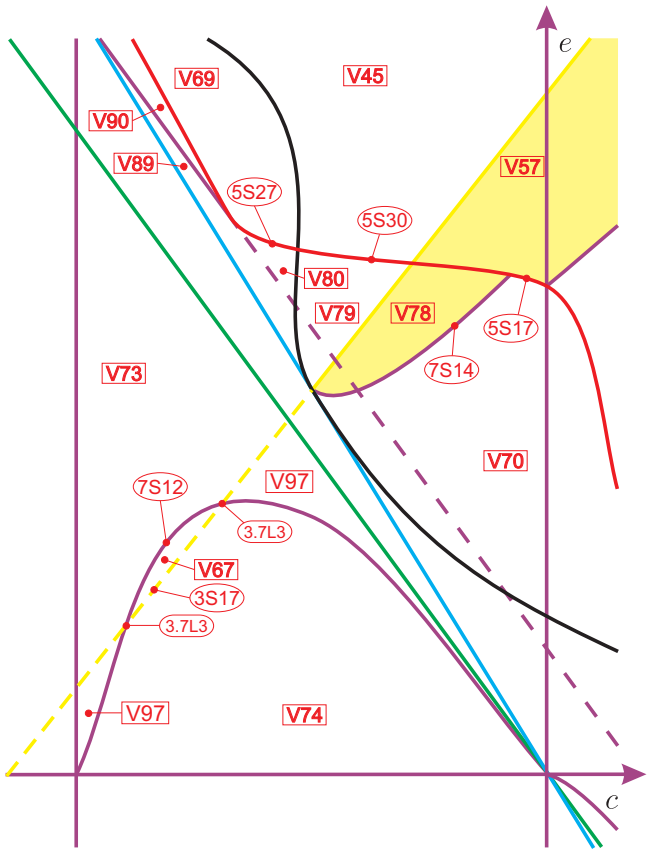

Figure 71 – Slice of parameter space when $m = -1 - \varepsilon_9$ (see Fig. 70)

On the other hand, as it was expected, due to the movement of these surfaces, there must exist a singular value $m = -1 - \varepsilon_9^*$ in which V_{67} vanishes. In fact, it is reduced to the curve $3.7L_3$ as in Fig. 72.

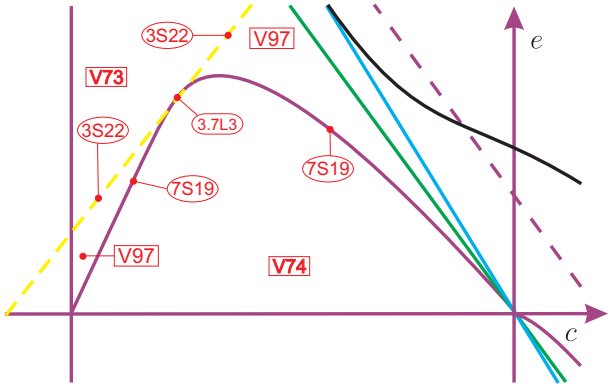

Figure 72 – Slice of parameter space when $m = -1 - \varepsilon_9^*$ (see Fig. 71)

When we keep going down with the parameter m, we detect that for $m = -1 - \varepsilon_{10}$ the nonalgebraic surface $7S_{19}$ no longer intersects $3S_{22}$. In fact, we describe this situation in Fig. 73.

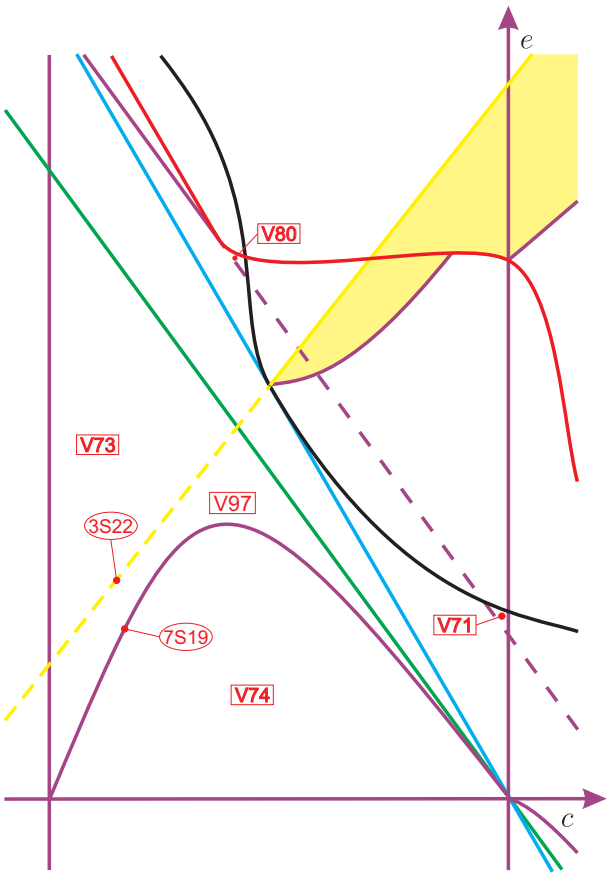

Figure 73 – Slice of parameter space when $m = -1 - \varepsilon_{10}$ (see Fig. 72)

We draw special attention for the fact that, up to here, the volume regions V_{71} and V_{80} have become even smaller (see Fig. 73). Indeed, when we have the algebraic singular slice $m = -5/4$, such regions are reduced to the points P_{18} and P_{17}, respectively, as in Fig. 74.

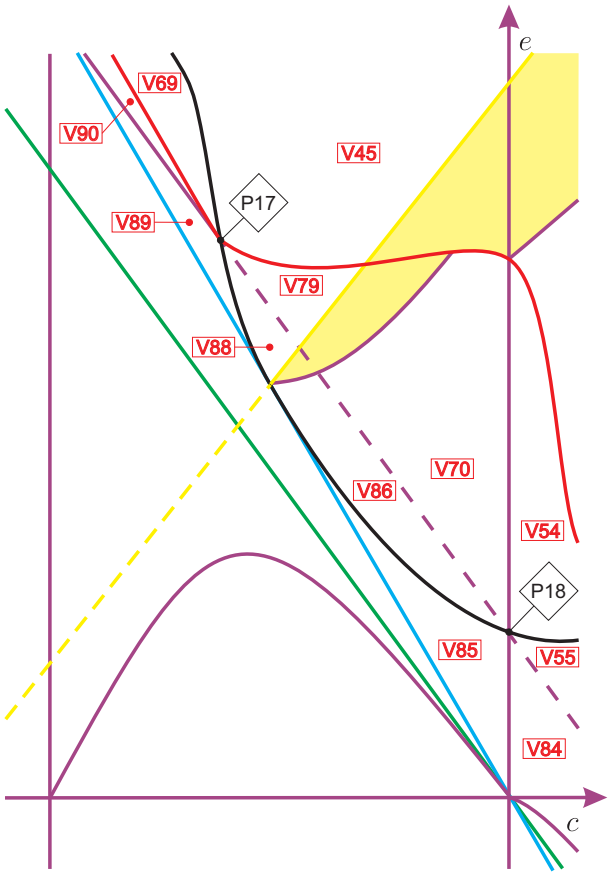

Figure 74 – Slice of parameter space when $m = -5/4$ (see Fig. 73)

In the generic slice $m = -13/10$, we observe that from the points P_{18} and P_{17} the volume regions V_{99} and V_{100} arise, respectively. Such regions, and their respective borders are presented in Fig. 75 in which we intend to show all the volume regions (modulo islands) in this slice.

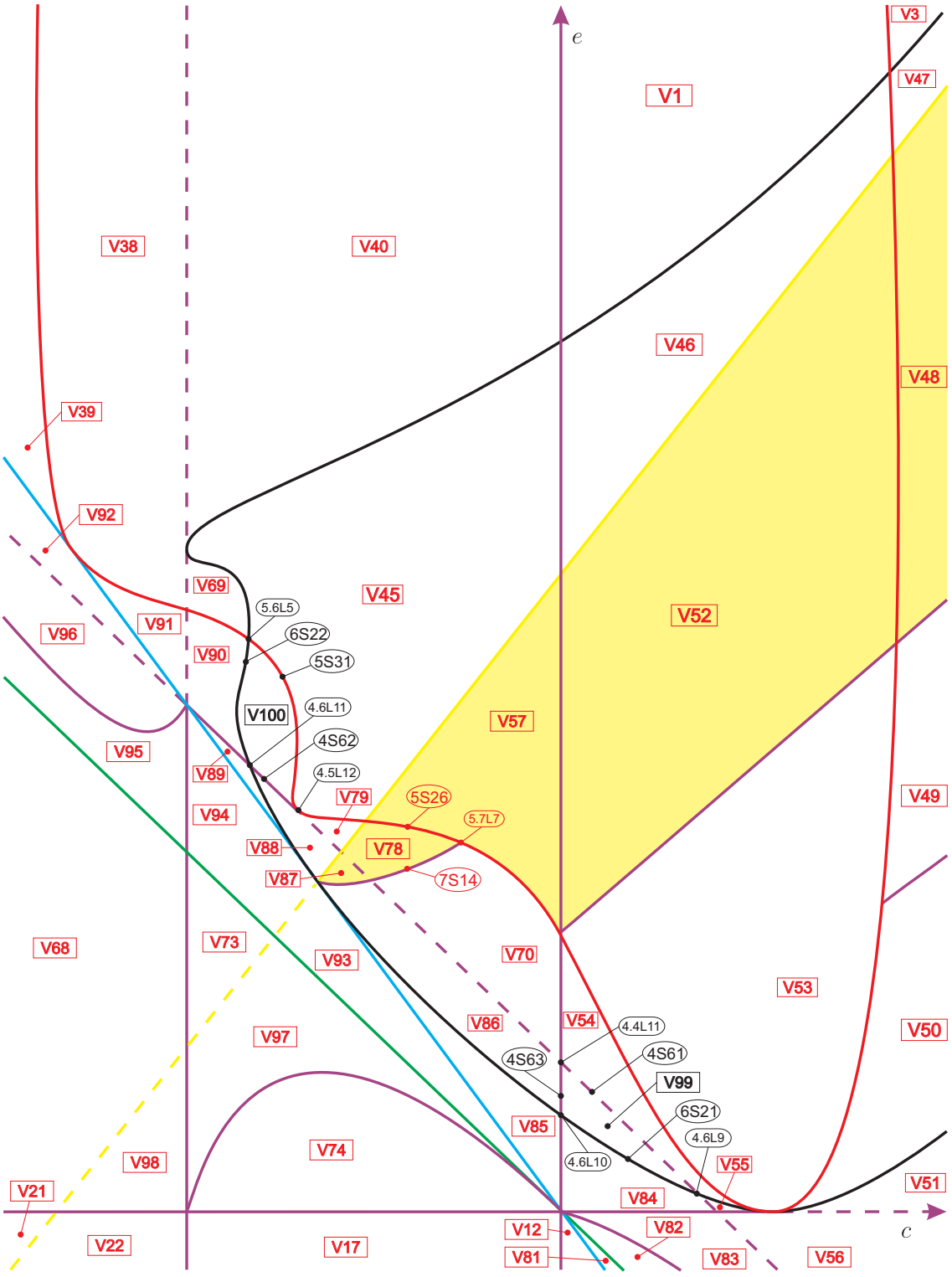

Figure 75 – Slice of parameter space when $m = -13/10$ (see Fig. 74)

By performing the study of the next singular slice, namely, $m = -3/2$, we only have one significant change in the bifurcation diagram. In fact, for this value of the parameter m the volume region V_{79} reduces to the point P_{19}, as in Fig. 76.

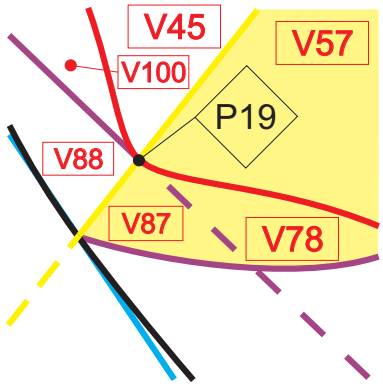

Figure 76 – Slice of parameter space when $m = -3/2$ (see Fig. 75)

Due to the displacement of all the surfaces, as it was expected, from the point P_{19} a new volume region arises, which we denote by V_{101}. In Fig. 77 we present a piece of the bifurcation diagram containing V_{101} when we consider the generic value $m = -7/4$.

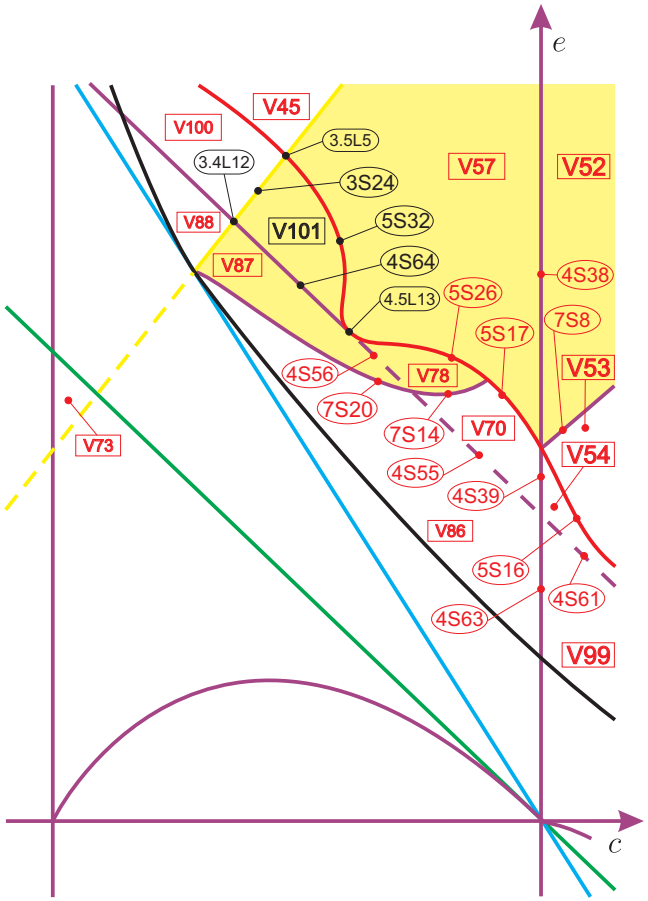

Figure 77 – Slice of parameter space when $m = -7/4$ (see Fig. 76)

Now when we go to the singular slice $m = -2$, we detect that the volume regions V_{70} (together with V_{78}) and V_{73} are reduced to the points P_{20} and P_{21}, respectively. The

remaining bifurcation diagram does not present any other significant change, see Fig. 78.

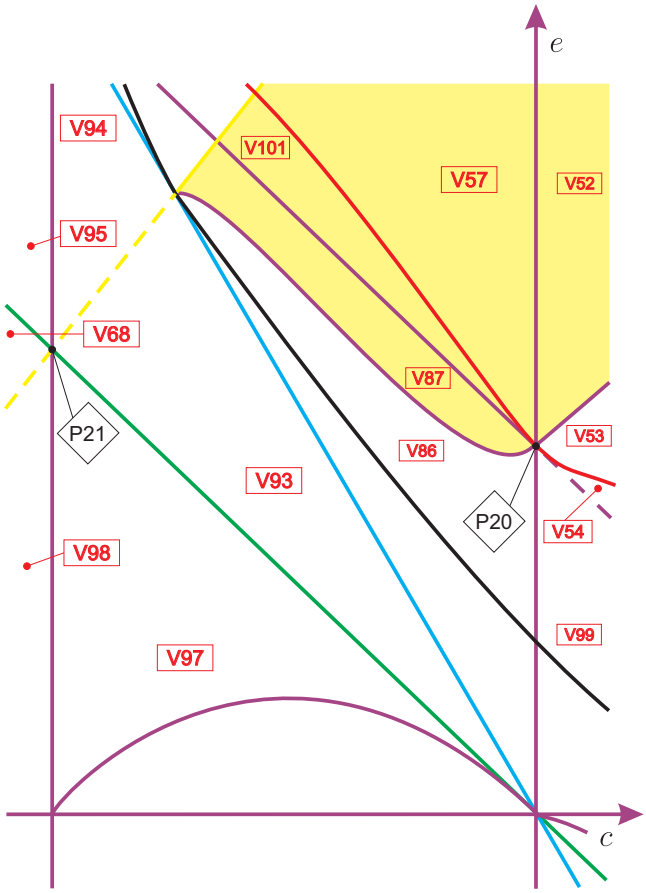

Figure 78 – Slice of parameter space when $m = -2$ (see Fig. 76)

By studying the next generic slice, $m = -5/2$, we observe that due to the displacement of the yellow surface, from the point P_{21} a new volume region arises and we denote it by V_{103}. Moreover, due to the displacement of the purple surface (which is parallel to the green one) and the red surface, we detect the birth of two new volume regions, namely, V_{102} and V_{104}. In what follows, we explain about the existence of this two volume regions, in particular, we explain why there exists the respective nonalgebraic surface $7S_{22}$. In fact, when we approach $4S_{67}$ to the right hand side we obtain a phase portrait that is topologically equivalent to V_{104}. On the other hand, when we approach $4S_{65}$ over it we obtain a phase portrait that is topologically equivalent to V_{102}. Then, there must exist a piece of surface $(\mathscr{S}_7)$ being a common border of these two regions. We denote this piece of nonalgebraic surface by $7S_{22}$, which corresponds to a loop–type bifurcation (of the finite saddle–node to itself). When we parametrize and make a study of the red surface, we obtain $5S_{33}$ being a border of V_{102} and $5S_{34}$ being a border of V_{104}, respectively. Then the nonalgebraic surface $7S_{22}$ has one of its endpoints on the red surface, more precisely, at $5.7L_{11}$. In fact, since $5S_{33}$ is a border of V_{53} and $5S_{34}$ is a border of V_{52}, we conclude that $7S_{22}$ is a continuation of the nonalgebraic surface $7S_8$. We claim that the other endpoint of

$7S_{22}$ is $4.4L_{12}$. Indeed, if the other endpoint of $7S_{22}$ is on $4S_{67}$, then the invariant straight line should be broken in order to make the respective loop–type bifurcation happens. For the same reason the endpoint of $7S_{22}$ cannot be in $4S_{65}$, see this slice in Fig. 79.

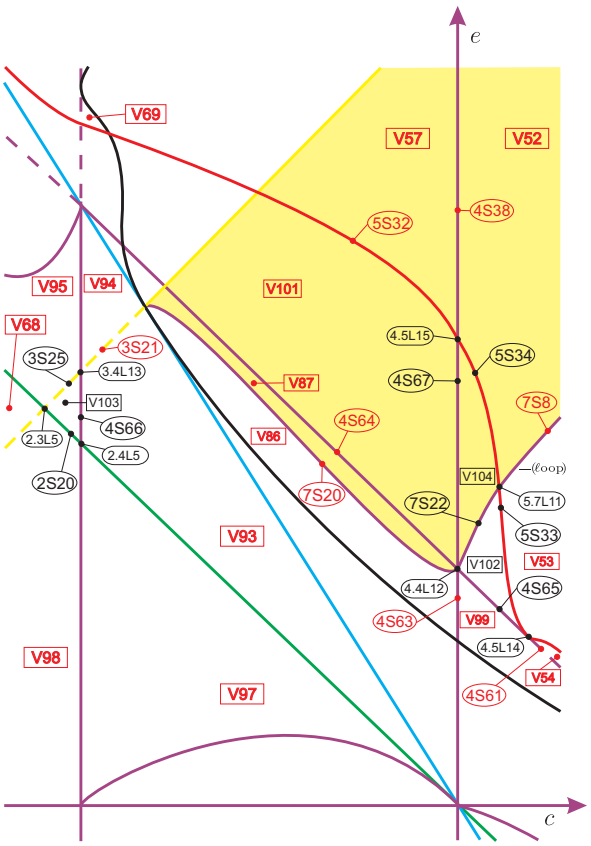

Figure 79 – Slice of parameter space when $m = -5/2$ (see Fig. 78)

For a better comprehension of the graphics producing limit cycles in perturbations, in Fig. 80 we present an amplification of the neighborhood in the parameter space of the curve $4.4L_{12}$ (see Fig. 79) with the corresponding phase portraits.

In Rmk. 4.3.2 we have concluded that the equation $\mathscr{T}_4 = \mathscr{F}_1 = 0$ has one double root if $\Delta = 0$, i.e. $m = \left(\pm 2\sqrt{2} - 3\right)/2$. In this way, the slice $m = \left(-2\sqrt{2} - 3\right)/2$ is singular. In fact, at this value of the parameter m we have a double curve $3.10L_3$, which in this case indicates a weak saddle of order two. This point splits surface $3S_{21}$ into two parts. Since these two pieces of surface $(\mathscr{S}_3)$ clearly produce topologically equivalent phase portraits, we denote both pieces by $3S_{21}$. The result can be seen in Fig. 81.

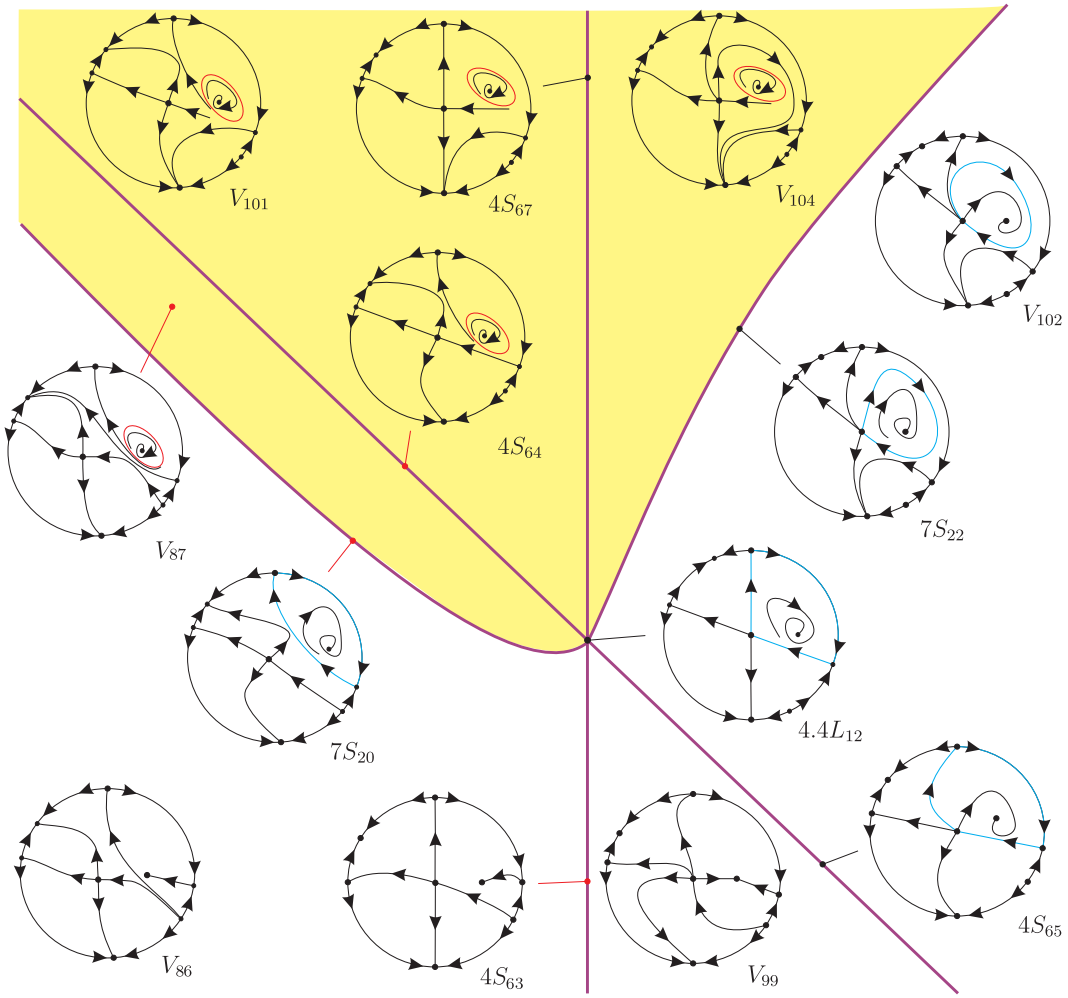

Figure 80 – Graphics producing limit cycles: neighborhood of $4.4L_{12}$ (see Fig. 79)

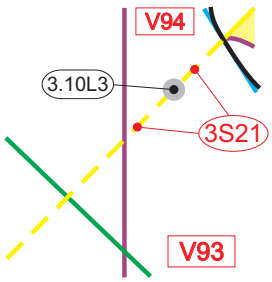

Figure 81 – Slice of parameter space when $m = \left(-2\sqrt{2}-3\right)/2$ (see Fig. 79)

Again according to Rmk. 4.3.2, the equation $\mathscr{T}_4 = \mathscr{F}_1 = 0$ has two real roots for $\Delta > 0$, i.e. for $m \notin \left(\left(-2\sqrt{2}-3\right)/2, \left(2\sqrt{2}-3\right)/2\right)$. Therefore, on the next generic slice, namely, $m = -295/100$, the curve $3.10L_3$ becomes two, creating surface $3S_{26}$, as in Fig. 82.

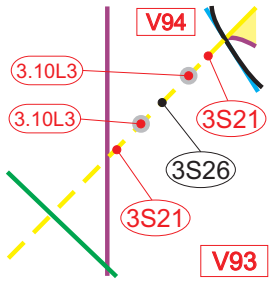

Figure 82 – Slice of parameter space when $m = -295/100$ (see Fig. 81)

Proceeding the study of the next singular slice, $m = -3$, we observe that here the curved triangle V_{69} (see Fig. 79) coalesces in a point, namely P_{22}. This is caused by the displacement of the black and red surfaces. Moreover, we also note that the two curves $3.10L_3$ moved themselves, causing the death of both pieces of surface $3S_{21}$. Then we have the corresponding points P_{23} and P_{24}. We present this result in Fig. 83.

Figure 83 – Slice of parameter space when $m = -3$ (see Fig. 82)

When we make a study of values of the parameter m less than $m = -3$, but very close to it, up to $m = -7/2$ we detect three important facts: first, from the point P_{22} a new volume region arises and we denote it by V_{105}. Second, from P_{23} a piece of surface $(\mathscr{S}_3)$ is

born, namely, $3S_{29}$. The third fact (which is the most interesting one) is that from P_{24} two pieces of surface ($\mathscr{S}_3$) are born, namely, $3S_{28}$ (without limit cycle) and $3S_{27}$ (with limit cycle). We observe that both pieces of surface must have an endpoint of surface $7S_{20}$ (which refers to a connection between a separatrix of the infinite saddle–node and a separatrix of the infinite saddle) being a common edge. In fact, numerical analysis supports this claim. We note that there must exist a continuation of the nonalgebraic surface $7S_{20}$. Indeed, we start by approaching $3S_{28}$ over it and then we obtain a phase portrait V_{106}, which contains a limit cycle. However, when we approach $4S_{62}$ and also $6S_{19}$ we obtain (in both cases) a phase portrait that is topologically equivalent to V_{88} (without limit cycles). Then we must have an element of surface ($\mathscr{S}_7$), namely, $7S_{23}$, which corresponds to a bifurcation due to a connection between a separatrix of the infinite saddle–node and a separatrix of the infinite saddle. Therefore, $7S_{23}$ is indeed a continuation of $7S_{20}$. Due to our numerical analysis described above and due to the fact that on black surfaces we can only have a $\mathscr{C}^\infty$ node–focus bifurcation, we conclude that the other endpoint of $7S_{23}$ is $7.8L_5$ and $7S_{23}$ is a border of the new volume region V_{106}.

On the other hand, surface $3S_{27}$ has $3.10L_5$ (the gray surface of $f^{(2)}$) being a common edge with $3S_{20}$. As surface $3S_{27}$ contains a limit cycle and we know that on surface ($\mathscr{S}_3$) one can have Hopf bifurcation, we can expect that in some neighborhood of this surface we have a region containing two limit cycles. Indeed, when we approach such a surface under we obtain a phase portrait that is topologically equivalent to V_{87} (i.e. containing only one limit cycle) and, on the other hand, when we approach $3S_{27}$ over it we obtain a phase portrait V_{107}, which contains two limit cycles surrounding the same focus. However, when we approach $4S_{62}$ and also $6S_{19}$ we obtain (in both cases) a phase portrait that is topologically equivalent to V_{88} (without limit cycles). Then there must exist an element $10S_1$ of surface ($\mathscr{S}_{10}$) which corresponds to a bifurcation of double limit cycle in order to keep the coherence in the bifurcation diagram. Lemma 4.3.45 assures the existence of such a surface and there we indicate its endpoints.

Lemma 4.3.45. Surface $10S_1$ corresponds to a bifurcation of a double limit cycle and its endpoints are on $7.8L_5$ and $3.10L_5$.

Proof. We consider Fig. 84. Part V_{87} first appeared in slice when $m = -1 - \varepsilon_6$ and its corresponding phase portrait possesses a limit cycle. We note that on surfaces $3S_{20}$, $3S_{27}$, $3S_{28}$ and on their linking points the phase portraits possess a weak focus of order at least one and, consequently, they refer to a Hopf bifurcation. If we are in part V_{87} and cross surface $3S_{20}$, we enter part V_{88} and the limit cycle is lost. Following this idea, the same should happen if we cross surface $3S_{27}$, but it is not what happens. After crossing this surface, the limit cycle persists when entering part V_{107}. In fact the Hopf bifurcation creates a second limit cycle. We note that these two limit cycles surrounds a unique focus. Then, as in part V_{88} we do not have limit cycles and in V_{107} we have two of them (around

the same focus), and there must exist at least one element $10S_1$ of surface $(\mathscr{S}_{10})$ dividing these two parts and corresponding to the presence of a double limit cycle. Now, it remains to prove where $10S_1$ starts from. We know that curve $3.10L_5$ corresponds to the presence of a weak focus of order two. With this in mind, it is more comprehensible that leaving part V_{87} and crossing the yellow surface, we enter in two topologically distinct parts, one with limit cycles and the other without them. The linking curve $3.10L_5$ of surfaces $3S_{20}$ and $3S_{27}$ is responsible for this, i.e. if we "walk" along surface $3S_{20}$, which does not possess limit cycle, and cross $3.10L_5$, the focus becomes weaker and a Hopf bifurcation happens, implying the birth of a limit cycle in the representatives of $3S_{27}$. Then, by this argument and by numerical evidences, surface $10S_1$ starts from $3.10L_5$. Moreover, since surface $3S_{27}$ has a limit cycle and this limit cycle is lost when we pass by the curve $3.7L_4$, and if we take several parallel straight lines sufficiently close to $3S_{28}$ and $3S_{27}$ over it, we detect numerically that the other endpoint of surface $10S_1$ is $7.8L_5$. □

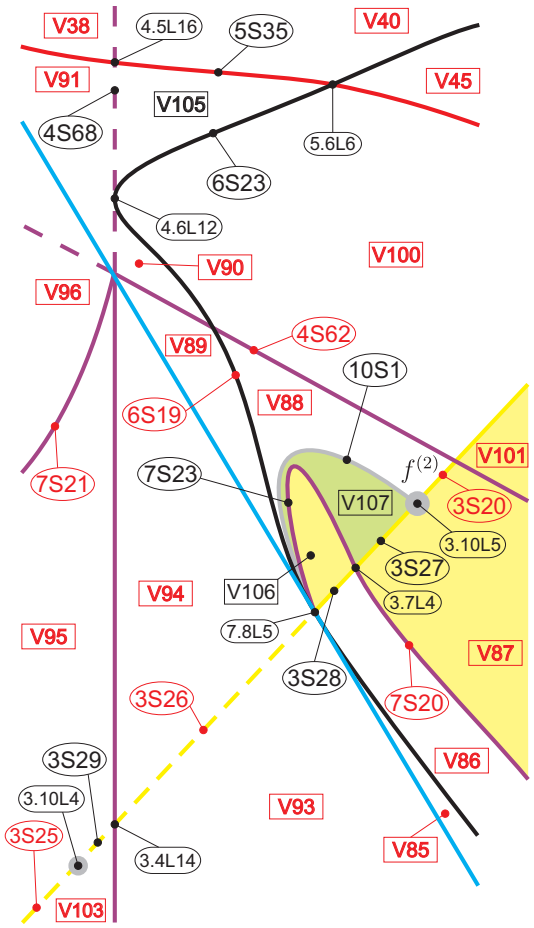

Figure 84 – Slice of parameter space when $m = -7/2$ (see Fig. 83)

We presented the slice $m = -7/2$ in Fig. 84 and we show in Fig. 85 an amplification of the neighborhood in the parameter space of the curve $3.7L_4$ with the corresponding

phase portraits. In these and in the next figures we have colored in light green the regions whose respective phase portraits possess two limit cycles.

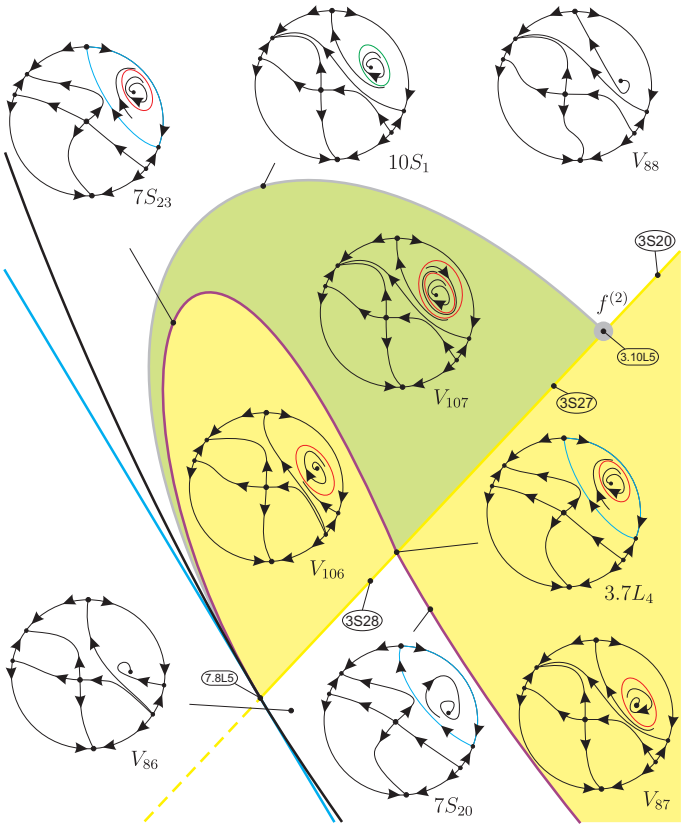

Figure 85 – Neighborhood in the parameter space of the curve $3.7L_4$ with the corresponding phase portraits: the existence of double limit cycle from a $f^{(2)}$

Regarding the previous lemma, we have to show three impossible situations:

1. surfaces $10S_1$ and $7S_{23}$ cannot intersect each other, since otherwise we would necessarily have a region containing 3 limit cycles (1 from V_{106} plus 2 generated by a piece of surface $10S_1$) being neighbor of V_{88}, which does not contain limit cycles, a contradiction. In Fig. 86 we present this hypothetic situation indicating only the respective number of limit cycles in each region (we do the same in the next two figures). In this and in the next figures we have colored in light purple the regions whose the respective phase portraits possess three limit cycles;

2. surface $10S_1$ cannot have an endpoint on $7S_{23}$, since otherwise we would have a piece of $7S_{23}$ with one (simple) limit cycle and other piece without limit cycles. Then the linking point would be a bifurcation due to a double limit cycle. See Fig. 87;

3. the endpoint of $10S_1$ cannot be on $3.7L_4$, due to the different stability of the antisaddles on the neighbors of $3.7L_4$. In fact, this situation could happen unless we have a singularity of center type. But, according to Vulpe (2011, Main Theorem,

item (b_4)), for the normal form (4.1) we do not have such a singularity, since on Rmk. 4.3.2 we see that $\mathscr{F}_3\mathscr{F}_4 \neq 0$. In Fig. 88 we present this hypothetic situation.

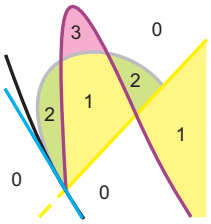

Figure 86 – Hypothetic situation of intersection between $7S_{23}$ and $10S_1$. We indicate the respective number of limit cycles that each region possesses (see Fig. 85)

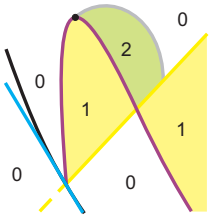

Figure 87 – Hypothetic situation in which surface $10S_1$ has an endpoint on $7S_{23}$. We indicate the respective number of limit cycles that each region possesses (see Fig. 85)

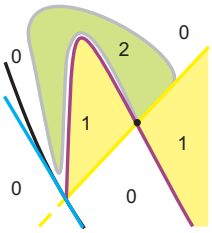

Figure 88 – Hypothetic situation in which surface $10S_1$ has an endpoint on $3.7L_4$. We indicate the respective number of limit cycles that each region possesses (see Fig. 85)

The next important value of the parameter m to be considered is $m = -4$. At this level, the volume region V_{57} (see Fig. 79) reduces to the point P_{25} as in Fig. 89.

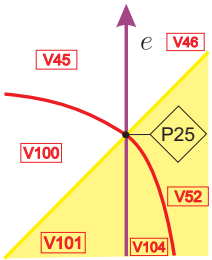

Figure 89 – Slice of parameter space when $m = -4$ (see Fig. 84)

By studying values of the parameter m less than but closer to $m=-4$, namely $m=-4-\varepsilon_{11}$, we observe that from the point P_{25} a new volume region arises and we denote it by V_{108} as in Fig. 90.

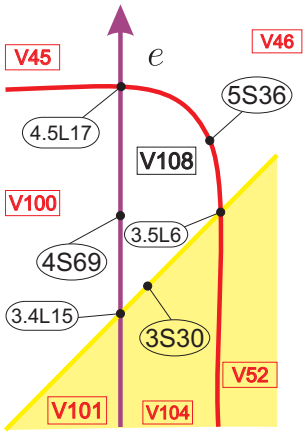

Figure 90 – Slice of parameter space when $m=-4-\varepsilon_{11}$ (see Fig. 89)

Regarding Rmk. 4.3.2, we know that for $m=-21/5$ we have a third order weak singularity. In fact, as we saw in such a remark, this singularity comes from equation

$$\mathscr{T}_4=\mathscr{F}_1=\mathscr{F}_2=0,$$

then if we move down from $m=-7/2$ (see Fig. 84) towards $m=-21/5$, we observe that the curve $3.10L_5$ (which was indicating a weak focus of second order) for $m=-7/2$ represents a weak focus of third order. As we saw in Rmk. 4.3.2, this situation happens for only one value of the parameter m, i.e. we have a point that represents this weak focus of third order. We denote such a point by P_{26}, see Fig. 91.

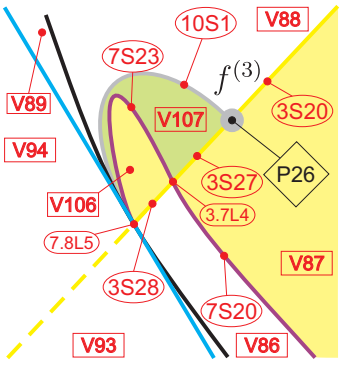

Figure 91 – Slice of parameter space when $m=-21/5$ (see Fig. 90)

Now, for smaller values of m, close to $m=-21/5$, the weak singularity is again of order two. Moreover, if we parametrize the yellow surface and "walk" on it, by starting on

the piece that represents $3S_{20}$ and move down with the parameter c, at a certain moment we pass by a bifurcation that allows us to detect the existence of two limit cycles on a portion of the yellow surface. After that we pass by another bifurcation that gives us a phase portrait that is topologically equivalent to $3S_{27}$. We denote the portion containing two limit cycles by $3S_{31}$. As this surface contains two limit cycles and we know that on surface $(\mathscr{S}_3)$ one can have Hopf bifurcation, we can expect that in some neighborhood of this surface we have a region containing three limit cycles. Indeed, we already know that over this surface we have a phase portrait corresponding to V_{107}, i.e. containing two limit cycles. When we approach such a surface under it we obtain a phase portrait V_{109}, which contains three limit cycles surrounding the same focus. However, when we approach $3S_{20}$, $3S_{27}$ (under) and also in a (over) neighborhood of the nonalgebraic border $7S_{20}$ we obtain (in all the cases) a phase portrait that is topologically equivalent to V_{87} (with only one limit cycle). Then there must exist an element $10S_2$ of surface $(\mathscr{S}_{10})$ which corresponds to a bifurcation of double limit cycle in order to keep the coherence in the bifurcation diagram. In fact, we detect that $10S_2$ is a continuation of $10S_1$. Lemma 4.3.46 assures the existence of such a surface and there we indicate its endpoints.

Lemma 4.3.46. Surface $10S_2$ corresponds to a bifurcation of a double limit cycle and its endpoints are on $3.10L_6$ and $3.10L_7$.

Proof. We consider Fig. 92. Part V_{107} first appeared in slice when $m = -7/2$ and its corresponding phase portrait possesses two limit cycles. If we are in this part and cross surface $3S_{27}$, we enter part V_{87} and one of the limit cycles is lost. Following this idea, the same should happen if we cross surface $3S_{31}$, but that is not what happens. After crossing this surface, due to the presence of two limit cycles on this surface, the Hopf bifurcation creates a third limit cycle. We note that these three limit cycles are around the same focus, because there exists only one focus in this portion of the parameter space. Then, as in part V_{87} we have one limit cycle and in V_{109} we have three of them (around the same focus), there must exist at least one element $10S_2$ of surface $(\mathscr{S}_{10})$ dividing these two parts and corresponding to the presence of a double limit cycle.
Now, it remains to prove where $10S_2$ starts from. We know that curve $3.10L_7$ corresponds to the presence of a weak focus of order two. With this in mind, it is more comprehensible that leaving part V_{107} and crossing the yellow surface, we enter in two topologically distinct parts, one with one limit cycle and the other with three of them. The linking curve $3.10L_7$ of surfaces $3S_{27}$ and $3S_{31}$ is responsible for this, i.e. if we "walk" along surface $3S_{27}$, which possesses one limit cycle, and cross $3.10L_7$, the focus becomes weaker and a Hopf bifurcation happens, implying the birth of second limit cycle in the representatives of $3S_{31}$. Then, by this argument and by numerical evidences, surface $10S_2$ starts from $3.10L_7$. Moreover, since surface $3S_{31}$ has two limit cycles and one of them is lost when we pass by the curve $3.10L_7$, and (on the bifurcation diagram) if we take several parallel

straight lines sufficiently close to $3S_{31}$ and $3S_{20}$ over and under, we detect numerically that, in fact, the other endpoint of surface $10S_2$ is $3.10L_6$ and therefore such a surface is a continuation of surface $10S_1$. □

We present the generic slice $m = -21/5 - \varepsilon_{12}$ in Fig. 92 as an amplification of the neighborhood in the parameter space of the curve $3.10L_7$ with the corresponding phase portraits.

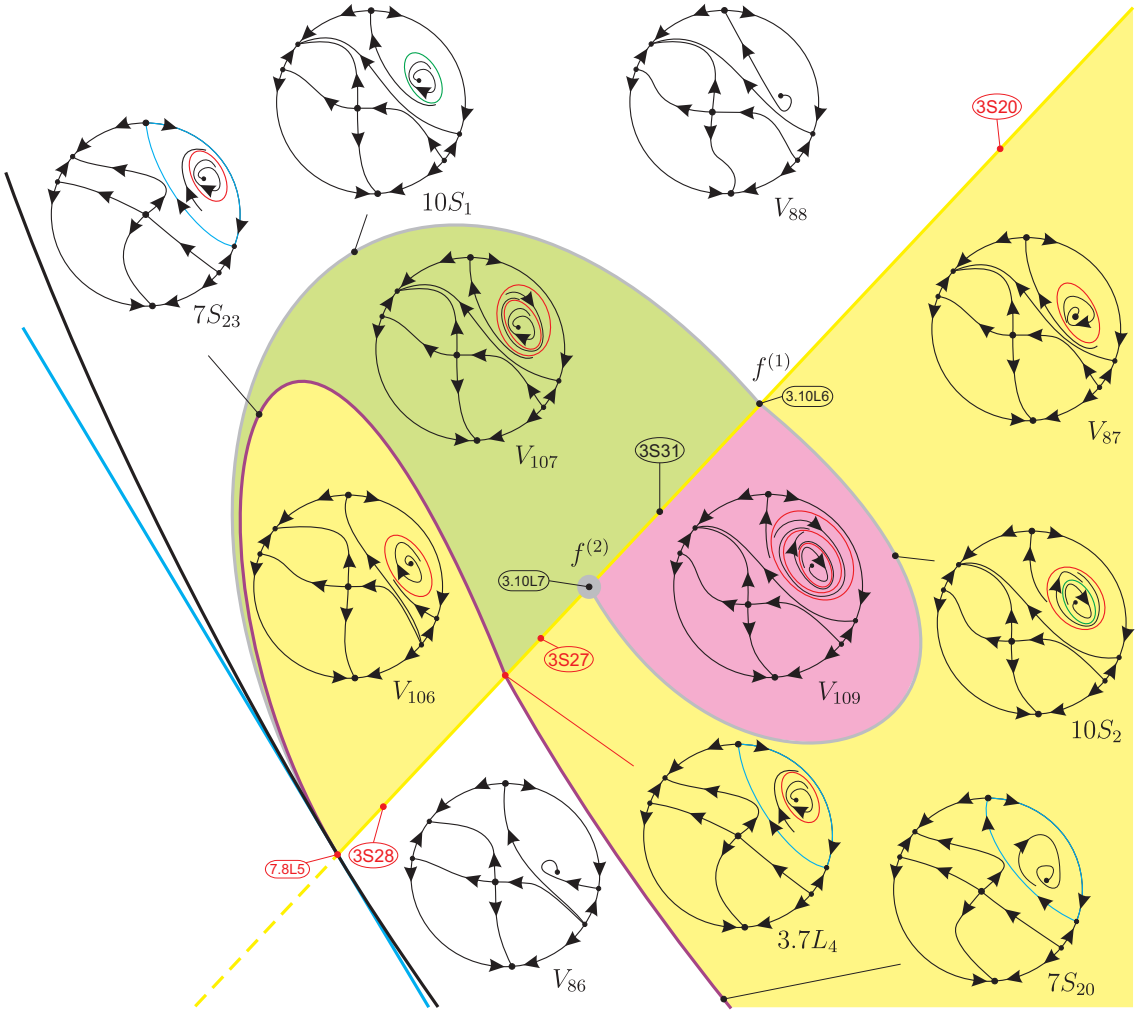

Figure 92 – Slice of parameter space when $m = -21/5 - \varepsilon_{12}$ (see Fig. 91)

When we keep going down, by performing the study of values of the parameter m less than $m = -21/5$, but very close to it, numerical analysis suggests that for some singular nonalgebraic value $m = -21/5 - \varepsilon_{12}^*$, the curves $3.10L_7$ and $3.7L_4$ coalesce, creating the point P_{27}, which represents a weak focus of order two, see Fig. 93.

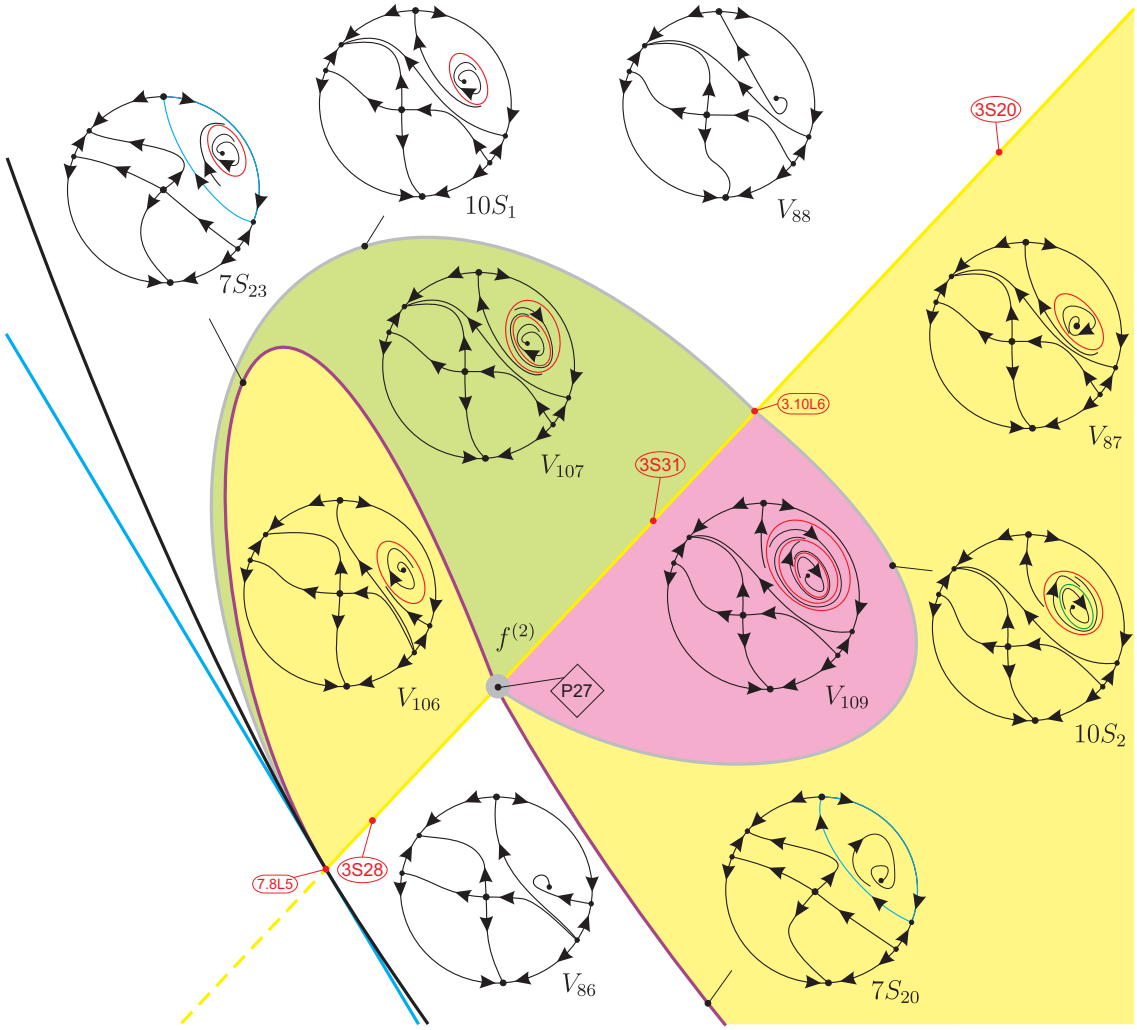

Figure 93 – Slice of parameter space when $m = -21/5 - \varepsilon_{12}^*$ (see Fig. 92)

Having analyzed the next generic slice (modulo islands) $m = -21/5 - \varepsilon_{13}$ we note that from the point P_{27} a new piece of surface $(\mathscr{S}_3)$ arises, namely, $3S_{32}$, which contains a limit cycle. Such a piece of surface has an endpoint on $3.7L_5$ (the connection between $3S_{31}$ and $3S_{32}$, which refers to a connection between a separatrix of the infinite saddle–node and a separatrix of the infinite saddle) and its another endpoint is the gray curve $3.10L_8$, which is a weak focus of order two. As surface $3S_{32}$ contains a limit cycle and we know that on surface $(\mathscr{S}_3)$ we can have Hopf bifurcation, we can expect that in some neighborhood of this surface we have a region containing two limit cycles. Indeed, when we approach such a surface over it we obtain a phase portrait that is topologically equivalent to V_{106} (i.e. containing only one limit cycle). On the other hand, when we approach $3S_{32}$ under it we obtain a phase portrait V_{110}, which contains two limit cycles surrounding the same focus. However, when we approach $3S_{28}$ (under it) and $6S_{18}$ (over it) we get (in both cases) a phase portrait that is topologically equivalent to V_{86} (without limit cycles). Then we must have an element $10S_3$ of surface $(\mathscr{S}_{10})$ which corresponds to a bifurcation of double limit

cycle in order to keep the coherence in the bifurcation diagram. We observe that surface $10S_3$ is a continuation of surface $10S_2$. Lemma 4.3.47 assures the existence of surface $10S_3$ and there we prove where its endpoints are located. As we do not have other significant change in the bifurcation diagram, here we only present in Fig. 94 an amplification of the neighborhood in the parameter space of the curve $3.7L_5$ with the corresponding phase portraits.

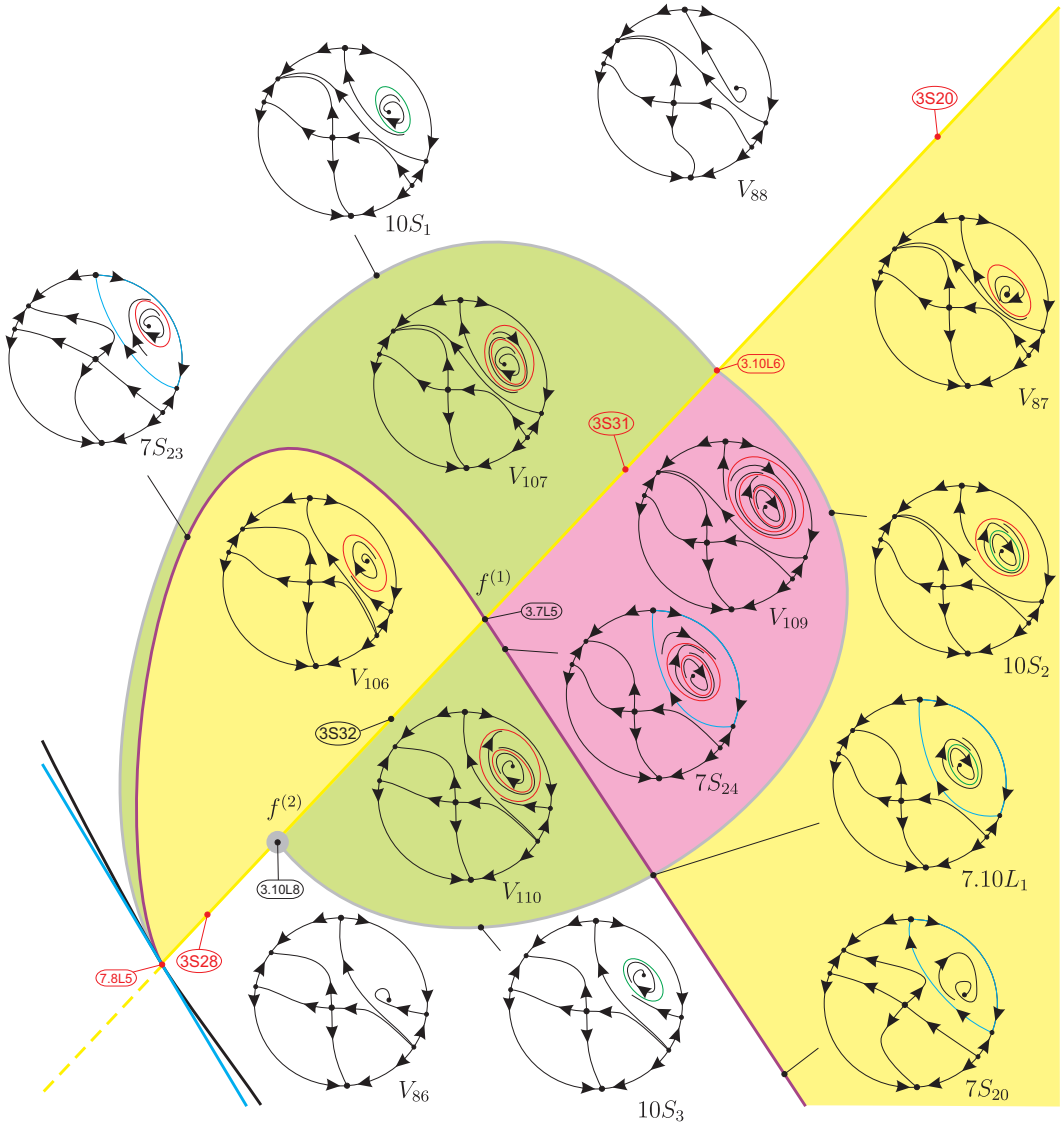

Figure 94 – Neighborhood in the parameter space of the curve $3.7L_5$ with the corresponding phase portraits: the existence of double limit cycle from $f^{(2)}$ and for $m = -21/5 - \varepsilon_{13}$

Lemma 4.3.47. Surface $10S_3$ corresponds to a bifurcation of a double limit cycle and its endpoints are on $7.10L_1$ and $3.10L_8$.

Proof. We consider Fig. 94. Part V_{106} first appeared in slice when $m = -7/2$ and its corresponding phase portrait possesses one limit cycle. We note that on surfaces $3S_{28}$, $3S_{32}$ and at their linking curve $3.10L_8$, the respective phase portraits possess a weak focus of order

at least one and, consequently, they refer to a Hopf bifurcation. If we are in part V_{106} and cross the surface $3S_{28}$, we enter part V_{86} and the limit cycle is lost. Following this idea, the same should happen if we cross the surface $3S_{32}$, but that is not what happens. After crossing this surface, the limit cycle persists when entering part V_{110}. In fact the Hopf bifurcation creates a second limit cycle. We note that these two limit cycles are around the same focus, because there exists only one focus in this portion of the parameter space. Then, as in part V_{86} we do not have limit cycles and in V_{110} we have two of them (around the same focus), there must exist at least one element $10S_3$ of surface $(\mathscr{S}_{10})$ dividing these two parts and corresponding to the presence of a double limit cycle.
Now, it remains to prove where $10S_3$ starts from. We know that the curve $3.10L_8$ corresponds to a presence of a weak focus of order two. With this in mind, it is more comprehensible that leaving part V_{106} and crossing the yellow surface, we enter into two topologically distinct parts, one of them with limit cycles and the other one without limit cycles. The linking curve $3.10L_8$ of the surfaces $3S_{28}$ and $3S_{32}$ is responsible for this, i.e. if we "walk" along the surface $3S_{28}$, which does not possess limit cycles, and cross $3.10L_8$, the focus becomes weaker and a Hopf bifurcation happens, implying the birth of a limit cycle in the representatives of $3S_{32}$. Then, by this argument and by numerical evidences, surface $10S_3$ starts from $3.10L_8$. Moreover, since surface $3S_{32}$ has one limit cycle and when we pass by the curve $3.7L_5$ we have two of them, and (on the bifurcation diagram) if we take several parallel straight lines sufficiently close to $3S_{32}$ and $3S_{31}$ (under), we detect that there is no element of V_{86} neither of V_{87} between V_{110} and V_{109}. Therefore the other endpoint of surface $10S_3$ is $7.10L_1$ and such a surface is a continuation of surface $10S_2$. □

When we perform the study of the values of the parameter m smaller but very close to $m = -21/5 - \varepsilon_{13}$, we observe that there must exist a nonalgebraic singular value $m = -21/5 - \varepsilon_{13}^*$ in which the nonalgebraic surface $7S_{21}$ is tangent to the piece of surface $3S_{29}$ (see Fig. 84) at $3.7L_6$. We present this fact in Fig. 95.

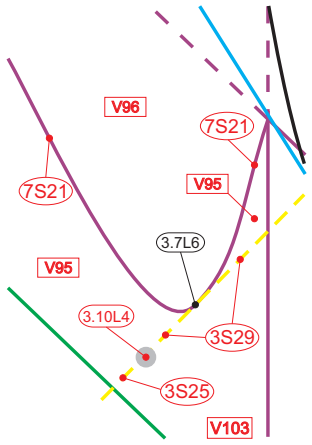

Figure 95 – Slice of parameter space when $m = -21/5 - \varepsilon_{13}^*$ (see Fig. 94)

Now, for some generic nonalgebraic value $m = -21/5 - \varepsilon_{14}$, as it was expected, from $3.7L_6$ a new volume region arises and we denote it by V_{111}, see Fig. 96.

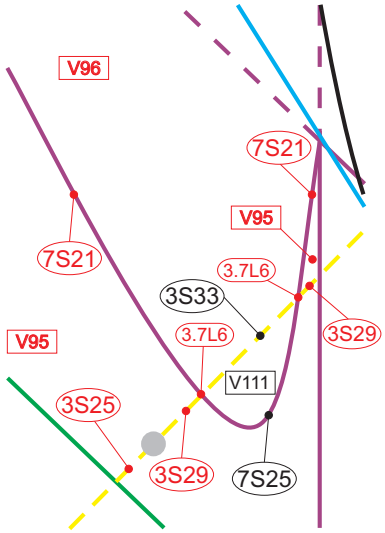

Figure 96 – Slice of parameter space when $m = -21/5 - \varepsilon_{14}$ (see Fig. 95)

The last singular slice ($m = -8$) describes the death of the volume region V_{45} (see for instance Fig. 75). Indeed, it reduces to the point P_{28} as in Fig. 97.

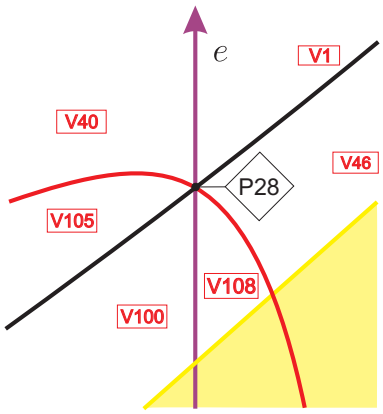

Figure 97 – Slice of parameter space when $m = -8$ (see Fig. 96)

We finally arrive at the last generic slice, namely, $m = -10$. Here, the only important fact is that from the point P_{28} we have the birth of the volume region V_{112}. The remaining bifurcation diagram does not present any other significant change. We show this new volume region (and its borders) in Fig. 98. In such a figure we intend to give an idea of the entire bifurcation diagram for $m = -10$.

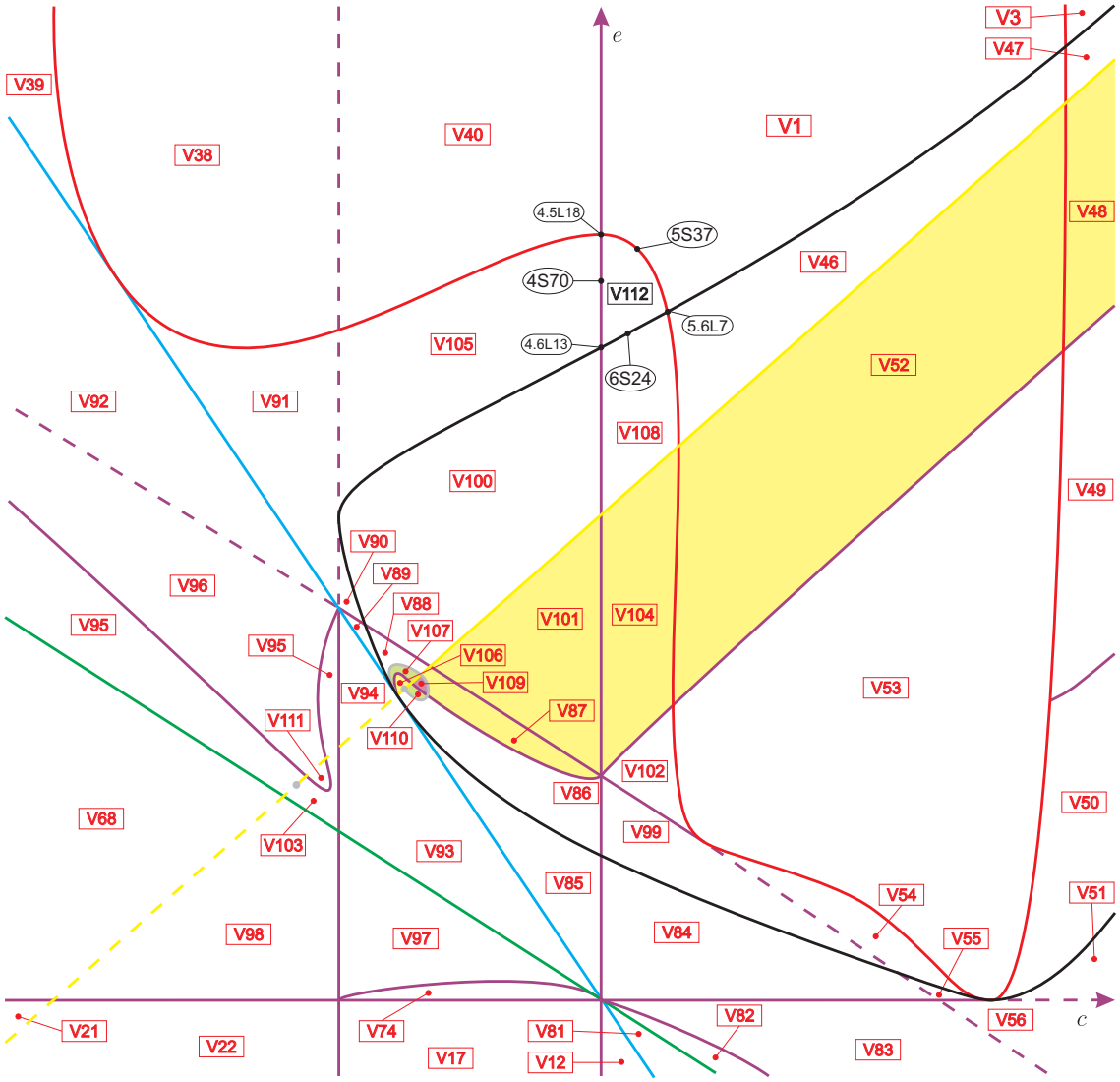

Figure 98 – Slice of parameter space when $m = -10$ (see Fig. 97)

After having finished the study of all values of the parameter m presented in (4.6), when we compare the two finite extreme values of such a parameter, i.e. $m = 4$ and $m = -10$, we observe that the regions $V_1, V_3, V_{12}, V_{17}, V_{21}, V_{22}, V_{38}, V_{39}$, and V_{40} appear in all slices.

We point out that the slice $m = -\infty$ is easily obtained from the slice $m = +\infty$. In fact, due to the symmetry in h (see page 122), the slices $m = +\infty$ and $m = -\infty$ are symmetrical. These slices correspond to $h = 0$ and $m = \pm 1$, respectively. Setting $h = 0$ and $m = -1$, systems (4.1) become

$$\dot{x} = cx + cy - cx^2,$$
$$\dot{y} = ex + ey - ex^2 - 2xy,$$

which differs from (4.7) only by the sign of the parameter m (i.e. by the sign of $2xy$).

Due to the symmetry in discussion, in Fig. 99 we present the slice when $m = -\infty$ properly labeled. As we mentioned before for the slice $m = +\infty$, here we draw special attention for the fact that the nonalgebraic surfaces (numeric detected and which existence was proved before) still remain at this slice and they "follow the movements" of the algebraic surfaces during the transition between the slices $m = -10$ and $m = -\infty$. Moreover, in Table 11 we indicate the death of all volume parts from slice $m = -10$ to $m = -\infty$. Then we have established the correspondence between the phase portraits of the slices $m = -10$ and $m = -\infty$.

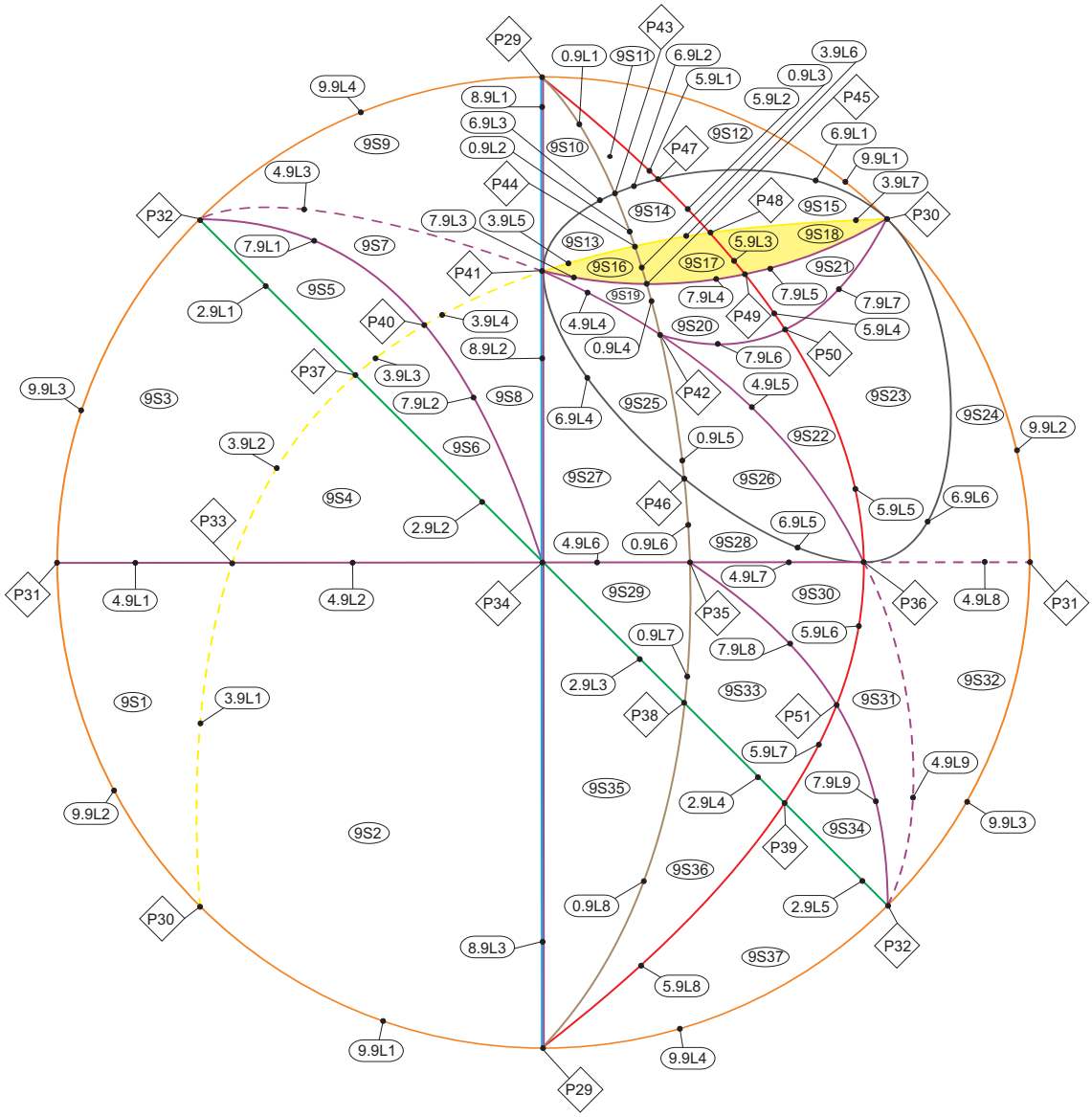

Figure 99 – Slice of parameter space when $m = -\infty$

Since there is coherence among the generic slices bordering the most singular slices $m = 1$, $m = 0$ and $m = -1$, with their respective generic side slices, no more slices are needed for the complete coherence of the bifurcation diagram. So, all the values of m in (4.6) are

Table 11 – Transition from slice $m = -10$ to $m = -\infty$. Here we present the correspondence between the volume regions from slice $m = -10$ and the respective parts from slice $m = -\infty$

Parts in slice $m = -10$	Parts in slice $m = -\infty$	Parts in slice $m = -10$	Parts in slice $m = -\infty$
V_1	$5.9L_1$	V_{86}	P_{41}
V_3	$9S_{12}$	V_{87}	P_{41}
V_{12}	$8.9L_3$	V_{88}	P_{41}
V_{17}	$8.9L_3$	V_{89}	P_{41}
V_{21}	$9S_1$	V_{90}	P_{41}
V_{22}	$9S_2$	V_{91}	$8.9L_1$
V_{38}	$5.9L_1$	V_{92}	$9S_9$
V_{39}	$8.9L_1$	V_{93}	P_{34}
V_{40}	$5.9L_1$	V_{94}	P_{41}
V_{46}	$5.9L_2$	V_{95}	$9S_5$
V_{47}	$9S_{15}$	V_{96}	$9S_7$
V_{48}	$9S_{18}$	V_{97}	P_{34}
V_{49}	$9S_{21}$	V_{98}	$9S_4$
V_{50}	$9S_{23}$	V_{99}	$9S_{25}$, $9S_{26}$
V_{51}	$9S_{24}$	V_{100}	P_{41}
V_{52}	$5.9L_3$	V_{101}	P_{41}
V_{53}	$5.9L_4$, P_{50}, $5.9L_5$	V_{102}	$9S_{19}$, $9S_{20}$, $9S_{22}$
V_{54}	P_{36}	V_{103}	$9S_6$
V_{55}	P_{36}	V_{104}	$9S_{16}$, $9S_{17}$
V_{56}	$9S_{32}$	V_{105}	$8.9L_1$
V_{68}	$9S_3$	V_{106}	P_{41}
V_{74}	P_{34}	V_{107}	P_{41}
V_{81}	$9S_{35}$, $9S_{36}$, $9S_{37}$	V_{108}	$9S_{13}$, $9S_{14}$
V_{82}	$9S_{29}$, $9S_{33}$, $9S_{34}$	V_{109}	P_{41}
V_{83}	$9S_{30}$, $9S_{31}$	V_{110}	P_{41}
V_{84}	$9S_{27}$, $9S_{28}$	V_{111}	$9S_8$
V_{85}	$8.9L_2$, P_{34}, P_{41}	V_{112}	$9S_{10}$, $9S_{11}$

sufficient for the coherence of the bifurcation diagram. Thus, we can affirm that we have described a complete bifurcation diagram for class $\overline{\mathbf{QsnSN_{11}(B)}}$ modulo islands, as we discuss in Sec. 4.4.

4.4 Other relevant facts about the bifurcation diagrams

The bifurcation diagram we have obtained for the class $\overline{\mathbf{QsnSN_{11}(B)}}$ is completely coherent, i.e. in this family, by taking any two points in the parameter space and joining them by a continuous curve, along this curve the changes in phase portraits that occur when crossing the different bifurcation surfaces we mention can be completely explained.

Nevertheless, we cannot be sure that this bifurcation diagram is the complete bifurcation diagram for $\overline{\mathbf{QsnSN_{11}(B)}}$ due to the possibility of the existence of "islands" inside the parts bordered by unmentioned bifurcation surfaces. In case they exist, these "islands" would not mean any modification of the nature of the singular points. So, on the border of these "islands" we could only have bifurcations due to saddle connections or multiple limit cycles.

In case there were more bifurcation surfaces, we should still be able to join two representatives of any two parts of the 631 parts of $\overline{\mathbf{QsnSN_{11}(B)}}$ found until now with a continuous curve either without crossing such a bifurcation surface or, in case the curve crosses it, it must do it an even number of times without tangencies, otherwise one must take into account the multiplicity of the tangency, so the total number must be even. This is why we call these potential bifurcation surfaces "*islands*".

However, we have not found a different phase portrait which could fit in such an island. A potential "island" would be the set of parameters for which the phase portraits possess a double limit cycle and this "island" would be inside the parts where $W_4 < 0$ since we have the presence of a focus.

The topological study that we do in the next chapter solves partially this problem, since there we prove that all the realizable phase portraits of class (AB) are, in fact, all the 40 generic phase portraits obtained in this chapter. But the possible existence of "islands" in the bifurcation diagram still persists since they can be related to the existence of double limit cycles, as we discussed in the previous paragraph.

4.5 Completion of the proof of the main theorem

In the bifurcation diagram we may have topologically equivalent phase portraits belonging to distinct parts of the parameter space. As here we have 631 distinct parts of the parameter space, to help us identify or distinguish phase portraits, we need to introduce some invariants and we actually choose integer valued, character and symbol invariants. Some of them were already used in Artés, Rezende and Oliveira (2013), Artés, Rezende and Oliveira (2014), Artés, Rezende and Oliveira (2015), and Artés, Mota and Rezende (2021a), but we recall them and introduce some needed ones. These invariants yield a classification which is easier to grasp.

Definition 4.5.1. We denote by $I_1(S)$ a symbol from the set $\{\emptyset, [\times], [\cup], [)(]\}$ which indicate the following configuration of curves filled up with singularities, respectively: none (non–degenerate systems – in this case all systems do not contain a curve filled up with singularities), two real straight lines intersecting at a finite point, a parabola, and an hyperbola. This invariant only makes sense to distinguish the degenerate phase portrait obtained.

Definition 4.5.2. We denote by $I_2(S)$ the sum of the indices of the isolated real finite singular points.

Definition 4.5.3. We denote by $I_3(S)$ the number of the real infinite singular points. We note that this number can also be infinity, which is represented by ∞.

Definition 4.5.4. For a given infinite singularity s of a system S, let ℓ_s be the number of global or local separatrices beginning or ending at s and which do not lie on the line at infinity. We have $0 \leq \ell_s \leq 4$. We denote by $I_4(S)$ the sequence of all such ℓ_s when s moves in the set of infinite singular points of system S. We start the sequence at the infinite singular point which receives (or sends) the greatest number of separatrices and take the direction which yields the greatest absolute value, e.g. the values 2110 and 2011 for this invariant are symmetrical (and, therefore, they are the same), so we consider 2110.

Definition 4.5.5. We denote by $I_5(S)$ the total number of local or global separatrices of the finite multiple singularity which link it with the infinite multiple singular points.

Definition 4.5.6. We denote by $I_6(S)$ a character from the set $\{\overline{sn}_{(2)}, \widehat{cp}_{(2)}\}$ which describes the type of the multiple singularity located at the origin.

Definition 4.5.7. We denote by $I_7(S)$ the number of local or global separatrices starting or ending at the nodal sector of the finite saddle–node.

Definition 4.5.8. We denote by $I_8(S)$ a character from the set $\{n, y\}$ which indicates if the separatrix of the infinite saddle–node $\overline{\binom{1}{1}}\,SN$ has the same limit of a separatrix of the finite saddle–node $\overline{sn}_{(2)}$.

Definition 4.5.9. We denote by $I_9(S)$ a character from the set $\{n, y\}$ describing the nonexistence ("n") or the existence ("y") of basins (see page 148).

Definition 4.5.10. We denote by $I_{10}(S)$ a character from the set $\{n, y\}$ describing the nonexistence ("n") or the existence ("y") of graphics.

Definition 4.5.11. We denote by $I_{11}(S)$ the number of local or global separatrices starting or ending at the finite antisaddle.

Definition 4.5.12. We denote by $I_{12}(S)$ the total number of local or global separatrices linking the finite simple singularity to the infinite saddle–node $\overline{\binom{1}{1}}\,SN$.

Definition 4.5.13. We denote by $I_{13}(S)$ the number of limit cycles around a focus.

Definition 4.5.14. In case there exist an infinite singularity which does not belong to the hyperbola filled up with singularities, we denote by $I_{14}(S)$ a character from the set $\{n, y\}$ (for **n**o or **y**es, respectively) describing if the infinite singularity is located between two other infinite singularities which belong to the same branch of the hyperbola filled up with singularities.

As we have noted previously in Rmk. 4.3.34, we do not distinguish between phase portraits whose only difference is that in one we have a finite node and in the other a focus. Both phase portraits are topologically equivalent and they can only be distinguished within the $\mathscr{C}^1$ class. In case we may want to distinguish between them, a new invariant may easily be introduced.

Theorem 4.5.15. Consider the class $\overline{\mathbf{QsnSN_{11}(B)}}$ and all the phase portraits that we have obtained for this family. The values of the affine invariant

$$\mathscr{I} = (I_1, I_2, I_3, I_4, I_5, I_6, I_7, I_8, I_9, I_{10}, I_{11}, I_{12}, I_{13}, I_{14})$$

given in the diagram from Tables 12 to 17 yield a partition of these phase portraits of the class $\overline{\mathbf{QsnSN_{11}(B)}}$.

Furthermore, for each value of $\mathscr{I}$ in this diagram there corresponds a single phase portrait; i.e. S and S' are such that $\mathscr{I}(S) = \mathscr{I}(S')$, if and only if S and S' are topologically equivalent.

The bifurcation diagram for $\overline{\mathbf{QsnSN_{11}(B)}}$ has 631 parts which produce 226 topologically different phase portraits as described in Tables 12 to 32. The remaining 405 parts do not produce any new phase portrait which was not included in the 226 previous ones. The difference is basically the presence of a strong focus instead of a node and vice versa and weak singular points.

The phase portraits having neither limit cycle nor graphic have been denoted surrounded by parenthesis, for example (V_{77}); the phase portraits having one, two or three limit cycles have been denoted surrounded by brackets, for example $[V_{57}]$ possessing one limit cycle, $[[V_{107}]]$ possessing two limit cycles, and $[[[V_{109}]]]$ possessing three limit cycles; the phase portraits having one graphic have been denoted surrounded by $\{*\}$ and those ones having two or more graphics have been denoted surrounded by $\{\{*\}\}$, for example $\{5S_{17}\}$ and $\{\{9S_{10}\}\}$, respectively. Moreover, the phase portraits having one limit cycle and one (respectively more than one) graphic have been denoted surrounded by $[\{*\}]$ (respectively $[\{\{*\}\}]$), for example $[\{7S_{23}\}]$ (respectively $[\{\{9S_{17}\}\}]$). In addition, the phase portraits possessing a double limit cycle have been denoted surrounded by $[*]^2$ and those ones which possesses a double limit cycle and also a simple one have been denoted surrounded by $[[*]^2]$, for instance $[10S_1]^2$ and $[[10S_2]^2]$, respectively.

Proof of Thm. 4.5.15. The mentioned result follows from the results in the previous sections and a careful analysis of the bifurcation diagrams given in Sec. 4.3, in Figs. 28 to 99, the definition of the invariants I_j and their explicit values for the corresponding phase portraits. □

We recall some facts regarding the equivalence relations used in this study: the affine and time rescaling, $\mathscr{C}^1$ and topological equivalences.

The coarsest one among these three is the topological equivalence and the finest is the affine equivalence. We can have two systems which are topologically equivalent but not $\mathscr{C}^1-$equivalent. For example, we could have a system with a finite antisaddle which is a structurally stable node and in another system with a focus, the two systems being topologically equivalent but belonging to distinct $\mathscr{C}^1-$equivalence classes, separated by the surface $(\mathscr{S}_6)$ on which the node turns into a focus.

In Tables 18 to 32 we list in the first column 226 parts with all the distinct phase portraits of Figs. 15 to 21. Corresponding to each part listed in column one we have in each row all parts whose phase portraits are topologically equivalent to the phase portrait appearing in column one of the same row.

In the second column we set all the parts whose systems yield topologically equivalent phase portraits to those in the first column, but which may have some algebro–geometric features related to the position of the orbits. In the third column we present all the parts which are topologically equivalent to the ones from the first column having a focus instead of a node.

In the fourth (respectively fifth and sixth) column we list all parts whose phase portraits have a node which is at a bifurcation point producing focus close to the node in perturbations, a node–focus to shorten (respectively a finite weak singular point; and possess an invariant curve not yielding a connection of separatrices).

The last column refers to other reasons associated to different geometric aspects and they are described as follows:

(1) the degenerate phase portrait possesses either a weak finite singular point, or a node–focus, or a cusp–type singularity, or an invariant line, or even a combination of these elements;

(2) the phase portrait possesses a singularity of type $\left(\widehat{\begin{smallmatrix}1\\2\end{smallmatrix}}\right) E-H$ at infinity;

(3) the phase portraits correspond to symmetric parts of the bifurcation diagram.

Whenever phase portraits appear in a row in a specific column, the listing is done according to the decreasing dimension of the parts where they appear, always placing the lower dimensions on lower lines.

Table 12 – Geometric classification for the family $\mathbf{QsnSN_{11}(B)}$

$$
I_1 = \begin{cases}
\emptyset \;\&\; I_2 = \begin{cases}
-1 \;\&\; I_3 = \begin{cases}
2 \;\&\; I_4 = \begin{cases}
2210\ \{\{4.9L_1\}\}, \\
3101\ \{\{7.9L_1\}\}, \\
3201 \;\&\; I_5 = \begin{cases} 1 \;\&\; I_6 = \begin{cases} \overline{sn}_{(2)}\ \{\{9S_7\}\}, \\ \widehat{cp}_{(2)}\ \{\{2.9L_1\}\}, \end{cases} \\ 2\ \{\{9S_1\}\}, \end{cases} \\
3310\ \{\{9S_3\}\}, \\
4201\ \{\{9S_5\}\},
\end{cases} \\
3 \;\&\; I_4 = \begin{cases}
111110\ (4.4L_6), \\
111111\ (4S_{34}), \\
211011\ (2.4L_4), \\
211101 \;\&\; I_5 = \begin{cases} 1\ (4S_{17}), \\ 2\ (4S_3), \end{cases} \\
211111 \;\&\; I_7 = \begin{cases} 0\ (7S_{12}), \\ 2\ (V_{13}), \end{cases} \\
211210\ (4S_{37}), \\
211211\ (V_{63}), \\
212110\ (7S_{21}), \\
221101\ (4S_{42}), \\
221110\ (7S_1), \\
221201\ (2S_{16}), \\
221210 \;\&\; I_8 = \begin{cases} n\ (V_{21}), \\ y\ (V_{10}), \end{cases} \\
311011\ (4S_{50}), \\
311110\ (4S_6), \\
311111\ (2S_{17}), \\
312110 \;\&\; I_5 = \begin{cases} 0\ (V_{92}), \\ 1\ (V_4), \end{cases} \\
321021\ (V_{95}), \\
321110\ (2S_5), \\
311111\ (V_{73}), \\
321201\ (V_{68}), \\
331110\ (V_8), \\
411111\ (V_{93}), \\
421110\ (V_6),
\end{cases}
\end{cases} \\
1 \;\&\; I_3 = \mathscr{A}_1\ \textit{(next page)},
\end{cases} \\
[\times] \;\&\; I_3 = \begin{cases} 2\ \{\{P_3\}\}, \\ 3\ \{\{4.8L_1\}\}, \end{cases} \\
[\cup] \;\&\; I_3 = \begin{cases} 1\ \{\{P_{29}\}\}, \\ 2\ \{\{9.9L_1\}\}, \end{cases} \\
[)(] \;\&\; I_3 = \begin{cases} 2\ \{\{5.8L_1\}\}, \\ 3 \;\&\; I_{14} = \begin{cases} n\ \{\{8S_1\}\}, \\ y\ (8S_2), \end{cases} \end{cases}
\end{cases}
$$

Table 13 – Geometric classification for the family **QsnSN$_{11}$(B)** *(cont.)*

$$
I_1=\left\{\begin{array}{l}
\mathscr{A}_1\\
\begin{bmatrix} I_1=\emptyset,\\ I_2=1\end{bmatrix}\ \&\ I_3=\left\{\begin{array}{l}
1\ \&\ I_4=\left\{\begin{array}{l}
11\ \&\ I_5=\left\{\begin{array}{l}
1\ \&\ I_6=\left\{\begin{array}{l}
\overline{sn}_{(2)}\ \&\ I_7=\left\{\begin{array}{l} 0\ \&\ I_{13}=\left\{\begin{array}{l}(0)\ (V_{33}),\\ (1)\ [V_{60}],\end{array}\right.\\ 1\ \{7S_8\},\\ 2\ \{V_{53}\},\end{array}\right.\\
\widehat{cp}_{(2)}\ \&\ I_{13}=\left\{\begin{array}{l}(0)\ (2S_2),\\ (1)\ [2S_{11}],\end{array}\right.
\end{array}\right.\\
2\ \&\ I_{13}=\left\{\begin{array}{l}(0)\ (4S_1),\\ (1)\ [4S_{38}],\end{array}\right.
\end{array}\right.\\
21\ \&\ I_7=\left\{\begin{array}{l}
0\ \&\ I_{13}=\left\{\begin{array}{l}(0)\ \&\ I_9=\left\{\begin{array}{l} n\ (P_{51}),\\ y\ (V_{38}),\end{array}\right.\\ (1)\ [V_{57}],\end{array}\right.\\
1\ \&\ I_{13}=\left\{\begin{array}{l}(0)\ \&\ I_{10}=\left\{\begin{array}{l} n\ (V_1),\\ y\ \{P_{50}\},\end{array}\right.\\ (1)\ [V_{52}],\end{array}\right.
\end{array}\right.\\
22\ \&\ I_6=\left\{\begin{array}{l}
\overline{sn}_{(2)}\ \&\ I_7=\left\{\begin{array}{l} 0\ (5.9L_7),\\ 1\ \{P_{49}\},\\ 2\ \{5.9L_4\},\end{array}\right.\\
\widehat{cp}_{(2)}\ (P_{39}),
\end{array}\right.\\
31\ \&\ I_{10}=\left\{\begin{array}{l} n\ (5.9L_6),\\ y\ \{5.9L_5\},\end{array}\right.\\
32\ \&\ I_7=\left\{\begin{array}{l}
0\ (5.9L_8),\\
1\ \&\ I_{13}=\left\{\begin{array}{l}(0)\ (5.9L_1),\\ (1)\ [5.9L_3],\end{array}\right.
\end{array}\right.
\end{array}\right.\\
2\ \&\ I_4=\left\{\begin{array}{l}
1110\ \&\ I_7=\left\{\begin{array}{l} 0\ \{\{4.9L_6\}\},\\ 1\ \{\{4.9L_4\}\},\end{array}\right.\\
1111\ \&\ I_5=\left\{\begin{array}{l}
2\ \&\ I_7=\left\{\begin{array}{l} 0\ (4.5L_3),\\ 2\ \{4.5L_{14}\},\end{array}\right.\\
3\ \{P_{20}\},
\end{array}\right.\\
2100\ \&\ I_7=\left\{\begin{array}{l} 0\ (7.9L_9),\\ 1\ \{7.9L_7\},\end{array}\right.\\
2101\ \&\ I_5=\left\{\begin{array}{l}
0\ (9S_{24}),\\
1\ \&\ I_6=\left\{\begin{array}{l}
\overline{sn}_{(2)}\ \&\ I_7=\left\{\begin{array}{l} 0\ \{\{9S_{29}\}\},\\ 1\ \{\{7.9L_3\}\},\\ 2\ \{\{9S_{19}\}\},\end{array}\right.\\
\widehat{cp}_{(2)}\ \{\{2.9L_3\}\},
\end{array}\right.\\
2\ \{\{9S_{27}\}\},
\end{array}\right.\\
2110\ \&\ I_{12}=\left\{\begin{array}{l} 0\ (4.5L_8),\\ 1\ (4.5L_4),\end{array}\right.\\
\mathscr{A}_2\ \textit{(next page)},
\end{array}\right.\\
3\ \&\ I_4=\mathscr{A}_3\ \textit{(next page)},\\
\infty\ \{\{P_{36}\}\},
\end{array}\right.
\end{array}\right.
$$

Table 14 – Geometric classification for the family **QsnSN$_{11}$(B)** *(cont.)*

$$
I_1=\left\{\begin{array}{l}
\mathscr{A}_2\ \begin{bmatrix} I_1=\emptyset, \\ I_2=1, \\ I_3=2 \end{bmatrix}\ \&\ I_4=\left\{\begin{array}{l}
2111\ \&\ I_5=\left\{\begin{array}{l}
1\ \&\ I_6=\left\{\begin{array}{l}
\overline{sn}_{(2)}\ \&\ I_7=\left\{\begin{array}{l} 0\ (5S_5), \\ 1\ \{\{4.9L_7\}\}, \\ 2\ \&\ I_{11}=\left\{\begin{array}{l} 0\ \{5.7L_{11}\}, \\ 2\ \{\{4.9L_5\}\}, \end{array}\right. \\ 3\ \{5S_{33}\}, \end{array}\right. \\
\widehat{cp}_{(2)}\ (2.5L_2),
\end{array}\right. \\
2\ \&\ I_7=\left\{\begin{array}{l} 0\ (4.5L_1), \\ 1\ \&\ I_{13}=\left\{\begin{array}{l} (0)\ \&\ I_{11}=\left\{\begin{array}{l} 1\ (4.5L_{18}), \\ 3\ (5S_4), \end{array}\right. \\ (1)\ [4.5L_{15}], \end{array}\right. \\ 2\ \{5S_{16}\}, \end{array}\right. \\
3\ \&\ I_7=\left\{\begin{array}{l} 0\ \{P_{14}\}, \\ 1\ \&\ I_{13}=\left\{\begin{array}{l} (0)\ \&\ I_{10}=\left\{\begin{array}{l} n\ (4.5L_{10}), \\ y\ \{4.5L_9\}, \end{array}\right. \\ (1)\ [4.5L_{13}], \end{array}\right. \end{array}\right.
\end{array}\right. \\
2120\ \&\ I_7=\left\{\begin{array}{l} 0\ (5.7L_1), \\ 1\ \{5.7L_3\}, \end{array}\right. \\
2121\ \&\ I_{11}=\left\{\begin{array}{l}
0\ \&\ I_{13}=\left\{\begin{array}{l} (0)\ \{5.7L_7\}, \\ (1)\ [5.7L_8], \end{array}\right. \\
1\ \&\ I_5=\left\{\begin{array}{l} 2\ \{\{7.9L_6\}\}, \\ 3\ (5.7L_9), \end{array}\right. \\
3\ \&\ I_5=\left\{\begin{array}{l} 2\ \{\{9S_{28}\}\}, \\ 3\ \{\{7.9L_8\}\}, \end{array}\right.
\end{array}\right. \\
2200\ \&\ I_{11}=\left\{\begin{array}{l} 0\ \{7.9L_5\}, \\ 1\ \{9S_{21}\}, \\ 2\ (2.9L_5), \\ 3\ (9S_{34}), \end{array}\right. \\
2211\ \&\ I_{13}=\left\{\begin{array}{l}
(0)\ \&\ I_{12}=\left\{\begin{array}{l} 0\ (5S_8), \\ 1\ (5S_{28}), \end{array}\right. \\
(1)\ [5S_{32}],
\end{array}\right. \\
3101\ \&\ I_7=\left\{\begin{array}{l} 0\ \{\{9S_{35}\}\}, \\ 1\ \&\ I_{13}=\left\{\begin{array}{l} (0)\ \{\{9S_{10}\}\}, \\ (1)\ [\{\{9S_{16}\}\}], \end{array}\right. \end{array}\right. \\
3111\ \&\ I_5=\left\{\begin{array}{l}
2\ \&\ I_6=\left\{\begin{array}{l}
\overline{sn}_{(2)}\ \&\ I_7=\left\{\begin{array}{l} 0\ (5S_6), \\ 2\ \&\ I_{13}=\left\{\begin{array}{l} (0)\ (5S_{37}), \\ (1)\ [5S_{34}], \end{array}\right. \end{array}\right. \\
\widehat{cp}_{(2)}\ \{P_7\},
\end{array}\right. \\
3\ \{5.7L_4\},
\end{array}\right. \\
3120\ \&\ I_5=\left\{\begin{array}{l}
1\ \&\ I_6=\left\{\begin{array}{l}
\overline{sn}_{(2)}\ \&\ I_7=\left\{\begin{array}{l} 0\ (5S_2), \\ 2\ \{5S_{14}\}, \end{array}\right. \\
\widehat{cp}_{(2)}\ (2.5L_1),
\end{array}\right. \\
2\ \&\ I_{10}=\left\{\begin{array}{l} n\ (5S_3), \\ y\ \&\ I_{11}=\left\{\begin{array}{l} 0\ \{5.7L_2\}, \\ 2\ \{5S_{15}\}, \end{array}\right. \end{array}\right.
\end{array}\right. \\
\mathscr{A}_4\ \textit{(next page)},
\end{array}\right.
\end{array}\right.
$$

Table 15 – Geometric classification for the family **QsnSN$_{11}$(B)** *(cont.)*

$$
I_1=\left\{\begin{array}{l}
\begin{bmatrix}\mathscr{A}_4\\ I_1=\emptyset,\\ I_2=1,\\ I_3=2\end{bmatrix}\ \&\ I_4=\left\{\begin{array}{l}
3121\ \&\ I_5=\left\{\begin{array}{l}
1\ \&\ I_6=\left\{\begin{array}{l}\overline{sn}_{(2)}\ \&\ I_7=\left\{\begin{array}{l}1\ \{\{9S_{33}\}\},\\ 3\ \{\{9S_{20}\}\},\end{array}\right.\\ \widehat{cp}_{(2)}\ \{\{2.9L_4\}\},\end{array}\right.\\
2\ \&\ I_{13}=\left\{\begin{array}{l}(0)\ \&\ I_{11}=\left\{\begin{array}{l}0\ \{\{7.9L_4\}\},\\ 1\ (2.5L_7),\\ 2\ \{\{9S_{22}\}\},\\ 3\ \{\{9S_{30}\}\},\end{array}\right.\\ (1)\ [2.5L_5],\end{array}\right.\\
3\ \&\ I_{13}=\left\{\begin{array}{l}(0)\ \&\ I_{10}=\left\{\begin{array}{l}n\ (5S_{27}),\\ y\ \{5S_{17}\},\end{array}\right.\\ (1)\ [5S_{26}],\end{array}\right.
\end{array}\right.\\
3200\ \&\ I_{13}=\left\{\begin{array}{l}(0)\ \&\ I_{11}=\left\{\begin{array}{l}1\ (9S_{12}),\\ 2\ (9S_{37}),\end{array}\right.\\ (1)\ [9S_{18}],\end{array}\right.\\
3211\ \{5.7L_6\},\\
3221\ \&\ I_{13}=\left\{\begin{array}{l}(0)\ (5S_{25}),\\ (1)\ [5S_{23}],\end{array}\right.\\
4111\ \&\ I_5=\left\{\begin{array}{l}2\ \{2.5L_4\},\\ 3\ \{5.7L_5\},\end{array}\right.\\
4120\ \&\ I_7=\left\{\begin{array}{l}0\ (5S_1),\\ 1\ \&\ I_{13}=\left\{\begin{array}{l}(0)\ (5S_9),\\ (1)\ [5S_{13}],\end{array}\right.\end{array}\right.\\
4121\ \&\ I_5=\left\{\begin{array}{l}2\ \&\ I_7=\left\{\begin{array}{l}0\ \{\{9S_{36}\}\},\\ 2\ \&\ I_{13}=\left\{\begin{array}{l}(0)\ \{\{9S_{11}\}\},\\ (1)\ [\{\{9S_{17}\}\}],\end{array}\right.\end{array}\right.\\
3\ \&\ I_{13}=\left\{\begin{array}{l}(0)\ (5S_{22}),\\ (1)\ [5S_{20}],\end{array}\right.\end{array}\right.\\
4211\ \{5S_{18}\},\\
5111\ \{5S_{19}\},
\end{array}\right.\\
\begin{bmatrix}\mathscr{A}_3\\ I_1=\emptyset,\\ I_2=1,\\ I_3=3\end{bmatrix}\ \&\ I_4=\left\{\begin{array}{l}
110110\ \&\ I_5=\left\{\begin{array}{l}1\ \&\ I_7=\left\{\begin{array}{l}0\ (4S_8),\\ 2\ \{4S_{65}\},\end{array}\right.\\ 2\ \{4.4L_{12}\},\end{array}\right.\\
111010\ \&\ I_5=\left\{\begin{array}{l}0\ (4S_{22}),\\ 1\ (4S_{33}),\end{array}\right.\\
\mathscr{A}_5\ \textit{(next page)},
\end{array}\right.
\end{array}\right.
$$

Table 16 – Geometric classification for the family **QsnSN$_{11}$(B)** *(cont.)*

$$
I_1 = \left\{ \begin{array}{l}
\mathscr{A}_5 \\
\begin{bmatrix} I_1 = \emptyset, \\ I_2 = 1, \\ I_3 = 3 \end{bmatrix}
\end{array} \right. \;\&\; I_4 = \left\{ \begin{array}{l}
111110 \;\&\; I_5 = \left\{ \begin{array}{l}
0 \;\&\; I_7 = \left\{ \begin{array}{l} 0\ (7S_5), \\ 1\ \{7S_7\}, \end{array} \right. \\
1 \;\&\; I_7 = \left\{ \begin{array}{l} 0\ \{7.7L_1\}, \\ 1 \;\&\; I_{13} = \left\{ \begin{array}{l} (0) \;\&\; I_{11} = \left\{ \begin{array}{l} 1\ (4S_{59}), \\ 3\ (V_{14}), \end{array} \right. \\ (1)\ [4S_{64}], \end{array} \right. \\ 2\ (V_{55}), \end{array} \right. \\
2\ (4S_{40}),
\end{array} \right. \\
111111 \;\&\; I_7 = \left\{ \begin{array}{l}
0 \;\&\; I_{13} = \left\{ \begin{array}{l} (0)\ (7S_{17}), \\ (1)\ [7S_{15}], \end{array} \right. \\
1 \;\&\; I_{13} = \left\{ \begin{array}{l} (0)\ \{7S_{14}\} \\ (1)\ [\{7S_{23}\}], \\ (2)\ [[\{7S_{24}\}]] \\ (1)^2\ [\{7.10L_1\}]^2, \end{array} \right.
\end{array} \right. \\
210110 \;\&\; I_5 = \left\{ \begin{array}{l}
1 \;\&\; I_6 = \left\{ \begin{array}{l} \overline{sn}_{(2)} \;\&\; I_{11} = \left\{ \begin{array}{l} 0\ \{7S_{22}\}, \\ 1\ \{V_{102}\}, \\ 3\ (V_{29}), \end{array} \right. \\ \widehat{cp}_{(2)}\ (2S_3), \end{array} \right. \\
2 \;\&\; I_{13} = \left\{ \begin{array}{l} (0) \;\&\; I_{11} = \left\{ \begin{array}{l} 1\ (4S_{70}), \\ 2\ (4S_2), \end{array} \right. \\ (1)\ [4S_{67}], \end{array} \right.
\end{array} \right. \\
211010 \;\&\; I_7 = \left\{ \begin{array}{l} 0\ (7S_{18}), \\ 1\ \{7S_4\}, \end{array} \right. \\
211011 \;\&\; I_6 = \left\{ \begin{array}{l} \overline{sn}_{(2)}\ (7S_9), \\ \widehat{cp}_{(2)}\ \{2.7L_1\}, \end{array} \right. \\
211101 \;\&\; I_6 = \left\{ \begin{array}{l}
\overline{sn}_{(2)} \;\&\; I_7 = \left\{ \begin{array}{l} 0\ (V_{35}), \\ 1\ \{7S_6\}, \\ 2\ \{V_{49}\}, \end{array} \right. \\
\widehat{cp}_{(2)}\ (2S_1),
\end{array} \right. \\
211110 \;\&\; I_5 = \left\{ \begin{array}{l}
0 \;\&\; I_{12} = \left\{ \begin{array}{l} 0\ (V_{51}), \\ 1\ (V_{20}), \end{array} \right. \\
1 \;\&\; I_{13} = \left\{ \begin{array}{l} (0)\ (V_{90}), \\ (1)\ [V_{101}], \end{array} \right. \\
2\ (V_2),
\end{array} \right. \\
\mathscr{A}_6 \textit{ (next page)},
\end{array} \right.
$$

Table 17 – Geometric classification for the family **QsnSN$_{11}$(B)** *(cont.)*

$$
I_1=\left\{\begin{array}{l}
\mathscr{A}_6\ \begin{bmatrix} I_1=\emptyset, \\ I_2=1, \\ I_3=3 \end{bmatrix}\ \&\ I_4=\left\{\begin{array}{l}
211111\ \&\ I_6=\left\{\begin{array}{l}
\overline{sn}_{(2)}\ \&\ I_{13}=\left\{\begin{array}{l}
(0)\ \&\ I_{12}=\left\{\begin{array}{l} 0\ (V_{71}), \\ 1\ (V_{80}), \end{array}\right. \\
(1)\ \&\ I_7=\left\{\begin{array}{l} n\ [V_{78}], \\ y\ [V_{106}], \end{array}\right. \\
(1)^2\ \&\ I_7=\left\{\begin{array}{l} n\ [10S_1]^2, \\ y\ [10S_3]^2, \end{array}\right. \\
(2)\ \&\ I_7=\left\{\begin{array}{l} n\ [[V_{107}]], \\ y\ [[V_{110}]], \end{array}\right. \\
(1),(1)^2\ \left[[10S_2]^2\right], \\
(3)\ [[[V_{109}]]], \end{array}\right. \\
\widehat{cp}_{(2)}\ \&\ I_{13}=\left\{\begin{array}{l} (0)\ (2S_{15}), \\ (1)\ [2S_{13}], \end{array}\right.
\end{array}\right. \\
221101\ \{7S_{13}\}, \\
221111\ \&\ I_{13}=\left\{\begin{array}{l} (0)\ (V_{77}), \\ (1)\ [V_{75}], \end{array}\right. \\
310110\ \&\ I_7=\left\{\begin{array}{l}
0\ (V_{36}), \\
2\ \&\ I_{13}=\left\{\begin{array}{l} (0)\ (V_{112}), \\ (1)\ [V_{104}], \end{array}\right.
\end{array}\right. \\
311010\ \&\ I_6=\left\{\begin{array}{l}
\overline{sn}_{(2)}\ \&\ I_7=\left\{\begin{array}{l} 0\ (V_{82}), \\ 1\ \{7S_3\}, \\ 2\ \{V_{26}\}, \end{array}\right. \\
\widehat{cp}_{(2)}\ (2S_{19}),
\end{array}\right. \\
311011\ \&\ I_6=\left\{\begin{array}{l} \overline{sn}_{(2)}\ \{7S_{11}\}, \\ \widehat{cp}_{(2)}\ (2S_9), \end{array}\right. \\
311101\ \&\ I_{11}=\left\{\begin{array}{l} 0\ [V_{48}], \\ 1\ (V_3), \\ 2\ (V_{39}), \end{array}\right. \\
311111\ \&\ I_{13}=\left\{\begin{array}{l} (0)\ (V_{65}), \\ (1)\ [V_{72}], \end{array}\right. \\
321011\ (V_{59}), \\
411010\ \&\ I_7=\left\{\begin{array}{l}
0\ (V_{81}), \\
1\ \&\ I_{13}=\left\{\begin{array}{l} (0)\ (V_{23}), \\ (1)\ [V_{25}], \end{array}\right.
\end{array}\right. \\
411011\ (V_{62}).
\end{array}\right.
\end{array}\right.
$$

Table 18 – Topological equivalences for the family **QsnSN$_{11}$(B)**

Presented phase portrait	Identical under perturbations	Finite antisaddle focus	Finite antisaddle node–focus	Finite weak point	Possessing invariant curve (no separatrix)	Other reasons
V_1		V_{46}	$6S_7$	$3S_{12}$		
V_2						
V_3		V_{47}	$6S_6$	$3S_{11}$		
V_4	V_5			$3S_1$		
V_6	V_7			$3S_2$, $3S_3$ $3.10L_1$		
V_8	V_9			$3S_4$		
V_{10}	V_{11}, V_{12}			$3S_5$	$4S_{19}$	
V_{13}	V_{15}, V_{16}, V_{17}			$3S_6$, $3S_7$, $3S_8$ $3.4L_3$, $3.10L_2$	$4S_{20}$, $4S_{21}$	
V_{14}	V_{18}, V_{19}, V_{31}, V_{43}	V_{27}	$6S_2$, $6S_3$ $4.6L_2$		$4S_{10}$, $4S_{15}$, $4S_{16}$, $4S_{29}$, $4S_{30}$ $4.4L_4$	
V_{20}	V_{32}, V_{34}	V_{28}	$6S_1$		$4S_{11}$, $4S_{26}$	

Table 19 – Topological equivalences for the family **QsnSN$_{11}$(B)** *(cont.)*

Presented phase portrait	Identical under perturbations	Finite antisaddle focus	Finite antisaddle node–focus	Finite weak point	Possessing invariant curve (no separatrix)	Other reasons
V_{21}	V_{22}			$3S_9$		
V_{23}		V_{24}	$6S_4$	$3S_{10}$		
V_{25}						
V_{26}						
V_{29}	V_{30}				$4S_{14}$	
V_{33}	V_{41}, V_{42}	V_{44}	$6S_9$, $6S_{10}$ $4.6L_4$	$3S_{14}$	$4S_{27}$, $4S_{28}$	
V_{35}						
V_{36}	V_{37}				$4S_{13}$	
V_{38}	V_{40}, V_{69}	V_{45}	$6S_8$, $6S_{16}$ $4.6L_6$	$3S_{13}$	$4S_{12}$, $4S_{43}$	
V_{39}						
V_{48}						
V_{49}						
V_{51}	V_{56}, V_{83}	V_{50}	$6S_5$		$4S_{32}$, $4S_{52}$	
V_{52}						
V_{53}						
V_{55}	V_{84}	V_{54}, V_{99}	$6S_{11}$, $6S_{21}$ $4.6L_9$		$4S_{53}$, $4S_{61}$	

Table 20 – Topological equivalences for the family **QsnSN$_{11}$(B)** *(cont.)*

Presented phase portrait	Identical under perturbations	Finite antisaddle focus	Finite antisaddle node–focus	Finite weak point	Possessing invariant curve (no separatrix)	Other reasons
V_{57}						
V_{59}		V_{58}	$6S_{13}$			
V_{60}						
V_{62}		V_{61}	$6S_{14}$			
V_{63}	V_{66}, V_{67}, V_{74}			$3S_{16}$, $3S_{17}$ $3.4L_7$	$4S_{41}$, $4S_{44}$	
V_{65}		V_{64}	$6S_{15}$	$3S_{15}$		
V_{68}	V_{98}			$3S_{23}$		
V_{71}	V_{85}	V_{70}, V_{86}	$6S_{12}$, $6S_{18}$ $4.6L_7$	$3S_{28}$ $3.10L_8$	$4S_{54}$, $4S_{55}$	
V_{72}						
V_{73}	V_{97}			$3S_{22}$		
V_{75}						
V_{77}		V_{76}	$6S_{17}$	$3S_{18}$		
V_{78}	V_{87}			$3S_{27}$ $3.10L_7$	$4S_{56}$	

Table 21 – Topological equivalences for the family **QsnSN$_{11}$(B)** *(cont.)*

Presented phase portrait	Identical under perturbations	Finite antisaddle focus	Finite antisaddle node–focus	Finite weak point	Possessing invariant curve (no separatrix)	Other reasons
V_{80}	V_{89}	V_{79}, V_{88}	$6S_{19}$, $6S_{20}$ $4.6L_8$	$3S_{19}$, $3S_{20}$ $3.4L_9$, $3.10L_5$ P_{26}	$4S_{57}$, $4S_{58}$	
V_{81}						
V_{82}						
V_{90}	V_{91}, V_{105}	V_{100}	$6S_{22}$, $6S_{23}$ $4.6L_{12}$	$3S_{24}$	$4S_{51}$, $4S_{68}$	
V_{92}	V_{96}, V_{111}			$3S_{33}$	$4S_{60}$	
V_{93}	V_{94}			$3S_{21}$, $3S_{26}$ $3.10L_3$		
V_{95}	V_{103}			$3S_{25}$, $3S_{29}$ $3.10L_4$		
V_{101}						
V_{102}						
V_{104}						
V_{106}				$3S_{32}$		
V_{107}				$3S_{31}$		
V_{109}						
V_{110}						

Table 22 – Topological equivalences for the family **QsnSN$_{11}$(B)** *(cont.)*

Presented phase portrait	Identical under perturbations	Finite antisaddle focus	Finite antisaddle node–focus	Finite weak point	Possessing invariant curve (no separatrix)	Other reasons
V_{112}		V_{108}	$6S_{24}$	$3S_{30}$		
$2S_1$						
$2S_2$	$2S_7$, $2S_{12}$	$2S_8$	$2.6L_1$, $2.6L_3$ P_4	$2.3L_2$	$2.4L_2$, $2.4L_3$	
$2S_3$	$2S_4$				$2.4L_1$	
$2S_5$	$2S_6$			$2.3L_1$		
$2S_9$		$2S_{10}$	$2.6L_2$			
$2S_{11}$						
$2S_{13}$						
$2S_{15}$		$2S_{14}$	$2.6L_4$	$2.3L_3$		
$2S_{16}$	$2S_{20}$			$2.3L_5$		
$2S_{17}$	$2S_{18}$			$2.3L_4$		
$2S_{19}$						
$4S_1$		$4S_{31}$	$4.6L_3$	$3.4L_5$		
$4S_2$						
$4S_3$	$4S_4$, $4S_5$			$3.4L_2$	$4.4L_1$	

Table 23 – Topological equivalences for the family **QsnSN$_{11}$(B)** *(cont.)*

Presented phase portrait	Identical under perturbations	Finite antisaddle focus	Finite antisaddle node–focus	Finite weak point	Possessing invariant curve (no separatrix)	Other reasons
$4S_6$	$4S_7$			$3.4L_1$		
$4S_8$	$4S_9$				$4.4L_3$	
$4S_{17}$	$4S_{18}$			$3.4L_4$		
$4S_{22}$	$4S_{24}$, $4S_{25}$	$4S_{23}$	$4.6L_1$		$4.4L_2$	
$4S_{33}$	$4S_{47}$				$4.4L_8$	
$4S_{34}$	$4S_{35}$, $4S_{36}$, $4S_{45}$			$3.4L_6$, $3.4L_8$	$4.4L_5$, $4.4L_7$ P_6	
$4S_{37}$	$4S_{48}$			$3.4L_{11}$		
$4S_{38}$						
$4S_{40}$	$4S_{46}$	$4S_{39}$, $4S_{63}$	$4.6L_5$, $4.6L_{10}$ P_{18}		$4.4L_{10}$, $4.4L_{11}$	
$4S_{42}$	$4S_{49}$			$3.4L_{10}$		
$4S_{50}$	$4S_{66}$			$3.4L_{13}$, $3.4L_{14}$ P_{23}		
$4S_{59}$		$4S_{62}$	$4.6L_{11}$	$3.4L_{12}$		

Table 24 – Topological equivalences for the family **QsnSN$_{11}$(B)** *(cont.)*

Presented phase portrait	Identical under perturbations	Finite antisaddle focus	Finite antisaddle node–focus	Finite weak point	Possessing invariant curve (no separatrix)	Other reasons
$4S_{64}$						
$4S_{65}$						
$4S_{67}$						
$4S_{70}$		$4S_{69}$	$4.6L_{13}$	$3.4L_{15}$		
$5S_1$						
$5S_2$						
$5S_3$						
$5S_4$	$5S_{11}$				$4.5L_7$	
$5S_5$	$5S_{10}$				$4.5L_5$	
$5S_6$	$5S_7$				$4.5L_2$	
$5S_8$						
$5S_9$	$5S_{12}$		$5.6L_1$	$3.5L_1$		
$5S_{13}$						
$5S_{14}$						
$5S_{15}$						
$5S_{16}$						
$5S_{17}$						
$5S_{18}$						
$5S_{19}$						
$5S_{20}$						

Table 25 – Topological equivalences for the family **QsnSN$_{11}$(B)** *(cont.)*

Presented phase portrait	Identical under perturbations	Finite antisaddle focus	Finite antisaddle node–focus	Finite weak point	Possessing invariant curve (no separatrix)	Other reasons
$5S_{22}$		$5S_{21}$	$5.6L_2$	$3.5L_2$		
$5S_{23}$						
$5S_{25}$		$5S_{24}$	$5.6L_3$	$3.5L_3$		
$5S_{26}$						
$5S_{27}$		$5S_{30}$	$5.6L_4$	$3.5L_4$		
$5S_{28}$	$5S_{29}$, $5S_{35}$	$5S_{31}$	$5.6L_5$, $5.6L_6$ P_{22}	$3.5L_5$	$4.5L_{11}$, $4.5L_{16}$	
$5S_{32}$						
$5S_{33}$						
$5S_{34}$						
$5S_{37}$		$5S_{36}$	$5.6L_7$	$3.5L_6$		
$7S_1$	$7S_2$			$3.7L_1$		
$7S_3$						
$7S_4$						
$7S_5$						
$7S_6$						
$7S_7$						
$7S_8$						
$7S_9$	$7S_{10}$		$6.7L_1$			
$7S_{11}$						

Table 26 – Topological equivalences for the family **QsnSN$_{11}$(B)** *(cont.)*

Presented phase portrait	Identical under perturbations	Finite antisaddle focus	Finite antisaddle node–focus	Finite weak point	Possessing invariant curve (no separatrix)	Other reasons
$7S_{12}$	$7S_{19}$			$3.7L_3$		
$7S_{13}$						
$7S_{14}$	$7S_{20}$			P_{27}	$4.7L_1$	
$7S_{15}$						
$7S_{17}$		$7S_{16}$	$6.7L_2$	$3.7L_2$		
$7S_{18}$						
$7S_{21}$	$7S_{25}$			$3.7L_6$		
$7S_{22}$						
$7S_{23}$				$3.7L_4$, $3.7L_5$		
$7S_{24}$						
$8S_1$						$8S_4^{(1)}$, $8S_5^{(1)}$, $8S_6^{(1)}$, $8S_7^{(1)}$ $8S_8^{(1)}$, $8S_9^{(1)}$, $8S_{11}^{(1)}$, $8S_{12}^{(1)}$ $8S_{14}^{(1)}$, $8S_{15}^{(1)}$, $8S_{16}^{(1)}$ $4.8L_3^{(1)}$, $4.8L_5^{(1)}$, $4.8L_8^{(1)}$ $4.8L_9^{(1)}$, $4.8L_{10}^{(1)}$, $4.8L_{11}^{(1)}$ $7.8L_1^{(1)}$, $7.8L_2^{(1)}$, $7.8L_3^{(1)}$ $7.8L_4^{(1)}$, $7.8L_5^{(1)}$ $P_{11}^{(1)}$, $P_{24}^{(1)}$

Table 27 – Topological equivalences for the family **QsnSN$_{11}$(B)** *(cont.)*

Presented phase portrait	Identical under perturbations	Finite antisaddle focus	Finite antisaddle node–focus	Finite weak point	Possessing invariant curve (no separatrix)	Other reasons
$8S_2$						$8S_3{}^{(1)}$, $8S_{10}{}^{(1)}$, $8S_{13}{}^{(1)}$ $4.8L_4$
$9S_1$	$9S_2$			$3.9L_1$		
$9S_3$	$9S_4$			$3.9L_2$		
$9S_5$	$9S_6$			$3.9L_3$		
$9S_7$	$9S_8$, $9S_9$			$3.9L_4$	$4.9L_3$	
$9S_{10}$		$9S_{13}$	$6.9L_3$	$3.9L_5$		$0.9L_1{}^{(2)}$, $0.9L_2{}^{(2)}$ $P_{43}{}^{(2)}$, $P_{44}{}^{(2)}$
$9S_{11}$		$9S_{14}$	$6.9L_2$	$3.9L_6$		
$9S_{12}$		$9S_{15}$	$6.9L_1$	$3.9L_7$		
$9S_{16}$						$0.9L_3{}^{(2)}$
$9S_{17}$						
$9S_{18}$						
$9S_{19}$						$0.9L_4{}^{(2)}$
$9S_{20}$						
$9S_{21}$						
$9S_{22}$						

Table 28 – Topological equivalences for the family **QsnSN$_{11}$(B)** *(cont.)*

Presented phase portrait	Identical under perturbations	Finite antisaddle focus	Finite antisaddle node–focus	Finite weak point	Possessing invariant curve (no separatrix)	Other reasons
$9S_{24}$	$9S_{31}$, $9S_{32}$	$9S_{23}$	$6.9L_6$		$4.9L_8$, $4.9L_9$	
$9S_{27}$		$9S_{25}$	$6.9L_4$			$0.9{L_5}^{(2)}$, $0.9{L_6}^{(2)}$ ${P_{46}}^{(2)}$
$9S_{28}$		$9S_{26}$	$6.9L_5$			
$9S_{29}$						$0.9{L_7}^{(2)}$
$9S_{30}$						
$9S_{33}$						
$9S_{34}$						
$9S_{35}$						$0.9{L_8}^{(2)}$
$9S_{36}$						
$9S_{37}$						
$10S_1$				$3.10L_6$		
$10S_2$						
$10S_3$						
$2.4L_4$	$2.4L_5$			P_{21}		
$2.5L_1$						
$2.5L_2$	$2.5L_3$				P_1	
$2.5L_4$						

Table 29 – Topological equivalences for the family **QsnSN$_{11}$(B)** *(cont.)*

Presented phase portrait	Identical under perturbations	Finite antisaddle focus	Finite antisaddle node–focus	Finite weak point	Possessing invariant curve (no separatrix)	Other reasons
$2.5L_5$						
$2.5L_7$		$2.5L_6$	P_9	P_8		
$2.7L_1$						
$2.9L_1$	$2.9L_2$			P_{37}		
$2.9L_3$						$P_{38}{}^{(2)}$
$2.9L_4$						
$2.9L_5$						
$4.4L_6$	$4.4L_9$			P_{13}		
$4.4L_{12}$						
$4.5L_1$						
$4.5L_3$			$4.5L_6$ P_2			
$4.5L_4$						
$4.5L_8$						
$4.5L_9$						
$4.5L_{10}$		$4.5L_{12}$	P_{17}	P_{19}		
$4.5L_{13}$						
$4.5L_{14}$						
$4.5L_{15}$						
$4.5L_{18}$		$4.5L_{17}$	P_{28}	P_{25}		

Table 30 – Topological equivalences for the family **QsnSN$_{11}$(B)** *(cont.)*

Presented phase portrait	Identical under perturbations	Finite antisaddle focus	Finite antisaddle node–focus	Finite weak point	Possessing invariant curve (no separatrix)	Other reasons
$4.8L_1$						$4.8L_2{}^{(1)}$, $4.8L_6{}^{(1)}$, $4.8L_7{}^{(1)}$ $4.8L_{12}{}^{(1)}$, $4.8L_{13}{}^{(1)}$ $P_5{}^{(1)}$, $P_{12}{}^{(1)}$
$4.9L_1$	$4.9L_2$			P_{33}		
$4.9L_4$						$P_{42}{}^{(2)}$
$4.9L_5$						
$4.9L_6$						$P_{35}{}^{(2)}$
$4.9L_7$						
$5.7L_1$						
$5.7L_2$						
$5.7L_3$						
$5.7L_4$						
$5.7L_5$						
$5.7L_6$						
$5.7L_7$						
$5.7L_8$						
$5.7L_9$		$5.7L_{10}$	P_{16}	P_{15}		
$5.7L_{11}$						
$5.8L_1$						$5.8L_2{}^{(1)}$, $5.8L_3{}^{(1)}$ $8.9L_1{}^{(1)}$, $8.9L_2{}^{(1)}$, $8.9L_3{}^{(1)}$
$5.9L_1$		$5.9L_2$	P_{47}, P_{48}			

Table 31 – Topological equivalences for the family **QsnSN$_{11}$(B)** *(cont.)*

Presented phase portrait	Identical under perturbations	Finite antisaddle focus	Finite antisaddle node–focus	Finite weak point	Possessing invariant curve (no separatrix)	Other reasons
5.9L_3						
5.9L_4						
5.9L_5						
5.9L_6						
5.9L_7						
5.9L_8						
7.7L_1						
7.9L_1	7.9L_2			P_{40}		
7.9L_3						$P_{45}{}^{(2)}$
7.9L_4						
7.9L_5						
7.9L_6						
7.9L_7						
7.9L_8						
7.9L_9						
7.10L_1						
9.9L_1						9.9$L_2{}^{(3)}$, 9.9$L_3{}^{(3)}$, 9.9$L_4{}^{(3)}$ $P_{30}{}^{(3)}$, $P_{31}{}^{(3)}$, $P_{32}{}^{(3)}$
P_3						$P_{10}{}^{(1)}$, $P_{34}{}^{(1)}$, $P_{41}{}^{(1)}$
P_7						
P_{14}						
P_{20}						
P_{29}						

Table 32 – Topological equivalences for the family $\mathbf{QsnSN_{11}(B)}$ *(cont.)*

Presented phase portrait	Identical under perturbations	Finite antisaddle focus	Finite antisaddle node–focus	Finite weak point	Possessing invariant curve (no separatrix)	Other reasons
P_{36}						
P_{39}						
P_{49}						
P_{50}						
P_{51}						

4.5.1 Proof of the main theorem

The bifurcation diagram described in Sec. 4.3, plus Tables 12 to 17 of the geometrical invariants distinguishing the 226 phase portraits, plus Tables 18 to 32 giving the equivalences with the remaining phase portraits lead to the proof of the main statement of Thm. 4.1.1.

As it was expected, in the class $\overline{\mathbf{QsnSN_{11}(B)}}$, all the unfoldings of the phase portraits corresponding to parts of volume regions yield a phase portrait of codimension one from sets (A) and (C) (i.e. with a finite saddle–node $\overline{sn}_{(2)}$ and with a infinite saddle–node of type $\overline{\binom{1}{1}}SN$, respectively, see page 47 for the description of these sets and also Artés *et al.* (2021) for more details). In Tables 33 and 34 we present the correspondence between the phase portraits of the volume regions with their respective unfoldings of codimension one. In such tables, on the first column we present all the topologically distinct phase portraits of the volume regions from the class $\overline{\mathbf{QsnSN_{11}(B)}}$. On the second (respectively third, fourth and fifth) column we present the phase portrait obtained after we perform a perturbation of the respective phase portrait from the first column in order to split the finite saddle–node $\overline{sn}_{(2)}$ into a saddle plus a node (respectively to make the finite saddle–node $\overline{sn}_{(2)}$ disappears, to make the infinite saddle–node $\overline{\binom{1}{1}}SN$ looses a saddle (respectively a node) for the finite part). In all of these columns, when the phase portrait possesses a limit cycle, we indicate the corresponding phase portrait which does not possess limit cycle (for instance, $V_{25} \equiv V_{23}(L.C.)$ means that the phase portrait V_{25} is topologically equivalent to V_{23} with limit cycle). Moreover, we indicate Artés, Llibre and Rezende (2018) for the notation and respective phase portraits of codimension one that appear as unfoldings on these tables.

Table 33 – The respective unfoldings of codimension one of the phase portraits corresponding to parts of volume

Phase portrait from $\overline{\mathbf{QsnSN_{11}(B)}}$	Unfoldings of codimension one: Splitting $\overline{sn}_{(2)}$	Disappearing $\overline{sn}_{(2)}$	Splitting $\overline{\binom{1}{1}}SN\ (\downarrow s)$	Splitting $\overline{\binom{1}{1}}SN\ (\downarrow n)$
V_1	$\mathbb{U}^1_{C,2}$	$\mathbb{U}^1_{C,1}$	$\mathbb{U}^1_{A,3}$	$\mathbb{U}^1_{A,12}$
V_2	$\mathbb{U}^1_{C,23}$	$\mathbb{U}^1_{C,17}$	$\mathbb{U}^1_{A,32}$	$\mathbb{U}^1_{A,61}$
V_3	$\mathbb{U}^1_{C,26}$	$\mathbb{U}^1_{C,16}$	$\mathbb{U}^1_{A,23}$	$\mathbb{U}^1_{A,66}$
V_4	$\mathbb{U}^1_{C,7}$	$\mathbb{U}^1_{C,4}$	$\mathbb{U}^1_{A,15}$	$\mathbb{U}^1_{A,32}$
V_6	$\mathbb{U}^1_{C,6}$	$\mathbb{U}^1_{C,4}$	$\mathbb{U}^1_{A,18}$	$\mathbb{U}^1_{A,27}$
V_8	$\mathbb{U}^1_{C,10}$	$\mathbb{U}^1_{C,4}$	$\mathbb{U}^1_{A,17}$	$\mathbb{U}^1_{A,42}$
V_{10}	$\mathbb{U}^1_{C,12}$	$\mathbb{U}^1_{C,4}$	$\mathbb{U}^1_{A,16}$	$\mathbb{U}^1_{A,52}$
V_{13}	$\mathbb{U}^1_{C,14}$	$\mathbb{U}^1_{C,4}$	$\mathbb{U}^1_{A,14}$	$\mathbb{U}^1_{A,55}$
V_{14}	$\mathbb{U}^1_{C,22}$	$\mathbb{U}^1_{C,17}$	$\mathbb{U}^1_{A,55}$	$\mathbb{U}^1_{A,61}$
V_{20}	$\mathbb{U}^1_{C,30}$	$\mathbb{U}^1_{C,16}$	$\mathbb{U}^1_{A,51}$	$\mathbb{U}^1_{A,67}$
V_{21}	$\mathbb{U}^1_{C,12}$	$\mathbb{U}^1_{C,4}$	$\mathbb{U}^1_{A,15}$	$\mathbb{U}^1_{A,53}$
V_{23}	$\mathbb{U}^1_{C,18}$	$\mathbb{U}^1_{C,15}$	$\mathbb{U}^1_{A,28}$	$\mathbb{U}^1_{A,57}$
$V_{25} \equiv V_{23}(L.C.)$	$\mathbb{U}^1_{C,18}(L.C.)$	$\mathbb{U}^1_{C,15}(L.C.)$	$\mathbb{U}^1_{A,28}(L.C.)$	$\mathbb{U}^1_{A,57}(L.C.)$
V_{26}	$\mathbb{U}^1_{C,24}$	$\mathbb{U}^1_{C,15}(L.C.)$	$\mathbb{U}^1_{A,43}$	$\mathbb{U}^1_{A,64}$
V_{29}	$\mathbb{U}^1_{C,20}$	$\mathbb{U}^1_{C,17}$	$\mathbb{U}^1_{A,42}$	$\mathbb{U}^1_{A,60}$
V_{33}	$\mathbb{U}^1_{C,3}$	$\mathbb{U}^1_{C,1}$	$\mathbb{U}^1_{A,9}$	$\mathbb{U}^1_{A,11}$
V_{35}	$\mathbb{U}^1_{C,31}$	$\mathbb{U}^1_{C,16}$	$\mathbb{U}^1_{A,36}$	$\mathbb{U}^1_{A,69}$
V_{36}	$\mathbb{U}^1_{C,21}$	$\mathbb{U}^1_{C,17}$	$\mathbb{U}^1_{A,27}$	$\mathbb{U}^1_{A,60}$
V_{38}	$\mathbb{U}^1_{C,2}$	$\mathbb{U}^1_{C,1}$	$\mathbb{U}^1_{A,2}$	$\mathbb{U}^1_{A,11}$
V_{39}	$\mathbb{U}^1_{C,26}$	$\mathbb{U}^1_{C,16}$	$\mathbb{U}^1_{A,22}$	$\mathbb{U}^1_{A,65}$
$V_{48} \equiv V_3(L.C.)$	$\mathbb{U}^1_{C,26}(L.C.)$	$\mathbb{U}^1_{C,16}(L.C.)$	$\mathbb{U}^1_{A,23}(L.C.)$	$\mathbb{U}^1_{A,66}(L.C.)$
V_{49}	$\mathbb{U}^1_{C,31}$	$\mathbb{U}^1_{C,16}(L.C.)$	$\mathbb{U}^1_{A,37}$	$\mathbb{U}^1_{A,70}$
V_{51}	$\mathbb{U}^1_{C,30}$	$\mathbb{U}^1_{C,15}$	$\mathbb{U}^1_{A,52}$	$\mathbb{U}^1_{A,68}$
$V_{52} \equiv V_1(L.C.)$	$\mathbb{U}^1_{C,2}(L.C.)$	$\mathbb{U}^1_{C,1}(L.C.)$	$\mathbb{U}^1_{A,3}(L.C.)$	$\mathbb{U}^1_{A,12}(L.C.)$
V_{53}	$\mathbb{U}^1_{C,3}$	$\mathbb{U}^1_{C,1}(L.C.)$	$\mathbb{U}^1_{A,10}$	$\mathbb{U}^1_{A,13}$
V_{55}	$\mathbb{U}^1_{C,22}$	$\mathbb{U}^1_{C,15}$	$\mathbb{U}^1_{A,55}$	$\mathbb{U}^1_{A,62}$
$V_{57} \equiv V_{38}(L.C.)$	$\mathbb{U}^1_{C,2}(L.C.)$	$\mathbb{U}^1_{C,1}(L.C.)$	$\mathbb{U}^1_{A,2}(L.C.)$	$\mathbb{U}^1_{A,11}(L.C.)$
V_{59}	$\mathbb{U}^1_{C,25}$	$\mathbb{U}^1_{C,15}$	$\mathbb{U}^1_{A,41}$	$\mathbb{U}^1_{A,63}$
$V_{60} \equiv V_{33}(L.C.)$	$\mathbb{U}^1_{C,3}(L.C.)$	$\mathbb{U}^1_{C,1}(L.C.)$	$\mathbb{U}^1_{A,9}(L.C.)$	$\mathbb{U}^1_{A,11}(L.C.)$
V_{62}	$\mathbb{U}^1_{C,19}$	$\mathbb{U}^1_{C,15}$	$\mathbb{U}^1_{A,25}$	$\mathbb{U}^1_{A,56}$
V_{63}	$\mathbb{U}^1_{C,13}$	$\mathbb{U}^1_{C,4}$	$\mathbb{U}^1_{A,16}$	$\mathbb{U}^1_{A,54}$
V_{65}	$\mathbb{U}^1_{C,27}$	$\mathbb{U}^1_{C,16}$	$\mathbb{U}^1_{A,39}$	$\mathbb{U}^1_{A,65}$
V_{68}	$\mathbb{U}^1_{C,11}$	$\mathbb{U}^1_{C,4}$	$\mathbb{U}^1_{A,18}$	$\mathbb{U}^1_{A,45}$

Table 34 – The respective unfoldings of codimension one of the phase portraits corresponding to parts of volume

Phase portrait from $\overline{\mathbf{QsnSN_{11}(B)}}$	Unfoldings of codimension one			
	Splitting $\overline{sn}_{(2)}$	Disappearing $\overline{sn}_{(2)}$	Splitting $\overline{\binom{1}{1}}\,SN\ (\downarrow s)$	Splitting $\overline{\binom{1}{1}}\,SN\ (\downarrow n)$
V_{71}	$\mathbb{U}^1_{C,28}$	$\mathbb{U}^1_{C,15}$	$\mathbb{U}^1_{A,54}$	$\mathbb{U}^1_{A,68}$
$V_{72} \equiv V_{65}(L.C.)$	$\mathbb{U}^1_{C,27}(L.C.)$	$\mathbb{U}^1_{C,16}(L.C.)$	$\mathbb{U}^1_{A,39}(L.C.)$	$\mathbb{U}^1_{A,65}(L.C.)$
V_{73}	$\mathbb{U}^1_{C,9}$	$\mathbb{U}^1_{C,4}$	$\mathbb{U}^1_{A,17}$	$\mathbb{U}^1_{A,41}$
$V_{75} \equiv V_{77}(L.C.)$	$\mathbb{U}^1_{C,32}(L.C.)$	$\mathbb{U}^1_{C,16}(L.C.)$	$\mathbb{U}^1_{A,30}(L.C.)$	$\mathbb{U}^1_{A,69}(L.C.)$
V_{77}	$\mathbb{U}^1_{C,32}$	$\mathbb{U}^1_{C,16}$	$\mathbb{U}^1_{A,30}$	$\mathbb{U}^1_{A,69}$
$V_{78} \equiv V_{80}(L.C.)$	$\mathbb{U}^1_{C,29}(L.C.)$	$\mathbb{U}^1_{C,16}(L.C.)$	$\mathbb{U}^1_{A,26}(L.C.)$	$\mathbb{U}^1_{A,67}(L.C.)$
V_{80}	$\mathbb{U}^1_{C,29}$	$\mathbb{U}^1_{C,16}$	$\mathbb{U}^1_{A,26}$	$\mathbb{U}^1_{A,67}$
V_{81}	$\mathbb{U}^1_{C,18}$	$\mathbb{U}^1_{C,15}$	$\mathbb{U}^1_{A,27}$	$\mathbb{U}^1_{A,56}$
V_{82}	$\mathbb{U}^1_{C,24}$	$\mathbb{U}^1_{C,15}$	$\mathbb{U}^1_{A,42}$	$\mathbb{U}^1_{A,63}$
V_{90}	$\mathbb{U}^1_{C,23}$	$\mathbb{U}^1_{C,17}$	$\mathbb{U}^1_{A,31}$	$\mathbb{U}^1_{A,61}$
V_{92}	$\mathbb{U}^1_{C,7}$	$\mathbb{U}^1_{C,4}$	$\mathbb{U}^1_{A,16}$	$\mathbb{U}^1_{A,33}$
V_{93}	$\mathbb{U}^1_{C,5}$	$\mathbb{U}^1_{C,4}$	$\mathbb{U}^1_{A,18}$	$\mathbb{U}^1_{A,25}$
V_{95}	$\mathbb{U}^1_{C,8}$	$\mathbb{U}^1_{C,4}$	$\mathbb{U}^1_{A,17}$	$\mathbb{U}^1_{A,35}$
$V_{101} \equiv V_{90}(L.C.)$	$\mathbb{U}^1_{C,23}(L.C.)$	$\mathbb{U}^1_{C,17}(L.C.)$	$\mathbb{U}^1_{A,31}(L.C.)$	$\mathbb{U}^1_{A,61}(L.C.)$
V_{102}	$\mathbb{U}^1_{C,20}$	$\mathbb{U}^1_{C,17}(L.C.)$	$\mathbb{U}^1_{A,43}$	$\mathbb{U}^1_{A,59}$
$V_{104} \equiv V_{112}(L.C.)$	$\mathbb{U}^1_{C,21}(L.C.)$	$\mathbb{U}^1_{C,17}(L.C.)$	$\mathbb{U}^1_{A,28}(L.C.)$	$\mathbb{U}^1_{A,58}(L.C.)$
$V_{106} \equiv V_{71}(L.C.)$	$\mathbb{U}^1_{C,28}(L.C.)$	$\mathbb{U}^1_{C,15}(L.C.)$	$\mathbb{U}^1_{A,54}(L.C.)$	$\mathbb{U}^1_{A,68}(L.C.)$
$V_{107} \equiv V_{80}(2\ L.C.)$	$\mathbb{U}^1_{C,29}(2\ L.C.)$	$\mathbb{U}^1_{C,16}(2\ L.C.)$	$\mathbb{U}^1_{A,26}(2\ L.C.)$	$\mathbb{U}^1_{A,67}(2\ L.C.)$
$V_{109} \equiv V_{80}(3\ L.C.)$	$\mathbb{U}^1_{C,29}(3\ L.C.)$	$\mathbb{U}^1_{C,16}(3\ L.C.)$	$\mathbb{U}^1_{A,26}(3\ L.C.)$	$\mathbb{U}^1_{A,67}(3\ L.C.)$
$V_{110} \equiv V_{71}(2\ L.C.)$	$\mathbb{U}^1_{C,28}(2\ L.C.)$	$\mathbb{U}^1_{C,15}(2\ L.C.)$	$\mathbb{U}^1_{A,54}(2\ L.C.)$	$\mathbb{U}^1_{A,68}(2\ L.C.)$
V_{112}	$\mathbb{U}^1_{C,21}$	$\mathbb{U}^1_{C,17}$	$\mathbb{U}^1_{A,28}$	$\mathbb{U}^1_{A,58}$

CHAPTER

5

STRUCTURALLY UNSTABLE QUADRATIC VECTOR FIELDS OF CODIMENSION TWO: FAMILIES POSSESSING A FINITE SADDLE–NODE AND AN INFINITE SADDLE–NODE

In this chapter we present the topological classification of phase portraits belonging to the sets (AB) and (AC), as we described at the end of Chap. 1.

5.1 Introduction and statement of the main results

In Chap. 1 we saw a little bit about the context of the classification of quadratic systems modulo limit cycles according to the structural stability. In Chap. 3 and 4 we have used a more geometrical and algebraic approach in order to study the entire bifurcation diagram of the families $\mathbf{QsnSN_{11}(A)}$ and $\mathbf{QsnSN_{11}(B)}$. In this chapter we use a more topological approach. Our main goal is to obtain all the potential topological phase portraits of the set (AB) and also all the potential phase portraits possessing the set of saddle–nodes $\left\{\overline{sn}_{(2)} + \overline{\binom{1}{1}}\, SN\right\}$ from the set (AC), and then study the realization of all of them. Here we use effectively the results from Chap. 4 and also the results from Artés, Rezende and Oliveira (2015). Therefore, with this chapter we contribute significantly to the classification of quadratic systems of codimension two modulo limit cycles.

We point out that in each picture representing a phase portrait we only draw the *skeleton of separatrices* (see page 45). Additionally, in what follows, instead of talking about codimension one modulo limit cycles, we simply say *codimension one**. Analogously we simply say *codimension two** instead of talking about codimension two modulo limit

cycles.

Let $\sum_0^2$ denote the set of all planar structurally stable vector fields and $\sum_i^2(S)$ denote the set of all structurally unstable vector fields $X \in P_2(\mathbb{R}^2)$ of codimension i, modulo limit cycles belonging to the set S, where S is a set of vector fields with the same type of instability modulo orientation. For instance, in Artés, Llibre and Rezende (2018) the authors classified the sets $\sum_1^2(A)$, $\sum_1^2(B)$, $\sum_1^2(C)$, and $\sum_1^2(D)$. In Artés, Oliveira and Rezende (2020) the authors classified the set $\sum_2^2(AA)$ and in this study we consider the sets $\sum_2^2(AB)$ and $\sum_2^2(AC)$, which denote, respectively, the set of all structurally unstable vector fields $X \in P_2(\mathbb{R}^2)$ of *codimension two** belonging to the sets (AB) and (AC).

Theorem 5.1.1. If $X \in \sum_2^2(AB)$, then its phase portrait on the Poincaré disc is topologically equivalent modulo orientation and modulo limit cycles to one of the 71 phase portraits of Figs. 100 to 102.

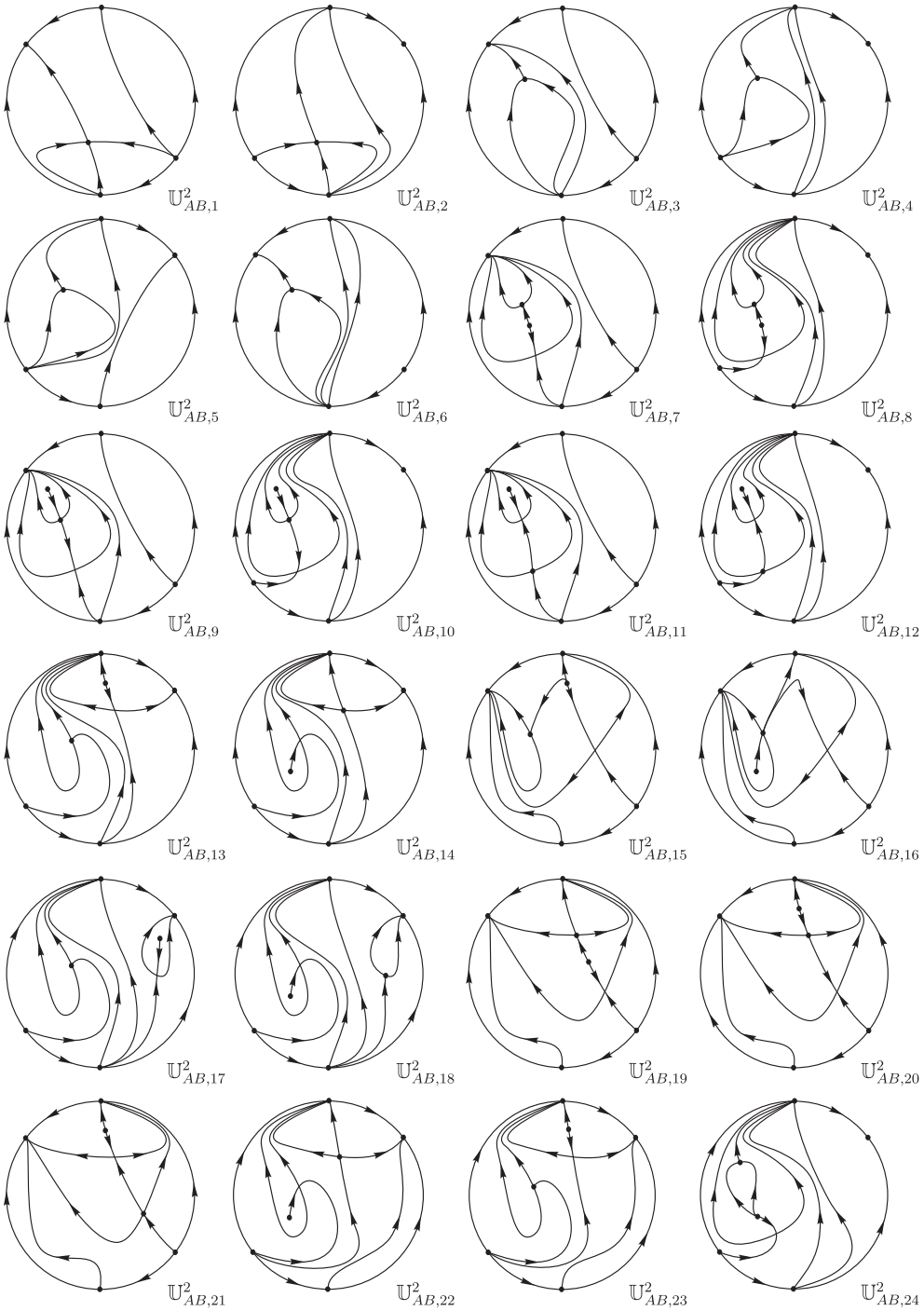

Figure 100 – Structurally unstable quadratic phase portraits of *codimension two** of the set (AB)

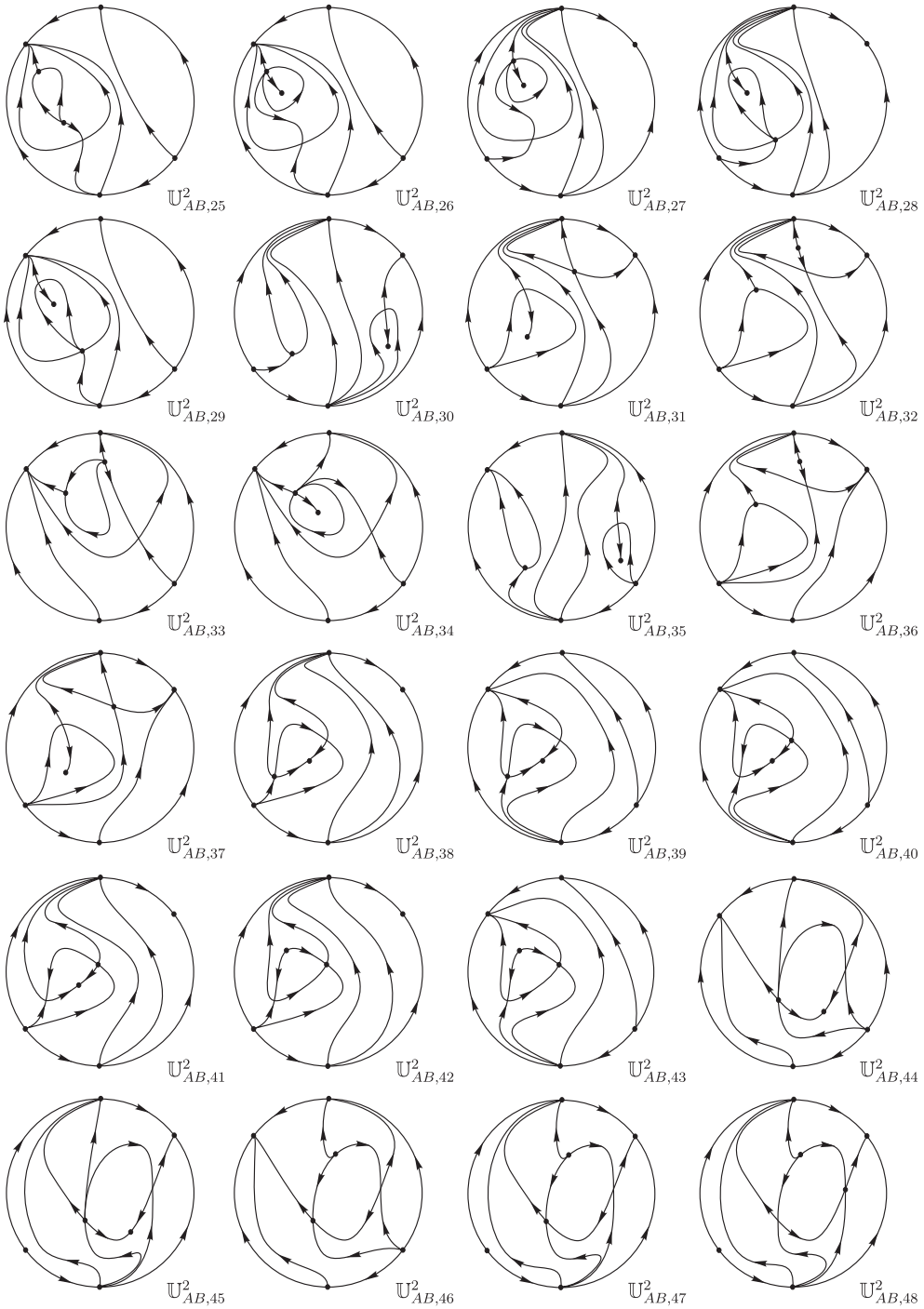

Figure 101 – *(Cont.)* Structurally unstable quadratic phase portraits of *codimension two** of the set (***AB***)

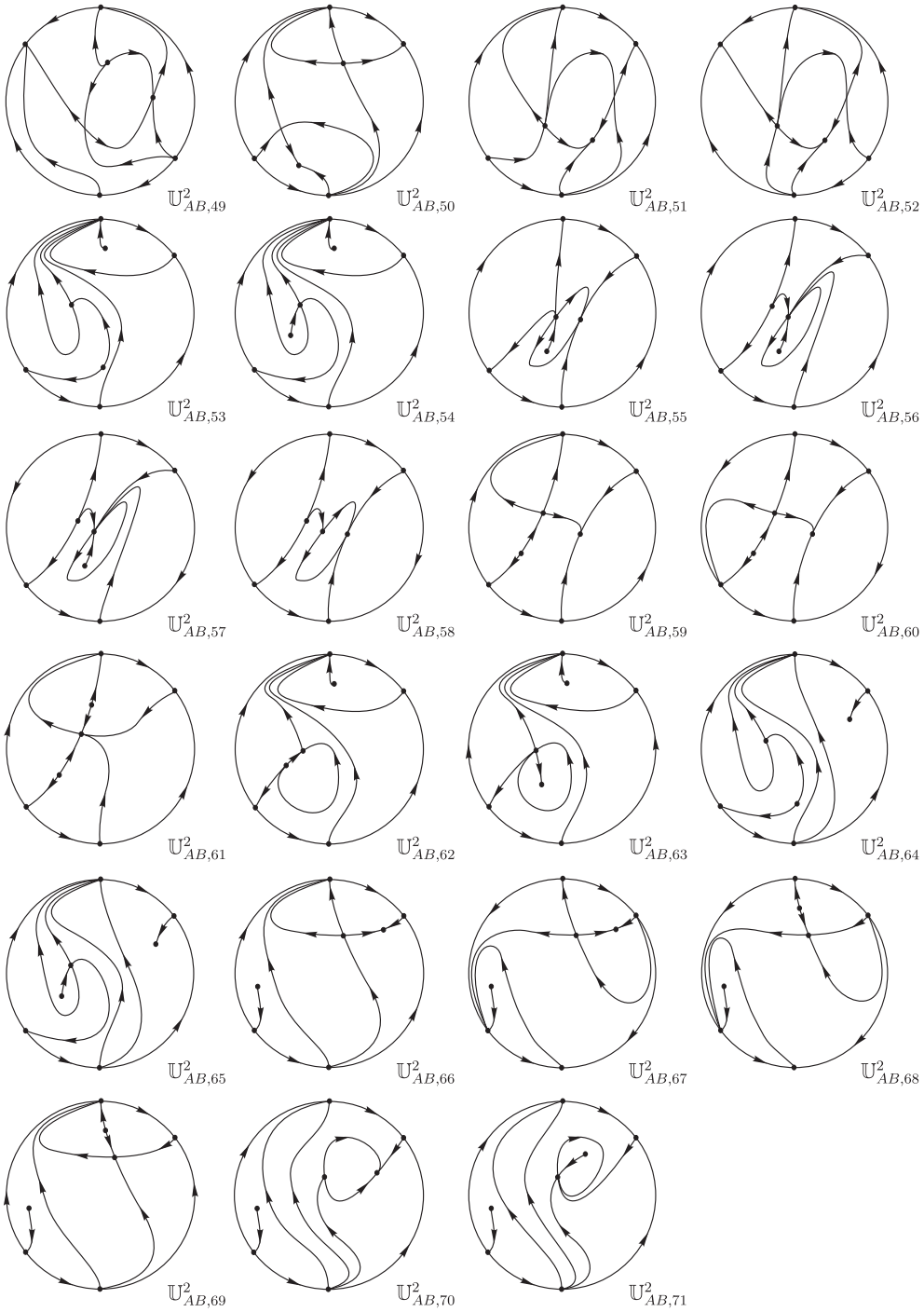

Figure 102 – *(Cont.)* Structurally unstable quadratic phase portraits of *codimension two** of the set (***AB***)

Theorem 5.1.2. If $X \in \sum_2^2(AC)$, then its phase portrait on the Poincaré disc is topologically equivalent modulo orientation and modulo limit cycles to one of the 40 phase portraits of Figs. 103 and 104.

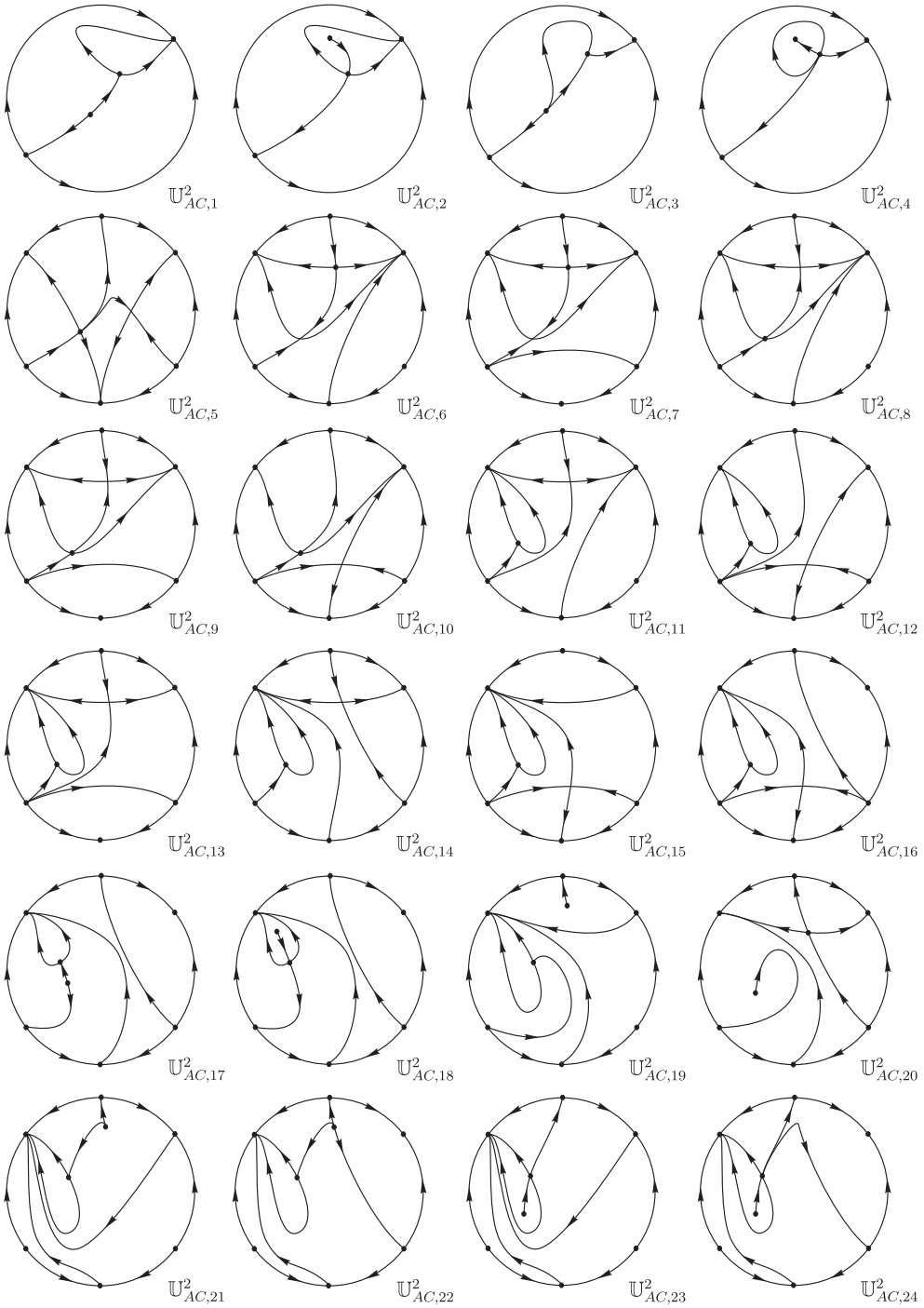

Figure 103 – Structurally unstable quadratic phase portraits of *codimension two** of the set (AC)

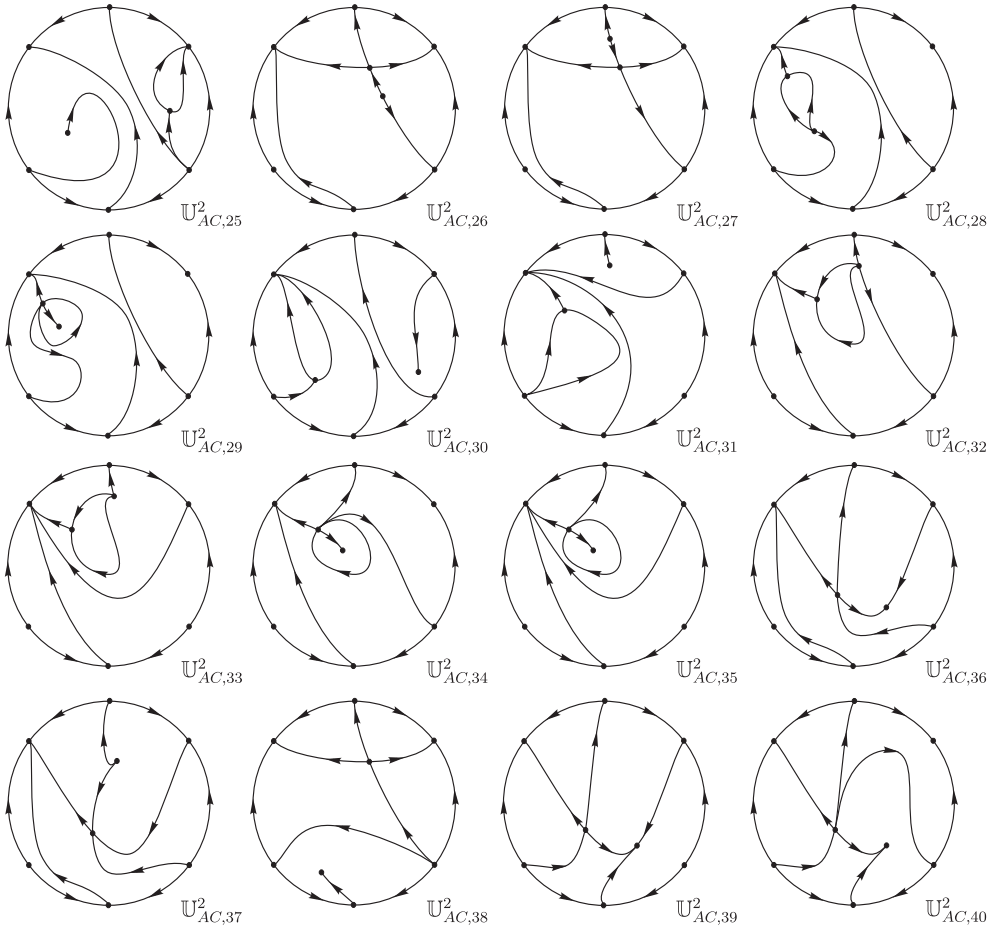

Figure 104 – *(Cont.)* Structurally unstable quadratic phase portraits of *codimension two** of the set (*AC*)

This chapter is organized as follows. In Sec. 5.2 we make a brief description of phase portraits of codimensions zero and one that are needed in this chapter.

In Sec. 5.3 we prove Thm. 5.1.1 and in Sec. 5.4 we prove Thm. 5.1.2. In order to verify the realization of the corresponding phase portraits we compute each one of them with the numerical program P4 (see Artés *et al.* (2005)).

Once again, remember that by modulo limit cycles we mean all nests with limit cycles are assimilated with the unique singular point (a focus) within such an nest, i.e. we may say that the phase portraits are *blind* to limit cycles. Additionally, the phase portraits are also blind with respect to distinguishing if a singular point is a focus or a node, because these are not topological properties. But as the phase portraits are not blind to detecting other important features like various types of graphics, in Sec. 5.5 we discuss about the existence of graphics and also limit cycles in this study.

5.2 Quadratic vector fields of codimension zero and one

In this section we summarize all the needed results from the book of Artés, Llibre and Rezende (2018). The following three results are the restriction of Thm. 1.1 from

the mentioned book to the sets (A), (B), and (C), respectively. We denote by $\sum_1^2(A)$ (respectively $\sum_1^2(B)$ and $\sum_1^2(C)$) the set of all structurally unstable vector fields $X \in \mathscr{P}_2(\mathbb{R}^2)$ of *codimension one** belonging to the set (A) (respectively (B) and (C)).

Theorem 5.2.1. If $X \in \sum_1^2(A)$, then its phase portrait on the Poincaré disc is topologically equivalent modulo orientation and modulo limit cycles to one of the 69 phase portraits of Figs. 105 to 107, and all of them are realizable.

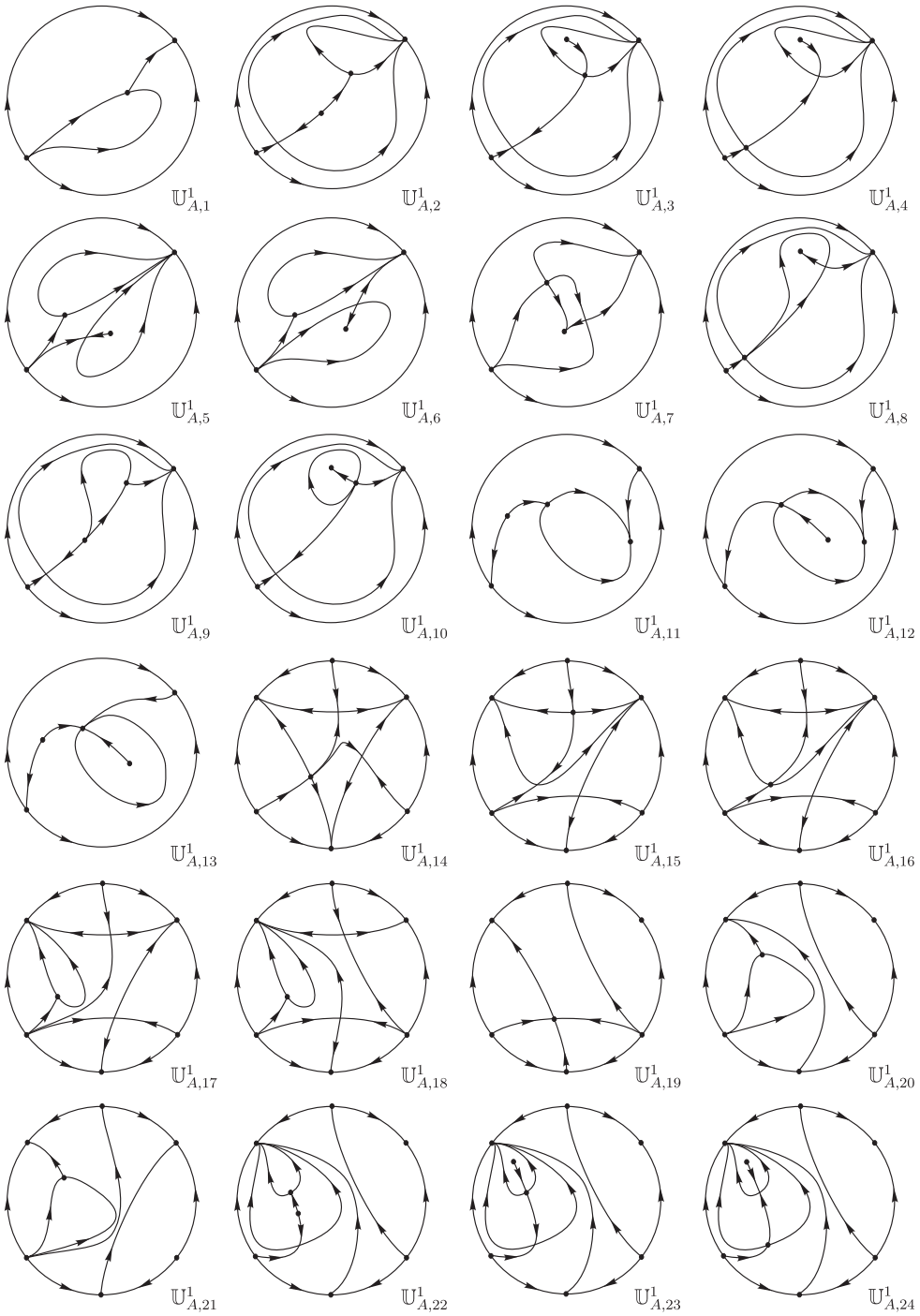

Figure 105 – Unstable quadratic systems of *codimension one** of the set (A) (cases with a finite saddle–node $\overline{sn}_{(2)}$)

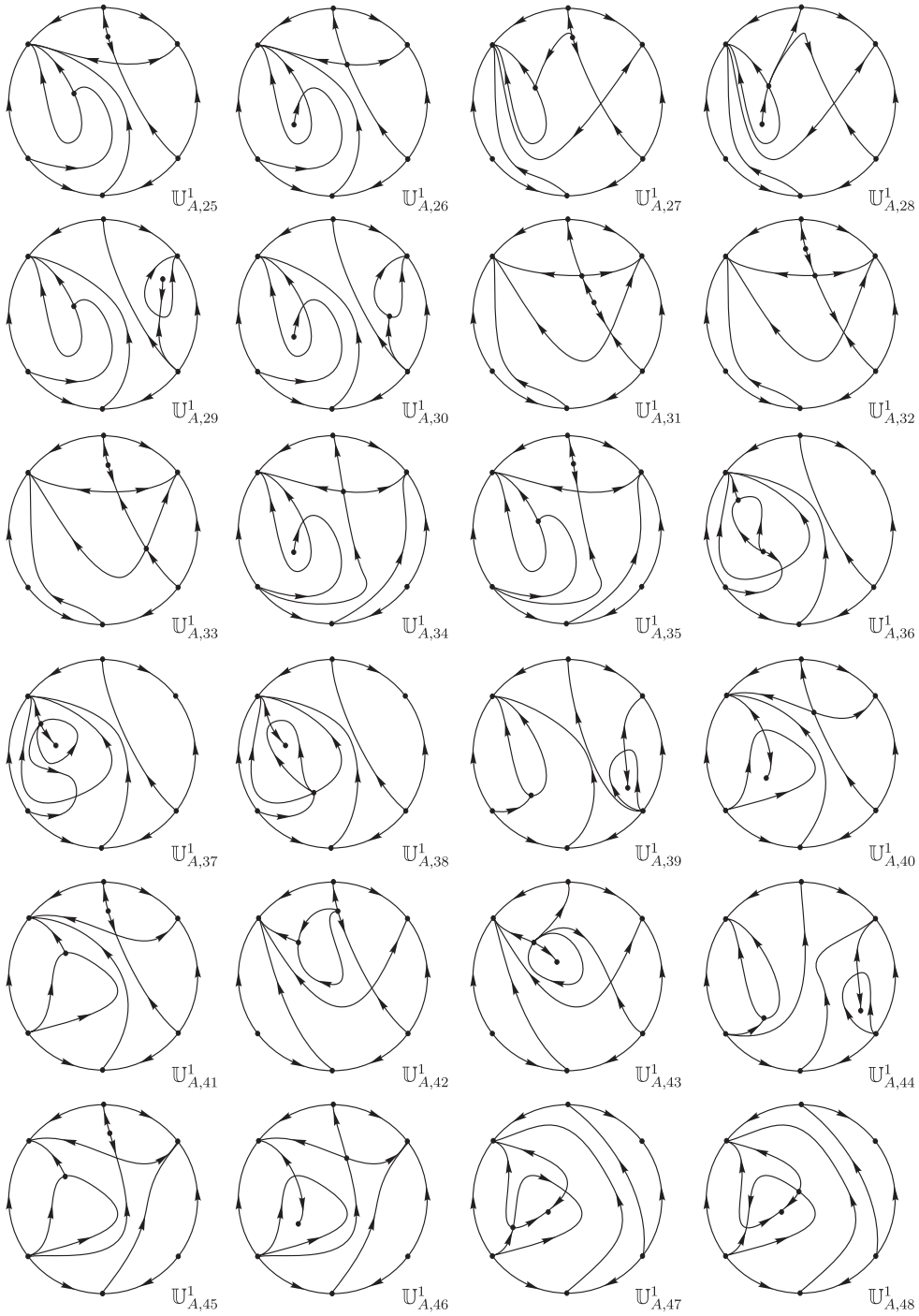

Figure 106 – *(Cont.)* Unstable quadratic systems of *codimension one** of the set (A) (cases with a finite saddle–node $\overline{sn}_{(2)}$)

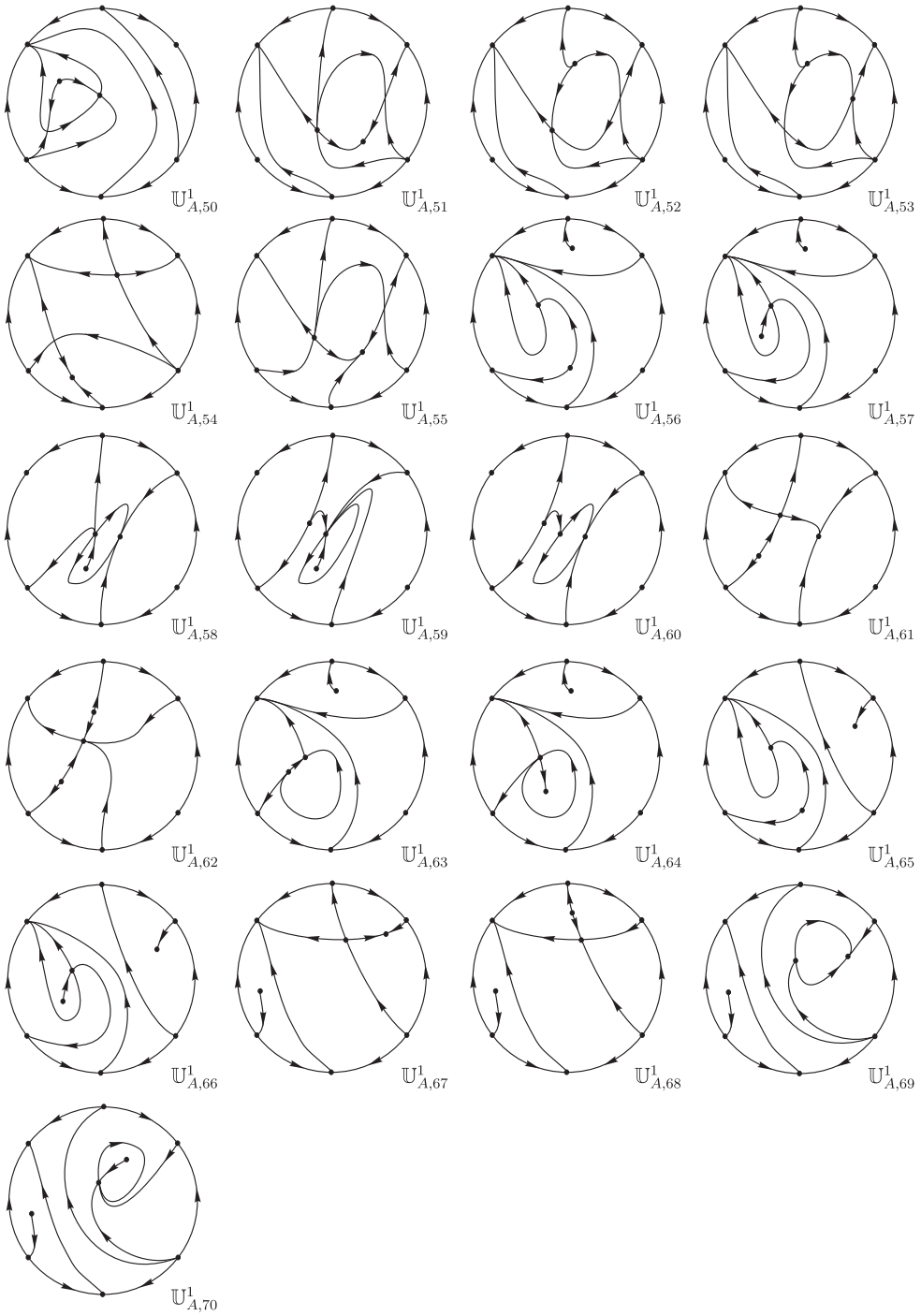

Figure 107 – *(Cont.)* Unstable quadratic systems of *codimension one** of the set (A) (cases with a finite saddle–node $\overline{sn}_{(2)}$)

Remark 5.2.2. In Artés, Oliveira and Rezende (2020) the authors have proved that phase portrait $\mathbb{U}^1_{A,49}$ from Fig. 1.4 of Artés, Llibre and Rezende (2018) is actually impossible. Therefore, in our Figs. 105 to 107 we have simply "skipped" this phase portrait, since all of the remaining ones are indeed realizable. We present this impossible phase portrait in Fig. 112 and there we denote it by $\mathbb{U}^{1,I}_{A,49}$.

Theorem 5.2.3. If $X \in \sum_1^2(B)$, then its phase portrait on the Poincaré disc is topologically equivalent modulo orientation and modulo limit cycles to one of the 40 phase portraits of Figs. 108 and 109, and all of them are realizable.

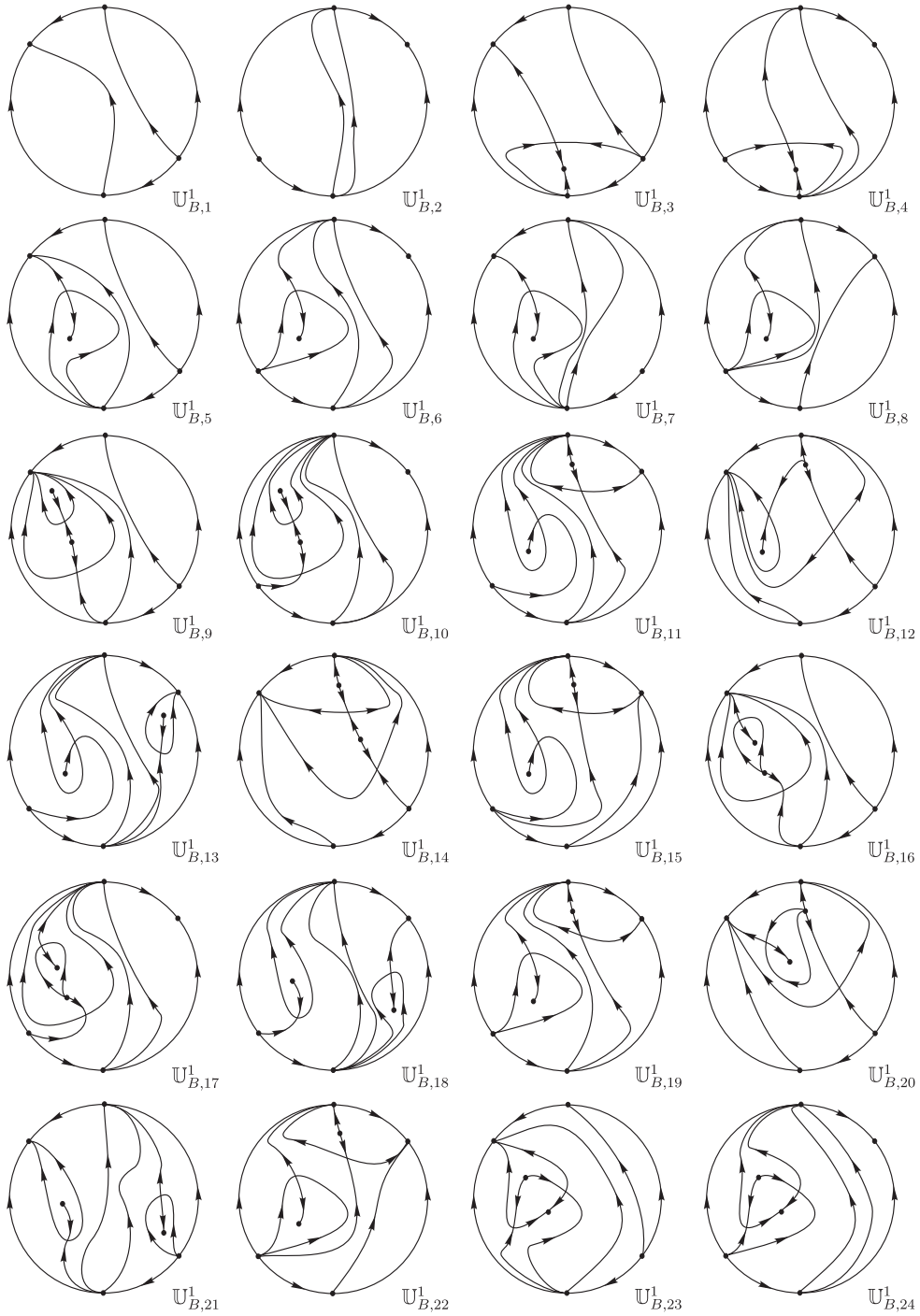

Figure 108 – Unstable quadratic systems of *codimension one** of the set (B) (cases with an infinite saddle–node of type $\overline{\binom{0}{2}}\,SN$)

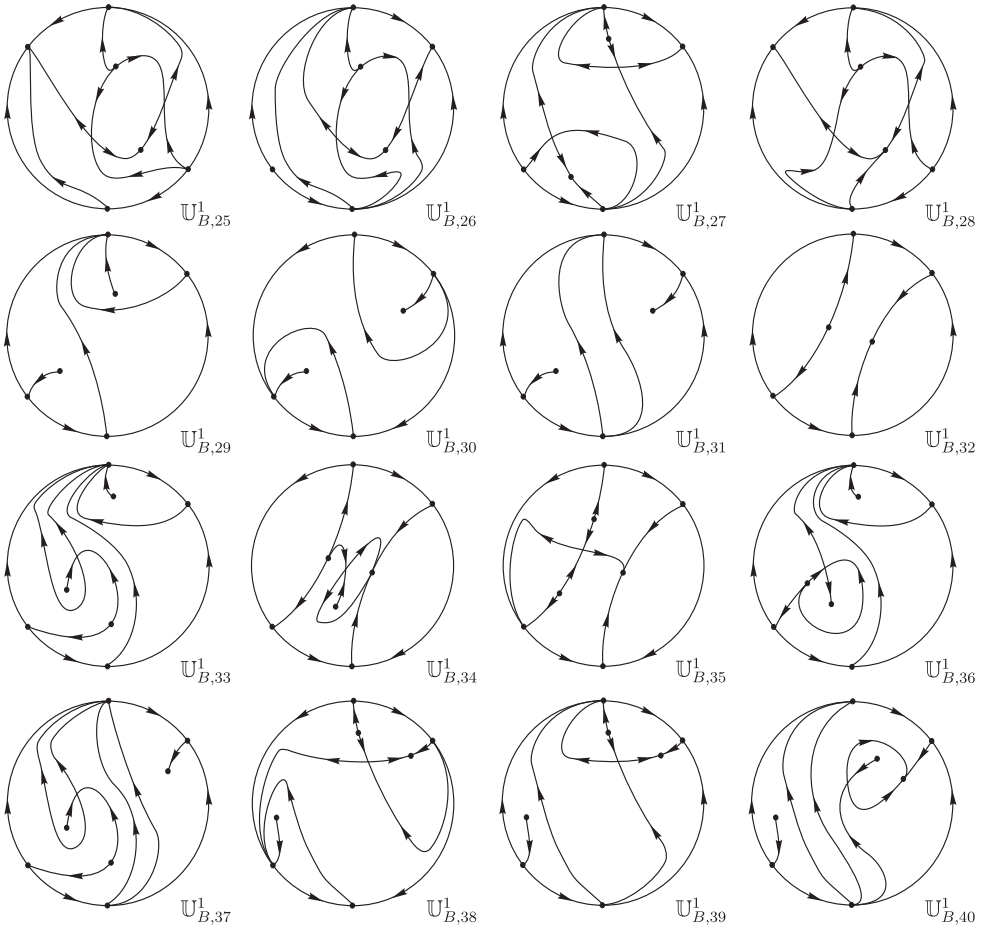

Figure 109 – *(Cont.)* Unstable quadratic systems of *codimension one** of the set (B) (cases with an infinite saddle–node of type $\overline{\binom{0}{2}}\,SN$)

Theorem 5.2.4. If $X \in \sum_1^2(C)$, then its phase portrait on the Poincaré disc is topologically equivalent modulo orientation and modulo limit cycles to one of the 32 phase portraits of Figs. 110 to 111, and all of them are realizable.

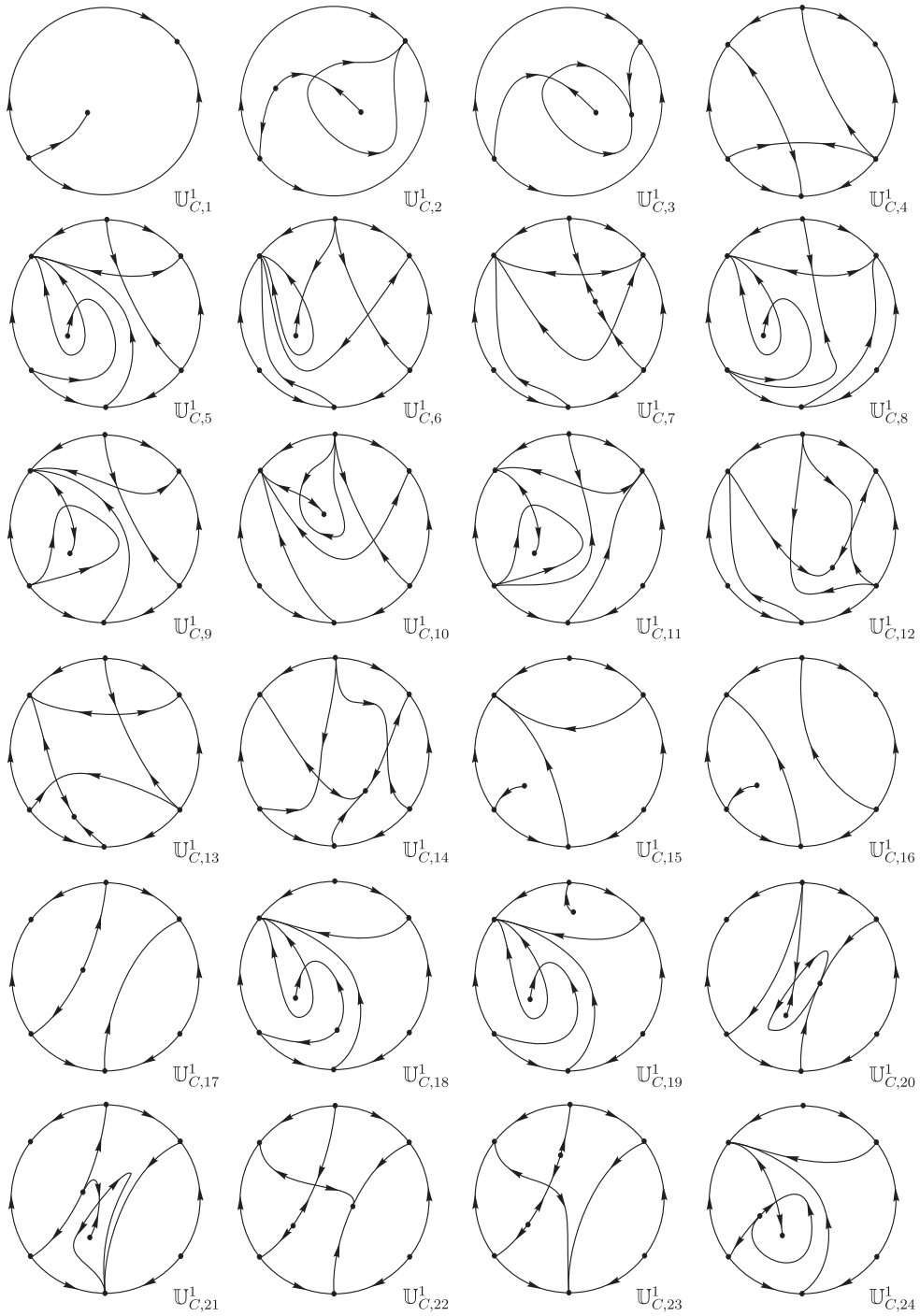

Figure 110 – Unstable quadratic systems of *codimension one** of the set (C) (cases with an infinite saddle–node of type $\overline{\binom{1}{1}}\,SN$)

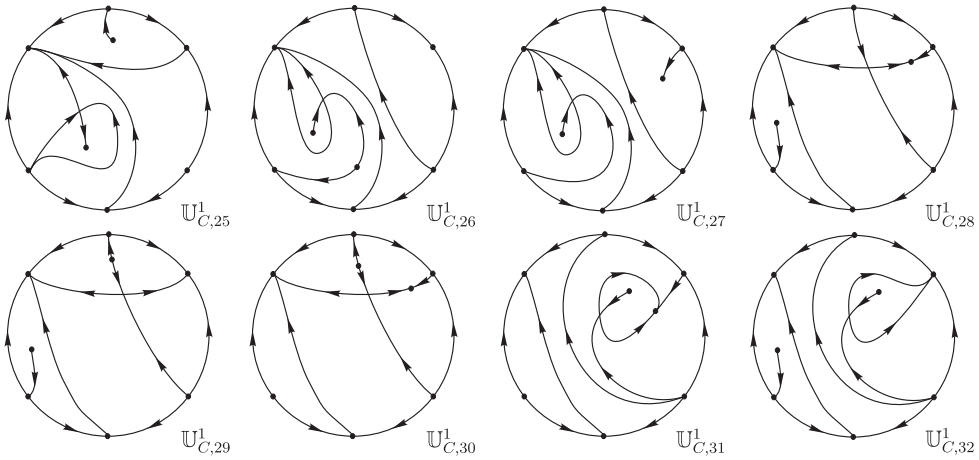

Figure 111 – *(Cont.)* Unstable quadratic systems of *codimension one** of the set (C) (cases with an infinite saddle–node of type $\overline{\binom{1}{1}}\,SN$)

Before we state our next theorem, consider the following remark.

Remark 5.2.5. Consider all the impossible phase portraits from the book Artés, Llibre and Rezende (2018). In that book these phase portraits are described with a specific notation. However, here we changed a little bit their notation in order to associate each impossible phase portrait with the set in which such a phase portrait is proved to be impossible, but we keep the respective indexes. For instance, in that book we have the presence of the impossible phase portrait $\mathbb{U}^1_{I,105}$, which is a non–realizable case from the set (A). Such a phase portrait is denoted here by $\mathbb{U}^{1,I}_{A,105}$. We also use this new notation for phase portraits which are proved to be impossible in the sets (B) and (C).

The next result describes which phase portraits were discarded in the set (A) in Artés, Llibre and Rezende (2018) because they were not realizable, but their role now is important in the process of discarding impossible phase portraits of *codimension two**.

Theorem 5.2.6. In order to obtain a phase portrait of a structurally unstable quadratic vector field of *codimension one** from the set (A) it is necessary and sufficient to coalesce a finite saddle and a finite node from a structurally stable quadratic vector field, which leads to a finite saddle–node, and after some small perturbation it disappears. For the vector fields in set (A), the following statements hold.

(a) In Table 35 we may see in the first and fifth columns the structurally stable quadratic vector fields (following the notation present in Artés, Kooij and Llibre (1998) and Artés, Llibre and Rezende (2018)) which, after the coalescence of singularities mentioned before, lead to at least one phase portrait of *codimension one** from the set (A).

(b) Inside this set (A), we have a total of 77 topologically distinct phase portraits according to the different α–limit or ω–limit of the separatrices of their saddles, seven

of which are proved non–realizable in Artés, Llibre and Rezende (2018) and another one is proved non–realizable in Artés, Oliveira and Rezende (2020) (all of these eight non–realizable phase portraits are given in Table 36). These numbers are given in the second and sixth columns of Table 35.

(c) From these potential phase portraits, most of them are realizable. That is, even though there is the topological possibility of their existence, some of them break some analytical property which makes them not realizable inside quadratic vector fields. We have a total of 69 realizable phase portraits. In the third and seventh columns of Table 35 we present the number of realizable cases coming from the bifurcation of each structurally stable phase portrait, and in the fourth and eighth columns we present the bifurcated phase portraits of *codimension one** associated to each one.

(d) There are then eight non–realizable cases from the set (A) which we now collect in a single picture (see Fig. 112) and denote by $\mathbb{U}^{1,I}_{A,k}$, where $\mathbb{U}^{1,I}_{A}$ stands for Impossible of *codimension one** from the set (A) and $k \in \{1,2,3,49,103,104,105,106\}$, see Remark 5.2.5. These phase portraits are all drawn in Artés, Llibre and Rezende (2018). Anyway, we provide Table 36 in order to relate easily (giving also the page where they appear first and the page they are proved to be impossible).

Table 35 – Potential and realizable bifurcated phase portraits for a given structurally stable quadratic vector field. In this table, **SSQVF** stands for structurally stable quadratic vector fields (according to Artés, Kooij and Llibre (1998)), $\#_p$ (respectively $\#_r$) for the number of topologically potential (respectively realizable) phase portraits of *codimension one** bifurcated from the respective **SSQVF**, and **SU1** for the respective phase portraits of *codimension one** (according to Artés, Llibre and Rezende (2018))

SSQVF	$\#_p$	$\#_r$	**SU1**	**SSQVF**	$\#_p$	$\#_r$	**SU1**
$\mathbb{S}^2_{2,1}$	1	1	$\mathbb{U}^1_{A,1}$	$\mathbb{S}^2_{10,6}$	2	2	$\mathbb{U}^1_{A,34}, \mathbb{U}^1_{A,35}$
$\mathbb{S}^2_{3,1}$	3	3	$\mathbb{U}^1_{A,2}, \mathbb{U}^1_{A,3}, \mathbb{U}^1_{A,4}$	$\mathbb{S}^2_{10,7}$	4	3	$\mathbb{U}^1_{A,36}, \mathbb{U}^1_{A,37}, \mathbb{U}^1_{A,38}$
$\mathbb{S}^2_{3,2}$	1	1	$\mathbb{U}^1_{A,5}$	$\mathbb{S}^2_{10,8}$	1	1	$\mathbb{U}^1_{A,39}$
$\mathbb{S}^2_{3,3}$	1	1	$\mathbb{U}^1_{A,6}$	$\mathbb{S}^2_{10,9}$	2	2	$\mathbb{U}^1_{A,40}, \mathbb{U}^1_{A,41}$
$\mathbb{S}^2_{3,4}$	1	1	$\mathbb{U}^1_{A,7}$	$\mathbb{S}^2_{10,10}$	4	2	$\mathbb{U}^1_{A,42}, \mathbb{U}^1_{A,43}$
$\mathbb{S}^2_{3,5}$	3	3	$\mathbb{U}^1_{A,8}, \mathbb{U}^1_{A,9}, \mathbb{U}^1_{A,10}$	$\mathbb{S}^2_{10,11}$	1	1	$\mathbb{U}^1_{A,44}$
$\mathbb{S}^2_{5,1}$	3	3	$\mathbb{U}^1_{A,11}, \mathbb{U}^1_{A,12}, \mathbb{U}^1_{A,13}$	$\mathbb{S}^2_{10,12}$	2	2	$\mathbb{U}^1_{A,45}, \mathbb{U}^1_{A,46}$
$\mathbb{S}^2_{7,1}$	1	1	$\mathbb{U}^1_{A,14}$	$\mathbb{S}^2_{10,13}$	4	4	$\mathbb{U}^1_{A,47}, \mathbb{U}^1_{A,48}, \mathbb{U}^1_{A,50}$
$\mathbb{S}^2_{7,2}$	2	2	$\mathbb{U}^1_{A,15}, \mathbb{U}^1_{A,16}$	$\mathbb{S}^2_{10,14}$	4	3	$\mathbb{U}^1_{A,51}, \mathbb{U}^1_{A,52}, \mathbb{U}^1_{A,53}$
$\mathbb{S}^2_{7,3}$	1	1	$\mathbb{U}^1_{A,17}$	$\mathbb{S}^2_{10,15}$	1	1	$\mathbb{U}^1_{A,54}$
$\mathbb{S}^2_{7,4}$	1	1	$\mathbb{U}^1_{A,18}$	$\mathbb{S}^2_{10,16}$	1	1	$\mathbb{U}^1_{A,55}$
$\mathbb{S}^2_{9,1}$	1	1	$\mathbb{U}^1_{A,19}$	$\mathbb{S}^2_{12,1}$	2	2	$\mathbb{U}^1_{A,56}, \mathbb{U}^1_{A,57}$
$\mathbb{S}^2_{9,2}$	1	1	$\mathbb{U}^1_{A,20}$	$\mathbb{S}^2_{12,2}$	3	3	$\mathbb{U}^1_{A,58}, \mathbb{U}^1_{A,59}, \mathbb{U}^1_{A,60}$
$\mathbb{S}^2_{9,3}$	1	1	$\mathbb{U}^1_{A,21}$	$\mathbb{S}^2_{12,3}$	2	2	$\mathbb{U}^1_{A,61}, \mathbb{U}^1_{A,62}$
$\mathbb{S}^2_{10,1}$	3	3	$\mathbb{U}^1_{A,22}, \mathbb{U}^1_{A,23}, \mathbb{U}^1_{A,24}$	$\mathbb{S}^2_{12,4}$	3	2	$\mathbb{U}^1_{A,63}, \mathbb{U}^1_{A,64}$
$\mathbb{S}^2_{10,2}$	2	2	$\mathbb{U}^1_{A,25}, \mathbb{U}^1_{A,26}$	$\mathbb{S}^2_{12,5}$	2	2	$\mathbb{U}^1_{A,65}, \mathbb{U}^1_{A,66}$
$\mathbb{S}^2_{10,3}$	3	2	$\mathbb{U}^1_{A,27}, \mathbb{U}^1_{A,28}$	$\mathbb{S}^2_{12,6}$	2	2	$\mathbb{U}^1_{A,67}, \mathbb{U}^1_{A,68}$
$\mathbb{S}^2_{10,4}$	2	2	$\mathbb{U}^1_{A,29}, \mathbb{U}^1_{A,30}$	$\mathbb{S}^2_{12,7}$	3	2	$\mathbb{U}^1_{A,69}, \mathbb{U}^1_{A,70}$
$\mathbb{S}^2_{10,5}$	3	3	$\mathbb{U}^1_{A,31}, \mathbb{U}^1_{A,32}, \mathbb{U}^1_{A,33}$				

Table 36 – Non–realizable phase portraits from the set (A) which could bifurcate (if existed) from structurally stable quadratic vector fields. The first and fourth columns indicate the structurally stable quadratic vector field (**SSQVF** from Artés, Kooij and Llibre (1998)) which suffers a bifurcation, the second and fifth columns indicate the pages where they appear in Artés, Llibre and Rezende (2018) and the third and sixth columns present the corresponding impossible phase portraits (remember that phase portrait $\mathbb{U}^1_{A,49}$ from Fig. 1.4 of Artés, Llibre and Rezende (2018) is proved to be impossible in Artés, Oliveira and Rezende (2020))

SSQVF	**Page**	**Impossible**	**SSQVF**	**Page**	**Impossible**
$\mathbb{S}^2_{10,3}$	70	$\mathbb{U}^{1,I}_{A,1}$	$\mathbb{S}^2_{10,14}$	77	$\mathbb{U}^{1,I}_{A,3}$
$\mathbb{S}^2_{10,7}$	(73) 190	$\mathbb{U}^{1,I}_{A,103}$	$\mathbb{S}^2_{12,4}$	(80) 191	$\mathbb{U}^{1,I}_{A,105}$
$\mathbb{S}^2_{10,10}$	75; 191	$\mathbb{U}^{1,I}_{A,2}$;$\mathbb{U}^{1,I}_{A,104}$	$\mathbb{S}^2_{12,7}$	(82) 188	$\mathbb{U}^{1,I}_{A,106}$
$\mathbb{S}^2_{10,13}$	76	$\mathbb{U}^{1,I}_{A,49}$			

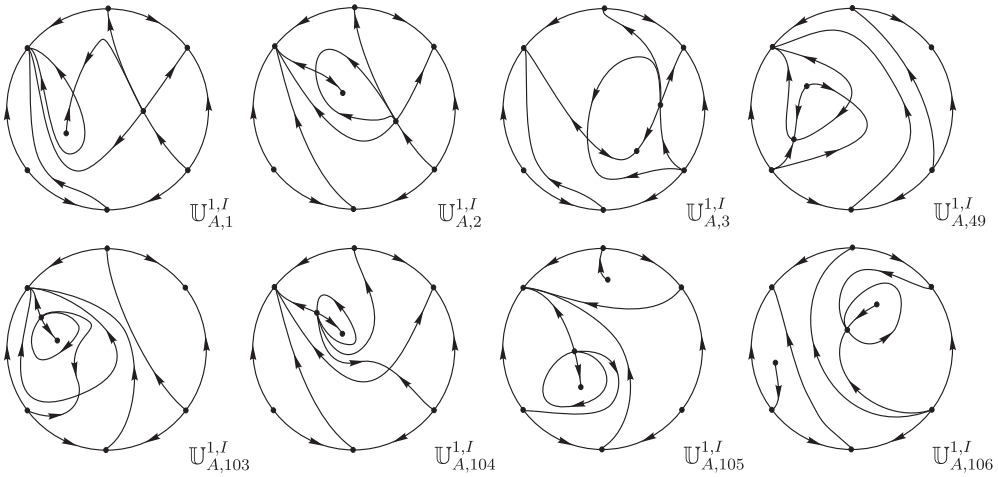

Figure 112 – Phase portraits of the non–realizable structurally unstable quadratic vector fields of *codimension one** from the set (A)

In what follows we present an analogous theorem regarding discarded phase portraits from the set (B) in Artés, Llibre and Rezende (2018).

Theorem 5.2.7. In order to obtain a phase portrait of a structurally unstable quadratic vector field of *codimension one** from the set (B) it is necessary and sufficient to coalesce an infinite saddle with an infinite node from a structurally stable quadratic vector field, which leads to an infinite saddle–node of type $\overline{\binom{0}{2}}\,SN$, and after some small perturbation it disappears. For the vector fields in set (B), the following statements hold.

(a) In Table 37 we may see in the first and fifth columns the structurally stable quadratic vector fields (following the notation present in Artés, Kooij and Llibre (1998) and Artés, Llibre and Rezende (2018)) which, after the coalescence of singularities mentioned before, lead to at least one phase portrait of *codimension one** from the set (B).

(b) Inside this set (B), we have a total of 55 topologically distinct phase portraits according to the different α–limit or ω–limit of the separatrices of their saddles, 15 of which are non–realizable (they are given in Table 38). These numbers are given in the second and sixth columns of Table 37.

(c) From these potential phase portraits, most of them are realizable. That is, even though there is the topological possibility of their existence, some of them break some analytical property which makes them not realizable inside quadratic vector fields. We have a total of 40 realizable phase portraits. In the third and seventh columns of Table 37 we present the number of realizable cases coming from the bifurcation of each structurally stable phase portrait, and in the fourth and eighth columns we present the bifurcated phase portraits of *codimension one** associated to each one.

(d) There are then **15** non–realizable cases from the set $(\boldsymbol{B})$ which we now collect in a single picture (see Fig. 113) and denote by $\mathbb{U}^{1,I}_{B,k}$, where $\mathbb{U}^{1,I}_{B}$ stands for Impossible of *codimension one** from the set $(\boldsymbol{B})$ and

$$k \in \{4,5,6,7,107,108,109,110,111,112,113,114,115,116,117\},$$

see Rmk. 5.2.5. These phase portraits are all drawn in Artés, Llibre and Rezende (2018). Anyway, we provide Table 38 in order to relate easily (giving also the page where they appear first and the page they are proved to be impossible).

Table 37 – Potential and realizable bifurcated phase portraits for a given structurally stable quadratic vector field. In this table, **SSQVF** stands for structurally stable quadratic vector fields (according to Artés, Kooij and Llibre (1998)), $\#_p$ (respectively $\#_r$) for the number of topologically potential (respectively realizable) phase portraits of *codimension one** bifurcated from the respective **SSQVF**, and **SU1** for the respective phase portraits of *codimension one** (according to Artés, Llibre and Rezende (2018))

SSQVF	$\#_p$	$\#_r$	**SU1**	**SSQVF**	$\#_p$	$\#_r$	**SU1**
$\mathbb{S}^2_{8,1}$	2	2	$\mathbb{U}^1_{B,1}, \mathbb{U}^1_{B,2}$	$\mathbb{S}^2_{10,12}$	2	1	$\mathbb{U}^1_{B,22}$
$\mathbb{S}^2_{9,1}$	2	2	$\mathbb{U}^1_{B,3}, \mathbb{U}^1_{B,4}$	$\mathbb{S}^2_{10,13}$	2	2	$\mathbb{U}^1_{B,23}, \mathbb{U}^1_{B,24}$
$\mathbb{S}^2_{9,2}$	2	2	$\mathbb{U}^1_{B,5}, \mathbb{U}^1_{B,6}$	$\mathbb{S}^2_{10,14}$	2	2	$\mathbb{U}^1_{B,25}, \mathbb{U}^1_{B,26}$
$\mathbb{S}^2_{9,3}$	2	2	$\mathbb{U}^1_{B,7}, \mathbb{U}^1_{B,8}$	$\mathbb{S}^2_{10,15}$	2	1	$\mathbb{U}^1_{B,27}$
$\mathbb{S}^2_{10,1}$	2	2	$\mathbb{U}^1_{B,9}, \mathbb{U}^1_{B,10}$	$\mathbb{S}^2_{10,16}$	1	1	$\mathbb{U}^1_{B,28}$
$\mathbb{S}^2_{10,2}$	2	1	$\mathbb{U}^1_{B,11}$	$\mathbb{S}^2_{11,1}$	1	1	$\mathbb{U}^1_{B,29}$
$\mathbb{S}^2_{10,3}$	2	1	$\mathbb{U}^1_{B,12}$	$\mathbb{S}^2_{11,2}$	2	2	$\mathbb{U}^1_{B,30}, \mathbb{U}^1_{B,31}$
$\mathbb{S}^2_{10,4}$	2	1	$\mathbb{U}^1_{B,13}$	$\mathbb{S}^2_{11,3}$	1	1	$\mathbb{U}^1_{B,32}$
$\mathbb{S}^2_{10,5}$	2	1	$\mathbb{U}^1_{B,14}$	$\mathbb{S}^2_{12,1}$	2	1	$\mathbb{U}^1_{B,33}$
$\mathbb{S}^2_{10,6}$	2	1	$\mathbb{U}^1_{B,15}$	$\mathbb{S}^2_{12,2}$	1	1	$\mathbb{U}^1_{B,34}$
$\mathbb{S}^2_{10,7}$	2	2	$\mathbb{U}^1_{B,16}, \mathbb{U}^1_{B,17}$	$\mathbb{S}^2_{12,3}$	1	1	$\mathbb{U}^1_{B,35}$
$\mathbb{S}^2_{10,8}$	2	1	$\mathbb{U}^1_{B,18}$	$\mathbb{S}^2_{12,4}$	2	1	$\mathbb{U}^1_{B,36}$
$\mathbb{S}^2_{10,9}$	2	1	$\mathbb{U}^1_{B,19}$	$\mathbb{S}^2_{12,5}$	2	1	$\mathbb{U}^1_{B,37}$
$\mathbb{S}^2_{10,10}$	2	1	$\mathbb{U}^1_{B,20}$	$\mathbb{S}^2_{12,6}$	2	2	$\mathbb{U}^1_{B,38}, \mathbb{U}^1_{B,39}$
$\mathbb{S}^2_{10,11}$	2	1	$\mathbb{U}^1_{B,21}$	$\mathbb{S}^2_{12,7}$	2	1	$\mathbb{U}^1_{B,40}$

Table 38 – Non–realizable phase portraits from the set (B) which could bifurcate (if existed) from structurally stable quadratic vector fields. The first and fourth columns indicate the structurally stable quadratic vector field (**SSQVF** from Artés, Kooij and Llibre (1998)) which suffers a bifurcation, the second and fifth columns indicate the pages where they appear in Artés, Llibre and Rezende (2018) and the third and sixth columns present the corresponding impossible phase portraits

SSQVF	**Page**	**Impossible**	**SSQVF**	**Page**	**Impossible**
$\mathbb{S}^2_{10,2}$	86; 200	$\mathbb{U}^{1,I}_{B,107}$	$\mathbb{S}^2_{10,11}$	90; 200	$\mathbb{U}^{1,I}_{B,115}$
$\mathbb{S}^2_{10,3}$	86; 203	$\mathbb{U}^{1,I}_{B,108}$	$\mathbb{S}^2_{10,12}$	91; 200	$\mathbb{U}^{1,I}_{B,116}$
$\mathbb{S}^2_{10,4}$	87; 200	$\mathbb{U}^{1,I}_{B,109}$	$\mathbb{S}^2_{10,15}$	92; 200	$\mathbb{U}^{1,I}_{B,117}$
$\mathbb{S}^2_{10,5}$	87; 207	$\mathbb{U}^{1,I}_{B,110}$	$\mathbb{S}^2_{12,1}$	94	$\mathbb{U}^{1,I}_{B,4}$
$\mathbb{S}^2_{10,6}$	88; 200	$\mathbb{U}^{1,I}_{B,111}$	$\mathbb{S}^2_{12,4}$	96	$\mathbb{U}^{1,I}_{B,5}$
$\mathbb{S}^2_{10,8}$	89; 200	$\mathbb{U}^{1,I}_{B,112}$	$\mathbb{S}^2_{12,5}$	96	$\mathbb{U}^{1,I}_{B,6}$
$\mathbb{S}^2_{10,9}$	89; 200	$\mathbb{U}^{1,I}_{B,113}$	$\mathbb{S}^2_{12,7}$	97	$\mathbb{U}^{1,I}_{B,7}$
$\mathbb{S}^2_{10,10}$	90; 203	$\mathbb{U}^{1,I}_{B,114}$			

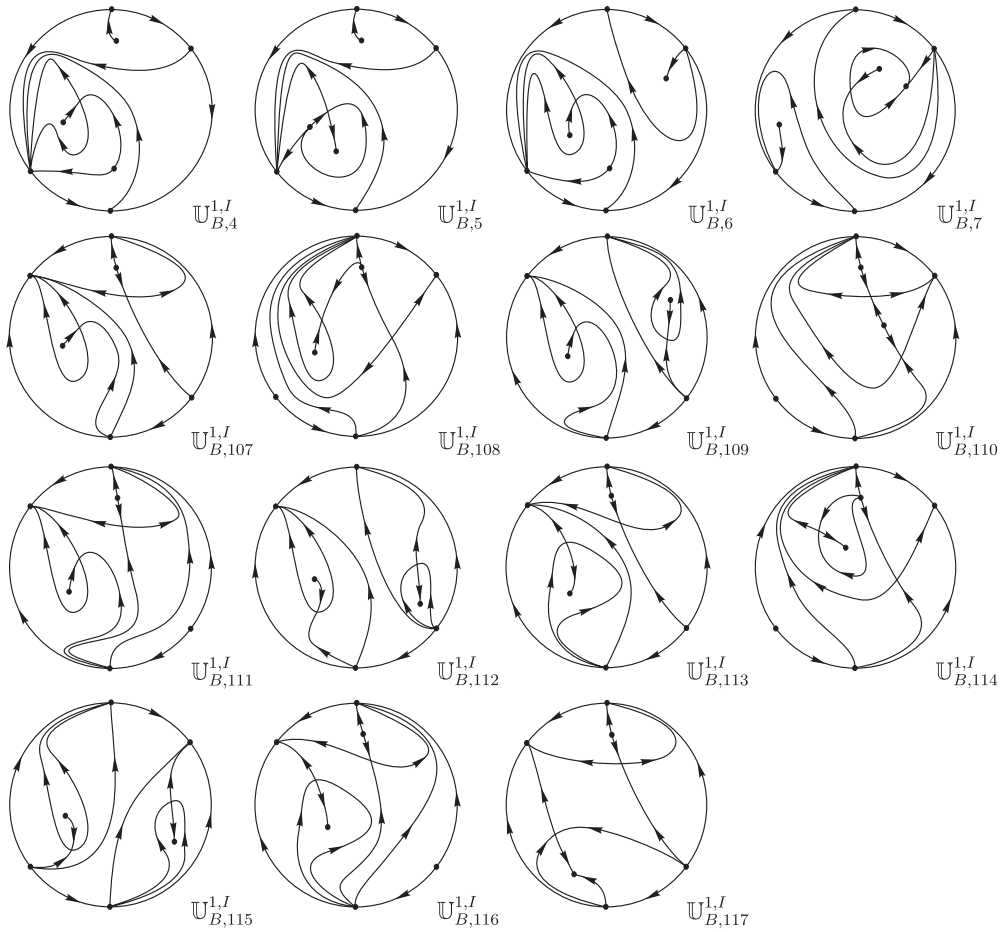

Figure 113 – Phase portraits of the non–realizable structurally unstable quadratic vector fields of *codimension one** from the set (B)

Finally, we present an analogous theorem regarding discarded phase portraits from the set (C) in Artés, Llibre and Rezende (2018).

Theorem 5.2.8. In order to obtain a phase portrait of a structurally unstable quadratic vector field of *codimension one** from the set (C) it is necessary and sufficient to coalesce a finite node (respectively a finite saddle) with an infinite saddle (respectively an infinite node) from a structurally stable quadratic vector field, which leads to an infinite saddle–node of type $\overline{\binom{1}{1}}$ SN, and after some small perturbation, this saddle–node is split into a finite saddle (respectively a finite node) and an infinite node (respectively an infinite saddle). For the vector fields in set (C), the following statements hold.

(a) In Table 39 we may see in the first and fifth columns the structurally stable quadratic vector fields (following the notation present in Artés, Kooij and Llibre (1998) and Artés, Llibre and Rezende (2018)) which, after the coalescence of singularities mentioned before, lead to at least one phase portrait of *codimension one** from the set (C).

(b) Inside this set (C), we have a total of 34 topologically distinct phase portraits according to the different α–limit or ω–limit of the separatrices of their saddles, two of which are non–realizable (they are given in Table 40). These numbers are given in the second and sixth columns of Table 39.

(c) From these potential phase portraits, only two of them are not realizable. That is, even though there is the topological possibility of their existence, two of them break some analytical property which makes them not realizable inside quadratic vector fields. We have a total of 32 realizable phase portraits. In the third and seventh columns of Table 39 we present the number of realizable cases coming from the bifurcation of each structurally stable phase portrait, and in the fourth and eighth columns we present the bifurcated phase portraits of *codimension one** associated to each one.

(d) There are then two non–realizable cases from the set (C) which we present in Fig. 114 and denote by $\mathbb{U}^{1,I}_{C,k}$, where $\mathbb{U}^{1,I}_{C}$ stands for Impossible of *codimension one** from the set (C) and $k \in \{8,9\}$, see Rmk. 5.2.5. These phase portraits are all drawn in Artés, Llibre and Rezende (2018). Anyway, we provide Table 40 in order to relate easily (giving also the page where they appear first and the page they are proved to be impossible).

Table 39 – Potential and realizable bifurcated phase portraits for a given structurally stable quadratic vector field. In this table, **SSQVF** stands for structurally stable quadratic vector fields (according to Artés, Kooij and Llibre (1998)), $\#_p$ (respectively $\#_r$) for the number of topologically potential (respectively realizable) phase portraits of *codimension one** bifurcated from the respective **SSQVF**, and **SU1** for the respective phase portraits of *codimension one** (according to Artés, Llibre and Rezende (2018))

SSQVF	$\#_p$	$\#_r$	**SU1**	**SSQVF**	$\#_p$	$\#_r$	**SU1**
$\mathbb{S}^2_{4,1}$	1	1	$\mathbb{U}^1_{C,1}$	$\mathbb{S}^2_{10,16}$	1	1	$\mathbb{U}^1_{C,14}$
$\mathbb{S}^2_{5,1}$	2	2	$\mathbb{U}^1_{C,2}, \mathbb{U}^1_{C,3}$	$\mathbb{S}^2_{11,1}$	1	1	$\mathbb{U}^1_{C,15}$
$\mathbb{S}^2_{9,1}$	1	1	$\mathbb{U}^1_{C,4}$	$\mathbb{S}^2_{11,2}$	1	1	$\mathbb{U}^1_{C,16}$
$\mathbb{S}^2_{10,2}$	2	1	$\mathbb{U}^1_{C,5}$	$\mathbb{S}^2_{11,3}$	1	1	$\mathbb{U}^1_{C,17}$
$\mathbb{S}^2_{10,3}$	1	1	$\mathbb{U}^1_{C,6}$	$\mathbb{S}^2_{12,1}$	2	2	$\mathbb{U}^1_{C,18}, \mathbb{U}^1_{C,19}$
$\mathbb{S}^2_{10,5}$	1	1	$\mathbb{U}^1_{C,7}$	$\mathbb{S}^2_{12,2}$	2	2	$\mathbb{U}^1_{C,20}, \mathbb{U}^1_{C,21}$
$\mathbb{S}^2_{10,6}$	1	1	$\mathbb{U}^1_{C,8}$	$\mathbb{S}^2_{12,3}$	2	2	$\mathbb{U}^1_{C,22}, \mathbb{U}^1_{C,23}$
$\mathbb{S}^2_{10,9}$	2	1	$\mathbb{U}^1_{C,9}$	$\mathbb{S}^2_{12,4}$	2	2	$\mathbb{U}^1_{C,24}, \mathbb{U}^1_{C,25}$
$\mathbb{S}^2_{10,10}$	1	1	$\mathbb{U}^1_{C,10}$	$\mathbb{S}^2_{12,5}$	2	2	$\mathbb{U}^1_{C,26}, \mathbb{U}^1_{C,27}$
$\mathbb{S}^2_{10,12}$	1	1	$\mathbb{U}^1_{C,11}$	$\mathbb{S}^2_{12,6}$	3	3	$\mathbb{U}^1_{C,28}, \mathbb{U}^1_{C,29}, \mathbb{U}^1_{30}$
$\mathbb{S}^2_{10,14}$	1	1	$\mathbb{U}^1_{C,12}$	$\mathbb{S}^2_{12,7}$	2	2	$\mathbb{U}^1_{C,31}, \mathbb{U}^1_{C,32}$
$\mathbb{S}^2_{10,15}$	1	1	$\mathbb{U}^1_{C,13}$				

Table 40 – Non–realizable phase portraits from the set (C) which could bifurcate (if existed) from structurally stable quadratic vector fields. The first column indicates the structurally stable quadratic vector field (**SSQVF** from Artés, Kooij and Llibre (1998)) which suffers a bifurcation, the second column indicates the pages where they appear in Artés, Llibre and Rezende (2018) and the third column present the corresponding impossible phase portrait

SSQVF	**Page**	**Impossible**
$\mathbb{S}^2_{10,2}$	101	$\mathbb{U}^{1,I}_{C,8}$
$\mathbb{S}^2_{10,9}$	103	$\mathbb{U}^{1,I}_{C,9}$

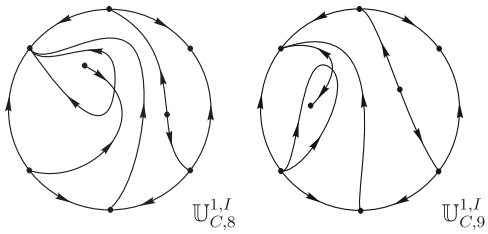

Figure 114 – Phase portraits of the non–realizable structurally unstable quadratic vector fields of *codimension one** from the set (C)

An important result to study the impossibility of some phase portraits is Cor. 3.29 of Artés, Llibre and Rezende (2018), which we state as follows.

Corollary 5.2.9. If one of the structurally stable vector fields that bifurcates from a potential structurally unstable vector field of *codimension one** is not realizable, then this

unstable system is also not realizable.

Our aim is to prove the following result, which is the analogous of the previous corollary for the sets (AB) and (AC).

Theorem 5.2.10. If one of the phase portraits of *codimension one** that bifurcates from a potential *codimension two** phase portrait from the sets (AB) and (AC) is not realizable, then this latter phase portrait is also not realizable.

Proof. In what follows we prove the equivalent statement: If a potential *codimension two** phase portrait X from the sets (AB) and (AC) is realizable, then the phase portraits of *codimension one** that bifurcates from X are also realizable.

We start from the set (AB). We already know that a realizable phase portrait belongs to the set (AB) if and only if it has a finite saddle–node $\overline{sn}_{(2)}$ and an infinite saddle–node of type $\overline{\binom{0}{2}}\,SN$ obtained by the coalescence of an infinite saddle with an infinite node. In Artés, Rezende and Oliveira (2015) the authors classified the set of all real quadratic polynomial differential systems with a finite semi–elemental saddle–node $\overline{sn}_{(2)}$ located at the origin of the plane and an infinite saddle–node of type $\overline{\binom{0}{2}}\,SN$ located in the bisector of first and third quadrants. Such a classification was done with respect to the normal form

$$\begin{aligned} \dot{x} &= gx^2 + 2hxy + (n-g-2h)y^2, \\ \dot{y} &= y + lx^2 + (2g+2h-2l-n)xy + (l-2g-2h+2n)y^2, \end{aligned} \tag{5.1}$$

where g, h, l, and n are real parameters. The parameter space of this normal form is a four–dimensional space, which can be projectivized, as it was done in Artés, Rezende and Oliveira (2015) and the authors proved that all generic phenomena occur for $g = 1$. In the paper under discussion the authors used the Invariant Theory in order to construct and study their bifurcation diagram. In Lemma 5.5 from the book Artés *et al.* (2021) the authors proved that a necessary and sufficient condition for a generic quadratic system to possess an infinite saddle–node of type $\overline{\binom{0}{2}}\,SN$ and another simple infinite singularity is that the comitants η and $\widetilde{M}$ verify the conditions

$$\eta = 0, \quad \widetilde{M} \neq 0,$$

for all the possible values of the parameters of the system. Additionally, in Table 5.1 from that book the authors present the invariant polynomials which are responsible for the number, kinds (real or/and complex), and multiplicities of finite singularities of a generic quadratic system. In particular, they show that if the invariant polynomial $\mathbb{D}$ verifies the condition

$$\mathbb{D} = 0,$$

then we have a finite singularity of multiplicity at least two. In fact, for systems (5.1) calculations show that these systems verify such conditions, since for that normal form (with $g=1$) we obtain

$$\eta = 0, \quad \widetilde{M} = -8(1+2h+l-n)^2(x-y)^2 \neq 0, \quad \mathbb{D} = 0.$$

Now, for $g=1$, consider the perturbation of systems (5.1)

$$\begin{aligned} \dot{x} &= (1-\varepsilon)x^2 + 2hxy + (n-1-2h)y^2, \\ \dot{y} &= y + l(1-\varepsilon)x^2 + ((2+2h-n)(1-\varepsilon) - 2l)xy + (l-2-2h+2n)y^2, \end{aligned} \tag{5.2}$$

where $|\varepsilon|$ is small enough. For these systems, calculations show that

$$\eta = 4\varepsilon((1+2h+l-n)^2 - (-1-2h+n)^2\varepsilon)^2 \neq 0, \quad \mathbb{D} = 0.$$

So, according to Lemma 5.5 from the mentioned book, we have three distinct infinite singularities (all of them are real if $\varepsilon > 0$ and, if $\varepsilon < 0$, we have one real infinite singularity and two complex ones). Additionally, as $\mathbb{D} = 0$, perturbation (5.2) leaves unperturbed the finite saddle–node.

On the other hand, for $g=1$ consider the perturbation of systems (5.1)

$$\begin{aligned} \dot{x} &= -\varepsilon + x^2 + 2hxy + (n-1-2h)y^2, \\ \dot{y} &= -\varepsilon l + y + lx^2 + (2+2h-2l-n)xy + (l-2-2h+2n)y^2, \end{aligned} \tag{5.3}$$

where $|\varepsilon|$ is small enough. For systems (5.3) we have

$$\eta = 0, \quad \widetilde{M} = -8(1+2h+l-n)^2(x-y)^2 \neq 0,$$

and

$$\mathbb{D} = -768\varepsilon(-1+(2(1+h)(-1+l)+n)^2\varepsilon)^2(1+2h+h^2-n+n^2((-1+l)(1+2h+l)+n)\varepsilon).$$

According to Lemma 5.5 mentioned before, the perturbation (5.3) has not affected the infinite singular points and, according to Table 5.1 from the mentioned book, we no longer have finite multiple singularities, i.e. the perturbation splits the origin into two points (which are real or complex, depending on the sign of ε).

Therefore the result holds for the set (AB).

Now, consider the set (AC). A realizable phase portrait belongs to the set (AC) if and only if it has a finite saddle–node $\overline{sn}_{(2)}$ and an infinite saddle–node of type $\overline{\binom{1}{1}}SN$, obtained by the coalescence of a finite saddle (respectively, finite node) with an infinite node (respectively, infinite saddle). Remember that, as we discussed in page 26, the case in which the finite saddle–node is the finite singularity that coalesces with an infinite singularity will be considered in the future during the study of the set (CC). In Chap. 4 we classified the set

of all real quadratic polynomial differential systems with a finite semi–elemental saddle–node $\overline{sn}_{(2)}$ located at the origin of the plane and an infinite saddle–node of type $\overline{\binom{1}{1}}\,SN$. Such a classification was done with respect to the normal form (4.1), i.e.

$$\begin{aligned}\dot{x} &= cx + cy - cx^2 + 2hxy,\\ \dot{y} &= ex + ey - ex^2 + 2mxy,\end{aligned}$$

where c, h, e, and m are real parameters, with the (non–degeneracity) condition $eh \neq cm$. The parameter space of this normal form is a four–dimensional space, which can be projectivized, as it was done in that chapter where we proved that all generic phenomena occur for $h = 1$. In Lemma 5.2 from the book Artés *et al.* (2021) the authors proved that a necessary and sufficient condition for a generic quadratic system to possess an infinite saddle–node of type $\overline{\binom{1}{1}}\,SN$ is that the comitants μ_0 and μ_1 verify the conditions

$$\mu_0 = 0, \quad \mu_1 \neq 0,$$

for all the possible values of the parameters of the system. Additionally, as in the previous case, from Table 5.1 it is possible to conclude that if the invariant polynomial $\mathbb{D}$ verifies the condition

$$\mathbb{D} = 0,$$

then we have a finite singularity of multiplicity at least two. Indeed, for systems (4.1) with $h = 1$ calculations show that such conditions are fulfilled, since

$$\mu_0 = 0, \quad \mu_1 = -8(e - cm)^2 x \neq 0, \quad \mathbb{D} = 0.$$

Now, for $h = 1$, consider the perturbation of systems (4.1)

$$\begin{aligned}\dot{x} &= cx + cy - cx^2 + 2xy + \varepsilon y^2,\\ \dot{y} &= ex + ey - ex^2 + 2mxy + \varepsilon y^2,\end{aligned} \tag{5.4}$$

where $|\varepsilon|$ is small enough, calculations show that for systems (5.4) the comitant μ_0 is given by

$$\mu_0 = \varepsilon(-4(1 - m)(e - cm) + (c - e)^2\varepsilon).$$

So the perturbation under consideration splits the infinite saddle–node $\overline{\binom{1}{1}}\,SN$. Additionally, we conclude that the perturbation maintains the finite saddle–node, since for systems (5.4) calculations show that the invariant polynomial $\mathbb{D}$ vanishes.

Finally, for $h = 1$ (as we did for the set (AB)), consider the perturbation of systems (4.1)

$$\begin{aligned}\dot{x} &= -\varepsilon + cx + cy - cx^2 + 2xy,\\ \dot{y} &= -\varepsilon e + ex + ey - ex^2 + 2mxy,\end{aligned} \tag{5.5}$$

where $|\varepsilon|$ is small enough. For systems (5.5) we have

$$\mu_0 = 0, \quad \mu_1 = -4(e - cm)^2 x \neq 0,$$

and

$$\begin{aligned}\mathbb{D} =& 768\varepsilon(e-cm)^3\left(16\varepsilon^2(e-m)^3-8(c-1)e(e-cm)^2\right)\\ &+768\varepsilon^2(e-cm)^4\left((9c(3c-2)-13)e^2+4(11-9c)em-4m^2\right).\end{aligned}$$

According to the results (from the book Artés *et al.* (2021)) presented before, we conclude that systems (5.5) have the infinite saddle–node $\overline{\binom{1}{1}}SN$ and do not have the finite saddle–node $\overline{sn}_{(2)}$, i.e. the perturbation (5.5) of systems (4.1) keeps the infinite saddle–node and splits the finite saddle–node.

Then the theorem also holds for the set (AC), as we wanted to prove.

□

In Artés, Mota and Rezende (2021c) the authors present a conjecture, which is the general case of the previous theorem.

Conjecture 5.2.11. If one of the phase portraits of codimension k that bifurcates from a potential codimension $k+1$ phase portrait is not realizable, then this latter phase portrait is also not realizable.

Remark 5.2.12. In Qualitative Theory of Ordinary Differential Equations is quite common to use the term "perturbation" to denote an infinitesimal modification of the parameters of a system such that a different phase portrait bifurcates from it. In this thesis we use the term "evolution" in order to say that we "move a *codimension one** phase portrait to its border and detect which phase portraits are in the other side of this border", so with an evolution of a *codimension one** phase portrait we produce a *codimension two** phase portrait. In this sense we mean that we modify (in a continuous way) the first system inside the region of parameters in which it is defined up to the other side of the border of this region where we obtain a system having one codimension more. In a certain way, with this modification we are provoking an "evolution" of the first system. Note that we *contrast* "perturbation" with "evolution".

5.3 Proof of Thm. 5.1.1

In this section we present the proof of Thm. 5.1.1. More precisely, in Subsection 5.3.1 we obtain all the topologically potential phase portraits belonging to the set (AB) (we have 110 topologically distinct phase portraits) and we prove that 39 of them are impossible. In Subsec. 5.3.2 we show the realization of each one of the remaining 71 phase portraits.

5.3.1 The topologically potential phase portraits

The main goal of this subsection is to obtain all the topologically potential phase portraits from the set (AB).

We already know that in the set (AB), the unstable objects of *codimension two** belong to the set of saddle–nodes $\left\{\overline{sn}_{(2)}+\overline{\binom{0}{2}}\,SN\right\}$. Considering all the different ways of obtaining phase portraits belonging to the set (AB) of *codimension two**, we have to consider all the possible ways of coalescing specific singular points in both sets (A) and (B). However, as the sets (AB) and (BA) are the same (i.e. their elements are obtained independently of the order of the evolution in the elements of the sets (A) or (B)), it is necessary to consider only all the possible ways of obtaining an infinite saddle–node of type $\overline{\binom{0}{2}}\,SN$ in each element from the set (A) (phase portraits possessing a finite saddle–node $\overline{sn}_{(2)}$). Anyway, in order to make things clear, in page 295 we discuss briefly how do we should perform if we start by considering the set (B).

In order to obtain phase portraits from the set (AB) by starting our study from the set (A), we have to consider Thm. 5.2.7 and also Lemma 3.25 from Artés, Llibre and Rezende (2018) (regarding phase portraits from the set (B)) which we state as follows.

Lemma 5.3.1. Suppose that a polynomial vector field X of *codimension one** has an infinite saddle–node p of multiplicity two with $\rho_0 = (\partial P/\partial x + \partial Q/\partial y)_p \neq 0$ and first eigenvalue equal to zero.

(a) Any perturbation of X in a sufficiently small neighborhood of this point will produce a structurally stable system (with one infinite saddle and one infinite node, or with no singular points in the neighborhood) or a system topologically equivalent to X.

(b) Both possibilities of structurally stable system (with one saddle and one node at infinity, or with no singular points in the neighborhood) are realizable.

Here we consider all 69 realizable structurally unstable quadratic vector fields of *codimension one** from the set (A). In order to obtain a phase portrait of *codimension two** belonging to the set (AB) starting from a phase portrait of *codimension one** of the set (A), we keep the existing finite saddle–node and using Lemma 5.3.1 we build an infinite saddle–node of type $\overline{\binom{0}{2}}\,SN$ by the coalescence of an infinite saddle with an infinite node. On the other hand, from the phase portraits of *codimension two** from the set (AB), one can obtain phase portraits of *codimension one** belonging to the set (A) after perturbation of the infinite saddle–node $\overline{\binom{0}{2}}\,SN$ into an infinite saddle and an infinite node, or into complex singularities.

In what follows we denote by $\mathbb{U}^2_{AB,k}$, where $\mathbb{U}^2_{AB}$ stands for structurally unstable quadratic vector field of *codimension two** from the set (AB) and $k \in \{1,\ldots,71\}$. The

impossible phase portraits will be denoted by $\mathbb{U}^{2,I}_{AB,j}$, where $\mathbb{U}^{2,I}_{AB}$ stands for *Impossible of codimension two* from the set (AB)* and $j \in \mathbb{N}$. We need to enumerate also the impossible phase portraits, not for the completeness of this classification, but for the future studies in which someone will study *codimension three** families. Just in the same way as impossible *codimension one** phase portraits are a crucial tool for the study of our families.

Note that phase portraits $\mathbb{U}^1_{A,1}$ to $\mathbb{U}^1_{A,13}$ cannot have a phase portrait possessing an infinite saddle–node of type $\overline{\binom{0}{2}}\,SN$ as an evolution, since each one of them has only one infinite singularity. Analogously, phase portraits $\mathbb{U}^1_{A,14}$ to $\mathbb{U}^1_{A,18}$ cannot have a phase portrait possessing an infinite saddle–node of type $\overline{\binom{0}{2}}\,SN$ as an evolution, since each one of them has three infinite singularities (which are nodes).

Phase portrait $\mathbb{U}^1_{A,19}$ has phase portraits $\mathbb{U}^2_{AB,1}$ and $\mathbb{U}^2_{AB,2}$ as evolution (see Fig. 115, where the arrows starting from the phase portrait $\mathbb{U}^1_{A,19}$ and pointing towards the phase portraits $\mathbb{U}^2_{AB,1}$ and $\mathbb{U}^2_{AB,2}$ indicate that these last two phase portraits are evolution of the phase portrait $\mathbb{U}^1_{A,19}$). After bifurcation we get phase portrait $\mathbb{U}^1_{A,1}$, in both cases, by making the infinite saddle–node $\overline{\binom{0}{2}}\,SN$ disappears (split into two complex singularities). In Fig. 115 we present the corresponding unfoldings on the right–hand side of the *codimension two** phase portraits.

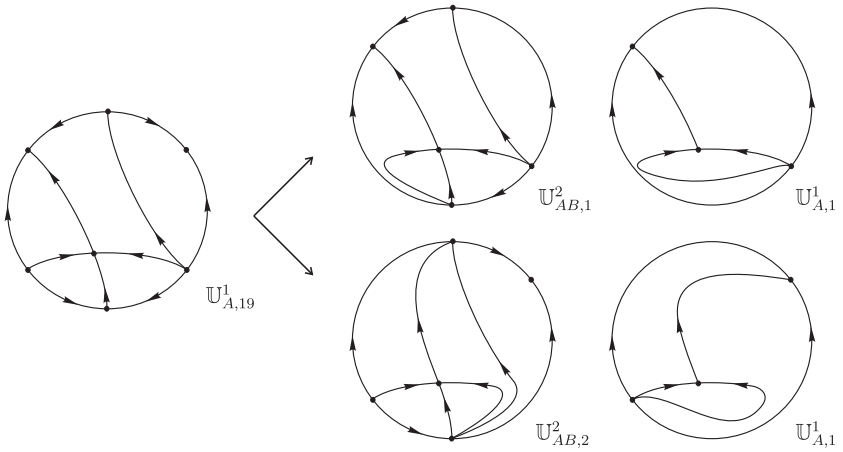

Figure 115 – Unstable systems $\mathbb{U}^2_{AB,1}$ and $\mathbb{U}^2_{AB,2}$

Note that $\mathbb{U}^1_{A,19}$ possesses two pairs of infinite nodes and only one pair of infinite saddles, so from $\mathbb{U}^1_{A,19}$ there are only two ways of obtaining a phase portrait possessing an infinite saddle–node of type $\overline{\binom{0}{2}}\,SN$, and these cases are represented exactly by the phase portraits $\mathbb{U}^2_{AB,1}$ and $\mathbb{U}^2_{AB,2}$ from Fig. 115. From now on, we will always omit the proof of the nonexistence of other cases apart from those ones that we discuss by words or by presenting in figures, since the argument of nonexistence is in general quite simple.

Before we continue with the study of the remaining *codimension one** phase portraits, we highlight that it is very important to have the "structure" of all the figures very well understood, since the proofs of Thm. 5.1.1 and Thm. 5.1.2 require and are done

based on several figures. So, in this paragraph we discuss about it. In the next cases, when from a *codimension one** phase portrait we have more than one *codimension two** phase portraits which are evolution of the *codimension one** phase portrait, we will present figures with the same "structure" of Fig. 115. More precisely, all the arrows that appear starting from an unstable phase portrait of *codimension one** will have the same meaning as explained for Fig. 115, i.e., they will point towards the phase portraits of *codimension two** which are evolution of the respective *codimension one** phase portrait. Moreover, we will present the corresponding unfoldings on the right–hand side of the *codimension two** phase portraits. On the other hand, when from a *codimension one** phase portrait we have only one *codimension two** phase portrait which is an evolution of the *codimension one** phase portrait, we will present figures like Fig. 121, for instance, where on the left–hand side we have a *codimension one** phase portrait, on the center we have the corresponding *codimension two** phase portrait and on the right–hand side we have the respective unfolding of the *codimension two** phase portrait.

Phase portrait $\mathbb{U}^1_{A,20}$ has phase portraits $\mathbb{U}^2_{AB,3}$ and $\mathbb{U}^2_{AB,4}$ as evolution (see Fig. 116). After bifurcation we get phase portrait $\mathbb{U}^1_{A,1}$, in both cases, by making the infinite saddle–node $\overline{\binom{0}{2}}\,SN$ disappears.

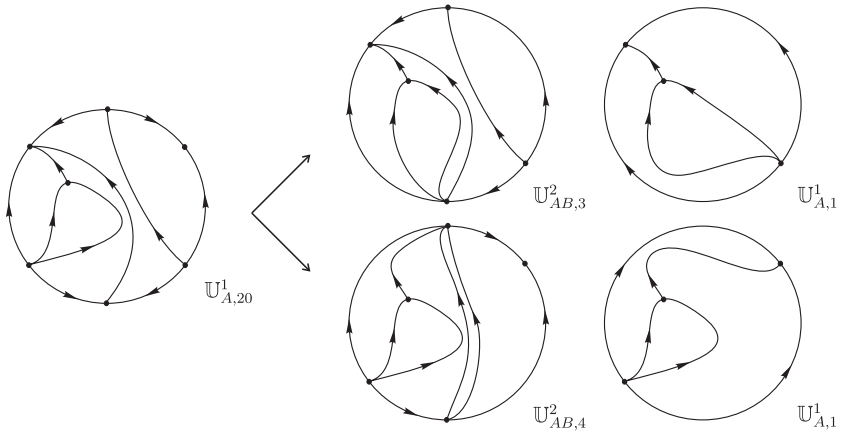

Figure 116 – Unstable systems $\mathbb{U}^2_{AB,3}$ and $\mathbb{U}^2_{AB,4}$

Phase portrait $\mathbb{U}^1_{A,21}$ has phase portraits $\mathbb{U}^2_{AB,5}$ and $\mathbb{U}^2_{AB,6}$ as evolution (see Fig. 117). After bifurcation we get phase portrait $\mathbb{U}^1_{A,1}$, in both cases, by making the infinite saddle–node $\overline{\binom{0}{2}}\,SN$ disappears.

Phase portrait $\mathbb{U}^1_{A,22}$ has phase portraits $\mathbb{U}^2_{AB,7}$ and $\mathbb{U}^2_{AB,8}$ as evolution (see Fig. 118). After bifurcation we get phase portrait $\mathbb{U}^1_{A,2}$, in both cases, by making the infinite saddle–node $\overline{\binom{0}{2}}\,SN$ disappears.

Phase portrait $\mathbb{U}^1_{A,23}$ has phase portraits $\mathbb{U}^2_{AB,9}$ and $\mathbb{U}^2_{AB,10}$ as evolution (see Fig. 119). After bifurcation we get phase portrait $\mathbb{U}^1_{A,3}$, in both cases, by making the infinite saddle–node $\overline{\binom{0}{2}}\,SN$ disappears.

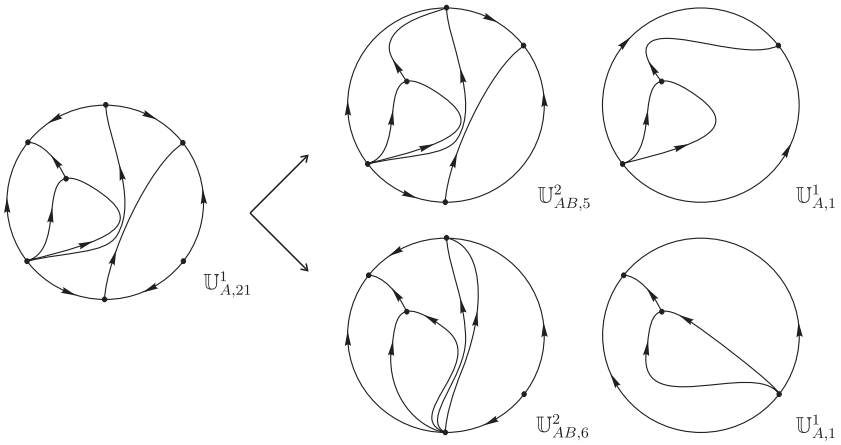

Figure 117 – Unstable systems $\mathbb{U}^2_{AB,5}$ and $\mathbb{U}^2_{AB,6}$

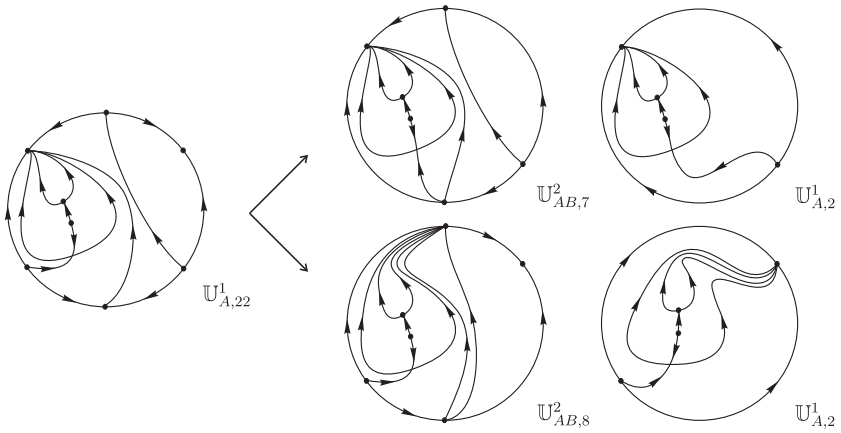

Figure 118 – Unstable systems $\mathbb{U}^2_{AB,7}$ and $\mathbb{U}^2_{AB,8}$

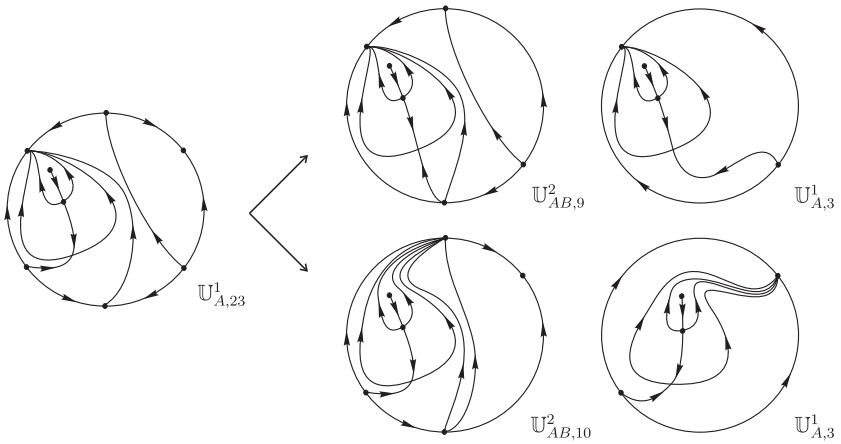

Figure 119 – Unstable systems $\mathbb{U}^2_{AB,9}$ and $\mathbb{U}^2_{AB,10}$

Phase portrait $\mathbb{U}^1_{A,24}$ has phase portraits $\mathbb{U}^2_{AB,11}$ and $\mathbb{U}^2_{AB,12}$ as evolution (see Fig. 120). After bifurcation we get phase portrait $\mathbb{U}^1_{A,4}$, in both cases, by making the infinite saddle–node $\overline{\binom{0}{2}}\,SN$ disappears.

Phase portrait $\mathbb{U}^1_{A,25}$ has phase portrait $\mathbb{U}^2_{AB,13}$ as an evolution (see Fig. 121). Af-

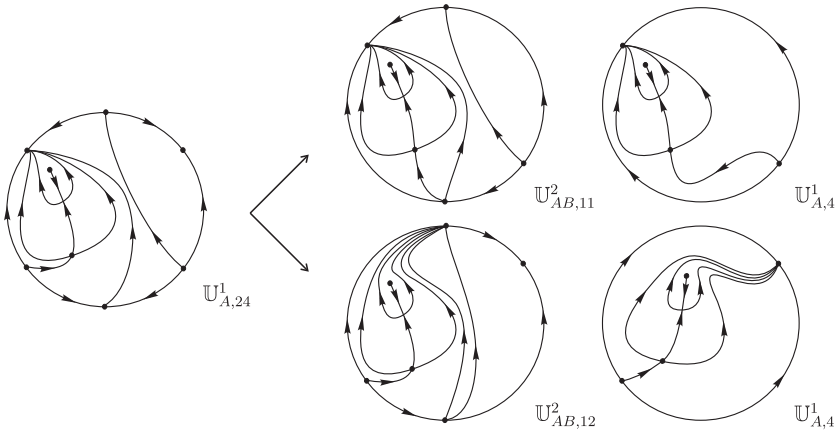

Figure 120 – Unstable systems $\mathbb{U}^2_{AB,11}$ and $\mathbb{U}^2_{AB,12}$

ter bifurcation we get phase portrait $\mathbb{U}^1_{A,5}$, by making the infinite saddle–node $\overline{\binom{0}{2}}$ *SN* disappears. Moreover, $\mathbb{U}^1_{A,25}$ has the impossible phase portrait $\mathbb{U}^{2,I}_{AB,1}$ as an evolution. By Thm. 5.2.10 such a phase portrait is impossible because by splitting the original finite saddle–node into a saddle and a node we obtain the impossible phase portrait $\mathbb{U}^{1,I}_{B,107}$ of *codimension one**, see Fig. 122. We observe that, in the set (A), $\mathbb{U}^{2,I}_{AB,1}$ unfolds in $\mathbb{U}^1_{A,5}$.

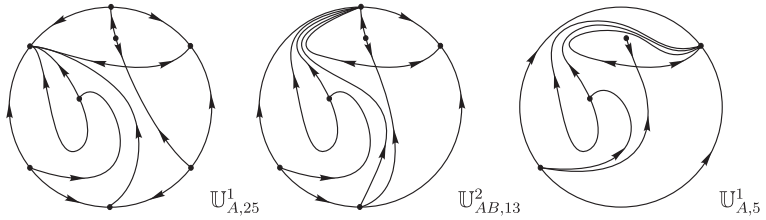

Figure 121 – Unstable system $\mathbb{U}^2_{AB,13}$

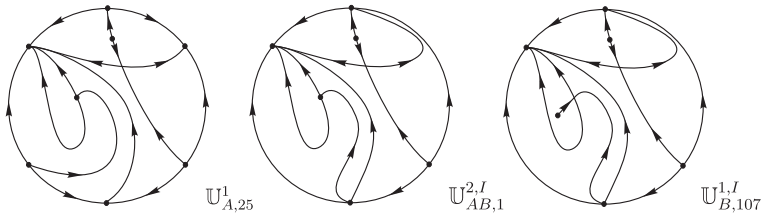

Figure 122 – Impossible unstable phase portrait $\mathbb{U}^{2,I}_{AB,1}$

Phase portrait $\mathbb{U}^1_{A,26}$ has phase portrait $\mathbb{U}^2_{AB,14}$ as an evolution (see Fig. 123). After bifurcation we get phase portrait $\mathbb{U}^1_{A,5}$, by making the infinite saddle–node $\overline{\binom{0}{2}}$ *SN* disappears. Moreover, $\mathbb{U}^1_{A,26}$ has the impossible phase portrait $\mathbb{U}^{2,I}_{AB,2}$ as an evolution. By Thm. 5.2.10 such a phase portrait is impossible because by splitting the original finite saddle–node into a saddle and a node we obtain the impossible phase portrait $\mathbb{U}^{1,I}_{B,107}$ of *codimension one**, see Fig. 124. We observe that, in the set (A), $\mathbb{U}^{2,I}_{AB,2}$ unfolds in $\mathbb{U}^1_{A,5}$.

Phase portrait $\mathbb{U}^1_{A,27}$ has phase portrait $\mathbb{U}^2_{AB,15}$ as an evolution (see Fig. 125). After bifurcation we get phase portrait $\mathbb{U}^1_{A,2}$, by making the infinite saddle–node $\overline{\binom{0}{2}}$ *SN*

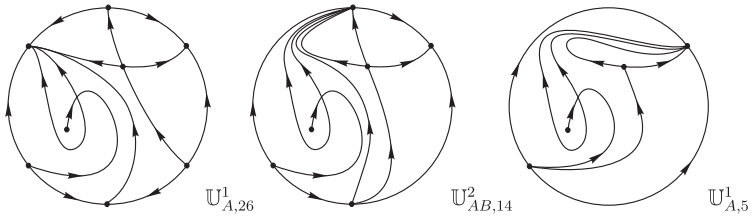

Figure 123 – Unstable system $\mathbb{U}^2_{AB,14}$

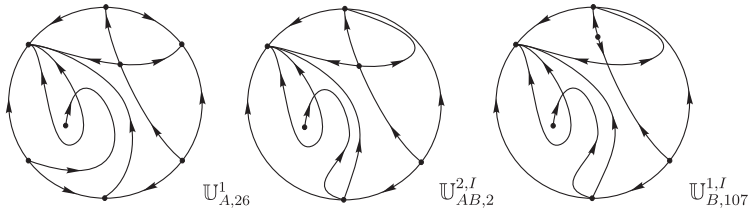

Figure 124 – Impossible unstable phase portrait $\mathbb{U}^{2,I}_{AB,2}$

disappears. Moreover, $\mathbb{U}^1_{A,27}$ has the impossible phase portrait $\mathbb{U}^{2,I}_{AB,3}$ as an evolution. By Thm. 5.2.10 such a phase portrait is impossible because by splitting the original finite saddle–node into a saddle and a node we obtain the impossible phase portrait $\mathbb{U}^{1,I}_{B,108}$ of *codimension one**, see Fig. 126. We observe that, in the set (A), $\mathbb{U}^{2,I}_{AB,3}$ unfolds in $\mathbb{U}^1_{A,2}$.

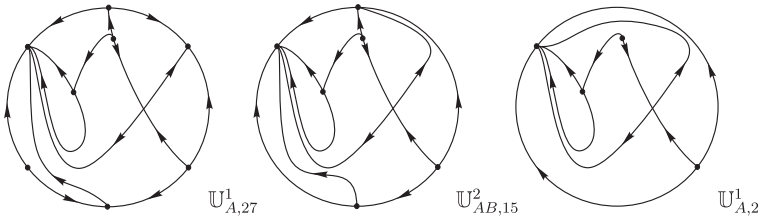

Figure 125 – Unstable system $\mathbb{U}^2_{AB,15}$

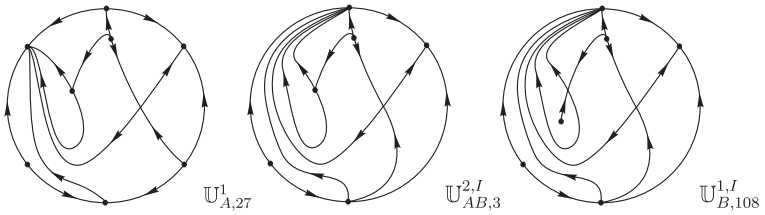

Figure 126 – Impossible unstable phase portrait $\mathbb{U}^{2,I}_{AB,3}$

Phase portrait $\mathbb{U}^1_{A,28}$ has phase portrait $\mathbb{U}^2_{AB,16}$ as an evolution (see Fig. 127). After bifurcation we get phase portrait $\mathbb{U}^1_{A,3}$, by making the infinite saddle–node $\overline{\binom{0}{2}}$ *SN* disappears. Moreover, $\mathbb{U}^1_{A,28}$ has the impossible phase portrait $\mathbb{U}^{2,I}_{AB,4}$ as an evolution. By Thm. 5.2.10 such a phase portrait is impossible because by splitting the original finite saddle–node into a saddle and a node we obtain the impossible phase portrait $\mathbb{U}^{1,I}_{B,108}$ of *codimension one**, see Fig. 128. We observe that, in the set (A), $\mathbb{U}^{2,I}_{AB,4}$ unfolds in $\mathbb{U}^1_{A,3}$.

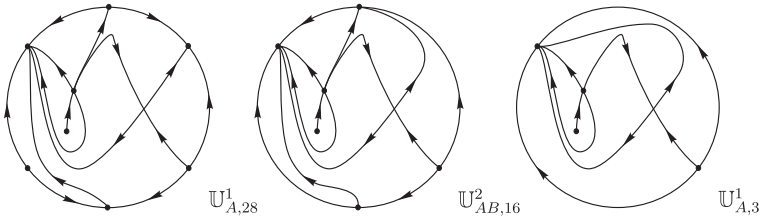

Figure 127 – Unstable system $\mathbb{U}^2_{AB,16}$

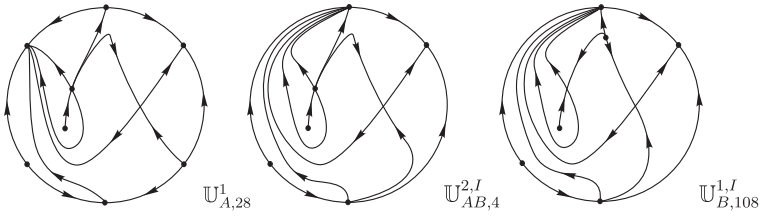

Figure 128 – Impossible unstable phase portrait $\mathbb{U}^{2,I}_{AB,4}$

Phase portrait $\mathbb{U}^1_{A,29}$ has phase portrait $\mathbb{U}^2_{AB,17}$ as an evolution (see Fig. 129). After bifurcation we get phase portrait $\mathbb{U}^1_{A,5}$, by making the infinite saddle–node $\overline{\binom{0}{2}}$ *SN* disappears. Moreover, $\mathbb{U}^1_{A,29}$ has the impossible phase portrait $\mathbb{U}^{2,I}_{AB,5}$ as an evolution. By Thm. 5.2.10 such a phase portrait is impossible because by splitting the original finite saddle–node into a saddle and a node we obtain the impossible phase portrait $\mathbb{U}^{1,I}_{B,109}$ of *codimension one**, see Fig. 130. We observe that, in the set (A), $\mathbb{U}^{2,I}_{AB,5}$ unfolds in $\mathbb{U}^1_{A,5}$.

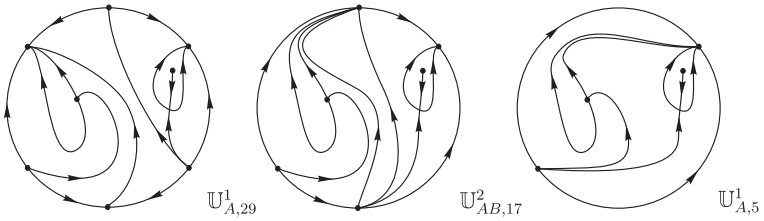

Figure 129 – Unstable system $\mathbb{U}^2_{AB,17}$

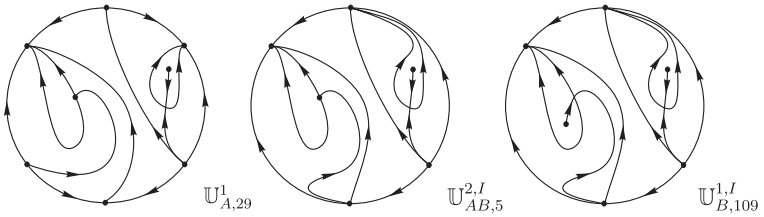

Figure 130 – Impossible unstable phase portrait $\mathbb{U}^{2,I}_{AB,5}$

Phase portrait $\mathbb{U}^1_{A,30}$ has phase portrait $\mathbb{U}^2_{AB,18}$ as an evolution (see Fig. 131). After bifurcation we get phase portrait $\mathbb{U}^1_{A,5}$, by making the infinite saddle–node $\overline{\binom{0}{2}}$ *SN* disappears. Moreover, $\mathbb{U}^1_{A,30}$ has the impossible phase portrait $\mathbb{U}^{2,I}_{AB,6}$ as an evolution. By Thm. 5.2.10 such a phase portrait is impossible because by splitting the original finite

saddle–node into a saddle and a node we obtain the impossible phase portrait $\mathbb{U}^{1,I}_{B,109}$ of *codimension one**, see Fig. 132. We observe that, in the set (A), $\mathbb{U}^{2,I}_{AB,6}$ unfolds in $\mathbb{U}^{1}_{A,5}$.

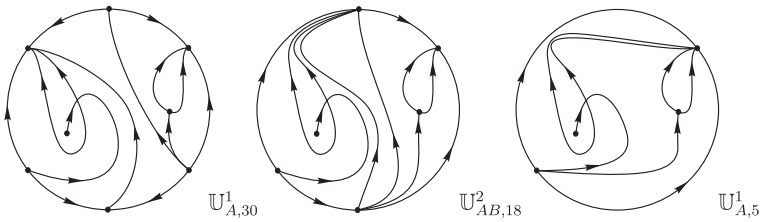

Figure 131 – Unstable system $\mathbb{U}^{2}_{AB,18}$

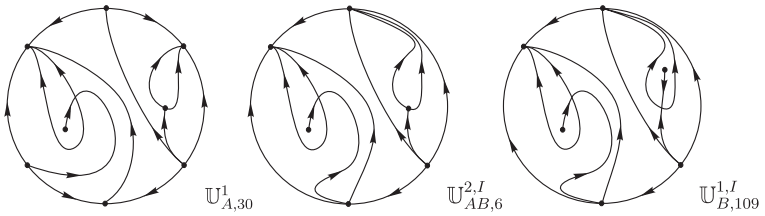

Figure 132 – Impossible unstable phase portrait $\mathbb{U}^{2,I}_{AB,6}$

Phase portrait $\mathbb{U}^{1}_{A,31}$ has phase portrait $\mathbb{U}^{2}_{AB,19}$ as an evolution (see Fig. 133). After bifurcation we get phase portrait $\mathbb{U}^{1}_{A,2}$, by making the infinite saddle–node $\overline{\binom{0}{2}}$ *SN* disappears. Moreover, $\mathbb{U}^{1}_{A,31}$ has the impossible phase portrait $\mathbb{U}^{2,I}_{AB,7}$ as an evolution. By Thm. 5.2.10 such a phase portrait is impossible because by splitting the original finite saddle–node into a saddle and a node we obtain the impossible phase portrait $\mathbb{U}^{1,I}_{B,110}$ of *codimension one**, see Fig. 134. We observe that, in the set (A), $\mathbb{U}^{2,I}_{AB,7}$ unfolds in $\mathbb{U}^{1}_{A,2}$.

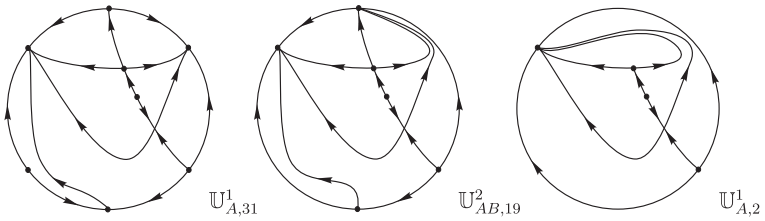

Figure 133 – Unstable system $\mathbb{U}^{2}_{AB,19}$

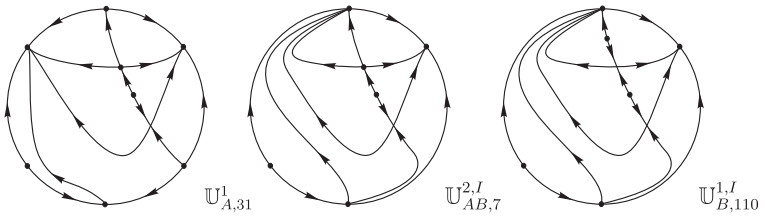

Figure 134 – Impossible unstable phase portrait $\mathbb{U}^{2,I}_{AB,7}$

Phase portrait $\mathbb{U}^{1}_{A,32}$ has phase portrait $\mathbb{U}^{2}_{AB,20}$ as an evolution (see Fig. 135). After bifurcation we get phase portrait $\mathbb{U}^{1}_{A,3}$, by making the infinite saddle–node $\overline{\binom{0}{2}}$ *SN*

disappears. Moreover, $\mathbb{U}^1_{A,32}$ has the impossible phase portrait $\mathbb{U}^{2,I}_{AB,8}$ as an evolution. By Thm. 5.2.10 such a phase portrait is impossible because by splitting the original finite saddle–node into a saddle and a node we obtain the impossible phase portrait $\mathbb{U}^{1,I}_{B,110}$ of *codimension one**, see Fig. 136. We observe that, in the set (A), $\mathbb{U}^{2,I}_{AB,8}$ unfolds in $\mathbb{U}^1_{A,3}$.

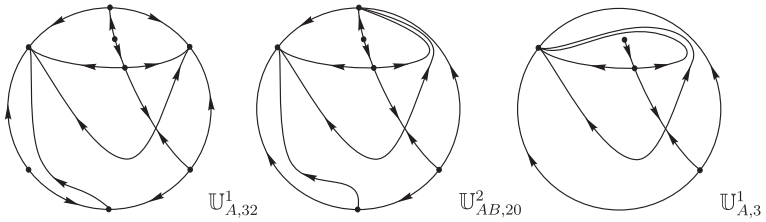

Figure 135 – Unstable system $\mathbb{U}^2_{AB,20}$

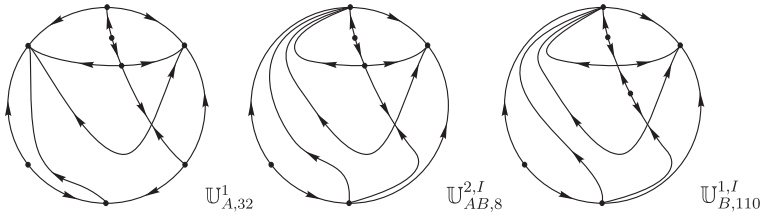

Figure 136 – Impossible unstable phase portrait $\mathbb{U}^{2,I}_{AB,8}$

Phase portrait $\mathbb{U}^1_{A,33}$ has phase portrait $\mathbb{U}^2_{AB,21}$ as an evolution (see Fig. 137). After bifurcation we get phase portrait $\mathbb{U}^1_{A,4}$, by making the infinite saddle–node $\overline{\binom{0}{2}}$ *SN* disappears. Moreover, $\mathbb{U}^1_{A,33}$ has the impossible phase portrait $\mathbb{U}^{2,I}_{AB,9}$ as an evolution. By Thm. 5.2.10 such a phase portrait is impossible because by splitting the original finite saddle–node into a saddle and a node we obtain the impossible phase portrait $\mathbb{U}^{1,I}_{B,110}$ of *codimension one**, see Fig. 138. We observe that, in the set (A), $\mathbb{U}^{2,I}_{AB,9}$ unfolds in $\mathbb{U}^1_{A,4}$.

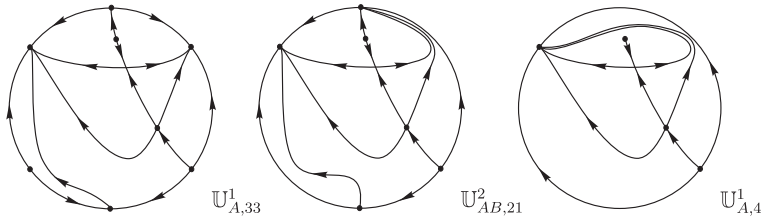

Figure 137 – Unstable system $\mathbb{U}^2_{AB,21}$

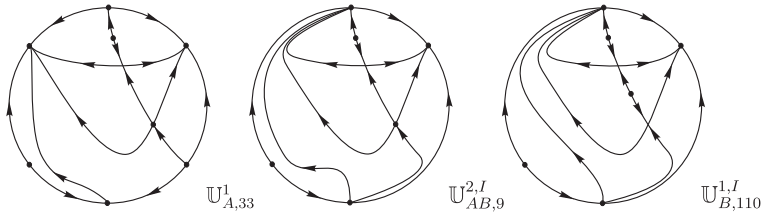

Figure 138 – Impossible unstable phase portrait $\mathbb{U}^{2,I}_{AB,9}$

Phase portrait $\mathbb{U}^1_{A,34}$ has phase portrait $\mathbb{U}^2_{AB,22}$ as an evolution (see Fig. 139). After bifurcation we get phase portrait $\mathbb{U}^1_{A,5}$, by making the infinite saddle–node $\binom{\overline{0}}{2}$ *SN* disappears. Moreover, $\mathbb{U}^1_{A,34}$ has the impossible phase portrait $\mathbb{U}^{2,I}_{AB,10}$ as an evolution. By Thm. 5.2.10 such a phase portrait is impossible because by splitting the original finite saddle–node into a saddle and a node we obtain the impossible phase portrait $\mathbb{U}^{1,I}_{B,111}$ of *codimension one**, see Fig. 140. We observe that, in the set (A), $\mathbb{U}^{2,I}_{AB,10}$ unfolds in $\mathbb{U}^1_{A,5}$.

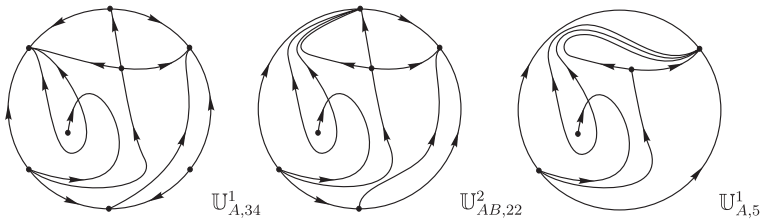

Figure 139 – Unstable system $\mathbb{U}^2_{AB,22}$

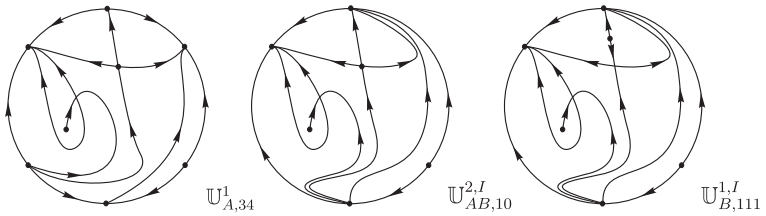

Figure 140 – Impossible unstable phase portrait $\mathbb{U}^{2,I}_{AB,10}$

Phase portrait $\mathbb{U}^1_{A,35}$ has phase portrait $\mathbb{U}^2_{AB,23}$ as an evolution (see Fig. 141). After bifurcation we get phase portrait $\mathbb{U}^1_{A,5}$, by making the infinite saddle–node $\binom{\overline{0}}{2}$ *SN* disappears. Moreover, $\mathbb{U}^1_{A,35}$ has the impossible phase portrait $\mathbb{U}^{2,I}_{AB,11}$ as an evolution. By Thm. 5.2.10 such a phase portrait is impossible because by splitting the original finite saddle–node into a saddle and a node we obtain the impossible phase portrait $\mathbb{U}^{1,I}_{B,111}$ of *codimension one**, see Fig. 142. We observe that, in the set (A), $\mathbb{U}^{2,I}_{AB,11}$ unfolds in $\mathbb{U}^1_{A,5}$.

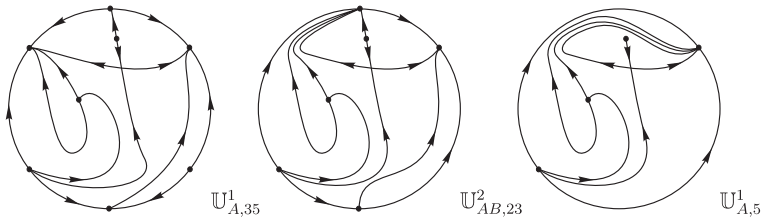

Figure 141 – Unstable system $\mathbb{U}^2_{AB,23}$

Phase portrait $\mathbb{U}^1_{A,36}$ has phase portraits $\mathbb{U}^2_{AB,24}$ and $\mathbb{U}^2_{AB,25}$ as evolution (see Fig. 143). After bifurcation we get phase portrait $\mathbb{U}^1_{A,9}$, in both cases, by making the infinite saddle–node $\binom{\overline{0}}{2}$ *SN* disappears.

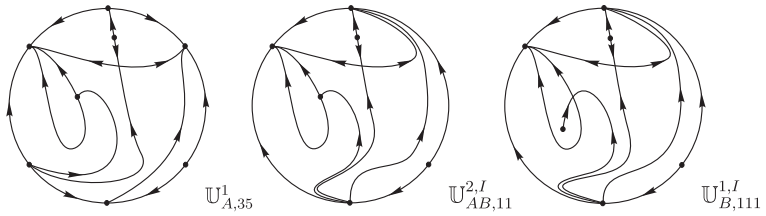

Figure 142 – Impossible unstable phase portrait $\mathbb{U}^{2,I}_{AB,11}$

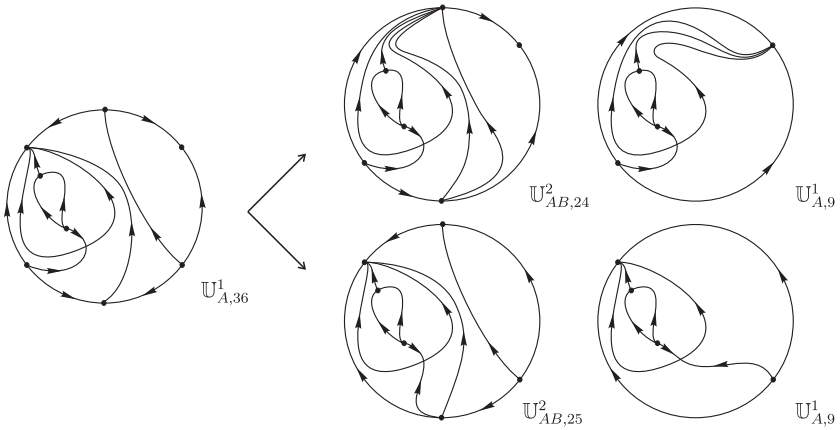

Figure 143 – Unstable systems $\mathbb{U}^2_{AB,24}$ and $\mathbb{U}^2_{AB,25}$

Phase portrait $\mathbb{U}^1_{A,37}$ has phase portraits $\mathbb{U}^2_{AB,26}$ and $\mathbb{U}^2_{AB,27}$ as evolution (see Fig. 144). After bifurcation we get phase portrait $\mathbb{U}^1_{A,10}$, in both cases, by making the infinite saddle–node $\overline{\binom{0}{2}}\,SN$ disappears.

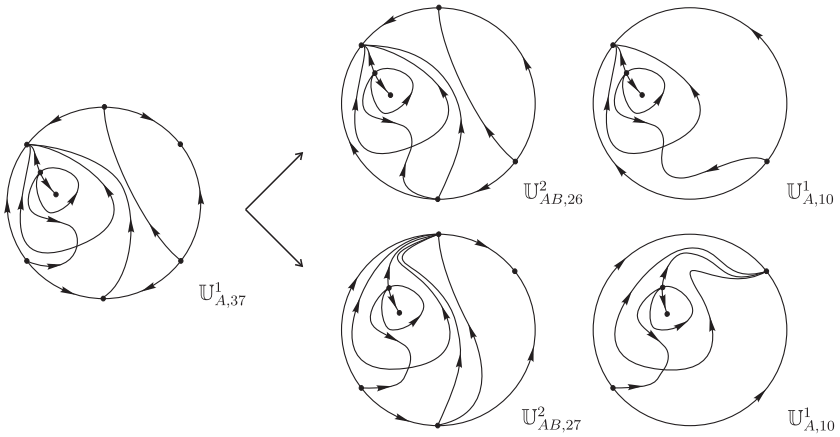

Figure 144 – Unstable systems $\mathbb{U}^2_{AB,26}$ and $\mathbb{U}^2_{AB,27}$

Phase portrait $\mathbb{U}^1_{A,38}$ has phase portraits $\mathbb{U}^2_{AB,28}$ and $\mathbb{U}^2_{AB,29}$ as evolution (see Fig. 145). After bifurcation we get phase portrait $\mathbb{U}^1_{A,8}$, in both cases, by making the infinite saddle–node $\overline{\binom{0}{2}}\,SN$ disappears.

Phase portrait $\mathbb{U}^1_{A,39}$ has phase portrait $\mathbb{U}^2_{AB,30}$ as an evolution (see Fig. 146). After bifurcation we get phase portrait $\mathbb{U}^1_{A,6}$, by making the infinite saddle–node $\overline{\binom{0}{2}}\,SN$ disappears. Moreover, $\mathbb{U}^1_{A,39}$ has the impossible phase portrait $\mathbb{U}^{2,I}_{AB,12}$ as an evolution. By

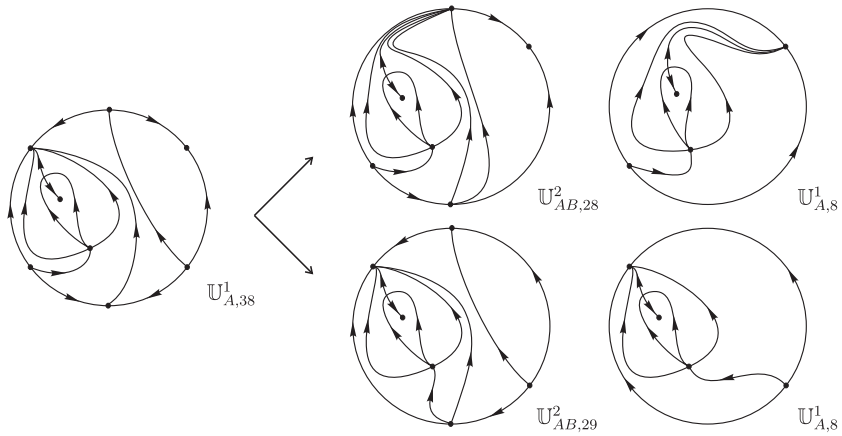

Figure 145 – Unstable systems $\mathbb{U}^2_{AB,28}$ and $\mathbb{U}^2_{AB,29}$

Thm. 5.2.10 such a phase portrait is impossible because by splitting the original finite saddle–node into a saddle and a node we obtain the impossible phase portrait $\mathbb{U}^{1,I}_{B,112}$ of *codimension one**, see Fig. 147. We observe that, in the set (A), $\mathbb{U}^{2,I}_{AB,12}$ unfolds in $\mathbb{U}^1_{A,6}$.

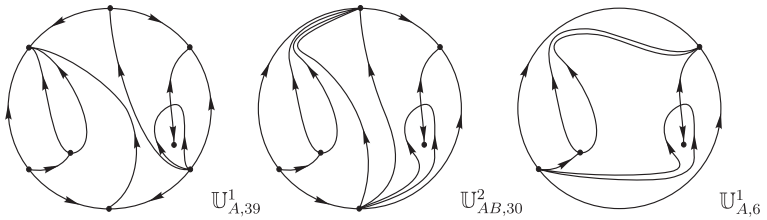

Figure 146 – Unstable system $\mathbb{U}^2_{AB,30}$

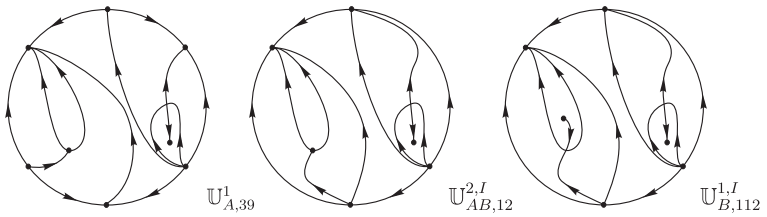

Figure 147 – Impossible unstable phase portrait $\mathbb{U}^{2,I}_{AB,12}$

Phase portrait $\mathbb{U}^1_{A,40}$ has phase portrait $\mathbb{U}^2_{AB,31}$ as an evolution (see Fig. 148). After bifurcation we get phase portrait $\mathbb{U}^1_{A,6}$, by making the infinite saddle–node $\binom{\overline{0}}{2}$ *SN* disappears. Moreover, $\mathbb{U}^1_{A,40}$ has the impossible phase portrait $\mathbb{U}^{2,I}_{AB,13}$ as an evolution. By Thm. 5.2.10 such a phase portrait is impossible because by splitting the original finite saddle–node into a saddle and a node we obtain the impossible phase portrait $\mathbb{U}^{1,I}_{B,113}$ of *codimension one**, see Fig. 149. We observe that, in the set (A), $\mathbb{U}^{2,I}_{AB,13}$ unfolds in $\mathbb{U}^1_{A,6}$.

Phase portrait $\mathbb{U}^1_{A,41}$ has phase portrait $\mathbb{U}^2_{AB,32}$ as an evolution (see Fig. 150). After bifurcation we get phase portrait $\mathbb{U}^1_{A,6}$, by making the infinite saddle–node $\binom{\overline{0}}{2}$ *SN* disappears. Moreover, $\mathbb{U}^1_{A,41}$ has the impossible phase portrait $\mathbb{U}^{2,I}_{AB,14}$ as an evolution. By Thm. 5.2.10 such a phase portrait is impossible because by splitting the original finite

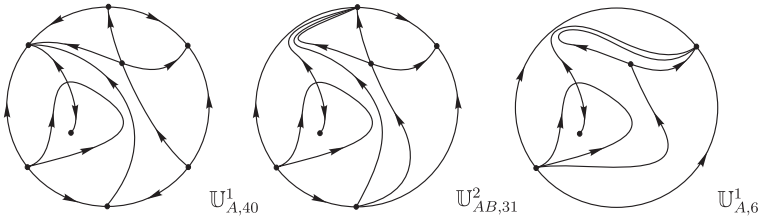

Figure 148 – Unstable system $\mathbb{U}^2_{AB,31}$

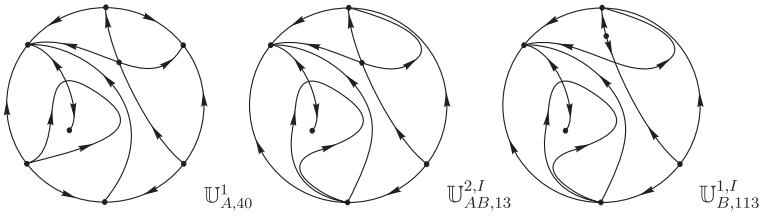

Figure 149 – Impossible unstable phase portrait $\mathbb{U}^{2,I}_{AB,13}$

saddle–node into a saddle and a node we obtain the impossible phase portrait $\mathbb{U}^{1,I}_{B,113}$ of *codimension one**, see Fig. 151. We observe that, in the set (A), $\mathbb{U}^{2,I}_{AB,14}$ unfolds in $\mathbb{U}^1_{A,6}$.

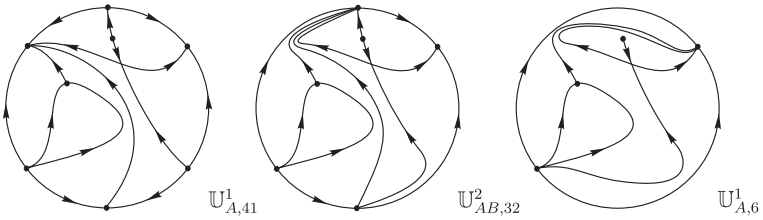

Figure 150 – Unstable system $\mathbb{U}^2_{AB,32}$

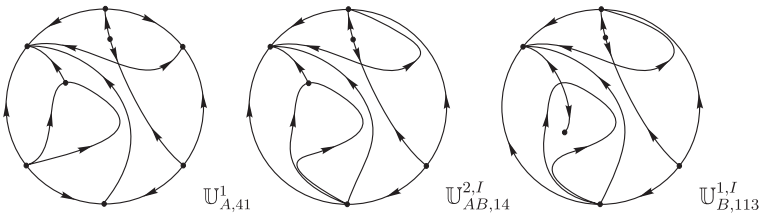

Figure 151 – Impossible unstable phase portrait $\mathbb{U}^{2,I}_{AB,14}$

Phase portrait $\mathbb{U}^1_{A,42}$ has phase portrait $\mathbb{U}^2_{AB,33}$ as an evolution (see Fig. 152). After bifurcation we get phase portrait $\mathbb{U}^1_{A,9}$, by making the infinite saddle–node $\overline{\binom{0}{2}}$ *SN* disappears. Moreover, $\mathbb{U}^1_{A,42}$ has the impossible phase portrait $\mathbb{U}^{2,I}_{AB,15}$ as an evolution. By Thm. 5.2.10 such a phase portrait is impossible because by splitting the original finite saddle–node into a saddle and a node we obtain the impossible phase portrait $\mathbb{U}^{1,I}_{B,114}$ of *codimension one**, see Fig. 153. We observe that, in the set (A), $\mathbb{U}^{2,I}_{AB,15}$ unfolds in $\mathbb{U}^1_{A,9}$.

Phase portrait $\mathbb{U}^1_{A,43}$ has phase portrait $\mathbb{U}^2_{AB,34}$ as an evolution (see Fig. 154). After bifurcation we get phase portrait $\mathbb{U}^1_{A,10}$, by making the infinite saddle–node $\overline{\binom{0}{2}}$ *SN*

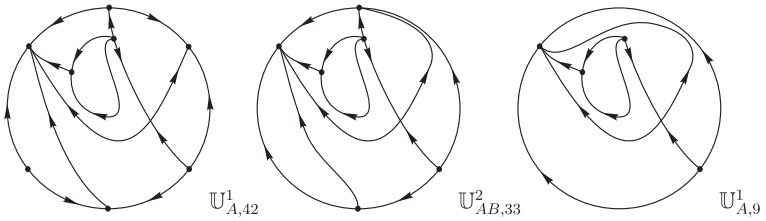

Figure 152 – Unstable system $\mathbb{U}^2_{AB,33}$

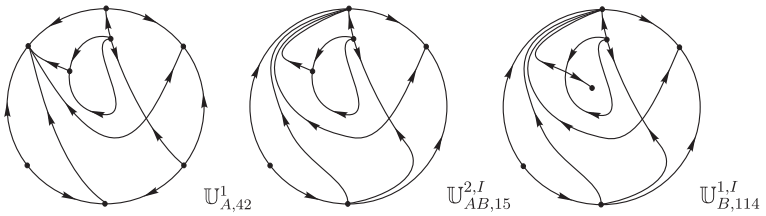

Figure 153 – Impossible unstable phase portrait $\mathbb{U}^{2,I}_{AB,15}$

disappears. Moreover, $\mathbb{U}^1_{A,43}$ has the impossible phase portrait $\mathbb{U}^{2,I}_{AB,16}$ as an evolution. By Thm. 5.2.10 such a phase portrait is impossible because by splitting the original finite saddle–node into a saddle and a node we obtain the impossible phase portrait $\mathbb{U}^{1,I}_{B,114}$ of *codimension one**, see Fig. 155. We observe that, in the set (A), $\mathbb{U}^{2,I}_{AB,16}$ unfolds in $\mathbb{U}^1_{A,10}$.

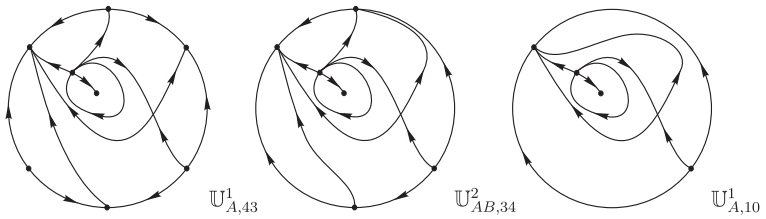

Figure 154 – Unstable system $\mathbb{U}^2_{AB,34}$

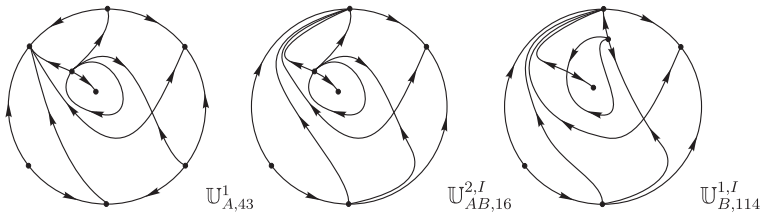

Figure 155 – Impossible unstable phase portrait $\mathbb{U}^{2,I}_{AB,16}$

Phase portrait $\mathbb{U}^1_{A,44}$ has phase portrait $\mathbb{U}^2_{AB,35}$ as an evolution (see Fig. 156). After bifurcation we get phase portrait $\mathbb{U}^1_{A,6}$, by making the infinite saddle–node $\overline{\binom{0}{2}}$ *SN* disappears. Moreover, $\mathbb{U}^1_{A,44}$ has the impossible phase portrait $\mathbb{U}^{2,I}_{AB,17}$ as an evolution. By Thm. 5.2.10 such a phase portrait is impossible because by splitting the original finite saddle–node into a saddle and a node we obtain the impossible phase portrait $\mathbb{U}^{1,I}_{B,115}$ of *codimension one**, see Fig. 157. We observe that, in the set (A), $\mathbb{U}^{2,I}_{AB,17}$ unfolds in $\mathbb{U}^1_{A,6}$.

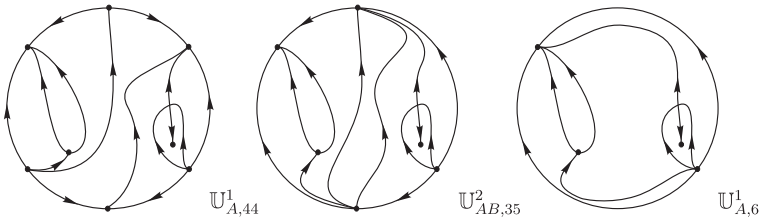

Figure 156 – Unstable system $\mathbb{U}^2_{AB,35}$

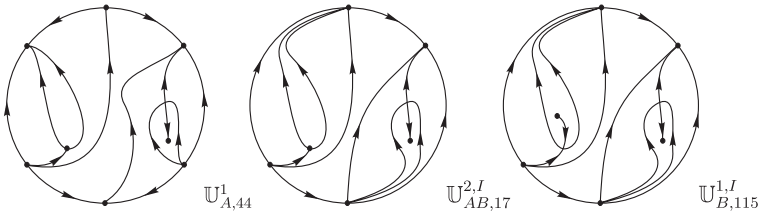

Figure 157 – Impossible unstable phase portrait $\mathbb{U}^{2,I}_{AB,17}$

Phase portrait $\mathbb{U}^1_{A,45}$ has phase portrait $\mathbb{U}^2_{AB,36}$ as an evolution (see Fig. 158). After bifurcation we get phase portrait $\mathbb{U}^1_{A,6}$, by making the infinite saddle–node $\overline{\binom{0}{2}}$ *SN* disappears. Moreover, $\mathbb{U}^1_{A,45}$ has the impossible phase portrait $\mathbb{U}^{2,I}_{AB,18}$ as an evolution. By Thm. 5.2.10 such a phase portrait is impossible because by splitting the original finite saddle–node into a saddle and a node we obtain the impossible phase portrait $\mathbb{U}^{1,I}_{B,116}$ of *codimension one**, see Fig. 159. We observe that, in the set (A), $\mathbb{U}^{2,I}_{AB,18}$ unfolds in $\mathbb{U}^1_{A,6}$.

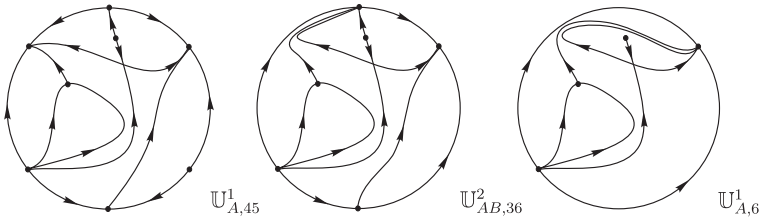

Figure 158 – Unstable system $\mathbb{U}^2_{AB,36}$

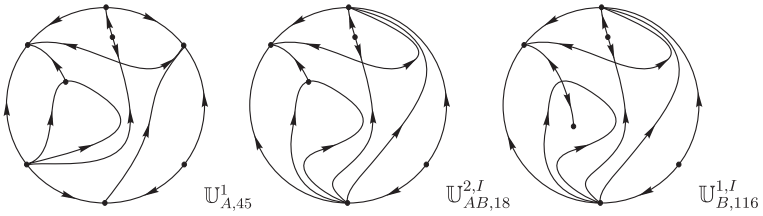

Figure 159 – Impossible unstable phase portrait $\mathbb{U}^{2,I}_{AB,18}$

Phase portrait $\mathbb{U}^1_{A,46}$ has phase portrait $\mathbb{U}^2_{AB,37}$ as an evolution (see Fig. 160). After bifurcation we get phase portrait $\mathbb{U}^1_{A,6}$, by making the infinite saddle–node $\overline{\binom{0}{2}}$ *SN* disappears. Moreover, $\mathbb{U}^1_{A,46}$ has the impossible phase portrait $\mathbb{U}^{2,I}_{AB,19}$ as an evolution. By Thm. 5.2.10 such a phase portrait is impossible because by splitting the original finite

saddle–node into a saddle and a node we obtain the impossible phase portrait $\mathbb{U}^{1,I}_{B,116}$ of *codimension one**, see Fig. 161. We observe that, in the set (A), $\mathbb{U}^{2,I}_{AB,19}$ unfolds in $\mathbb{U}^{1}_{A,6}$.

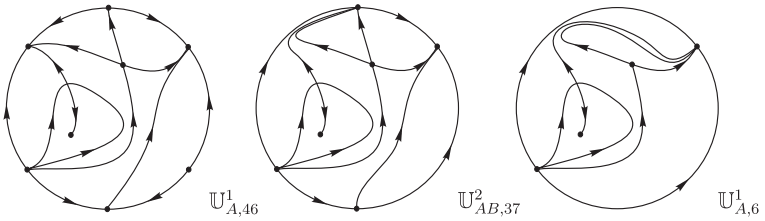

Figure 160 – Unstable system $\mathbb{U}^{2}_{AB,37}$

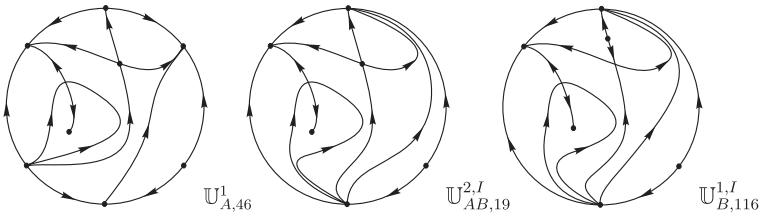

Figure 161 – Impossible unstable phase portrait $\mathbb{U}^{2,I}_{AB,19}$

Phase portrait $\mathbb{U}^{1}_{A,47}$ has phase portraits $\mathbb{U}^{2}_{AB,38}$ and $\mathbb{U}^{2}_{AB,39}$ as evolution (see Fig. 162). After bifurcation we get phase portrait $\mathbb{U}^{1}_{A,7}$, in both cases, by making the infinite saddle–node $\overline{\binom{0}{2}}\,SN$ disappears.

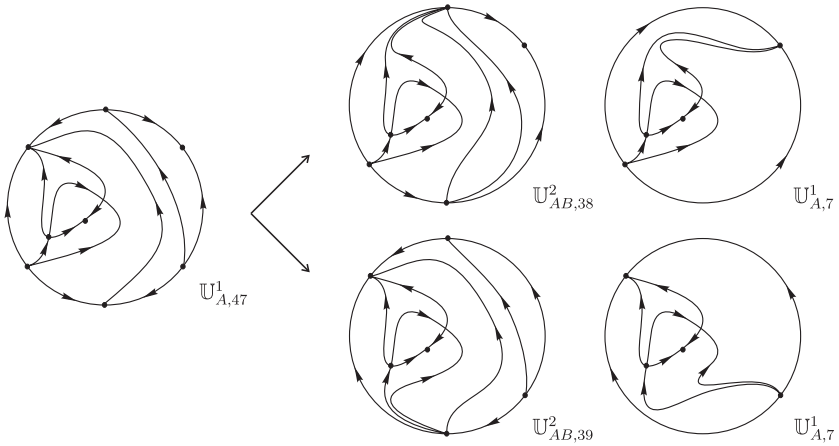

Figure 162 – Unstable systems $\mathbb{U}^{2}_{AB,38}$ and $\mathbb{U}^{2}_{AB,39}$

Phase portrait $\mathbb{U}^{1}_{A,48}$ has phase portraits $\mathbb{U}^{2}_{AB,40}$ and $\mathbb{U}^{2}_{AB,41}$ as evolution (see Fig. 163). After bifurcation we get phase portrait $\mathbb{U}^{1}_{A,7}$, in both cases, by making the infinite saddle–node $\overline{\binom{0}{2}}\,SN$ disappears.

Phase portrait $\mathbb{U}^{1}_{A,50}$ has phase portraits $\mathbb{U}^{2}_{AB,42}$ and $\mathbb{U}^{2}_{AB,43}$ as evolution (see Fig. 164). After bifurcation we get phase portrait $\mathbb{U}^{1}_{A,7}$, in both cases, by making the infinite saddle–node $\overline{\binom{0}{2}}\,SN$ disappears.

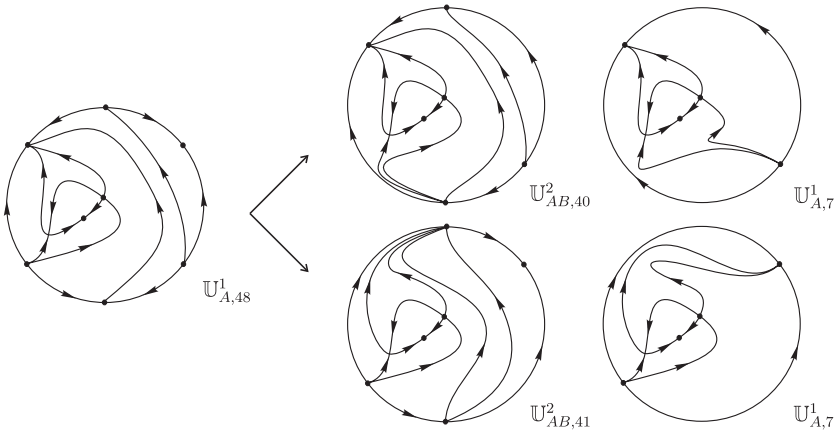

Figure 163 – Unstable systems $\mathbb{U}^2_{AB,40}$ and $\mathbb{U}^2_{AB,41}$

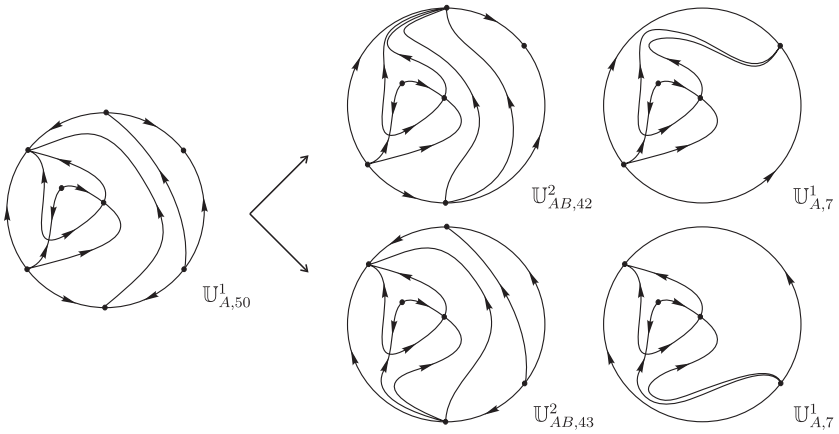

Figure 164 – Unstable systems $\mathbb{U}^2_{AB,42}$ and $\mathbb{U}^2_{AB,43}$

Phase portrait $\mathbb{U}^1_{A,51}$ has phase portraits $\mathbb{U}^2_{AB,44}$ and $\mathbb{U}^2_{AB,45}$ as evolution (see Fig. 165). After bifurcation we get phase portrait $\mathbb{U}^1_{A,7}$, in both cases, by making the infinite saddle–node $\overline{\binom{0}{2}}\,SN$ disappears.

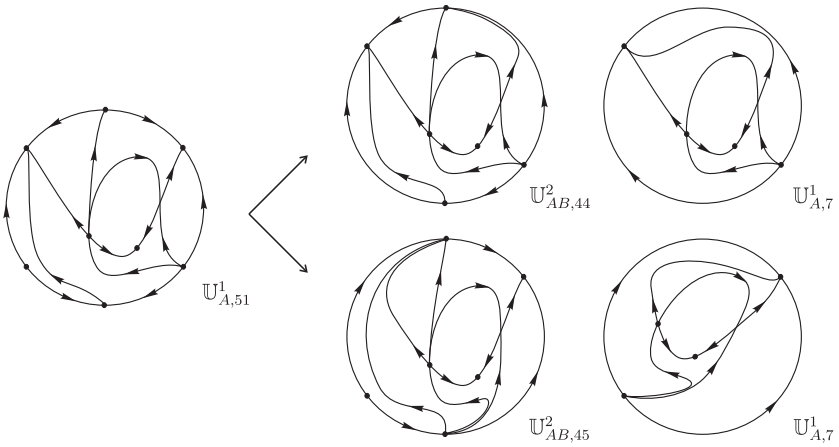

Figure 165 – Unstable systems $\mathbb{U}^2_{AB,44}$ and $\mathbb{U}^2_{AB,45}$

Phase portrait $\mathbb{U}^1_{A,52}$ has phase portraits $\mathbb{U}^2_{AB,46}$ and $\mathbb{U}^2_{AB,47}$ as evolution (see Fig. 166).

After bifurcation we get phase portrait $\mathbb{U}^1_{A,7}$, in both cases, by making the infinite saddle–node $\binom{\overline{0}}{2}$ *SN* disappears.

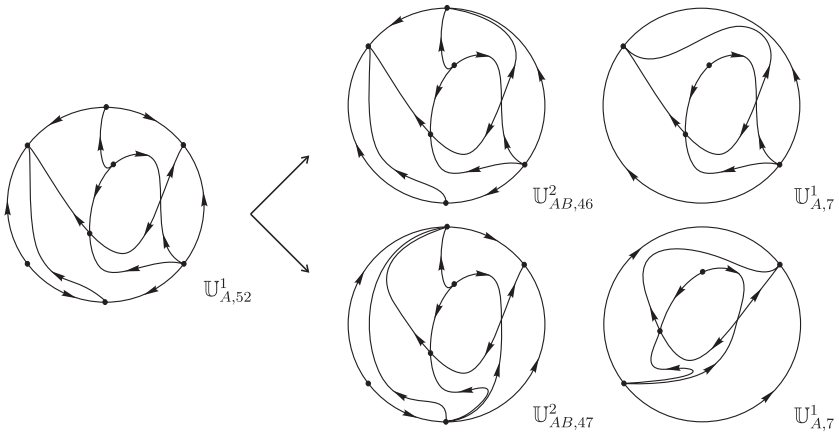

Figure 166 – Unstable systems $\mathbb{U}^2_{AB,46}$ and $\mathbb{U}^2_{AB,47}$

Phase portrait $\mathbb{U}^1_{A,53}$ has phase portraits $\mathbb{U}^2_{AB,48}$ and $\mathbb{U}^2_{AB,49}$ as evolution (see Fig. 167). After bifurcation we get phase portrait $\mathbb{U}^1_{A,7}$, in both cases, by making the infinite saddle–node $\binom{\overline{0}}{2}$ *SN* disappears.

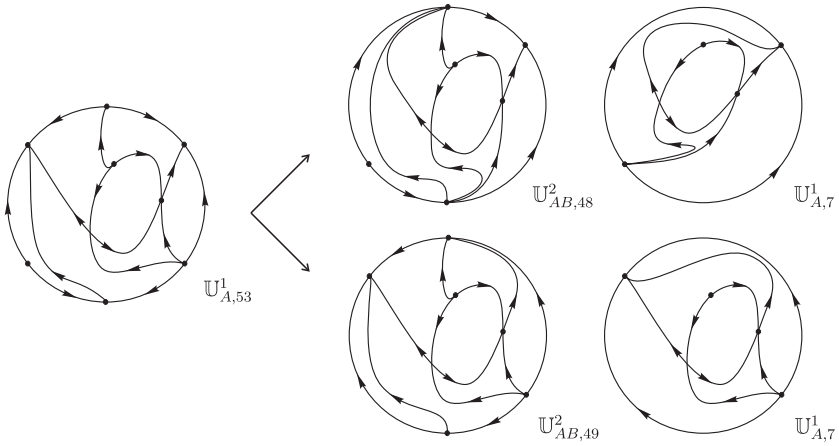

Figure 167 – Unstable systems $\mathbb{U}^2_{AB,48}$ and $\mathbb{U}^2_{AB,49}$

Phase portrait $\mathbb{U}^1_{A,54}$ has phase portrait $\mathbb{U}^2_{AB,50}$ as an evolution (see Fig. 168). After bifurcation we get phase portrait $\mathbb{U}^1_{A,6}$, by making the infinite saddle–node $\binom{\overline{0}}{2}$ *SN* disappears. Moreover, $\mathbb{U}^1_{A,54}$ has the impossible phase portrait $\mathbb{U}^{2,I}_{AB,20}$ as an evolution. By Thm. 5.2.10 such a phase portrait is impossible because by splitting the original finite saddle–node into a saddle and a node we obtain the impossible phase portrait $\mathbb{U}^{1,I}_{B,117}$ of *codimension one**, see Fig. 169. We observe that, in the set (A), $\mathbb{U}^{2,I}_{AB,20}$ unfolds in $\mathbb{U}^1_{A,6}$.

Phase portrait $\mathbb{U}^1_{A,55}$ has phase portraits $\mathbb{U}^2_{AB,51}$ and $\mathbb{U}^2_{AB,52}$ as evolution (see Fig. 170). After bifurcation we get phase portrait $\mathbb{U}^1_{A,7}$, in both cases, by making the infinite saddle–node $\binom{\overline{0}}{2}$ *SN* disappears.

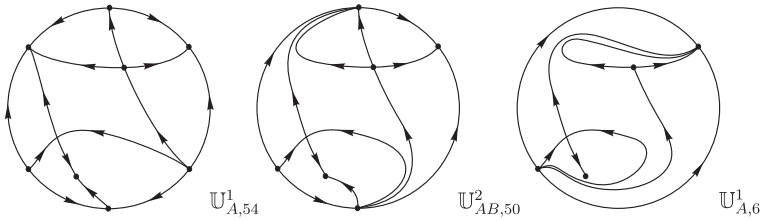

Figure 168 – Unstable system $\mathbb{U}^2_{AB,50}$

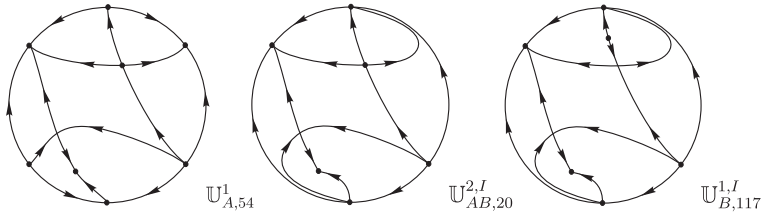

Figure 169 – Impossible unstable phase portrait $\mathbb{U}^{2,I}_{AB,20}$

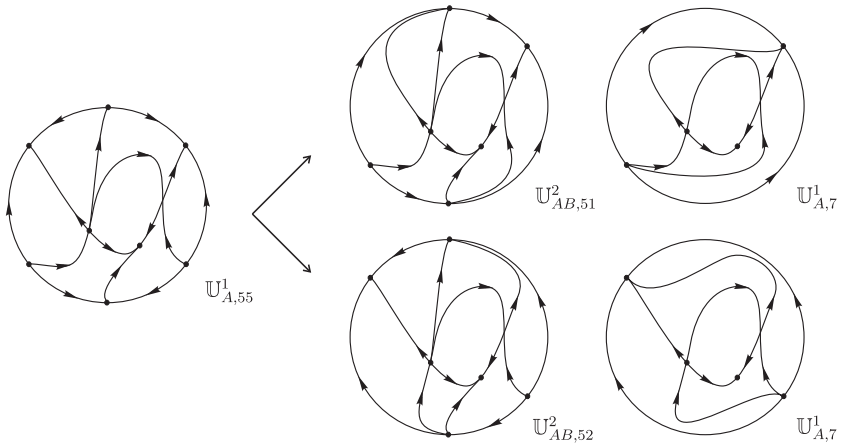

Figure 170 – Unstable systems $\mathbb{U}^2_{AB,51}$ and $\mathbb{U}^2_{AB,52}$

Phase portrait $\mathbb{U}^1_{A,56}$ has phase portrait $\mathbb{U}^2_{AB,53}$ as an evolution (see Fig. 171). After bifurcation we get phase portrait $\mathbb{U}^1_{A,11}$, modulo limit cycle, by making the infinite saddle–node $\binom{\overline{0}}{2}$ *SN* disappears. Moreover, $\mathbb{U}^1_{A,56}$ has the impossible phase portrait $\mathbb{U}^{2,I}_{AB,21}$ as an evolution. By Thm. 5.2.10 such a phase portrait is impossible because by splitting the original finite saddle–node into a saddle and a node we obtain the impossible phase portrait $\mathbb{U}^{1,I}_{B,4}$ of *codimension one**, see Fig. 172. We observe that, in the set (A), $\mathbb{U}^{2,I}_{AB,21}$ also unfolds in an impossible phase portrait because after bifurcation we would get a limit cycle surrounding more than one finite singular points, and this is not possible in quadratic systems (see Lemma 3.14 from Artés, Llibre and Rezende (2018)).

Phase portrait $\mathbb{U}^1_{A,57}$ has phase portrait $\mathbb{U}^2_{AB,54}$ as an evolution (see Fig. 173). After bifurcation we get phase portrait $\mathbb{U}^1_{A,12}$, modulo limit cycle, by making the infinite saddle–node $\binom{\overline{0}}{2}$ *SN* disappears. Moreover, $\mathbb{U}^1_{A,57}$ has the impossible phase portrait $\mathbb{U}^{2,I}_{AB,22}$ as an evolution. By Thm. 5.2.10 such a phase portrait is impossible because by splitting the

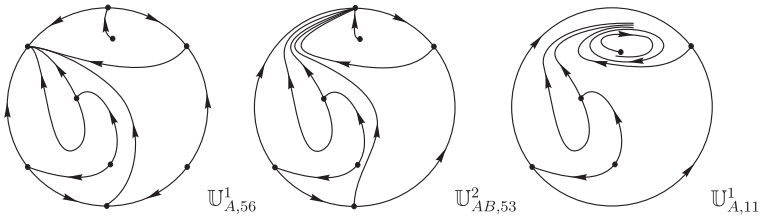

Figure 171 – Unstable system $\mathbb{U}^2_{AB,53}$

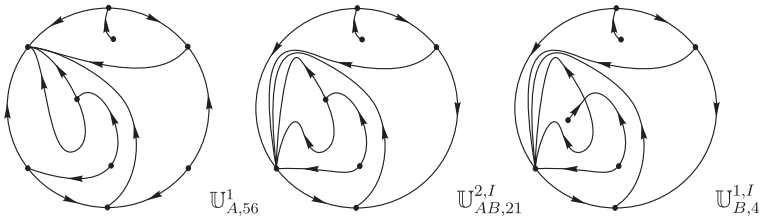

Figure 172 – Impossible unstable phase portrait $\mathbb{U}^{2,I}_{AB,21}$

original finite saddle–node into a saddle and a node we obtain the impossible phase portrait $\mathbb{U}^{1,I}_{B,4}$ of *codimension one**, see Fig. 174. We observe that, in the set (A), $\mathbb{U}^{2,I}_{AB,22}$ also unfolds in an impossible phase portrait, as in $\mathbb{U}^{2,I}_{AB,21}$.

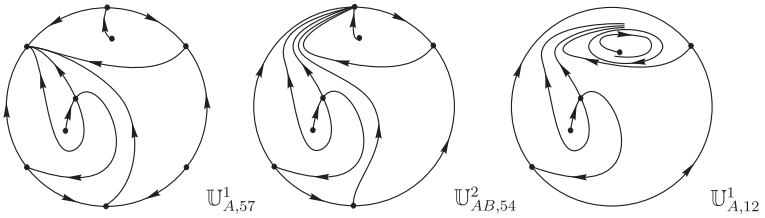

Figure 173 – Unstable system $\mathbb{U}^2_{AB,54}$

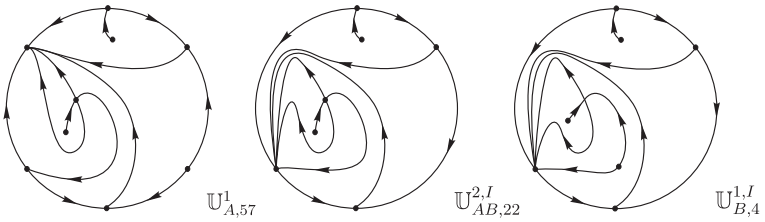

Figure 174 – Impossible unstable phase portrait $\mathbb{U}^{2,I}_{AB,22}$

Phase portrait $\mathbb{U}^1_{A,58}$ has phase portrait $\mathbb{U}^2_{AB,55}$ as an evolution (see Fig. 175). After bifurcation we get phase portrait $\mathbb{U}^1_{A,12}$, by making the infinite saddle–node $\overline{\binom{0}{2}}\,SN$ disappears. Moreover, $\mathbb{U}^1_{A,58}$ has a second phase portrait as an evolution which is not presented since it is topologically equivalent to $\mathbb{U}^2_{AB,55}$.

Phase portrait $\mathbb{U}^1_{A,59}$ has phase portraits $\mathbb{U}^2_{AB,56}$ and $\mathbb{U}^2_{AB,57}$ as evolution (see Fig. 176). After bifurcation we get phase portrait $\mathbb{U}^1_{A,13}$, in both cases, by making the infinite saddle–node $\overline{\binom{0}{2}}\,SN$ disappears.

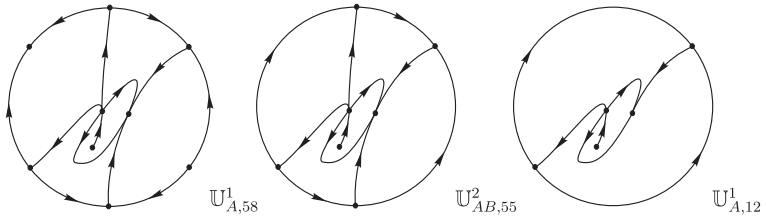

Figure 175 – Unstable system $\mathbb{U}^2_{AB,55}$

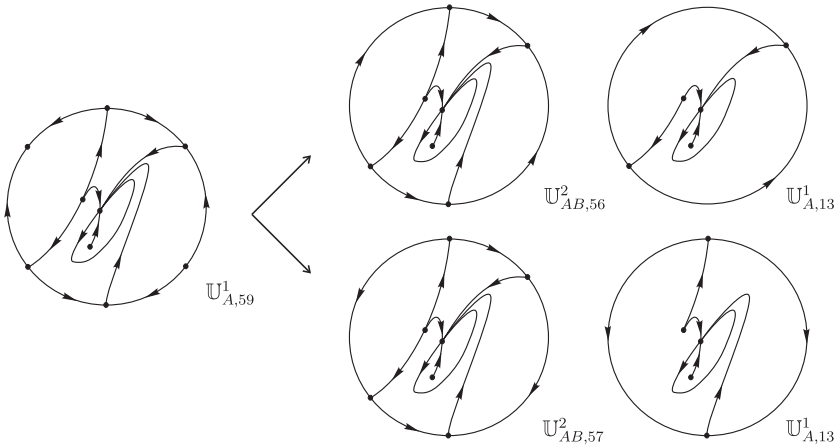

Figure 176 – Unstable systems $\mathbb{U}^2_{AB,56}$ and $\mathbb{U}^2_{AB,57}$

Phase portrait $\mathbb{U}^1_{A,60}$ has phase portrait $\mathbb{U}^2_{AB,58}$ as an evolution (see Fig. 177). After bifurcation we get phase portrait $\mathbb{U}^1_{A,11}$, by making the infinite saddle–node $\overline{\binom{0}{2}}\,SN$ disappears. Moreover, $\mathbb{U}^1_{A,60}$ has a second phase portrait as an evolution which is not presented since it is topologically equivalent to $\mathbb{U}^2_{AB,58}$.

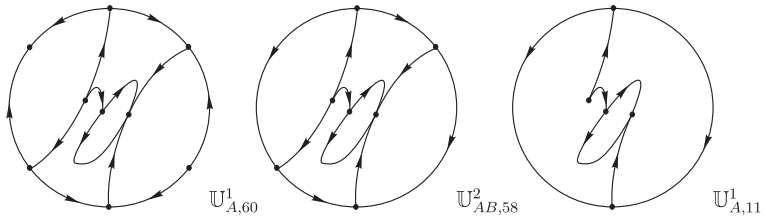

Figure 177 – Unstable system $\mathbb{U}^2_{AB,58}$

Phase portrait $\mathbb{U}^1_{A,61}$ has phase portraits $\mathbb{U}^2_{AB,59}$ and $\mathbb{U}^2_{AB,60}$ as evolution (see Fig. 178). After bifurcation we get phase portraits $\mathbb{U}^1_{A,11}$ and $\mathbb{U}^1_{A,12}$, respectively, by making the infinite saddle–node $\overline{\binom{0}{2}}\,SN$ disappears.

Phase portrait $\mathbb{U}^1_{A,62}$ has phase portrait $\mathbb{U}^2_{AB,61}$ as an evolution (see Fig. 179). After bifurcation we get phase portrait $\mathbb{U}^1_{A,13}$, by making the infinite saddle–node $\overline{\binom{0}{2}}\,SN$ disappears. Moreover, $\mathbb{U}^1_{A,62}$ has a second phase portrait as an evolution which is not presented since it is topologically equivalent to $\mathbb{U}^2_{AB,61}$.

Phase portrait $\mathbb{U}^1_{A,63}$ has phase portrait $\mathbb{U}^2_{AB,62}$ as an evolution (see Fig. 180). After

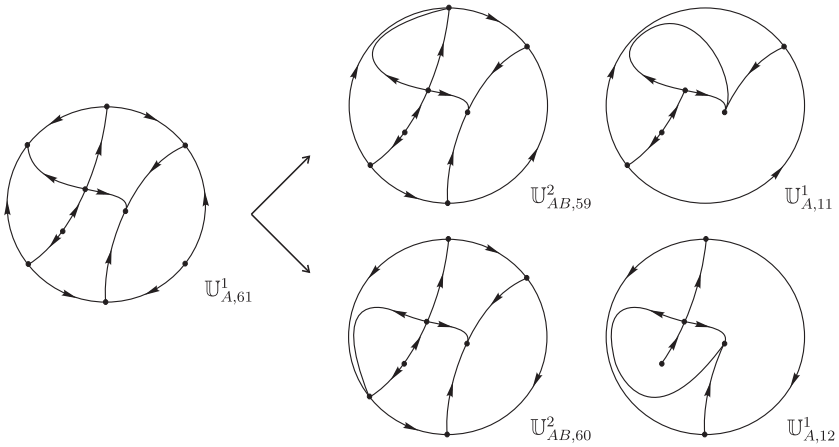

Figure 178 – Unstable systems $\mathbb{U}^2_{AB,59}$ and $\mathbb{U}^2_{AB,60}$

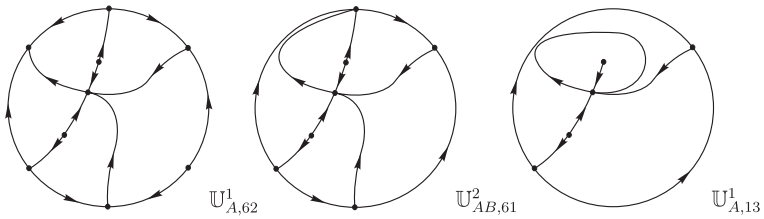

Figure 179 – Unstable system $\mathbb{U}^2_{AB,61}$

bifurcation we get phase portrait $\mathbb{U}^1_{A,11}$, modulo limit cycle, by making the infinite saddle–node $\overline{\binom{0}{2}}$ *SN* disappears. Moreover, $\mathbb{U}^1_{A,63}$ has the impossible phase portrait $\mathbb{U}^{2,I}_{AB,23}$ as an evolution. By Thm. 5.2.10 such a phase portrait is impossible because by splitting the original finite saddle–node into a saddle and a node we obtain the impossible phase portrait $\mathbb{U}^{1,I}_{B,5}$ of *codimension one**, see Fig. 181. We observe that, in the set (A), $\mathbb{U}^{2,I}_{AB,23}$ also unfolds in an impossible phase portrait, as in $\mathbb{U}^{2,I}_{AB,21}$.

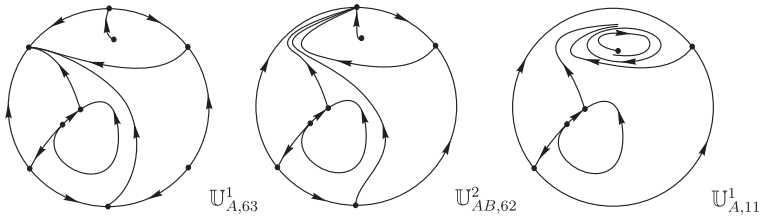

Figure 180 – Unstable system $\mathbb{U}^2_{AB,62}$

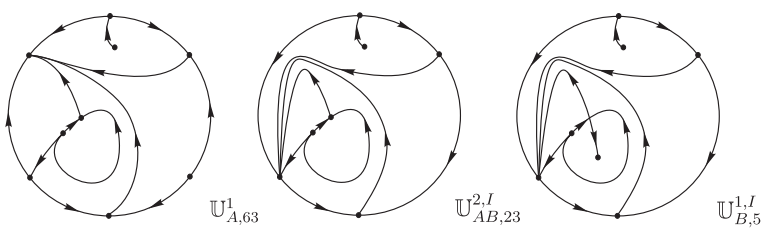

Figure 181 – Impossible unstable phase portrait $\mathbb{U}^{2,I}_{AB,23}$

Phase portrait $\mathbb{U}^1_{A,64}$ has phase portrait $\mathbb{U}^2_{AB,63}$ as an evolution (see Fig. 182). After bifurcation we get phase portrait $\mathbb{U}^1_{A,13}$, modulo limit cycle, by making the infinite saddle–node $\overline{\binom{0}{2}}$ *SN* disappears. Moreover, $\mathbb{U}^1_{A,64}$ has the impossible phase portrait $\mathbb{U}^{2,I}_{AB,24}$ as an evolution. By Thm. 5.2.10 such a phase portrait is impossible because by splitting the original finite saddle–node into a saddle and a node we obtain the impossible phase portrait $\mathbb{U}^{1,I}_{B,5}$ of *codimension one**, see Fig. 183. We observe that, in the set (A), $\mathbb{U}^{2,I}_{AB,24}$ also unfolds in an impossible phase portrait, as in $\mathbb{U}^{2,I}_{AB,21}$.

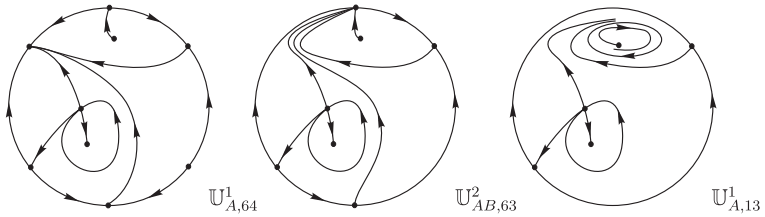

Figure 182 – Unstable system $\mathbb{U}^2_{AB,63}$

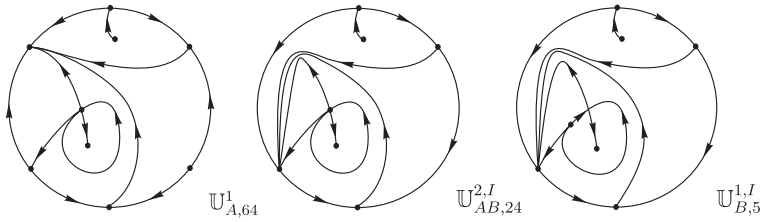

Figure 183 – Impossible unstable phase portrait $\mathbb{U}^{2,I}_{AB,24}$

Phase portrait $\mathbb{U}^1_{A,65}$ has phase portrait $\mathbb{U}^2_{AB,64}$ as an evolution (see Fig. 184). After bifurcation we get phase portrait $\mathbb{U}^1_{A,11}$, by making the infinite saddle–node $\overline{\binom{0}{2}}$ *SN* disappears. Moreover, $\mathbb{U}^1_{A,65}$ has the impossible phase portrait $\mathbb{U}^{2,I}_{AB,25}$ as an evolution. By Thm. 5.2.10 such a phase portrait is impossible because by splitting the original finite saddle–node into a saddle and a node we obtain the impossible phase portrait $\mathbb{U}^{1,I}_{B,6}$ of *codimension one**, see Fig. 185. We observe that, in the set (A), $\mathbb{U}^{2,I}_{AB,25}$ also unfolds in an impossible phase portrait, as in $\mathbb{U}^{2,I}_{AB,21}$.

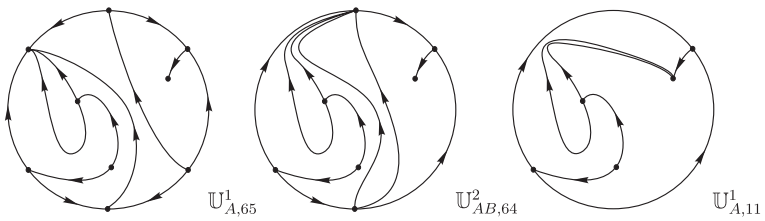

Figure 184 – Unstable system $\mathbb{U}^2_{AB,64}$

Phase portrait $\mathbb{U}^1_{A,66}$ has phase portrait $\mathbb{U}^2_{AB,65}$ as an evolution (see Fig. 186). After bifurcation we get phase portrait $\mathbb{U}^1_{A,12}$, by making the infinite saddle–node $\overline{\binom{0}{2}}$ *SN* disappears. Moreover, $\mathbb{U}^1_{A,66}$ has the impossible phase portrait $\mathbb{U}^{2,I}_{AB,26}$ as an evolution. By

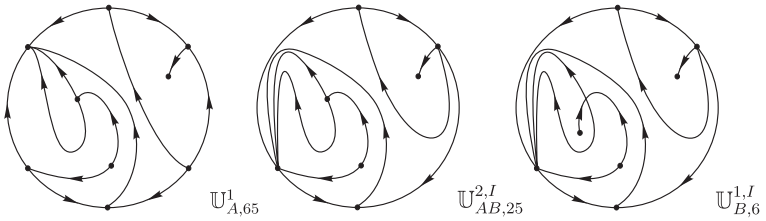

Figure 185 – Impossible unstable phase portrait $\mathbb{U}^{2,I}_{AB,25}$

Thm. 5.2.10 such a phase portrait is impossible because by splitting the original finite saddle–node into a saddle and a node we obtain the impossible phase portrait $\mathbb{U}^{1,I}_{B,6}$ of *codimension one**, see Fig. 187. We observe that, in the set (A), $\mathbb{U}^{2,I}_{AB,26}$ also unfolds in an impossible phase portrait, as in $\mathbb{U}^{2,I}_{AB,21}$.

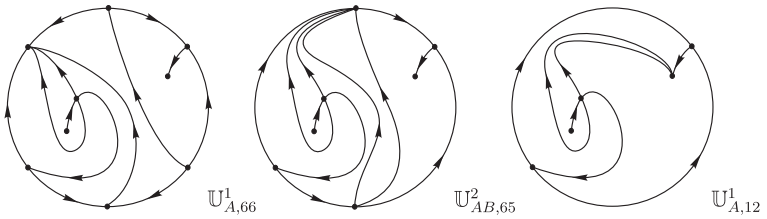

Figure 186 – Unstable system $\mathbb{U}^2_{AB,65}$

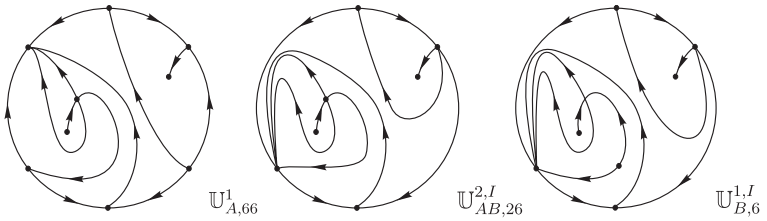

Figure 187 – Impossible unstable phase portrait $\mathbb{U}^{2,I}_{AB,26}$

Phase portrait $\mathbb{U}^1_{A,67}$ has phase portraits $\mathbb{U}^2_{AB,66}$ and $\mathbb{U}^2_{AB,67}$ as evolution (see Fig. 188). After bifurcation we get phase portraits $\mathbb{U}^1_{A,11}$ and $\mathbb{U}^1_{A,13}$ (being this last one modulo limit cycles), respectively, by making the infinite saddle–node $\overline{\binom{0}{2}}$ *SN* disappears.

Phase portrait $\mathbb{U}^1_{A,68}$ has phase portraits $\mathbb{U}^2_{AB,68}$ and $\mathbb{U}^2_{AB,69}$ as evolution (see Fig. 189). After bifurcation we get phase portraits $\mathbb{U}^1_{A,11}$ (modulo limit cycles) and $\mathbb{U}^1_{A,13}$, respectively, by making the infinite saddle–node $\overline{\binom{0}{2}}$ *SN* disappears.

Phase portrait $\mathbb{U}^1_{A,69}$ has phase portrait $\mathbb{U}^2_{AB,70}$ as an evolution (see Fig. 190). After bifurcation we get phase portrait $\mathbb{U}^1_{A,11}$, by making the infinite saddle–node $\overline{\binom{0}{2}}$ *SN* disappears. Moreover, $\mathbb{U}^1_{A,69}$ has the impossible phase portrait $\mathbb{U}^{2,I}_{AB,27}$ as an evolution. By Thm. 5.2.10 such a phase portrait is impossible because by splitting the original finite saddle–node into a saddle and a node we obtain the impossible phase portrait $\mathbb{U}^{1,I}_{B,7}$ of *codimension one**, see Fig. 191. We observe that, in the set (A), $\mathbb{U}^{2,I}_{AB,27}$ also unfolds in an impossible phase portrait, as in $\mathbb{U}^{2,I}_{AB,21}$.

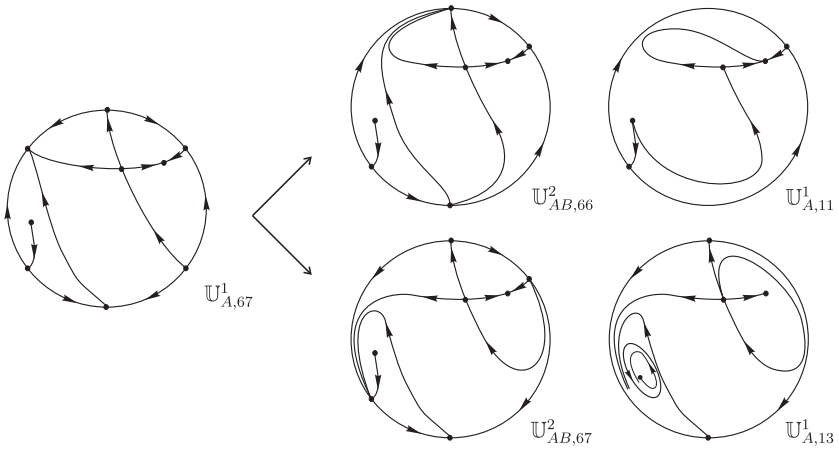

Figure 188 – Unstable systems $\mathbb{U}^2_{AB,66}$ and $\mathbb{U}^2_{AB,67}$

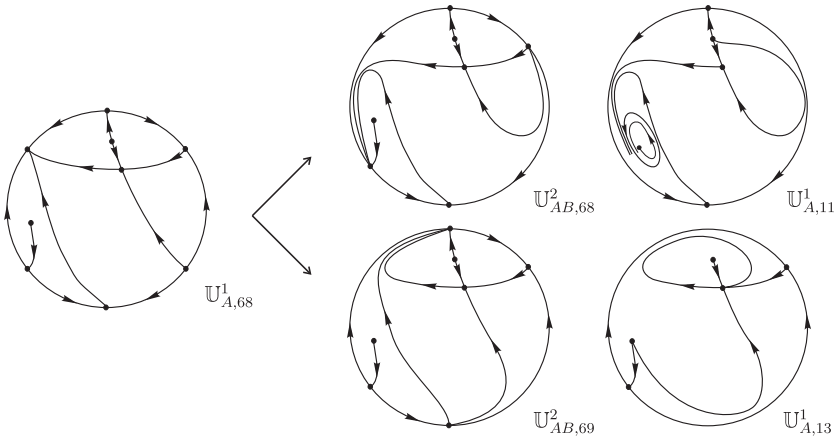

Figure 189 – Unstable systems $\mathbb{U}^2_{AB,68}$ and $\mathbb{U}^2_{AB,69}$

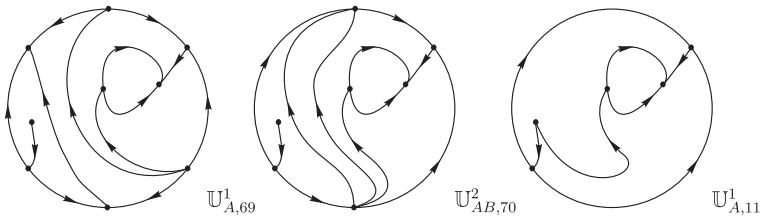

Figure 190 – Unstable system $\mathbb{U}^2_{AB,70}$

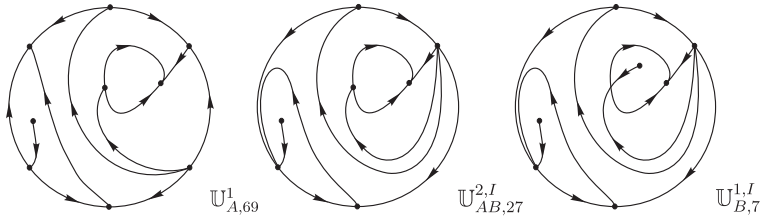

Figure 191 – Impossible unstable phase portrait $\mathbb{U}^{2,I}_{AB,27}$

Phase portrait $\mathbb{U}^1_{A,70}$ has phase portrait $\mathbb{U}^2_{AB,71}$ as an evolution (see Fig. 192). After bifurcation we get phase portrait $\mathbb{U}^1_{A,13}$, by making the infinite saddle–node $\overline{\binom{0}{2}}$ *SN*

disappears. Moreover, $\mathbb{U}^1_{A,70}$ has the impossible phase portrait $\mathbb{U}^{2,I}_{AB,28}$ as an evolution. By Thm. 5.2.10 such a phase portrait is impossible because by splitting the original finite saddle–node into a saddle and a node we obtain the impossible phase portrait $\mathbb{U}^{1,I}_{B,7}$ of *codimension one**, see Fig. 193. We observe that, in the set (A), $\mathbb{U}^{2,I}_{AB,28}$ also unfolds in an impossible phase portrait, as in $\mathbb{U}^{2,I}_{AB,21}$.

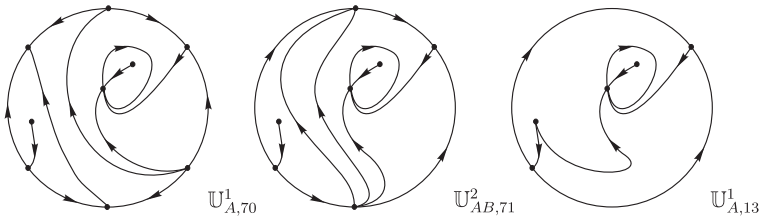

Figure 192 – Unstable system $\mathbb{U}^2_{AB,71}$

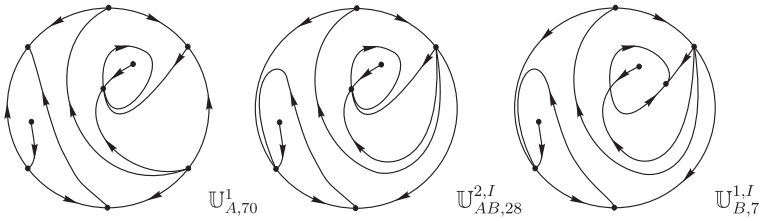

Figure 193 – Impossible unstable phase portrait $\mathbb{U}^{2,I}_{AB,28}$

Therefore, we have just finished obtaining all the 71 topologically potential phase portraits of *codimension two** from the set (AB) presented in Figs. 100 to 102.

Now we explain how one can obtain these 71 phase portraits by starting the study from the set (B). We consider all the 40 realizable structurally unstable quadratic vector fields of *codimension one** from the set (B). In order to obtain a phase portrait of *codimension two** belonging to the set (AB) starting from a phase portrait of *codimension one** of the set (B), we keep the existing infinite saddle–node $\binom{\overline{0}}{2}SN$ and by using Thm. 5.2.6 we build a finite saddle–node $\overline{sn}_{(2)}$ by the coalescence of a finite saddle with a finite node. On the other hand, from the phase portraits of *codimension two** from the set (AB), there exist two ways of obtaining phase portraits of *codimension one** also belonging to the set (B) after perturbation: splitting $\overline{sn}_{(2)}$ into a saddle and a node, or moving it to complex singularities (see Rmk. 5.3.2).

Remark 5.3.2. We recall that, in quadratic differential systems, the finite singular points are zeroes of a polynomial of degree four. Supposing that we have a singular point of multiplicity two, then the remaining singular points are zeroes of a quadratic polynomial. Therefore, these other two points can be two simple singular points, a double point (a saddle–node) or two complex conjugate singular points.

According to these facts, if a phase portrait does not possess finite singularities (for instance, $\mathbb{U}^1_{B,1}$ and $\mathbb{U}^1_{B,2}$) or if it possesses only two finite antisaddles (as for instance

$\mathbb{U}^1_{B,29}$ to $\mathbb{U}^1_{B,32}$), it is not possible to obtain a phase portrait from it which belongs to the set (AB).

The main goal of this section is to obtain all the topologically potential phase portraits from the set (AB) and then prove their realization or show that they are not possible. So we have to be sure that no other phase portrait can be found if one does some evolution in all elements of the set (B) in order to obtain a phase portrait belonging to the set (AB). We point out that we have done this verification, i.e. we have also considered each element from the set (B) and produced a coalescence (when it was possible) of a finite saddle with a finite node and we also have obtained the 71 topologically potential phase portraits of *codimension two** from the set (AB) presented in Figs. 100 to 102. In what follows we show the result (modulo limit cycles) of this study. We point out that we will not give all the details of this study. We will not even mention anything about why there are no more possible cases to be considered as evolution of a *codimension one** phase portrait, since we believe that this can be easily verified by the reader. Additionally, we will present pictures only of the impossible phase portraits obtained in order to explain their impossibility and we will not mention anything about phase portraits which are topologically equivalent to phase portraits already obtained.

It is important to remark that the realizable phase portraits that we will obtain from the set (B) to the set (AB) will coincide exactly with those ones previously found. However, the non–realizable ones that we will find from (B) will be different from those ones coming from (A). The reason is that the arguments used to prove the impossibility of those coming from (A) were precisely that they would bifurcate in some impossible from (B) and now, they will be those ones that bifurcate in some impossible from (A).

In Table 41 we present the study of phase portraits $\mathbb{U}^1_{B,3}$ to $\mathbb{U}^1_{B,11}$. In the first column we present the corresponding phase portrait from the set (B), in the second column we indicate its corresponding phase portrait belonging to the set (AB) i.e. after producing a finite saddle–node $\overline{sn}_{(2)}$, and in the third column we show the corresponding phase portrait after we make this finite saddle–node $\overline{sn}_{(2)}$ disappears.

Phase portrait $\mathbb{U}^1_{B,12}$ has phase portraits $\mathbb{U}^2_{AB,15}$ and $\mathbb{U}^2_{AB,16}$ as evolution. After bifurcation we get phase portrait $\mathbb{U}^1_{B,3}$ (for both cases) by making the finite saddle–node $\overline{sn}_{(2)}$ disappears. Moreover, $\mathbb{U}^1_{B,12}$ has the impossible phase portrait $\mathbb{U}^{2,I}_{AB,29}$ as an evolution. By Thm. 5.2.10 such a phase portrait is impossible because by splitting the original infinite saddle–node $\overline{\binom{0}{2}}\,SN$ into an infinite saddle and an infinite node we obtain the impossible phase portrait $\mathbb{U}^{1,I}_{A,1}$ of *codimension one**, see Fig. 194. We point out that, in the set (B), the corresponding unfolding of $\mathbb{U}^{2,I}_{AB,29}$ does not exist, since if such a phase portrait does exist, it would be an evolution of the impossible phase portrait $\mathbb{I}_{9,1}$ (see Fig. 4.4 from Artés, Llibre and Rezende (2018)), which contradicts Thm. 5.2.10.

In Table 42 we present the study of phase portraits $\mathbb{U}^1_{B,13}$ to $\mathbb{U}^1_{B,15}$. In the first

Table 41 – Phase portraits from the set (AB) obtained from evolution of elements of the set (B)

phase portrait from the set (B)	**phase portrait from the set (AB)**	**phase portrait from the set (B)**
$\mathbb{U}^1_{B,3}$	$\mathbb{U}^2_{AB,1}$	$\mathbb{U}^1_{B,1}$
$\mathbb{U}^1_{B,4}$	$\mathbb{U}^2_{AB,2}$	$\mathbb{U}^1_{B,2}$
$\mathbb{U}^1_{B,5}$	$\mathbb{U}^2_{AB,3}$	$\mathbb{U}^1_{B,1}$
$\mathbb{U}^1_{B,6}$	$\mathbb{U}^2_{AB,4}$	$\mathbb{U}^1_{B,2}$
$\mathbb{U}^1_{B,7}$	$\mathbb{U}^2_{AB,6}$	$\mathbb{U}^1_{B,2}$
$\mathbb{U}^1_{B,8}$	$\mathbb{U}^2_{AB,5}$	$\mathbb{U}^1_{B,1}$
$\mathbb{U}^1_{B,9}$	$\mathbb{U}^2_{AB,7}$ $\mathbb{U}^2_{AB,9}$ $\mathbb{U}^2_{AB,11}$	$\mathbb{U}^1_{B,8}$
$\mathbb{U}^1_{B,10}$	$\mathbb{U}^2_{AB,8}$ $\mathbb{U}^2_{AB,10}$ $\mathbb{U}^2_{AB,12}$	$\mathbb{U}^1_{B,7}$
$\mathbb{U}^1_{B,11}$	$\mathbb{U}^2_{AB,13}$ $\mathbb{U}^2_{AB,14}$	$\mathbb{U}^1_{B,4}$ $\mathbb{U}^1_{B,7}$

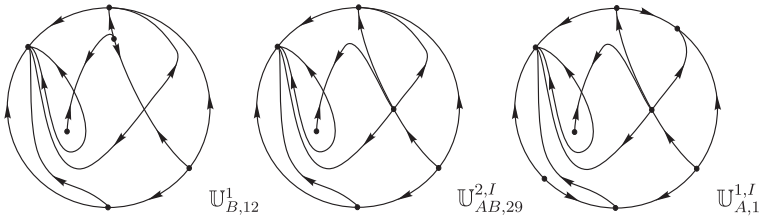

Figure 194 – Impossible unstable phase portrait $\mathbb{U}^{2,I}_{AB,29}$

column we present the corresponding phase portrait from the set (B), in the second column we indicate its corresponding phase portrait belonging to the set (AB) i.e. after producing a finite saddle–node $\overline{sn}_{(2)}$, and in the third column we show the corresponding phase portrait after we make this finite saddle–node $\overline{sn}_{(2)}$ disappears.

Table 42 – Phase portraits from the set (AB) obtained from evolution of elements of the set (B)

phase portrait from the set (B)	**phase portrait from the set (AB)**	**phase portrait from the set (B)**
$\mathbb{U}^1_{B,13}$	$\mathbb{U}^2_{AB,17}$ $\mathbb{U}^2_{AB,18}$	$\mathbb{U}^1_{B,6}$ $\mathbb{U}^1_{B,7}$
$\mathbb{U}^1_{B,14}$	$\mathbb{U}^2_{AB,19}$ $\mathbb{U}^2_{AB,20}$ $\mathbb{U}^2_{AB,21}$	$\mathbb{U}^1_{B,3}$
$\mathbb{U}^1_{B,15}$	$\mathbb{U}^2_{AB,23}$ $\mathbb{U}^2_{AB,22}$	$\mathbb{U}^1_{B,3}$ $\mathbb{U}^1_{B,5}$

Phase portrait $\mathbb{U}^1_{B,16}$ has phase portraits $\mathbb{U}^2_{AB,29}$, $\mathbb{U}^2_{AB,25}$, and $\mathbb{U}^2_{AB,26}$ as evolution. After bifurcation we get phase portraits $\mathbb{U}^1_{B,5}$, $\mathbb{U}^1_{B,8}$ and $\mathbb{U}^1_{B,8}$ (being this last one modulo limit cycle), respectively, by making the finite saddle–node $\overline{sn}_{(2)}$ disappears. Moreover, $\mathbb{U}^1_{B,16}$ has the impossible phase portrait $\mathbb{U}^{2,I}_{AB,30}$ as an evolution. By Thm. 5.2.10 such a phase portrait is impossible because by splitting the original infinite saddle–node $\overline{\binom{0}{2}}\,SN$ into an infinite saddle and an infinite node we obtain the impossible phase portrait $\mathbb{U}^{1,I}_{A,103}$ of *codimension one**, see Fig. 195. We observe that, in the set (B), $\mathbb{U}^{2,I}_{AB,30}$ unfolds in $\mathbb{U}^1_{B,8}$ (modulo limit cycles).

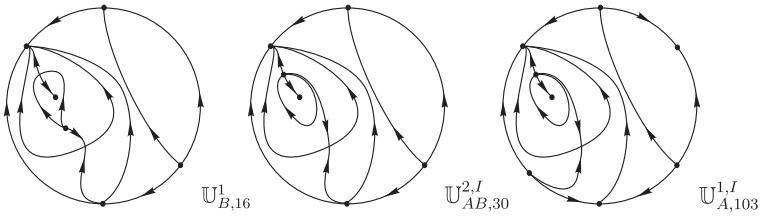

Figure 195 – Impossible unstable phase portrait $\mathbb{U}^{2,I}_{AB,30}$

Phase portrait $\mathbb{U}^1_{B,17}$ has phase portraits $\mathbb{U}^2_{AB,28}$, $\mathbb{U}^2_{AB,24}$, and $\mathbb{U}^2_{AB,27}$ as evolution. After bifurcation we get phase portraits $\mathbb{U}^1_{B,6}$, $\mathbb{U}^1_{B,7}$ and $\mathbb{U}^1_{B,7}$ (being this last one modulo limit cycle), respectively, by making the finite saddle–node $\overline{sn}_{(2)}$ disappears. Moreover, $\mathbb{U}^1_{B,17}$ has the impossible phase portrait $\mathbb{U}^{2,I}_{AB,31}$ as an evolution. By Thm. 5.2.10 such a phase portrait is impossible because by splitting the original infinite saddle–node $\overline{\binom{0}{2}}\,SN$ into an infinite saddle and an infinite node we obtain the impossible phase portrait $\mathbb{U}^{1,I}_{A,103}$ of *codimension one**, see Fig. 196. We observe that, in the set (B), $\mathbb{U}^{2,I}_{AB,31}$ unfolds in $\mathbb{U}^1_{B,7}$ (modulo limit cycles).

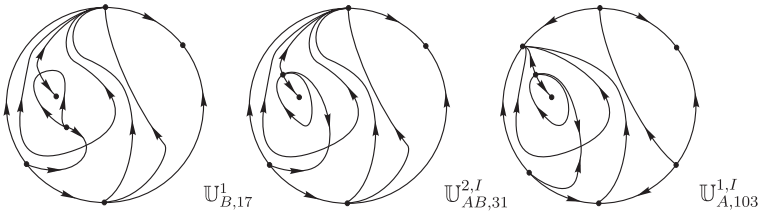

Figure 196 – Impossible unstable phase portrait $\mathbb{U}^{2,I}_{AB,31}$

Phase portrait $\mathbb{U}^1_{B,18}$ has phase portrait $\mathbb{U}^2_{AB,30}$ as an evolution and after bifurcation we get phase portrait $\mathbb{U}^1_{B,7}$, by making the finite saddle–node $\overline{sn}_{(2)}$ disappears. Moreover, $\mathbb{U}^1_{B,18}$ has a second phase portrait as an evolution which is topologically equivalent $\mathbb{U}^2_{AB,30}$.

Phase portrait $\mathbb{U}^1_{B,19}$ has phase portraits $\mathbb{U}^2_{AB,32}$ and $\mathbb{U}^2_{AB,31}$ as evolution. After bifurcation we get phase portraits $\mathbb{U}^1_{B,4}$ and $\mathbb{U}^1_{B,6}$, respective, by making the finite saddle–node $\overline{sn}_{(2)}$ disappears.

Phase portrait $\mathbb{U}^1_{B,20}$ has phase portraits $\mathbb{U}^2_{AB,33}$ and $\mathbb{U}^2_{AB,34}$ as evolution. After bifurcation we get phase portrait $\mathbb{U}^1_{B,3}$, in both cases (being one of them modulo limit cycles),

by making the finite saddle–node $\overline{sn}_{(2)}$ disappears. Moreover, $\mathbb{U}^1_{B,20}$ has the impossible phase portraits $\mathbb{U}^{2,I}_{AB,32}$ and $\mathbb{U}^{2,I}_{AB,33}$ as evolution. By Thm. 5.2.10 such phase portraits are impossible because by splitting the original infinite saddle–node $\overline{\binom{0}{2}}\,SN$ into an infinite saddle and an infinite node we obtain the impossible phase portraits $\mathbb{U}^{1,I}_{A,2}$ and $\mathbb{U}^{1,I}_{A,104}$, respectively, of *codimension one**, see Fig. 197. We point out that, in the set (B), the corresponding unfolding of $\mathbb{U}^{2,I}_{AB,32}$ does not exist (by the exactly same reason that we have discussed in $\mathbb{U}^{2,I}_{AB,29}$) and the corresponding unfolding of $\mathbb{U}^{2,I}_{AB,33}$ is $\mathbb{U}^1_{B,3}$ (modulo limit cycles).

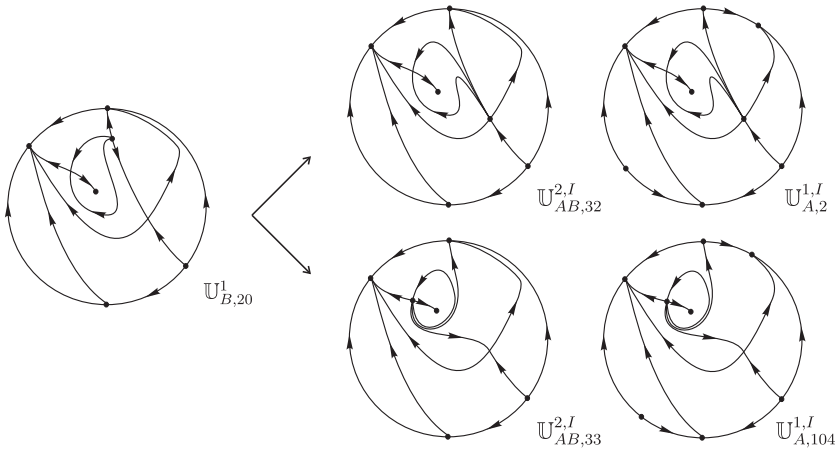

Figure 197 – Impossible unstable phase portraits $\mathbb{U}^{2,I}_{AB,32}$ and $\mathbb{U}^{2,I}_{AB,33}$

Phase portrait $\mathbb{U}^1_{B,21}$ has phase portrait $\mathbb{U}^2_{AB,35}$ as an evolution and after bifurcation we get phase portrait $\mathbb{U}^1_{B,6}$, by making the finite saddle–node $\overline{sn}_{(2)}$ disappears. Moreover, $\mathbb{U}^1_{B,21}$ has a second phase portrait as an evolution which is topologically equivalent $\mathbb{U}^2_{AB,35}$.

Phase portrait $\mathbb{U}^1_{B,22}$ has phase portraits $\mathbb{U}^2_{AB,36}$ and $\mathbb{U}^2_{AB,37}$ as evolution. After bifurcation we get phase portraits $\mathbb{U}^1_{B,3}$ and $\mathbb{U}^1_{B,8}$, respective, by making the finite saddle–node $\overline{sn}_{(2)}$ disappears.

Phase portrait $\mathbb{U}^1_{B,23}$ has phase portraits $\mathbb{U}^2_{AB,39}$, $\mathbb{U}^2_{AB,40}$, and $\mathbb{U}^2_{AB,43}$ as evolution. After bifurcation we get phase portraits $\mathbb{U}^1_{B,5}$ (for the two first cases) and $\mathbb{U}^1_{B,8}$ (for the third case), by making the finite saddle–node $\overline{sn}_{(2)}$ disappears. Moreover, $\mathbb{U}^1_{B,23}$ has the impossible phase portrait $\mathbb{U}^{2,I}_{AB,34}$ as an evolution. By Thm. 5.2.10 such a phase portrait is impossible because by splitting the original infinite saddle–node $\overline{\binom{0}{2}}\,SN$ into an infinite saddle and an infinite node we obtain the impossible phase portrait $\mathbb{U}^{1,I}_{A,49}$ of *codimension one**, see Fig. 198. We observe that, in the set (B), $\mathbb{U}^{2,I}_{AB,34}$ unfolds in $\mathbb{U}^1_{B,8}$.

Phase portrait $\mathbb{U}^1_{B,24}$ has phase portraits $\mathbb{U}^2_{AB,38}$, $\mathbb{U}^2_{AB,41}$, and $\mathbb{U}^2_{AB,42}$ as evolution. After bifurcation we get phase portraits $\mathbb{U}^1_{B,6}$ (for the two first cases) and $\mathbb{U}^1_{B,7}$ (for the third case), by making the finite saddle–node $\overline{sn}_{(2)}$ disappears. Moreover, $\mathbb{U}^1_{B,24}$ has the impossible phase portrait $\mathbb{U}^{2,I}_{AB,35}$ as an evolution. By Thm. 5.2.10 such a phase portrait is impossible because by splitting the original infinite saddle–node $\overline{\binom{0}{2}}\,SN$ into an infinite

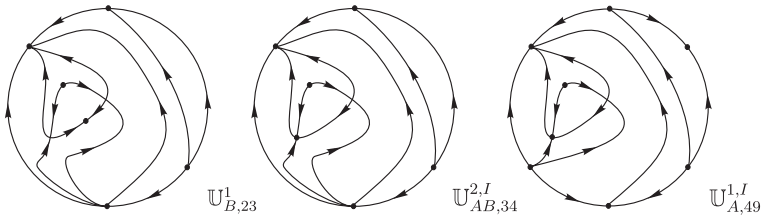

Figure 198 – Impossible unstable phase portrait $\mathbb{U}^{2,I}_{AB,34}$

saddle and an infinite node we obtain the impossible phase portrait $\mathbb{U}^{1,I}_{A,49}$ of *codimension one**, see Fig. 199. We observe that, in the set $(\boldsymbol{B})$, $\mathbb{U}^{2,I}_{AB,35}$ unfolds in $\mathbb{U}^{1}_{B,7}$.

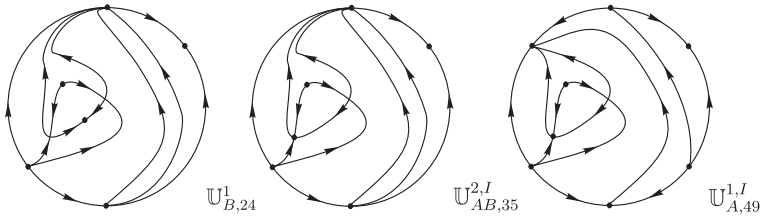

Figure 199 – Impossible unstable phase portrait $\mathbb{U}^{2,I}_{AB,35}$

Phase portrait $\mathbb{U}^{1}_{B,25}$ has phase portraits $\mathbb{U}^{2}_{AB,46}$, $\mathbb{U}^{2}_{AB,49}$, and $\mathbb{U}^{2}_{AB,44}$ as evolution. After bifurcation we get phase portraits $\mathbb{U}^{1}_{B,3}$ (for the two first cases) and $\mathbb{U}^{1}_{B,8}$ (for the third case), by making the finite saddle–node $\overline{sn}_{(2)}$ disappears. Moreover, $\mathbb{U}^{1}_{B,25}$ has the impossible phase portrait $\mathbb{U}^{2,I}_{AB,36}$ as an evolution. By Thm. 5.2.10 such a phase portrait is impossible because by splitting the original infinite saddle–node $\overline{\binom{0}{2}}\,SN$ into an infinite saddle and an infinite node we obtain the impossible phase portrait $\mathbb{U}^{1,I}_{A,3}$ of *codimension one**, see Fig. 200. We point out that, in the set $(\boldsymbol{B})$, the corresponding unfolding of $\mathbb{U}^{2,I}_{AB,36}$ does not exist (by the exactly same reason that we have discussed in $\mathbb{U}^{2,I}_{AB,29}$).

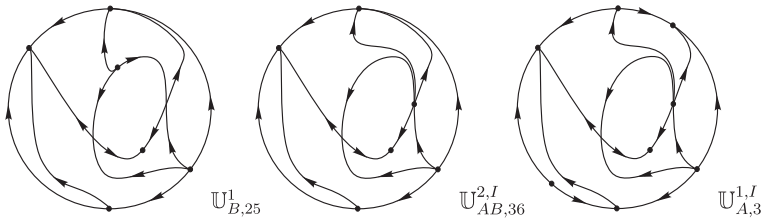

Figure 200 – Impossible unstable phase portrait $\mathbb{U}^{2,I}_{AB,36}$

Phase portrait $\mathbb{U}^{1}_{B,26}$ has phase portraits $\mathbb{U}^{2}_{AB,47}$, $\mathbb{U}^{2}_{AB,48}$, and $\mathbb{U}^{2}_{AB,45}$ as evolution. After bifurcation we get phase portraits $\mathbb{U}^{1}_{B,4}$ (for the two first cases) and $\mathbb{U}^{1}_{B,7}$ (for the third case), by making the finite saddle–node $\overline{sn}_{(2)}$ disappears. Moreover, $\mathbb{U}^{1}_{B,26}$ has the impossible phase portrait $\mathbb{U}^{2,I}_{AB,37}$ as an evolution. By Thm. 5.2.10 such a phase portrait is impossible because by splitting the original infinite saddle–node $\overline{\binom{0}{2}}\,SN$ into an infinite saddle and an infinite node we obtain the impossible phase portrait $\mathbb{U}^{1,I}_{A,3}$ of *codimension*

*one**, see Fig. 201. We point out that, in the set (B), the corresponding unfolding of $\mathbb{U}^{2,I}_{AB,37}$ does not exist (by the exactly same reason that we have discussed in $\mathbb{U}^{2,I}_{AB,29}$).

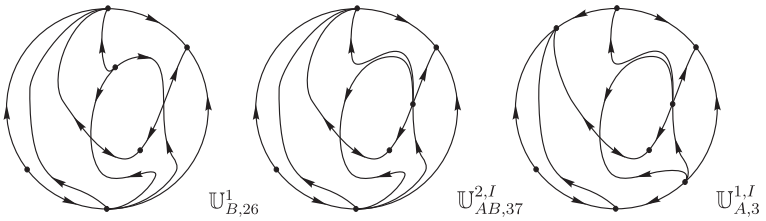

Figure 201 – Impossible unstable phase portrait $\mathbb{U}^{2,I}_{AB,37}$

In Table 43 we present the study of phase portraits $\mathbb{U}^{1}_{B,27}$ to $\mathbb{U}^{1}_{B,35}$, modulo symmetries and limit cycles. In the first column we present the corresponding phase portrait from the set (B), in the second column we indicate its corresponding phase portrait belonging to the set (AB) i.e. after producing a finite saddle–node $\overline{sn}_{(2)}$, and in the third column we show the corresponding phase portrait after we make this finite saddle–node $\overline{sn}_{(2)}$ disappears.

Table 43 – Phase portraits from the set (AB) obtained from evolution of elements of the set (B)

phase portrait from the set (B)	**phase portrait from the set (AB)**	**phase portrait from the set (B)**
$\mathbb{U}^{1}_{B,27}$	$\mathbb{U}^{2}_{AB,50}$	$\mathbb{U}^{1}_{B,4}$
$\mathbb{U}^{1}_{B,28}$	$\mathbb{U}^{2}_{AB,51}$ $\mathbb{U}^{2}_{AB,52}$	$\mathbb{U}^{1}_{B,3}$ $\mathbb{U}^{1}_{B,4}$
$\mathbb{U}^{1}_{B,33}$	$\mathbb{U}^{2}_{AB,53}$ $\mathbb{U}^{2}_{AB,54}$	$\mathbb{U}^{1}_{B,29}$
$\mathbb{U}^{1}_{B,34}$	$\mathbb{U}^{2}_{AB,55}$ $\mathbb{U}^{2}_{AB,56}$ $\mathbb{U}^{2}_{AB,57}$ $\mathbb{U}^{2}_{AB,58}$	$\mathbb{U}^{1}_{B,32}$
$\mathbb{U}^{1}_{B,35}$	$\mathbb{U}^{2}_{AB,61}$ $\mathbb{U}^{2}_{AB,59}$ $\mathbb{U}^{2}_{AB,60}$	$\mathbb{U}^{1}_{B,29}$ $\mathbb{U}^{1}_{B,32}$

Phase portrait $\mathbb{U}^{1}_{B,36}$ has phase portraits $\mathbb{U}^{2}_{AB,62}$ and $\mathbb{U}^{2}_{AB,63}$ as evolution. After bifurcation we get phase portrait $\mathbb{U}^{1}_{B,29}$, for both cases (being one of them modulo limit cycles), by making the finite saddle–node $\overline{sn}_{(2)}$ disappears. Moreover, $\mathbb{U}^{1}_{B,36}$ has the impossible phase portrait $\mathbb{U}^{2,I}_{AB,38}$ as an evolution. By Thm. 5.2.10 such a phase portrait is impossible because by splitting the original infinite saddle–node $\overline{\binom{0}{2}}$ *SN* into an infinite saddle and an infinite node we obtain the impossible phase portrait $\mathbb{U}^{1,I}_{A,105}$ of *codimension one**, see Fig. 202. We observe that, in the set (B), $\mathbb{U}^{2,I}_{AB,38}$ unfolds in $\mathbb{U}^{1}_{B,29}$ (modulo limit cycles).

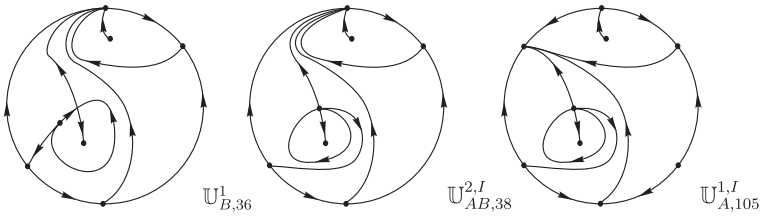

Figure 202 – Impossible unstable phase portrait $\mathbb{U}^{2,I}_{AB,38}$

Phase portrait $\mathbb{U}^1_{B,37}$ has phase portraits $\mathbb{U}^2_{AB,64}$ and $\mathbb{U}^2_{AB,65}$ as evolution. After bifurcation we get phase portrait $\mathbb{U}^1_{B,31}$, for both cases, by making the finite saddle–node $\overline{sn}_{(2)}$ disappears.

Phase portrait $\mathbb{U}^1_{B,38}$ has phase portraits $\mathbb{U}^2_{AB,68}$ and $\mathbb{U}^2_{AB,67}$ as evolution. After bifurcation we get phase portraits $\mathbb{U}^1_{B,29}$ and $\mathbb{U}^1_{B,30}$, respective, by making the finite saddle–node $\overline{sn}_{(2)}$ disappears.

Phase portrait $\mathbb{U}^1_{B,39}$ has phase portraits $\mathbb{U}^2_{AB,69}$ and $\mathbb{U}^2_{AB,66}$ as evolution. After bifurcation we get phase portraits $\mathbb{U}^1_{B,29}$ and $\mathbb{U}^1_{B,31}$, respective, by making the finite saddle–node $\overline{sn}_{(2)}$ disappears.

Phase portrait $\mathbb{U}^1_{B,40}$ has phase portraits $\mathbb{U}^2_{AB,70}$ and $\mathbb{U}^2_{AB,71}$ as evolution. After bifurcation we get phase portrait $\mathbb{U}^1_{B,31}$, for both cases (being one of them modulo limit cycles), by making the finite saddle–node $\overline{sn}_{(2)}$ disappears. Moreover, $\mathbb{U}^1_{B,40}$ has the impossible phase portrait $\mathbb{U}^{2,I}_{AB,39}$ as an evolution. By Thm. 5.2.10 such a phase portrait is impossible because by splitting the original infinite saddle–node $\overline{\binom{0}{2}}$ *SN* into an infinite saddle and an infinite node we obtain the impossible phase portrait $\mathbb{U}^{1,I}_{A,106}$ of *codimension one**, see Fig. 203. We observe that, in the set (B), $\mathbb{U}^{2,I}_{AB,39}$ unfolds in $\mathbb{U}^1_{B,31}$ (modulo limit cycles).

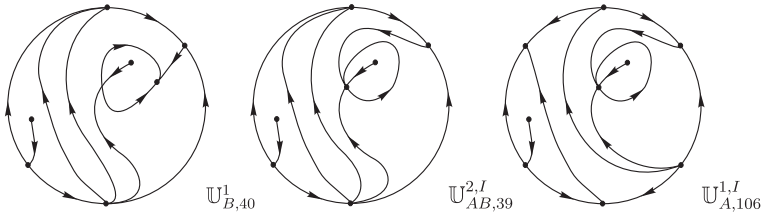

Figure 203 – Impossible unstable phase portrait $\mathbb{U}^{2,I}_{AB,39}$

5.3.2 The realization of the potential phase portraits

In the previous subsection we have produced all the topologically potential phase portraits for structurally unstable quadratic systems of *codimension two** belonging to the set $\sum^2_2(AB)$. And from them, we have discarded 33 which are not realizable due to their respective unfoldings of *codimension one** being impossible.

In this subsection we aim to give specific examples for the remaining 71 different topological classes of structurally unstable quadratic systems of *codimension two** belonging to the set $\sum_2^2(AB)$ and presented in Figs. 100 to 102.

In Artés, Kooij and Llibre (1998) the authors showed that for each structurally stable phase portrait with limit cycles there exists a realizable structurally stable phase portrait without limit cycles so that modulo limit cycles they are equivalent. On the contrary, due to the large number of cases, in Artés, Llibre and Rezende (2018) the authors did not follow the same procedure for the realizable structurally unstable phase portraits of *codimension one**. Since this present study is directly derived from this second study, here we have found examples of *codimension two** phase portraits with no evident limit cycles, but we have not proved the absence of the infinitesimal ones (i.e. the ones born by Hopf-bifurcation).

In Artés, Rezende and Oliveira (2015) the authors classified, with respect to a specific normal form, the set of all real quadratic polynomial differential systems with a finite semi–elemental saddle–node $\overline{sn}_{(2)}$ located at the origin of the plane and an infinite saddle–node of type $\overline{\binom{0}{2}}$ SN (obtained by the coalescence of an infinite saddle with an infinite node) located in the bisector of first and third quadrants. In Artés, Mota and Rezende (2021b) the authors show that phase portrait V_{171} from Artés, Rezende and Oliveira (2015) is not topologically equivalent to V_{170} (i.e. the equivalence presented in Table 65 from the mentioned paper is not correct) and in Artés, Mota and Rezende (2021b) the authors present the correct V_{171}.

Remark 5.3.3. The study of a bifurcation diagram of a certain family of quadratic systems, produces not only the class of phase portraits looked for, but also all those of their closure according to the normal form used. Even though the study is mainly algebraic, often, also analytic and numerical tools are required. This makes that these studies may be not complete and subject to the existence of possible "islands" which could contain an undetected phase portrait. The border of that "island" could mean the connection of two separatrices, and the interior contain a different phase portrait from the ones stated in the theorem. In Artés, Rezende and Oliveira (2015) the authors studied a bifurcation diagram in which the most generic phase portraits correspond to elements of the set (AB). In Section 7 of that paper the authors said that the bifurcation diagram they obtained is completely coherent, i.e. by taking any two points in the parameter space and joining them by a continuous curve, along this curve the changes in phase portraits that occur when crossing the different bifurcation surfaces they mentioned could be completely explained. Nevertheless, at that moment, the authors could not be sure that the bifurcation diagram was the complete bifurcation diagram for the family considered in their paper, due to the possibility of "islands" inside the bifurcation diagram. The topological study that we do here solves partially this problem, since we prove that all the realizable phase portraits of

class (AB) do really exists, and no other topological possibility does. However, the possible existence of "islands" in the bifurcation diagram still persists since they can be related with double limit cycles, as discussed in Section 7 of Artés, Rezende and Oliveira (2015).

By using the phase portraits of generic regions of the bifurcation diagram from Artés, Rezende and Oliveira (2015) plus the correct V_{171} presented in Artés, Mota and Rezende (2021b) we realize all the 71 unstable systems of *codimension two** of the set (AB), i.e. we can give specific examples of all structurally unstable phase portraits from the set (AB).

Consider systems

$$\begin{aligned} \dot{x} &= gx^2 + 2hxy + (n-g-2h)y^2, \\ \dot{y} &= y + \ell x^2 + (2g+2h-2\ell-n)xy + (2h+\ell+2(n-g-2h))y^2, \end{aligned} \tag{5.6}$$

where g, h, ℓ, and n are real parameters and $g \neq 0$.

Normal form (5.6) is studied in Artés, Rezende and Oliveira (2015) and it describes quadratic polynomial differential systems which have a finite semi–elemental saddle–node $\overline{sn}_{(2)}$ and an infinite saddle–node of type $\overline{\binom{0}{2}}\,SN$ located in the endpoints of the bisector of the first and third quadrants.

In Tables 44 and 45 we present one representative from each generic region of the bifurcation diagram of Artés, Rezende and Oliveira (2015) (as described before) corresponding to each phase portrait of *codimension two** from the set (AB) and, therefore, we conclude the proof of Thm. 5.1.1.

Table 44 – Correspondence between *codimension two** phase portraits of the set (AB) and phase portraits from generic regions of the bifurcation diagram presented in Artés, Rezende and Oliveira (2015). In the first column we present the *codimension two** phase portraits from the set (AB) obtained in this study, in the second column we show the corresponding phase portraits from Artés, Rezende and Oliveira (2015) given by normal form (5.6), and in the other columns we present the values of the parameters g, h, ℓ, and n of (5.6) which realizes such phase portrait (remember that the correct phase portrait V_{171} is presented in Artés, Mota and Rezende (2021b))

Cod 2^*	Phase Portrait	g	h	ℓ	n
$\mathbb{U}^2_{AB,1}$	V_{23}	1	0	1/2	10
$\mathbb{U}^2_{AB,2}$	V_{84}	1	91/100	1	2304/625
$\mathbb{U}^2_{AB,3}$	V_{22}	1	0	9/10	10
$\mathbb{U}^2_{AB,4}$	V_{85}	1	22/25	1	2304/625
$\mathbb{U}^2_{AB,5}$	V_{20}	1	0	18	10
$\mathbb{U}^2_{AB,6}$	V_{21}	1	−2	1	10
$\mathbb{U}^2_{AB,7}$	V_{1}	1	−21/5	18	10
$\mathbb{U}^2_{AB,8}$	V_{2}	1	−5	10	10
$\mathbb{U}^2_{AB,9}$	V_{190}	1	3/5	−33/10	−1
$\mathbb{U}^2_{AB,10}$	V_{191}	1	3/5	−3	−1
$\mathbb{U}^2_{AB,11}$	V_{25}	1	173/80	6	10
$\mathbb{U}^2_{AB,12}$	V_{31}	1	112/25	6	30
$\mathbb{U}^2_{AB,13}$	V_{9}	1	−5	11/10	10
$\mathbb{U}^2_{AB,14}$	V_{121}	1	−9999/100000	4/25	81/100
$\mathbb{U}^2_{AB,15}$	V_{147}	1	−6/5	5	−1
$\mathbb{U}^2_{AB,16}$	V_{66}	1	5	−15	10
$\mathbb{U}^2_{AB,17}$	V_{7}	1	−9/2	13/5	10
$\mathbb{U}^2_{AB,18}$	V_{136}	1	−59999/100000	7/10	4/25
$\mathbb{U}^2_{AB,19}$	V_{64}	1	11/5	−4	10
$\mathbb{U}^2_{AB,20}$	V_{145}	1	−4/5	5	−1
$\mathbb{U}^2_{AB,21}$	V_{13}	1	−5	1/2	10
$\mathbb{U}^2_{AB,22}$	V_{83}	1	9201/10000	−15	2304/625
$\mathbb{U}^2_{AB,23}$	V_{10}	1	−5	7/10	10
$\mathbb{U}^2_{AB,24}$	V_{141}	1	−69/100	601/1000	9/100
$\mathbb{U}^2_{AB,25}$	V_{144}	1	−7999/10000	6397/10000	1/25
$\mathbb{U}^2_{AB,26}$	V_{172}	1	−1/10	−3	−1
$\mathbb{U}^2_{AB,27}$	V_{173}	1	−7/100	−31/20	−1
$\mathbb{U}^2_{AB,28}$	V_{41}	1	44773/10000	11/5	30
$\mathbb{U}^2_{AB,29}$	V_{69}	1	11/5	6	10
$\mathbb{U}^2_{AB,30}$	V_{15}	1	−21/5	3	10
$\mathbb{U}^2_{AB,31}$	V_{114}	1	−211/2000	9549/50000	4/5
$\mathbb{U}^2_{AB,32}$	V_{109}	1	−41/400	99999/100000	4/5
$\mathbb{U}^2_{AB,33}$	V_{154}	1	−7/5	8/25	−1
$\mathbb{U}^2_{AB,34}$	V_{102}	1	481/2000	−10	1
$\mathbb{U}^2_{AB,35}$	V_{129}	1	−5499/10000	3/4	81/400
$\mathbb{U}^2_{AB,36}$	V_{108}	1	−41/400	11/10	4/5

Table 45 – Continuation of Table 44

Cod 2*	**Phase Portrait**	g	h	ℓ	n
$\mathbb{U}^2_{AB,37}$	V_{78}	1	9201/10000	−50	2304/625
$\mathbb{U}^2_{AB,38}$	V_{42}	1	44777/10000	203/100	30
$\mathbb{U}^2_{AB,39}$	V_{71}	1	223/100	6	10
$\mathbb{U}^2_{AB,40}$	V_{170}	1	−9/50	−3	−1
$\mathbb{U}^2_{AB,41}$	V_{171}	1	−3/40	−3/2	−1
$\mathbb{U}^2_{AB,42}$	V_{142}	1	−69/100	6007/10000	9/100
$\mathbb{U}^2_{AB,43}$	V_{143}	1	−7999/10000	27/50	1/25
$\mathbb{U}^2_{AB,44}$	V_{104}	1	573/1250	−8	19/10
$\mathbb{U}^2_{AB,45}$	V_{123}	1	−39/400	1/100	81/100
$\mathbb{U}^2_{AB,46}$	V_{155}	1	−7/5	3/10	−1
$\mathbb{U}^2_{AB,47}$	V_{165}	1	−1/5	−13/10	−1
$\mathbb{U}^2_{AB,48}$	V_{37}	1	3	11/10	10
$\mathbb{U}^2_{AB,49}$	V_{44}	1	22/5	2	10
$\mathbb{U}^2_{AB,50}$	V_{110}	1	−41/400	9/10	4/5
$\mathbb{U}^2_{AB,51}$	V_{46}	1	11/5	9/10	10
$\mathbb{U}^2_{AB,52}$	V_{49}	1	23/5	9/10	10
$\mathbb{U}^2_{AB,53}$	V_{6}	1	−5	3	10
$\mathbb{U}^2_{AB,54}$	V_{189}	1	37/50	−147/100	−1
$\mathbb{U}^2_{AB,55}$	V_{61}	1	4501/1000	−1	10
$\mathbb{U}^2_{AB,56}$	V_{53}	1	6	−1/10000	10
$\mathbb{U}^2_{AB,57}$	V_{107}	1	9/25	−1/2	41/25
$\mathbb{U}^2_{AB,58}$	V_{149}	1	−11/10	3/2	−1
$\mathbb{U}^2_{AB,59}$	V_{62}	1	3	−1	10
$\mathbb{U}^2_{AB,60}$	V_{198}	1	−2/5	11/10	−1
$\mathbb{U}^2_{AB,61}$	V_{51}	1	6	1/5	10
$\mathbb{U}^2_{AB,62}$	V_{138}	1	−3/5	7/10	9/100
$\mathbb{U}^2_{AB,63}$	V_{177}	1	3/100	−9/10	−1
$\mathbb{U}^2_{AB,64}$	V_{3}	1	−5	6	10
$\mathbb{U}^2_{AB,65}$	V_{192}	1	3/5	−123/50	−1
$\mathbb{U}^2_{AB,66}$	V_{122}	1	−39/400	31/1000	81/100
$\mathbb{U}^2_{AB,67}$	V_{169}	1	−1/5	−7/10	−1
$\mathbb{U}^2_{AB,68}$	V_{113}	1	−39/400	1/10	81/100
$\mathbb{U}^2_{AB,69}$	V_{166}	1	−1/5	−53/50	−1
$\mathbb{U}^2_{AB,70}$	V_{140}	1	−69/100	63/100	9/100
$\mathbb{U}^2_{AB,71}$	V_{174}	1	−41/1000	−133/100	−1

5.4 Proof of Thm. 5.1.2

In this section we present the proof of Thm. 5.1.2. The procedure is the same as used in the previous section. In Subsec. 5.4.1 we obtain all the topologically potential phase portraits possessing the saddle–nodes $\overline{sn}_{(2)}$ and $\overline{\binom{1}{1}}\,SN$ (we have 45 phase portraits) and we prove that five of them are impossible. In Subsec. 5.4.2 we show the realization of each one of the remaining 40 phase portraits.

5.4.1 The topologically potential phase portraits

The main goal of this subsection is to obtain all the topologically potential phase portraits from the set (AC).

As we said before, inside the set (AC), the unstable objects of *codimension two** that we are considering in this study belong to the set of saddle–nodes $\left\{\overline{sn}_{(2)}+\overline{\binom{1}{1}}\,SN\right\}$. Considering all the different ways of obtaining phase portraits belonging to the set (AC) of *codimension two**, we have to consider all the possible ways of coalescing specific singular points in both sets (A) and (C). However, as the sets (AC) and (CA) are the same (i.e. their elements are obtained independently of the order of evolution in elements of the sets (A) or (C)), it is necessary to consider only all the possible ways of obtaining an infinite saddle–node of type $\overline{\binom{1}{1}}\,SN$ in each element from the set (A) (phase portraits possessing a finite saddle–node $\overline{sn}_{(2)}$). Anyway, in order to make things clear, in page 321 we discuss briefly how we should perform if we start by considering the set (C).

In order to obtain phase portraits from the set (AC) by starting our study from the set (A), we have to consider Thm. 5.2.8 and also Lemma 3.26 from Artés, Llibre and Rezende (2018) (regarding phase portraits from the set (C)) which we state as follows.

Lemma 5.4.1. Assume that a *codimension one** polynomial vector field X has an infinite singular point p being a saddle–node of multiplicity two with $\rho_0 = (\partial P/\partial x + \partial Q/\partial y)_p \neq 0$ and second eigenvalue equal to zero.

(a) Any perturbation of X in a sufficiently small neighborhood of this point will produce a structurally stable system (with one infinite saddle and one finite node, or vice versa) or a system topologically equivalent to X.

(b) Both possibilities of structurally stable systems are realizable.

(c) If the saddle–node is the only unstable object in the region of definition and we consider the perturbation which leaves a saddle and a node in a small neighborhood, then the node is ω–limit or α–limit (depending on its stability) of at least one of the separatrices of the saddle.

(d) In the case that after bifurcation the node remains at infinity and the saddle moves to the finite plane, then the separatrices of this new saddle have their α– and ω–limits fixed according to next rule:

(1) The separatrix γ that corresponds to the one of the saddle–node different from the infinity line must maintain the same α– or ω–limit set.

(2) The separatrix (belonging to the same eigenspace of γ) which appears after bifurcation must go to the node that remains at infinity, and this will be the only separatrix which can arrive to this node in this side of the infinity.

(3) The two separatrices which correspond to the infinite line in the unstable phase portrait, and that now are two separatrices of the saddle drawn on the finite plane, must end at the same infinite node where they ended before the bifurcation (if a node was adjacent to the saddle–node) or in the same α– or ω–limit point of the finite separatrix of the adjacent infinite saddle. In case that the saddle–node is the only infinite singular point, then both separatrices go to the symmetric point which will remain as a node.

Here we consider all 69 realizable structurally unstable quadratic vector fields of *codimension one** from the set (A). In order to obtain a phase portrait of *codimension two** belonging to the set (AC) starting from a phase portrait of *codimension one** of the set (A), we keep the existing finite saddle–node and using Lemma 5.4.1 we build an infinite saddle–node of type $\binom{1}{1}SN$ by the coalescence of a finite node (respectively finite saddle) with an infinite saddle (respectively infinite node). As we said in the Introduction, we point out that the finite singularity that coalesces with an infinite singularity cannot be the finite saddle–node since then what we would obtain at infinity would not be a saddle–node of type $\binom{1}{1}SN$ but a multiplicity three singularity. Even though this is also a *codimension two** case and somehow can be considered inside the set (AC), we preferred to consider it into the set (CC) where two possibilities will be needed to be studied: either two finite singularities coalescing with different infinite singularities, or two finite singularities coalescing with the same infinite singularity. On the other hand, from the phase portraits of *codimension two** from the set (AC), one can obtain phase portraits of *codimension one** also belonging to the set (A) after perturbation by splitting the infinite saddle–node $\binom{1}{1}SN$ into a finite saddle (respectively finite node) and an infinite node (respectively infinite saddle). More precisely, after bifurcation the point that has arrived to infinity remains there with the same local behavior, and the one which was at infinity moves into the real plane at the other side of the infinity line.

As in the previous section, in what follows we denote by $\mathbb{U}^2_{AC,k}$, where $\mathbb{U}^2_{AC}$ stands for structurally unstable quadratic vector field of *codimension two** from the set (AC) and

$k \in \{1,\ldots,40\}$. The impossible phase portraits will be denoted by $\mathbb{U}^{2,I}_{AC,j}$, where $\mathbb{U}^{2,I}_{AC}$ stands for *Impossible of codimension two* from the set (AC)* and $j \in \mathbb{N}$.

We point out that in this study we do not present phase portraits which are topologically equivalent to phase portraits already obtained. Additionally, as we explained clearly about how we obtain an infinite saddle–node of type $\overline{\binom{1}{1}}\,SN$ from a phase portrait from the set (A), we will not mention anything about why we do not have no more possibilities (of obtaining an infinite saddle–node of type $\overline{\binom{1}{1}}\,SN$) beyond those ones that we will present.

Phase portrait $\mathbb{U}^1_{A,1}$ cannot have a phase portrait possessing an infinite saddle–node of type $\overline{\binom{1}{1}}\,SN$ as an evolution since it has only the finite saddle–node $\overline{sn}_{(2)}$ and only the infinite node.

Phase portrait $\mathbb{U}^1_{A,2}$ has phase portrait $\mathbb{U}^2_{AC,1}$ as an evolution (see Fig. 204). After bifurcation we get phase portrait $\mathbb{U}^1_{A,11}$ by splitting the infinite saddle–node $\overline{\binom{1}{1}}\,SN$.

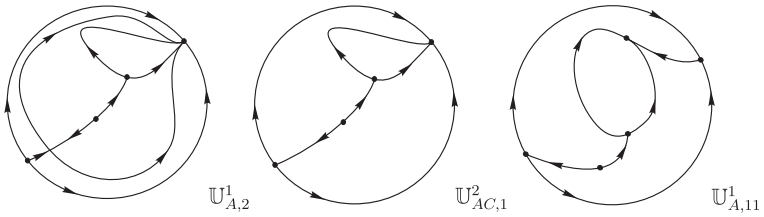

Figure 204 – Unstable system $\mathbb{U}^2_{AC,1}$

Phase portrait $\mathbb{U}^1_{A,3}$ has phase portrait $\mathbb{U}^2_{AC,2}$ as an evolution (see Fig. 205). After bifurcation we get phase portrait $\mathbb{U}^1_{A,12}$ by splitting the infinite saddle–node $\overline{\binom{1}{1}}\,SN$.

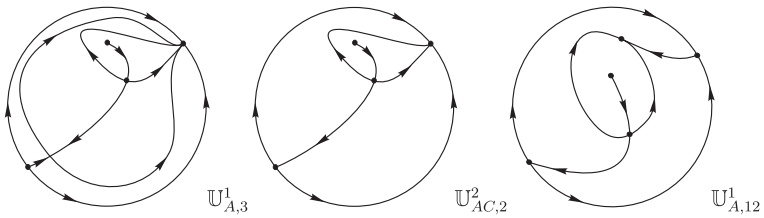

Figure 205 – Unstable system $\mathbb{U}^2_{AC,2}$

Phase portrait $\mathbb{U}^1_{A,4}$ cannot have a phase portrait possessing an infinite saddle–node of type $\overline{\binom{1}{1}}\,SN$ as an evolution. In fact, such a phase portrait possesses only an infinite node which receives four separatrices from finite singularities. Then by item $(d)-(2)$ of Lemma 5.4.1 the finite saddle cannot reach the infinite node. We point out that this same situation happens in many other phase portraits, such as in $\mathbb{U}^1_{A,5}$ to $\mathbb{U}^1_{A,8}$. Because it is quite simple to detect this phenomena, when we deal again with this situation we will skip all the details.

Phase portrait $\mathbb{U}^1_{A,9}$ has phase portrait $\mathbb{U}^2_{AC,3}$ as an evolution (see Fig. 206). After bifurcation we get phase portrait $\mathbb{U}^1_{A,11}$ by splitting the infinite saddle–node $\overline{\binom{1}{1}}\,SN$.

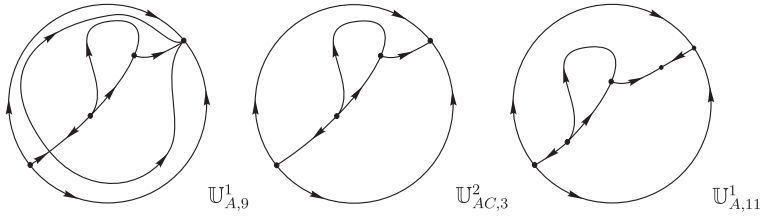

Figure 206 – Unstable system $\mathbb{U}^2_{AC,3}$

Phase portrait $\mathbb{U}^1_{A,10}$ has phase portrait $\mathbb{U}^2_{AC,4}$ as an evolution (see Fig. 207). After bifurcation we get phase portrait $\mathbb{U}^1_{A,13}$ by splitting the infinite saddle–node $\overline{\binom{1}{1}}\,SN$.

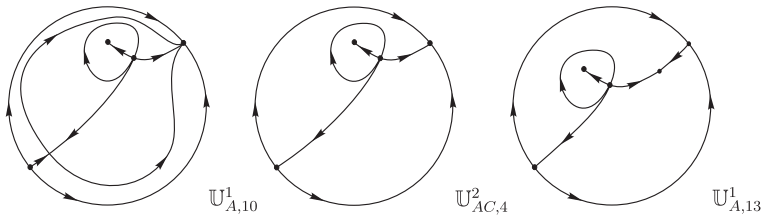

Figure 207 – Unstable system $\mathbb{U}^2_{AC,4}$

It is quite common that a given phase portrait of a certain codimension K be an unfolding of topologically distinct phase portraits of codimension $K+1$ (modulo limit cycles). This situation appears in this study. In the first column of Table 46 we present the phase portrait of the set (A), in the second column we indicate its corresponding phase portrait belonging to the set (AC), and in the third column we show the corresponding phase portrait after bifurcation. We point out that it is not necessary to present any explanation for the phase portraits present in the first column, since their corresponding elements from the third column already appeared and were explained before.

Table 46 – Phase portraits from the set (AC) obtained from evolution of some elements of the set (A)

phase portrait from the set (A)	**phase portrait from the set (AC)**	**phase portrait from the set (A)**
$\mathbb{U}^1_{A,11}$	$\mathbb{U}^2_{AC,1}$ $\mathbb{U}^2_{AC,3}$	$\mathbb{U}^1_{A,2}$ $\mathbb{U}^1_{A,9}$
$\mathbb{U}^1_{A,12}$	$\mathbb{U}^2_{AC,2}$	$\mathbb{U}^1_{A,3}$
$\mathbb{U}^1_{A,13}$	$\mathbb{U}^2_{AC,4}$	$\mathbb{U}^1_{A,10}$

Phase portrait $\mathbb{U}^1_{A,14}$ has phase portrait $\mathbb{U}^2_{AC,5}$ as an evolution (see Fig. 208). After bifurcation we get phase portrait $\mathbb{U}^1_{A,55}$ by splitting the infinite saddle–node $\overline{\binom{1}{1}}\,SN$.

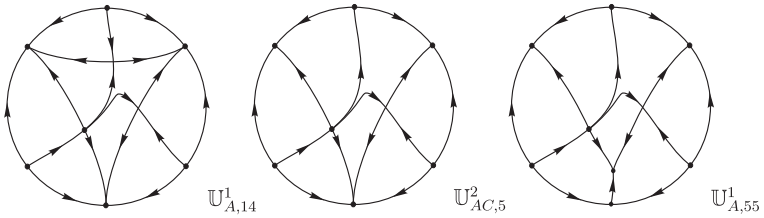

Figure 208 – Unstable system $\mathbb{U}^2_{AC,5}$

Phase portrait $\mathbb{U}^1_{A,15}$ has phase portraits $\mathbb{U}^2_{AC,6}$ and $\mathbb{U}^2_{AC,7}$ as evolution (see Fig. 209). After bifurcation we get phase portraits $\mathbb{U}^1_{A,32}$ and $\mathbb{U}^1_{A,53}$, respectively, by splitting the infinite saddle–node $\overline{\binom{1}{1}}\,SN$.

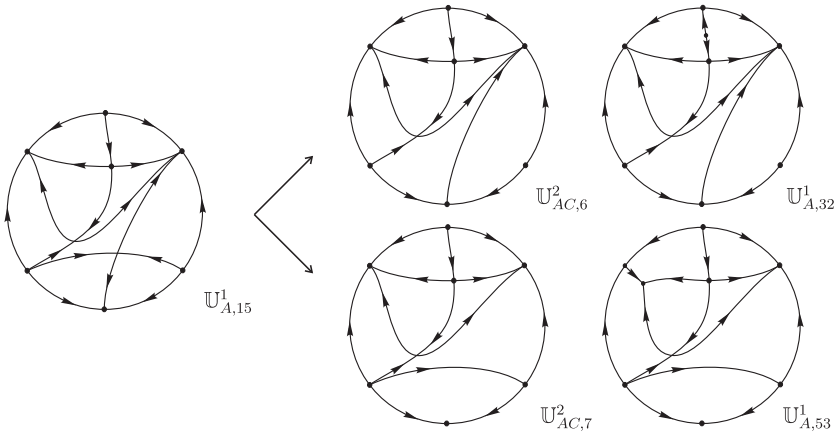

Figure 209 – Unstable systems $\mathbb{U}^2_{AC,6}$ and $\mathbb{U}^2_{AC,7}$

Phase portrait $\mathbb{U}^1_{A,16}$ has phase portraits $\mathbb{U}^2_{AC,8}$, $\mathbb{U}^2_{AC,9}$, and $\mathbb{U}^2_{AC,10}$ as evolution (see Fig. 210). After bifurcation we get phase portraits $\mathbb{U}^1_{A,33}$, $\mathbb{U}^1_{A,52}$, and $\mathbb{U}^1_{A,54}$, respectively, by splitting the infinite saddle–node $\overline{\binom{1}{1}}\,SN$.

Phase portrait $\mathbb{U}^1_{A,17}$ has phase portraits $\mathbb{U}^2_{AC,11}$, $\mathbb{U}^2_{AC,12}$, and $\mathbb{U}^2_{AC,13}$ as evolution (see Fig. 211). After bifurcation we get phase portraits $\mathbb{U}^1_{A,35}$, $\mathbb{U}^1_{A,41}$, and $\mathbb{U}^1_{A,42}$, respectively, by splitting the infinite saddle–node $\overline{\binom{1}{1}}\,SN$.

Phase portrait $\mathbb{U}^1_{A,18}$ has phase portraits $\mathbb{U}^2_{AC,14}$, $\mathbb{U}^2_{AC,15}$, and $\mathbb{U}^2_{AC,16}$ as evolution (see Fig. 212). After bifurcation we get phase portraits $\mathbb{U}^1_{A,25}$, $\mathbb{U}^1_{A,27}$, and $\mathbb{U}^1_{A,45}$, respectively, by splitting the infinite saddle–node $\overline{\binom{1}{1}}\,SN$.

Phase portraits $\mathbb{U}^1_{A,19}$, $\mathbb{U}^1_{A,20}$, and $\mathbb{U}^1_{A,21}$ cannot have a phase portrait possessing an infinite saddle–node of type $\overline{\binom{1}{1}}\,SN$ as an evolution since each one of them has only the finite saddle–node $\overline{sn}_{(2)}$.

Phase portrait $\mathbb{U}^1_{A,22}$ has phase portrait $\mathbb{U}^2_{AC,17}$ as an evolution (see Fig. 213). After bifurcation we get phase portrait $\mathbb{U}^1_{A,65}$ by splitting the infinite saddle–node $\overline{\binom{1}{1}}\,SN$.

Phase portrait $\mathbb{U}^1_{A,23}$ has phase portrait $\mathbb{U}^2_{AC,18}$ as an evolution (see Fig. 214). After

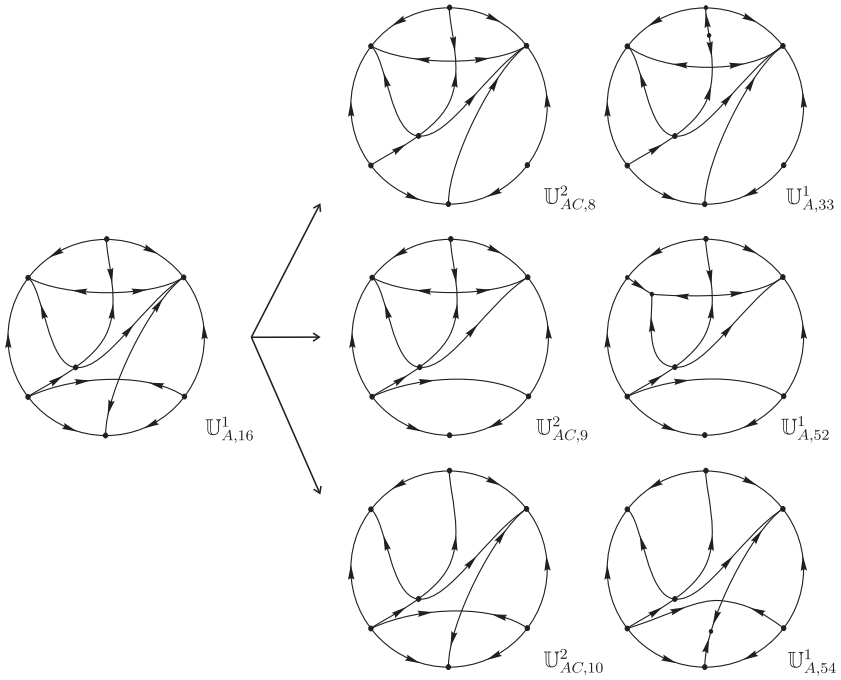

Figure 210 – Unstable systems $\mathbb{U}^2_{AC,8}$, $\mathbb{U}^2_{AC,9}$, and $\mathbb{U}^2_{AC,10}$

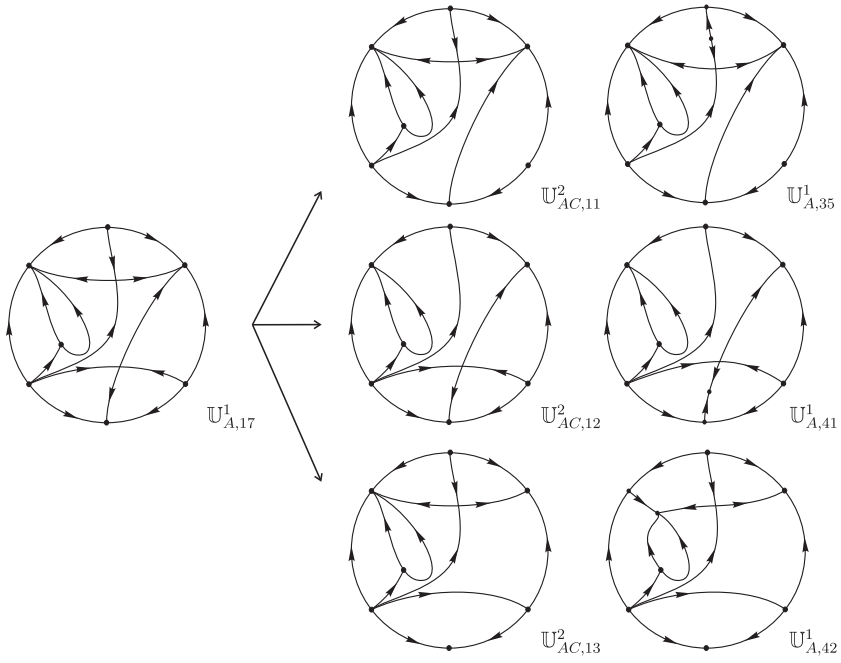

Figure 211 – Unstable systems $\mathbb{U}^2_{AC,11}$, $\mathbb{U}^2_{AC,12}$, and $\mathbb{U}^2_{AC,13}$

bifurcation we get phase portrait $\mathbb{U}^1_{A,66}$ by splitting the infinite saddle–node $\binom{\overline{1}}{1}SN$.

Phase portrait $\mathbb{U}^1_{A,24}$ cannot have a phase portrait possessing an infinite saddle–node of type $\binom{\overline{1}}{1}SN$ as an evolution since the finite saddle cannot reach the infinite node (by item $(d)-(2)$ of Lemma 5.4.1) and the finite node cannot reach the infinite saddle (because this elemental antisaddle is surrounded by the separatrices of the finite saddle).

Phase portrait $\mathbb{U}^1_{A,25}$ has three phase portraits as evolution.

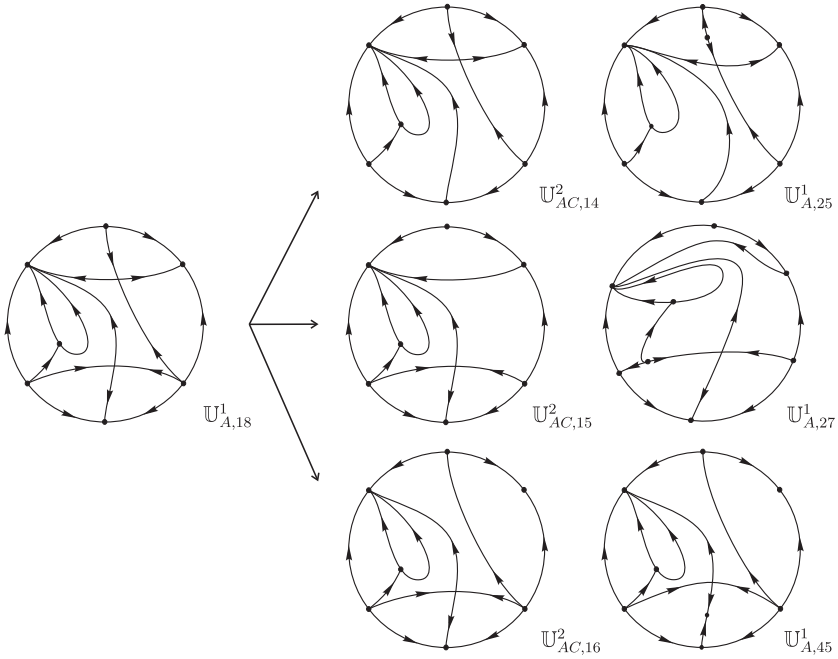

Figure 212 – Unstable systems $\mathbb{U}^2_{AC,14}$, $\mathbb{U}^2_{AC,15}$, and $\mathbb{U}^2_{AC,16}$

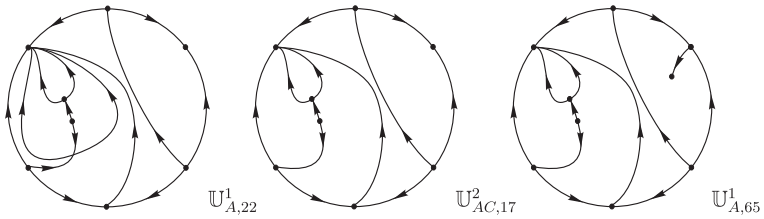

Figure 213 – Unstable system $\mathbb{U}^2_{AC,17}$

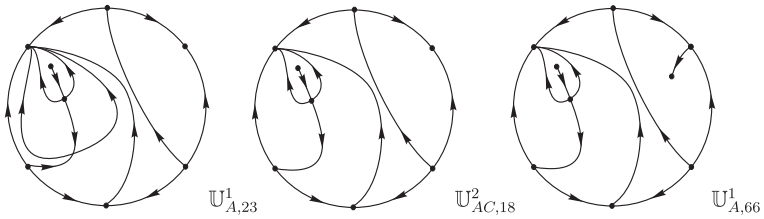

Figure 214 – Unstable system $\mathbb{U}^2_{AC,18}$

1. $\mathbb{U}^2_{AC,19}$, see Fig. 215, and after bifurcation we get phase portrait $\mathbb{U}^1_{A,56}$;

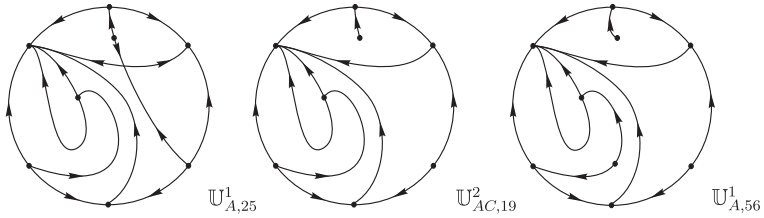

Figure 215 – Unstable system $\mathbb{U}^2_{AC,19}$

2. $\mathbb{U}^2_{AC,14}$, and its study was done when we spoke about $\mathbb{U}^1_{A,18}$;

3. impossible phase portrait $\mathbb{U}^{2,I}_{AC,1}$. By Thm. 5.2.10 such a phase portrait is impossible because by splitting the original finite saddle–node into a saddle and a node we obtain the impossible phase portrait $\mathbb{U}^{1,I}_{C,8}$ of *codimension one**, see Fig. 216. We point out that, in the set (A), the corresponding unfolding of $\mathbb{U}^{2,I}_{AC,1}$ does not exist, since if such a phase portrait does exist, it would be an evolution of the impossible phase portrait $\mathbb{I}_{12,3}$ (see Fig. 4.4 from Artés, Llibre and Rezende (2018)), which contradicts Thm. 5.2.10.

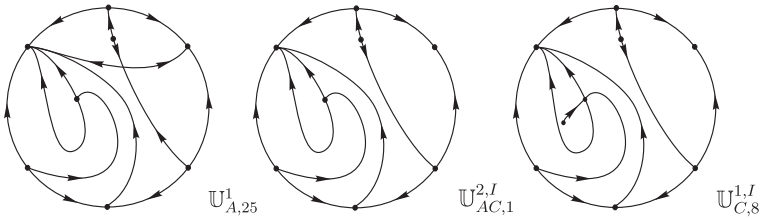

Figure 216 – Impossible unstable phase portrait $\mathbb{U}^{2,I}_{AC,1}$

Phase portrait $\mathbb{U}^{1}_{A,26}$ has phase portrait $\mathbb{U}^{2}_{AC,20}$ as an evolution (see Fig. 217). After bifurcation we get phase portrait $\mathbb{U}^{1}_{A,67}$ by splitting the infinite saddle–node $\overline{\binom{1}{1}}\,SN$.

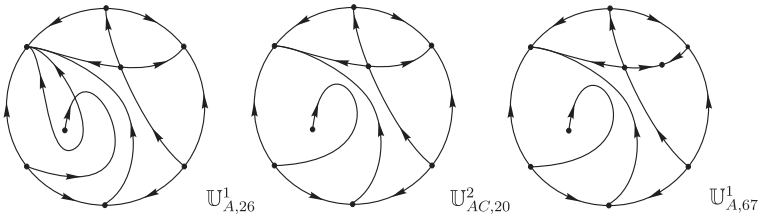

Figure 217 – Unstable system $\mathbb{U}^{2}_{AC,20}$

Phase portrait $\mathbb{U}^{1}_{A,27}$ has phase portraits $\mathbb{U}^{2}_{AC,21}$ and $\mathbb{U}^{2}_{AC,22}$ as evolution (see Fig. 218). After bifurcation we get phase portraits $\mathbb{U}^{1}_{A,56}$ and $\mathbb{U}^{1}_{A,60}$, respectively, by splitting the infinite saddle–node $\overline{\binom{1}{1}}\,SN$. Moreover, $\mathbb{U}^{1}_{A,27}$ also has $\mathbb{U}^{2}_{AC,15}$ as an evolution, and this last one was mentioned before during the study of $\mathbb{U}^{1}_{A,18}$.

Phase portrait $\mathbb{U}^{1}_{A,28}$ has phase portraits $\mathbb{U}^{2}_{AC,23}$ and $\mathbb{U}^{2}_{AC,24}$ as evolution (see Fig. 219). After bifurcation we get phase portraits $\mathbb{U}^{1}_{A,57}$ and $\mathbb{U}^{1}_{A,58}$, respectively, by splitting the infinite saddle–node $\overline{\binom{1}{1}}\,SN$.

Phase portrait $\mathbb{U}^{1}_{A,29}$ cannot have a phase portrait possessing an infinite saddle–node of type $\overline{\binom{1}{1}}\,SN$ as an evolution since the finite saddle cannot reach the infinite node (by item $(d)-(2)$ of Lemma 5.4.1), the finite node cannot reach the infinite saddle (because this elemental antisaddle is surrounded by the separatrices of the finite saddle) and the finite saddle–node cannot go to infinity (as we have discussed during the analysis of $\mathbb{U}^{1}_{A,1}$).

Phase portrait $\mathbb{U}^{1}_{A,30}$ has phase portrait $\mathbb{U}^{2}_{AC,25}$ as an evolution (see Fig. 220). After bifurcation we get phase portrait $\mathbb{U}^{1}_{A,69}$ by splitting the infinite saddle–node $\overline{\binom{1}{1}}\,SN$.

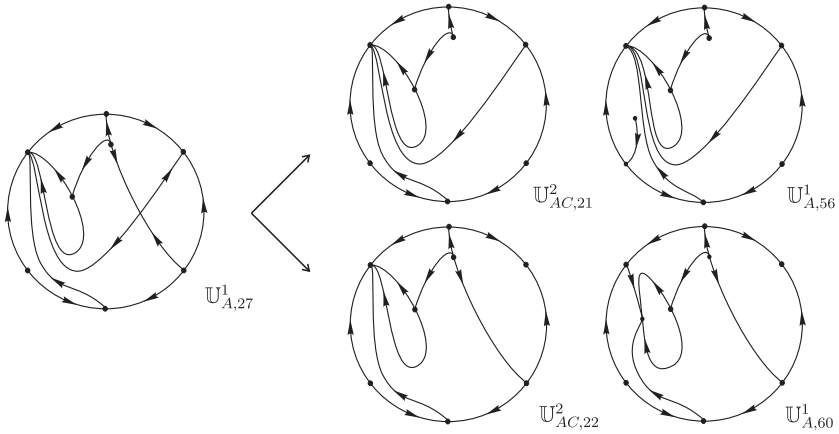

Figure 218 – Unstable systems $\mathbb{U}^2_{AC,21}$ and $\mathbb{U}^2_{AC,22}$

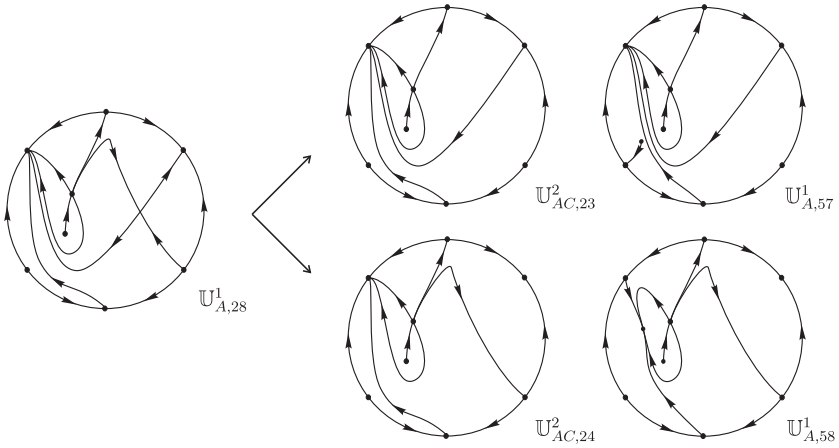

Figure 219 – Unstable systems $\mathbb{U}^2_{AC,23}$ and $\mathbb{U}^2_{AC,24}$

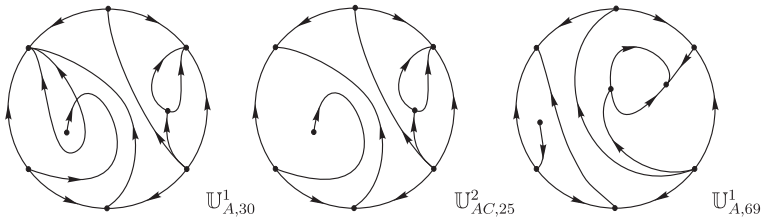

Figure 220 – Unstable system $\mathbb{U}^2_{AC,25}$

Phase portrait $\mathbb{U}^1_{A,31}$ has phase portrait $\mathbb{U}^2_{AC,26}$ as an evolution (see Fig. 221). After bifurcation we get phase portrait $\mathbb{U}^1_{A,61}$ by splitting the infinite saddle–node $\overline{\binom{1}{1}}\,SN$.

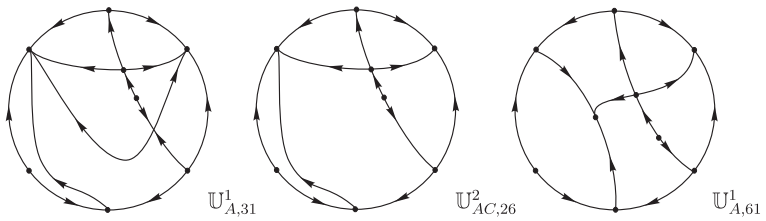

Figure 221 – Unstable system $\mathbb{U}^2_{AC,26}$

Phase portrait $\mathbb{U}^1_{A,32}$ has phase portrait $\mathbb{U}^2_{AC,27}$ as an evolution (see Fig. 222). After bifurcation we get phase portrait $\mathbb{U}^1_{A,61}$ by splitting the infinite saddle–node $\overline{\binom{1}{1}}\,SN$. Moreover, $\mathbb{U}^1_{A,32}$ also has $\mathbb{U}^2_{AC,6}$ as an evolution, and this last one was mentioned before during the study of $\mathbb{U}^1_{A,15}$.

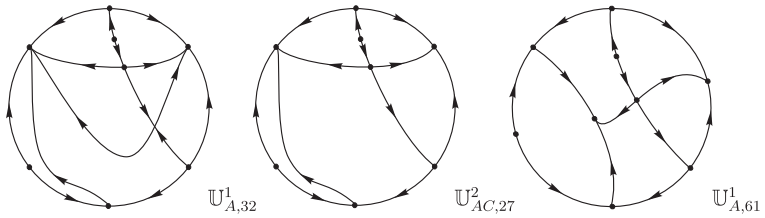

Figure 222 – Unstable system $\mathbb{U}^2_{AC,27}$

Phase portrait $\mathbb{U}^1_{A,33}$ has phase portrait $\mathbb{U}^2_{AC,8}$ as an evolution and this last one was mentioned before during the study of $\mathbb{U}^1_{A,16}$.

Phase portrait $\mathbb{U}^1_{A,34}$ cannot have a phase portrait possessing an infinite saddle–node of type $\overline{\binom{1}{1}}\,SN$ as an evolution, we can conclude this fact by using the same arguments as used for $\mathbb{U}^1_{A,29}$.

Phase portrait $\mathbb{U}^1_{A,35}$ has phase portrait $\mathbb{U}^2_{AC,11}$ as an evolution and this last one was mentioned before during the study of $\mathbb{U}^1_{A,17}$.

Phase portrait $\mathbb{U}^1_{A,36}$ has phase portrait $\mathbb{U}^2_{AC,28}$ as an evolution (see Fig. 223). After bifurcation we get phase portrait $\mathbb{U}^1_{A,69}$ by splitting the infinite saddle–node $\overline{\binom{1}{1}}\,SN$.

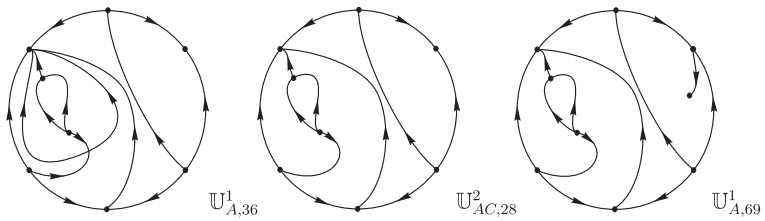

Figure 223 – Unstable system $\mathbb{U}^2_{AC,28}$

Phase portrait $\mathbb{U}^1_{A,37}$ has phase portrait $\mathbb{U}^2_{AC,29}$ as an evolution (see Fig. 224). After bifurcation we get phase portrait $\mathbb{U}^1_{A,70}$ by splitting the infinite saddle–node $\overline{\binom{1}{1}}\,SN$.

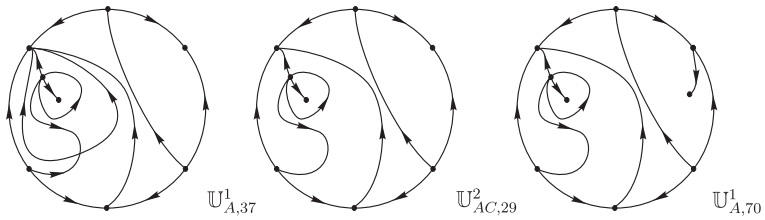

Figure 224 – Unstable system $\mathbb{U}^2_{AC,29}$

Phase portrait $\mathbb{U}^1_{A,38}$ cannot have a phase portrait possessing an infinite saddle–node of type $\overline{\binom{1}{1}}\,SN$ as an evolution.

Phase portrait $\mathbb{U}^1_{A,39}$ has phase portrait $\mathbb{U}^2_{AC,30}$ as an evolution (see Fig. 225). After bifurcation we get phase portrait $\mathbb{U}^1_{A,65}$ by splitting the infinite saddle–node $\overline{\binom{1}{1}}\,SN$.

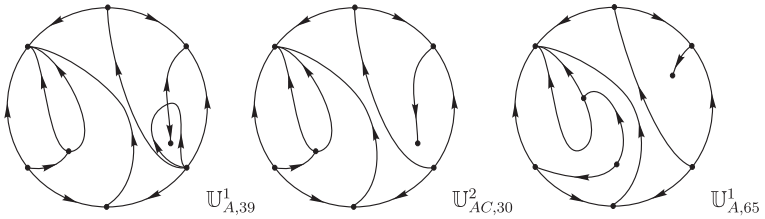

Figure 225 – Unstable system $\mathbb{U}^2_{AC,30}$

Phase portrait $\mathbb{U}^1_{A,40}$ cannot have a phase portrait possessing an infinite saddle–node of type $\overline{\binom{1}{1}}\,SN$ as an evolution.

Phase portrait $\mathbb{U}^1_{A,41}$ has three phase portraits as evolution.

1. $\mathbb{U}^2_{AC,31}$, see Fig. 226, and after bifurcation we get phase portrait $\mathbb{U}^1_{A,63}$;

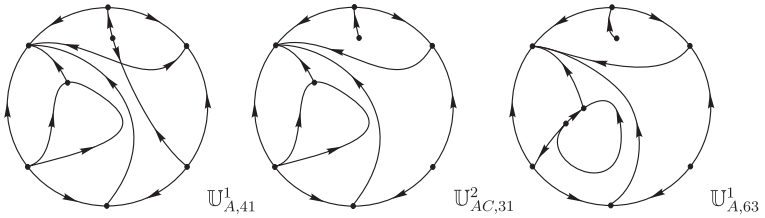

Figure 226 – Unstable system $\mathbb{U}^2_{AC,31}$

2. $\mathbb{U}^2_{AC,12}$, and its study was done when we spoke about $\mathbb{U}^1_{A,17}$;

3. impossible phase portrait $\mathbb{U}^{2,I}_{AC,2}$. By Thm. 5.2.10 such a phase portrait is impossible because by splitting the original finite saddle–node into a saddle and a node we obtain the impossible phase portrait $\mathbb{U}^{1,I}_{C,9}$ of *codimension one**, see Fig. 227. We point out that, in the set (A), the corresponding unfolding of $\mathbb{U}^{2,I}_{AC,2}$ does not exist, since if such a phase portrait does exist, it would be an evolution of the impossible phase portrait $\mathbb{I}_{12,2}$ (see Fig. 4.4 from Artés, Llibre and Rezende (2018)), which contradicts Thm. 5.2.10.

Phase portrait $\mathbb{U}^1_{A,42}$ has phase portraits $\mathbb{U}^2_{AC,32}$ and $\mathbb{U}^2_{AC,33}$ as evolution (see Fig. 228). After bifurcation we get phase portraits $\mathbb{U}^1_{A,60}$ and $\mathbb{U}^1_{A,63}$, respectively, by splitting the infinite saddle–node $\overline{\binom{1}{1}}\,SN$. Moreover, $\mathbb{U}^1_{A,42}$ also has $\mathbb{U}^2_{AC,13}$ as an evolution, and this last one was mentioned before during the study of $\mathbb{U}^1_{A,17}$.

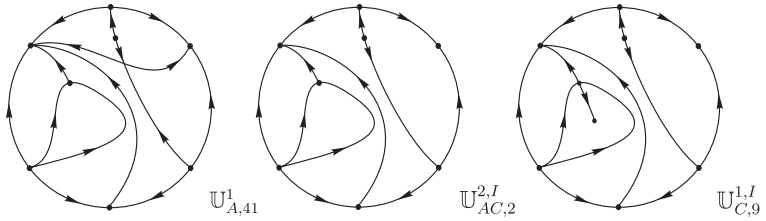

Figure 227 – Impossible unstable phase portrait $\mathbb{U}^{2,I}_{AC,2}$

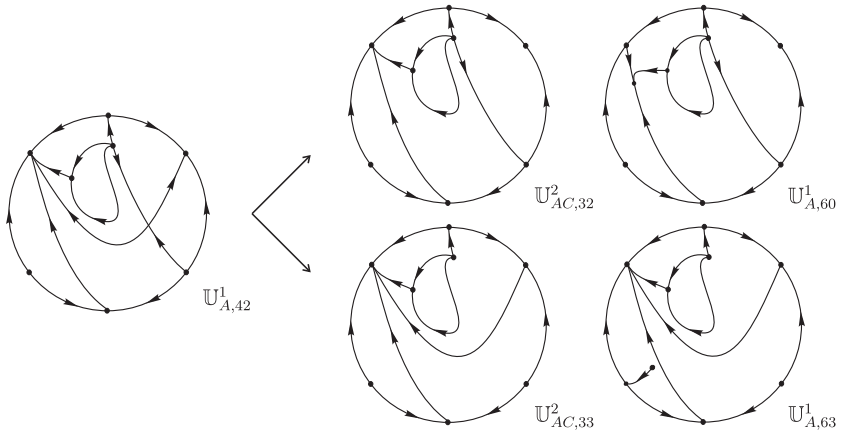

Figure 228 – Unstable systems $\mathbb{U}^2_{AC,32}$ and $\mathbb{U}^2_{AC,33}$

Phase portrait $\mathbb{U}^1_{A,43}$ has phase portraits $\mathbb{U}^2_{AC,34}$ and $\mathbb{U}^2_{AC,35}$ as evolution (see Fig. 229). After bifurcation we get phase portraits $\mathbb{U}^1_{A,59}$ and $\mathbb{U}^1_{A,64}$, respectively, by splitting the infinite saddle–node $\binom{\overline{1}}{1}SN$.

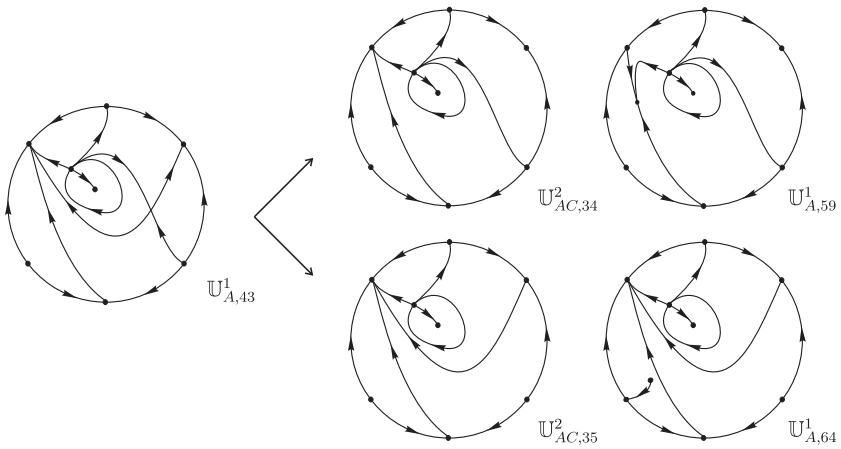

Figure 229 – Unstable systems $\mathbb{U}^2_{AC,34}$ and $\mathbb{U}^2_{AC,35}$

Phase portrait $\mathbb{U}^1_{A,44}$ cannot have a phase portrait possessing an infinite saddle–node of type $\binom{\overline{1}}{1}SN$ as an evolution.

Phase portrait $\mathbb{U}^1_{A,45}$ has phase portrait $\mathbb{U}^2_{AC,16}$ as an evolution and this last one was mentioned before during the study of $\mathbb{U}^1_{A,18}$.

Phase portraits $\mathbb{U}^1_{A,46}$ to $\mathbb{U}^1_{A,48}$ and also $\mathbb{U}^1_{A,50}$ cannot have a phase portrait possess-

ing an infinite saddle–node of type $\overline{\binom{1}{1}}\,SN$ as an evolution.

Phase portrait $\mathbb{U}^1_{A,51}$ has phase portrait $\mathbb{U}^2_{AC,36}$ as an evolution (see Fig. 230). After bifurcation we get phase portrait $\mathbb{U}^1_{A,67}$ by splitting the infinite saddle–node $\overline{\binom{1}{1}}\,SN$.

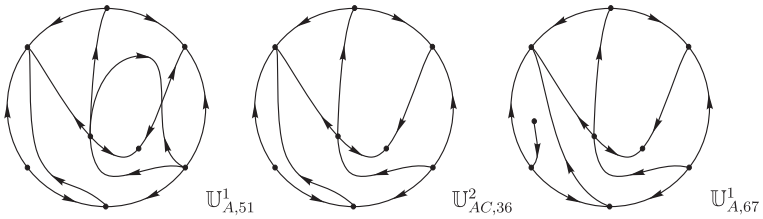

Figure 230 – Unstable system $\mathbb{U}^2_{AC,36}$

Phase portrait $\mathbb{U}^1_{A,52}$ has phase portrait $\mathbb{U}^2_{AC,37}$ as an evolution (see Fig. 231). After bifurcation we get phase portrait $\mathbb{U}^1_{A,68}$, by splitting the infinite saddle–node $\overline{\binom{1}{1}}\,SN$. Moreover, $\mathbb{U}^1_{A,52}$ also has $\mathbb{U}^2_{AC,9}$ as an evolution, and this last one was mentioned before during the study of $\mathbb{U}^1_{A,16}$.

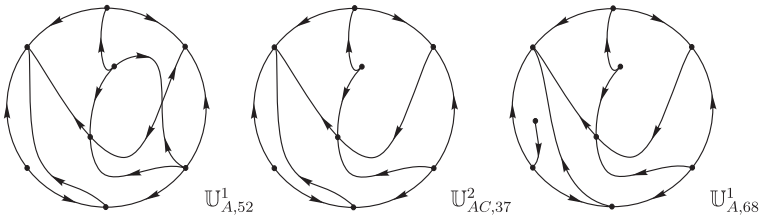

Figure 231 – Unstable system $\mathbb{U}^2_{AC,37}$

Phase portrait $\mathbb{U}^1_{A,53}$ has phase portrait $\mathbb{U}^2_{AC,7}$ as an evolution, and this last one was mentioned before during the study of $\mathbb{U}^1_{A,15}$.

Phase portrait $\mathbb{U}^1_{A,54}$ has phase portrait $\mathbb{U}^2_{AC,38}$ as an evolution (see Fig. 232). After bifurcation we get phase portrait $\mathbb{U}^1_{A,68}$, by splitting the infinite saddle–node $\overline{\binom{1}{1}}\,SN$. Moreover, $\mathbb{U}^1_{A,54}$ also has $\mathbb{U}^2_{AC,10}$ as an evolution, and this last one was mentioned before during the study of $\mathbb{U}^1_{A,16}$.

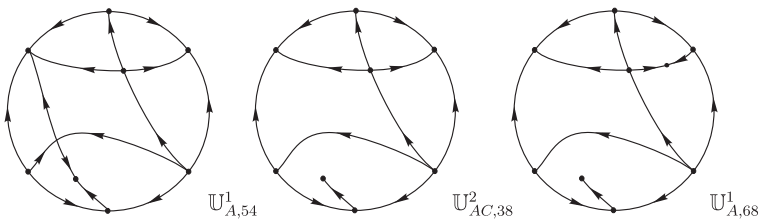

Figure 232 – Unstable system $\mathbb{U}^2_{AC,38}$

Phase portrait $\mathbb{U}^1_{A,55}$ has phase portraits $\mathbb{U}^2_{AC,39}$ and $\mathbb{U}^2_{AC,40}$ as evolution (see Fig. 233). After bifurcation we get phase portraits $\mathbb{U}^1_{A,61}$ and $\mathbb{U}^1_{A,62}$, respectively, by splitting the infinite saddle–node $\overline{\binom{1}{1}}\,SN$. Moreover, $\mathbb{U}^1_{A,55}$ also has $\mathbb{U}^2_{AC,5}$ as an evolution, and this last one was mentioned before during the study of $\mathbb{U}^1_{A,14}$.

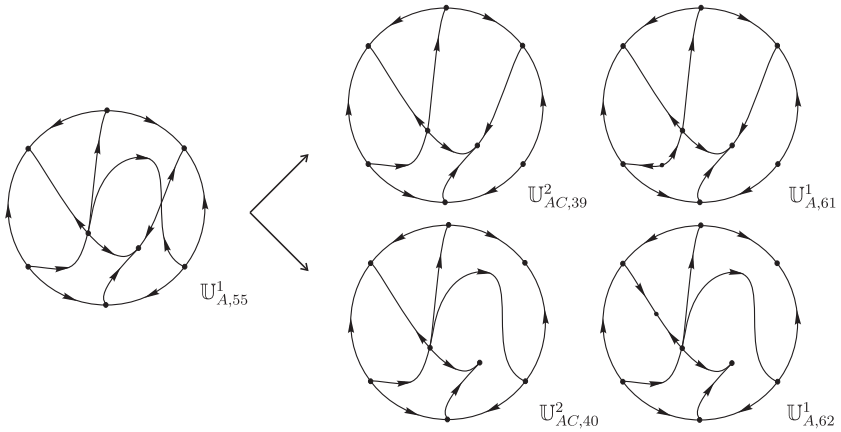

Figure 233 – Unstable systems $\mathbb{U}^2_{AC,39}$ and $\mathbb{U}^2_{AC,40}$

Phase portrait $\mathbb{U}^1_{A,56}$ has phase portraits $\mathbb{U}^2_{AC,19}$ and $\mathbb{U}^2_{AC,21}$ as evolution. These two phase portraits were obtained during the study of $\mathbb{U}^1_{A,25}$ and $\mathbb{U}^1_{A,27}$, respectively.

Phase portrait $\mathbb{U}^1_{A,57}$ has phase portrait $\mathbb{U}^2_{AC,23}$ as an evolution and this last one was obtained during the study of $\mathbb{U}^1_{A,28}$.

Phase portrait $\mathbb{U}^1_{A,58}$ has phase portrait $\mathbb{U}^2_{AC,24}$ as an evolution and this last one was obtained during the study of $\mathbb{U}^1_{A,28}$. Moreover, $\mathbb{U}^1_{A,58}$ has a second phase portrait as an evolution which is topologically equivalent to $\mathbb{U}^2_{AC,24}$.

Phase portrait $\mathbb{U}^1_{A,59}$ has phase portrait $\mathbb{U}^2_{AC,34}$ as an evolution and this last one was obtained during the study of $\mathbb{U}^1_{A,43}$. Moreover, $\mathbb{U}^1_{A,59}$ has the impossible phase portrait $\mathbb{U}^{2,I}_{AC,3}$ as an evolution. By Thm. 5.2.10 such a phase portrait is impossible because by splitting the obtained infinite saddle–node $\overline{\binom{1}{1}}\,SN$ into a finite saddle and an infinite node we obtain the impossible phase portrait $\mathbb{U}^{1,I}_{A,104}$ of *codimension one**, see Fig. 234. We observe that, in the set (C), $\mathbb{U}^{2,I}_{AC,3}$ unfolds in $\mathbb{U}^1_{C,17}$ (modulo limit cycles).

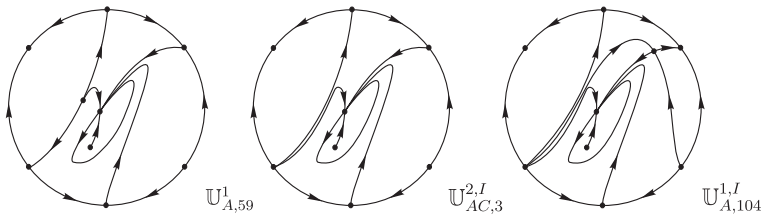

Figure 234 – Impossible unstable phase portrait $\mathbb{U}^{2,I}_{AC,3}$

In the first column of Table 47 we present the remaining phase portraits of the set (A), in the second column we indicate its corresponding phase portrait belonging to the set (AC), and in the third column we show the corresponding phase portrait after bifurcation. We point out that it is not necessary to present any explanation for the phase portraits present in the first column, since their corresponding elements from the third column already appeared and were explained before.

Table 47 – Phase portraits from the set (*AC*) obtained from evolution of some elements of the set (*A*)

phase portrait from the set (*A*)	**phase portrait from the set (*AC*)**	**phase portrait from the set (*A*)**
$\mathbb{U}^1_{A,60}$	$\mathbb{U}^2_{AC,22}$ $\mathbb{U}^2_{AC,32}$	$\mathbb{U}^1_{A,27}$ $\mathbb{U}^1_{A,42}$
$\mathbb{U}^1_{A,61}$	$\mathbb{U}^2_{AC,26}$ $\mathbb{U}^2_{AC,27}$ $\mathbb{U}^2_{AC,39}$	$\mathbb{U}^1_{A,31}$ $\mathbb{U}^1_{A,32}$ $\mathbb{U}^1_{A,55}$
$\mathbb{U}^1_{A,62}$	$\mathbb{U}^2_{AC,40}$	$\mathbb{U}^1_{A,55}$
$\mathbb{U}^1_{A,63}$	$\mathbb{U}^2_{AC,31}$ $\mathbb{U}^2_{AC,33}$	$\mathbb{U}^1_{A,41}$ $\mathbb{U}^1_{A,42}$
$\mathbb{U}^1_{A,64}$	$\mathbb{U}^2_{AC,35}$	$\mathbb{U}^1_{A,43}$
$\mathbb{U}^1_{A,65}$	$\mathbb{U}^2_{AC,17}$ $\mathbb{U}^2_{AC,30}$	$\mathbb{U}^1_{A,22}$ $\mathbb{U}^1_{A,39}$
$\mathbb{U}^1_{A,66}$	$\mathbb{U}^2_{AC,18}$	$\mathbb{U}^1_{A,23}$
$\mathbb{U}^1_{A,67}$	$\mathbb{U}^2_{AC,20}$ $\mathbb{U}^2_{AC,36}$	$\mathbb{U}^1_{A,26}$ $\mathbb{U}^1_{A,51}$
$\mathbb{U}^1_{A,68}$	$\mathbb{U}^2_{AC,37}$ $\mathbb{U}^2_{AC,38}$	$\mathbb{U}^1_{A,52}$ $\mathbb{U}^1_{A,54}$
$\mathbb{U}^1_{A,69}$	$\mathbb{U}^2_{AC,25}$ $\mathbb{U}^2_{AC,28}$	$\mathbb{U}^1_{A,30}$ $\mathbb{U}^1_{A,36}$
$\mathbb{U}^1_{A,70}$	$\mathbb{U}^2_{AC,29}$	$\mathbb{U}^1_{A,37}$

Therefore, we have just finished obtaining all the 40 topologically potential phase portraits of *codimension two** from the set (*AC*) presented in Figs. 103 and 104.

Now we explain how one can obtain these 40 phase portraits by starting the study from the set (*C*). We consider all 32 realizable structurally unstable quadratic vector fields of *codimension one** from the set (*C*). In order to obtain a phase portrait of *codimension two** belonging to the set (*AC*) starting from a phase portrait of *codimension one** of the set (*C*), we keep the existing infinite saddle–node $\binom{1}{1}$ *SN* and by using Thm. 5.2.6 we build a finite saddle–node $\overline{sn}_{(2)}$ by the coalescence of a finite node with a finite saddle. On the other hand, from the phase portraits of *codimension two** from the set (*AC*), there exist two ways of obtaining phase portraits of *codimension one** also belonging to the set (*C*) after perturbation: splitting $\overline{sn}_{(2)}$ into a saddle and a node, or moving it to complex singularities (remember Rmk. 5.3.2).

According to these facts, if a phase portrait possesses only a finite saddle–node, as $\mathbb{U}^1_{C,1}$ for instance, it is not possible to obtain a phase portrait from it which belongs to the set (*AC*). Moreover, in some cases when one makes the finite saddle–node disappears, it is possible to find a phase portrait possessing a limit cycle, as happens for instance with

phase portrait $\mathbb{U}^1_{C,3}$ (see Fig. 235). In such a figure we present the two potential phase portraits which can be obtained by forming a finite saddle–node and then by making it disappears. Indeed, phase portrait $\mathbb{U}^1_{C,3}$ has phase portraits $\mathbb{U}^2_{AC,3}$ and $\mathbb{U}^2_{AC,4}$ as evolution, respectively, by the coalescence of the finite saddle with each one of the two finite nodes. After bifurcation, by making the finite saddle–node disappears, $\mathbb{U}^2_{AC,3}$ generates $\mathbb{U}^1_{C,1}$ and $\mathbb{U}^2_{AC,4}$ generates $\mathbb{U}^1_{C,1}$, being this last one with a limit cycle. However, as our classification of phase portraits is always done modulo limit cycles we simply say that in this case $\mathbb{U}^2_{AC,4}$ generates $\mathbb{U}^1_{C,1}$. This situation also happens when we perform analogous studies of phase portraits $\mathbb{U}^1_{C,20}$, $\mathbb{U}^1_{C,24}$, and $\mathbb{U}^1_{C,31}$, as we will see in the sequence.

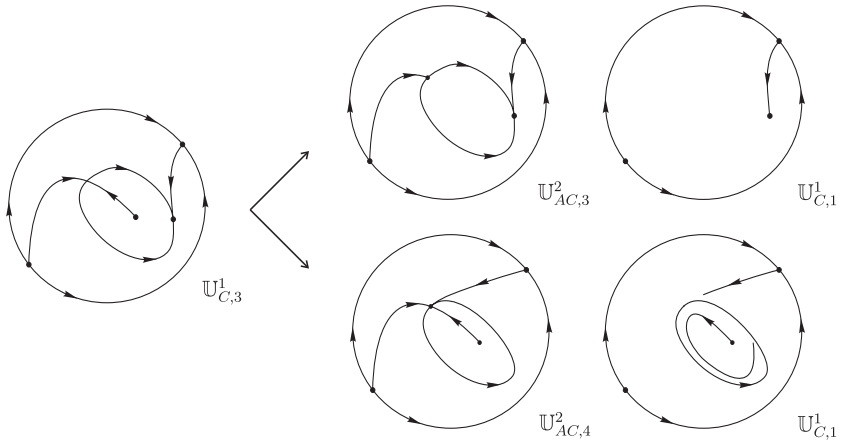

Figure 235 – Unstable systems $\mathbb{U}^2_{AC,3}$ and $\mathbb{U}^2_{AC,4}$ from phase portrait $\mathbb{U}^1_{C,3}$

The main goal of this section is to obtain all the topologically potential phase portraits from the set (AC) and then prove their realization or show that they are not possible. So we have to be sure that no other phase portrait can be found if one does some evolution in all elements of the set (C) in order to obtain a phase portrait belonging to the set (AC). We point out that we have done this verification, i.e. we have also considered each element from the set (C) and produced a coalescence (when it was possible) of a finite node with a finite saddle and we also have obtained the 40 topologically potential phase portraits of *codimension two** from the set (AC) presented in Figs. 103 and 104. Moreover, doing this verification we have not found the impossible phase portraits $\mathbb{U}^{2,I}_{AC,1}$ and $\mathbb{U}^{2,I}_{AC,2}$ (this was expected since the corresponding unfoldings of *codimension one** are impossible in the set (C)). In Table 48 we present the study of phase portraits $\mathbb{U}^1_{C,2}$ to $\mathbb{U}^1_{C,19}$. In the first column of the mentioned table we present the phase portrait of the set (C), in the second column we indicate its corresponding phase portrait belonging to the set (AC) i.e. after producing a finite saddle–node $\overline{sn}_{(2)}$, and in the third column we show the corresponding phase portrait after we make this finite saddle–node $\overline{sn}_{(2)}$ disappears. Note that the sequence of indexes in the first column is not consecutive since in some phase portraits from the set (C) it is not possible to produce a finite saddle–node $\overline{sn}_{(2)}$ and then it is not possible to obtain a phase portrait belonging to the set (AC).

Table 48 – Phase portraits from the set (AC) obtained from evolution of elements of the set (C)

phase portrait from the set (C)	**phase portrait from the set (AC)**	**phase portrait from the set (C)**
$\mathbb{U}^1_{C,2}$	$\mathbb{U}^2_{AC,1}$ $\mathbb{U}^2_{AC,2}$	$\mathbb{U}^1_{C,1}$
$\mathbb{U}^1_{C,3}$	$\mathbb{U}^2_{AC,3}$ $\mathbb{U}^2_{AC,4}$	$\mathbb{U}^1_{C,1}$
$\mathbb{U}^1_{C,5}$	$\mathbb{U}^2_{AC,14}$	$\mathbb{U}^1_{C,4}$
$\mathbb{U}^1_{C,6}$	$\mathbb{U}^2_{AC,15}$	$\mathbb{U}^1_{C,4}$
$\mathbb{U}^1_{C,7}$	$\mathbb{U}^2_{AC,6}$ $\mathbb{U}^2_{AC,8}$	$\mathbb{U}^1_{C,4}$
$\mathbb{U}^1_{C,8}$	$\mathbb{U}^2_{AC,11}$	$\mathbb{U}^1_{C,4}$
$\mathbb{U}^1_{C,9}$	$\mathbb{U}^2_{AC,12}$	$\mathbb{U}^1_{C,4}$
$\mathbb{U}^1_{C,10}$	$\mathbb{U}^2_{AC,13}$	$\mathbb{U}^1_{C,4}$
$\mathbb{U}^1_{C,11}$	$\mathbb{U}^2_{AC,16}$	$\mathbb{U}^1_{C,4}$
$\mathbb{U}^1_{C,12}$	$\mathbb{U}^2_{AC,7}$ $\mathbb{U}^2_{AC,9}$	$\mathbb{U}^1_{C,4}$
$\mathbb{U}^1_{C,13}$	$\mathbb{U}^2_{AC,10}$	$\mathbb{U}^1_{C,4}$
$\mathbb{U}^1_{C,14}$	$\mathbb{U}^2_{AC,5}$	$\mathbb{U}^1_{C,4}$
$\mathbb{U}^1_{C,18}$	$\mathbb{U}^2_{AC,21}$ $\mathbb{U}^2_{AC,23}$	$\mathbb{U}^1_{C,15}$
$\mathbb{U}^1_{C,19}$	$\mathbb{U}^2_{AC,19}$	$\mathbb{U}^1_{C,15}$

Phase portrait $\mathbb{U}^1_{C,20}$ has phase portraits $\mathbb{U}^2_{AC,32}$ and $\mathbb{U}^2_{AC,34}$ as evolution. After bifurcation we get phase portrait $\mathbb{U}^1_{C,17}$ for both cases (being one of them modulo limit cycles), by making the finite saddle–node $\overline{sn}_{(2)}$ disappears. Moreover, phase portrait $\mathbb{U}^1_{C,20}$ also has a phase portrait as an evolution which is topologically equivalent to impossible phase portrait $\mathbb{U}^{2,I}_{AC,3}$, obtained before during the study of phase portrait $\mathbb{U}^{1,I}_{A,59}$. Again, by Thm. 5.2.10 such a phase portrait is impossible because by splitting the original infinite saddle–node $\overline{\binom{1}{1}}SN$ into a finite saddle and an infinite node we obtain the impossible phase portrait $\mathbb{U}^{1,I}_{A,104}$ of *codimension one**, see Fig. 236. Also, in the set (C), $\mathbb{U}^{2,I}_{AC,3}$ unfolds in $\mathbb{U}^1_{C,17}$ (modulo limit cycles).

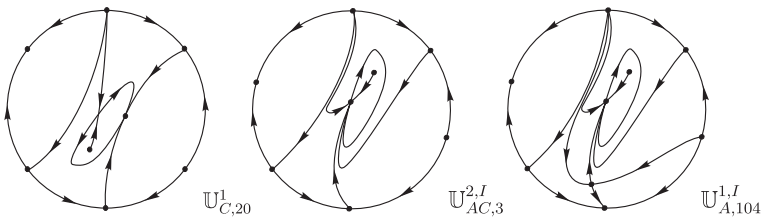

Figure 236 – Impossible unstable phase portrait $\mathbb{U}^{2,I}_{AC,3}$ (see again Fig. 234)

Phase portrait $\mathbb{U}^1_{C,21}$ has phase portraits $\mathbb{U}^2_{AC,22}$ and $\mathbb{U}^2_{AC,24}$ as evolution. After

bifurcation we get phase portrait $\mathbb{U}^1_{C,17}$ for both cases, by making the finite saddle–node $\overline{sn}_{(2)}$ disappears.

Phase portrait $\mathbb{U}^1_{C,22}$ has phase portraits $\mathbb{U}^2_{AC,40}$ and $\mathbb{U}^2_{AC,39}$ as evolution. After bifurcation we get phase portraits $\mathbb{U}^1_{C,15}$ and $\mathbb{U}^1_{C,17}$, respectively, by making the finite saddle–node $\overline{sn}_{(2)}$ disappears.

Phase portrait $\mathbb{U}^1_{C,23}$ has phase portraits $\mathbb{U}^2_{AC,26}$ and $\mathbb{U}^2_{AC,27}$ as evolution. After bifurcation we get phase portrait $\mathbb{U}^1_{C,17}$ for both cases, by making the finite saddle–node $\overline{sn}_{(2)}$ disappears.

Phase portrait $\mathbb{U}^1_{C,24}$ has phase portraits $\mathbb{U}^2_{AC,33}$ and $\mathbb{U}^2_{AC,35}$ as evolution. After bifurcation we get phase portrait $\mathbb{U}^1_{C,15}$ for both cases (being one of them modulo limit cycles), by making the finite saddle–node $\overline{sn}_{(2)}$ disappears. Moreover, phase portrait $\mathbb{U}^1_{C,24}$ also has the impossible phase portrait $\mathbb{U}^{2,I}_{AC,4}$ as an evolution. By Thm. 5.2.10 such a phase portrait is impossible because by splitting the original infinite saddle–node $\overline{\binom{1}{1}}\,SN$ into a finite saddle and an infinite node we obtain the impossible phase portrait $\mathbb{U}^{1,I}_{A,104}$ of *codimension one**, see Fig. 237. We observe that, in the set (C), $\mathbb{U}^{2,I}_{AC,4}$ unfolds in $\mathbb{U}^1_{C,15}$ (modulo limit cycles).

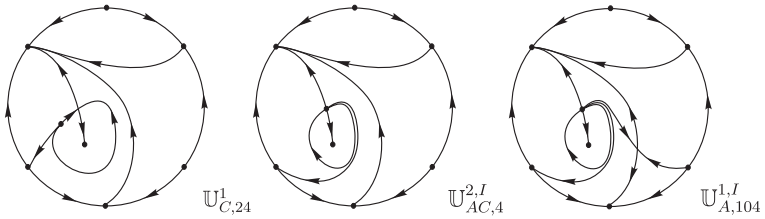

Figure 237 – Impossible unstable phase portrait $\mathbb{U}^{2,I}_{AC,4}$

In Table 49 we present the study of phase portraits $\mathbb{U}^1_{C,25}$ to $\mathbb{U}^1_{C,30}$ and we follow the same pattern used in Table 48.

Table 49 – Phase portraits from the set (AC) obtained from evolution of elements of the set (C)

phase portrait from the set (C)	**phase portrait from the set (AC)**	**phase portrait from the set (C)**
$\mathbb{U}^1_{C,25}$	$\mathbb{U}^2_{AC,31}$	$\mathbb{U}^1_{C,15}$
$\mathbb{U}^1_{C,26}$	$\mathbb{U}^2_{AC,17}$ $\mathbb{U}^2_{AC,18}$	$\mathbb{U}^1_{C,16}$
$\mathbb{U}^1_{C,27}$	$\mathbb{U}^2_{AC,30}$	$\mathbb{U}^1_{C,16}$
$\mathbb{U}^1_{C,28}$	$\mathbb{U}^2_{AC,38}$	$\mathbb{U}^1_{C,15}$
$\mathbb{U}^1_{C,29}$	$\mathbb{U}^2_{AC,20}$	$\mathbb{U}^1_{C,16}$
$\mathbb{U}^1_{C,30}$	$\mathbb{U}^2_{AC,37}$ $\mathbb{U}^2_{AC,36}$	$\mathbb{U}^1_{C,15}$ $\mathbb{U}^1_{C,16}$

Phase portrait $\mathbb{U}^1_{C,31}$ has phase portraits $\mathbb{U}^2_{AC,28}$ and $\mathbb{U}^2_{AC,29}$ as evolution. After bifurcation we get phase portrait $\mathbb{U}^1_{C,16}$ for both cases (being one of them modulo limit cycles), by making the finite saddle–node $\overline{sn}_{(2)}$ disappears. Moreover, phase portrait $\mathbb{U}^1_{C,31}$ also has the impossible phase portrait $\mathbb{U}^{2,I}_{AC,5}$ as an evolution. By Thm. 5.2.10 such a phase portrait is impossible because by splitting the original infinite saddle–node $\overline{\binom{1}{1}}\,SN$ into an infinite saddle and a finite node we obtain the impossible phase portrait $\mathbb{U}^{1,I}_{A,106}$ of *codimension one**, see Fig. 238. We observe that, in the set (C), $\mathbb{U}^{2,I}_{AC,5}$ unfolds in $\mathbb{U}^1_{C,16}$ (modulo limit cycles).

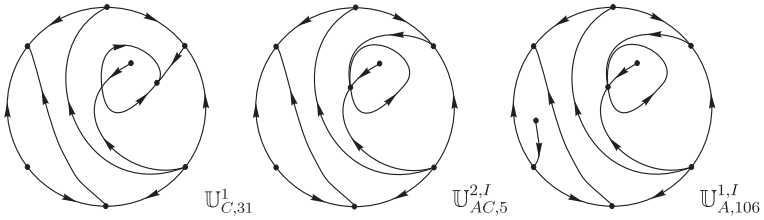

Figure 238 – Impossible unstable phase portrait $\mathbb{U}^{2,I}_{AC,5}$

5.4.2 The realization of the potential phase portraits

In the previous subsection we have produced all the 42 topologically potential phase portraits for structurally unstable quadratic systems of *codimension two** belonging to the set $\sum^2_2(AC)$. And from them, we have already discarded two which are not realizable due to their respective unfoldings of *codimension one** being impossible.

In this subsection we aim to give specific examples for the 40 different topological classes of structurally unstable quadratic systems of *codimension two** belonging to the set $\sum^2_2(AC)$ and presented in Figs. 103 and 104. As in the previous section, we point out that we have found examples with no signals of limit cycles, but we have not proved the absence of infinitesimal ones.

In Chap. 4 we classified, with respect to a specific normal form, the set of all real quadratic polynomial differential systems with a finite semi–elemental saddle–node $\overline{sn}_{(2)}$ located at the origin of the plane and an infinite saddle–node of type $\overline{\binom{1}{1}}\,SN$ obtained by the coalescence of a finite antisaddle (respectively finite saddle) with an infinite saddle (respectively infinite node).

As we have discussed in the previous section, the study of bifurcation diagrams of a certain family of quadratic systems, produces not only the class of phase portraits looked for, but also all those of their closure according to the normal form used. Even though the study is mainly algebraic, often, also analytic and numerical tools are required. This makes that these studies may be not complete and subject to the existence of possible "islands" which contain an undetected phase portrait. The border of that "island" could mean the

connection of two separatrices, and the interior contain a different phase portrait from the ones stated in the theorem. The topological study that we do here solves partially this problem, since we prove that all the realizable phase portraits of class (*AC*) do really exists, and no other topological possibility does. However, the possible existence of "islands" in the bifurcation diagram still persists since they can be related with double limit cycles, as we discussed in Sec. 4.4 of Chap. 4.

By using the phase portraits of generic regions of the bifurcation diagram presented in Chap. 4 we realize all the 40 unstable systems of *codimension two** of the set (*AC*), i.e. we can give specific examples of all structurally unstable phase portraits from the set (*AC*). In fact, consider systems (4.1), i.e.

$$\dot{x} = cx + cy - cx^2 + 2hxy,$$
$$\dot{y} = ex + ey - ex^2 + 2mxy,$$

where c, e, h and m are real parameters and $eh - cm \neq 0$. This normal form was studied in Chap. 4 and it describes quadratic polynomial differential systems which have a finite semi–elemental saddle–node $\overline{sn}_{(2)}$, a finite elemental singularity and an infinite saddle–node of type $\overline{\binom{1}{1}}\,SN$.

In Table 50 we present one representative from each generic region of the bifurcation diagram from Chap. 4 corresponding to each phase portrait of *codimension two** from the set (*AC*) and, therefore, we conclude the proof of Thm. 5.1.2.

5.5 Graphics and limit cycles

Even though the goal of this chapter deals little with graphics and limit cycles, there is no doubt that these are two of the most important elements in Qualitative Theory of Ordinary Differential Equations.

Limit cycles are the most elusive phenomena in phase portraits. They may appear either by a bifurcation of a weak focus (Hopf bifurcation), by a bifurcation of a graphic, or by a bifurcation of a multiple limit cycle, and only the first case can be fully algebraically controlled. The other cases are generically nonalgebraic. In fact, weak foci can be considered among graphics, since they can be seen as graphics reduced to a single point.

Our goal to find all the topologically different phase portraits modulo limit cycles bypasses this big problem, but it is not an irrelevant goal. Whenever the mathematical community finally gets the complete set of phase portraits of quadratic systems (or whatever other family), the subset of the phase portraits modulo limit cycles will be the base for such a classification. It is expected to obtain more than one thousand (maybe even up to 2000) different phase portraits of quadratic systems modulo limit cycles. For quite

Table 50 – Correspondence between *codimension two** phase portraits of the set (*AC*) and phase portraits from Figs. 15 and 16. In the first column we present the *codimension two** phase portraits from the set (*AC*), in the second column we show the corresponding phase portraits from Figs. 15 and 16, and in the other columns we present the values of the parameters c, e, h, and m of (4.1) which realizes the phase portrait

Cod 2*	**Phase Portrait**	c	e	h	m
$\mathbb{U}^2_{AC,1}$	V_{38}	-10	30	1	4
$\mathbb{U}^2_{AC,2}$	V_1	6	81/2	1	4
$\mathbb{U}^2_{AC,3}$	V_{33}	-7	5/2	1	4
$\mathbb{U}^2_{AC,4}$	V_{53}	2	47/50	1	37/100
$\mathbb{U}^2_{AC,5}$	V_{13}	-1	-10	1	4
$\mathbb{U}^2_{AC,6}$	V_4	7	15	1	4
$\mathbb{U}^2_{AC,7}$	V_{21}	$-9/4$	-10	1	4
$\mathbb{U}^2_{AC,8}$	V_{92}	-3	7/2	1	$-6/5$
$\mathbb{U}^2_{AC,9}$	V_{10}	1/2	$-11/2$	1	4
$\mathbb{U}^2_{AC,10}$	V_{63}	$-2/5$	1/50	1	$-1/4$
$\mathbb{U}^2_{AC,11}$	V_{95}	-3	31/10	1	$-6/5$
$\mathbb{U}^2_{AC,12}$	V_{73}	$-19/10$	17/20	1	$-3/4$
$\mathbb{U}^2_{AC,13}$	V_8	3/2	$-9/2$	1	4
$\mathbb{U}^2_{AC,14}$	V_{93}	-1	11/10	1	$-6/5$
$\mathbb{U}^2_{AC,15}$	V_6	24/5	$-4/5$	1	4
$\mathbb{U}^2_{AC,16}$	V_{68}	-3	2/5	1	$-1/4$
$\mathbb{U}^2_{AC,17}$	V_{39}	-25	30	1	4
$\mathbb{U}^2_{AC,18}$	V_3	45/2	98	1	4
$\mathbb{U}^2_{AC,19}$	V_{62}	$-1/40$	1/50	1	$-1/4$
$\mathbb{U}^2_{AC,20}$	V_{80}	$-6/5$	1207/1000	1	-1
$\mathbb{U}^2_{AC,21}$	V_{81}	29/50	$-3/5$	1	$-6/5$
$\mathbb{U}^2_{AC,22}$	V_{36}	-1	4	1	4
$\mathbb{U}^2_{AC,23}$	V_{23}	$-9/2$	-17	1	4
$\mathbb{U}^2_{AC,24}$	V_{112}	1/2	42	1	-10
$\mathbb{U}^2_{AC,25}$	V_{77}	$-5/4$	629/500	1	$-49/50$
$\mathbb{U}^2_{AC,26}$	V_{90}	$-9/5$	881/400	1	$-6/5$
$\mathbb{U}^2_{AC,27}$	V_2	1	7	1	4
$\mathbb{U}^2_{AC,28}$	V_{35}	$-1747/50$	30	1	4
$\mathbb{U}^2_{AC,29}$	V_{49}	10	5156/625	1	51/100
$\mathbb{U}^2_{AC,30}$	V_{65}	$-23/50$	1151/10000	1	$-1/4$
$\mathbb{U}^2_{AC,31}$	V_{59}	$-1/50$	1/40	1	$-1/4$
$\mathbb{U}^2_{AC,32}$	V_{29}	$-3/2$	1/2	1	4
$\mathbb{U}^2_{AC,33}$	V_{82}	1341/2000	$-3/5$	1	$-6/5$
$\mathbb{U}^2_{AC,34}$	V_{102}	1/100	31/10	1	$-5/2$
$\mathbb{U}^2_{AC,35}$	V_{26}	$-687/50$	-17	1	4
$\mathbb{U}^2_{AC,36}$	V_{20}	$-21/10$	$-41/5$	1	4
$\mathbb{U}^2_{AC,37}$	V_{51}	10	151/20	1	3/4
$\mathbb{U}^2_{AC,38}$	V_{71}	$-1/10000$	3/125	1	$-1/4$
$\mathbb{U}^2_{AC,39}$	V_{14}	$-3/2$	-4	1	4
$\mathbb{U}^2_{AC,40}$	V_{55}	1/100	1/100	1	$-1/4$

many of them it will be trivial to determine that they will not have limit cycles (in the case they do not have a finite antisaddle). But for all the others, it will be necessary to determine exactly how many different phase portraits can be obtained from that skeleton by adding limit cycles. Up to now and up to our knowledge, there are very few nontrivial skeletons of phase portraits which could theoretically have limit cycles, and for which the absence of limit cycles has been proved. To be more precise, we are only completely sure of one of them, namely the structurally stable phase portrait $\mathbb{S}^2_{7,1}$. This phase portrait was obtained in Artés, Kooij and Llibre (1998) and was conjectured by statistical tools to be incompatible with limit cycles in Artés and Llibre (2003) and this conjecture was proved in Artés, Llibre and Medrado (2007). Also in Artés and Llibre (2003) some other phase portraits are conjectured (by statistical data) to be incompatible with limit cycles, but no proof is available yet. Apart from these last ones, other candidates can be found in Class I of Ye and Lo (1986). In that paper the authors produce three normal forms (denoted by I, II and III) and they prove that any system with limit cycle can be transformed in an element of them. The three classes have no intersection since they deal with the number of finite singularities that have gone to infinity (≥ 2, 1 and 0, respectively). And in Ye and Lo (1986) it is also proved that systems from Class I have at most one limit cycle. There is still no conclusive study of phase portraits from Class I, but some phase portraits of this class have already been found having one limit cycle and some others with no limit cycle (see Coll (1987), Jia, Chen and Chen (2020), Reyn and Kooij (1997)). For the cases with limit cycle, it is closed the fact that such phase portraits can have at most one limit cycle, and if a conclusive study is done and results are confirmed, the cases with no limit cycle would add to the phase portrait $\mathbb{S}^2_{7,1}$ as skeletons of phase portraits without limit cycles. For all other skeletons of phase portraits found up to now, there is not a single proof determining which is the maximum number of limit cycles that each one may have. There are many other papers related to the maximum number of limit cycles, but they are mostly linked to a certain normal form. Most of them simply prove that a specific normal form may have just one limit cycle. But this does not imply that the skeletons of phase portraits obtained in that normal form may have more limit cycles in the entire classification.

Up to now, it is known that there are examples of phase portraits of quadratic systems with four limit cycles distributed into two nests around two foci, more precisely, three limit cycles in one nest and the fourth limit cycle in the other nest (see, for instance, Songling (1981) where the author provided one of the first quadratic systems proved to have 4 limit cycles). And even though it is conjectured that the effective maximum is four with the distribution just mentioned, there is still no conclusive proof. The phase portraits for which there are examples with four limit cycles belong to three skeletons of phase portraits, namely, the structurally stables $\mathbb{S}^2_{4,1}$ and $\mathbb{S}^2_{11,2}$ from Artés, Kooij and Llibre (1998), and the *codimension one** $\mathbb{U}^1_{B,31}$ from Artés, Llibre and Rezende (2018).

The proof that they may have at least four limit cycles appears in several papers since they appear in classifications with a weak focus of order three, already having a limit cycle around a strong focus.

But not even if the maximum bound was four, we would not be close to obtain all the phase portraits of quadratic systems. Any of the three skeletons mentioned before may have the topologically different configurations $(0,0)$, $(1,0)$, $(2,0)$, $(3,0)$, $(1,1)$, $(2,1)$, and $(3,1)$. That is, seven different configurations. But even that is not a criterion (that is, multiply the number of skeletons by 7) to obtain a simple upper bound for the total number of phase portraits. There are phase portraits like $\mathbb{S}^2_{5,1}$ from Artés, Kooij and Llibre (1998) which has three finite antisaddles. One of them receives (or emits) a single separatrix, the second one receives (or emits) exactly two separatrices, and the third one receives (or emits) exactly three separatrices. So, the fact that a limit cycle could be surrounding any of the three antisaddles would generate a topologically different phase portrait. And in case there were two nests of limit cycles, and assuming that they could have up to four limit cycles, the number of cases would increase up to 25 possibilities. But from these 25 possibilities, up to now only six have been confirmed to exist. We are collecting a large database and recording the maximum number of limit cycles found in each one of the skeletons classified up to now.

With all these facts we want to remark that the topological classification of phase portraits modulo limit cycles is important since it produces a complete set of skeletons from which all the complete set of phase portraits must be located. For each particular skeleton, it must be studied if it contains none, one, two or up to three antisaddles around which the limit cycles may be located. If there is a complete collection of phase portraits modulo limit cycles, and if an upper bound of limit cycles is found, it will give a quite rough upper bound for the number of different phase portraits. But the real number will need a deeper study case by case. Nowadays, the moment that we could have a complete topological classification is quite far away. However, the topological classification modulo limit cycles is within reach, although they are not easily reachable yet.

We now talk about graphics. Graphics are also very important because they can become the bifurcation edge which leads to the birth of limit cycles. There has been a lot of literature related to graphics, and one of the most relevant papers is the one from Dumortier, Roussarie and Rousseau (1994) where the authors list a set of 121 different graphics whose finite cyclicity needs to be proved in order to prove the finiteness part of Hilbert 16th problem for quadratic systems. The graphics in this list can be of different types. Many of them imply the connection of one (or more) couple of separatrices, finite or infinite. Other graphics are formed simply because a separatrix arrives to the nodal part of a saddle–node (finite or infinite) or an even more degenerate singularity in coexistence with other properties of the phase portrait. Unfortunately, most of these graphics cannot

be detected by means of algebraic tools. In many studies of families of systems where a complete bifurcation is given in the parameter space, after all the algebraic bifurcations are given, the use of continuity and coherence arguments allows the detection of some other nonalgebraic bifurcations where these graphics appear.

Our methodical study of phase portraits of quadratic systems modulo limit cycles started with codimension zero (structurally stable) (see Artés, Kooij and Llibre (1998)) and of course these phase portraits cannot have any graphic at all. The second step was the classification of codimension–one phase portraits (modulo limit cycles), and in that study we could start finding some graphics, but not too many. Precisely, we found graphic (F_2^1) from Dumortier, Roussarie and Rousseau (1994) in $\mathbb{U}^1_{A,37}$, $\mathbb{U}^1_{A,43}$, $\mathbb{U}^1_{A,64}$, and $\mathbb{U}^1_{A,70}$. This graphic is formed simply by one finite saddle–node which sends its center manifold (separatrix of zero eigenvalue) to its own nodal part. We also have graphic (I^2_{19}) from Dumortier, Roussarie and Rousseau (1994) in $\mathbb{U}^1_{B,29}$, $\mathbb{U}^1_{B,30}$ (twice), $\mathbb{U}^1_{B,33}$, $\mathbb{U}^1_{B,36}$, and $\mathbb{U}^1_{B,38}$. This graphic is formed by one elemental infinite saddle which sends one of its separatrices to the nodal part of an infinite adjacent saddle–node formed by the coalescence of two infinite singularities. There are no graphics in the set $(\boldsymbol{C})$ of codimension–one phase portraits (modulo limit cycles, see page 47). Finally, in the set $(\boldsymbol{D})$ (see again page 47) we found the graphics (F_1^1), (H_1^1), and (I_1^2) from Dumortier, Roussarie and Rousseau (1994). The first one is just a loop of a finite elemental saddle, the second one is a separatrix connection between opposite infinite elemental saddles, and the third one is a separatrix connection between adjacent infinite elemental saddles. The loop is present in $\mathbb{U}^1_{D,1}$, $\mathbb{U}^1_{D,6}$, $\mathbb{U}^1_{D,7}$, $\mathbb{U}^1_{D,8}$, $\mathbb{U}^1_{D,9}$, $\mathbb{U}^1_{D,12}$, $\mathbb{U}^1_{D,19}$, $\mathbb{U}^1_{D,20}$, $\mathbb{U}^1_{D,22}$, $\mathbb{U}^1_{D,23}$, $\mathbb{U}^1_{D,30}$, $\mathbb{U}^1_{D,31}$, $\mathbb{U}^1_{D,32}$, $\mathbb{U}^1_{D,46}$, $\mathbb{U}^1_{D,47}$, $\mathbb{U}^1_{D,48}$, $\mathbb{U}^1_{D,49}$, $\mathbb{U}^1_{D,50}$, $\mathbb{U}^1_{D,51}$, $\mathbb{U}^1_{D,52}$, $\mathbb{U}^1_{D,53}$, and $\mathbb{U}^1_{D,54}$. The second graphic appears in $\mathbb{U}^1_{D,10}$ and $\mathbb{U}^1_{D,11}$. And the third one can be seen in $\mathbb{U}^1_{D,28}$, $\mathbb{U}^1_{D,29}$, $\mathbb{U}^1_{D,37}$, $\mathbb{U}^1_{D,38}$, and $\mathbb{U}^1_{D,39}$. No other graphic from these last five may appear, since all the remaining 116 imply higher codimension.

Thus, in our current study of phase portraits of *codimension two** with a finite saddle–node and an infinite saddle–node, the only graphics that we can see will be those ones which are inherited from the respective phase portraits of *codimension one** already having a graphic. No new graphic may appear from the consolidation of the two different instabilities we mix here. In the studies of the sets $(\boldsymbol{AD})$, $(\boldsymbol{BD})$, and $(\boldsymbol{CD})$ we will start incorporating more graphics from Dumortier, Roussarie and Rousseau (1994), since we will find, for example, saddle–nodes forming a loop instead of an elemental saddle. Also the set $(\boldsymbol{DD})$ will provide graphics with two separatrix connections. Anyway, the graphics will appear in larger numbers when *codimension three** is studied.

There is another important fact, related to stability and graphics, to comment about the classification that we are working with. As we mentioned in the Introduction, in Artés, Llibre and Rezende (2018) it is claimed that there are at least 204 structurally

unstable phase portraits of *codimension one** and at most 211. Two papers have found two mistakes in that book and the newly proved numbers are 202 and 209, respectively. The seven cases that have not been found correspond to cases which are conjectured as impossible and some arguments are given to support that conjecture. We point out that all the seven cases conjectured impossible contain a graphic, more precisely the polycycles (F_2^1) or (H_1^1). These phase portraits consist in an skeleton of separatrices which depending on the stability of the focus inside the polycycle (compared to other stabilities outside it) may lead or not to a realizable phase portrait. That is, they lead to a phase portrait which is already known to exist, or lead to a phase portrait which (up to our knowledge) never appeared before in any paper. The normal techniques which have allowed us to prove the impossibility of hundreds of phase portraits are useless in these seven cases. All we can say about these seven phase portraits is that in case they exist, some perturbations from them would produce phase portraits with a limit cycle that we have not found anywhere. Using the tools of perturbations related to stability that we use in this chapter, we may claim that if one of those phase portraits with a limit cycle could be proven impossible, then the related unstable phase portrait with a polycycle would be also impossible. However, the opposite is not true. If the phase portrait with a limit cycle does exist, it is not sure that the related unstable phase portrait with a polycycle may exist. There is the possibility that by means of a rotated vector field one could pass from one to the other, but it is not guaranteed.

So, we see once more the importance of graphics and limit cycles in the classification of phase portraits. The fact that we talk so little about limit cycles is simply because we want to do the classification modulo limit cycles in order to have a good base upon which we or others may add the limit cycles. And the fact that we talk so little about graphics is because at the level of codimension that we are in this stage, there appear very few of the 121 graphics described in Dumortier, Roussarie and Rousseau (1994).

CHAPTER

6

GEOMETRIC ANALYSIS OF QUADRATIC DIFFERENTIAL SYSTEMS WITH INVARIANT ELLIPSES

In this chapter we use extensively the theory developed in Chap. 2 in order to study quadratic systems possessing invariant ellipses.

6.1 Introduction and statement of the main results

As before, here we consider planar polynomial differential systems

$$dx/dt = p(x,y), \quad dy/dt = q(x,y) \tag{6.1}$$

where $p,q \in \mathbb{R}[x,y]$.

Lets us recall two important definitions.

Definition 6.1.1 (Darboux)**.** An algebraic curve $f(x,y) = 0$, where $f \in \mathbb{C}[x,y]$, is an invariant curve of the planar polynomial system (6.1) if and only if there exists a polynomial $k(x,y) \in \mathbb{C}[x,y]$ such that

$$p(x,y)\frac{\partial f}{\partial x} + q(x,y)\frac{\partial f}{\partial y} = k(x,y)f(x,y).$$

Definition 6.1.2 (Darboux)**.** We call algebraic solution of a planar polynomial system an invariant algebraic curve over $\mathbb{C}$ which is irreducible.

One of the main motivations for this chapter comes from integrability problems related to the work of Darboux (see Darboux (1878)).

Theorem 6.1.3 (Darboux)**.** Suppose that a polynomial system (6.1) has m invariant algebraic curves $f_i(x,y) = 0$, $i \le m$, with $f_i \in \mathbb{C}[x,y]$ and with $m > n(n+1)/2$, where n is

the degree of the system. Then there exist complex numbers $\lambda_1,\ldots,\lambda_m$ such that $f_1^{\lambda_1}\ldots f_m^{\lambda_m}$ is a first integral of the system.

The condition in Darboux's theorem is only sufficient for Darboux integrability (integrability in terms of invariant algebraic curves) and it is not also necessary. Thus the lower bound on the number of invariant curves sufficient for Darboux integrability stated in the theorem of Darboux is larger than necessary. Darboux's theory has been improved by including for example the multiplicities of the curves (Llibre and Zhang (2009)). Also, the number of invariant algebraic curves needed was reduced but by adding some conditions, in particular the condition that any two of the curves be transversal. But a deeper understanding about Darboux integrability is still lacking. Algebraic integrability, which intervenes in the open problem stated by Poincaré in 1891 (see Poincaré (1891a) and Poincaré (1891b)), and which means the existence of a rational first integral for the system, is a particular case of Darboux integrability.

Theorem 6.1.4 (See Jouanolou (1979))**.** Suppose that a polynomial system (6.1), defined by polynomials $p(x,y)$, $q(x,y)\in\mathbb{C}[x,y]$, has m invariant algebraic curves $f_i(x,y)=0$, $i\le m$, with $f_i\in\mathbb{C}[x,y]$ and with $m\ge n(n+1)/2+2$, where n is the degree of the system. Then the system has a rational first integral $h(x,y)/g(x,y)$ where $h(x,y),g(x,y)\in\mathbb{C}[x,y]$.

To advance knowledge on algebraic or more generally Darboux integrability it is necessary to have a large number of examples to analyze. In the literature, scattered isolated examples were analyzed but a more systematic approach was still needed. Schlomiuk and Vulpe initiated a systematic program to construct such a data base for quadratic differential systems. Since the simplest case is of systems with invariant straight lines, their first works involved only invariant lines for quadratic systems (see Schlomiuk and Vulpe (2004), Schlomiuk and Vulpe (2008b), Schlomiuk and Vulpe (2008d), Schlomiuk and Vulpe (2008c) and Schlomiuk and Vulpe (2010)). One of the next steps is to study classes of quadratic systems with invariant conics. In this sense, in Oliveira *et al.* (2017) the authors started these studies by considering the class **QSH** of non–degenerate quadratic differential systems having invariant hyperbolas. In this chapter we discuss the study of a class of quadratic systems with an invariant conic, namely the class **QSE** of non–degenerate (i.e. p and q are relatively prime) quadratic differential systems having an invariant ellipse. Such systems could also have some invariant lines and in many cases the presence of these invariant curves turns them into Darboux integrable systems. We always assume here that systems (6.1) are non–degenerate because otherwise doing a time rescaling, they can be reduced to linear or constant systems. Under this assumption all the systems in **QSE** have a finite number of finite singularities.

The irreducible affine conics over the field $\mathbb{R}$ are the hyperbolas, ellipses and parabolas. One way to distinguish them is to consider their points at infinity (see Abhyankar

(1988)). The term hyperbola is used for a real irreducible affine conic which has two real points at infinity. This distinguishes it from the other two irreducible real conics: the parabola has just one real point at infinity at which the multiplicity of intersection of the conic with the line at infinity is two, and the ellipse which has two complex points at infinity.

In the theory of Darboux the invariant algebraic curves are considered (and rightly so) over the complex field $\mathbb{C}$. We may extend the notion of hyperbola (parabola or ellipse) for conics over $\mathbb{C}$. A hyperbola (respectively parabola or ellipse) is an algebraic curve C in $\mathbb{C}^2$, $C : f(x,y) = 0$ with $f \in \mathbb{C}[x,y]$, $\deg(f) = 2$ which is irreducible and which has two real points at infinity (respectively one real point at infinity with intersection multiplicity two, or two complex (non–real) points at infinity).

Remark 6.1.5. We draw attention to the fact that if we have a curve $C : f(x,y) = 0$ over $\mathbb{C}$ it could happen that multiplying the equation by a number $\lambda \in \mathbb{C}^* = \mathbb{C}\backslash\{0\}$, the coefficients of the new equation become real. In this case, to the equation $f(x,y) = 0$ we can associate two curves: one real $\{(x,y) \in \mathbb{R}^2 | \lambda f(x,y) = 0\}$ and one complex $\{(x,y) \in \mathbb{C}^2 | f(x,y) = 0\}$. In particular, if $f(x,y) \in \mathbb{R}[x,y]$ then we could talk about two curves, one in the real and the other in the complex plane. If the coefficients of an algebraic curve $C : f(x,y) = 0$ cannot be made real by multiplication with a constant, then clearly to the equation $f(x,y) = 0$ we can associate just one curve, namely the complex curve $\{(x,y) \in \mathbb{C}^2 | f(x,y) = 0\}$.

In this chapter (in fact, in the entire thesis) we consider real polynomial differential equations. To each such system of equations there corresponds the complex system with the same coefficients to which we can apply the theory of Darboux using complex invariant algebraic curves. Some of these curves may turn out to be with real coefficients in which case they also yield, as in the previous remark, invariant algebraic curves in $\mathbb{R}^2$ of the real differential system. It is one way, but not the only way, in which the theory of Darboux yields applications to real systems. It is by juggling both with complex and real systems and their invariant complex or real algebraic curves that we get a full understanding of the classification problem we consider here.

We suppose that a polynomial differential system has an algebraic solution $f(x,y) = 0$ where $f(x,y) \in \mathbb{C}[x,y]$ is of degree n, $f(x,y) = a_{00} + a_{10}x + a_{01}y + \cdots + a_{n0}x^n + a_{n-1,1}x^{n-1}y + \cdots + a_{0n}y^n$ with $\hat{a} = (a_{00}, \ldots, a_{0n}) \in \mathbb{C}^N$ where $N = (n+1)(n+2)/2$. We note that the equation $\lambda f(x,y) = 0$ where $\lambda \in \mathbb{C}^* = \mathbb{C}\backslash\{0\}$ yields the same locus of complex points in the plane as the locus induced by $f(x,y) = 0$. So, a curve of degree n defined by $\hat{a}$ can be identified with a point $[\hat{a}] = [a_{00} : a_{10} : \cdots : a_{0n}]$ in $\mathbb{P}_{N-1}(\mathbb{C})$. We say that a sequence of curves $f_i(x,y) = 0$ of degree n converges to a curve $f(x,y) = 0$ if and only if the sequence of points $[a_i] = [a_{i00} : a_{i10} : \cdots : a_{i0n}]$ converges to $[\hat{a}] = [a_{00} : a_{10} : \cdots : a_{0n}]$ in the topology

of $\mathbb{P}_{N-1}(\mathbb{C})$.

On the class **QS** acts the group of real affine transformations and time rescaling and because of this, modulo this group action quadratic systems ultimately depend on five parameters. In particular, restricting this group action on **QSE**, modulo this action the **QSE** is a union of one–dimensional, two–dimensional and three–dimensional families of systems as it can be seen from the normal forms obtained in Oliveira *et al.* (2021) for this class.

We observe that if we rescale the time $t' = \lambda t$ by a positive constant λ the geometry of systems (6.1) does not change. So, for our purposes we can identify a system (6.1) of degree n with a point $[a_{00}, a_{10}, \ldots, a_{0n}, b_{00}, \ldots, b_{0n}]$ in $\mathbb{S}^{N-1}(\mathbb{R})$, with $N = (n+1)(n+2)$.

We compactify the space of all the polynomial differential systems of degree n on $\mathbb{S}^{N-1}$ with $N = (n+1)(n+2)$ by multiplying the coefficients of each systems with $1/(\sum(a_{ij}^2 + b_{ij}^2))^{1/2}$.

Definition 6.1.6. (1) We say that an invariant curve $\mathscr{L} : f(x,y) = 0$, $f \in \mathbb{C}[x,y]$, for a polynomial system (S) of degree n has *multiplicity* m if there exists a sequence of real polynomial systems (S_k) of degree n converging to (S) in the topology of $\mathbb{S}^{N-1}$, $N = (n+1)(n+2)$, such that each (S_k) has m distinct invariant curves $\mathscr{L}_{1,k} : f_{1,k}(x,y) = 0, \ldots, \mathscr{L}_{m,k} : f_{m,k}(x,y) = 0$ over $\mathbb{C}$, $\deg(f) = \deg(f_{i,k}) = r$, converging to $\mathscr{L}$ as $k \to \infty$, in the topology of $\mathbb{P}_{R-1}(\mathbb{C})$, with $R = (r+1)(r+2)/2$ and this does not occur for $m+1$.

(2) We say that the line at infinity $\mathscr{L}_\infty : Z = 0$ of a polynomial system (S) of degree n has *multiplicity* m if there exists a sequence of real polynomial systems (S_k) of degree n converging to (S) in the topology of $\mathbb{S}^{N-1}$, $N = (n+1)(n+2)$, such that each (S_k) has $m-1$ distinct invariant lines $\mathscr{L}_{1,k} : f_{1,k}(x,y) = 0, \ldots, \mathscr{L}_{m-1,k} : f_{m-1,k}(x,y) = 0$ over $\mathbb{C}$, converging to the line at infinity $\mathscr{L}_\infty$ as $k \to \infty$, in the topology of $\mathbb{P}_2(\mathbb{C})$ and this does not occur for m.

Remark 6.1.7. (a) In order to describe the various kinds of multiplicities for infinite singularities we use the concepts and notations introduced in Schlomiuk and Vulpe (2004). Thus we denote by "(a,b)" the maximum number a (respectively b) of infinite (respectively finite) singularities which can be obtained by perturbation of a multiple infinite singularity.

(b) In the diagram of Fig. 242 we draw the multiple curves with bold lines and we place a number without parentheses next to the curve which corresponds to its multiplicity (see for example *Config. E.24*). However, there exist two configurations in which we draw the invariant ellipse with thicker line (without a number next to it) in order to indicate that it is a limit cycle (see *Config. E.5* and *Config. E.9*).

An important tool in this chapter is the notion of *configuration of algebraic solutions* of a polynomial differential system. This notion appeared for the first time in Schlomiuk and Vulpe (2004).

Definition 6.1.8. Consider a planar polynomial system which has a finite number of algebraic solutions and a finite number of singularities, finite or infinite. By a *configuration of algebraic solutions* of this system we mean the set of algebraic solutions over $\mathbb{C}$ of the system, each one of these curves endowed with its own multiplicity and together with all the real singularities of this system located on these curves, each one of these singularities endowed with its own multiplicity.

We may have two distinct systems which may be non–equivalent modulo the action of the group but which may have "the same configuration" of invariant ellipses and straight lines. We need to say when two configurations are "the same" or equivalent.

Definition 6.1.9. Suppose we have two systems (S_1) and (S_2) in **QSE** with a finite number of singularities, finite or infinite, a finite set of invariant ellipses $\mathscr{E}_i : e_i(x,y) = 0$, $i = 1,\ldots,k$, of (S_1) (respectively $\mathscr{E}_i' : e_i'(x,y) = 0$, $i = 1,\ldots,k$, of (S_2)) and a finite set (which could also be empty) of invariant straight lines $\mathscr{L}_j : f_j(x,y) = 0$, $j = 1,2,\ldots,k'$, of (S_1) (respectively $\mathscr{L}_j' : f_j'(x,y) = 0$, $j = 1,2,\ldots,k'$, of (S_2)). We say that the two configurations C_1 and C_2 of ellipses and lines of these systems are equivalent if there is a one–to–one correspondence ϕ_e between the ellipses of C_1 and C_2 and a one–to–one correspondence ϕ_l between the lines of C_1 and C_2 such that:

(i) the correspondences conserve the multiplicities of the ellipses and lines and also send a real invariant curve to a real invariant curve and a complex invariant curve to a complex invariant curve;

(ii) for each ellipse $\mathscr{E} : e(x,y) = 0$ of C_1 (respectively each line $\mathscr{L} : f(x,y) = 0$) we have a one–to–one correspondence between the real singularities on $\mathscr{E}$ (respectively on $\mathscr{L}$) and the real singularities on $\phi_e(\mathscr{E})$ (respectively $\phi_l(\mathscr{L})$) conserving their multiplicities and their location;

(iii) furthermore, consider the total curves $\mathscr{F} : \prod E_i(X,Y,X)\prod F_j(X,Y,Z)Z = 0$ (respectively $\mathscr{F}' : \prod E_i'(X,Y,X)\prod F_j'(X,Y,Z)Z = 0$ where $E_i(X,Y,X) = 0$ and $F_j(X,Y,X) = 0$ (respectively $E_i'(X,Y,X) = 0$ and $F_j'(X,Y,X) = 0$) are the projective completions of $\mathscr{E}_i$ and $\mathscr{L}_j$ (respectively $\mathscr{E}_i'$ and $\mathscr{L}_j'$). Then, there is a correspondence ψ between the singularities of the curves $\mathscr{F}$ and $\mathscr{F}'$ conserving their multiplicities as singularities of the total curves.

In the family **QSE** we also have cases where we have an infinite number of ellipses. Thus, according to the theorem of Jouanolou (Thm. 6.1.4), we have a rational first integral. In this case the multiplicity of an ellipse in the family is either considered to be undefined or we may say that this multiplicity is infinite. Such situations occur either when we

have (*i*) a finite number of singularities, finite or infinite, or (*ii*) an infinite number of singularities which could only be at infinity (recall that the systems in **QSE** are non–degenerate). In both cases however we show that we have a finite number of invariant affine straight lines with finite multiplicities. In fact it was proved in Schlomiuk and Vulpe (2008a) that all quadratic systems which have the line at infinity filled up with singularities have invariant affine straight lines of total multiplicity three. Furthermore, the multiplicities of singularities of the systems are finite in the case (*i*) and this is also true in the case (*ii*) if we only take into consideration the affine lines. We therefore can talk about the *configuration of invariant affine lines associated to the system*. Two such configurations of invariant affine lines C_{1L} and C_{2L} associated to systems (S_1) and (S_2) are said to be equivalent if and only if there is a one–to–one correspondence ϕ_l between the lines of C_{1L} and C_{2L} such that:

(i) the correspondence conserves the multiplicities of lines and also sends a real invariant line to a real invariant line and a complex invariant line to a complex invariant line;

(ii) for each line $\mathscr{L} : f(x,y) = 0$ we have a one–to–one correspondence between the real singularities on $\mathscr{L}$ and the real singularities on $\phi_l(\mathscr{L})$ conserving their multiplicities and their order on the lines.

We use this to extend Def. 6.1.9 to include these cases.

Definition 6.1.10. Suppose we have two systems (S_1) and (S_2) in **QSE**, each one with a finite number of finite singularities and an infinite number of invariant ellipses. Suppose we have a nonempty finite set of invariant affine straight lines $\mathscr{L}_j : f_j(x,y) = 0,\ j = 1,2,\ldots,k$, of (S_1) (respectively $\mathscr{L}'_j : f'_j(x,y) = 0,\ j = 1,2,\ldots,k$, of (S_2)). We now consider only the two configurations C_{1L} and C_{2L} of invariant affine lines of (S_1) and (S_2) associated to the systems, respectively. We say that the two configurations C_{1L} and C_{2L} are *equivalent with respect to the ellipses of the systems* if and only if (*i*) they are equivalent as configurations of invariant lines and in addition the following property (ii) is satisfied: we take any ellipse $\mathscr{E} : e(x,y) = 0$ of (S_1) and any ellipse $\mathscr{E}' : e'(x,y) = 0$ of (S_2). Then, we must have a one–to–one correspondence between the real singularities of system (S_1) located on $\mathscr{E}$ and of real singularities of system (S_2) located on $\mathscr{E}'$, conserving their multiplicities and their location. Furthermore, consider the curves $\mathscr{F} : \prod e(x,y) \prod f_j(x,y) = 0$ and $\mathscr{F}' : \prod e'(x,y) \prod f'_j(x,y) = 0$. Then we have a one–to–one correspondence between the singularities of the curve $\mathscr{F}$ with those of the curve $\mathscr{F}'$ conserving their multiplicities as singularities of these curves.

It can be shown that this definition is independent of the choice of the two ellipses $\mathscr{E} : e(x,y) = 0$ of (S_1) and $\mathscr{E}' : e'(x,y) = 0$ of (S_2).

Here we are interested in systems possessing an invariant ellipse. The conics $f(x,y) = 0$ with $f(x,y) \in \mathbb{R}[x,y]$ are classified via the group action of real affine transforma-

tion. The conics for which $f(x,y)$ is an irreducible polynomial over $\mathbb{C}$ can be brought by a real affine transformation to one of the following four forms: 1) $x^2+y^2-1=0$ (ellipses); 2) $x^2-y^2-1=0$ (hyperbolas); 3) $y-x^2=0$ (parabolas); 4) $x^2+y^2+1=0$, these are empty in $\mathbb{R}^2$ with points only in $\mathbb{C}^2$. Some authors call these conics *complex ellipses* (see Cairó and Llibre (2002), for instance). These complex ellipses play a helpful role in our classification problem.

Definition 6.1.11. By an ellipse we mean a conic $f(x,y)=0$ with real coefficients which can be brought by a real affine transformation to an equation $x^2+y^2+a=0$ with $a=-1$ (a real ellipse) or $a=1$ (a complex ellipse).

Remark 6.1.12. In the family **QSE** we can have cases of systems which possess simultaneously an infinite number of real ellipses as well as an infinite number of complex ellipses. For such systems we present the respective configurations containing only real ellipses (besides, of course, the corresponding invariant lines, if there are any).

In Oliveira *et al.* (2021) the authors provide necessary and sufficient affine invariant conditions for a non–degenerate quadratic differential system to have at least one invariant ellipse and these conditions are expressed in terms of the coefficients of the systems. In this chapter we denote by $\mathbf{QSE}_{(\eta<0)}$ the family of non–degenerate quadratic systems in **QSE** possessing two complex singularities at infinity and by $\mathbf{QSE}_{(C_2=0)}$ the systems in **QSE** possessing the line at infinity filled up with singularities. We classify these families of systems, modulo the action of the group of real affine transformations and time rescaling, according to their geometric properties encoded in the configurations of invariant ellipses and/or invariant straight lines which these systems possess.

As we want this classification to be intrinsic, independent of the normal form given to the systems, we use here geometric invariants and invariant polynomials for the classification. For example, it is clear that the configuration of algebraic solutions of a system in **QSE** is an affine invariant. The classification is done according to the configurations of invariant ellipses and straight lines encountered in systems belonging to **QSE**. We put in the same equivalence class systems which have equivalent configurations of invariant ellipses and lines (in the sense of Def. 6.1.9 and 6.1.10). In particular the notion of multiplicity in Def. 6.1.6 is invariant under the group action, i.e. if a quadratic system S has an invariant curve $\mathscr{L}=0$ of multiplicity m, then each system S' in the orbit of S under the group action has a corresponding invariant line $\mathscr{L}'=0$ of the same multiplicity m. To distinguish configurations of algebraic solutions we need some geometric invariants, and we also use invariant polynomials both of which are introduced in our Sec. 6.2.

Main Theorem. *Consider the class* **QSE** *of all non–degenerate quadratic differential systems* (6.1) *possessing an invariant ellipse.*

(*A*) *This family is classified according to the configurations of invariant ellipses and of invariant straight lines of the systems, yielding 35 distinct such configurations, 30 of which belong to the class* $\mathbf{QSE}_{(\eta<0)}$ *and 5 to* $\mathbf{QSE}_{(C_2=0)}$. *This geometric classification is described in Thm. 6.3.1.*

(*B*) *Using invariant polynomials, we obtain the bifurcation diagram in the space* $\mathbb{R}^{12}$ *of the coefficients of systems in* **QS** *according to their configurations of invariant ellipses and invariant straight lines (this diagram is presented in part (B) of Thm. 6.3.1). Moreover, this diagram gives an algorithm to compute the configuration of a system with an invariant ellipse for any quadratic differential system, presented in any normal form.*

This chapter is organized as follows: In Sec. 6.2 we define all the geometric and algebraic invariants used along the chapter and we introduce the basic auxiliary results we need for the proof of our theorems. In Sec. 6.3 we consider the class $\mathbf{QSE}_{(\eta<0)}$ (respectively $\mathbf{QSE}_{(C_2=0)}$) of all non–degenerate quadratic differential systems (6.1) possessing exactly one real singularity at infinity (respectively all non–degenerate quadratic differential systems (6.1) possessing an invariant ellipse and the line at infinity filled up with singularities) and we classify this family according to the geometric configurations of invariant ellipses and invariant straight lines which they possess. We also give their bifurcation diagram in the 12–dimensional space $\mathbb{R}^{12}$ of the coefficients of quadratic systems, in terms of invariant polynomials. In Sec. 6.4 we give some concluding comments, stressing the fact that the bifurcation diagrams in $\mathbb{R}^{12}$ give us an algorithm to compute the configuration of a system with an invariant ellipse for any system presented in any normal form.

6.2 Basic concepts and auxiliary results

In this section we define all the geometric invariants we use in the Main Theorem and we state some auxiliary results. A quadratic system possessing an invariant ellipse could also possesses invariant lines. We classify the systems possessing an invariant ellipse in terms of their configurations of invariant ellipses and invariant lines. Each one of these invariant curves has a multiplicity in the sense of Def. 6.1.6 (see also Christopher, Llibre and Pereira (2007)). We encode this picture in the multiplicity divisor of invariant ellipses and lines. For the definition of zero–cycles and divisors see Sec. 2.1.3.

We define the geometric invariants needed for distinguishing the configurations given by the Main Theorem.

Definition 6.2.1. We denote the number of invariant ellipses by N_ε, which assumes the value 1 if the systems possess only one invariant ellipse or ∞ if they possess a family of invariant ellipses (real or complex ones).

Definition 6.2.2. 1. Suppose that a real quadratic system has a finite number of invariant ellipses $\mathscr{E}_i : f_i(x,y) = 0$ and a finite number of invariant affine lines $\mathscr{L}_j$. We denote the line at infinity $\mathscr{L}_\infty : Z = 0$. We assume that on the line at infinity we have a finite number of singularities. The divisor of invariant ellipses and invariant lines on the complex projective plane of the system is the following:

$$ICD = n_1\mathscr{E}_1 + \cdots + n_k\mathscr{E}_k + m_1\mathscr{L}_1 + \cdots + m_k\mathscr{L}_k + m_\infty\mathscr{L}_\infty,$$

where n_j (respectively m_i) is the multiplicity of the ellipse $\mathscr{E}_j$ (respectively of the line $\mathscr{L}_i$), and m_∞ is the multiplicity of $\mathscr{L}_\infty$. We also mark the complex (non–real) invariant ellipses (respectively lines) denoting them by $\mathscr{E}_i^C$ (respectively $\mathscr{L}_i^C$). We denote by ILD the invariant lines divisor, i.e.

$$ILD = m_\infty\mathscr{L}_\infty + m_1\mathscr{L}_1 + \cdots + m_k\mathscr{L}_k.$$

2. The zero–cycle on the real projective plane, of real singularities of a system (6.1) located on the configuration of invariant lines and invariant ellipses, is given by:

$$MS_{0C} = l_1U_1 + \cdots + l_kU_k + m_1s_1 + \cdots + m_ns_n,$$

where U_i (respectively s_j) are all the real infinite (respectively finite) such singularities of the system and l_i (respectively m_j) are their corresponding multiplicities.

The *zero–cycle on the real affine plane*, of real singularities of a quadratic system located on the configuration of invariant lines and invariant ellipses, is given by:

$$MS_{0C}^{Af} = m_1s_1 + \cdots + m_ns_n,$$

where s_j are all the real finite such singularities of the system and m_j are their corresponding multiplicities.

In case we have a real finite singularity located on invariant curves we denote it by $\overset{j}{s}_r$, where $j \in \{e, l, el, ll, \ldots\}$. Here e (respectively $l, el, ll, \ldots$) means that the singular point s_r is located on an ellipse (respectively located on a line, on the intersection of an ellipse and a line, on the intersection of two lines, etc.).

Here we indicate Sec. 2.2.5 for more definitions and results which play an important role in the proof of the part (B) of the Main Theorem.

According to the definition of an invariant curve (see Defnition 6.1.1) a conic $\Phi(x,y) = 0$ must satisfy the identity

$$\frac{\partial\Phi}{\partial x}P(x,y) + \frac{\partial\Phi}{\partial y}Q(x,y) = \Phi(x,y)(Ux + Vy + W). \tag{6.2}$$

for some polynomial $K = Ux + Vy + W \in \mathbb{C}[x,y]$, called the *cofactor* of the invariant conic $\Phi(x,y) = 0$.

Remark 6.2.3. The cofactor K has degree at most 1 because in the previous equation we have

$$\deg(K)+\deg(\Phi)=\max\{\deg(P(x,y))+\deg(\Phi)-1,\deg(Q(x,y))+\deg(\Phi)-1\}\leq\deg(\Phi)+1,$$

since (6.1) is a quadratic system, the degree of the corresponding vector field is two, so $\deg(K)\leq 1$ and, therefore, without loss of generality we can assume that the cofactor is of the form $K(x,y)=Ux+Vy+W$.

According to Oliveira *et al.* (2021) a conic which is not a parabola can be written as

$$\Phi(x,y)\equiv p+qx+ry+sx^2+2vxy+uy^2=0.$$

Remark 6.2.4. The identity (6.2) involves several types of parameters:

- the 12 coefficients of systems (6.1);
- the 6 coefficients the conic Φ;
- the 3 coefficients U,V,W of the cofactor $K(x,y)$.

For a conic $\Phi(x,y)=0$ of the previous form the identity (6.2) yields 10 nonlinear equations for determining the 9 unknown coefficients p, q, r, s, v, u, U, V, W as functions of the coefficients of the systems:

$$\begin{aligned}
Eq_1 &\equiv s(2g-U)+2lv=0,\\
Eq_2 &\equiv 2v(g+2m-U)+s(4h-V)+2lu=0,\\
Eq_3 &\equiv 2v(2h+n-V)+u(4m-U)+2ks=0,\\
Eq_4 &\equiv u(2n-V)+2kv=0,\\
Eq_5 &\equiv q(g-U)+s(2c-W)+2ev+lr=0,\\
Eq_6 &\equiv r(2m-U)+q(2h-V)+2v(c+f-W)+2(ds+eu)=0,\\
Eq_7 &\equiv r(n-V)+u(2f-W)+2dv+kq=0,\\
Eq_8 &\equiv q(c-W)+2(as+bv)+er-pU=0,\\
Eq_9 &\equiv r(f-W)+2(bu+av)+dq-pV=0,\\
Eq_{10} &\equiv aq+br-pW=0.
\end{aligned}\tag{6.3}$$

The next result, based on the previous identities and proved in Oliveira *et al.* (2021), gives us for non–degenerate quadratic systems (6.1) the necessary and sufficient conditions for the existence of at least one invariant ellipse. The invariant polynomials which appear in the next theorem and in the corresponding diagrams are presented later.

Theorem 6.2.5 (Oliveira *et al.* (2021))**.** Consider a non–degenerate quadratic system.

(*A*) The conditions $\widehat{\gamma}_1 = \widehat{\gamma}_2 = 0$ and either $\eta < 0$ or $C_2 = 0$ are necessary for this system to possess at least one invariant ellipse. Assume that $\widehat{\gamma}_1 = \widehat{\gamma}_2 = 0$ holds.

(A_1) If $\eta < 0$ and $\widetilde{N} \neq 0$, then the system could possesses at most one invariant ellipse. Moreover, the necessary and sufficient conditions for the existence of such an ellipse are given in the diagram of Fig. 239.

(A_2) If $\eta < 0$ and $\widetilde{N} = 0$, then the system either has no invariant ellipse or it has an infinite family of invariant ellipses. The necessary and sufficient conditions for the existence of a family of invariant ellipses are given in the diagram of Fig. 239.

(A_3) If $C_2 = 0$, then the system either has no invariant ellipse or it has an infinite family of invariant ellipses. Moreover, the necessary and sufficient conditions for the existence of a family of invariant ellipses are given in the diagram of Fig. 241.

(*B*) A non–degenerate quadratic system possesses an algebraic limit cycle, which is an ellipse, if and only if $\widehat{\gamma}_1 = \widehat{\gamma}_2 = 0$, $\eta < 0$, $\mathscr{T}_3\mathscr{F} < 0$, $\widehat{\beta}_1\widehat{\beta}_2 \neq 0$, and one of the following sets of conditions is satisfied:

(B_1) $\theta \neq 0$, $\widehat{\beta}_3 \neq 0$, $\widehat{\mathscr{R}}_1 < 0$;

(B_2) $\theta \neq 0$, $\widehat{\beta}_3 = 0$, $\widehat{\gamma}_3 = 0$, $\widehat{\mathscr{R}}_1 < 0$;

(B_3) $\theta = 0$, $\widehat{\gamma}_6 = 0$, $\widehat{\mathscr{R}}_5 < 0$.

(*C*) The diagrams of Fig. 239 and 241 actually contain the global "bifurcation" diagram in the 12–dimensional space of parameters of non–degenerate systems which possess at least one invariant ellipse. The corresponding conditions are given in terms of 37 invariant polynomials with respect to affine transformations and time rescaling.

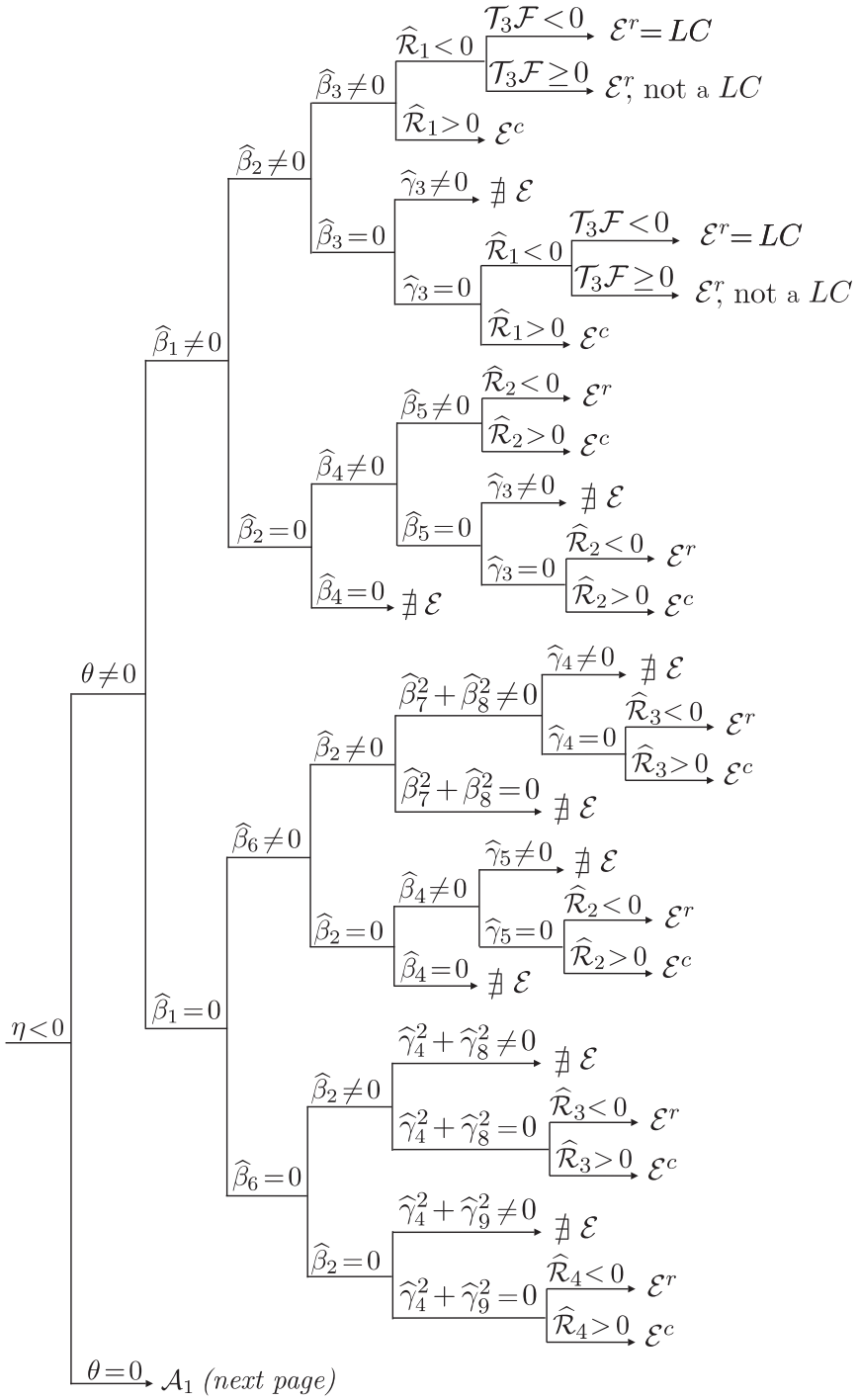

Figure 239 – Diagram of existence of invariant ellipse: the case $\eta<0$

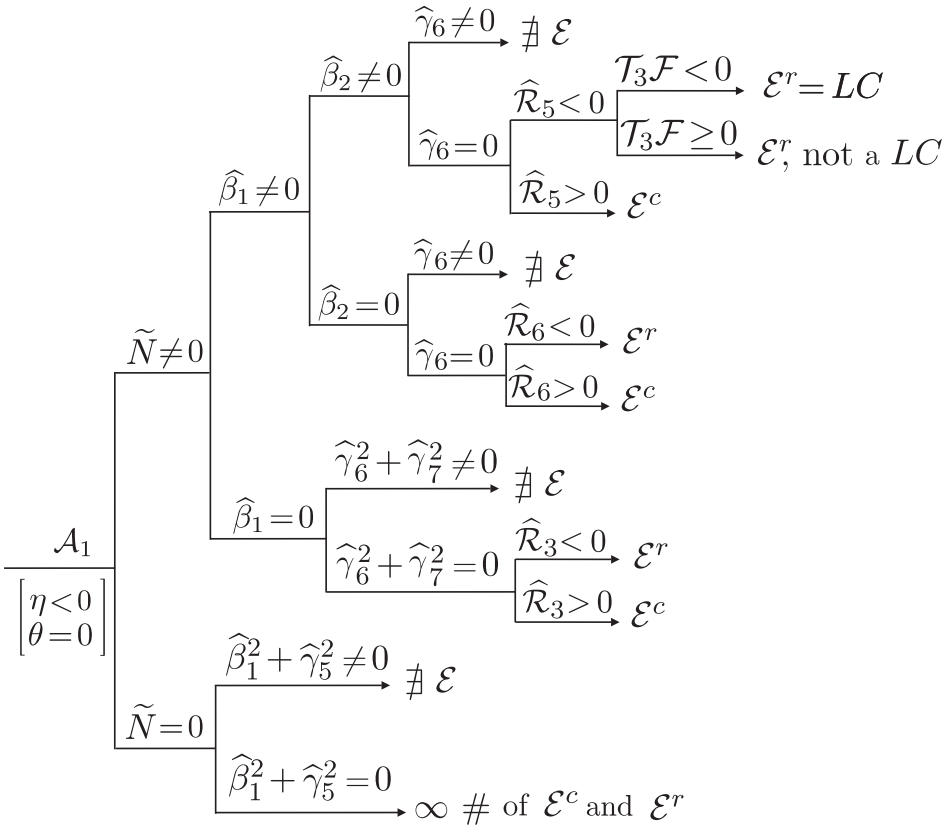

Figure 240 – *(Cont.)* Diagram of existence of invariant ellipse: the case $\eta < 0$

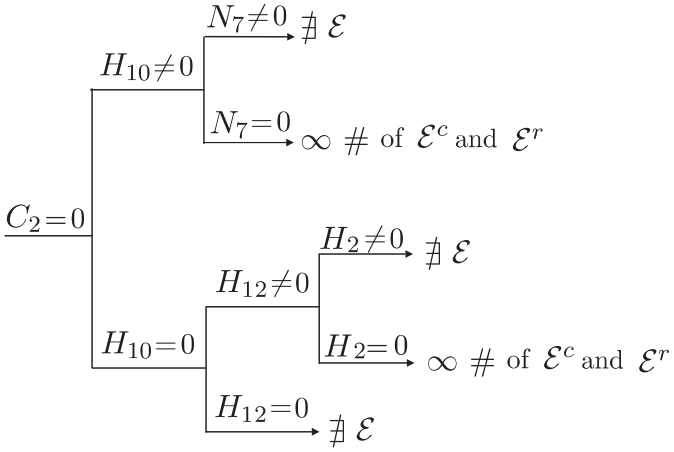

Figure 241 – Diagram of existence of invariant ellipse: the case $C_2 = 0$

Remark 6.2.6. An invariant ellipse is denoted by $\mathscr{E}^r$ if it is real and by $\mathscr{E}^c$ if it is complex. In the case of an $\mathscr{E}^r$ when the drawing is done with thicker line it means that this ellipse is a limit cycle (see Rmk. 6.1.7 (b)).

The following result is included in Oliveira *et al.* (2021) as a corollary of Thm. 6.2.5.

Corollary 6.2.7 (Oliveira *et al.* (2021))**.** Consider a non–degenerate quadratic system with the coefficients corresponding to a point $\tilde{a} \in \mathbb{R}^{12}$. According to Oliveira *et al.* (2021)

this system could possess an invariant ellipse only if the conditions $\widehat{\gamma}_1(\tilde{a}) = \widehat{\gamma}_2(\tilde{a}) = 0$ and either $\eta(\tilde{a}) < 0$ or $C_2(\tilde{a},x,y) = 0$ in the ring $\mathbb{R}[x,y]$ are satisfied. So we define the following two affine invariant subsets in $\mathbb{R}^{12}$, which must contain all quadratic systems (1) possessing an invariant ellipse:

$$\begin{aligned}\mathfrak{B} =&\{\tilde{a} \in \mathbb{R}^{12} \big|\ \widehat{\gamma}_1(\tilde{a}) = \widehat{\gamma}_2(\tilde{a}) = 0, \eta(\tilde{a}) < 0\};\\ \mathfrak{C} =&\{\tilde{a} \in \mathbb{R}^{12} \big|\ \widehat{\gamma}_1(\tilde{a}) = \widehat{\gamma}_2(\tilde{a}) = 0, C_2(\tilde{a},x,y) = 0\}.\end{aligned}$$

Next, following the diagrams of Fig. 239 and Fig. 241 we split the invariant sets $\mathfrak{B}$ and $\mathfrak{C}$ into affine invariant subsets $\mathfrak{B}_i$ and $\mathfrak{C}_j$ (defined in the sequence):

$$\mathfrak{B} = \bigcup_{i=1}^{12} \mathfrak{B}_i,\ \mathfrak{B}_i \bigcap_{i\neq j} \mathfrak{B}_j = \emptyset; \quad \mathfrak{C} = \bigcup_{j=1}^{2} \mathfrak{C}_j,\ \mathfrak{C}_1 \bigcap \mathfrak{C}_2 = \emptyset,$$

and we define the corresponding invariant subsets $\widetilde{\mathfrak{B}}_i$ $(i = 1,2,\ldots,12)$ and $\widetilde{\mathfrak{C}}_j$ $(j = 1,2)$:

$$\begin{array}{ll}
(\mathfrak{B}_1):\ \theta \neq 0, \widehat{\beta}_1 \neq 0, \widehat{\beta}_2 \neq 0, \widehat{\beta}_3 \neq 0; & (\widetilde{\mathfrak{B}}_1):\ \widehat{\mathscr{R}}_1 \neq 0;\\
(\mathfrak{B}_2):\ \theta \neq 0, \widehat{\beta}_1 \neq 0, \widehat{\beta}_2 \neq 0, \widehat{\beta}_3 = 0, & (\widetilde{\mathfrak{B}}_2):\ \widehat{\gamma}_3 = 0, \widehat{\mathscr{R}}_1 \neq 0;\\
(\mathfrak{B}_3):\ \theta \neq 0, \widehat{\beta}_1 \neq 0, \widehat{\beta}_2 = 0, \widehat{\beta}_5 \neq 0, & (\widetilde{\mathfrak{B}}_3):\ \widehat{\mathscr{R}}_2 \neq 0;\\
(\mathfrak{B}_4):\ \theta \neq 0, \widehat{\beta}_1 \neq 0, \widehat{\beta}_2 = 0, \widehat{\beta}_5 = 0, & (\widetilde{\mathfrak{B}}_4):\ \widehat{\gamma}_3 = 0, \widehat{\mathscr{R}}_2 \neq 0;\\
(\mathfrak{B}_5):\ \theta \neq 0, \widehat{\beta}_1 = 0, \widehat{\beta}_6 \neq 0, \widehat{\beta}_2 \neq 0, & (\widetilde{\mathfrak{B}}_5):\ \widehat{\beta}_7^2 + \widehat{\beta}_8^2 \neq 0, \widehat{\gamma}_4 = 0, \widehat{\mathscr{R}}_3 \neq 0;\\
(\mathfrak{B}_6):\ \theta \neq 0, \widehat{\beta}_1 = 0, \widehat{\beta}_6 \neq 0, \widehat{\beta}_2 = 0, & (\widetilde{\mathfrak{B}}_6):\ \widehat{\gamma}_5 = 0, \widehat{\mathscr{R}}_2 \neq 0;\\
(\mathfrak{B}_7):\ \theta \neq 0, \widehat{\beta}_1 = 0, \widehat{\beta}_6 = 0, \widehat{\beta}_2 \neq 0, & (\widetilde{\mathfrak{B}}_7):\ \widehat{\gamma}_4^2 + \widehat{\gamma}_8^2 = 0, \widehat{\mathscr{R}}_3 \neq 0;\\
(\mathfrak{B}_8):\ \theta \neq 0, \widehat{\beta}_1 = 0, \widehat{\beta}_6 = 0, \widehat{\beta}_2 = 0, & (\widetilde{\mathfrak{B}}_8):\ \widehat{\gamma}_4^2 + \widehat{\gamma}_9^2 = 0, \widehat{\mathscr{R}}_4 \neq 0;\\
(\mathfrak{B}_9):\ \theta = 0, \widetilde{N} \neq 0, \widehat{\beta}_1 \neq 0, \widehat{\beta}_2 \neq 0, & (\widetilde{\mathfrak{B}}_9):\ \widehat{\gamma}_6 = 0, \widehat{\mathscr{R}}_5 \neq 0;\\
(\mathfrak{B}_{10}):\ \theta = 0, \widetilde{N} \neq 0, \widehat{\beta}_1 \neq 0, \widehat{\beta}_2 = 0, & (\widetilde{\mathfrak{B}}_{10}):\ \widehat{\gamma}_6 = 0, \widehat{\mathscr{R}}_6 \neq 0;\\
(\mathfrak{B}_{11}):\ \theta = 0, \widetilde{N} \neq 0, \widehat{\beta}_1 = 0, & (\widetilde{\mathfrak{B}}_{11}):\ \widehat{\gamma}_6^2 + \widehat{\gamma}_7^2 = 0, \widehat{\mathscr{R}}_3 \neq 0;\\
(\mathfrak{B}_{12}):\ \theta = 0, \widetilde{N} = 0, & (\widetilde{\mathfrak{B}}_{12}):\ \widehat{\beta}_1^2 + \widehat{\gamma}_5^2 = 0;\\
(\mathfrak{C}_1):\ C_2 = 0, H_{10} \neq 0, & (\widetilde{\mathfrak{C}}_1):\ N_7 = 0;\\
(\mathfrak{C}_2):\ C_2 = 0, H_{10} = 0, & (\widetilde{\mathfrak{C}}_2):\ H_{12} \neq 0, H_2 = 0.
\end{array}$$

Then according to the mentioned diagrams, a quadratic system, corresponding to a point $\tilde{a} \in \mathbb{R}^{12}$, possesses:

- an invariant ellipse which is unique if and only if $\tilde{a} \in \mathfrak{B}_i \cap \widetilde{\mathfrak{B}}_i$ $(i = 1,2,\ldots,11)$; moreover this ellipse is real (respectively complex) if the corresponding invariant polynomial $\widehat{\mathscr{R}}_s \neq 0$, $(s = 1,\ldots,6)$, which belongs to the set of polynomials defining $\widetilde{\mathfrak{B}}_i$ $(i = 1,2,\ldots,11)$, is negative (respectively positive);
- an infinite number of invariant ellipses if and only if either $\tilde{a} \in \mathfrak{B}_{12} \cap \widetilde{\mathfrak{B}}_{12}$ or $\tilde{a} \in \mathfrak{C}_j \cap \widetilde{\mathfrak{C}}_j$ $(j = 1,2)$. The ellipses could be real or/and complex.

We point out that most of the invariants which appeared in these results are stated in Sec. 2.2.5. Using the elements of the minimal polynomial basis given in such a section we construct the affine invariant polynomials:

$$
\begin{aligned}
\widehat{\gamma}_1(\tilde{a}) &= A_1^2(3A_6+2A_7)-2A_6(A_8+A_{12}),\\
\widehat{\gamma}_2(\tilde{a}) &= 9A_1^2A_2(23252A_3+23689A_4)-1440A_2A_5(3A_{10}+13A_{11})\\
&\quad -1280A_{13}(2A_{17}+A_{18}+23A_{19}-4A_{20})-320A_{24}(50A_8+3A_{10}\\
&\quad +45A_{11}-18A_{12})+120A_1A_6(6718A_8+4033A_9+3542A_{11}\\
&\quad +2786A_{12})+30A_1A_{15}(14980A_3-2029A_4-48266A_5)\\
&\quad -30A_1A_7(76626A_1^2-15173A_8+11797A_{10}+16427A_{11}-30153A_{12})\\
&\quad +8A_2A_7(75515A_6-32954A_7)+2A_2A_3(33057A_8-98759A_{12})\\
&\quad -60480A_1^2A_{24}+A_2A_4(68605A_8-131816A_9+131073A_{10}+129953A_{11})\\
&\quad -2A_2(141267A_6^2-208741A_5A_{12}+3200A_2A_{13}),\\
\widehat{\gamma}_3(\tilde{a}) &= 843696A_5A_6A_{10}+A_1(-27(689078A_8+419172A_9-2907149A_{10}\\
&\quad -2621619A_{11})A_{13}-26(21057A_3A_{23}+49005A_4A_{23}-166774A_3A_{24}\\
&\quad +115641A_4A_{24})),\\
\widehat{\gamma}_4(\tilde{a}) &= -488A_2^3A_4+A_2(12(4468A_8^2+32A_9^2-915A_{10}^2+320A_9A_{11}-3898A_{10}A_{11}\\
&\quad -3331A_{11}^2+2A_8(78A_9+199A_{10}+2433A_{11}))+2A_5(25488A_{18}\\
&\quad -60259A_{19}-16824A_{21})+779A_4A_{21})+4(7380A_{10}A_{31}\\
&\quad -24(A_{10}+41A_{11})A_{33}+A_8(33453A_{31}+19588A_{32}-468A_{33}-19120A_{34})\\
&\quad +96A_9(-A_{33}+A_{34})+556A_4A_{41}-A_5(27773A_{38}+41538A_{39}\\
&\quad -2304A_{41}+5544A_{42})),\\
\widehat{\gamma}_5(\tilde{a}) &= A_{22},\\
\widehat{\gamma}_6(\tilde{a}) &= A_1(64A_3-541A_4)A_7+86A_8A_{13}+128A_9A_{13}-54A_{10}A_{13}\\
&\quad -128A_3A_{22}+256A_5A_{22}+101A_3A_{24}-27A_4A_{24},\\
\widehat{\gamma}_7(\tilde{a}) &= A_2\big[2A_3(A_8-11A_{10})-18A_7^2-9A_4(2A_9+A_{10})+22A_8A_{22}+26A_{10}A_{22},\\
\widehat{\gamma}_8(\tilde{a}) &= A_6,\\
\widehat{\gamma}_9(\tilde{a}) &= 12A_1^2+12A_8+5A_{10}+17A_{11},\\
\widehat{\beta}_1(\tilde{a}) &= 3A_1^2-2A_8-2A_{12},\\
\widehat{\beta}_2(\tilde{a}) &= 2A_{13},\\
\widehat{\beta}_3(\tilde{a}) &= 8A_3+27A_4-54A_5,\\
\widehat{\beta}_4(\tilde{a}) &= A_4,\\
\widehat{\beta}_5(\tilde{a}) &= 8A_5-5A_4,\\
\widehat{\beta}_6(\tilde{a}) &= A_3,\\
\widehat{\beta}_7(\tilde{a}) &= 24A_3+11A_4+20A_5,\\
\widehat{\beta}_8(\tilde{a}) &= 41A_8+44A_9+32A_{10},
\end{aligned}
$$

$$
\begin{aligned}
\widehat{\mathscr{R}}_1(\tilde{a}) &= \theta A_6\big[5A_6(A_{10}+A_{11})-2A_7(12A_1^2+A_8+A_{12})-2A_1(A_{23}-A_{24})\\
&\quad +2A_5(A_{14}+A_{15})+A_6(9A_8+7A_{12})\big],\\
\widehat{\mathscr{R}}_2(\tilde{a}) &= \widehat{\beta}_4\widehat{\beta}_6(2A_{10}-A_8-A_9),\\
\widehat{\mathscr{R}}_3(\tilde{a}) &= \widehat{\beta}_2\big[A_2(80A_3-3A_4-54A_5)-80A_{22}+708A_{23}-324A_{24}\big],\\
\widehat{\mathscr{R}}_4(\tilde{a}) &= T_{11},\\
\widehat{\mathscr{R}}_5(\tilde{a}) &= 12A_1^2+12A_8+5A_{10}+17A_{11},\\
\widehat{\mathscr{R}}_6(\tilde{a}) &= 2A_{10}-A_8-A_9,\\
\widehat{\mathscr{R}}_7(\tilde{a}) &= 4A_8-3A_9,\\
\nu_1 &= -A_6\big(A_1A_2-2A_{15}\big)\big(3A_1^2-2A_8-2A_{12}\big),\\
\nu_2 &= A_1(-461A_2A_4+183A_2A_5-296A_{22}+122A_{24})+A_4(467A_{14}+922A_{15})\\
&\quad +2A_6\big(553A_8+183A_9-100A_{10}-39A_{11}+144A_{12}\big)\\
&\quad +A_7\big(5790A_1^2-1531A_8-140A_9+177A_{10}+947A_{11}-2791A_{12}\big),\\
\nu_3 &= A_4\big(18A_1^2-5A_8+A_{10}+3A_{11}-9A_{12}\big),\\
\widetilde{N}(\tilde{a},x,y) &= (D_2^2+T_8-2T_9)/9,\\
\theta(\tilde{a}) &= 2A_5-A_4\equiv \mathrm{Discrim}[\widetilde{N},x]/(16y^2),\\
\mathscr{F}(\tilde{a}) &= A_7,\\
\mathscr{T}_3(\tilde{a}) &= 8A_{15}-4A_1A_2,\\
H_2(\tilde{a},x,y) &= \big(C_1,-8\widehat{H}-\widetilde{N}\big)^{(1)}-2D_1\widetilde{N},\\
H_9(\tilde{a}) &= -\big[\big[\widehat{D},\widehat{D}\big)^{(2)},\widehat{D}\big)^{(1)},\widehat{D}\big)^{(3)},\\
H_{10}(\tilde{a}) &= \big[\big[\widehat{D},\widetilde{N}\big)^{(2)},D_2\big)^{(1)},\\
H_{11}(\tilde{a},x,y) &= -32\widehat{H}\Big[\big(C_2,\widehat{D}\big)^{(2)}+8\big(\widehat{D},D_2\big)^{(1)}\Big]+3\Big[\big(C_1,-8\widehat{H}-\widetilde{N}\big)^{(1)}-2D_1\widetilde{N}\Big]^2,\\
H_{12}(\tilde{a},x,y) &= \big(\widehat{D},\widehat{D}\big)^{(2)},\\
N_7(\tilde{a}) &= 12D_1\big(C_0,D_2\big)^{(1)}+2D_1^3+9D_1\big(C_1,C_2\big)^{(2)}+36\big[\big[C_0,C_1\big)^{(1)},D_2\big)^{(1)}.
\end{aligned}
$$

We remark that the last six invariant polynomials H_2, H_9 to H_{12}, and N_7 are constructed in Schlomiuk and Vulpe (2008a), whereas $\mathscr{F}$ and $\mathscr{T}_3$ are defined in Vulpe (2011).

6.3 Configurations of invariant ellipses for the classes $\mathbf{QSE}_{(\eta<0)}$ and $\mathbf{QSE}_{(C_2=0)}$

Theorem 6.3.1. Consider the classes $\mathbf{QSE}_{(\eta<0)}$ and $\mathbf{QSE}_{(C_2=0)}$ of all non–degenerate quadratic differential systems (6.1) possessing one real and two complex singularities at

infinity, and the quadratic differential systems possessing the line at infinity filled up with singularities, respectively.

(A) These families are classified according to the configurations of invariant ellipses and of invariant straight lines of the systems, yielding 30 distinct such configurations for the class $\mathbf{QSE}_{(\eta<0)}$ and 5 for the class $\mathbf{QSE}_{(C_2=0)}$. This geometric classification appears in the diagrams of Fig. 242 and Fig. 244. More precisely:

(A1) For the class $\mathbf{QSE}_{(\eta<0)}$, there exist exactly 3 configurations of systems possessing an infinite number of ellipses. More precisely two of them contain only real ellipses and the third one contains simultaneously an infinite number of real and an infinite number of complex ellipses. The remaining 27 configurations possess exactly one invariant ellipse, (real for 21 of them) or complex (for another 6).

(A2) For the class $\mathbf{QSE}_{(C_2=0)}$ all the 5 configurations of systems possess an infinite number of ellipses (four of them with three simple invariant lines and one of them with a triple invariant line). More precisely three of the configurations contain only real ellipses, one contains only complex ones and the remaining configuration contains simultaneously an infinite number of real and an infinite number of complex ellipses.

(B) The bifurcation diagrams for systems in $\mathbf{QSE}_{(\eta<0)}$ and $\mathbf{QSE}_{(C_2=0)}$ done in the coefficient space $\mathbb{R}^{12}$ in terms of invariant polynomials appear in the diagrams of Fig. 245 to Fig. 248. In these diagrams we have necessary and sufficient conditions for the realization of each one of the configurations.

Remark 6.3.2. We note that on the expressions of the divisors *ICD* and *ILD* as well of the zero–cycles MS_{0C} and MS_{0C}^{Af} appearing in the diagrams of Fig. 242 and Fig. 244, we can read their types help in this classification and furthermore they are affinely invariant.

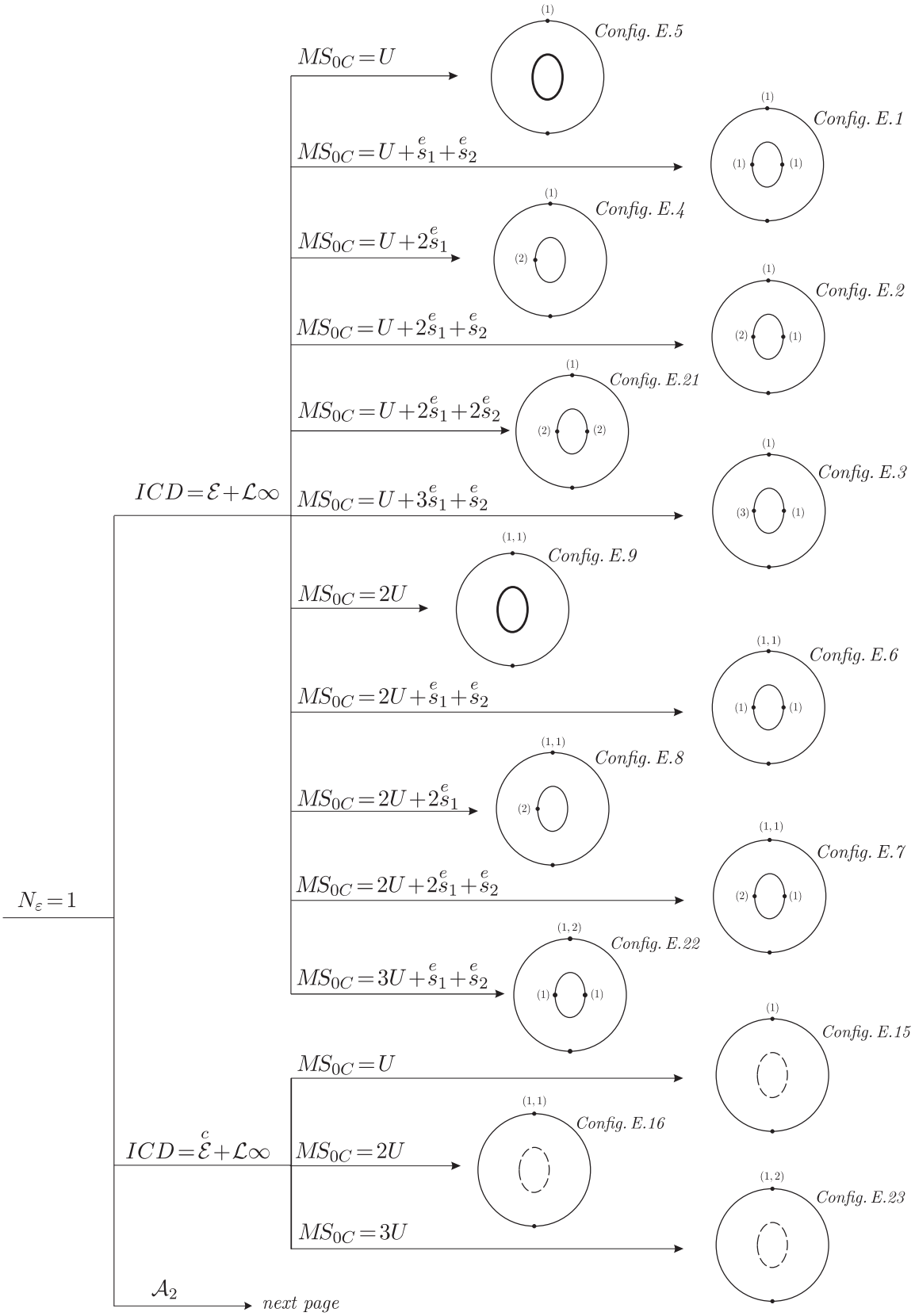

Figure 242 – Diagram of configurations with one invariant ellipse

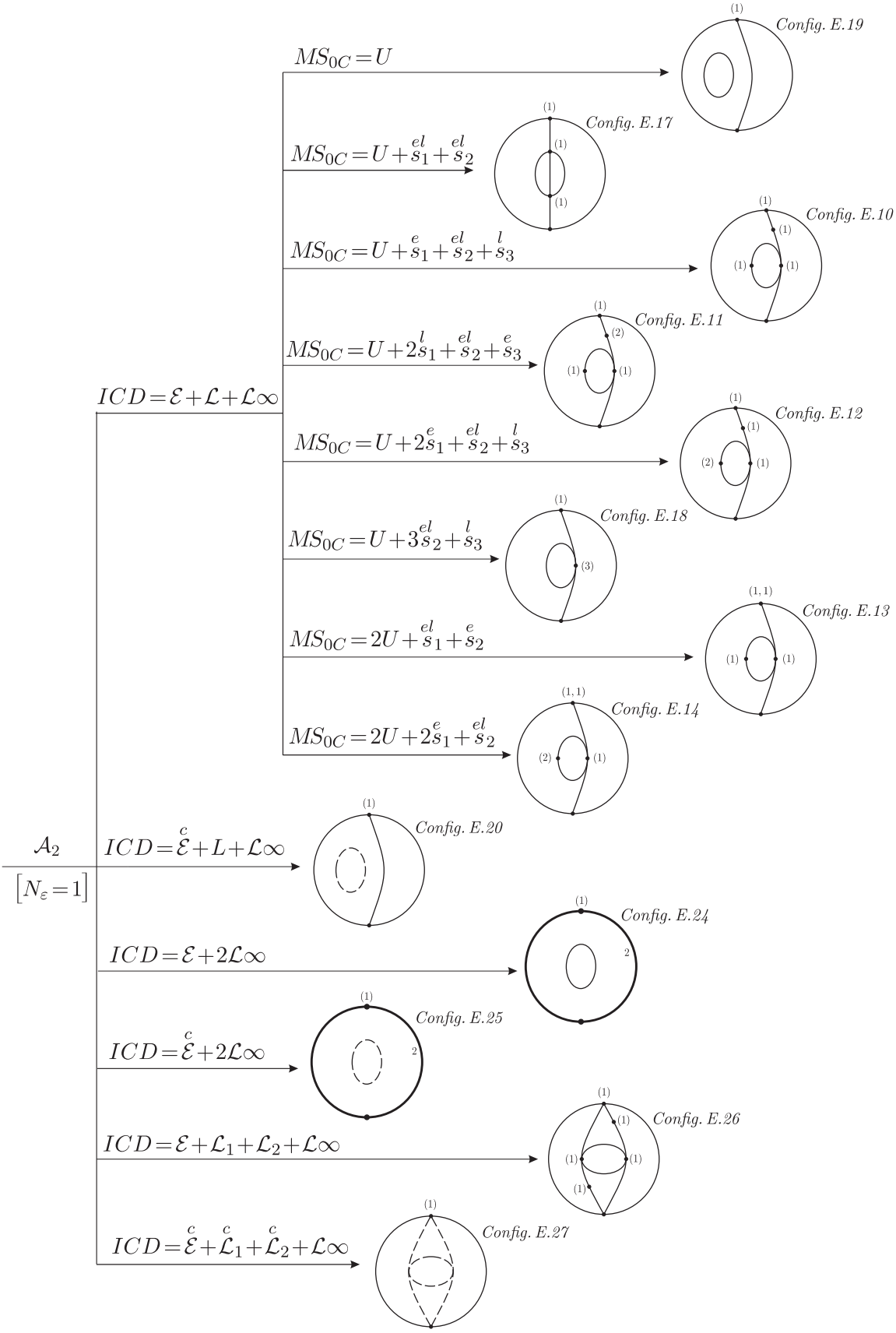

Figure 243 – *(Cont.)* Diagram of configurations with one invariant ellipse

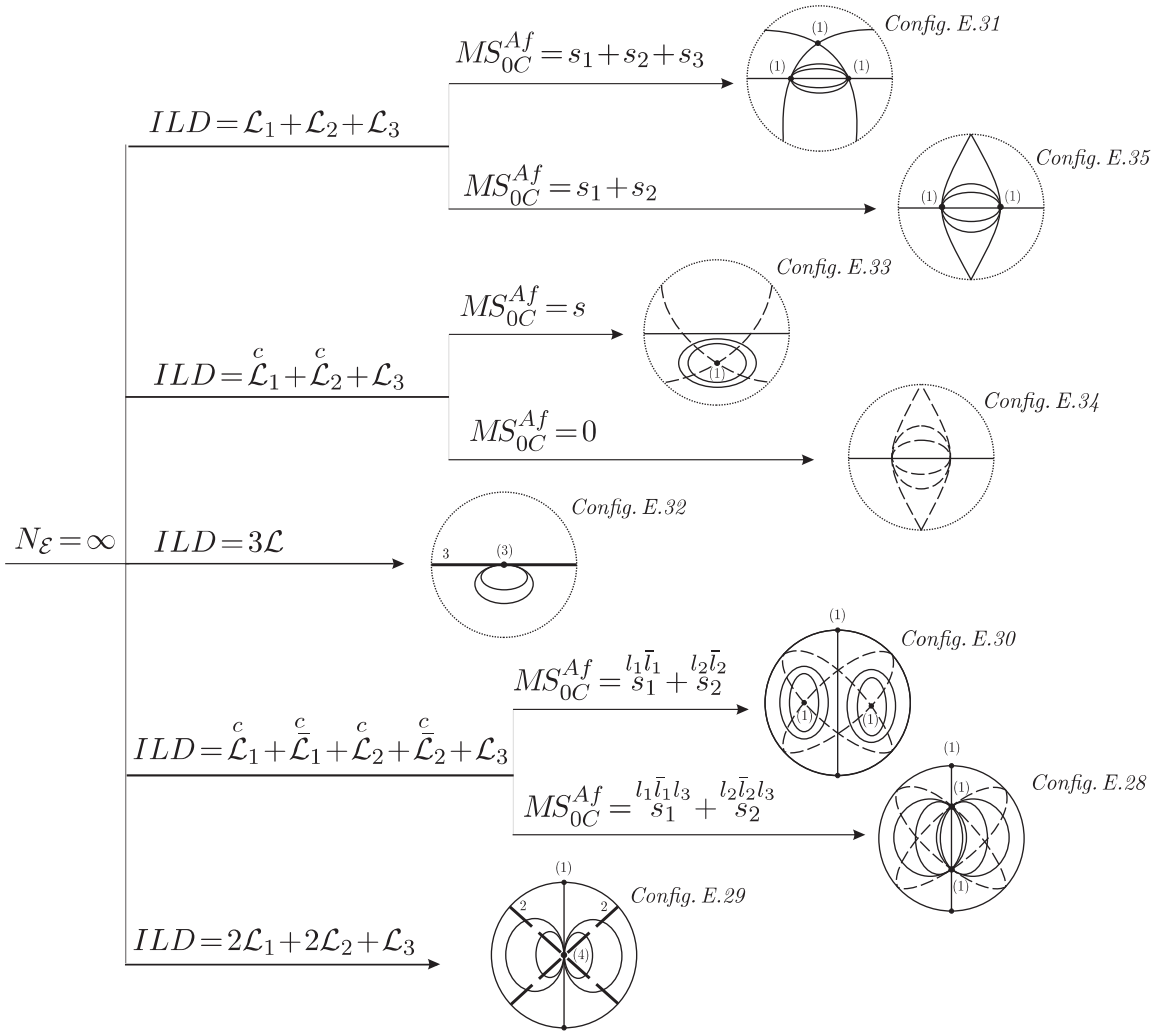

Figure 244 – Diagram of configurations with a family of invariant ellipses

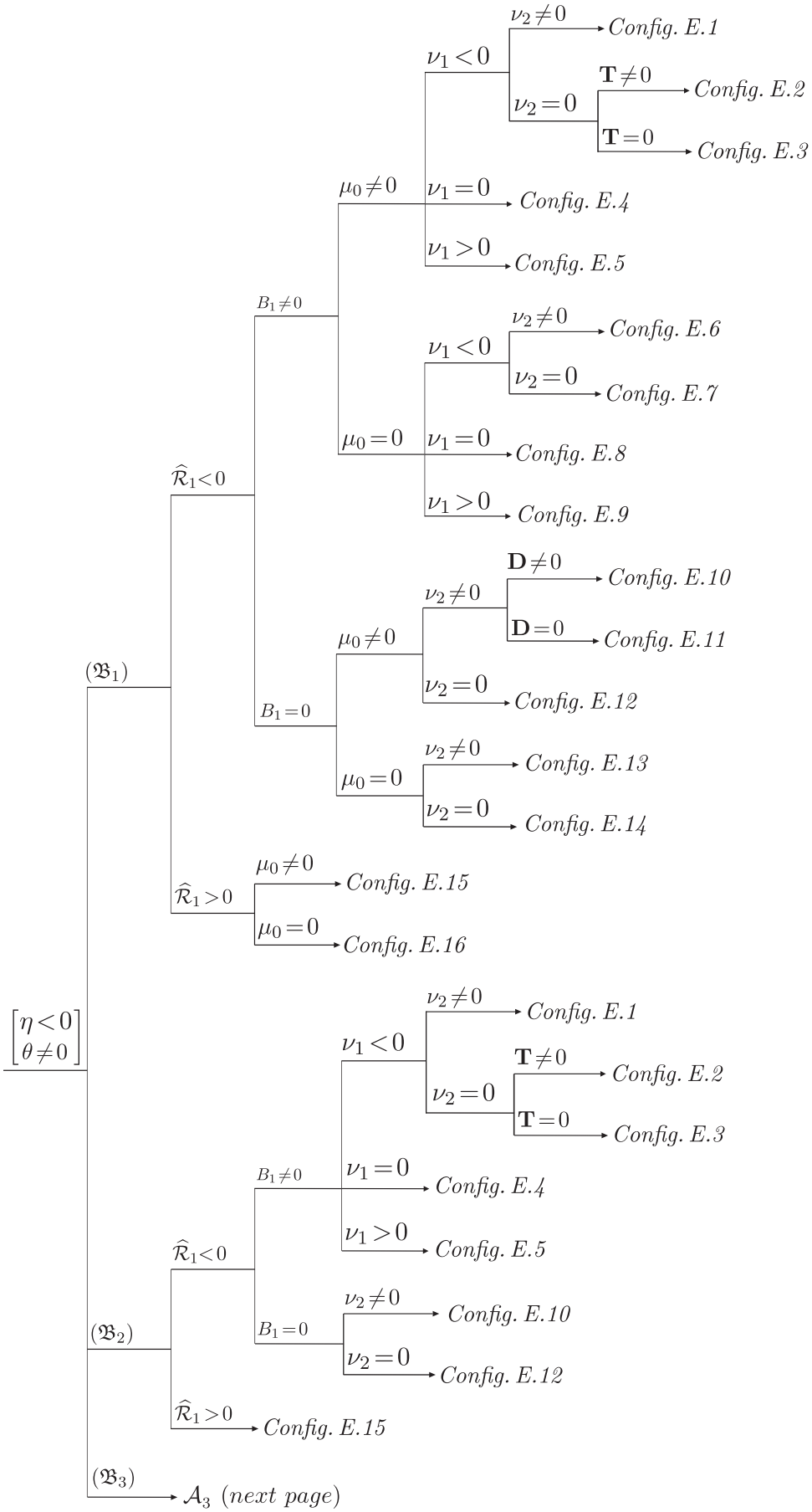

Figure 245 – Bifurcation diagram in $\mathbb{R}^{12}$ of the configurations: Case $\eta < 0$, $\theta \neq 0$

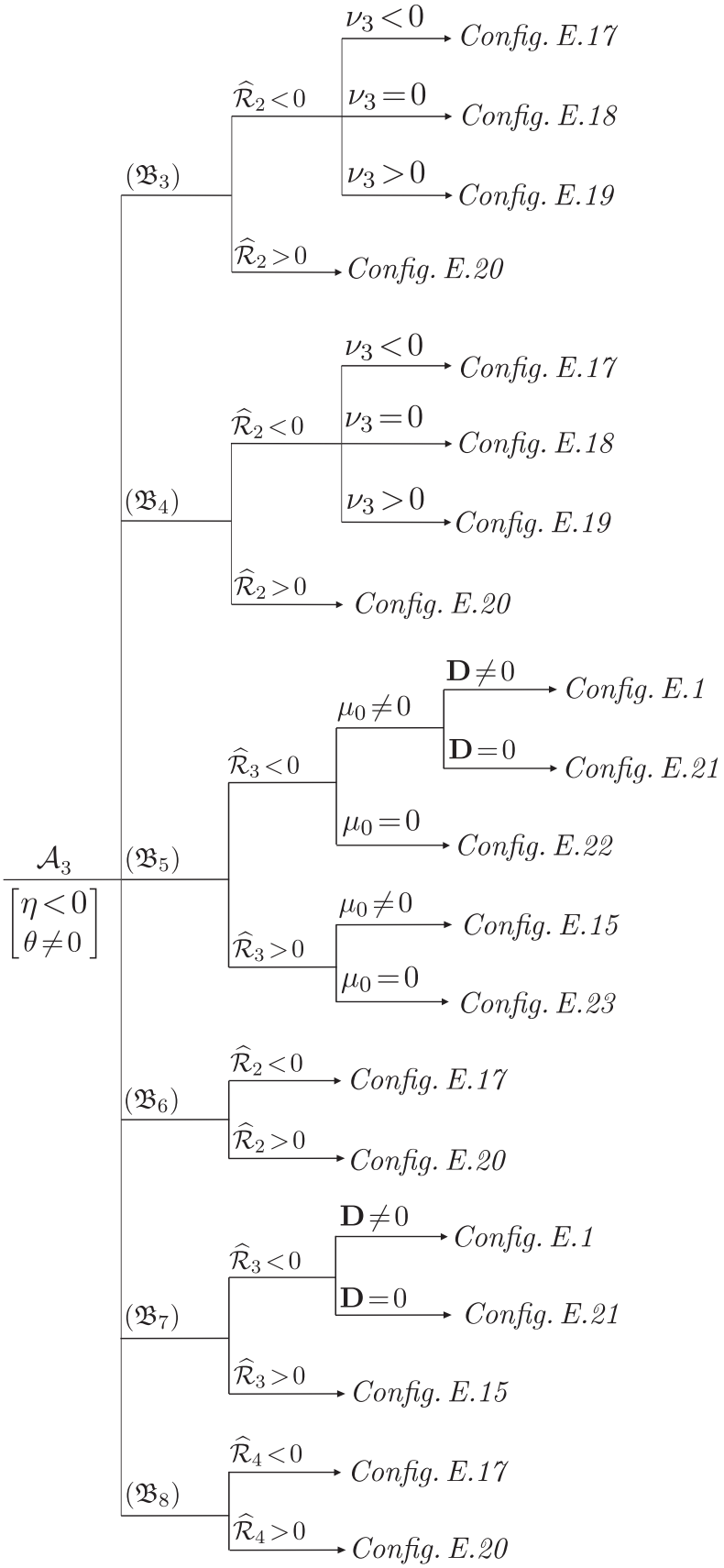

Figure 246 – *(Cont.)* Bifurcation diagram in $\mathbb{R}^{12}$ of the configurations: Case $\eta<0$, $\theta\neq0$

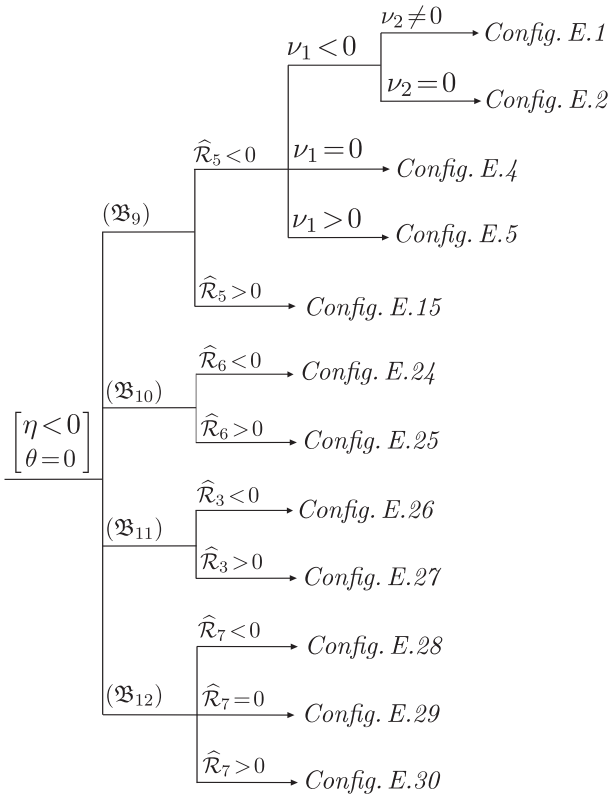

Figure 247 – Bifurcation diagram in $\mathbb{R}^{12}$ of the configurations: Case $\eta<0$, $\theta=0$

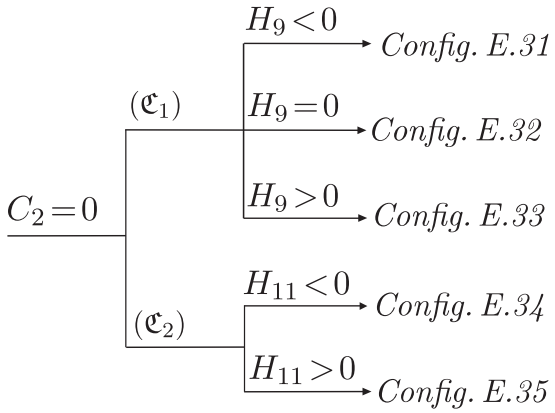

Figure 248 – Bifurcation diagram in $\mathbb{R}^{12}$ of the configurations: Case $C_2=0$

Proof of part (A). We prove part (A) under the assumption that part (B) is already proved. Later we prove part (B).

We first need to make sure that the concepts introduced before gave us a sufficient number of invariants under the action of the affine group and time rescaling so as to be able to classify geometrically the classes $\mathbf{QSE}_{(\eta<0)}$ and $\mathbf{QSE}_{(C_2=0)}$ according to their configurations of their invariant ellipses and lines.

Fixing the values of N_ε and using the types of the divisors *ICD* in the diagram of Fig. 242 (respectively *ILD* in the diagram of Fig. 244) we split all the corresponding

configurations in 8 (respectively in 5) groups. We observe that some groups have only one configuration. For the groups which possess more than one configuration we use the types of zero–cycles MS_{0C} and MS_{0C}^{Af}, correspondingly. This suffices for distinguishing all the configurations.

As a result we obtain the 35 geometric configurations displayed in the diagrams of Fig. 242 and Fig. 244. This proves statement (A) of this theorem. □

Proof of part (B). According to Oliveira *et al.* (2021) a quadratic system could have an invariant ellipse only if $\widehat{\gamma}_1 = \widehat{\gamma}_2 = 0$ and either $\eta < 0$ or $C_2 = 0$. We examine the cases $\eta < 0$ and $C_2 = 0$ separately.

6.3.1 The case $\eta < 0$

According to Lemma 2.2.14 a quadratic system with the condition $\eta < 0$ could be brought via an affine transformation and time rescaling to the following canonical form:

$$\begin{aligned} \dot{x} &= a + cx + dy + gx^2 + (h+1)xy, \\ \dot{y} &= b + ex + fy - x^2 + gxy + hy^2, \end{aligned} \tag{6.4}$$

with $C_2 = x(x^2+y^2)$, i.e. this system possesses at infinity one real and two complex infinity singularities. Following the diagram of Fig. 239 (see also Oliveira *et al.* (2021)) we discuss two subcases: $\theta \neq 0$ and $\theta = 0$.

6.3.1.1 The subcase $\theta \neq 0$

We examine step by step each one of the possibilities presented in Cor. 6.2.7.

6.3.1.1.1 The possibility $(\mathfrak{B}_1)$: $\widehat{\beta}_1\widehat{\beta}_2\widehat{\beta}_3 \neq 0$.

As it was proved in Oliveira *et al.* (2021) in this case by an affine transformation and time rescaling, systems (6.4) could be brought to the canonical form

$$\begin{aligned} \dot{x} &= a + dy + gx^2 + (h+1)xy, \\ \dot{y} &= \frac{ah}{g} - dx - x^2 + gxy + hy^2, \quad g \neq 0, \end{aligned} \tag{6.5}$$

which possesses an invariant conic

$$\Phi(x,y) = \frac{a}{g} + x^2 + y^2 = 0. \tag{6.6}$$

This conic is irreducible if and only if $a \neq 0$. For systems (6.5) we calculate

$$\begin{gathered} \theta = (h+1)\left[g^2 + (h-1)^2\right]/2, \quad \widehat{\beta}_1 = -d^2\left[g^2 + (h-1)^2\right]\left[9g^2 + (3h+1)^2\right]/16, \\ \widehat{\beta}_2 = -g\left[9g^2 + (3h+1)^2\right]/2, \quad \widehat{\beta}_3 = (3h-1)\left[9g^2 + (3h+5)^2\right]/2, \end{gathered}$$

and therefore we conclude that for systems (6.5) the condition $\theta\widehat{\beta}_1\widehat{\beta}_2\widehat{\beta}_3\widehat{\mathscr{R}}_1 \neq 0$ is equivalent to the condition

$$adg(h+1)(3h-1) \neq 0. \tag{6.7}$$

We observe that

$$\widehat{\mathscr{R}}_1 = 3agd^2(1+h)^2\left[g^2+(h-1)^2\right]^4\left[9g^2+(3h+1)^2\right]/128 \;\Rightarrow\; \operatorname{sign}(ag) = \operatorname{sign}(\widehat{\mathscr{R}}_1).$$

The case $\widehat{\mathscr{R}}_1 < 0$. Then $ag < 0$ and clearly the ellipse (6.6) is real.

Taking into account Lemma 2.2.17 we examine if systems (6.5) could possess at least one invariant line. Calculations yield

$$B_1 = -\frac{a^2}{g^2}(g^2+h^2)\left[g^2+(h-1)^2\right]^2\left[a(h+1)^2+d^2g\right], \tag{6.8}$$

and we consider two subcases: $B_1 \neq 0$ and $B_1 = 0$.

1) *The subcase* $B_1 \neq 0$. Then by Lemma 2.2.17 systems (6.5) could not possess invariant lines. For these systems we calculate $\mu_0 = -h\left[g^2+(h+1)^2\right]$ and we examine two possibilities: $\mu_0 \neq 0$ and $\mu_0 = 0$.

a) *The possibility* $\mu_0 \neq 0$. Then by Lemma 2.2.13 systems (6.5) have finite singularities of total multiplicity 4. We detect that two of these singularities are located on the ellipse (6.6), more exactly such singularities are $M_{1,2}\left(x_{1,2}, y_{1,2}\right)$ with

$$x_{1,2} = -\frac{d(h+1)\pm\sqrt{Z_1}}{g^2+(h+1)^2}, \quad y_{1,2} = \frac{dg^2\mp(h+1)\sqrt{Z_1}}{g\left[g^2+(h+1)^2\right]}, \quad Z_1 = -g\left[a\left[g^2+(1+h)^2\right]+d^2g\right]. \tag{6.9}$$

Other two singularities of systems (6.5) are $M_{3,4}\left(x_{3,4}, y_{3,4}\right)$ (generically located outside the ellipse) with

$$x_{3,4} = -\frac{dg\pm\sqrt{Z_2}}{2g}, \quad y_{3,4} = \frac{dg\pm\sqrt{Z_2}}{2h}, \quad Z_2 = g(d^2g+4ah). \tag{6.10}$$

On the other hand for systems (6.5) we calculate

$$\nu_1 = -d^4\left[g^2+(h-1)^2\right]^2\left[9g^2+(3h+1)^2\right]Z_1/256.$$

We observe that

$$\operatorname{sign}(\nu_1) = -\operatorname{sign}(Z_1),$$

and this means that this invariant polynomial is responsible for what kind of singularities are $M_{1,2}$: are they real or complex, distinct or coinciding.

*a.***1)** *The case* $\nu_1 < 0$. Then $Z_1 > 0$ and we obtain that the singularities $M_{1,2}$ located on the invariant ellipse are real. We need to determine the conditions when at least one

of the singularities $M_{3,4}$ also lies on the ellipse. For this, considering (6.6), we calculate

$$\Phi(x,y)|_{\{x=x_{3,4},\ y=y_{3,4}\}} = \frac{d^2g\left(g^2+h^2\right) \pm d\left(g^2+h^2\right)\sqrt{g\left(4ah+d^2g\right)}+2ah\left(g^2+h^2+h\right)}{2gh^2}$$
$$\equiv \Omega_{3,4}(a,g,h).$$

It is clear that at least one of the singularities $M_3(x_3,y_3)$ or $M_4(x_4,y_4)$ belongs to the ellipse (6.6) if and only if

$$\Omega_3\Omega_4 = \frac{aZ_3}{g^2h^2} = 0, \qquad Z_3 = d^2g\left(g^2+h^2\right)+a\left(g^2+h^2+h\right)^2.$$

On the other hand for systems (6.5) we have

$$\nu_2 = -105d\left[9g^2+(3h+1)^2\right]Z_3,$$

and clearly by (6.7) the condition $\nu_2 = 0$ is equivalent to $Z_3 = 0$. So we conclude that the following remark is valid:

Remark 6.3.3. Assume that for systems (6.5) the conditions (6.7) and $h \neq 0$ (i.e. $\mu_0 \neq 0$) hold. Then at least one of the singularities M_3, M_4 belongs to the ellipse if and only if $\nu_2 = 0$.

Next we examine two subcases: $\nu_2 \neq 0$ and $\nu_2 = 0$.

α) *The subcase* $\nu_2 \neq 0$. In this case we have *Config. E.1* since another singularity belongs to ellipse if and only if $\nu_2 = 0$ (example: $a = 1, d = -1, g = -1, h = -2$).

β) *The subcase* $\nu_2 = 0$. In this case we have $Z_3 = 0$, i.e. at least one of the two other singular points also lies on the ellipse. Moreover $g^2+h^2+h \neq 0$ otherwise we obtain a contradiction with the conditions stated at (6.7). So the condition $Z_3 = 0$ implies $a = -\dfrac{d^2g\left(g^2+h^2\right)}{\left(g^2+h^2+h\right)^2}$. In this case two singularities coalesce, namely $M_4 \equiv M_2$ and considering the coordinates of $M_i, i = 1,2,3,4$, we obtain three singularities

$$(x_1,y_1) = \left(-\frac{d[h+(2+h)(g^2+h^2)]}{(g^2+h^2+h)[g^2+(h+1)^2]},\ \frac{dg\left(g^2+h^2-1\right)}{\left(g^2+h^2+h\right)\left[g^2+(h+1)^2\right]}\right)$$

and

$$(x_2,y_2) = \left(-\frac{dh}{g^2+h^2+h},\ \frac{dg}{g^2+h^2+h}\right), \quad (x_3,y_3) = \left(-\frac{d\left(g^2+h^2\right)}{g^2+h^2+h},\ \frac{dg\left(g^2+h^2\right)}{h\left(g^2+h^2+h\right)}\right).$$

Therefore we have located on the ellipse a double singularity M_2 and a simple singularity M_1. On the other hand we have

$$\Phi(x,y)|_{\{x=x_3,y=y_3\}} = \frac{d^2(g^2+h^2)(g^2+h^2-h)}{h^2(g^2+h+h^2)} \equiv \frac{d^2(g^2+h^2)Z_3'}{h^2(g^2+h+h^2)}.$$

Thus we conclude that the singularity M_3 belongs to the ellipse if and only if $Z_3'=0$. Now taking into consideration Prop. 2.2.21 (see Table 1), for systems (6.5) in this case we calculate

$$\mathbf{D}=0,\ \mathbf{T}=\frac{12d^6g^2\left(Z_3'\right)^2}{-\left(g^2+h^2+h\right)^4}(gy-hx-x)^2(gx+hy)^2\left[gx\left(g^2+h^2+1\right)+hy\left(g^2+h^2-1\right)\right]^2,$$

and due to (6.7) the condition $\mathbf{T}=0$ is equivalent to $Z_3'=0$, i.e. the invariant polynomial $\mathbf{T}$ indicates if the third singularity belongs to the ellipse or not. We discuss two possibilities:

$\beta.1$) *The possibility* $\boldsymbol{T}\neq 0$. In this case we obtain *Config. E.2* (example: $a=5/9,d=-1,g=-1,h=-2$).

$\beta.2$) *The possibility* $\boldsymbol{T}=0$. In this case we have $Z_3'=0$, i.e. $g^2+h^2=h$. Substituting this expression in the coordinates (x_3,y_3) we obtain that M_3 coincides with M_2. So we deduce that we have one triple and one simple singularities located on the ellipse. As a result we arrive at *Config. E.3* (example: $a=-1,d=-1,g=4/17,h=1/17$).

***a*.2)** *The case* $\nu_1=0$. In this case we have $Z_1=0$ (see (6.9)), i.e. the two singularities which belong to the ellipse coalesce. On the other hand the two singularities which are located outside the ellipse remains outside the ellipse because the condition $Z_1=0$ implies $a=-\dfrac{d^2g}{g^2+(h+1)^2}$ and for this value of the parameter a we obtain $Z_3=\dfrac{d^2g^3}{g^2+(h+1)^2}\neq 0$. In such a way we get *Config. E.4* (example: $a=1/2,d=-1,g=-1,h=-2$).

***a*.3)** *The case* $\nu_1>0$. Then $Z_1<0$, i.e. the two singularities which belong to the ellipse are complex. We note that the condition $Z_1<0$ implies $Z_3\neq 0$, because if $Z_3=0$ we found $Z_1=\frac{d^2g^4}{\left(g^2+h^2+h\right)^2}>0$. This leads to *Config. E.5* (example: $a=1/4,d=-1,g=-1,h=-2$).

We claim that in this configuration the invariant ellipse is a limit cycle drown in diagram in boldface (see Rmk. 6.1.7 (b)). Indeed taking into consideration Thm. 6.2.5 (see statement (B_1)) we conclude that in the case under examination for the existence of limit cycles the following conditions must be satisfied:

$$\eta<0,\quad \theta\widehat{\beta}_1\widehat{\beta}_2\widehat{\beta}_3\neq 0,\ \widehat{\gamma}_1=\widehat{\gamma}_2=0,\ \widehat{\mathscr{R}}_1<0,\quad \mathscr{T}_3\mathscr{F}<0. \tag{6.11}$$

Clearly all the conditions are satisfied except the last one. So it remains to verify that $\mathscr{T}_3\mathscr{F}<0$ is fulfilled, too. For systems (6.5) we calculate

$$\begin{aligned}\mathscr{T}_3\mathscr{F}&=-\frac{1}{8}d^2g\left[(9g^2+(3h+1)^2\right]^2\left(ag^2+ah^2+2ah+a+d^2g\right),\\ \nu_1&=\frac{1}{256}d^4g\left[(g^2+(h-1)^2\right]^2\left[(9g^2+(3h+1)^2\right]^2\left(ag^2+ah^2+2ah+a+d^2g\right),\end{aligned}$$

and evidently the condition $\nu_1>0$ implies $\mathscr{T}_3\mathscr{F}<0$. This completes the proof of our claim.

b) *The possibility* $\mu_0 = 0$. This condition implies $h = 0$ and the condition (6.7) becomes $adg \neq 0$. In this case we obtain $\mu_1 = dg(g^2+1)x \neq 0$. According to Lemma 2.2.13 we conclude that exactly one of the four finite singularities has gone to infinity and coalesced with the real infinity singularity. So we obtain one real infinite singularity of multiplicity two which is of type $(1,1)$ (i.e. one finite and one infinity singularities coalesced, see Rmk. 6.1.7).

For $h = 0$ considering the coordinates of $M_{1,2}(x_{1,2}, y_{1,2})$ (see (6.9)) we obtain that these two singularities remain located on the ellipse (6.6). On the other hand from (6.10) it is not so difficult to determine that the singularity M_3 has gone to infinity and a straightforward calculation gives us the coordinates of the fourth singularity: $M_4\left(0, -\frac{a}{d}\right)$.

Again we consider the value of ν_1 and we examine three cases:

***b*.1)** *The case* $\nu_1 < 0$. Then we have $Z_1 > 0$ and this implies the existence of two real distinct singularities located on the ellipse. On the other hand considering (6.6) we have

$$\Phi(x,y)|_{\{x=x_4, y=y_4\}} = \frac{a\left(d^2+ag\right)}{d^2 g},$$

and since $a \neq 0$ the singularity M_4 belongs to the ellipse if and only if $d^2 + ag = 0$. Calculating $\nu_2 = -105dg^3\left(9g^2+1\right)\left(d^2+ag\right)$ we conclude that the singularity M_4 belongs to the ellipse if and only if $\nu_2 = 0$. So we discuss two subcases: $\nu_2 \neq 0$ and $\nu_2 = 0$.

α) *The subcase* $\nu_2 \neq 0$. Then the singularity M_4 remains outside the ellipse and we arrive at *Config. E.6* (example: $a = 5/8, d = -1, g = -1$).

β) *The subcase* $\nu_2 = 0$. This implies $a = -\frac{d^2}{g}$ and we obtain that the singularity M_4 coincides with M_2. As a result we arrive at *Config. E.7* (example: $a = -1, d = -1, g = 1$).

***b*.2)** *The case* $\nu_1 = 0$. In this case we have $Z_1 = 0$, i.e. $a = -\frac{d^2 g}{g^2+1}$ (see (6.9)) and therefore the two singularities which belong to the ellipse coalesce. On the other hand we calculate $\nu_2 = -\frac{105d^3g^3\left(9g^2+1\right)}{g^2+1} \neq 0$ and this means that M_4 remains outside the ellipse. So we arrive at *Config. E.8* (example: $a = 1/2, d = -1, g = -1$).

***b*.3)** *The case* $\nu_1 > 0$. In this case we have $Z_1 < 0$, i.e. the two singularities which belong to the ellipse are complex. On the other hand this fact implies that $\nu_2 \neq 0$. Therefore we have *Config. E.9* (example: $a = 1/4, d = -1, g = -1$).

We claim that in this configuration the invariant ellipse is a limit cycle, too (see Rmk. 6.1.7 (b)). For this it is sufficient to show that the conditions (6.11) are satisfied in this particular case, when $\mu_0 = 0$ (i.e. $h = 0$). Indeed, for systems (6.5) with $h = 0$ we

obtain

$$\mathscr{T}_3\mathscr{F} = -\frac{1}{8}d^2g\left(9g^2+1\right)^2\left(ag^2+a+d^2g\right),$$
$$\nu_1 = \frac{1}{256}d^4g\left(g^2+1\right)^2\left(9g^2+1\right)^2\left(ag^2+a+d^2g\right)$$

and clearly the condition $\nu_1 > 0$ implies $\mathscr{T}_3\mathscr{F} < 0$, i.e. our claim is proved.

2) *The subcase* $B_1 = 0$. Considering the condition (6.7) we obtain that $B_1 = 0$ (see (6.8)) is equivalent to $a = -\dfrac{d^2g}{(h+1)^2}$ which implies the existence of the invariant line

$$\mathscr{L}(x,y) = (h+1)x + d = 0.$$

On the other hand for this value of the parameter a we obtain

$$B_2 = -\frac{648d^4\left[g^2+(h-1)^2\right]^2\left(g^2+h^2\right)x^4}{(h+1)^4},$$

which is nonzero due to condition (6.7). It follows from Lemma 2.2.17 and Lemma 2.2.16 that the conditions $B_1 = 0$, $B_2 \neq 0$ and $\theta \neq 0$ implies that there exists at most one simple invariant straight line of systems (6.5). On the other hand for these systems we have $\mu_0 = -h\left[g^2+(h+1)^2\right]$ and we examine two possibilities: $\mu_0 \neq 0$ and $\mu_0 = 0$.

a) *The possibility* $\mu_0 \neq 0$. Then the condition $\mu_0 = -h\left[g^2+(h+1)^2\right] \neq 0$ gives $h \neq 0$ and considering condition (6.7) by Lemma 2.2.13, systems (6.5) have finite singularities of total multiplicity 4. Taking into account the coordinates of the singularities $M_{i,j}(x_{i,j},y_{i,j})$ $(i=j=1,2,3,4)$ mentioned before (see page 357) in this particular case these singularities have the following real coordinates

$$\begin{gathered}(x_1,y_1) = \left(-\frac{d}{h+1},0\right), \quad (x_2,y_2) = \left(\frac{d\left[g^2-(h+1)^2\right]}{(h+1)\left[g^2+(h+1)^2\right]}, \frac{2dg}{g^2+(h+1)^2}\right), \\ (x_3,y_3) = \left(-\frac{dh}{h+1}, \frac{dg}{h+1}\right), \quad (x_4,y_4) = \left(-\frac{d}{h+1}, \frac{dg}{h(h+1)}\right).\end{gathered} \tag{6.12}$$

We observe that due to $a = -\dfrac{d^2g}{(h+1)^2}$ the invariant ellipse for systems (6.5) becomes

$$\Phi(x,y) = x^2+y^2-\frac{d^2}{(h+1)^2}.$$

As it was shown before, the singularities $M_{1,2}\left(x_{1,2},y_{1,2}\right)$ are located on the ellipse and the singularities $M_{3,4}\left(x_{3,4},y_{3,4}\right)$ are generically located outside the ellipse. We also determine that the singularities M_1 and M_4 are located on the invariant line. On the other hand in generic case the singularities M_2 and M_3 could not belong to the line since calculations yield

$$\mathscr{L}(x_2,y_2) = \frac{2dg^2}{g^2+(h+1)^2}, \qquad \mathscr{L}(x_3,y_3) = d(1-h).$$

Due to the condition (6.7) we get $\mathscr{L}(x_2,y_2)\neq 0$, i.e. the ellipse and the invariant line have M_1 as the unique common point at which a line is tangent to the ellipse.

Considering Rmk. 6.3.3 we conclude that one of the singularities M_3 or M_4 belongs to the ellipse if and only if $\nu_2=0$. So, in what follows we discuss two cases: $\nu_2\neq 0$ and $\nu_2=0$.

a.1) *The case* $\nu_2\neq 0$. Then according to Rmk. 6.3.3 neither the singularity M_3 nor M_4 could belong to the ellipse. On the other hand the singularity M_4 is located on the invariant line whereas the singularity M_3 belongs to the invariant line if and only if $\mathscr{L}(x_3,y_3)=d(1-h)=0$. Due to $d\neq 0$ we obtain the condition $h=1$. We observe that this condition is governed by the invariant polynomial $\mathbf{D}$ because for systems (6.5) in the case $a=-\dfrac{d^2g}{(h+1)^2}$ we calculate

$$\nu_2=\frac{105d^3g^3\left(g^2+h^2-1\right)\left[9g^2+(3h+1)^2\right]}{(h+1)^2},\quad \mathbf{D}=-\frac{192d^8g^6(h-1)^2\left(g^2+h^2-1\right)^2}{(h+1)^8}, \tag{6.13}$$

and due to the condition $\nu_2\neq 0$ we obtain that the condition $\mathbf{D}=0$ is equivalent to $h=1$. We examine two subcases: $\mathbf{D}\neq 0$ and $\mathbf{D}=0$.

α) *The subcase* $\boldsymbol{D\neq 0}$. Then $h\neq 1$, i.e. the singularity M_3 remains outside the invariant curves and this leads to *Config. E.10* (example: $d=-1,g=1,h=-2$).

β) *The subcase* $\boldsymbol{D=0}$. In this case we have $h=1$ and considering (6.10) we obtain that M_3 coalesces with M_4 which is located on the invariant line and we arrive at *Config. E.11* (example: $d=1,g=1,h=1$).

a.2) *The case* $\nu_2=0$. Due to (6.7), from (6.13) we obtain that the condition $\nu_2=0$ gives $g^2+h^2-1=0$. This implies $\mathbf{D}=0$, and moreover we have $h\neq 1$ due to $g\neq 0$. We observe that setting $g^2=1-h^2$ in the expressions of the coordinates of (x_2,y_2) from (6.12) we obtain that $(x_2,y_2)=(x_3,y_3)$. So on the ellipse we get a double singularity and this leads to *Config. E.12* (example: $d=-1,g=\sqrt{3}/2,h=-1/2$).

b) *The possibility* $\mu_0=0$. Then the condition $\mu_0=-h\left[g^2+(h+1)^2\right]=0$ implies $h=0$ and we obtain $\mu_1=dg(g^2+1)x\neq 0$. According to Lemma 2.2.13 we conclude that exactly one of the four finite singularities has gone to infinity and coalesced with the real infinite singularity. So we obtain one real infinite singularity of multiplicity two which is of type $(1,1)$ (see Rmk. 6.1.7). Considering the coordinates of the finite singularities given in (6.12) we observe that M_4 has gone to infinity along the invariant line $\mathscr{L}=0$ and the remaining real finite singularities are

$$(x_1,y_1)=(-d,0),\quad (x_2,y_2)=\left(\frac{d\left(g^2-1\right)}{g^2+1},\frac{2dg}{g^2+1}\right),\quad (x_3,y_3)=(0,dg). \tag{6.14}$$

In order to determine the position of the singularity M_3 we calculate

$$\mathscr{L}(x_3,y_3)=d,\quad \Phi(x_3,y_3)=d^2(g^2-1).$$

Due to the condition (6.7) we obtain $\mathscr{L}(x_3,y_3)\neq 0$, i.e. M_3 could not belong to the invariant line. On the other hand $\Phi(x_3,y_3)=0$ if and only if $g^2-1=0$. We observe that systems (6.5) in the case under examination (i.e. $h=0$ and $a=-d^2g$) become

$$\dot{x}=-d^2g+dy+gx^2+xy,\quad \dot{y}=-dx+gxy-x^2. \tag{6.15}$$

We determine that the condition $g^2-1=0$ is equivalent to $\nu_2=0$ because for systems (6.15) we have

$$\nu_2=105d^3g^3\left(9g^2+1\right)\left(g^2-1\right).$$

So we discuss two cases: $\nu_2\neq 0$ and $\nu_2=0$.

b.**1)** *The case* $\nu_2\neq 0$. In this case the singularity M_3 remains outside the invariant curves and this leads to *Config. E.13* (example: $d=-1,g=-2,h=0$).

b.**2)** *The case* $\nu_2=0$. This implies $g=\pm 1$. However we can consider $g=1$ due to the rescaling $(x,y,t)\mapsto(x,-y,-t)$ in systems (6.15) which changes the sign of the parameter g. In this case considering (6.14) we obtain $(x_3,y_3)=(x_2,y_2)$ and as a result we get *Config. E.14* (example: $d=-1,g=1,h=0$).

The case $\widehat{\mathscr{R}}_1>0$**.** This condition implies $ag>0$ and clearly the ellipse (6.6) is complex. On the other hand considering (6.8) we observe that for systems (6.5) the conditions (6.7) and $ag>0$ imply $B_1\neq 0$. Then by Lemma 2.2.17 systems (6.5) could not possess invariant lines.

For these systems we calculate $\mu_0=-h\left[g^2+(h+1)^2\right]$ and we examine two subcases: $\mu_0\neq 0$ and $\mu_0=0$.

1) *The subcase* $\mu_0\neq 0$. Then by Lemma 2.2.13, systems (6.5) have finite singularities of total multiplicity 4 and their coordinates are given in (6.9). We observe that the condition $ag>0$ implies $Z_1<0$, i.e. the singularities $M_{1,2}\left(x_{1,2},y_{1,2}\right)$ are complex and as it was proved before they belong to the complex ellipse.

On the other hand the condition $ag>0$ implies

$$Z_3=d^2g\left(g^2+h^2\right)+a\left(g^2+h^2+h\right)^2\neq 0.$$

This fact implies that the singularities $M_{3,4}\left(x_{3,4},y_{3,4}\right)$ remain outside the complex ellipse. Therefore the unique possible configuration is *Config. E.15* (example: $a=-1,d=-1,g=-1,h=-2$).

2) *The subcase* $\mu_0=0$. This condition implies $h=0$. In this case we obtain $\mu_1=dg(g^2+1)x\neq 0$ and by Lemma 2.2.13 only one finite singularity coalesced with the real

infinite singularity which has multiplicity $(1,1)$ (see Rmk. 6.1.7). Therefore we arrive at *Config. E.16* (example: $a=-1,d=-1,g=-1$).

Thus, we have all the configurations indicated in the diagram of Fig. 245 in the block corresponding to the possibility $(\mathfrak{B}_1)$.

6.3.1.1.2 The possibility $(\mathfrak{B}_2)$: $\widehat{\beta}_1\widehat{\beta}_2\neq 0,\widehat{\beta}_3=0$.

According to Oliveira *et al.* (2021) in this case by an affine transformation and time rescaling systems (6.4) could be brought to the canonical form (6.5) with $h=1/3$, i.e. we get a subfamily of (6.5) which was investigated in the previous subsection. As it was shown, for $h\neq 1/3$ systems (6.5) possess 16 configurations *Config. E.1* – *Config. E.16*. Moreover it is necessary to highlight that the value $h=1/3$ is not a bifurcation value for distinguishing these configurations.

It remains to find out which conditions defining each one of the configurations are compatible in this case. We claim that the configurations (i) *Config. E.6* – *Config. E.9*, *Config. E.13*, *Config. E.14*, *Config. E.16* and (ii) *Config. E.11*, could not be realizable for systems (6.5) with $h=1/3$.

Indeed, for each one of the configuration from the group (i) condition $\mu_0=0$ is necessary. However, for $h=1/3$ we have $\mu_0=-\left(9g^2+16\right)/27\neq 0$, i.e. the configurations from the group (i) could not be realized for $h=1/3$.

Secondly, as it was shown in the previous subsection, a system (6.5) possesses the configuration *Config. E.11* if and only if the following conditions hold:

$$B_1=0,\quad \mu_0\neq 0,\quad \nu_2\neq 0,\quad \mathbf{D}=0.$$

However, in the case $h=1/3$ the condition $B_1=0$ yields $a=-\left(9d^2g\right)/16$ and then we calculate

$$\nu_2=\frac{105d^3g^3\left(9g^2-8\right)\left(9g^2+4\right)}{16},\quad \mathbf{D}=-\frac{-27d^8g^6\left(9g^2-8\right)^2}{256}.$$

Evidently, the condition $\nu_2\neq 0$ implies $\mathbf{D}\neq 0$, and this completes the proof of our claim.

Therefore in this case (i.e. for $h=1/3$) we have *Config. E.1* (example: $a=1,d=-1,g=-1$), *Config. E.2* (example: $a=90/169,d=-1,g=-1$), *Config. E.3* (example: $a=\sqrt{2}/4,d=-1,g=-\sqrt{2}/3$), *Config. E.4* (example: $a=9/25,d=-1,g=-1$), *Config. E.5* (example: $a=1/4,d=-1,g=-1$), *Config. E.10* (example: $a=-1,d=-1,g=1/2$), *Config. E.12* (example: $a=-1,d=-1,g=2\sqrt{2}/3$) and *Config. E.15* (example: $a=-1,d=-1,g=-1$).

Next we discuss the existence of limit cycle for this subfamily of systems (6.5) defined by $h=1/3$. We observe that due to $\widehat{\beta}_3=0$ the conditions (6.11) are not satisfied.

On the other hand according to Thm. 6.2.5, statement (B_2) we have the following necessary and sufficient conditions for existence of limit cycles:

$$\eta<0,\quad \theta\widehat{\beta}_1\widehat{\beta}_2\neq 0,\ \widehat{\beta}_3=\widehat{\gamma}_1=\widehat{\gamma}_2=\widehat{\gamma}_3=0,\ \widehat{\mathscr{R}}_1<0,\quad \mathscr{T}_3\mathscr{F}<0. \tag{6.16}$$

Since for the configuration *Config. E.5* the conditions $\widehat{\mathscr{R}}_1<0$ and $\nu_1>0$ hold, considering Rmk. 6.2.7 we deduce that so far for systems (6.5) with $h=1/3$ all the previous conditions with the exception of $\mathscr{T}_3\mathscr{F}<0$ are fulfilled. We now calculate

$$\mathscr{T}_3\mathscr{F}=-\frac{1}{72}d^2g\left(9g^2+4\right)^2\left(9ag^2+16a+9d^2g\right),$$
$$\nu_1=\frac{d^4g\left(9g^2+4\right)^4\left(9ag^2+16a+9d^2g\right)}{186624},$$

and evidently the condition $\nu_1>0$ implies $\mathscr{T}_3\mathscr{F}<0$. So the conditions (6.16) are satisfied and the ellipse from *Config. E.5* is a limit cycle.

It is not too difficult to determine that for the remaining configurations (i.e. excluding the configurations of the groups (i) and (ii) defined before) all the corresponding conditions are compatible and this is confirmed by the examples presented before.

Thus, for all the realizable configurations for systems (6.5) with $h=1/3$ we obtain the conditions presented in the diagram of Fig. 245 in the block corresponding to the possibility $(\mathfrak{B}_2)$.

6.3.1.1.3 The possibility $(\mathfrak{B}_3)$: $\widehat{\beta}_1\neq 0,\widehat{\beta}_2=0,\widehat{\beta}_5\neq 0$.

As it was proved in Oliveira *et al.* (2021), in this case by an affine transformation and time rescaling systems (6.4) could be brought to the canonical form

$$\dot{x}=dy+(h+1)xy,\qquad \dot{y}=b-dx-x^2+hy^2, \tag{6.17}$$

which possesses an invariant conic

$$\Phi(x,y)=\frac{b}{h}+x^2+y^2=0,\quad h\neq 0. \tag{6.18}$$

This conic is irreducible if and only if $b\neq 0$. For systems (6.17) we calculate

$$\theta=(h+1)(h-1)^2/2,\quad \widehat{\beta}_1=-d^2(h-1)^2(3h+1)^2/16,$$
$$\widehat{\beta}_5=-2(h+1)(3h-1),\quad \widehat{\mathscr{R}}_2=bh(h+1)^2(h-1)^2(3h+1)^4/8,$$

and therefore we conclude that for systems (6.17) the condition $\theta\widehat{\beta}_1\widehat{\beta}_5\widehat{\mathscr{R}}_2\neq 0$ is equivalent to the condition

$$bdh(h-1)(h+1)(3h-1)(3h+1)\neq 0. \tag{6.19}$$

On the other hand we have

$$\widehat{\mathscr{R}}_2=bh(h+1)^2(h-1)^2(3h+1)^4/8\ \Rightarrow\ \operatorname{sign}(bh)=\operatorname{sign}(\widehat{\mathscr{R}}_2).$$

The case $\widehat{\mathscr{R}}_2 < 0$. Then $bh < 0$ and clearly the ellipse (6.18) is real.

We observe that systems (6.17) possess the invariant line

$$\mathscr{L}(x,y) = (h+1)x + d = 0. \tag{6.20}$$

Then by Lemma 2.2.17 the condition $B_1 = 0$ is satisfied. Moreover, since $\theta \neq 0$, by Lemmas 2.2.17 and 2.2.16 systems (6.17) could possess another invariant straight line only if $B_2 = 0$. We calculate

$$B_2 = -648b^2(h-1)^4x^4,$$

and due to condition (6.19) we have $B_2 \neq 0$. So systems (6.17) possess exactly one invariant straight line $\mathscr{L}(x,y) = 0$.

For these systems we calculate $\mu_0 = -h(h+1)^2$ and due to condition (6.19) we have $\mu_0 \neq 0$. Considering Lemma 2.2.13, systems (6.17) have finite singularities of total multiplicity 4. We observe that two of these singularities are located on the ellipse (6.18) as well as on the invariant line (6.20). More precisely these are the singularities $M_{1,2}\big(x_{1,2}, y_{1,2}\big)$ with

$$x_{1,2} = -\frac{d}{h+1}, \quad y_{1,2} = \pm\frac{\sqrt{Z_1'}}{h+1}, \quad Z_1' = -\Big[d^2 + \frac{b}{h}(h+1)^2\Big]. \tag{6.21}$$

Other two singularities of systems (6.17) are $M_{3,4}\big(x_{3,4}, y_{3,4}\big)$ (generically located outside both invariant curves) with

$$x_{3,4} = \frac{-d \pm \sqrt{Z_2'}}{2}, \quad y_{3,4} = 0, \quad Z_2' = 4b + d^2. \tag{6.22}$$

On the other hand for systems (6.17) we calculate

$$\nu_3 = -2h^2(h+1)^2(3h+1)^2Z_1'.$$

We observe that

$$\operatorname{sign}(\nu_3) = -\operatorname{sign}(Z_1'),$$

and this means that the invariant polynomial ν_3 determines if the singularities $M_{1,2}$ are either real or complex, distinct or coinciding.

1) *The subcase* $\nu_3 < 0$. Then $Z_1' > 0$ and the singularities $M_{1,2}$ are real. We need to determine the conditions when at least one of the singularities $M_{3,4}$ located outside the invariant curves coincides with one of their points. In this sense considering (6.18) and (6.20) we calculate

$$\Phi(x,y)|_{\{x=x_{3,4},\ y=y_{3,4}\}} = \frac{2bh + 2b + d^2h \mp dh\sqrt{Z_2'}}{2h} \equiv \Omega_{3,4}'(b,d,h),$$
$$\mathscr{L}(x,y)|_{\{x=x_{3,4},\ y=y_{3,4}\}} = \frac{d(1-h) \pm (h+1)\sqrt{Z_2'}}{2} \equiv \mathscr{L}_{3,4}'(b,d,h).$$

It is clear that at least one of the singularities $M_3(x_3,y_3)$ or $M_4(x_4,y_4)$ belongs to the ellipse (6.18) or to the line (6.20) if and only if the conditions

$$\Omega_3'\Omega_4' = \frac{b\left[b(h+1)^2+d^2h\right]}{h^2} = \frac{-bZ_1'}{h^2} = 0 \quad \text{or} \quad \mathscr{L}_3'\mathscr{L}_4' = -\left[d^2h+b(h+1)^2\right] = Z_1' = 0, \tag{6.23}$$

are satisfied, respectively.

We observe that the conditions $Z_1' \neq 0$ and (6.19) imply $\Omega_3'\Omega_4'\mathscr{L}_3'\mathscr{L}_4' \neq 0$. Therefore none of the points $M_{3,4}$ could belong to the ellipse or to the line. So we arrive at *Config. E.17* (example: $b=-1, d=-1, h=1/4$).

2) *The subcase* $\nu_3 = 0$. Then $Z_1' = 0$ which implies $b = -\dfrac{d^2h}{(h+1)^2}$ and therefore the singularities M_1 and M_2 coalesce. It is clear that in this case the invariant line and the ellipse have a unique common point at which they are tangent and this point is a double singularity. However according to (6.23) in this case we have $\Omega_3'\Omega_4' = 0$ and $\mathscr{L}_3'\mathscr{L}_4' = 0$, and this imply that the singularity M_3 also belongs to both curves. More exactly we obtain $M_3 = M_2 = M_1$ which leads to a triple singularity. On the other hand due to the condition (6.19) we obtain

$$\Phi(x,y)|_{\{x=x_4,\ y=y_4\}} = \frac{d^2(h-1)}{h+1} \neq 0, \quad \mathscr{L}(x,y)|_{\{x=x_4,\ y=y_4\}} = d(1-h) \neq 0,$$

i.e. the singularity M_4 remains outside both invariant curves. So the only possible configuration is *Config. E.18* (example: $b=2, d=-1, h=-2$).

3) *The subcase* $\nu_3 > 0$. Then $Z_1' < 0$ and this implies that the singularities M_1 and M_2 located at the intersections of the invariant ellipse with the invariant line are complex. On the other hand we observe that due to conditions (6.19) and (6.23) we have $\Omega_3'\Omega_4'\mathscr{L}_3'\mathscr{L}_4' \neq 0$ and therefore none of the points $M_{3,4}$ could belong to the ellipse or to the line. It is not difficult to convince ourselves that in the case under examination we obtain *Config. E.19* (example: $b=-1/8, d=-1, h=1/4$).

We claim that in this configuration the invariant ellipse is not a limit cycle. Indeed since for systems (6.17) we have $\mathscr{T}_3\mathscr{F} = 0$, by Thm. 6.2.5 (see statement **(B)**) we conclude that our claim is valid.

The case $\widehat{\mathscr{R}}_2 > 0$. Then $bh > 0$ and in this case the ellipse (6.18) is complex. According to (6.21) the condition $bh > 0$ implies $Z_1' < 0$, i.e. evidently the singularities $M_{1,2}$ located on the ellipse also are complex. Therefore we arrive at *Config. E.20* (example: $b=1, d=-1, h=1/6$).

Thus we have all the configurations indicated in the diagram of Fig. 245 in the block corresponding to the possibility $(\mathfrak{B}_3)$.

6.3.1.1.4 The possibility $(\mathfrak{B}_4)$: $\widehat{\beta}_1 \neq 0, \widehat{\beta}_2 = \widehat{\beta}_5 = 0$.

According to Oliveira *et al.* (2021) in this case by an affine transformation and time rescaling systems (6.4) could be brought to the canonical form (6.17) with $h = 1/3$, i.e. we get a subfamily of (6.17) which was investigated in the previous subsection. As it was shown, for $h \neq 1/3$ systems (6.17) possess four configurations, namely *Config. E.17*, *Config. E.18*, *Config. E.19* and *Config. E.20*. Moreover it is necessary to point out that the value $h = 1/3$ is not a bifurcation value for the corresponding configurations.

It is not too difficult to determine that all the configurations are realizable in the case $h = 1/3$, too. In fact, for *Config. E.17* we take $b = -11/16$ and $d = -1$, for *Config. E.18* we put $b = -3/16$ and $d = -1$, for *Config. E.19* we write $b = -3/32$ and $d = -1$ and finally for *Config. E.20* we consider $b = 1$ and $d = -1$.

So we obtain the condition presented in the diagram of Fig. 245 in the block corresponding to the possibility $(\mathfrak{B}_4)$.

6.3.1.1.5 The possibility $(\mathfrak{B}_5)$: $\widehat{\beta}_1 = 0, \widehat{\beta}_6 \neq 0, \widehat{\beta}_2 \neq 0$.

As it was proved in Oliveira *et al.* (2021) in this case by an affine transformation and time rescaling systems (6.4) could be brought to the canonical form

$$\dot{x} = a + gx^2 + (h+1)xy, \qquad \dot{y} = \frac{ah}{g} - x^2 + gxy + hy^2, \tag{6.24}$$

which possesses an invariant conic (of the elliptic type)

$$\Phi(x,y) = \frac{a}{g} + x^2 + y^2 = 0, \quad g \neq 0. \tag{6.25}$$

This conic is irreducible if and only if $a \neq 0$. For systems (6.24) we calculate

$$\theta = \frac{1}{2}(h+1)\left[g^2 + (h-1)^2\right], \quad \widehat{\beta}_6 = (3h+1)\left[9g^2 + (3h+1)^2\right]/8,$$
$$\widehat{\beta}_2 = -g\left[g^2 + (3h+1)^2\right]/2, \quad \widehat{\mathscr{R}}_3 = 160ag\left(g^2+h^2\right)\left[g^2 + (3h+1)^2\right],$$

and therefore we conclude that for systems (6.24) the condition $\theta\widehat{\beta}_2\widehat{\beta}_6\widehat{\mathscr{R}}_3 \neq 0$ is equivalent to the condition

$$ag(h+1)(3h+1) \neq 0. \tag{6.26}$$

Taking into account Lemma 2.2.17 we examine if systems (6.24) could possess at least one invariant line. Calculations yield

$$B_1 = -\frac{a^3(h+1)^2\left[g^2 + (h-1)^2\right]^2\left(g^2+h^2\right)}{g^2},$$

and due to condition (6.26) we obtain $B_1 \neq 0$. In this case by Lemma 2.2.17 we can conclude that systems (6.24) could not possess invariant lines.

On the other hand we have

$$\widehat{\mathscr{R}}_3 = 160ag\left(g^2+h^2\right)\left[g^2+(3h+1)^2\right] \;\Rightarrow\; \operatorname{sign}(ag)=\operatorname{sign}(\widehat{\mathscr{R}}_3).$$

The case $\widehat{\mathscr{R}}_3<0$. Then $ag<0$ and clearly the ellipse (6.25) is real.

For systems (6.24) we calculate $\mu_0=-h\left[g^2+(h+1)^2\right]$ and we examine two subcases: $\mu_0\neq 0$ and $\mu_0=0$.

1) *The subcase* $\mu_0\neq 0$. Then by Lemma 2.2.13 the systems have finite singularities of total multiplicity 4. We detect that two of these singularities are located on the ellipse (6.25), more exactly such singularities are $M_{1,2}\left(x_{1,2},y_{1,2}\right)$ with

$$x_{1,2}=\pm\frac{\sqrt{Z_1}}{g^2+(h+1)^2},\quad y_{1,2}=\pm\frac{(h+1)\sqrt{Z_1}}{g\left[g^2+(h+1)^2\right]},\quad Z_1=-ag\left[g^2+(h+1)^2\right]. \tag{6.27}$$

Other two singularities of systems (6.24) are $M_{3,4}\left(x_{3,4},y_{3,4}\right)$ (generically located outside the ellipse) with

$$x_{3,4}=\pm\frac{\sqrt{Z_2}}{g},\quad y_{3,4}=\mp\frac{\sqrt{Z_2}}{h},\quad Z_2=agh. \tag{6.28}$$

Since $\operatorname{sign}(\widehat{\mathscr{R}}_3)=-\operatorname{sign}(Z_1)$, the condition $\widehat{\mathscr{R}}_3<0$ implies $Z_1>0$. In this case we have two real distinct singularities on the ellipse, namely $M_{1,2}$.

We need to determine the conditions when at least one of the singularities $M_{3,4}$ located outside the ellipse coincide with its points. In this order considering (6.25) we calculate

$$\Phi(x,y)|_{\{x=x_{3,4},\ y=y_{3,4}\}}=\frac{aZ_3}{gh},\quad Z_3=g^2+h(h+1).$$

It is clear that at least one of the singularities $M_3(x_3,y_3)$ or $M_4(x_4,y_4)$ belongs to the ellipse (6.25) if and only if $Z_3=0$.

On the other hand for systems (6.24) we have

$$\mathbf{D}=\frac{768a^4h\left[g^2+(h+1)^2\right]Z_3^4}{g^4},$$

and clearly due to the conditions (6.26) and $\mu_0\neq 0$ the condition $\mathbf{D}=0$ is equivalent to $Z_3=0$.

a) *The possibility* $\boldsymbol{D}\neq 0$. Then $Z_3\neq 0$ and the singularities $M_{3,4}$ remain outside the ellipse and we have *Config. E.1* (example: $a=1,g=-3/2,h=-2$).

b) *The possibility* $\boldsymbol{D}=0$. Then $Z_3=0$, i.e. $g^2+h(h+1)=0$. In order to use this relation, due to $h\neq 0$ we apply the following parametrization: $g=g_1h$ and then $h=-1/(g_1^2+1)$. Considering the coordinates (6.27) and (6.28) we obtain

$$x_{1,2}=\pm\frac{\sqrt{ag_1}}{g_1},\quad y_{1,2}=\mp\sqrt{ag_1};\quad x_{3,4}=\mp\frac{\sqrt{ag_1}}{g_1},\quad y_{3,4}=\pm\sqrt{ag_1},$$

and we observe that M_3 coincides with M_2 and M_4 coincides with M_1. As a result we arrive at *Config. E.21* (example: $a=-1, g=1/4, h=-(2+\sqrt{3})/4$).

2) *The subcase* $\mu_0=0$. In this subcase we get $h=0$ and this implies $\mu_1=0$ and $\mu_2=ag\left(g^2+1\right)x^2\neq 0$ due to the condition (6.26). Therefore by Lemma 2.2.13 exactly two finite singularities have gone to infinity. More exactly according to the factorization of μ_2 by the same lemma we deduce that both points coalesced with the infinite singularity $[0:1:0]$. So we obtain a triple singularity at infinity of the type $(1,2)$ (see Rmk. 6.1.7), and this leads to *Config. E.22* (example: $a=1, g=-1$).

The case $\widehat{\mathscr{R}}_3>0$**.** This condition implies $ag>0$ and clearly the ellipse (6.25) is complex. For systems (6.24) we have $\mu_0=-h\left[g^2+(h+1)^2\right]$ and we examine two subcases: $\mu_0\neq 0$ and $\mu_0=0$.

1) *The subcase* $\mu_0\neq 0$. Then by Lemma 2.2.13, systems (6.24) have finite singularities of total multiplicity 4 and their coordinates are given in (6.27). We observe that the condition $ag>0$ implies $Z_1<0$, i.e. the singularities $M_{1,2}\left(x_{1,2},y_{1,2}\right)$ are complex and as it was proved before they belong to a complex ellipse.

It is not to difficult to determine that the condition $Z_3=0$ in this case implies $h<0$ and due to $ag>0$ we obtain that the singularities $M_{3,4}$ are also complex. Moreover the condition $Z_3=0$ forces them to coalesce with the two complex singularities on the ellipse. Therefore on the complex ellipse we get two double complex singularities. This is however irrelevant in view of the definition of a configuration (see Def. 6.1.8).

Thus we conclude that in both cases $Z_3\neq 0$ and $Z_3=0$ we arrive at the same configuration, namely *Config. E.15* (examples: $a=-1, g=-3/2, h=-2$ and $a=-1, g=-249/512, h=-(256+\sqrt{3535})/512$, respectively).

2) *The subcase* $\mu_0=0$. In this case we have $h=0$ and as it was shown in the case $\widehat{\mathscr{R}}_3<0$ we get at infinity a triple singularity of the type $(1,2)$ (see Rmk. 6.1.7), and this leads to *Config. E.23* (example: $a=-1, g=-1$).

In this way we have all the configurations indicated in the diagram of Fig. 245 in the block corresponding to the possibility $(\mathfrak{B}_5)$.

6.3.1.1.6 The possibility $(\mathfrak{B}_6)$: $\widehat{\beta}_1=0, \widehat{\beta}_6\neq 0, \widehat{\beta}_2=0$.

As it was proved in Oliveira *et al.* (2021) in this case by an affine transformation and time rescaling systems (6.4) could be brought to the canonical form

$$\dot{x}=(h+1)xy, \qquad \dot{y}=b-x^2+hy^2, \tag{6.29}$$

which possesses an invariant conic (of the elliptic type)

$$\Phi(x,y)=\frac{b}{h}+x^2+y^2=0,\quad h\neq 0. \tag{6.30}$$

This conic is irreducible if and only if $b\neq 0$. For systems (6.29) we calculate

$$\theta=(h+1)(h-1)^2/2,\quad \widehat{\beta}_6=(3h+1)^3/8,\quad \widehat{\mathscr{R}}_2=bh(3h+1)^4\left(h^2-1\right)^2/8,$$

and therefore we conclude that for systems (6.29) the condition $\theta\widehat{\beta}_6\widehat{\mathscr{R}}_2\neq 0$ is equivalent to the condition

$$bh(h+1)(h-1)(3h+1)\neq 0. \tag{6.31}$$

On the other hand we have

$$\operatorname{sign}(bh)=\operatorname{sign}(\widehat{\mathscr{R}}_2).$$

The case $\widehat{\mathscr{R}}_2<0$. This condition implies $bh<0$ and clearly the ellipse (6.30) is real.

Taking into account Lemma 2.2.17 we examine if systems (6.29) could possess at least one invariant line. Calculations yield $B_1=0$ and $B_2=-648b^2(h-1)^4x^4$ which is nonzero due to condition (6.31). It follows from Lemma 2.2.17 and Lemma 2.2.16 that the conditions $B_1=0$, $B_2\neq 0$ and $\theta\neq 0$ imply that there exists exactly one simple invariant straight line of systems (6.29), namely

$$\mathscr{L}(x,y)=x=0. \tag{6.32}$$

Moreover for these systems we have $\mu_0=-h(h+1)^2$ which is nonzero due to condition (6.31). Therefore in this case the coordinates of the finite singularities for systems (6.29) could be obtained from the coordinates described in (6.21) and (6.22) setting $d=0$:

$$\begin{gathered} x_{1,2}=0,\quad y_{1,2}=\pm\sqrt{Z_1},\quad Z_1=-\frac{b}{h},\\ x_{3,4}=\pm\sqrt{Z_2},\quad y_{3,4}=0,\quad Z_2=b. \end{gathered} \tag{6.33}$$

We observe that the singularities $M_{1,2}$ belong to the ellipse as well as to the invariant line, and the singularities $M_{3,4}$ are generically located outside both invariant curves.

Since $\operatorname{sign}(\widehat{\mathscr{R}}_2)=-\operatorname{sign}(Z_1)$, the condition $\widehat{\mathscr{R}}_2<0$ implies $Z_1>0$. In this case the singularities $M_{1,2}$ are real and distinct.

We need to determine the conditions when at least one of the singularities $M_{3,4}$, in general located outside the invariant curves, lies on these curves. In this order considering (6.30), (6.32) and (6.33) we calculate

$$\Phi(x,y)|_{\{x=x_{3,4},\ y=y_{3,4}\}}=\frac{b(h+1)}{h}\equiv\Omega,\quad \mathscr{L}(x,y)|_{\{x=x_{3,4},\ y=y_{3,4}\}}=\pm\sqrt{b}\equiv\mathscr{L}_{3,4}.$$

It is clear that at least one of the singularities M_3 or M_4 belongs to the ellipse (6.30) and the invariant line (6.32) if and only if $\Omega=0$ or $\mathscr{L}_3\mathscr{L}_4=0$, respectively. Due to conditions (6.31) none of these conditions could hold. As a result we arrive at *Config. E.17* (example: $b=1,h=-2$).

The case $\widehat{\mathscr{R}}_2 > 0$. This condition implies $bh > 0$ and clearly the ellipse (6.30) is complex. According to (6.33) the condition $bh > 0$ implies $Z_1 < 0$, i.e. evidently the singularities $M_{1,2}$ located on the ellipse are also complex. Thus we arrive at *Config. E.20* (example: $b = 1, h = 1/2$).

So we have all the configurations indicated in the diagram of Fig. 245 in the block corresponding to the possibility $(\mathfrak{B}_6)$.

6.3.1.1.7 The possibility $(\mathfrak{B}_7)$: $\widehat{\beta}_1 = \widehat{\beta}_6 = 0, \widehat{\beta}_2 \neq 0$.

As it was proved in Oliveira *et al.* (2021) in this case by an affine transformation and time rescaling systems (6.4) could be brought to the canonical form

$$\dot{x} = a + gx^2 + \frac{2xy}{3}, \quad \dot{y} = -\frac{a}{3g} - x^2 - \frac{y^2}{3} + gxy, \tag{6.34}$$

which possesses an invariant conic (of the elliptic type)

$$\Phi(x,y) = \frac{a}{g} + x^2 + y^2 = 0, \quad g \neq 0. \tag{6.35}$$

This conic is irreducible if and only if $a \neq 0$. For systems (6.34) we calculate

$$\theta = \left(9g^2 + 16\right)/27, \quad \widehat{\beta}_2 = -g^3/2, \quad \widehat{\mathscr{R}}_3 = 160ag^3\left(9g^2 + 1\right)/9,$$

and therefore we conclude that for systems (6.34) the condition $\theta\widehat{\beta}_2\widehat{\mathscr{R}}_3 \neq 0$ is equivalent to the condition $ag \neq 0$. Moreover we clearly have $\mathbf{sign}(ag) = \mathbf{sign}(\widehat{\mathscr{R}}_3)$.

On the other hand for systems (6.34) we calculate

$$B_1 = -\frac{4a^3\left(9g^2+1\right)\left(9g^2+16\right)^2}{6561g^2} \neq 0,$$

due to $ag \neq 0$. Therefore by Lemma 2.2.17 we conclude that systems (6.34) could not possess invariant lines.

The case $\widehat{\mathscr{R}}_3 < 0$. Then $ag < 0$ and clearly the ellipse (6.35) is real.

For systems (6.34) we calculate $\mu_0 = \left(9g^2 + 4\right)/27 \neq 0$. Then by Lemma 2.2.13 the systems have finite singularities of total multiplicity 4. We detect that two of these singularities are located on the ellipse (6.35), more exactly such singularities are $M_{1,2}\left(x_{1,2}, y_{1,2}\right)$ with

$$x_{1,2} = \pm\frac{3\sqrt{Z_1}}{9g^2+4}, \quad y_{1,2} = \pm\frac{2\sqrt{Z_1}}{g\left(9g^2+4\right)}, \quad Z_1 = -ag\left(9g^2+4\right). \tag{6.36}$$

Other two singularities of systems (6.34) are $M_{3,4}\left(x_{3,4}, y_{3,4}\right)$ (generically located outside the ellipse) with

$$x_{3,4} = \pm\frac{\sqrt{-3ag}}{3g}, \quad y_{3,4} = \pm\sqrt{-3ag}. \tag{6.37}$$

Since $\operatorname{sign}(\widehat{\mathscr{R}}_3) = -\operatorname{sign}(Z_1)$, the condition $\widehat{\mathscr{R}}_3 < 0$ implies $Z_1 > 0$. In this case we have two real distinct singularities on the ellipse, namely $M_{1,2}$.

We need to determine the conditions when at least one of the singularities $M_{3,4}$, in general located outside the ellipse, lies on the ellipse. In this order considering (6.35) we calculate

$$\Phi(x,y)|_{\{x=x_{3,4},\ y=y_{3,4}\}} = aZ_3, \quad Z_3 = -\frac{9g^2-2}{3g}.$$

It is clear that at least one of the singularities $M_3(x_3,y_3)$ or $M_4(x_4,y_4)$ belongs to the ellipse (6.35) if and only if $Z_3 = 0$. We observe that the invariant polynomial $\mathbf{D}$ is responsible for this condition because for systems (6.34) we have

$$\mathbf{D} = -\frac{256a^4\left(9g^2+4\right)Z_3^4}{59049g^4}, \quad ag \neq 0.$$

1) *The subcase* $\boldsymbol{D \neq 0}$. Then $Z_3 \neq 0$ and the singularities $M_{3,4}$ remain outside the ellipse and we have *Config. E.1* (example: $a = -1, g = 1/4$).

2) *The subcase* $\boldsymbol{D = 0}$. Then $Z_3 = 0$, i.e. $9g^2 - 2 = 0$. In this case we have $g = \pm\sqrt{2}/3$. Without loss of generality we can assume $g = \sqrt{2}/3$ since the rescaling $(x,y,t) \to (-x,y,t)$ simultaneously change the signs of the parameters a and g of systems (6.34). So $g = \sqrt{2}/3$ and for the coordinates of the singularities $M_{1,2}$ and $M_{3,4}$ of these systems we have

$$x_{1,2} = \pm\frac{\sqrt{-a}}{\sqrt[4]{2}} = x_{3,4}, \quad y_{1,2} = \pm\sqrt[4]{2}\sqrt{-a} = y_{3,4}.$$

So we obtain that the singularity M_3 (respectively M_4) coalesces with M_1 (respectively M_2). As a result we have two double singularities located on the ellipse which leads to *Config. E.21* (example: $a = -75, g = \sqrt{2}/3$).

The case $\widehat{\mathscr{R}}_3 > 0$. This condition implies $ag > 0$ and clearly the ellipse (6.35) is complex. Since for systems (6.34) we have $\mu_0 \neq 0$, by Lemma 2.2.13 these systems have finite singularities of total multiplicity 4 and their coordinates are given in (6.36) and (6.37). We observe that the condition $ag > 0$ implies $Z_1 < 0$, i.e. the singularities $M_{1,2}\left(x_{1,2}, y_{1,2}\right)$ are complex and as it was proved before they belong to the complex ellipse.

It is not to difficult to determine that the singularities $M_{3,4}$ are also complex. Moreover the condition $\mathbf{D} = 0$ forces them to coalesce with the two complex singularities on the ellipse as we discussed in the case $\widehat{\mathscr{R}}_3 < 0$. So we get two double complex singularities located on the complex ellipse.

Thus considering Def. 6.1.8 we conclude that in both cases, i.e. $\mathbf{D} \neq 0$ and $\mathbf{D} = 0$, we arrive at the same configuration, namely *Config. E.15* (examples: $a = -1, g = -1$ and $a = 27, g = \sqrt{2}/3$, respectively).

Therefore we have all the configurations indicated in the diagram of Fig. 245 in the block corresponding to the possibility $(\mathfrak{B}_7)$.

6.3.1.1.8 The possibility $(\mathfrak{B}_8)$: $\widehat{\beta}_1 = \widehat{\beta}_6 = \widehat{\beta}_2 = 0$.

As it was proved in Oliveira *et al.* (2021) in this case by an affine transformation and time rescaling, systems (6.4) could be brought to the canonical form

$$\dot{x} = 2xy/3, \qquad \dot{y} = b - x^2 - y^2/3, \tag{6.38}$$

which possesses an invariant conic

$$\Phi(x,y) = -3b + x^2 + y^2 = 0. \tag{6.39}$$

This conic is irreducible if and only if $b \neq 0$. For systems (6.38) we calculate

$$\theta = 16/27, \quad \widehat{\mathscr{R}}_4 = -32b\left(3x^2 + y^2\right)/9,$$

and therefore we conclude that for systems (6.38) the condition $\widehat{\mathscr{R}}_4 \neq 0$ is equivalent to the condition $b \neq 0$. On the other hand we have $\mathbf{sign}(b) = -\mathbf{sign}(\widehat{\mathscr{R}}_4)$.

The case $\widehat{\mathscr{R}}_4 < 0$. This condition implies $b > 0$ and clearly the ellipse (6.39) is real.

We observe that systems (6.38) possess the invariant line $x = 0$. Then by Lemma 2.2.17 the condition $B_1 = 0$ is satisfied. Moreover by this lemma systems (6.38) could not possess another invariant line because $B_2 = -2048b^2x^4 \neq 0$ due to the condition $b \neq 0$. So systems (6.38) possess exactly one invariant line $x = 0$. For these systems we have $\mu_0 = 4/27 \neq 0$.

On the other hand in this case the coordinates of the finite singularities for systems (6.38) could be obtained from the coordinates described in (6.33) setting $h = -1/3$:

$$x_{1,2} = 0, \quad y_{1,2} = \pm\sqrt{3b}; \qquad x_{3,4} = \pm\sqrt{b}, \quad y_{3,4} = 0. \tag{6.40}$$

We detect that the singularities $M_{1,2}$ belong to the ellipse as well as to the invariant line $x = 0$. Since $b > 0$ all four singularities are real and $M_{3,4}$ are located outside the invariant curves. As a result we arrive at *Config. E.17* (example: $b = 1$).

The case $\widehat{\mathscr{R}}_4 > 0$. This condition implies $b < 0$ and clearly the ellipse (6.39) is complex. According to (6.40) the condition $b < 0$ implies that the singularities $M_{1,2}$ located on the ellipse also are complex. Thus we arrive at *Config. E.20* (example: $b = -1$).

Then we have all the configurations indicated in the diagram of Fig. 245 in the block corresponding to the possibility $(\mathfrak{B}_8)$.

6.3.1.2 The subcase $\theta = 0$

We examine step by step each one of the possibilities presented in Cor. 6.2.7 and corresponding to this case.

6.3.1.2.1 The possibility $(\mathfrak{B}_9)$: $\widetilde{N}\neq 0, \widehat{\beta}_1\neq 0, \widehat{\beta}_2\neq 0$.

As it was proved in Oliveira *et al.* (2021) in this case by an affine transformation and time rescaling systems (6.4) could be brought to the canonical form

$$\begin{aligned} \dot{x} &= a+dy+gx^2,\\ \dot{y} &= -\frac{a}{g}-dx-x^2+gxy-y^2, \quad g\neq 0, \end{aligned} \tag{6.41}$$

which possesses an invariant conic

$$\Phi(x,y)=\frac{a}{g}+x^2+y^2=0. \tag{6.42}$$

This conic is irreducible if and only if $a\neq 0$. For systems (6.41) we calculate

$$\widetilde{N}=\left(g^2+4\right)x^2, \quad \widehat{\beta}_1=-d^2\left(g^2+4\right)\left(9g^2+4\right)/16,$$
$$\widehat{\beta}_2=-g\left(g^2+4\right)/2, \quad \widehat{\mathscr{R}}_5=12ag\left(g^2+4\right),$$

and therefore we conclude that for systems (6.41) the condition $\widetilde{N}\widehat{\beta}_1\widehat{\beta}_2\widehat{\mathscr{R}}_5\neq 0$ is equivalent to the condition $adg\neq 0$. On the other hand we observe that $\mathrm{sign}(ag)=\mathrm{sign}(\widehat{\mathscr{R}}_5)$.

Taking into account Lemma 2.2.17 we calculate

$$B_1=-\frac{a^2d^2\left(g^2+1\right)\left(g^2+4\right)^2}{g}\neq 0,$$

due to condition $adg\neq 0$, and we conclude that systems (6.41) could not possess invariant lines.

The case $\widehat{\mathscr{R}}_5<0$. Then $ag<0$ and clearly the ellipse (6.42) is real.

For systems (6.41) we calculate $\mu_0=g^2\neq 0$ and therefore by Lemma 2.2.13 the systems have finite singularities of total multiplicity 4.

We detect that two of these singularities are located on the ellipse (6.42), more exactly the singularities $M_{1,2}\left(x_{1,2},y_{1,2}\right)$, with

$$x_{1,2}=\pm\frac{\sqrt{Z_1}}{g}, \quad y_{1,2}=\frac{d}{g}, \quad Z_1=-(ag+d^2). \tag{6.43}$$

Other two singularities of systems (6.41) are $M_{3,4}\left(x_{3,4},y_{3,4}\right)$ (generically located outside the ellipse), with

$$x_{3,4}=-\frac{dg\pm\sqrt{Z_2}}{2g}, \quad y_{3,4}=-\frac{1}{2}\left(dg\pm\sqrt{Z_2}\right), \quad Z_2=g\left(d^2g-4a\right). \tag{6.44}$$

On the other hand for systems (6.41) we calculate

$$\nu_1=-d^4g^2\left(g^2+4\right)^2\left(9g^2+4\right)^2Z_1/256.$$

We observe that

$$\operatorname{sign}(\nu_1) = -\operatorname{sign}(Z_1),$$

and this means that the singularities $M_{1,2}$ are real (respectively complex or coinciding) if $\nu_1 < 0$ (respectively $\nu_1 > 0$ or $\nu_1 = 0$).

1) *The subcase* $\nu_1 < 0$. Then the singularities $M_{1,2}$ located on the invariant ellipse are real. We need to determine the conditions when at least one of the singularities $M_{3,4}$ located outside the ellipse lies on the ellipse. For this, considering (6.42) and (6.44), we calculate

$$\Phi(x,y)|_{\{x=x_{3,4},\ y=y_{3,4}\}} = \frac{d^2\left(g^3+g\right) - 2ag^2 \pm d\left(g^2+1\right)\sqrt{g\left(d^2g-4a\right)}}{2g} \equiv \Omega_{3,4}(a,d,g).$$

It is clear that at least one of the singularities $M_3(x_3,y_3)$ or $M_4(x_4,y_4)$ belongs to the ellipse (6.42) if and only if

$$\Omega_3\Omega_4 = \frac{aZ_3}{g} = 0, \qquad Z_3 = ag^3 + d^2\left(g^2+1\right).$$

On the other hand for systems (6.41) we have

$$\nu_2 = -105dg\left(9g^2+4\right)Z_3,$$

and clearly since $adg \neq 0$ the condition $\nu_2 = 0$ is equivalent to $Z_3 = 0$.

Next we examine two possibilities: $\nu_2 \neq 0$ and $\nu_2 = 0$.

a) *The possibility* $\nu_2 \neq 0$. In this case we have *Config. E.1* since other singularities could belong to ellipse if and only if $\nu_2 = 0$ (example: $a = 5/4, d = 1, g = -1$).

b) *The possibility* $\nu_2 = 0$. In this case we have $Z_3 = 0$ and since $g \neq 0$ this condition gives $a = -\dfrac{d^2\left(g^2+1\right)}{g^3}$. Therefore we obtain the following coordinates of the singularities $M_i, i = 1,2,3,4$:

$$(x_1,y_1) = \left(\frac{d}{g^2},\frac{d}{g}\right), \quad (x_2,y_2) = \left(-\frac{d}{g^2},\frac{d}{g}\right),$$
$$(x_3,y_3) = \left(-\frac{d\left(g^2+1\right)}{g^2},-\frac{d\left(g^2+1\right)}{g}\right), \quad (x_4,y_4) = \left(\frac{d}{g^2},\frac{d}{g}\right).$$

As we can observe, the singularity M_4 coalesced with M_1. Therefore on the ellipse we have a double singularity M_1 and a simple singularity M_2. On the other hand we have

$$\Phi(x,y)|_{\{x=x_3,y=y_3\}} = \frac{d^2\left(g^4+3g^2+2\right)}{g^2} \neq 0,$$

due to $d \neq 0$. Hence the singularity M_3 remains outside the ellipse and we arrive at *Config. E.2* (example: $a = -1, d = \sqrt{2}/2, g = 1$).

2) *The subcase* $\nu_1 = 0$. In this case we have $Z_1 = 0$, i.e. $a = -d^2 g$ and this implies $Z_3 = d^2 \neq 0$. Therefore the two singularities which belong to the ellipse coalesce, whereas other two singularities remain outside the ellipse. In this way we get *Config. E.4* (example: $a = 1, d = 1, g = -1$).

3) *The subcase* $\nu_1 > 0$. Then we have $Z_1 < 0$, i.e. the two singularities which belong to the ellipse are complex. We note that the condition $Z_1 < 0$ implies $Z_3 \neq 0$, because if $Z_3 = 0$ we found $Z_1 = d^2/g^2 > 0$. This leads to *Config. E.5* (example: $a = 1/2, d = 1, g = -1$).

We claim that in this configuration the invariant ellipse is a limit cycle. Indeed, taking into consideration Thm. 6.2.5 (see statement (B_3)) we conclude that in the case under examination, for the existence of limit cycles the following conditions must be satisfied:

$$\eta < 0,\ \theta = \widehat{\gamma}_1 = \widehat{\gamma}_2 = \widehat{\gamma}_6 = 0, \widehat{\beta}_1 \widehat{\beta}_2 \neq 0,\ \widehat{\mathscr{R}}_5 < 0,\ \mathscr{T}_3 \mathscr{F} < 0.$$

Clearly all the conditions are satisfied except the last one. So it remains to verify that $\mathscr{T}_3 \mathscr{F} < 0$ is fulfilled, too. For systems (6.41) we calculate

$$\nu_1 = \frac{1}{256} d^4 g^2 \left(g^2+4\right)^2 \left(9g^2+4\right)^2 \left(ag+d^2\right), \quad \mathscr{T}_3 \mathscr{F} = -\frac{1}{8} d^2 g^2 \left(9g^2+4\right)^2 \left(ag+d^2\right),$$

and evidently the condition $\nu_1 > 0$ implies $\mathscr{T}_3 \mathscr{F} < 0$. This completes the proof of our claim.

The case $\widehat{\mathscr{R}}_5 > 0$**.** This condition implies $ag > 0$ and clearly the ellipse (6.42) is complex.

As we discuss on the case $\widehat{\mathscr{R}}_5 < 0$ for these systems we have $\mu_0 \neq 0$. Then by Lemma 2.2.13, systems (6.41) have finite singularities of total multiplicity 4 and the coordinates are given in (6.43) and (6.44). We observe that the condition $ag > 0$ implies $Z_1 < 0$, i.e. the singularities $M_{1,2}(x_{1,2}, y_{1,2})$ are complex and as it was proved before they belong to the complex ellipse.

On the other hand the condition $ag > 0$ yields $Z_3 = ag^3 + d^2\left(g^2+1\right) \neq 0$. This fact implies that the singularities $M_{3,4}(x_{3,4}, y_{3,4})$ remain outside the complex ellipse. Therefore the unique possible configuration is *Config. E.15*, detected before (example: $a = -1, d = 1, g = -1$).

Thus, we have all the configurations indicated in the diagram of Fig. 247 in the block corresponding to the possibility $(\mathfrak{B}_9)$.

6.3.1.2.2 The possibility $(\mathfrak{B}_{10})$: $\widetilde{N} \neq 0, \widehat{\beta}_1 \neq 0, \widehat{\beta}_2 = 0$.

As it was proved in Oliveira *et al.* (2021) in this case by an affine transformation and time rescaling systems (6.4) could be brought to the two–parameter family of systems

$$\dot{x} = dy, \qquad \dot{y} = b - dx - x^2 - y^2, \qquad d \neq 0, \tag{6.45}$$

which is a subfamily of (6.17) defined by the condition $h = -1$. Clearly these systems possess the same invariant ellipse (6.18) which in this particular case takes the form

$$\Phi(x,y) = -b + x^2 + y^2 = 0. \tag{6.46}$$

This conic is irreducible if and only if $b \neq 0$.

We claim that the infinite invariant line $Z = 0$ for systems (6.45) is of multiplicity 2. Indeed considering Lemma 2.2.19 for these systems we calculate:

$$\gcd(\mathscr{E}_1, \mathscr{E}_2) = dZ,$$

and by Lemma 2.2.19, statement *(3)*, the line $Z = 0$ is a double one. This completes the proof of our claim.

For systems (6.45) we calculate

$$\widetilde{N} = 16bd^2x^2, \quad \widehat{\beta}_1 = -d^2, \quad \widehat{\mathscr{R}}_6 = -4b,$$

and therefore we conclude that for these systems the condition $\widetilde{N}\widehat{\beta}_1\widehat{\mathscr{R}}_6 \neq 0$ is equivalent to the condition $bd \neq 0$. On the other hand we have $\operatorname{sign}(b) = -\operatorname{sign}(\widehat{\mathscr{R}}_6)$.

The case $\widehat{\mathscr{R}}_6 < 0$. Then $b > 0$ and clearly the ellipse (6.46) is real.

Considering Lemma 2.2.17 we examine if systems (6.45) could possess at least one invariant affine line. Calculations yield $B_1 = 0$, however we claim that this condition is implied by the existence of the double line at the infinity. Indeed, the coefficients of systems (6.45) could be perturbed with a small parameter $0 < \varepsilon \ll 1$ as follows:

$$\dot{x} = (d + \varepsilon x)y, \qquad \dot{y} = b - dx - x^2 - y^2.$$

Evidently, these systems possess the invariant line $d + \varepsilon x = 0$ and hence by Lemma 2.2.17 we have $B_1 = 0$ (this could also be checked directly).

On the other hand, by Lemma 2.2.17, systems (6.45) could not possess any finite invariant lines because $B_2 = -10368b^2x^4 \neq 0$, due to condition $bd \neq 0$.

For these systems we calculate $\mu_0 = \mu_1 = 0$ and $\mu_2 = d^2(x^2 + y^2) \neq 0$. According to Lemma 2.2.13, two finite singularities coalesced with infinite singularities, namely with the complex singularities $[\pm i : 1 : 0]$.

Therefore on the line $Z = 0$ we get two double complex infinite singularities. This is however irrelevant in view of the definition of a configuration (see Def. 6.1.8). So the unique real singularity at infinity is of multiplicity one.

On the other hand, by Lemma 2.2.13, systems (6.45) have finite singularities of total multiplicity 2. We detect that these singularities are located outside the ellipse (6.46) and their coordinates are $M_{1,2}\left(x_{1,2},y_{1,2}\right)$, with

$$x_{1,2}=-\frac{d\pm\sqrt{4b+d^2}}{2},\quad y_{1,2}=0.$$

For these singularities we calculate

$$\Phi(x,y)|_{\{x=x_{1,2},\ y=y_{1,2}\}}=\frac{d(d\pm\sqrt{4b+d^2})}{2}\equiv\Omega_{1,2}(b,d),\quad \Omega_1\Omega_2=-bd^2\neq 0.$$

We conclude that neither M_1 nor M_2 could belong to the ellipse. As a result we arrive at *Config. E.24* (example: $b=1,d=-1$).

The case $\widehat{\mathscr{R}}_6>0$. Then $b<0$ and clearly the ellipse (6.46) is complex. Since none of the singularities $M_{1,2}$ could be on the ellipse, we obtain *Config. E.25* (example: $b=-1,d=-1$).

So we have all the configurations indicated in the diagram of Fig. 247 in the block corresponding to the possibility $(\mathfrak{B}_{10})$.

6.3.1.2.3 The possibility $(\mathfrak{B}_{11})$: $\widetilde{N}\neq 0,\widehat{\beta}_1=0$.

As it was proved in Oliveira *et al.* (2021) in this case by an affine transformation and time rescaling, systems (6.4) could be brought to the canonical form (6.5) with $h=-1$ and $d=0$. So we consider the following systems

$$\dot{x}=a+gx^2,\quad \dot{y}=-\frac{a}{g}-x^2+gxy-y^2,\quad g\neq 0, \tag{6.47}$$

which possess the invariant ellipse (6.6), i.e.

$$\Phi(x,y)=\frac{a}{g}+x^2+y^2=0, \tag{6.48}$$

which is irreducible if and only if $a\neq 0$.

We observe that systems (6.47) possess the invariant lines $\mathscr{L}_{1,2}(x,y)=a+gx^2=0$, i.e.

$$\mathscr{L}_1(x,y)=x-\frac{\sqrt{-ag}}{g}=0,\quad \mathscr{L}_2(x,y)=x+\frac{\sqrt{-ag}}{g}=0. \tag{6.49}$$

Then by Lemma 2.2.17 the condition $B_1=0$ is satisfied. Moreover by this lemma, systems (6.47) could possess an invariant line in another direction only if $B_2=0$. However, for these systems we have

$$B_2=-\frac{648a^2\left(g^2+1\right)\left(g^2+4\right)^2x^4}{g^2}\neq 0.$$

So we conclude that systems (6.47) possess exactly two invariant lines (6.49), which are distinct due to $ag \neq 0$ and they could be real or complex, depending on $\mathbf{sign}(ag)$.

For systems (6.47) we calculate

$$\widetilde{N} = \left(g^2+4\right)x^2, \quad \widehat{\mathscr{R}}_3 = 160ag\left(g^2+1\right)\left(g^2+4\right),$$

and therefore we conclude that $\mathbf{sign}(ag) = \mathbf{sign}(\widehat{\mathscr{R}}_3)$.

The case $\widehat{\mathscr{R}}_3 < 0$. Then $ag < 0$ which implies that the ellipse (6.48) as well as the invariant lines (6.49) are real.

For systems (6.47) we calculate $\mu_0 = g^2 \neq 0$ due to the condition $g \neq 0$. Then by Lemma 2.2.13 the mentioned systems have finite singularities of total multiplicity 4.

We detect that two of these singularities are located on the ellipse (6.48), more exactly such singularities are $M_{1,2}\left(x_{1,2}, y_{1,2}\right)$, with

$$x_{1,2} = \pm\frac{\sqrt{-ag}}{g}, \quad y_{1,2} = 0.$$

Other two singularities of systems (6.47) are $M_{3,4}\left(x_{3,4}, y_{3,4}\right)$ (generically located outside the ellipse), with

$$x_{3,4} = \pm\frac{\sqrt{-ag}}{g}, \quad y_{3,4} = \pm\sqrt{-ag}. \tag{6.50}$$

We also detect that the singularities $M_{1,3}$ (respectively $M_{2,4}$) belong to the line $\mathscr{L}_1(x,y) = 0$ (respectively $\mathscr{L}_2(x,y) = 0$).

For the singularities $M_{3,4}$ we calculate

$$\Phi(x,y)|_{\{x=x_{3,4},\ y=y_{3,4}\}} = -ag \neq 0,$$

and we conclude that neither $M_3(x_3,y_3)$ nor $M_4(x_4,y_4)$ belong to the ellipse (6.48). According to (6.50) we observe that $y_3 > 0$ and $y_4 < 0$, which leads to *Config. E.26* (example: $a = 1, g = -1$).

The case $\widehat{\mathscr{R}}_3 > 0$. Then $ag > 0$ and this implies that the ellipse (6.48) as well as the invariant lines (6.49) and the four singularities of systems (6.47) are complex. Therefore we obtain *Config. E.27* (example: $a = -1, g = -1$).

Therefore we have all the configurations indicated in the diagram of Fig. 247 in the block corresponding to the possibility $(\mathfrak{B}_{11})$.

6.3.1.2.4 The possibility $(\mathfrak{B}_{12})$: $\widetilde{N}=0$.

As it was proved in Oliveira *et al.* (2021) in this case by an affine transformation and time rescaling systems (6.4) could be brought to the systems

$$\dot{x}=2xy, \quad \dot{y}=b-x^2+y^2, \tag{6.51}$$

which possess the family of invariant ellipses

$$\Phi(x,y)=b+qx+x^2+y^2=0, \quad q\in\mathbb{R}, \tag{6.52}$$

depending on the parameter q and having the corresponding determinant $\Delta=(4b-q^2)/4$. So for any fixed value of the parameter q, the ellipses from the family (6.52) are irreducible if and only if $\Delta\neq 0$.

Since for systems (6.51) we have $B_1=B_2=B_3=0$, by Lemma 2.2.17 these systems could possess invariant lines in three different directions. We verify that these systems indeed possess the following five invariant lines:

$$\mathscr{L}_1(x,y)=x=0, \quad \mathscr{L}_{2,4}(x,y)=(x-iy)^2-b=0, \quad \mathscr{L}_{3,5}(x,y)=(x+iy)^2-b=0. \tag{6.53}$$

Since $\mu_0=-4\neq 0$ systems (6.51) possess finite singularities of total multiplicity four and their coordinates are

$$x_{1,2}=0, \quad y_{1,2}=\pm\sqrt{-b}, \qquad x_{3,4}=\pm\sqrt{b}, \quad y_{3,4}=0.$$

We observe that if $b\neq 0$ systems (6.51) have two real and two complex singularities. Moreover we have that the real singularities are located on the real invariant line $\mathscr{L}_1(x,y)=0$ if $b<0$ (namely $M_{1,2}$) and outside this invariant line if $b>0$ (in this case the real singularities are M_3 and M_4). In the case $b=0$ all four singularities coincide and we have one real singularity of multiplicity four.

On the other hand for systems (6.51) we calculate $\widehat{\mathscr{R}}_7=32b$, which implies $\mathbf{sign}(b)=\mathbf{sign}(\widehat{\mathscr{R}}_7)$. It is clear that if $\widehat{\mathscr{R}}_7\leq 0$ the invariant ellipses from the family (6.52) are real and if $\widehat{\mathscr{R}}_7>0$ they could be real or complex, depending on the parameter q in (6.52). So, if $\widehat{\mathscr{R}}_7<0$ we arrive at *Config. E.28* (example: $b=-75, q\in\mathbb{R}$) and if $\widehat{\mathscr{R}}_7=0$ the complex invariant lines (6.53) become double and we obtain *Config. E.29* (example: $b=0, q\neq 0$). In the case $\widehat{\mathscr{R}}_7>0$ we observe that for any fixed value of parameter b, any ellipse from the family (6.52) is invariant for systems (6.51). In other words, for any $b>0$ we have that such systems possess simultaneously an infinite number of real ellipses as well as an infinite number of complex ellipses. Therefore, taking into consideration Rmk. 6.1.12 we arrive at *Config. E.30* (example: $b=1/8, |q|>\sqrt{2}/2$).

Thus, we have all the configurations indicated in the diagram of Fig. 247 in the block corresponding to the possibility $(\mathfrak{B}_{12})$.

6.3.2 The case $C_2 = 0$

According to Lemma 2.2.14 a quadratic system with the condition $C_2 = 0$ could be brought via an affine transformation and time rescaling to the following canonical form:

$$\dot{x} = a + cx + dy + x^2, \quad \dot{y} = b + ex + fy + xy,$$

with $C_2 \equiv 0$, i.e. the line at infinity of this system is filled up with singularities. Following Oliveira *et al.* (2021) (see the diagram of Fig. 239) and Cor. 6.2.7 we discuss two possibilities.

6.3.2.1 The possibility $(\mathfrak{C}_1)$: $H_{10} \neq 0$.

As it was proved in Oliveira *et al.* (2021) in this case we have the systems

$$\dot{x} = a + y + x^2, \quad \dot{y} = xy, \tag{6.54}$$

which possess the family of invariant ellipses

$$\Phi(x,y) = a + 2y + x^2 + m^2y^2 = 0, \quad m \neq 0. \tag{6.55}$$

We observe that for any fixed value of the parameter a, the ellipses from the family (6.55) are irreducible if and only if $\Delta = am^2 - 1 \neq 0$.

Since for systems (6.54) we have $B_1 = B_2 = B_3 = 0$, by Lemma 2.2.17 these systems could possess invariant lines in three different directions. We verify that these systems indeed possess the following three invariant lines:

$$\mathscr{L}_1(x,y) = y = 0, \quad \mathscr{L}_{2,3}(x,y) = y \pm \sqrt{-a}x + a = 0.$$

It is clear that the invariant lines $\mathscr{L}_2(x,y)$ and $\mathscr{L}_3(x,y)$ are real, coinciding or complex if $a < 0$, $a = 0$ or $a > 0$, respectively.

Since $\mu_0 = 0$ and $\mu_1 = x \neq 0$, Lemma 2.2.13 tells us that there exist exactly three finite singularities. Their coordinates are given by

$$x_{1,2} = \pm\sqrt{-a}, \quad y_{1,2} = 0, \qquad x_3 = 0, \quad y_3 = -a.$$

For each fixed value of the parameter a we observe that if $a < 0$ (respectively $a > 0$) the singularities $M_{1,2}$ are real (respectively complex) and they verify the equalities

$$\Phi(x_1,y_1) = \mathscr{L}_1(x_1,y_1) = \mathscr{L}_2(x_1,y_1) = 0, \quad \Phi(x_2,y_2) = \mathscr{L}_1(x_2,y_2) = \mathscr{L}_3(x_2,y_2) = 0,$$

respectively. Moreover we detect that the singularity M_3 belongs to the invariant lines $\mathscr{L}_2(x,y)$ and $\mathscr{L}_3(x,y)$ and this singularity belongs to the irreducible invariant ellipse $\Phi(x,y) = 0$ if and only if $a = 0$. In such a case (i.e. when $a = 0$) all three singularities

coincide (as well the three invariant lines $\mathscr{L}_1$, $\mathscr{L}_2$ and $\mathscr{L}_3$) and we have one real singularity of multiplicity three located on a triple invariant line.

On the other hand for systems (6.54) we calculate $H_9 = 2304a^3$, which implies $\mathrm{sign}(a) = \mathrm{sign}(H_9)$. It is clear that if $H_9 \leq 0$ then the irreducible conics from the family (6.55) are real and if $H_9 > 0$ they could be real or complex, depending on the parameter m in (6.55). So, if $H_9 < 0$ we arrive at *Config. E.31* (example: $a = -75, m \in \mathbb{R}\backslash\{0\}$) and if $H_9 = 0$ we obtain *Config. E.32* (example: $a = 0, m \in \mathbb{R}\backslash\{0\}$). In the case $H_9 > 0$, as we discussed before, for any fixed value of the parameter a, systems (6.54) possess simultaneously an infinite number of real ellipses as well as an infinite number of complex ellipses. Then, based on Rmk. 6.1.12 we obtain *Config. E.33* (example: $a = 1/2, |m| < \sqrt{2}$).

Thus, we have all the configurations indicated in the diagram of Fig. 248 in the block corresponding to the possibility $(\mathfrak{C}_1)$.

6.3.2.2 *The possibility* $(\mathfrak{C}_2)$: $H_{10} = 0$.

As it was proved in Oliveira *et al.* (2021) in this case we have the systems

$$\dot{x} = a + x^2, \qquad \dot{y} = xy, \qquad a \neq 0, \tag{6.56}$$

which possess the family of invariant ellipses

$$\Phi(x,y) = a + x^2 + m^2y^2 = 0, \quad m \in \mathbb{R}\backslash\{0\}. \tag{6.57}$$

Since for this family of ellipses we have $\Delta = am^2 \neq 0$ due to $am \neq 0$, we deduce that the family (6.57) cannot contain any reducible conic.

For systems (6.56) we calculate $B_1 = B_2 = B_3 = 0$ and hence, by Lemma 2.2.17, these systems could possess invariant lines in three different directions. We verify that these systems possess the following three invariant lines:

$$\mathscr{L}_1(x,y) = y = 0, \quad \mathscr{L}_{2,3}(x,y) = x \mp \sqrt{-a} = 0.$$

It is clear that the invariant lines $\mathscr{L}_2(x,y)$ and $\mathscr{L}_3(x,y)$ are real if $a < 0$ and complex if $a > 0$.

Since $\mu_0 = \mu_1 = 0$ and $\mu_2 = ax^2 \neq 0$, Lemma 2.2.13 tells us that there exist exactly two finite singularities. Their coordinates are

$$x_{1,2} = \pm\sqrt{-a}, \quad y_{1,2} = 0.$$

We observe that if $a < 0$ (respectively $a > 0$) the singularities $M_{1,2}$ are real (respectively complex) and they are located on each one of the invariant ellipse of the family $\Phi(x,y) = 0$ from (6.57). Moreover we observe that

$$\mathscr{L}_1(x_1,y_1) = \mathscr{L}_2(x_1,y_1) = 0, \quad \mathscr{L}_1(x_2,y_2) = \mathscr{L}_3(x_2,y_2) = 0.$$

On the other hand for systems (6.56) we calculate $H_{11} = -192ax^4$, which implies $\mathrm{sign}(a) = -\mathrm{sign}(H_{11})$. So, we arrive at *Config. E.34* if $H_{11} < 0$ (example: $a = 27, m \in \mathbb{R}$) and *Config. E.35* if $H_{11} > 0$ (example: $a = -75, m \in \mathbb{R}$).

Thus, we have all the configurations indicated in the diagram of Fig. 248 in the block corresponding to the possibility $(\mathfrak{C}_2)$.

Since all the affine invariant subsets in $\mathbb{R}^{12}$ defined in Cor. 6.2.7 are examined, we conclude that Thm. 6.3.1 is proved.

6.4 Concluding comments

Now we present some conclusions about the 35 configurations obtained and their realization. The diagrams of Figs. 245, 247 and 248 give an algorithm to compute for any system possessing an invariant ellipse, presented in any normal form, its configuration. Moreover the diagrams of Figs. 245, 247 and 248 are the bifurcation diagrams of the configurations of such systems, done in the 12–parameter space of the coefficients of these systems.

6.4.1 Concluding comments for $\eta < 0$

According to Thm. 6.3.1, each non–degenerate quadratic system in the class $\mathbf{QSE}_{(\eta<0)}$ possesses either exactly one invariant ellipse or a family of invariant ellipses. This class yields 30 distinct configurations which can be split into the following cases according to their geometry:

α_1) Fourteen configurations with exactly one ellipse and no invariant lines other that a line at infinity, which is simple. Among these we only have three cases where the ellipse is complex. The configurations are split into subsets by the total multiplicity of the real singularities located on them, whose maximum is 5 in the case of real ellipses and 3 in the case of complex ellipses.

We point out that in this class we have the only two configurations with limit cycles occurring in the family **QSE**. In both configurations we only have one real singular point located on the configuration, on the line of infinity. The two configurations whit the ellipse as a limit cycle are distinguished by the multiplicity of this singularity which could be one or two.

α_2) Eleven configurations with exactly one ellipse and invariant lines of total multiplicity 2, including the line at infinity. Among these we only have two configurations with complex ellipses, distinguished by the number of invariant lines, which could be 2 or 1. The remaining configurations are distinguished by the number of invariant lines (1 or

2) and by the geometry of the positions of the invariant lines with respect to the ellipses as well as the multiplicities of the real singularities located on the configurations.

α_3) Two configurations of systems possessing exactly one invariant ellipse (real or complex) and three simple invariant lines, including the line at infinity, the two affine lines being real or complex.

α_4) Three configurations, each one of them possessing an infinite family of invariant ellipses. Two of them possess only real ellipses (*Config. E.28* and *Config. E.29*) and one of them (*Config. E.30*) possesses simultaneously an infinity of real ellipses and an infinity of complex ellipses (according to Rmk. 6.1.12 we only placed the real ellipses on the drawing of this configuration). All three configurations possess invariant lines of total multiplicity 6, including the line at infinity and they are distinguished by the number of singular points located on the real invariant lines of the configurations.

6.4.2 Concluding comments for $C_2 = 0$

According to Thm. 6.3.1, each non–degenerate quadratic system in the class $\mathbf{QSE}_{(C_2=0)}$ possesses an infinite family of invariant ellipses and in addition its line at infinity is filled up with singularities. This class yields five distinct configurations which can be split into the following cases according to their geometry:

β_1) Three configurations possessing an infinity of real ellipses (*Config. E.31*, *Config. E.33* and *Config. E.35*), have affine invariant lines (real) of total multiplicity 3. These configurations are distinguished by the number of singular points located on these invariant lines.

β_2) One configuration (*Config. E.34*) has an infinity of only complex ellipses and three invariant lines two of them complex parallel lines.

β_3) One configuration (*Config. E.33*) possesses simultaneously an infinity of real ellipses and an infinity of complex ellipses (according to Rmk. 6.1.12 we only placed the real ellipses on the drawing of this configuration). This configuration also possesses three invariant lines, two of them complex intersecting at a real singular point.

CONCLUSION

In this thesis we have seen some applications of the Invariant Theory in the study of quadratic differential systems on the plane. By using this tool we could perform a complete study of the bifurcation diagram corresponding to the class $\overline{\mathbf{QsnSN_{11}}}$ of all quadratic systems possessing a finite saddle–node $\overline{sn}_{(2)}$ located at the origin of the plane and an infinite saddle–node of type $\overline{\binom{1}{1}}\,SN$. This class is divided into families $\mathbf{QsnSN_{11}(A)}$ and $\mathbf{QsnSN_{11}(B)}$, as described in Chap. 3 and 4, respectively.

With the study of the bifurcation diagram of family $\mathbf{QsnSN_{11}(B)}$ we could obtain all the representatives for the phase portraits from the set (AC), as we have described in Chap. 5. In addition, we have proved that all the generic phase portraits obtained in the bifurcation diagram described in Artés, Rezende and Oliveira (2015) are indeed all the representatives for the phase portraits from the set (AB).

The study of the bifurcation diagram of family $\mathbf{QsnSN_{11}(A)}$ will be very useful in a near future when someone performs the classification of all the phase portraits of codimension three, modulo limit cycles. Moreover, with this study we had the possibility of starting the analysis of a higher dimension bifurcation diagram, for future studies it is important to have clear ideas about how we work in such levels of dimensions.

The study presented in the final chapter, also done with help of the Invariant Theory, is very interesting in the sense of classification of quadratic systems with invariant conics. Also, this study is closely related to the problem of classification of phase portraits, since the knowledge of algebraic invariant curves can help us to draw phase portraits. In a near future we intend to continue collaborating with Professor Nicolae Vulpe and Professor Dana Schlomiuk in the study of quadratic systems with invariant parabolas.

Therefore, with this thesis we have contributed a little bit to the classification of quadratic systems.

In conclusion, in order to continue contributing to the classification of quadratic systems, in a near future we intent to continue studying other families of quadratic systems of codimension two and higher. Additionally, we intend to contribute in the study of the integrability of quadratic systems possessing invariant ellipses and invariant parabolas, as it was done in Oliveira, Schlomiuk and Travaglini (2021), where the authors studied the integrability of quadratic systems possessing invariant hyperbolas.

BIBLIOGRAPHY

ABHYANKAR, S. What is the difference between a parabola and a hyperbola? **The Mathematical Intelligencer**, v. 10, n. 4, p. 36–43, 1988. Citation on page 335.

ANDRONOV, A. A.; LEONTOVICH, E. A.; GORDON, I. I.; MAIER, A. G. **Qualitative theory of second-order dynamic systems**. NY-Toronto, Ontario: Halsted Press, A division of John Wiley & Sons, 1973. Citation on page 42.

ARTÉS, J. C.; DUMORTIER, F.; HERSSENS, C.; LLIBRE, J. **Computer program P4 to study phase portraits of planar polynomial differential equations**. 2005. Available: <mat.uab.es/~artes/p4/p4.html>. Citations on pages 94, 148, 186, and 251.

ARTÉS, J. C.; KOOIJ, R.; LLIBRE, J. **Structurally stable quadratic vector fields**. [S.l.]: Memoires Amer. Math. Soc., 1998. ISBN 0-8218-0796-X. Citations on pages 24, 25, 46, 47, 258, 260, 261, 262, 263, 264, 265, 303, 328, 329, and 330.

ARTÉS, J. C.; LLIBRE, J. Quadratic hamiltonian vector fields. **J. Differential Equations**, v. 107, p. 80–95, 1994. ISSN 0022-0396. Citation on page 99.

_____. Quadratic vector fields with a weak focus of third order. **Publ. Mat.**, v. 41, p. 7–39, 1997. Citation on page 24.

_____. Statistical measure of quadratic vector fields. **Resenhas**, v. 6, p. 85–97, 2003. Citation on page 328.

ARTÉS, J. C.; LLIBRE, J.; MEDRADO, J. C. Nonexistence of limit cycles for a class of structurally stable quadratic vector fields. **Discrete Contin. Dyn. Syst.**, v. 17, p. 259–271, 2007. Citation on page 328.

ARTÉS, J. C.; LLIBRE, J.; REZENDE, A. C. **Structurally unstable quadratic vector fields of codimension one**. [S.l.]: Birkhäuser, 2018. ISBN 978-3-319-92116-7. Citations on pages 25, 42, 47, 48, 101, 110, 242, 246, 251, 254, 258, 259, 260, 261, 262, 263, 264, 265, 270, 288, 296, 303, 307, 314, 317, 328, and 330.

ARTÉS, J. C.; LLIBRE, J.; SCHLOMIUK, D. The geometry of quadratic differential systems with a weak focus of second order. **Internat. J. Bifur. Chaos Appl. Sci. Engrg.**, v. 16, p. 3127–3194, 2006. Citations on pages 42, 56, 58, 61, 66, 81, 83, 84, 86, 89, 91, and 117.

ARTÉS, J. C.; LLIBRE, J.; SCHLOMIUK, D.; VULPE, N. From topological to geometric equivalence in the classification of singularities at infinity for quadratic vector fields. **Rocky Mountain J. Math.**, v. 45, p. 29–113, 2015. Citation on page 44.

_____. Global topological configurations of singularities for the whole family of quadratic differential systems. **Qualitative Theory on Dynamical Systems**, v. 51, 2020. Citations on pages 29 and 99.

_____. **Geometrical configurations of singularities of planar polynomial differential systems - A global classification in the quadratic case**. [S.l.]: Birkhäuser Basel, 2021. ISBN 978-3-030-50570-7. Citations on pages 44, 45, 66, 74, 82, 86, 87, 89, 123, 124, 125, 127, 128, 129, 156, 157, 242, 266, 268, and 269.

ARTÉS, J. C.; LLIBRE, J.; VULPE, N. Singular points of quadratic systems: a complete classification in the coefficient space $\mathbb{R}^{12}$. **Internat. J. Bifur. Chaos Appl. Sci. Engrg.**, v. 18, p. 313–362, 2008. Citations on pages 82, 119, 123, 128, and 157.

ARTÉS, J. C.; MOTA, M. C.; REZENDE, A. C. Quadratic differential systems with a finite saddle–node and an infinite saddle–node (1,1)SN - (A). **Internat. J. Bifur. Chaos Appl. Sci. Engrg.**, v. 31, n. 2, p. 24, 2021. Citations on pages 110 and 217.

_____. Quadratic differential systems with a finite saddle–node and an infinite saddle–node (1,1)SN - (B). **to appear at Internat. J. Bifur. Chaos Appl. Sci. Engrg.**, 2021. Citations on pages 303, 304, and 305.

_____. Structurally unstable quadratic vector fields of codimension two: families possessing a finite saddle-node and an infinite saddle-node. **to appear at Electron. J. Qual. Theo.**, 2021. Citation on page 269.

ARTÉS, J. C.; OLIVEIRA, R. D. S.; REZENDE, A. C. Topological classification of quadratic polynomial differential systems with a finite semi-elemental triple saddle. **Int. J. Bifurcation and Chaos**, v. 26, 2016. Citation on page 49.

_____. Structurally unstable quadratic vector fields of codimension two: families possessing either a cusp point or two finite saddle-nodes. **J. Dyn. Differ. Equ.**, p. 43, 2020. Citations on pages 21, 25, 26, 51, 246, 254, 259, and 260.

ARTÉS, J. C.; REZENDE, A. C.; OLIVEIRA, R. D. S. Global phase portraits of quadratic polynomial differential systems with a semi-elemental triple node. **Internat. J. Bifur. Chaos Appl. Sci. Engrg.**, v. 23, 2013. Citations on pages 49, 147, and 217.

_____. The geometry of quadratic polynomial differential systems with a finite and an infinite saddle-node (A,B). **Internat. J. Bifur. Chaos Appl. Sci. Engrg.**, v. 24, 2014. Citations on pages 147 and 217.

_____. The geometry of quadratic polynomial differential systems with a finite and an infinite saddle-node C. **Internat. J. Bifur. Chaos Appl. Sci. Engrg.**, v. 25, n. 3, 2015. Citations on pages 26, 61, 66, 78, 81, 83, 84, 88, 89, 91, 101, 110, 117, 125, 217, 245, 266, 303, 304, 305, and 387.

BALTAG, V. A. Algebraic equations with invariant coefficients inqualitative study of the polynomial homogeneous differential systems. **Bull. of Acad. of Sci. of Moldova. Mathematics**, v. 2, p. 31–46, 2003. Citation on page 71.

BALTAG, V. A.; VULPE, N. Total multiplicity of all finite critical points of the polynomial differential system. **Differ. Equ. Dyn. Syst.**, v. 5, p. 455–471, 1997. Citation on page 71.

BAUTIN, N. N. On periodic solutions of a system of differential equations. **Prikl. Mat. Meh.**, v. 18, 1954. Citation on page 43.

BULARAS, D.; CALIN, I.; TIMOCHOUK, L.; VULPE, N. T-comitants of quadratic systems: a study via the translation invariants. **Delft University of Technology, Faculty of Technical Mathematics and Informatics**, n. 96-90, 1996. Citation on page 70.

CAIRÓ, L.; LLIBRE, J. Darbouxian first integrals and invariants for real quadratic systems having an invariant conic. **J. Phys. A: Math. Gen.**, v. 35, p. 589–608, 2002. Citation on page 339.

CHICONE, C. **Ordinary differential equations with applications**. [S.l.]: Springer Science & Business Media, 2006. Citation on page 35.

CHRISTOPHER, C.; LLIBRE, J.; PEREIRA, J. V. Multiplicity of invariant algebraic curves in polynomial vector fields. **Pacific J. Math.**, v. 229, p. 63–117, 2007. Citation on page 340.

COLL, B. **Estudi qualitatu d'algunes classes de camps vectorials al pla**. Phd Thesis (PhD Thesis) — Universitat Autònoma of Barcelona, 1987. Citation on page 328.

COLL, B.; LLIBRE, J. Limit cycles for a quadratic system with an invariant straight line and some evolution of phase portraits. **Qualitative Theory of Differential Equations, Colloq. Math. Soc. János Bolyai, Bolyai Institut, Szeged, Hungria**, v. 53, p. 111–123, 1988. Citation on page 43.

COPPEL, W. A. A survey of quadratic systems. **J. Differential Equations**, v. 2, p. 293–304, 1966. Citations on pages 23, 24, 40, and 43.

DARBOUX, G. Mémoire sur les équations différentielles du premier ordre et du premier degré. **Bull. Sci. Math.**, v. 2, p. 60–96; 123–144; 151–200, 1878. Citation on page 333.

DUMORTIER, F.; FIDDELAERS, P. Quadratic models for generic local 3-parameter bifurcations on the plane. **T. Am. Math. Soc.**, v. 326, p. 101–126, 1991. Citation on page 23.

DUMORTIER, F.; LLIBRE, J.; ARTÉS, J. C. **Qualitative theory of planar differential systems**. New York: Universitext, Springer-Verlag, 2008. Citations on pages 31, 34, 40, 42, 44, 46, 94, 148, and 186.

DUMORTIER, F.; ROUSSARIE, R.; ROUSSEAU, C. Hilbert's 16th problem for quadratic vector fields. **J. Differential Equations**, v. 110, p. 66–133, 1994. Citations on pages 45, 46, 329, 330, and 331.

FULTON, W. **Algebraic curves: an introduction to algebraic geometry**. [S.l.: s.n.], 2008. Citations on pages 53 and 56.

GARCIA, A.; LEQUAIN, Y. **Elementos de álgebra**. 6. ed. [S.l.]: IMPA, 2012. Citations on pages 56 and 57.

GASULL, A.; REN, S. L.; LLIBRE, J. Chordal quadratic systems. **Rocky Mountain J. Math.**, v. 16, n. 4, p. 751–782, 1986. Citation on page 24.

GONZÁLEZ, E. A. Generic properties of polynomial vector fields at infinity. **Trans. Amer. Math. Soc.**, v. 143, p. 201–222, 1969. Citation on page 42.

HARTSHORNE, R. **Algebraic geometry**. [S.l.]: Springer, 1977. (Graduate Texts in Math., v. 52). Citation on page 58.

HILBERT, D. Mathematische probleme. **In Nachr. Ges. Wiss., editor, Second Internat. Congress Math. Paris. Göttingen Math.-Phys. Kl.**, p. 253–297, 1900. Citation on page 22.

_____. Mathematical problems. **Bull. Amer. Math. Soc.**, v. 8, p. 437–479, 1902. Citation on page 22.

HIRSCH, M. W. **Differential topology**. Berlin-Heidelberg-New York: Springer-Verlag, 1976. Citation on page 46.

HIRSCH, M. W.; SMALE, S.; DEVANEY, R. L. **Differential Equations, Dynamical Systems, and an Introduction to Chaos**. 2. ed. [S.l.]: Elsevier Academic Press Inc., 2004. Citation on page 34.

JAGER, P. Phase portraits for quadratics systems with a higher order singularity with two zero eigenvalues. **J. Diff. Eqns.**, v. 87, p. 169–204, 1990. Citation on page 24.

JIA, M.; CHEN, H.; CHEN, H. Bifurcation diagram and global phase portraits of a family of quadratic vector fields in class I. **Qual. Theo. Dyn. Syst.**, v. 19, p. 64–122, 2020. Citation on page 328.

JOUANOLOU, J. P. **Equations de pfaff algébriques**. New York: Springer, 1979. (Lecture Notes in Math., v. 708). Citation on page 334.

LI, C. Non-existence of limit cycles around a weak focus of order three for any quadratic system. **Chinese Ann. Math. Series B**, v. 7, n. 2, p. 174–190, 1986. Citation on page 43.

LLIBRE, J.; SCHLOMIUK, D. Geometry of quadratic differential systems with a weak focus of third order. **Canad. J. of Math.**, v. 56, n. 2, p. 310–343, 2004. Citations on pages 24, 43, 58, and 74.

LLIBRE, J.; ZHANG, X. Darboux theory of integrability in $\mathbb{C}^n$ taking into account the multiplicity. **J. Differential Equations**, v. 246, n. 2, p. 541–551, 2009. Citation on page 334.

NEUMANN, D. Classification of continuous flows on 2-manifolds. **Proc. Amer. Math. Soc.**, v. 48, p. 73–81, 1975. Citation on page 45.

OLIVEIRA, R. D. S.; REZENDE, A. C.; SCHLOMIUK, D.; VULPE, N. Geometric and algebraic classification of quadratic differential systems with invariant hyperbolas. **Electron. J. Differential Equations**, v. 295, 2017. Citations on pages 28 and 334.

_____. The family of quadratic differential systems with irreducible invariant ellipses: a complete classification in the space $\mathbb{R}^{12}$. **preprint**, 2021. Citations on pages 28, 336, 339, 342, 345, 356, 364, 365, 368, 370, 372, 374, 375, 377, 379, 381, 382, and 383.

OLIVEIRA, R. D. S.; SCHLOMIUK, D.; TRAVAGLINI, A. M. Geometry and integrability of quadratic systems with invariant hyperbolas. **Electron. J. Qual. Theo.**, n. 6, p. 1–56, 2021. Citation on page 387.

OLVER, P. J. **Classical invariant theory**. [S.l.]: Cambridge University Press, 1999. (London Mathematical Society Student Sexts, v. 44). Citations on pages 59 and 69.

PEIXOTO, M. M. Structural stability on two-dimensional manifolds. **Topology**, v. 1, p. 101–120, 1962. Citation on page 46.

POINCARÉ, H. Mémoire sur les courbes définies par une équation differentielle. **J. Math. Pures Appl.**, v. 1, p. 167–244, 1885. Citation on page 21.

_____. Sur l'intégration algébrique des équations différentielles. **C. R. Acad. Sci. Paris**, v. 112, p. 761–764, 1891. Citation on page 334.

_____. Sur l'intégration algébrique des équations différentielles du premier ordre et du premier degré. **I. Rend. Circ. Mat. Palermo**, v. 5, p. 169–191, 1891. Citation on page 334.

REYN, J. W. Phase portraits of a quadratic system of differential equations occurring frequently in applications. **Nieuw Arch. Wisk.**, v. 5, n. 2, p. 107–151, 1987. Citations on pages 23 and 24.

_____. Phase portraits of quadratic systems without finite critical points. **Faculty of Technical Mathematics and Informatics, Delft University of Technology, Delft, The Netherlands**, v. 36, 1991. Citation on page 24.

_____. A bibliography of the qualitative theory of quadratic systems of differential equations in the plane. **Faculty of Technical Mathematics and Informatics, Delft University of Technology, Delft, The Netherlands**, v. 2, 1994. Citation on page 23.

_____. Phase portraits of quadratic systems without finite critical points. **Nonlinear Anal-Theor.**, v. 27, 1996. Citation on page 23.

_____. Phase portraits of quadratic systems with finite multiplicity one. **Nonlinear Anal-Theor.**, v. 28, 1997. Citation on page 23.

_____. **Phase portraits of planar quadratic systems**. New York: Springer, 2007. (Mathematics and its Applications, v. 583). Citation on page 23.

REYN, J. W.; KOOIJ, R. E. Phase portraits of non-degenerate quadratic systems with finite multiplicity two. **Differential Equations Dynam. Systems**, v. 5, p. 355–414, 1997. Citation on page 328.

SCHLOMIUK, D.; PAL, J. On the geometry in the neighborhood of infinity of quadratic differential systems with a weak focus. **Qual. Theory Dyn. Syst.**, v. 2, n. 1, p. 01–43, 2001. Citations on pages 58 and 74.

SCHLOMIUK, D.; VULPE, N. Planar quadratic vector fields with invariant lines of total multiplicity at least five. **Qualitative Theory of Dynamical Systems**, v. 5, p. 135–194, 2004. Citations on pages 28, 72, 73, 74, 88, 126, 334, 336, and 337.

_____. Geometry of quadratic differential systems in the neighborhood of the infinity. **J. Differential Equations**, v. 215, p. 357–400, 2005. Citation on page 123.

_____. The full study of planar quadratic differential systems possessing a line of singularities at infinity. **J. Dynam. Differential Equations**, v. 20, n. 4, p. 737–775, 2008. Citations on pages 338 and 348.

_____. Integrals and phase portraits of planar quadratic differential systems with invariant lines of at least five total multiplicity. **Rocky Mountain J. Math.**, v. 38, p. 01–60, 2008. Citations on pages 28 and 334.

_____. Integrals and phase portraits of planar quadratic differential systems with invariant lines of total multiplicity four. **Bull. of Acad. of Sci. of Moldova. Mathematics**, v. 56, n. 1, p. 27–83, 2008. Citations on pages 28 and 334.

_____. Planar quadratic differential systems with invariant straight lines of total multiplicity four. **Nonlinear Anal.**, v. 68, n. 4, p. 681–715, 2008. Citations on pages 28 and 334.

_____. Global classification of the planar Lotka-Volterra differential systems according to their configurations of invariant straight lines. **J. Fixed Point Theory Appl.**, v. 8, n. 1, p. 177–245, 2010. Citations on pages 28, 72, and 334.

SIBIRSKY, K. S. **Introduction to the algebraic theory of invariants of differential equations**. Manchester University Press, Manchester: Translated from the Russian. Nonlinear Science: Theory and Applications, 1988. Citations on pages 61, 65, 66, and 67.

SONGLING, S. On limit cycles of plane quadratic systems. **Sci. Sin.**, v. 24, n. 2, p. 7, Feb. 1981. Citation on page 328.

SOTOMAYOR, J. **Curvas definidas por equações diferenciais no plano**. Rio de Janeiro: Instituto de Matemática Pura e Aplicada, 1979. Citation on page 42.

_____. **Equações diferenciais ordinárias**. 1. ed. ed. São Paulo: Livraria da Física, 2011. Citation on page 31.

VULPE, N. Affine-invariant conditions for the topological distinction of quadratic systems with a center. **J. Differential Equations**, v. 19, n. 3, p. 273–280, 1983. Citations on pages 24 and 48.

_____. **Polynomial bases of comitants of differential systems and their applications in qualitative theory**. Kishinev: Shtiintsa, 1986. Russian. Citations on pages 68 and 69.

_____. Characterization of the finite weak singularities of quadratic systems via invariant theory. **Nonlinear Anal.**, v. 74, p. 6553–6582, 2011. Citations on pages 74, 123, 125, 126, 127, 155, 205, and 348.

YE, Y. Q.; LO, C. Theory of limit cycles. **Transl. Math. Monogr.**, American Mathematical Society, v. 66, mar 1986. Citation on page 328.

ZHANG, P. Quadratic systems with a 3rd-order (or 2nd-order) weak focus. **Ann. Differential Equations**, v. 17, p. 287–294, 2001. Citation on page 43.

ŻOŁADEK, H. Quadratic systems with center and their perturbations. **J. Differential Equations**, v. 109, p. 223–273, 1994. Citation on page 24.

INDEX


ICMC
USP
SÃO CARLOS